THE MOTION DAMPING CHARACTERISTICS OF WIND ENERGY DEVICES

by

Fiona Mary Sinclair

A thesis submitted for the degree of

Doctor of Philosophy

in the

Faculty of Engineering

UNIVERSITY OF LONDON

February 1991

Department of Mechanical Engineering

University College London

Torrington Place

London WC1E 7JE

Abstract

Wind Assisted Ship Propulsion (WASP) uses wind energy devices such as wingsails, boundary layer control systems, wind turbines and others to augment the thrust provided by the ship's propeller. Ship motions in a seaway, particularly roll motions, can be reduced with consequent reductions in added hydrodynamic resistance, to yield fuel savings exceeding those predicted on the basis of thrust augmentation alone. Some wind assist devices compare favourably with the responses of conventional roll stabilisers. Attention is restricted to devices which are exterior to the hull and which apply direct aerodynamic forces or moments to the hull.

A theoretical analysis has been developed to examine wingsails for roll, pitch and yaw derivatives (both damping and inertia) due to harmonic excitation in roll at different headings and frequencies. Unsteady lifting surface theory has been used, linearised to first order in motion velocity. The theory has been augmented by experiments in the wind tunnel. Some measurements from a fishing boat with and without sails are also included. Other devices - wind turbines, Flettner rotors, Cousteau Turbosails and conventional roll stabilisers have been examined theoretically in roll only, using a quasisteady version of the above theory, as a comparison. Published data on steady lift and drag curves have been used, but these do not account for the motion of the separation point on the surface of the rotor and cylinder in unsteady motion.

Although offshore wind turbines are stationary, which makes resistance and propulsion irrelevant, they suffer from excitations due to wave motion which are unknown on land-based wind turbines, and also from shallow water effects and interractions with the aerodynamics which are unknown to deep-water offshore installations. The aerodynamic damping provided by the wind turbine will reduce the induced motions of the supporting structure.

The emphasis has been on the aerodynamics, rather than the hydrodynamics, because the hydrodynamic components of roll damping have been extensively researched elsewhere, and have proved impossible to evaluate in any generally applicable manner.

Contents

Acknowledgements

Much of this work has been funded by the SERC (Marine Technology Directorate Ltd.) under grant no. GR/D/8580.8, between 1/9/86 and 31/8/89. It has been performed at University College London under the supervision of Dr. B.R. Clayton.

Assistance has also been provided by the Amateur Yacht Research Society, especially James Byam Shaw, and the owner and crew of *M.F.V. Resolution*.

List of Figures

Nomenclature.

a_{mn} Non-dimensional inertia derivative coefficient in mode m due to motion in mode n

$a(\eta)$ Steady section lift curve slope $\partial C_L/\partial\alpha$

A Projected plan area (or swept area for wind turbine)

A_A, A_H Aero- and hydrodynamic components of inertia derivative

A_i Coefficients defined in Chapter 5

A_{mn} Aerodynamic inertia derivative in mode m due to motion in mode n

AR Aspect ratio = span^2/area

$A(\eta)$ Induced drag curve slope (i.e. $\partial C_D/\partial\alpha^2$)

b_{mn} Non-dimensional damping coefficients in mode m due to motion in mode n:

$b_{\phi n}$ $= B_{\phi n} / 0.5\rho V_A Ah^2$

$b_{\theta n}$ $= B_{\theta n} / 0.5\rho V_A Ah^2$

$b_{\psi n}$ $= B_{\psi n} / 0.5\rho V_A A\hat{c}h$

B Aerodynamic damping force

B_A, B_H Aero- and hydrodynamic components of $B_{\phi\phi}$

B_{mn} Aerodynamic damping force or moment derivative in mode m due to motion in mode n

B_s Structural damping force

B^* Critical damping force

$c(\eta)$ Local chord length of aerofoil

$\hat{c}$ Mean chord length

C Position of hull centre of gravity in body axes (Cx, Cy, Cz)

C_A Active damping derivative = $B / 0.5\,\rho V_A\, Ah^2$

C_B $B / 0.5\,\rho V_A\, Ah^2$ = passive damping derivative

C_D Drag coefficient, $D / 0.5\rho V_A^2 A$

C_{d0} Section form drag coefficient

C_H Static heel coefficient = roll moment / $0.5\,\rho\, V^2\, Ah$

$C(k)$ Theodorsen's function = $K_1 / (K_0 + K_1)$

C_L Lift coefficient, $L / 0.5\rho V_A^2 A$

C_{l0} Section lift coefficient at $\alpha = 0$

C_{m0} Section moment coefficient at $\alpha = 0$

C_M Inertia coefficient in Morison's equation

C_P Power coefficient = $P / 0.5\rho V^3 \pi R^2$

C_Q Torque coefficient = $Q / 0.5\rho V^2 \pi R^3$

C_q Suction coefficient (for Cousteau device)

C_T Thrust coefficient = $T / 0.5\rho V^2 A$

C_X, C_Y Coefficients of X and Y forces, = $X / 0.5\rho V_A^2 \pi R^2$

Cx,Cy,Cz Hull body axes centred at C

d Distance from roll bearing to top of aerofoil

d Mean water depth (still water level)

dV	Increment in velocity from roll motion
$d\alpha$	Increment in incidence from roll motion
$D(\eta)$	Aerodynamic section drag force
$D'(\eta)$	Aerodynamic force parallel to V_A
D_i	Induced drag force
$D(z)$, D_1	Wind turbine tower outside diameter
D_2	Wind turbine tower inside diameter
E	Young's modulus of elasticity
E_i	Load grading integrals (see Appendix 1 for definition)
f	Roll frequency (Hz)
f_n	Natural frequency (Hz)
F	Resultant driving force
F	Wave force on tower
F_A,F_H	Aero- and hydrodynamic components of F
F_D	Drag term in Morison's equation
F_M	Inertia term in Morison's equation
$F(k)$	Real part of C(k)
F_o	Steady component of aerodynamic force on aerofoil
F_1	Unsteady component of aerodynamic force on aerofoil
g	Accelleration due to gravity
$G(k)$	Imaginary part of C(k)
h	Lever arm of roll moment
H_ϕ	Defined in Chapter 5
I	Second moment of area
k	Wave number = $2\pi / \lambda$ where $k \tanh kd = \omega^2 / g$
k	Reduced frequency, $k = \omega c/2V$
K	Stiffness of tower
$L(\eta)$	Aerodynamic section lift force
$L'(\eta)$	Aerodynamic force perpendicular to V_A
m	Mass per unit length of tower
m_k	Spectral moment about origin = $\int_0^\infty \omega^k S_\xi(\omega)\, d\omega$
m_o	Variance = area under curve.
M	Mass of ship or floating structure
$M_\psi(\eta)$	Aerodynamic section yawing moment
N_B	Number of blades for wind turbine
P	Rotary power output of wind turbine = torque x angular velocity
q_n	Non-dimensional velocity ratio (= $h\omega\phi$ / V for active stabiliser)
q_ϕ	$= ih\omega\underline{\phi}/V_A = (ih\omega/V_A)\ \phi_o \exp(i\varepsilon_\phi)$
q_θ	$= ih\omega\underline{\theta}/V_A = (ih\omega/V_A)\ \theta_o \exp(i\varepsilon_\theta)$
Q	Torque = (Tangential force) x radius

$Q_m(t)$ Aerodynamic force component in direction of mode m,
$= Q_{ms} + dQ_m(t)$,where $dQ_m(t) = \Sigma\, Q_{mn} q_n \tau$

Q_{ms} Steady part of Q_m

Q_{mn} Derivative for rate of change of Q_m with respect to $q_n = \partial Q_m / \partial(q_n \tau)$
$= \partial Q_m / \partial r_n = -\omega^2 A_{mn} + i\omega B_{mn} + C_{mn}$

r Gap between bottom of aerofoil and sea surface, as fraction of span

R Radius of wind turbine

Re Reynolds number = V D / ν.

R_{mn} $= \sqrt{c^2(\xi_m - \xi_n)^2 + s^2(\eta_m - \eta_n)^2}$

R^* $= \sqrt{c^2(\xi_m - \xi_n)^2 + y^2 + s^2(\eta_m - \eta_n)^2}$

s Span of aerofoil

S_A, S_H Aero- and hydrodynamic forces along Cy

S_A^*, S_H^* Aero- and hydrodynamic forces perpendicular to motion

$S(\omega)$ Spectral density = energy per unit frequency

t Time interval

T Kinetic energy

T_A, T_H Aero- and hydrodynamic forces along Cx

T_A^*, T_H^* Aero- and hydrodynamic forces in direction of motion

u Velocity ratio, v / V_A

v_ϕ, v_θ Linear roll and pitch velocities

V Free stream velocity

V Potential energy

V_A Steady apparent wind speed (freestream velocity)

V_E Effective wind velocity

V_S Ship speed

V_T True wind speed

V_U Unsteady apparent wind velocity

x_A, x_H Distance between centre of aero- or hydrodynamic force and C.

X Force in wave direction on offshore wind turbine

y Deflection of tower or shaft

y_A, y_H Distance between centre of aero- or hydrodynamic force and C.

Y Force perpendicular to wave direction on offshore wind turbine

z Coordinate along shaft of aerofoil or wind turbine, origin at free end

z_A, z_H Distance between centre of aero- or hydrodynamic force and C.

α Steady mean angle of incidence (radians)

α_e Effective angle of incidence on aerofoil = α + dα

α_{max} Maximum possible value of α

α_{stall} Stall angle of aerofoil

β^* Angle between apparent wind direction and x axis of the ship

β Angle between apparent wind direction and direction of motion (= β^* +)

γ Angle between true wind direction and direction of motion of the ship

γ Inclination of fin stabiliser to vertical

γ Wave angle for offshore wind turbine

δ Yaw angle of HAWT

δ Mean yaw angle of sail (setting angle) = $\beta^* - \alpha$

= angle between chord line of aerofoil and x axis of ship

δ Deflection angle of rudder or fin stabiliser

ε Phase angle

ζ Distance from shaft to leading edge of aerofoil, as fraction of chord length.

η Coordinate along aerofoil span as fraction of h, origin at sea level

θ Chordwise coordinate, $\xi = 0.5(1 + \cos\theta)$

or spanwise coordinate, $\eta = 0.5(1 - \cos\theta)$

θ Pitch angle of ship

θ Blade azimuthal position

λ Wavelength = $2\pi/k = \lambda_o \tanh(kd)$, where λ_o = deep water value

λ Tip-speed to wind speed ratio, $\Omega c/2V_A$ for Flettner rotor

λ $\Omega R/V_A$ (tip-speed ratio) for wind turbine

Λ Leeway angle, i.e. angle between Cx axis and direction of motion

μ^* Angle between direction of wave propagation and x axis of the ship

μ Angle between direction of wave propagation and direction of motion (= $\mu^* + \lambda$)

ν_m Dimensionless damping coefficient $= \dfrac{B_{mm}}{B_{crit}} = \dfrac{B_{mm}}{2A_{mm}\omega_m}$

= fraction of critical damping

ξ Coordinate along aerofoil chord as fraction of $c(\eta)$, origin at shaft

ξ Surface elevation = $\xi_o \exp(i\theta)$

ρ Density of air = 1.225 kg/m^3

ρ Density of seawater = 1025 kg/m^3

σ Solidity of wind turbine = total blade area / swept area

σ Ratio of ship speed to true wind speed at midspan or hub = V_S / V_T

τ $\exp(i\omega t)$

ϕ Roll angle

ϕ_s Static heel angle = roll moment / Δ GM

χ Chordwise position of centre of pressure of the aerofoil, measured from the shaft

ψ Yaw angle of ship

ψ Root pitch angle of wind turbine blade

ψ_o Active oscillation amplitude for pitch angle of wind turbine blade

ω Wave frequency

ω Angular frequency of excitation (radians/sec)

ω_n Natural frequency in mode n

Ω Angular velocity of rotation of Flettner rotor or wind turbine

Subscript

a	Added mass component
A	Aerodynamic
f	Full scale
H	Hydrodynamic
m	Model scale
q	Quasisteady component
s	Steady component

Abbreviations

HAWT	Horizontal axis wind turbine
VAWT	Vertical axis wind turbine
WASP	Wind assisted ship propulsion

1. INTRODUCTION

1.1 Wind Assisted Ship Propulsion.

Wind assisted ship propulsion (WASP) uses wind energy devices in conjunction with the ship's engine to propel the ship. The economic viability of WASP depends mainly on the price of oil, which is subject to sudden unpredictable fluctuations not usually related to the cost of production. The sudden oil price rise of 1973, coupled with fears that supplies from the Middle East would be interrupted, was responsible for starting extensive research on WASP worldwide, as demonstrated at international symposia and conferences in London (1980), Florida (1983), Southampton (1985) and Manila (1985). Financial investment then dwindled with the corresponding fall in the oil price in 1986. Commercial interest in WASP is at present as low as the price of oil, which however is starting to rise again, so there is hope of obtaining funds for further research, or for implementing the findings of current research, when the price rises. Fluctuations in the oil price (and/or the U.S. dollar) cannot be forseen accurately over the life-expectancy of the ship, so it is not always possible to predict whether the installation of a wind-assist device will be economic, i.e. pay for itself in saved fuel or other benefits.

The problems of the cost and supply of fuel are always more acute for offshore islands and regions remote from the principal oil sources. Commercial sail flourishes in many parts of the Third World, e.g. in Fiji and Indonesia, where many small short-distance inter-island traders and fishing boats, built in the days of cheap oil, have been retro-fitted with cloth sails, as their owners can no longer afford to import fuel. It should be recognised that in many developing countries, imported oil is the only available fuel. It is expected that, for the near future, the prospects for WASP lie in retrofitting devices to existing hulls, rather than optimising hull design, which should be the ultimate aim. When WASP devices are retrofitted onto motorboats with shallow keels and small rudders, problems may arise due to leeway.

Between 1973 and 1986, there was an increasing awareness of the important contribution to energy conservation, in the form of fuel saving, that could be made by installing WASP systems on conventional displacement vessels. Research was mainly concerned with using wind energy devices to augment the thrust of the ship directly, either by using the aerodynamic forces or by driving a propeller. Little emphasis was placed on motion damping effects, but recent research has re-discovered the principle that marine aerofoils can improve ship motions. Japanese designers during the early 1980s initially only considered thrust augmentation as a means of reducing the fuel consumption, but it was found that twice as much fuel was saved as had been predicted by this theory. Also, the unsteady motions in rough water were greatly reduced and a significant increase in speed resulted. Container ships often travel at low speeds to save fuel, if the cargo is cheap and non-perishable. As roll can be far worse at low ship speeds, a significant saving can be made by using WASP on these ships. Many devices do not produce a net thrust

when travelling directly to windward, and are therefore not suitable for very fast ships, where roll is less of a problem and little benefit would result.

The fringe benefits which come from reducing the ship's motions include greater comfort for the crew, which is particularly vital for long transit times in a heavy swell where fatigue and exhaustion may lead to accidents. The increased stability of the working area will lead to higher productivity on fishing and research vessels. It also makes a much more pleasant journey for the passengers and a safer journey for delicate cargoes, and there will be reduced noise and vibrations from the engine. A reduction in the motions is always beneficial, even if no direct thrust is generated. The most significant reduction is in the rolling motion, and so it is roll damping that is primarily expected from a WASP device. Additional fringe benefits from installing WASP systems are directional stability and improved course keeping due to less rudder resistance (but only if the device is positioned appropriately and has the ability to be actively controlled). A carefully positioned rig can greatly improve the manoeuvrability of the ship. Ships fitted with WASP systems can continue operating through worse weather conditions when stability is important - e.g. for passenger ferries.

The fuel saving resulting from damping the motions of a ship using a WASP device could outweigh the saving from the thrust of the device. A small decrease in hull resistance coefficient yields a large reduction in resistance, owing to the high density of water, whereas an equivalent aerodynamic force requires large sail area despite apparent wind speed to ship speed ratios of two or more. Optimising marine aerofoil design by maximising the thrust of the device, which has been the aim of much previously published work, may not give the maximum possible fuel saving.

Wind energy is not only free, but also environmentally clean and virtually inexhaustible. It's use does not deplete national resources, and is not subject to price fluctuations, nor does it have to be imported, stored or processed, and therefore needs no on-land space for storage or processing. However, it is not available on demand, nor is it reliable or steady. The supply of wind energy may range from a level near zero to that causing total destruction over a short period of time. WASP devices can be used either to save fuel at the same service speed, (although engines are usually less fuel-efficient when run off their optimum speed and load conditions), or to increase the service speed for the same fuel usage. However, it is not necessarily advantageous to alter the journey time of a cargo ship on a tight schedule.

However, the wind is never steady or uniform in either speed or direction, and also introduces further difficulties for the naval architect because of its influence on surface wave generation. A WASP device will be subjected to a wide range of constantly varying windspeeds and directions, which generally reduces the theoretical efficiency of the device, due to unsteady flow.

The wind rig may be larger than the equivalent engine, and has a much higher centre of gravity, which may adversely affect the static stability. Its presence on deck may interfere with cargo loading, unless cranes can also be used as masts. The air draught may cause problems going under bridges, although it is possible to build folding masts. Existing crews may not be able to cope with the operation and maintenance of unfamiliar equipment. The addition of the device to a ship increases its displacement, leeway, heel, drag and their associated resistances, and also creates a sideforce which needs to be balanced by an induced hydrodynamic sideforce on the hull, whose induced drag component also increases the resistance. However, there is still a net resistance decrease in a seaway. The hydrodynamic side force causes the ship to move at an angle of leeway and with an angle of heel. These departures from symmetry will increase the resistance, so for a device to be effective this increase will need to be outweighed by the reductions in motion resistance and the thrust of the device. Modern ships have higher hull efficiency than formerly, with lower resistance and fins to counterract the side forces and yawing moments.

Until recently, sail technology lagged behind engine development. However, advances in sail technology have enabled more aerodynamically efficient devices to be built using new materials and techniques at lower cost, and also to be controlled automatically from the ship's bridge or by a microprocessor. Reefing and furling may also be mechanised. There have also been advances in satellite weather forecasting, navigation and communications. Ships may therefore be comparatively unmanned, although this is not likely to be popular with the crews, as it may lead to unemployment. However, this fine tuning may be unnecessarily expensive, and may not pay for itself on commercial ships.

1.1.1 Devices.

Suitable devices need to provide benefits at a wide range of wind angles and speeds. The requirements for a good device are:

a) It needs to produce a steady and continuous net forward thrust and positive roll damping at all true wind angles and velocities, but most importantly at those where the ship motions create problems.
b) It needs to produce a resultant thrust whose magnitude and direction can be varied, and to produce a stern thrust also.
c) It needs to match the performance of the engine and propeller, and be compatible with the design, operating conditions and performance of the vessel. (i.e. maximum efficiencies of WASP device, engine and propeller must coincide).
d) It needs to have good dynamic stability and control.
e) Symmetric devices are required, to give equal response to winds from either side of the ship.

f) It must not obstruct the handling of the ship's cargo.
g) It should not require any increase in crew.
h) For fishing boats particularly, it needs to cope with the changes in displacement and draught for different cargo loadings.

There are a wide variety of WASP devices being investigated in various parts of the world at present. Those which will be covered here are shown in Fig. 1. They are:
a) Rigid wingsails (marine aerofoils)
b) Horizontal axis wind turbines (HAWT)
c) Vertical axis wind turbines (VAWT)
d) Flettner rotors (rotating cylinders)
e) Cousteau Turbosails (boundary-layer control suction cylinders).
Soft sails have not been considered here, as they have already been extensively researched elsewhere. Kites have not been included as they would have required a fundamentally different theoretical treatment.

The driving force (or power) to propel the ship is generated by transferring momentum between streams of air and water relative to the ship. This can be achieved by either:
a) Applying opposite deflections to the two streams, (as in sails and autogyros). The two relative streams must be in different directions to produce a net thrust (i.e. no upwind sailing). Any difference in their velocities does not affect it.
b) The difference in velocities can be used - e.g. the faster stream (air) is slowed down by the turbine and the slower stream (water) is speeded up by a propeller. By this method, a ship can be propelled straight upwind.
When sailing straight downwind, the apparent wind is lower than the true wind, and ship speed will be also, usually.

All of these devices can be used to propel the ship by direct aerodynamic force, but wind turbines can also be used more efficiently to turn a propeller, in which case they can produce a forward thrust directly upwind, even with no motor present, because the momentum given to the water is larger than that extracted from the air, although the kinetic energies are equal. The close-reaching performance (sailing into the wind) of many devices is still in need of improvement - particularly the Flettner rotor, which produces high drag when sailing to windward. It should also be noted that all these devices are difficult to reef (reduce effective area) to any great extent, and most are impossible to furl (remove effective area), so other means must be used to reduce forces in high winds.

The direction of the resultant aerodynamic force can be controlled by adjusting the angle of incidence to the apparent wind (for wingsails, HAWTs and Cousteau Turbosails), the blade pitch angle (for VAWTs) or the rotational speed (for Flettner rotors). This can be used to

manoeuvre the ship as well as to alter the thrust or stabilising forces. The Walker Wingsail installed on the *M.V. Ashington* of Stephenson Clarke Ltd. not only showed good fuel savings, but also greatly reduced tug charges, as it could berth itself using the sails.

It is not easy to rank the devices in order of merit, as no single parameter can be used to measure the efficiency of a device. It is necessary to consider the device and hull in combination, and to optimise a combination of thrust, seakeeping, fuel economy, routeing, reliability, capital, operating and maintenance costs, directional stability, size and weight of rig and ease of maintenance. It may be possible to select the optimum for a particular ship on a particular route, but not an overall winner. Obviously, the gain on the downwind course must more than outweigh any loss on the upwind course.

To optimise the performance of a combination of device and hull, it would be necessary to combine the hull motion derivatives for existing ships with the damping coefficients calculated here. Hull derivatives are usually obtained either from experiments or by using strip or boundary element theories. These methods are not adequate for roll damping, where the damping is mainly viscous and too much scatter is present in the data. Calculations of added mass are often difficult to obtain and strip theory approximations can introduce significant errors owing to the presence of a three-dimensional wave pattern generated by the hull. Ships suitable for wind assistance need high block coefficients and low slenderness ratios to give an acceptable margin of stability when WASP devices operate in a combination of strong winds and large waves. Unfortunately, roll derivative measurements for this hull geometry are scarce and large discrepancies often occur within published data even for similar hull shapes.

Aerodynamics and hydrodynamics are both important features of wind assisted ship propulsion. The conventional methods of aero- and hydrodynamics have much in common, as is shown in the literature survey. Much may be gained by treating the hull and wind-assist device by the same method.

1.2 Offshore wind turbines.

In order to supply a reasonable proportion of Britain's electricity demand from the wind, it would be necessary to build a large number of wind turbines spread over a considerable area in locations with high average windspeeds. Britain, unlike the U.S.A., does not have large unused areas of land on which to locate windfarms, but it does have a large amount of coastline and the Continental Shelf offshore, where average windspeeds are higher than on land. As the difficulties in building wind turbines on hills in remote locations have not prevented their development so far, the additional difficulties of building offshore should also be overcome. Maintenance will be a great problem, and therefore machines with lower maintenance requirements need to be developed.

At the 1988 British Wind Energy Association Conference, Michael Spicer, the Secretary of State for Energy, announced a large wind power programme, which included a £ 2 million project financed by the Department of Energy and the EEC to build the world's first ever offshore wind turbine in the Wash, 5 km from the North Norfolk coast. Wind speeds in the Wash are not particularly high, and shallow water effects will be pronounced, but it was considered a suitable site for a prototype. The Central Electricity Generating Board and the Eastern Electricity Board were originally collaborating with James Howden Wind Turbines Ltd. to design and build it, but the latter company ceased to manufacture wind turbines in 1989, and future plans are as yet unsettled. Uncertainties concerning the privatisation of the C.E.G.B. have frozen all wind energy development in Britain for the moment. Swedish plans for offshore wind turbines are still progressing, and the world's first offshore wind turbine will probably be Scandinavian.

Offshore wind turbines are likely to suffer from difficulties unknown to their land-based counterparts, arising mainly from wave motion, as well as tidal movements, currents, spray impact, wave scour at the foundations and corrosion. Wind turbines are likely to be located in much shallower water than oil platforms, and so weather conditions should be less extreme, i.e. modest sea states. Nevertheless, fixed installations will be affected by wave loading along most of the submerged length of the tower as well as wave slamming, vortex shedding and many of the other effects known on deep sea installations. Water depth may vary considerably with the tide. The distance from the wave crests to the lowest path of the turbine blades will vary with the tide.

The standard methods for the hydrodynamics of oil platforms, adapted to include shallow water effects, are used to calculate the wave forcing loads. The roll, pitch and yaw derivatives are calculated theoretically, based on the overall turbine lift and drag forces and structural responses due to elasticity are included. The vibrations of the structure give vortex shedding effects, in addition to aeroelastic blade flapping effects. The aerodynamic damping from the blades is of the order of magnitude of the structural damping, for a fixed tower, which means that the towers may be made less stiff, and therefore cheaper.

1.3 Outline of the research programme

The effects of rigid body motions on the unsteady aerodynamics of the wind energy devices are studied here. Unsteady motions may be caused by response to wave excitations or by operation of the ship's controls, (e.g. rudder, stabilisers or the device itself) for the manoeuvring of ships, or by changes of wind heading or speed, gusts, turbulence, etc. The aerodynamic forces on the device introduce stabilising forces and moments to the ship or tower.

For ships, only the rigid body modes (i.e. seakeeping) are considered. For offshore wind turbines, the tower bending motions are also considered. The principal motions which affect the aerodynamic forces and moments on the device are forward motion (of ship) and the wave-induced oscillatory motions of roll, pitch, yaw, surge and sway.

A theoretical analysis has been developed to examine the effect of harmonic excitation on the aerodynamics (and particularly the motion damping) of wingsails. Derivatives (both damping and inertia) in surge, sway, roll, pitch and yaw due to roll and pitch motions have been determined for marine aerofoils of different planforms, aspect ratios at different headings and frequencies. Unsteady lifting surface theory has been used, linearised to first order in roll velocity. The theory has been augmented by experiments in an open-jet wind tunnel. Other devices - wind turbines, Flettner rotors, Cousteau Turbosails and conventional roll stabilisers have been examined theoretically in roll only, using a quasisteady version of the above theory, as a comparison. Published data on steady lift and drag curves have been used, but these do not account for the motion of the separation point on the surface of the rotor and cylinder in unsteady motion. For ships, it is necessary to quantify the relative importance of the thrust and damping characteristics of the device.

The appropriate input data needed were not available in most cases, and so experimental results were required for incorporation into the theory. Data which are required are dynamic loads and load gradings of all the wind energy devices as functions of frequency, mean incidence, motion amplitude, and angle between the motion axis and the wind, for the various devices. These parameters have been measured experimentally or calculated theoretically as relevant data are largely unavailable or inapplicable. Interractions between several devices, boundary layer effects and gap effects could not be measured at the scale of the laboratory equipment. Sea spectra, wind shear and hydrodynamic derivatives were taken from existing literature. Aerodynamic damping coefficients were calculated which can then be combined with existing hydrodynamic and structural coefficients, assuming these to be independent and therefore able to be superposed.

The emphasis throughout has been on the aerodynamic components rather than the hydrodynamics, because hydrodynamic roll derivatives are uncertain quantities, even for a given hull in a given sea state.

2. COMPARISON WITH OTHER RELATED PROBLEMS AND EXISTING TECHNOLOGIES

2.1 Marine aerofoils and aircraft wings.

Marine aerofoils can be treated similarly to low-speed aircraft wings, with lower Reynolds number and higher incidence, and with pitch and yaw angles interchanged. The heel angle of the ship corresponds to dihedral or bank; trim to sweepback and leeway to drift. The equivalent 'apparent wind angle' will usually be either 0 or 90^{o} for an aircraft, but may be anywhere from 0 to $\pm 180^{o}$ for a ship. The free water surface boundary and wind shear gradient present additional problems for marine aerofoils.

2.2 Wind turbines and ship propellers.

Ship's propellers have very low aspect ratio, highly cambered and twisted blades at high pitch angles, and the boss forms a major part of the construction. The loading depends largely on the trailing vortices from the tips, so lifting line theories are inadequate, and lifting surface theories need a large number of steps for accuracy.

Wind turbine blades are of high aspect ratio, thin with low camber (at tips), low solidity and rotate at high speeds. They may be thick and highly twisted and cambered at the root, but the loading on the inner portions can usually be neglected in the analysis. High aspect ratio lifting line theories may be valid here, and most end effects can be ignored.

The efficiency requirements are opposite: A propeller gives a high thrust for a given applied torque. Since efficiency is expressed as (thrust) / (torque), high solidity is required to achieve high efficiency. A wind turbine gives a high torque for a given applied thrust. In this case efficiency is expressed as (torque) / (thrust), and so low solidity is required.

2.3 Ship-board and land-based wind turbines

Unlike land-based electricity-generating wind turbines, there will be no problems of energy storage or generation of electricity, as the wind energy is converted directly into propulsive thrust. Optimum blade shapes, pitch settings, tip speed ratios etc. may be different for this mode of use than for use in electricity generation. The lower power rating means that the support structure can be lighter too. The generation of thrust must be effectively optimised to yield propulsion, rather than torque of a turbine shaft. The siteing problem becomes a routeing problem, and careful monitoring of the weather along the whole route is necessary. In general, winds at sea behave less erratically than those on land, but the laws governing the meteorology near to sea level are not so well understood, as data are lacking for weather

conditions offshore. Some measurements have been taken on offshore structures but data acquisition techniques rarely conform to Meteorological Office quality control procedures. Trinity House give offshore data from lightships, but these are manually recorded at low altitudes from the ship's deck. There are very few continuous readings, particularly from offshore weather stations. Power fluctuations are less important thanb for electricity generation - it does not matter much if the ship speed varies as the wind varies.

2.4 Offshore and land-based wind turbines

Wind speeds are higher offshore, but the support structure needs to be longer and stronger per unit swept area. The survival wind speed is higher also. The costs and difficulties of maintenance and of transmitting the electricity to land have not yet been resolved.

As can be seen from Fig. 2a, the tower is proportionally longer for an offshore wind turbine, with wave loading over the lower part. Offshore wind turbines have more demanding loading conditions and much greater uncertainties of loading. Dynamic loading and fatigue present much greater physical problems than for land-based applications, as wave-induced oscillations give unwanted accelerations on the entire rotating part of the structure.

Meteorological and oceanographic data are required for accurate predictions of loads, but accurate data are scarce for offshore sites. Some records are available from coastal stations on land (e.g. Bell Rock), from ocean weather ships and from offshore structures in deep water, and a few measurements may be obtained from other ships, but not usually in the relevant areas. As a result, the design problems include:

a) Maximum expected waveheights cannot be predicted with great confidence from the sparse available data.

b) Two-dimensional wave theories provide poor predictions of velocities and accelerations in an irregular and turbulent sea and particularly in shallow water.

c) Morison's and other empirical equations are often inadequate, particularly when marine corrosion has given a surface of varying roughness.

A horizontal-axis wind turbine needs to be yawed into the wind, which will not be possible on a floating platform, as there is nothing to react the force against, so vertical-axis machines will probably be necessary for floating locations. For floating platforms, the weight will be critical, and particularly the vertical centre of gravity.

Offshore structures are subjected to both steady and time-varying forces, which are caused by wind, waves, currents, tides and passing vessels. The wind loading consists of a large, fairly constant force plus oscillatory components due to cyclic overall forces (for two-bladed machines particularly), and time-varying components due to wave loading, turbulence and gust

loads. Wave loading is mainly periodic and presents the most serious problem, causing blade flapping and tower vibrations. The tower must be designed so that its natural frequency, and possibly the first harmonic, does not coincide with the dominant wave frequencies or the blade passing frequency.

2.5 Offshore wind turbines and oil rigs

As can be seen from Fig. 2b, the major part of an oil rig tower is under water, and so the water not only provides some support, but also gives considerable hydrodynamic damping for the wave induced vibrations. Wave loading is only significant over the portion near the waterline, and the foundations are undisturbed. Space is available for a wider tower structure, as there is no question of blade interference. For a wind turbine, the major part of the tower is above water, so support and damping must be provided by other means. The seabed is not always geologically sound in conveniently windy places, and may be subject to scour and subsidence. Fatigue will be more critical than for oil rigs, because the unsteady aerodynamic loads from the blades will make up a higher proportion of the total force. The natural frequency of the tower must be designed to avoid the blade passing frequency as well as the dominant wave frequencies.

Wind turbines will be located in much shallower seas than oil platforms, so the weather conditions should be less extreme, i.e. modest sea states. However, wave loading will occur over the entire submerged structure, with wave scour at the sea bed for a fixed tower. In deep water, the foundations are undisturbed, but in shallow water all the underwater parts will be in the boundary layer of the sea bed. Wave motion is affected by the presence of the sea bed, so there will also be a sheared current, arising from friction effects, and the slope of the sea bed near to the shore will cause wave refraction (change of direction), which further modifies the wave spectrum. Wave shear behaves like wind shear on a hill (sloped profile). Waves slow down on approaching shallow water and the wave height increases as the water depth reduces, so the wave breaks. The tide and current (which is sheared) modify the wave spectrum and cause vortex shedding effects. Marine growths and ice will affect the weight of the floating structure, but these can be catered for by releasing ballast.

The seabed is not always geologically sound in conveniently windy places, and may subside under the weight of a gravity structure. Unlike oil platforms, wind turbines have no risers to bend or pull out, and so they do not have to be fixed quite so rigidly in position. Slack cables, which only prevent steady drifting and not first order responses, may be adequate for this. Tension leg concepts will be inadequate because of the tidal variation in depth.

2.6 Conventional methods of roll stabilisation

Transverse stability first became a problem when steam replaced sail, as sails had previously provided significant roll damping. There is a conflict between low resistance in calm water and roll damping in a seaway. Only stabilising tanks can work well at low ship speeds, as they derive their damping moment from their own inertia - all other devices depend on the forward velocity of the ship.

As the bare hull roll damping is inherently light, or even negligible, and restoring forces are small, large responses occur at resonance, which can be decreased considerably by the use of stabilisers. In fact, most of the roll damping on a ship comes from the stabilisers. As the energy required to roll a ship is low, the energy needed to reduce the roll is also small. However, to reduce the roll by a large proportion, active means are required such as active fins which apply an opposite heeling moment to the ship. The damping provided per unit area by active fins is high, so fairly small areas are sufficient. Active fin control may depend on the roll angle, velocity and acceleration and gives fine tuning but at a high cost. On low speed ships, passive stabilisers are often used as active stabilisation becomes ineffective. Bilge keels can double the bare hull roll damping moment, and so halve the resonant roll amplitude, but their effectiveness varies with position and size. Segmented bilge keels are less effective, as vortex cancellation occurs, which reduces the damping. Active fins reduce the resonant roll by about 90% at the natural frequency, and are usually shaply tuned about the natural roll frequency.

To stabilise pitch or heave would require drastic changes in the ship form to make a significant impression on the bare-hull damping, but roll can be stabilised with quite small changes, e.g. bilge keels (which cause drag), tanks (which take up internal space), active fins (which use power from the engine), or by increasing the metacentric height. The natural period depends on the metacentric height and the radius of gyration. Altering the mass distribution to give a higher moment of inertia about the roll axis (e.g. by the installation of a mast) increases the natural roll period and gives additional inertial damping by acting as a pendulum.

3. Literature survey

3.1 Damping effects from WASP

There is extensive modern literature concerning hull motions in a seaway. A large amount of data is available for hull motion derivatives, but for roll damping the results are scattered and conflicting. Each set of results refers to a particular hull shape, many of which are for slender hulls or deep keeled yachts, which are not suitable for wind-assist applications where high block coefficients are generally required. Consistant estimates of the roll damping available from relevant hull forms appear to be unavailable in any generally applicable form. Therefore the additional aerodynamic damping provided by the WASP device cannot generally be presented as a percentage increase of the ship's original hydrodynamic damping, except in a few specific cases. It can, however, be presented as a coefficient for comparison with the coefficients for hulls and other stabilisers, which however will be specific to each particular hull/device combination.

Modern wind-assisted vessels have rediscovered the fact that sails improve a ship's motion. In 'Nicholl's seamanship and Nautical knowledge' (**Brown, 1953**) it was stated that: 'A steamer's sails, if she has any, are principally for steadying her in a seaway. With a strong beam wind the side pressure on the sails moderates rolling. They also have some propelling power, and thus help her along. They are very useful in the case of an accident to the engines or propeller.' **Mandel (1967)** pointed out that sailing ships possess stick-fixed directional stability because their propulsive force can introduce stabilising forces and moments which tend to return the path of the ship to its original direction after a momentary disturbance.

There has, however, been very little quantitative research into the benefits to be derived from the damping effect. **Watanabe et al. (1982)** reported that the installation of two wingsails on the Japanese wind-assisted oil tanker SHIN AITOKU MARU had improved its seakeeping considerably due to motion damping. The damping was expressed as proportional to the energy consumed by the motion, but was not evaluated numerically. **Matsumoto et al (1982)** also considered the effects of damping on the same ship, using quasistatic strip theory and wind tunnel tests to show that roll amplitudes were decreased by 20% owing to the presence of the sails. Unexpectedly good results were obtained due to reducing yaw and pitch motions as well as the roll reduction which had been expected.

Satchwell & Mays (1983) developed a linearised theory for analysing WASP ships with deep keels and high aspect ratio devices by treating them as a double wing problem, using lifting line theory and balancing the aerodynamic and induced hydrodynamic loads. However, this cannot be applied in this form to shallow-keeled container ships with low aspect ratio sails, as used in current practice. **Firestein (1985)** used lifting strip theory to calculate the aerodynamic

response of a high aspect ratio wingmast on a rolling ship. **Nance (1985)** remarked that low efficiency aerofoils made good dampers, but thought that higher efficiency ones might give problems with stalling. It was suggested that Flettner rotors might make good dampers, but no evidence was given. **Satchwell (1985)** compared different devices on the grounds of compactness and maximum lift, and indicated that, for the same lift force and height, rigid aerofoils produced less damping than sails, and that Flettner rotors have virtually none. **Skogman (1985)** determined the drift and rudder angles needed to balance the sail forces and moments, and showed that sails could increase manoeuvrability. If two sails are used, they can be set to thrust against each other to produce the required yawing moment.

Satchwell (1986) predicted the roll damping from rectangular wingsails as a fractional increment of an arbitrary estimate of hull roll damping. It was demonstrated that a conflict existed between setting the aerofoil for thrust or for roll damping. It was shown that it was possible under some conditions to develop negative roll damping in quartering seas. **Clayton and Sinclair (1988/9)** evaluated the roll and pitch damping derivatives and cross-coupling for marine aerofoils of various aspect ratios and planforms, and confirmed the conflict between damping and thrust augmentation. A conflict between pitch damping and roll damping was also shown. **Sinclair and Clayton (1988)** extended the above analysis to wind turbines, Flettner rotors and Cousteau Turbosails, and showed that horizontal-axis wind turbines make very effective stabilisers. It was demonstrated that roll damping in beam winds depends mainly on the drag force of the device. Therefore, devices with high lift-to-drag ratios cannot provide substantial damping moments. **Clayton and Sinclair (1990)** extended the preceeding analysis to compare the damping and added resistance of various WASP devices with the preformance of conventional ship stabilisers.

3.2 Added Resistance of ships in a seaway.

This survey concerns only the added resistance due to weather, e.g. diffraction and reflection of waves, damping of motions due to waves and drag due to wind, in oblique seas. Speed loss, resistance increase and power increase to maintain speed are complementary concepts, and are frequently accounted for only by an arbitrary weather margin. Added resistance due to wind can be measured quite easily in a wind tunnel, but the component due to waves is much more difficult to calculate. Practical knowledge of ship resistance is based mainly on tank tests, which are predominantly for head or following seas. In oblique seas, results from different authors are not in agreement, particularly for roll, where results are considerably scattered. Added resistance is independent of calm-water resistance, and depends on the wave-induced motions and their phase relationship to the wave field. It also depends non-linearly on wind speed, significant wave height, wave spectrum, motions and incident waves, all of which depend on the Beaufort number or the sea state. The literature concentrates on head seas and on the damping of forced motions and the diffraction of incident waves.

Hydrodynamic damping is the biggest source of uncertainty in estimating ship response. There has been very little work on added resistance due to rolling, or in an oblique seaway.

Those papers which have included roll are: **Aertssen (1969)**, who performed trials at sea on motor ships, and gave a formula for speed loss as a function of ship length, Beaufort number and wave heading, for fast ships of good form coefficient, but it does not account for ship type. These formulae are tabulated by **Townsin and Kwon (1983)**. **Baree (1985)** gives a similar formula for added resistance due to waves, and a different one for added resistance due to wind. **Jφrgensen & Prohaska (1966)** looked at wind forces on the superstructure of motor ships, and showed that the necessity to use the rudder to counterract drift in beam winds causes extra resistance. Resistance was decreased for ships with large superstructures at certain headings, where the superstructure acts as a sail. **Van Berlekom et al. (1975)** gave graphs for the speed loss owing to the rudder movements and leeway needed to counterract the sideforces on the superstructure and to keep the ship on a sraight course. **Van Berlekom (1981)** measured wind forces on non-sailing ships at various headings in a wind tunnel, showing that the superstructure produces a considerable amount of drag, but no lift.

3.3 Hydrodynamic (seakeeping) Theories

In merchant ship design, the early stages of the design process frequently consider only resistance and propulsion, with seakeeping taken into consideration only at the later stages. Calculation of added resistance usually requires knowledge of the inertia and damping derivatives of the ship's hull, which can be calculated by several methods. They are often measured in air, not in water, owing to problems of scaling the Reynolds number effects. **Brook (1989)** reviewed theoretical methods for calculating roll damping coefficients for vortex shedding from bilge keels, and compared them by reanalysing data from full scale forced roll trials. There is very little agreement, and measurements of roll decrement may not be very reliable. Froude's method gives different results to the forced roll method.
Those methods suitable for high block coefficient container ships are:

3.3.1 Strip Theory. Classical linear strip theories depended largely on two-dimensional added mass and damping coefficients as functions of frequency, and were only suitable for fairly slender ships. Empirical correction factors were used for end effects and forward velocity and three-dimensional effects were neglected. Later versions had corrections for forward-speed effects. These did not represent lateral forces accurately, as they did not account for any viscous effects. Therefore, these methods are not accurate enough for roll, or where drift forces are present, caused by second-order wave excitations.

There have been many calculations for the added mass in heave of cylinders of various cross sections, although Lewis's classical conformal transformation method is still often used. Many

others have developed more complicated transformations, but most results are only slightly better than Lewis's, for much more work. There are many numerical techniques which give accurate added mass derivatives, but they do not all give reliable damping derivatives, particularly in roll. Among those few which do attempt to include it are: **Frank (1967)** represented each section by a series of straight-line segments with a pulsating source on each. **Bishop et al (1980)** used conformal mapping and multipole expansion to calculate coefficients for roll and sway of various sections, with and without bilge keels, but it requires a large number of points to do roll damping accurately.

Tasai (1972) reviewed the state of the art of strip theories, and showed that pitch and heave could be predicted more precisely using two-dimensional hydrodynamic coefficients of ship cross-section and multiple coefficient transformation method. The 'ordinary strip method' (OSM) theory, which modifies the equations by adding corrections for advance speed from unsteady wing theory, was expanded for lateral motions. **Salvesen et al (1970)** used linearised analysis based on the complete three-dimensional boundary value theory and then approximated stripwise. A new strip theory was presented for heave, pitch, sway, roll & yaw with forward speed in a random, oblique seaway using the **Frank (1967)** close-fit source distribution method, which gives good results for amplitude and phase of pitch and heave. Forward-speed terms were included due to the lifting effect of the blunt stern, and also included an additional quasilinear damping coefficient, but lateral terms were not very well represented. This theory was extended by **Loukakis & Sclavounos (1978)** for oblique regular waves, including the effects of blunt afterbodies. The average relative velocity at each cross-section is calculated, and then the diffraction part of the exciting force according to the method of **Salvesen et al (1970)** Approximations are made for the interraction terms between oscillatory flow and ship forward motion. Formulae are given in terms of two-dimensional section coefficients, and include the effect of blunt ends. **Sakata et al (1983)** modified **Salvesen et al's (1970)** method for box-forms, taking longitudinal as well as transverse strips and correcting with empirical coefficients. However, this does not account for damping forces adequately, particularly in roll. **Fujino & Yoon (1986)** extended strip theory for the nonlinear response in waves, including nonlinear roll-heave coupling.

3.3.2 Wave Diffraction Theory (Boundary element methods or source techniques). This is potential flow theory, which ignores drag forces. There are no restrictions on validity for any body shape. For an exact solution it is necessary to calculate the velocity potential to satisfy boundary conditions on the moving hull surface and on the free water surface. This is a three-dimensional way of calculating added-mass and damping coefficients, used where two-dimensional methods are not valid. The boundary integral method reduces the original three-dimensional flow problem to a two-dimensional integral for the velocity potential over the wetted surface. The oscillating velocity potential due to wavemaking can be expressed as the potential due to a source distribution on the surface of the hull, given by a Green's function

which must be inverted numerically to find the sources from the boundary conditions. Pulsating sources are distributed over the hull surface with strengths to satisfy the boundary conditions. The potential due to each source is then derived by solving the Fredholm integral. The pressure distribution over the hull surface can then be integrated to obtain the forces. The wave-exciting force is computed using diffraction theory for restrained hull in waves, and the motion-induced forces are computed using diffraction theory for forced motions in still water. The major problem with this method is the evaluation of the integral, which has a pole at the measuring point. There are very few explicit solutions. Numerical methods of solution have been given by many, usually involving series expansions in terms of Bessel functions or Chebychev polynomials. **MacCamy and Fuchs (1954)** developed a Green's function method for calculating wave forces on piles which is still in common use.

3.4 Aerodynamic (lifting surface) methods.

Classical two-dimensional linear unsteady aerofoil theory was developed from thin aerofoil theory (linearised velocity potential theory), using small harmonic oscillations and usually assuming frozen convection (no curlup of wake). **Bratt (1950)** showed experimentally that this was reasonable for low frequencies only, but as most of the wake effect comes from the near wake, errors will be small. Unsteady effects are less significant for low aspect ratio aerofoils, i.e. damping coefficients are nearly independent of frequency. For three-dimensional calculations, exact closed-form solutions are not possible, and only numerical approximations can be found. The evaluation of Kussner's kernel gives the main difficulty. Integration of it gives problems owing to the singularity at the measuring point, which is usually tackled by taking Cauchy Principal values or series expansions. The circulation varies in both directions on a low aspect ratio wing.

3.4.1 Mode Function Method. Kussner's kernel is replaced by simpler functions, i.e. it is assumed that the lift can be expressed as a linear combination of N preselected functions, whose unknown coefficients are determined from the boundary conditions by solving at N points where the normal velocity is known. The functions are either polynomials, trigonometric series or Chebychev polynomials. These are not very effective for irregular planforms with flaps. **Davies (1978)** summarised all the unsteady mode-function methods, and the methods of numerical evaluation.

3.4.2 Discrete Element Methods. **Falkner (1947)** extended the steady vortex lattice method to oscillations. It concentrated loading as horseshoe vortices at discrete grid points and so reduced the double integral to a matrix. **Watkins et al (1955/9)** extended it to oscillating motions, using a power series form for the oscillatory kernel of the integral equation, but keeping the loading functions - doublet lattice method. The non-singular part of the kernel was expressed in terms of Bessel and Struve functions. **Lan (1974)** had a quasi-vortex lattice method which converges

faster than the original, using Chebychev polynomials. **Jordan (1978)** had a more accurate method of approximating the influence functions. **Desmarais (1979)** expanded some of the integrals as series. The Bessel functions are not suitable for numerical series evaluation, but their Laplace transforms are.

3.5 Other methods:

Three-dimensional numerical Green's theorem: **Hess & Smith (1966)** developed a numerical singularity-distribution solution for arbitrary oscillating bodies, developed originally for aircraft. This was further developed (for aerofoils only) by **Giesing (1968)** for unsteady motions and by **Smith (1968)** and **Basu & Hancock (1978)** for unsteady vorticity effects (Kutta condition). **Van Oortmersson (1972)** and **Faltinsen & Michelsen (1974)** investigated the forces on large stationery structures in waves, using this method.

Morino et al (1975) developed an unsteady time or frequency domain method using complex reduced frequencies based on Green's functions. The wake surface is assumed to be a sheet of zero thickness with a constant potential difference across it, consisting of streamlines issuing from the trailing edge, which is discretised as semi-infinite strips. The body is discretised also, and the Green's function integral reduces to a matrix inversion. **Rowe & Cunningham (1984)** showed that numerical methods can differ considerably in their results, and contrast the convergence of the doublet-lattice with other kernel function and panel methods.

3.6 Non-linear effects.

Roll in irregular seas cannot be superposed from regular tests, i.e. spectral analysis based on superposition is not valid for roll. Near resonance, the motions depend critically on the hydrodynamic damping, which depends on viscous and vortex shedding effects, which are inherently non-linear. Roll damping contains a non-linear component resulting from the influence of viscosity, and the calculated value from an inviscid cylinder is quite unsatisfactory, so empirical values are used instead. Non-linear behaviour is summarised by **Grim (1969)**. Even in regular waves, nonlinear effects on motions come from the nonlinear damping moment (viscosity and seperation), particularly from bilge keels, etc. The literature treats this mainly experimentally.

Kaplan (1966) defines the linear equivalent damping terms for irregular sea spectra. A similar method was used by **Vassilopoulos (1971)**. **Bearman et al (1983)** included vortex shedding from sharp-edged keels. **Denise (1983)** included nonlinear gyroscopic terms. **Robinson et al (1984)** use nonlinear vortex shedding from the corners of a barge. **Mathisen and Price (1985)** measured roll damping and fitted curves of quadratic and cubic type. There are also yaw motions in oblique waves characterised by the difference between mean course angle. Displacement of ship with

respect to wave by coupling and gyroscopic effects produces a moment which tries to yaw the ship, which needs counterraction by rudder. **Vaughan (1985)** calculated the angular motions and demonstrated the importance of their gyroscopic coupling on stationary bodies.

3.7 Experimental results.

Papers publishing experimental results do not usually give enough background information on those parameters which are not being varied for the results to be transferred to other cases. Published data on hull motion derivative coefficients are usually specific to one hull shape, and there are great discrepancies between different references on similar hulls. For roll, there is a lot of scatter even on the same hull. Damping and added mass derivatives for surface ships are usually calculated from model tests, not theory. A full-bodied ship with no deep keel cannot really be treated as a wing. Motion derivatives are measured on a planar motion mechanism or rotating arm. Different techniques give very different values for nonlinear damping for the same hull forms.

Excluding warships and sailing yachts, and considering only tests on full-form container ships where roll was included in the measurements, relevant data have been given by :
Lewis & Numata (1960) performed roll tests on Series 60 models in irregular seas at varying velocities, wavelengths and directions, and calculated derivatives for heave, pitch, roll & yaw against Froude number. The worst roll motions occurred in a quartering sea, not in a bow sea. In quartering sea there is often a mean heading angle of up to 5°. In their rolling records from irregular seas, almost all wave energy was at frequencies above those causing significant roll response. Cross-coupled damping effects are affected by velocity. The roll is highest in quartering seas. **Vossers, Swaan & Rijken (1960)** performed parametric tests on Series 60 models, varying block coefficient, ship geometry, wave length and direction in oblique regular waves, and measuring the response. There is little dependence on block coefficient, and the dependence on wavelength and ship geometry is only significant in quartering seas, where roll becomes a serious problem. **Ueno et al (1966)** measured the resistance increase in forced roll at various amplitudes, frequencies and speeds on ships of various block coefficient, and tried to fit curves as functions of velocity ratio, but results were so scattered as to be meaningless.
Yamanouchi & Ando (1966) tested high block coefficient Series 60 models in oblique regular waves and measured the responses at various speeds, wavelengths and directions. The highest roll responses occur at in beam seas. **Welnicki (1968)** performed model tests for aerodynamic side force, drag and yaw moment on Polish tourist ships with large superstructures travelling at low speeds and at leeway angles up to 30°, to calculate the effect of these forces on the steering. **Vugts (1969)** tested high block coefficient Series 60 models for forced oscillations at zero forward speed and measured the responses in roll, sway and yaw, from which the empirical coefficients needed for strip theory were calculated. **Takagi (1974)** compared experimental measurements with strip theories, modified for viscous roll damping and forward speed. Roll is

highest in beam seas. **Fujii & Takahashi (1975)** measured responses to lateral motions, and calculated viscous damping by subtracting the wavemaking and advance speed damping given by **Tasai (1972)**. **Inglis & Price (1982)** compared two and three dimensional theories with experimental results for a series 60 model. **Brown et al. (1983)** performed model tests on stationary barges and compared results with potential flow theory. Roll does not give a good comparison, although the other modes do. **Robinson & Stoddart (1987)** calculated the transfer functions for barges, both analytically and by model tests, and found a great difference between a linear analysis and experimental results, particularly for roll damping, which is mainly non-linear. **Kountzeris et al (1990)** analysed roll measurements on a restrained model in an irregular beam sea to calculate the roll derivatives.

3.8 Roll stabilisation.

Chadwick (1955) mentions that using underwater propellers instead of fins for roll stabilisation is more efficient at low speeds, though less so at high speeds.

Connolly (1969) performed forced roll tests for active fins, & has a one degree of freedom method using added mass, damping and natural frequency for roll from calm water model tests. Graphs for stabilised/unstabilised roll against speed are given. It was shown that fins are less effective than cavitation tunnel measurements predicted, with losses due to interraction between fins and bilge keels, partial immersion in boundary layer and coupling between roll, sway and yaw motions. The apparent lift coefficient is less than expected, and fins in wake of others are affected by trailing vortices. Bilge keels near fins get negative lift, due to trailing vortices from fins, and straighten out the flow before it reaches the next fin. Conventional fins project at 45°, and generate lift forces with lateral components, which causes sway and yaw, which in turn generate roll, reducing their stabilising efficiency.

Lloyd (1975) performed forced rolling tests on a ship with fins, and found that predicted results were too high. Transfer functions were obtained relating ship's roll angle to fin angle, with fins oscillated to get roll at natural frequency with amplitude 10°. Apparent fin lift is out of phase with nominal lift. **Cox & Lloyd (1977)** use a modification of Connoly's method, using semi-empirical methods for boundary layer effects, fin/bilge interraction etc. Roll response operators were derived using regular beam waves and forced roll in calm water, with slopes of 4°-5°. Behaviour is non-linear with wave slope - do not ignore low angles of roll in spectral analysis. Graphs are given as wave period as a function of roll angle for various headings, speeds and modes of motion, stabilised and unstabilised. **Carley (1975)** and **Cowley and Lambert (1975)** describe sea trials on rudder stabilisers. The rudder does not generate a large rolling moment, as its centre of action has a small lever arm about the roll axis.

Schmitke (1978) combined strip, lifting surface and viscous theories to calculate roll resopnse at different headings and speeds by considering the energy dissipated. For roll, the damping is mainly from lifting effects on appendages and from viscous effects. **Källström (1981)** considered the combined problem of course-keeping and roll stabilising, considering the control of roll and yaw simultaneously by a rudder/fin combination.

Broome (1982) assumed that all cross-coupled added-masses and all cross-coupling with roll are negligible, and calculated transfer functions for rudder response. To solve these, it is necessary to know the hydrodynamic coefficients of the hull (from model tests), and added mass and damping coefficients from computer programs. Roll/yaw coupling and yaw response to rudder angle transfer function were measured, and damping and restoring cross-coupling of roll, sway and yaw on model container ships.

3.9 Unsteady propeller lifting surface theories

The propeller can be modelled as an actuator disk, lifting line or vortex lattice. Planar thin aerofoil theory is not directly applicable to a propeller with a helicoidal surface and wake, but can be adapted. The inlet flow to a ship propeller is not uniformly distributed, so the blades experience cyclic loading. There have been a series of papers related to ship's propellers, which can be adapted to wind turbines, where the blades have higher aspect ratio, so chordwise effects can be omitted. **Jacobs and Tsakonas (1973)** summarise a study based on lifting surface theory. **Schwanecke (1975)** gives the state of the art and a comparative survey of different lifting surface methods. He used two-dimensional strip theory and Sears's gust function. **Kerwin & Lee (1978)** used a discrete vortex representation for the blades and wake, rotating with constant angular velocity in an unbounded fluid. These were replaced by a lattice of concentrated straight line elements of constant strength on the camber surface - vortex lattice method.

3.9.1 Wind turbines

Wind turbines are usually analysed by combining traditional blade element and momentum theories. Actuator disk theory only caters for axial flow, but blade element theory can be adapted for angles of yaw.
Anderson (1979) studied the aerodynamics of HAWTs in yaw using blade element theory modified for yaw, but with the momentum theory unmodified. **Anderson (1980)** used a modified blade element theory, i.e. a vortex wake model (a lifting line along the blade plus a helical vortex at the tip) to calculate the axial, radial and tangential induced velocities due to the vortices, for a single bladed rotor in axial flow.

Rainey (1980) used momentum theory to equate the aerodynamic and hydrodynamic forces on a wind turbine driven boat. W.S. Atkins's AWASH program and Musgrove's theory for VAWTs on ships were summarised.
Blackford (1983) compared wind turbines with wingsails, showing that wind turbines provide forward thrust in head winds, but wingsails give higher thrust in beam winds. **Blackford (1985)** compared his theory with experimental measurements, but only for axial flow, i.e. sailing directly upwind.
Small (1985) used propeller lifting line theory for a HAWT, with corrections for viscosity, tip losses and small number of blades. Momentum theory was ignored, and the induced velocities calculated iteratively.
Garrad (1987) describes the difficulties of using finite element methods to analyse wind turbines, due to the periodic aeroelastic loading.

3.10 Offshore wind turbines

Ewing (1974) and **Ochi (1979)** give details of the Joint North Sea Wave Project (JONSWAP) wave spectrum for use in the North Sea, by derived by linear regression of measured data. **The U.K. Dept. of Energy (1984)** gives guidance notes on the design and construction of offshore installations, including design windspeeds, tides and currents. **The British Standards Institution (1986)** also give basic data for evaluating wind loads on structures.

Previous workers in this field have usually considered only:
a) Turbines in offshore winds, neglecting the influence of the induced wave loading on the aerodynamics of the turbine altogether. **Hardell and Ljungstrom (1979)** designed floating platforms, but used scaled-up versions of turbines designed for use on land. **Davies (1988)** reported the intended use of a 45m diameter version of a standard on-shore design, grafted onto a separately designed base.
b) Wave effects on offshore towers, neglecting the aerodynamic influence of the turbine, or treating it as a stationary bluff body, and frequently neglecting shallow water effects altogether. **Swift and Dixon (1982)** and **Dixon and Swift (1982)** and **(1986)** considered storm waves and breaking waves in shallow waters, with their impact forces on the tower, but not their effect on the performance of the turbine. **Kerr (1986)** considered waves on support structures. The cyclic forces produced by two-bladed machines were mentioned , but the logical progression to eliminate them by using three-bladed machines was not made. **Simpson (1988)** evaluated wind and wave loads, but considered the wind loads to be steady. **Bauer (1988)** considered supports fairly thoroughly, but did not take the varying aerodynamic forces from the turbine into account. A separately designed turbine was to have been fitted onto this support.

Dixon (1981) reports the findings of four studies carried out in the U.K., the U.S.A., Sweden and the Netherlands on the economic feasibility of offshore wind farms, showing such great discrepancies between the four studies that no conclusions could be drawn.
Lindley et al (1980) and **Simpson and Lindley (1980)** surveyed various sites for suitability for an offshore windfarm, and selected Burnham Flats in the Wash and Shell Flat in Morecambe Bay.
Burton and Roberts (1985) looked at the possibilities for siting a turbine at Burnham Flats.
Satchwell (1988) suggested using the aerodynamic damping from the blades to reduce the oscillations of floating platforms, but gave no details, and did not consider fixed platforms. Several novel configurations for moored platforms were investigated.

Sinclair and Clayton (1989) combine the two effects, and show how the presence of the wave loading affects the performance of the turbine, and vice versa.

3.10.1 Measurements of yawed wind turbines

Clayton and Filby (1982) measured the effects of oblique flows on the wake profile. The tip-speed ratio at which stall occurs reduces with the yaw angle, decreasing the operating range as well as the maximum power coefficient.
Atkinson et al (1986) measured the variations of coning angle in a yawed HAWT to show the interraction of yaw with the blade dynamics. The yawing moment was due to wind shear, not to non-axial flow.
Atkinson et al (1987) studied the aerodynamics of HAWTs in yaw, measuring the pressure in the wake of a yawed wind turbine.
Dahlberg et al (1989) measured the forces and moments on yawed wind turbines in a wind tunnel. Yawing the turbine introduces gyroscopic moments on the hub, which can be reduced by teetering the hub.

3.11 WASP devices.

3.11.1 Wingsails use existing technology, and can be made light, strong and compact from composite laminates or light alloys, using methods based on long experience in severe wind and weather. They may be rigid and hollow, or flexible sheeting stretched over aerofoil ribs. The lift coefficient is 2 - 3 times that of a soft sail.

Wingmasts have proved very sucessful for racing yachts, from Austin Farrar's LADY HELMSMAN (una rig = profiled wing mast and fully battened soft sail), which won the Little America's cup, 1966/8, and CLIFTON FLASHER (5 rigid cambered wingsails in parallel) which held the catamaran world speed record for its sail area (1973 - 79), to STARS AND STRIPES (America's cup, 1988), and the concept should adapt to wind assist use also. However,

these racing yachts were all specialist high-performance one-off designs, to sail in one direction only, and are not mass produced or multi-purpose.

The apparent wind angle is low under normal conditions, and so those wingsails which cannot be reefed will cause drag on upwind courses. They need to be able to 'weathercock' in high winds, otherwise a very high static heel angle is produced. They need less area than an equivalent soft sail, and do not use rigging. The device is largely passive, and usually microprocessor controlled, and so has low running costs. A high stability ship is required, as the ship will travel at an angle of heel. For high lift, camber is needed, but for wind ship use, symmetry is needed, e.g. flaps or Wainsail variable-camber idea. Slotted flaps, as on the Walker Wingsail, may also be used to redirect the flow.

In 1978, the Japan Marine Machinery Development Assosciation (JAMDA) sponsored Nippon Kaiji Kyokai (NKK) to develop sail-assist devices. By 1986, they had twelve ships operating, all using symmetrically-cambered, square, rigid, non-reefable aerofoils consisting of sailcloth stretched over steel ribs. The high induced drag and delayed stall associated with low aspect ratio aerofoils ensures good roll damping. A higher aspect ratio aerofoil would provide stalling problems, aeroelastic problems and less roll damping, in return for its higher thrust.

Amongst those which have been built at large scale and have been operational, the following have been reported:
Murata et al (1981), Matsumoto et al (1982), Watanabe (1982) and **Hamada (1985)** all describe SHIN AITOKU MARU, a 66 m, 1600 dwt oil tanker with two rigid, symmetrically cambered plates made from polyester coated with P.V.C. stretched on steel frames. There is one at the bow and one amidships, each of height 12.15 m and chord 8 m. The devices are hydraulically furled by folding back about the mast. The ship was equipped with a very large rudder, as it had been thought that the sails might reduce the course stability.
Hamada (1985) also describes: AITOKU MARU, a 66 m, 1680 dwt chemical tanker, similar to SHIN AITOKU MARU, but with only one sail at the bow, of area 85m^2.
SENYO MARU and NISSAN MARU, 72 m, 2100 dwt bulk dry cargo carriers, each equipped with two rigid sails of canvas coated with polyester, of size 14.5 m by 9.5 m (fore), and 12 m by 8 m (aft).
AQUA CITY, a 31000 dwt bulk cargo ship, with two 176 m^2 rigid curved square sails, side by side at the bow. After suffering storm damage to one sail, both were removed.
USUKI PIONEER, a 154 m, 26000 dwt bulk carrier, with two 650 m^2 sails (1 fore, 1 amidships). It broke its moorings and damaged a Chinese harbour in a typhoon in 1985.

Manners-Spencer and Edmunds (1983) describe the GALLANT rig, built by Aerosystems, fitted on a 30 m, 3 ton boat. There are three 14 m sails, of sailcloth stretched over symmetrical wooden

NACA 0015 battens. The sails have elliptical planform, and reef like a Chinese junk (Concertina furling). **Nance (1985)** describes a similar 15 ton fishing boat for Clipper Cargos Ltd.,U.K.

Gifford (1983) describes the TUNNY RIG, a 10 m catamaran, with a variable camber wingsail of sailcloth stretched on adjustable battens. It was invented and built by the Combewright famity, who crossed the Atlantic in it.

Walker (1985 and 1986) describes the M.V. ASHINGTON, a 6500 dwt bulk dry cargo coasting vessel belonging to Stephenson Clarke, U.K., fitted with a Walker Wingsail, a 14m high Canard-vane triplane, trimmed by a tail vane and controlled by a microprocessor. This was designed as a high lift device, and also has high manoeuvrability. It saved 15% of the fuel costs, and also tuggage charges. The triplane provides much smaller heel angles than an equivalent soft sail would have given. He anticipates being able to use the device actively to reduce the roll motions considerably.

3.11.2 Wind turbines provide propulsion in all wind directions, including directly upwind. This can be particularly useful to sail upstream in rivers where the prevailing wind blows downstream. The device can be controlled safely in all conditions by pushing buttons on the ship's bridge, and can be reefed by altering the pitch in high winds. It can also be used to manoeuvre the ship. It is an active device, and therefore susceptible to mechanical breakdown. The technology already exists, but is not yet quite reliable enough for commercial use at sea. The efficiency is highest when the ship speed is lower than the windspeed, and it can give very high thrust at low ship speed, i.e. they could make good tugs. The aerodynamic force may be used directly, as an autogyro, but it is usually more efficient to use the device to drive a propeller. The heavy nacelle high in the air causes instability problems by raising the centre of gravity, and also introduces inertia effects, but when it is used to drive a propeller, the some of the gears may be placed lower down, so that this may be less of a problem in WASP use than when used for electricity generation. The drag force is far more important then for stationery wind turbines, and so the blade optimisation is different.

Horizontal axis wind turbines have only been fitted onto small boats so far. Those for which details have been published include:

Bose and Wilkinson (1985) descibe REVELATION, an 8 m Sirocco Catamaran based at Bradwell Marina. It has been fitted with a 3-bladed, 6.1 m diameter HAWT. The thrust coefficient is the same as for a sail of equal swept area. It reaches approximately the same boat speed in all wind directions, which is about 1/3 of the wind speed. **Wilkinson (1989)** revealed that Revelation had later been fitted with a six-bladed, 7.3 m diameter HAWT, but that subsequently three of these blades had been removed. Similar boat speeds are reached in all wind speeds, as well as all wind directions, because at high windspeeds, the fine pitch of the blades produces more drag. The machine needs a large hub to accomodate the bulky pitch-

change mechanism. When the HAWT is not turning, the boat begins to pitch. There have been problems owing to the fact that the drive shaft does not bend when the mast does.

Bose & Small (1985) describe FALCON, a 5.6 m Blackwater sloop, at Glasgow University, fitted with a 2 bladed, 2.5 m diameter HAWT with controllable pitch, blade section NACA 16-012 or 16-410. It uses the hub from a helicopter rotor. It reaches the same boat speeds in all wind directions.
Blackford (1985) describes a 4 m catamaran fitted with a 4 m diameter HAWT which can be used with 4 or 2 blades. The 4-bladed version has section NACA 4412, the 2-bladed has section Wortman FX63-137.

For vertical axis wind turbines, methods of calculation have been summarised by **Sinclair (1982)**. Multiple streamtube and double actuator disk theories have also been used, with flow expansion, flow curvature and dynamic stall, as described by **Sharpe (1984)** and **Strickland (1986)**. **Madsen (1985)** used an actuator cylinder as an extension of the actuator disk method.
VAWTs have low transmission losses, as they need no gears to transmit the rotary motion to the propeller. In beam winds, high thrust and low side force are produced. Voith-Schneider type give little or no across component of force, nearly all in wind direction. These have a lower centre of gravity than HAWTs, which makes them more stable statically.
The first paper to consider VAWTs for ship propulsion was **Bauer (1971)**.
Gigliobianco (1986) has a small Catamaran fitted with a conical VAWT with triangular semi-rigid sails, driving a Voith-Schneider propeller coupled onto the same shaft.

3.11.3 Flettner rotors are vertical rotating cylinders, and are very compact. They provide high lift, but also high drag, which is a drawback in head winds. They do not need to be trimmed when the wind direction changes, as the force stays the same when the wind velocity increases, as can be seen in Figure 24. They are lighter and have a lower centre of gravity than sails. The rotation of the cylinder induces a velocity difference across the cylinder, and therefore a pressure difference, which gives a lift force on the low-pressure side. Endplates are needed to maintain this pressure difference.
Flettner's original two boats were:
BUCHAU (1924-29) (renamed Baden Baden 1926), an existing 600 dwt ship which was retrofitted with two rotors of height 18.3 m and diameter 3 m. It crossed the Atlantic in 1926, passing through a hurricane with no ill effects.
BARBARA (1926-33) was a purpose built, 90 m, 3000 dwt. ship fitted with three rotors, of height = 16.7 m and diameter = 4m.

Swanson (1961) summarised investigations on the Magnus effect.
Williams & Liljenberg (1983) reported experiments with measurements of hull resistance, and compared the performance to that of sails. They describe CLIPPER PATRICIA, a 445 dwt

Bermudian Schooner belonging to Ocean Carriers Inc., which was fitted with a Flettner rotor as mizzen, of height 12.5 m, and diameter 1.4 m, rotating at 450 rpm.

Bergeson & Greenwald (1985) and **Clayton (1985)** reported measurements of lift and drag. There are no references on the damping effects of these devices.
Bergeson et al (1983) and **Bergeson and Greenwald (1985)** describe TRACKER, a 13 m, 18 ton launch belonging to Windship Co./ Windfree, U.S.A. with a SPINS'L rig , of height 7.2 m and diameter 1.16 m.

Morisseau (1983) reported that the Borg/Luther Group in California have been investigating the use of Flettner rotors as wind turbine blades, rudders and (underwater) roll stabiliser fins.

3.11.4 Cousteau 'Turbosail' - this concept was invented by a team led by Prof. Malavard at the French Academy of Sciences and developed by the Cousteau Foundation. It was designed as a high lift device, and consists of an elliptical cylindrical profile with a moveable flap, which provides a sharp trailing edge. The downstream boundary layer is extracted through vertical slots, which increase the transverse force and reduce the drag force. It is made of aluminium, and is structurally sound and compact. It generates no heel in a beam wind. The lift coefficient is 3-4 times that of soft sails. Stall can be delayed (up to an incidence of 30^{o}) by increasing the suction rate. **Malavard (1984)** describes the theory behind the concept, and the preliminary research behind the design.

Charrier et al (1985) describe two oceanographic research ships;
MOULIN A VENT, an already existing 20 m catamaran, which was retrofitted with a device of width 2.75 m by 1.5m, and height 13.5 m. It sank in 1983, after nearly crossing the Atlantic, owing to structural failure of the boat due to bad seakeeping..
ALCYONE, a specially designed 31 m aluminium hull fitted with two devices, of height 10.2 m, and width 2.05 m.
Constans (1985) reports that two 25.5 m by 5.1 m devices have been fitted onto a 4500 ton chemical tanker, and estimates a fuel saving of 32% in 25 knot winds.

4. ASSUMPTIONS IN THE ANALYSIS

The main assumptions in the analysis are listed as follows.

(1) The air and water are assumed to be homogeneous and incompressible. There is potential flow everywhere except in the boundary layer and wake regions. The freestream velocity is assumed steady in direction and magnitude and unsheared. Fluctuations in velocity and magnitude will need spectral analysis.

(2) The ship is driven by the engine on a straight course at constant speed at a small leeway angle, and small mean angles of heel and trim may also be present without affecting this analysis.

(3) Wingsails have a thin, symmetric cross-section with no spanwise twist, but sweep and taper may be present, and are set at a small angle of incidence so that the equations can be linearised. No flap effects or hull interference are included here. Finite span is assumed and so low aspect ratio effects are considered. The devices are considered to operate in a 'stick fixed' mode, that is, the angle δ in Fig. 3 is fixed during subsequent oscillations.

(4) Devices can be yawed into a favourable direction to the wind, in order to operate unstalled at all headings, and can be positioned either to maximise propulsive effect or to maximise roll damping.

(5) For a ship travelling in a seaway at service speed, motions are considered to be small harmonic perturbations of steady flow, giving small incremental forces and moments, so equations can be linearised and separate modes superposed. Ship response is a linear function of wave excitation. Most nonlinear and coupling effects are usually neglected.

(6) Steady and unsteady effects can be decoupled. For motions about a mean position, the angle of incidence and the apparent wwind velocity vary harmonically about mean values. The unsteady component can be considered, to first order, as analogous to the motion of a flat plate at zero mean incidence, as thickness effects are entirely steady and, for a rigid wing, camber effects are also steady. Motions can be decoupled from wave excitation , i.e. motions in calm water and excitation on a restrained ship can be superposed linearly.

(7) There are a number of separate interacting ship components, e.g. the device, hull, rudder and possibly fins, bilge keels, etc, and the motion derivative matrix will contain components from each of these. These devices are assumed to be retro-fitted to existing motor-driven ships, so no account is taken here of selecting hull shapes, engines or propellers for optimum combined effect. Only the rigid body motions of the ship (i.e. seakeeping) are considered.

(8) The still water surface is taken as an infinite plane parallel to Cxy, with the ship at rest, and a distance below the bottom of the aerofoil. The method of images is used to ensure that no flow crosses the water surface.

(9) The response to a random seaway can be calculated from transfer functions, i.e. from responses to sinusoidal motions of unit amplitude. Unidirectional, monochromatic incident waves of frequency ω can be superposed linearly to give spectra.

(10) The wake is convected downstream without altering its form (neglecting curlup) - frozen convection theory.

(11) Owing to the uncertainties reported recently concerning dynamic stall on rotating blades, only the unstalled conditions have been considered at present.

5. MOTION DAMPING OF WINGSAILS - THEORETICAL

The aerodynamic forces on the device introduce stabilising side forces and moments, which are not present in a motor - driven ship where the thrust is usually directed along the centreline. These forces and moments significantly reduce the ship's rolling motion in waves and consequently its associated resistance, thus providing an equivalent augment in thrust. This effect may be larger than the direct thrust from the device, because a small decrease in the hull resistance coefficient will yield a large reduction in resistance, owing to the high density of water. The longitudinal positioning of the device on the ship is also very important, as the sideforces will create yawing moments. This problem could be eased by positioning a device at each end of the ship or distributing several devices along the ship deck.

A sailing ship must develop a hydrodynamic sideforce to balance the sail forces. This can be generated either by using a high aspect ratio keel (as on a sailing yacht) or by travelling at an angle of leeway, as was done formerly on sailing ships.

A ship at leeway behaves like a low aspect ratio aerofoil at incidence. It develops lift (i.e. hydrodynamic sideforce S_H^*) to balance the aerodynamic sideforce, S_A^*, but at the expence of considerable induced drag. For optimising the upwind performance, minimising this induced hydrodynamic drag is more advantageous than maximising the aerodynamic thrust, which will then increase the side force, needing a higher rudder angle and caUsing more resistance. A device which reduces the hydrodynamic drag, by reducing the motions, and which produces less aerodynamic drag than this saving, is therefore required.

Further progress with wind assisted ship propulsion will probably be on the basis of retrofit of wind assist devices to existing ships, Using minimum modification, as in the case of the *M.V. ASHINGTON*. The ultimate goal, however, is to develop a rational approach to windship technology in order to optimise the design of a ship with integrated conventional engine and wind assist systems.

A simplified steady - state picture of the various velocity and force vectors for a ship carrying a marine aerofoil is shown in Fig. 3. The true wind velocity V_T, the apparent wind velocity V_A, the ship velocity V_S, the ship speed to true wind speed ratio $\sigma = V_S / V_T$ and the true and apparent wind angles γ and β^* relative to the ship's course are connected by the following equations;

$$\tan\beta = \sin\gamma / (\cos\gamma + \sigma) \qquad [5.1]$$

$$V_A = V_T \sin\gamma / \sin\beta = V_T \sqrt{1 + 2\sigma\cos\gamma + \sigma^2} \qquad [5.2]$$

In general, β^* may vary from 0 to 180°, i.e. from dead ahead to dead astern and from either port or starboard, and σ may vary between zero and 2.0 for cargo ship applications. At higher values of σ, there would be less benefit to be gained by Using the device, as the apparent wind would

be predominantly a head wind, and most devices (except HAWTs) do not produce positive thrust when travelling upwind.

The response of the aerofoil to V_A directed at a mean incidence angle α is, as shown in Fig. 3, to generate an aerodynamic force F_A which may be resolved into the components of lift L perpendicular to V_A and drag D parallel to V_A. The force combination L and D, transformed to dimensionless terms is usually used to describe the performance of the aerofoil. The alternative combination of thrust T_A along Cx and side force S_A along Cy is the more relevant for hull behaviour, being referred to hull body axes with origin at the centre of mass C, with thrust measured along the direction of the propeller shaft.

The aerodynamic forces act through the centre of effort, which is commonly taken as the centre of the sail area, but is in fact much further forward. The hydrodynamic forces act through the centre of lateral resistance which is also commonly taken as centre of the submerged area, but in fact moves backwards as speed increases. It also varies with heel and leeway. The centre of effort must be behind the centre of lateral resistance, so that the ship turns into the wind with the rudder amidships. The component of aerodynamic force perpendicular to the direction of motion, S_A^*, must be exactly balanced by an equal and opposite hydrodynamic side force S_H^*, during steady motion. Usually, the locations of the centres of action of these two forces can only be made to lie on a common axis parallel to Cz, thereby producing zero net moment about C for equilibrium in the Cxy plane, if the ship has a leeway angle Λ. The resultant of all the forces acts in the direction of motion.

The yawing moment about the centre of gravity C is given by

$M_\psi = S_H x_H + S_A x_A + S_R x_R$

as T_A and T_H are in the same line and $S_F = 0$.

In equilibrium, this will be zero, so if the longitudinal distances of the force centres from C, x_H, x_R and x_A, are given, then S_H can be calculated from the relation

$$S_H = - (S_A x_A + S_R x_R) / x_H \qquad [5.3]$$

The resultant side force perpendicular to the direction of motion is given by

$S^* = (T_H + T_A + T_F + T_R + Mg \sin\theta) \sin\Lambda - (S_H + S_A + S_R + Mg \sin\phi \cos\theta) \cos\Lambda$

which will always be zero, so the leeway angle, Λ is given by

$\tan\Lambda = (S_H + S_A + S_R + Mg \sin\phi \cos\theta) / (T_H + T_A + T_F + T_R + Mg \sin\theta)$

and substituting for S_H gives

$$\tan\Lambda = [S_A(1 - x_A/x_H) + S_R(1 - x_R/x_H) + Mg\,\phi) / (T_H + T_A + T_F + T_R + Mg\,\theta) \qquad [5.4]$$

To balance S_A^*, the ship turns to an angle of leeway Λ and hence has sideforce S_H^*, which is hydrodynamic lift due to leeway. The combination of S_A^* and S_H^* then produces a heel angle.

The resultant driving force in the direction of motion, (i.e. along the x* axis) is then

$$T^* = (T_H + T_A - T_F - T_R + Mg \sin\theta) \cos\Lambda + (S_H + S_A + S_R - Mg \sin\phi \cos\theta) \sin\Lambda$$

For some wind assist devices, S_A^* may be of larger magnitude than T_A^*, and the ship must generate a large S_H^* for equilibrium. These two side forces are generated by different velocity vectors. High block coefficient container ships have much shallower keels than sailing ships to generate sideforce, which is therefore largely provided by the rudder.

Ships travelling at an angle of leeway have a large S_H^* acting on the hull well forward. Therefore, positioning the wind assist device towards the bow will reduce the resultant yawing force, and therefore reduce the rudder force required to keep a straight course.

Equilibrium in the Cxy plane can only be sustained if an angle of heel ϕ is present. We are therefore concerned with oblique flow about a hull with leeway and heel, and possibly increased draught as a result of the additional mass of the WASP device, unless engine or stabiliser modifications dictate otherwise. Changes of trim are also possible but the hydrodynamic consequences are probably of considerably smaller magnitude owing to the normally large hull hydrodynamic stiffness in trim. In any event, these departures from the nominally symmetric flow about the hull of an unrigged ship travelling at a steady speed increase the resistance by an amount defined as the induced resistance. There is no doubt that the induced resistance is supplemented by contributions from aerodynamic interference between the air flow over the hull superstructure and the WASP device itself, although there is some evidence that deck - edge shed vorticity may enhance the thrust performance of a marine aerofoil. Clearly, for the device to be useful as a propulsor it is necessary for the net propulsive thrust to be positive so that the thrust T_H of the ship's propeller can be reduced to maintain a given ship speed or maintain the same T_H to provide an increased speed.

When the unrigged ship is in a seaway the wave induced motions increase the resistance at a given forward speed and distort the wake so that propeller efficiency reduces and overall fuel consumption increases. The induced resistance will doubtless increase when the WASP device is fitted, but the thrust T_A will also increase owing to the increase in V_A and α as a result of vector additions of angular velocity. Nevertheless, it is the reduction in resistance to near steady - motion values that predominate if the device is to be used as a motion damper and therefore fuel saver. In the context of the present study, a marine aerofoil must be capable of providing thrust and damping at all true wind angles and velocities, especially under resonant conditions. It is therefore necessary to quantify the relative importance of the thrust and damping characteristics of the aerofoil. To do so requires an examination of the assumptions consistent with physical reality.

5.1 Aerodynamic damping due to ship motions.

The damping forces involved have aerodynamic, hydrodynamic and structural components. Hydrostatic, gravitational and dynamic forces must all be taken into account.

To calculate the relative advantages of one device or device/hull combination over another, a non - dimensional coefficient is required. As there are few relevant experimental data for the roll damping of these devices, steady C_L and C_D data have been used to estimate the stabilising moments by quasistatic analysis.

The influence function Q_{mn} is defined as the increment in aerodynamic loading (force or moment) in mode m produced by unit velocity in mode n. Furthermore, modal symmetry or antisymmetry is assumed, i.e. $Q_{mn} = \pm Q_{nm}$. The generalised velocities q_n are complex, so

$q_n = i\,|q_n|\,\exp(i\varepsilon_n)$. [5.5]

where ε_n is the phase lag between the excitation and the response.

Therefore, the incremental force or moment component,

$dQ_m = \Sigma\, Q_{mn}\, \text{Real}(q_n t) = -\Sigma\, Q_{mn}\, |q_n|\, \sin(\omega t + \varepsilon_n)$.

As stated earlier, we only have need of the damping component, which is in phase with the velocity, and is given by $-\Sigma\, Q_{mn}\, |q_n|\, \cos(\varepsilon_n)$.

The aerodynamic component of Q_{mn} is $(i\omega A_{mn} + B_{mn})$ and the aerodynamic force in mode m is then given by

$Q_m = \Sigma_n\, Q_{mn}\, q_n$ [5.6]

The aerofoil adds aerodynamic virtual inertia and damping terms, A_A and B_A respectively, to the existing ship terms A_H, B_H and C_H (the hydrodynamic stiffness), related to the hull, rudder, keel, etc. These hydrodynamic terms will also have to account for the increased rudder forces needed to balance the aerodynamic load. The natural frequency of oscillation of the ship will therefore change from $\omega_n = \sqrt{C_H/A_H}$ for the unrigged ship to $\omega_n = \sqrt{C_H / (A_H + A_A)}$ with the aerofoil present. However, as A_A is usually much smaller than A_H, this change will be small, and so A_A will no longer be taken into consideration during the subsequent theoretical development.

The hydrodynamic component of the damping coefficient is given by $\nu_H \approx B_H / 2A_H\omega_n$, and the aerodynamic component by $\nu_A \approx B_A / 2A_H\omega_n = \nu_H (B_A / B_H)$. At the natural frequency, the magnification factor for the resonant amplitude is $1 / \omega_n (B_H + B_A)$. The fractional reduction in resonant amplitude caused by the aerofoil is $B_A / (B_H + B_A)$, which will be positive unless $-B_H < B_A < 0$, and then the effects of damping will be reduced. Care must be taken to ensure that the negative avalues of B_A do not fall within this range.

The ship motion will be dynamically stable if the energy dissipated aerodynamically by the aerofoil and hydrodynamically by the hull is greater than that of the wave excitation. To achieve dynamic stability, the marine aerofoil must impart positive damping to the hull motion.

Changes in circulation take place gradually and lag behind the excitation, so the quasi-steady flow must be modified by a phase lag when calculating the unsteady flow, which also depends on the time elapsed since the start of the motion.

From standard aerofoil theory, the quasi-steady sectional forces at height $z = s\eta$ are given by:

$$L_q(\eta) = 0.5\rho V_A^2 c(\eta)(C_{l0} + a(\eta) \sin \alpha_e) \quad [5.7]$$

$$D_q(\eta) = 0.5\rho V_A^2 c(\eta)(C_{d0} + A(\eta) \sin^2\alpha_e) \quad [5.8]$$

$$M_q(\eta) = 0.5\rho V_A^2 c^2(\eta)\{C_{m0} + (\zeta - \chi)\,[C_L \cos \alpha_e + C_D \sin \alpha_e]\}$$

$$= 0.5\rho V_A^2 c^2(\eta)\{C_{m0} + (\zeta - \chi)\,[a(\eta) \sin \alpha_e \cos \alpha_e + C_{d0} \sin \alpha_e + A(\eta) \sin^3\alpha_e]\} \quad [5.9]$$

For a symmetric aerofoil, C_{l0} and C_{m0} will be zero, but they may not be for the other devices.

The aerodynamic non-circulatory (added mass) component of the lift force is given by

$L_a = 0.125\ \rho c^2 a *$ (normal velocity)

Therefore, the added - mass effects are given by:

i) for roll, $L_{a\phi} = 0.125\ \rho c^2 a\ (z\phi'')\cos\delta \cos\alpha = 0.5\rho V_A^2 ca\ q_\phi \tau\ 0.5ik \cos\delta \cos\alpha$

$D_{a\phi} = 0.125\ \rho c^2 a\ (z\phi'')\cos\delta \sin\alpha = 0.5\rho V_A^2 ca\ q_\phi \tau\ 0.5ik \cos\delta \sin\alpha$

$M_{a\phi} = 0.125\ \rho c^3 a\ (z\phi'')\cos\delta\ (\zeta - 0.5)$

ii) for pitch, $L_{a\theta} = 0.125\ \rho c^2 a\ (z\theta'')\sin\delta \cos\alpha = 0.5\rho V_A^2 ca\ q_\theta \tau\ 0.5ik \sin\delta \cos\alpha$

$D_{a\theta} = 0.125\ \rho c^2 a\ (z\theta'')\sin\delta \sin\alpha = 0.5\rho V_A^2 ca\ q_\theta \tau\ 0.5ik \sin\delta \sin\alpha$

$M_{a\theta} = 0.125\ \rho c^3 a\ (z\theta'')\sin\delta\ (\zeta - 0.5)$

Then the unsteady lift force is given by $L = L_q\, C(k) + L_a$, where $C(k) = F(k) + i\, G(k)$.

For low aspect ratio aerofoils, F(k) is approximately constant.

For AR = 1, $F(k) \approx 0.5$, $G(k) \approx 0.5k$

For AR = 2, $F(k) \approx 0.8$, $G(k) \approx 0.8k$.

As the ship rolls, α and V_A vary sinusoidally about the mean, and so also do the forces and moments. Free vorticity is shed into the wake, as a vortex sheet from the trailing edge, to balance the change in bound vorticity. The normal velocity components of the aerofoil (i.e. the components perpendicular to the plane of the aerofoil resulting from the separate roll and pitch motions) are additive. This is not so for any of the aerodynamic forces and moments, owing to the inclusion of interaction terms.

For the purposes of the present analysis, the apparent wind angle β^*, measured relative to the Cx axis of the ship (see Fig. 3), is considered given. The mean setting angle of the aerofoil δ, is

chosen to give a desired steady state angle of incidence α, so the theory will be developed in terms of α and β^*.

5.2 Forces and Moments Induced by Roll Motion

The linear roll velocity is given by

$v_\phi = \text{Real}(V_A\, q_\phi \tau)$.

From Fig. 4(a) it is seen that

$$V_A \sin(d\alpha) = v_\phi \cos(\beta^* + d\alpha) \qquad [5.10]$$

so that

$$\tan(d\alpha) = \frac{v_\phi \cos\beta^*}{V_A + v_\phi \sin\beta^*} = \frac{q_\phi \tau \cos\beta^*}{1 + q_\phi \tau \sin\beta^*} \qquad [5.11]$$

Again referring to Fig. 4(a),

$$\begin{aligned} V_U &= V_A \cos(d\alpha) + v_\phi \sin(\beta^* + d\alpha) \\ &= V_A[\cos(d\alpha)(1 + q_\phi \tau \sin\beta^*) + \sin(d\alpha)\, q_\phi \tau \cos\beta^*] \\ &= V_A\, H_\phi. \end{aligned}$$

where

$$H_\phi = \sqrt{1 + 2\, q_\phi \tau \sin\beta^* + (q_\phi \tau)^2} \approx 1 + q_\phi \tau \sin\beta^* \qquad [5.12]$$

and so

$1/H_\phi \approx 1 - q_\phi \tau \sin\beta^*$.

The roll induced component of the quasi-steady section lift force measured perpendicular to the instantaneous apparent wind velocity vector V_U is given by,

$L_q(\eta) = 0.5\rho V_U^2 c\{C_{l0} + a\sin(\alpha + d\alpha)\}$.

Linearising to first order in q_ϕ yields

$$L_q(\eta) = 0.5\rho V_A^2 c H_\phi\{C_{l0} + a\sin\alpha + q_\phi\tau[C_{l0}\sin\beta^* + a\cos(\beta^* - \alpha)]\}. \qquad [5.13]$$

The corresponding component of quasi-steady section drag force is

$D_q(\eta) = 0.5\rho V_U^2 c\{C_{d0} + A\sin^2(\alpha + d\alpha)\}$

Linearising to first order in q_ϕ yields

$$\begin{aligned} D_q(\eta) \approx\ & 0.5\rho V_A^2 c H_\phi\{C_{d0} + A\sin^2\alpha + q_\phi\tau[C_{d0}\sin\beta^* + A\sin\alpha\,(2\cos\alpha\cos\beta^* \\ & - \sin\alpha\sin\beta^*)]\} \end{aligned} \qquad [5.14]$$

The corresponding quasi-steady section yaw moment about the shaft can be written as

$$\begin{aligned} M_q(\eta) =\ & 0.5\rho V_U^2 c^2(\eta)[C_{m0} + (\zeta - \chi)\,(a(\eta)\sin(\alpha + d\alpha)\cos(\alpha + d\alpha) + C_{d0}\sin(\alpha + d\alpha) \\ & + A(\eta)\sin^3(\alpha + d\alpha))] \end{aligned}$$

Linearising to first order in q_ϕ yields

$$\begin{aligned} M_q(\eta) =\ & 0.5\rho V_A^2 c^2(\eta)[C_{m0} + (\zeta - \chi)\,\{a(\eta)\sin\alpha\cos\alpha + C_{d0}\sin\alpha + A(\eta)\sin^3\alpha\} \\ & + q_\phi\tau[2\,C_{m0}\sin\beta^* + (\zeta - \chi)\,\{a(\eta)\cos(\beta^* - 2\alpha) + C_{d0}(\cos\beta^*\cos\alpha + 2\sin\beta^*\sin\alpha) \\ & + A(\eta)\sin^2\alpha\,(3\cos\beta^*\cos\alpha + 2\sin\alpha\sin\beta^*)\}]\,] \\ =\ & M_s + M_q\, q_\phi\tau. \end{aligned} \qquad [5.15]$$

The component of quasi-steady aerodynamic force perpendicular to the steady state apparent wind velocity vector V_A, becomes

$$\begin{aligned} L_q' &= L_q \cos(d\alpha) + D_q \sin(d\alpha) \\ &= 0.5\rho V_A^2 c\{C_{l0} + a\sin\alpha + q_\phi\tau[2C_{l0}\sin\beta^* + a(\cos\beta^*\cos\alpha + 2\sin\alpha\sin\beta^*) \\ &\quad + (C_{d0} + A\sin^2\alpha)\cos\beta^*)]\} \end{aligned} \qquad [5.16]$$

and the corresponding component of quasi-steady force parallel to V_A,

$$\begin{aligned} D_q' &= D_q \cos(d\alpha) - L_q \sin(d\alpha) \\ &= 0.5\rho V_A^2 c\{C_{d0} + A\sin^2\alpha + q_\phi\tau[-C_{l0}\cos\beta^* - a\sin\alpha\cos\beta^* + 2C_{d0}\sin\beta^* \\ &\quad + 2A\sin\alpha(\cos\beta^*\cos\alpha + \sin\beta^*\sin\alpha)]\} \end{aligned} \qquad [5.17]$$

Combining with the added - mass components are given above, the unsteady forces and moment are given by

$L_u'(\eta, k) = L_s + C(k)L_q' + L_a(\eta, k)$

$D_u'(\eta, k) = D_s + C(k)D_q' + D_a(\eta, k)$

$M_u(\eta, k) = M_s + C(k)M_q + M_a(\eta, k)$

5.2.1 Roll moment component

The section roll moment component about the Cy axis is given by

$s\eta(L_u'\cos\beta^* + D_u'\sin\beta^*)$

and so the total roll moment component may be written in the form

$$Q_\phi = s^2\int_r^{r+1} \eta(L_u'\cos\beta^* + D_u'\sin\beta^*)\,d\eta.$$

Linearising to first order in q_ϕ yields

$$\begin{aligned} Q_\phi = 0.5\rho V_A^2 s^2 \int_r^{r+1} & c\eta\,\{C_{l0}\cos\beta^* + a\sin\alpha\cos\beta^* + (C_{d0} + A\sin^2\alpha)\sin\beta^* \\ & + q_\phi\tau[C(k)\{C_{l0}\sin\beta^*\cos\beta^* + a\cos\delta\cos\beta^* + C_{d0}(\cos^2\beta^* + 2\sin^2\beta^*) \\ & + A\sin\alpha(\cos^2\beta^* + 2\cos\delta\sin\beta^*)\} + 0.5\,ika\cos^2\delta]\}\,d\eta \end{aligned} \qquad [5.18]$$

that is,

$Q_\phi = Q_{\phi s} + Q_{\phi\phi}(\alpha, \beta^*, k)\,\phi'.$

The damping derivative,

$$\begin{aligned} B_{\phi\phi} &= \text{Real}(Q_{\phi\phi}(\alpha, \beta^*, k)) \\ &= 0.5\rho V_A s^3 \int_r^{r+1} c\eta^2 F(k)\,[C_{l0}\sin\beta^*\cos\beta^* + a\cos\delta\cos\beta^* \\ &\qquad + C_{d0}(\cos^2\beta^* + 2\sin^2\beta^*) + A\sin\alpha(\cos^2\beta^* + 2\cos\delta\sin\beta^*)]\,d\eta. \end{aligned} \qquad [5.19]$$

Using load grading integrals (as defined in Appendix 1) and assuming small α, the derivative for roll damping due to roll velocity may be represented by

$$\begin{aligned} b_{\phi\phi}(\alpha, \beta^*, k) &= B_{\phi\phi} \,/\, 0.5\rho V_A \hat{c} s h^2 \\ &= F(k)\,\{E_0\cos\beta^*\sin\beta^* + E_1(\cos^2\beta^* + \alpha\sin\beta^*\cos\beta^*) + E_2(\cos^2\beta^* + 2\sin^2\beta^*) \\ &\qquad + E_3(\alpha\cos^2\beta^* + 2\alpha\cos\beta^*\sin\beta^* + 2\alpha^2\sin^2\beta^*)\} \\ &= F(k)\,\{(E_1 + E_2 + E_3\alpha^2)\cos^2\beta^* + [E_0 + (E_1 + 2E_3)\alpha]\cos\beta^*\sin\beta^* + 2(E_2 + E_3\alpha^2)\sin^2\beta^*\} \\ &= F(k)\,\{A_1\cos^2\beta^* + A_2\cos\beta^*\sin\beta^* + A_3\sin^2\beta^*\} \end{aligned}$$

$$= 0.5\,F(k)\,\{\sqrt{(A_1 - A_3)^2 + A_2^2}\,\cos 2(\beta^* - \varepsilon) + A_1 + A_3\} \qquad [5.20]$$

where

$A_1 = E_1 + E_2 + E_3\,\alpha^2, \quad A_2 = E_0 + (E_1 + 2E_3)\alpha, \quad A_3 = 2(E_2 + E_3\,\alpha^2)$

and

$\tan(2\varepsilon) = A_2 / (A_1 - A_3)$.

It can be seen that $b_{\phi\phi}$ may become negative in the region near $\beta^* = \pi/2 + \varepsilon$ if

$A_1 + A_3 < \sqrt{(A_1 - A_3)^2 + A_2^2}$

that is, if

$4A_1\,A_3 < A_2^2$.

For standard aerofoils with moderate to high lift - to - drag ratios, we have

$A_1 \approx E_1, \quad A_2 \approx E_1\alpha, \quad A_3 \approx 0,$

which imply that $\tan(2\varepsilon) \approx \alpha$, and therefore $\varepsilon \approx \alpha/2$, so that

$$b_{\phi\phi} = 0.5\,F(k)\,E_1[(1 + 0.5\alpha^2)\cos(2\beta^* - \alpha) + 1]. \qquad [5.21]$$

This expression is plotted in Fig. 5(a) and it is seen that negative damping will always occur near $\beta^* = (\pi + \alpha)/2$ and the minimum value will be $b_{\phi\phi\,min} = -0.25\,F(k)\,E_1\,\alpha^2$. The negative damping condition can be avoided by ensuring that α is positive for $\beta^* < \pi/2$ and negative for $\beta^* > \pi/2$.

Minimum damping then occurs at $\beta^* = \pi/2$ thus

$b_{\phi\phi\,min} = 2\,F(k)\,(E_2 + E_3\alpha^2)$

and this can be increased by Using a lower lift - to - drag ratio aerofoil. Maximum thrust, corresponding to the $\alpha = 20^o$ line, corresponds to large positive motion damping for $\beta^* < \pi/2$ but low positive damping for $\beta^* > \pi/2$.

The aerodynamic inertia derivative,

$$\omega A_{\phi\phi} = \mathrm{Imag}(Q_{\phi\phi}(\alpha, \beta^*, k)) = 0.5\rho V_A s^3 \int_r^{r+1} c\eta^2\,\{G(k)\,[C_{l0}\sin\beta^*\cos\beta^* + a\cos\delta\cos\beta^*$$
$$+ C_{d0}(\cos^2\beta^* + 2\sin^2\beta^*) + A\sin\alpha(\cos^2\beta^* + 2\cos\delta\sin\beta^*)] + 0.5ka\cos^2\delta\}\,d\eta. \qquad [5.22]$$

Using load grading integrals and assuming small α, the derivative for roll inertia due to roll velocity may be represented by

$$\omega\,a_{\phi\phi}(\alpha, \beta^*, k) = G(k)\,\{E_0\cos\beta^*\sin\beta^* + E_1(\cos^2\beta^* + \alpha\sin\beta^*\cos\beta^*) + E_2(\cos^2\beta^* + 2\sin^2\beta^*)$$
$$+ 2E_3(\alpha\cos\beta^*\sin\beta^* + \alpha^2\sin^2\beta^*)\} + 0.5\,E_1\,k\,(\cos^2\beta^* + 2\alpha\sin\beta^*\cos\beta^* + \alpha^2\sin^2\beta^*)$$
$$= G(k)\,\{(E_1 + E_2)\cos^2\beta^* + [E_0 + (E_1 + 2E_3)\alpha]\cos\beta^*\sin\beta^* + 2(E_2 + E_3\alpha^2)\sin^2\beta^*\}$$
$$+ 0.5\,E1\,k(\cos^2\beta^* + 2\,\alpha\cos\beta^*\sin\beta^* + \alpha^2\sin^2\beta^*)$$
$$= G(k)\{A_1\cos^2\beta^* + A_2\cos\beta^*\sin\beta^* + A_3\sin^2\beta^*\} + 0.5k\,\{B_1\cos^2\beta^* + B_2\cos\beta^*\sin\beta^*$$
$$+ B_3\sin^2\beta^*\}$$
$$= 0.5\,G(k)\,\{\sqrt{(A_1 - A_3)^2 + A_2^2}\quad\cos 2(\beta^* - \varepsilon) + A_1 + A_3\}$$
$$+ 0.25k\,\{\sqrt{(B_1 - B_3)^2 + B_2^2}\quad\cos 2(\beta^* - \varepsilon') + B_1 + B_3\} \qquad [5.23]$$

where

$B_1 = E_1, \quad B_2 = 2\,E_1\alpha, \quad B_3 = E_1\alpha^2$

and

$\tan(2\varepsilon') = B_2 / (B_1 - B_3) \approx 2\alpha / (1 - \alpha^2) \approx 2\alpha$ so $\varepsilon' \approx \alpha$,

so that

$$\omega a_{\phi\phi} = 0.5 E_1 \{G(k) \{(1 + 0.5\alpha^2) \cos(2\beta^* - \alpha) + 1\} + 0.5k (1 + \alpha^2) (\cos 2(\beta^* - \alpha) + 1) \quad [5.24]$$

This expression is plotted in Fig. 6(a), and is always negative.

5.2.2 Pitch moment component

The pitching moment component developed by an elementary section of the aerofoil is given by $s\eta(L_u' \sin\beta^* - D_u' \cos\beta^*)$, and so the total pitch component

$$Q_\theta = s^2 \int_r^{r+1} \eta(L_u' \sin\beta^* - D_u' \cos\beta^*)\, d\eta. \quad [5.25]$$

Linearising to first order in q_ϕ yields

$$\begin{aligned} Q_\theta = 0.5\rho V_A^2 s^2 \int_r^{r+1} c\eta \{&C_{l0} \sin\beta^* + a \sin\alpha \sin\beta^* - (C_{d0} + A \sin^2\alpha) \cos\beta^* + \\ &q_\phi \tau [C(k) \{C_{l0} (2 \sin^2\beta^* - \cos^2\beta^*) + a(\cos\beta^* \sin\beta^* \cos\alpha + 2 \sin\alpha \sin^2\beta^* \\ &+ \cos^2\beta^* \sin\alpha) - C_{d0} \sin\beta^* \cos\beta^* - A \sin\alpha \cos\beta^* (\sin\alpha \sin\beta^* + 2 \cos\beta^* \cos\alpha)\} \\ &+ 0.5ika \cos\delta \sin\delta]\}\, d\eta \end{aligned} \quad [5.26]$$

that is,

$Q_\theta = Q_{\theta s} + Q_{\theta\phi}(\alpha, \beta^*, k)\, \phi'$.

The damping derivative,

$$\begin{aligned} B_{\theta\phi} = \mathrm{Real}(Q_{\theta\phi}(\alpha, \beta^*, k)) = 0.5\rho V_A s^3 \int_r^{r+1} c\eta^2 F(k) [&C_{l0}(2 \sin^2\beta^* - \cos^2\beta^*) \\ &+ a(\cos\beta^* \cos\alpha \sin\beta^* + 2 \sin\alpha \sin^2\beta^* + \cos^2\beta^* \sin\alpha) - C_{d0} \sin\beta^* \cos\beta^* \\ &- A \sin\alpha \cos\beta^* (\sin\alpha \sin\beta^* + 2 \cos\beta^* \cos\alpha)]\, d\eta. \end{aligned} \quad [5.27]$$

Using load grading integrals and assuming small α, the coefficient of pitch damping derivative due to roll velocity may be represented by

$$\begin{aligned} b_{\theta\phi}(\alpha, \beta^*, k) &= F(k) \{E_0(2 \sin^2\beta^* - \cos^2\beta^*) + E_1(\cos\beta^* \sin\beta^* + 2\alpha \sin^2\beta^* + \alpha \cos^2\beta^*) \\ &\quad - E_2 \sin\beta^* \cos\beta^* - E_3 \alpha \cos\beta^* (\alpha \sin\beta^* + 2 \cos\beta^*)\} \\ &= F(k) \{[-E_0 + (E_1 - 2E_3)\alpha] \cos^2\beta^* + (E_1 - E_2 - E_3 \alpha^2) \sin\beta^* \cos\beta^* + 2(E_0 + E_1\alpha) \sin^2\beta^*\}. \end{aligned} \quad [5.28]$$

Putting

$A_1 = -E_0 + (E_1 - 2E_3)\alpha$, $A_2 = E_1 - E_2 - E_3 \alpha^2$, $A_3 = 2(E_0 + E_1\alpha)$,

and approximating again for standard aerofoils gives

$A_1 \approx E_1\alpha$, $A_2 \approx E_1$, $A_3 \approx 2E_1\alpha$

so that $\tan(2\varepsilon) \approx -1/\alpha$ and therefore $\varepsilon \approx \pi/4 + \alpha/2$, with the result

$b_{\theta\phi} \approx 0.5 F(k) E_1((1 + 0.5\alpha^2) \sin(2\beta^* - \alpha) + 3\alpha)$.

This expression is plotted in Fig. 5(b). It can be seen that minimum damping will occur at $\beta^* = \alpha/2 + 3\pi/4$, and at this point we need $\alpha > 0.355$ ($\approx 20^o$) for positive damping. If this is not the case, damping will be negative throughout the region where

$\sin(2\beta^* - \alpha) < -3\alpha/(1 + 0.5\alpha^2)$.

The inertia derivative,

$$\omega A_{\theta\phi} = \text{Imag}(Q_{\theta\phi}(\alpha, \beta^*, k)) = 0.5\rho V_A s^3 \int_r^{r+1} c\eta^2 \{G(k)[C_{l0}(2\sin^2\beta^* - \cos^2\beta^*) + a(\cos\beta^* \cos\alpha \sin\beta^* + 2\sin\alpha \sin^2\beta^* + \cos^2\beta^* \sin\alpha) - C_{d0} \sin\beta^* \cos\beta^* - A \sin\alpha \cos\beta^*(\sin\alpha \sin\beta^* + 2\cos\beta^* \cos\alpha)] + 0.5ka \cos\delta \sin\delta\} d\eta. \quad [5.29]$$

Using load grading integrals and assuming small α, the coefficient of pitch inertia derivative due to roll velocity may be represented by

$$\omega a_{\theta\phi}(\alpha, \beta^*, k) = G(k)\{E_0(2\sin^2\beta^* - \cos^2\beta^*) + E_1(\cos\beta^* \sin\beta^* + 2\alpha \sin^2\beta^* + \alpha \cos^2\beta^*) - E_2 \sin\beta^* \cos\beta^* - E_3 \alpha \cos\beta^*(\alpha \sin\beta^* + 2\cos\beta^*)\} + 0.5k E_1(\sin\beta^* \cos\beta^* + \alpha(\sin^2\beta^* - \cos^2\beta^*) - \alpha^2 \sin\beta^* \cos\beta^*)$$
$$= F(k)\{[-E_0 + (E_1 - 2E_3)\alpha] \cos^2\beta^* + (E_1 - E_2 - E_3\alpha^2) \sin\beta^* \cos\beta^* + 2(E_0 + E_1\alpha) \sin^2\beta^*\}.$$

Putting

$B_1 = -E_1 \alpha$, $B_2 = E_1(1 - \alpha^2)$, $B_3 = E_1\alpha$

then

$\tan(2\varepsilon') \approx -1/2\alpha$ and therefore $\varepsilon' \approx \pi/4 + \alpha$, with the result

$$\omega a_{\theta\phi} \approx 0.5 E_1 \{G(k)((1 + 0.5\alpha^2) \sin(2\beta^* - \alpha) + 3\alpha) + 0.5k(1 + \alpha^2) \sin 2(\beta^* - \alpha)\}. \quad [5.30]$$

This is plotted in Fig. 6(b), where it can be seen that positive values may occur in quartering winds.

5.2.3 Yaw moment component

The section yaw moment component is given by M, and so the total yaw component,

$$Q_\psi = s\int_r^{r+1} M_u \, d\eta.$$

Linearising to first order in q_ϕ yields

$$Q_\psi = 0.5\rho V_A^2 s \int_r^{r+1} c^2\{C_{m0} + (\zeta - \chi)\{a(\eta) \sin\alpha \cos\alpha + C_{d0} \sin\alpha + A(\eta) \sin^3\alpha\} + q_\phi\tau[C(k)\{2C_{m0} \sin\beta^* + (\zeta - \chi)\{a(\eta) \cos(\beta^* - 2\alpha) + C_{d0}(\cos\beta^* \cos\alpha + 2\sin\beta^* \sin\alpha) + A(\eta) \sin^2\alpha(3\cos\beta^* \cos\alpha + 2\sin\alpha \sin\beta^*)\}\} + 0.5ia(\eta)k(\zeta - 0.5) \cos\delta]\} d\eta \quad [5.31]$$
$$= Q_{\psi s} + Q_{\psi\phi}(\alpha, \beta^*, k)\, \phi'.$$

The damping derivative,

$$B_{\psi\phi} = \text{Real}(Q_{\psi\phi}(\alpha, \beta^*, k)) = 0.5\rho V_A s^2 \int_r^{r+1} c^2\eta \, F(k)[2C_{m0} \sin\beta^* + (\zeta - \chi)\{a(\eta) \cos(\beta^* - 2\alpha) + C_{d0}(\cos\beta^* \cos\alpha + 2\sin\beta^* \sin\alpha) + A(\eta) \sin^2\alpha(3\cos\beta^* \cos\alpha + 2\sin\alpha \sin\beta^*)\}] \, d\eta. \quad [5.32]$$

Using load grading integrals and assuming small α, the coefficient of yaw damping derivative due to roll velocity may be represented by

$$b_{\psi\phi}(\alpha, \beta^*, k) = F(k)[2E_4 \sin\beta^* + E_5(\cos\beta^* + 2\alpha \sin\beta^*) + E_6(\cos\beta^* + 2\alpha \sin\beta^*) + E_7\alpha^2(3\cos\beta^* + 2\alpha \sin\beta^*)]d\eta. \quad [5.33]$$

For symmetric aerofoils $E_4 = 0$, and E_6 and $E_7\alpha^2$ can be neglected in comparison with E_5, so

$$b_{\psi\phi}(\alpha, \beta^*, k) \approx F(k) E_5 \sqrt{1 + 4\alpha^2} \cos(\beta^* - \varepsilon)$$

where $\tan \varepsilon = 2\alpha \approx \varepsilon$.

The coefficient $b_{\psi\phi}$ will be negative for $\beta^* > \pi/2 + 2\alpha$.

This expression is plotted in Fig. 5(c), and it can be seen that negative damping will occur in following winds unless α is zero.

The inertia derivative,

$$\omega A_{\psi\phi} = \text{Imag}(Q_{\psi\phi}(\alpha, \beta^*, k) = 0.5\rho V_A s^2 \int_r^{r+1} c^2\eta \{G(k)\{2\, C_{m0} \sin \beta^* + (\zeta - \chi)\{a(\eta) \cos(\beta^* - 2\alpha) + C_{d0}(\cos \beta^* \cos \alpha + 2 \sin \beta^* \sin \alpha) + A(\eta) \sin^2\alpha (3 \cos \beta^* \cos \alpha + 2 \sin \alpha \sin \beta^*)\} + 0.5\, a(\eta) k(\zeta - 0.5) \cos \delta\}\, d\eta. \quad [5.34]$$

Using load grading integrals and assuming small α, the coefficient of yaw inertia derivative due to roll velocity may be represented by

$$\omega a_{\psi\phi}(\alpha, \beta^*, k) = G(k)\{2\, E_4 \sin \beta^* + E_5(\cos \beta^* + 2\alpha \sin \beta^*) + E_6(\cos \beta^* + 2\alpha \sin \beta^*) + E_7 \alpha^2 (3 \cos \beta^* + 2\alpha \sin \beta^*)\} + 0.5k(E_5 - 0.5\, E_8)(\cos \beta^* + \alpha \sin \beta^*)$$
$$\approx G(k)E_5(\cos \beta^* + 2\alpha \sin \beta^*) + 0.5k(E_5 - 0.5\, E_8)(\cos \beta^* + \alpha \sin \beta^*) \quad [5.35]$$

This is plotted in Fig. 6(c), where it can be seen that it will always be positive for $\beta < 90^o$.

5.3 Forces and Moments Induced by Pitch Motion.

The linear pitch velocity is given by

$v_\theta = \text{Real}(V_A\, q_\theta \tau)$.

In fact, this velocity varies across the chord, because the motion is angular, but is taken as constant here since small motions only are considered.

From Fig. 4(b), it is seen that

$V_U \cos(d\alpha) = V_A - v_\theta \cos \beta^*$

$V_U \sin(d\alpha) = v_\theta \sin \beta^*$

so that

$$\tan(d\alpha) = \frac{v_\theta \sin \beta^*}{VA - v_\theta \cos \beta^*} = \frac{q_\theta \tau \sin \beta^*}{1 - q_\theta \tau \cos \beta^*} \quad [5.36]$$

Again referring to Fig. 4(b),

$V_U = v_\theta \sin \beta^* / \sin d\alpha = V_A H_\theta$

where

$$H_\theta = \sqrt{1 - 2q_\theta \tau \cos \beta^* + (q_\theta \tau)^2} \approx 1 - q_\theta \tau \cos \beta^* \quad [5.37]$$

and

$1/H_\theta = 1 + q_\theta \tau \cos \beta^*$.

The roll induced component of the quasi-steady section lift force is given by

$$L_q(\eta) = 0.5\rho V_U^2 c[C_{l0} + a \sin(\alpha + d\alpha)]$$
$$= 0.5\rho V_A^2 c H_\theta [C_{l0} + a \sin \alpha + q_\theta \tau(-C_{l0} \cos \beta^* + a \sin \delta)] \quad [5.38]$$

and the corresponding component of quasi-steady section drag force is

$D_q(\eta) = 0.5\rho V_U^2 c[C_{d0} + A \sin^2(\alpha + d\alpha)]$

$$= 0.5\rho V_A^2 c[H_\theta^2 C_{d0} + A(\sin\alpha + q_\theta\tau \sin\delta)^2]$$

linearisation to first order in q_θ yields

$$D_q(\eta) \approx 0.5\rho V_A^2 c[C_{d0} + A\sin^2\alpha - 2\, q_\theta\tau(C_{d0}\cos\beta^* - A\sin\alpha\sin\delta)]$$

$$\approx 0.5\rho V_A^2 c H_\theta\{C_{d0} + A\sin^2\alpha - q_\theta\tau[C_{d0}\cos\beta^* - A\sin\alpha(2\sin\beta^*\cos\alpha - \sin\alpha\cos\beta^*)]\} \quad [5.39]$$

The corresponding section yaw moment about the shaft

$$M_q(\eta) = 0.5\rho V_U^2 c^2(\eta)[C_{m0} + (\zeta - \chi)\{a(\eta)\sin(\alpha + d\alpha)\cos(\alpha + d\alpha) + C_{d0}\sin(\alpha + d\alpha)$$

$$+ A(\eta)\sin^3(\alpha + d\alpha)\}]$$

and linearising to first order in q_θ yields

$$M_q(\eta) = 0.5\rho V_A^2 c^2(\eta)[C_{m0} + (\zeta - \chi)\{a(\eta)\sin\alpha\cos\alpha + C_{d0}\sin\alpha + A(\eta)\sin^3\alpha\}$$

$$+ q_\theta\tau[-2C_{m0}\cos\beta^* + (\zeta - \chi)\{a(\eta)\sin(\beta - 2\alpha) + C_{d0}\sin\beta^*\cos\alpha$$

$$+ A(\eta)\sin^2\alpha(3\sin\beta^*\cos\alpha - 2\sin\alpha\cos\beta^*)\}]] \quad [5.40]$$

$$= M_s + M_q q_\theta\tau.$$

The component of force perpendicular to V becomes

$$L_q' = L_q\cos(d\alpha) + D_q\sin(d\alpha)$$

$$\approx 0.5\rho V_A^2 c\{C_{l0} + a\sin\alpha + q_\theta\tau[-2C_{l0}\cos\beta^* + a(\sin\delta - \sin\alpha\cos\beta^*) + (C_{d0} + A\sin^2\alpha)\sin\beta^*]\}$$

$$= L_s + L_q q_\theta\tau$$

and the component of force parallel to V becomes

$$D_q' = D_q\cos(d\alpha) - L_q\sin(d\alpha)$$

$$\approx 0.5\rho V_A^2 c[C_{d0} + A\sin^2\alpha - q_\theta\tau(C_{l0}\sin\beta^* + a\sin\alpha\sin\beta^* + 2C_{d0}\cos\beta^* - 2A\sin\alpha\sin\delta)$$

$$= D_s + D_q q_\theta\tau.$$

5.3.1 Roll moment component

The section roll moment component about the Cy axis is given by

$$s\eta(L_u'\cos\beta^* + D_u'\sin\beta^*)$$

and so the total roll component may be written in the form

$$Q_\phi = h^2\int_r^{r+1} \eta(L_u'\cos\beta^* + D_u'\sin\beta^*)\, d\eta$$

Linearising to first order in q_θ yields

$$Q_\phi = 0.5\rho V_A s^2 h\int_r^{r+1} c\eta\,\{C_{l0}\cos\beta^* + a\sin\alpha\cos\beta^* + (C_{d0} + A\sin^2\alpha)\sin\beta^*$$

$$+ q_\theta\tau\{C(k)[-(C_{l0}(2\cos^2\beta^* + \sin^2\beta^*) + a(\cos\beta^*\sin\beta^*\cos\alpha - 2\sin\alpha\cos^2\beta^*$$

$$- \sin^2\beta^*\sin\alpha) - C_{d0}\sin\beta^*\cos\beta^* + A\sin\alpha\sin\beta^*(2\sin\beta^*\cos\alpha - \sin\alpha\cos\beta^*)]$$

$$+ 0.5ika\sin\delta\cos\delta\}\, d\eta \quad [5.41]$$

that is

$$Q_\phi = Q_{\phi s} + Q_{\phi\theta}(\alpha, \beta^*, k)\,\theta'.$$

The damping derivative,

$$B_{\phi\theta} = \text{Real}(Q_{\phi\theta}(\alpha, \beta^*, k) = 0.5\rho V_A s^3\int_r^{r+1} c\eta^2 F(k)\,[-C_{l0}(2\cos^2\beta^* + \sin^2\beta^*) +$$

$$a(\cos\beta^*\sin\beta^*\cos\alpha - 2\sin\alpha\cos^2\beta^* - \sin^2\beta^*\sin\alpha) - C_{d0\,\sin}\beta^*\cos\beta^*$$

$$+ A\sin\alpha\sin\beta^*(2\sin\beta^*\cos\alpha - \sin\alpha\cos\beta^*)]\, d\eta. \quad [5.42]$$

Using load grading integrals and assuming small α, the coefficient of roll damping due to pitch velocity may be written in the form

$$b_{\phi\theta}(\alpha, \beta^*, k) = F(k)\{ - E_0(2\cos^2\beta^* + \sin^2\beta^*) + E_1(\cos\beta^* \sin\beta^* - 2\alpha\cos^2\beta^* - \alpha\sin^2\beta^*) - E_2 \sin\beta^* \cos\beta^*$$
$$+ E_3 \alpha \sin\beta^*(2\sin\beta^* - \alpha\cos\beta^*)\}$$
$$= F(k)\{ - 2(E_0 + E_1\alpha)\cos^2\beta^* + (E_1 - E_2 - E_3\alpha^2)\sin\beta^*\cos\beta^* - [E_0 + (E_1 - 2E_3)\alpha]\sin^2\beta^*\} \quad [5.43]$$

where

$A_1 = - 2(E_0 + E_1\alpha)$, $A_2 = (E_1 - E_2 - E_3\alpha^2)$, $A_3 = - [E_0 + (E_1 - 2E_3)\alpha,]$

and applying the aerofoil approximation gives $A_1 = - 2E_1\alpha$, $A_2 \approx E_1$, $A_3 \approx - E_1\alpha$

so that $\tan(2\varepsilon) \approx - 1/\alpha$ and therefore $\varepsilon \approx \pi/4 + \alpha/2$.

The roll damping coefficient due to pitch motion is then

$$b_{\phi\theta} \approx 0.5\, F(k)\, E_1[(1 + 0.5\,\alpha^2)\sin(2\beta^* - \alpha) - 3\alpha]. \quad [5.44]$$

This expression is plotted in Fig. 5(d), and it can be seen that minimum damping occurs at $\beta^* = \alpha/2 + 3\pi/4$, where $b_{\phi\theta}$ will be negative unless $\alpha < - 0.355$ ($\approx - 20^o$). Otherwise, $b_{\phi\theta}$ will be negative throughout the region where

$\sin(2\beta^* - \alpha) < 3\alpha / (1 + 0.5\alpha^2)$.

The inertia derivative is given by

$$\omega A_{\phi\theta} = \text{Imag}(Q_{\phi\theta}(\alpha, \beta^*, k) = 0.5\rho V_A s^3 \int_r^{r+1} c\eta^2 \{G(k)[- C_{l0}(2\cos^2\beta^* + \sin^2\beta^*) +$$
$$a(\cos\beta^* \sin\beta^* \cos\alpha - 2\sin\alpha\cos^2\beta^* - \sin^2\beta^* \sin\alpha) - C_{d0} \sin\beta^* \cos\beta^*$$
$$+ A \sin\alpha \sin\beta^*(2\sin\beta^* \cos\alpha - \sin\alpha\cos\beta^*)] + 0.5ka(\sin\beta^* \cos\beta^* \cos^2\alpha + \sin\alpha\cos\alpha\sin^2\beta^*$$
$$- \sin\alpha\cos\alpha\cos^2\beta^* - \sin^2\alpha\sin\beta^*\cos\beta^*\}\, d\eta. \quad [5.45]$$

Using load grading integrals and assuming small α, the coefficient of roll damping due to pitch velocity may be written in the form

$$\omega\, a_{\phi\theta}(\alpha, \beta^*, k) = G(k)\{ - E_0(2\cos^2\beta^* + \sin^2\beta^*) + E_1(\cos\beta^* \sin\beta^* - 2\alpha\cos^2\beta^* - \alpha\sin^2\beta^*)$$
$$- E_2 \sin\beta^* \cos\beta^* + E_3 \alpha \sin\beta^*(2\sin\beta^* - \alpha\cos\beta^*)\} + 0.5k\, E_1 (- \alpha\cos^2\beta^*$$
$$+ (1 - \alpha^2)\sin\beta^*\cos\beta^* + \alpha\sin^2\beta^*)$$
$$= G(k)\{ - 2(E_0 + E_1\alpha)\cos^2\beta^* + (E_1 - E_2 - E_3\,\alpha^2)\sin\beta^*\cos\beta^* - [E_0 + (E_1 - 2E_3)\alpha]\sin^2\beta^*\}$$
$$+ 0.5k\, E_1 (- \alpha\cos^2\beta^* + (1 - \alpha^2)\sin\beta^*\cos\beta^* + \alpha\sin^2\beta^*) \quad [5.46]$$

and with

$B_1 = - E_1\,\alpha$, $B_2 = E_1(1 - \alpha^2)$, $B_3 = E_1\,\alpha$

then $\tan(2\varepsilon') \approx - 1/2\alpha$ and therefore $\varepsilon \approx \pi/4 + \alpha$.

We can thus write for the roll inertia coefficient due to pitch motion,

$$\omega\, a_{\phi\theta} \approx 0.5\, E_1(G(k)[(1 + 0.5\,\alpha^2)\sin(2\beta^* - A) - 3\alpha] + 0.5k(1 + \alpha^2)\sin 2(\beta^* - \alpha)) \quad [5.47]$$

This is plotted in Fig. 6(d) and, as for $a_{\theta\phi}$, positive values will occur in quartering winds.

5.3.2 Pitch moment component

The section pitch moment component about the Cx axis is given by $s\eta(L_u' \sin\beta^* - D_u' \cos\beta^*)$, and so the total pitch component may be written as

$$Q_\theta = s^2 \int_r^{r+1} \eta(L_u' \sin\beta^* - D_u' \cos\beta^*)\, d\eta$$

Linearising to first order in q_θ yields

$$Q_\theta = 0.5\rho V_A s^2 \int_r^{r+1} c\eta\{C_{l0}\sin\beta^* + a\sin\alpha\sin\beta^* - (C_{d0} + A\sin^2\alpha)\cos\beta^*$$
$$+ q_\theta\tau[C(k)\{-C_{l0}\sin\beta^*\cos\beta^* + a\sin\delta\sin\beta^* + C_{d0}(\sin^2\beta^* + 2\cos^2\beta^*) + A(\sin^2\alpha\sin^2\beta^*$$
$$- 2\sin\alpha\cos\beta^*\sin\delta)\} + 0.5ika\sin^2\delta]\}d\eta \qquad [5.48]$$
$$= Q_{\theta s} + Q_{\theta\theta}\,\theta'.$$

The damping derivative is

$$B_{\theta\theta} = \text{Real}(Q_{\theta\theta}(\alpha, \beta^*, k)) = 0.5\rho V_A s^3 \int_r^{r+1} c\eta^2\, F(k)\,[-C_{l0}\sin\beta^*\cos\beta^*$$
$$+ a(\sin^2\beta^*\cos\alpha - \cos\beta^*\sin\alpha\sin\beta^*) + C_{d0}(\sin^2\beta^* + 2\cos^2\beta^*) + A\sin\alpha(\sin\alpha\sin^2\beta^*$$
$$- 2\cos\beta^*\sin\delta)]\,d\eta \qquad [5.49]$$

Using load grading integrals and assuming small α, the coefficient of pitch damping derivative due to pitch velocity may be written as

$$b_{\theta\theta}(\alpha, \beta^*) = F(k)\{-E_0\sin\beta^*\cos\beta^* + E_1(\sin^2\beta^* - \alpha\cos\beta^*\sin\beta^*) + E_2(\sin^2\beta^* + 2\cos^2\beta^*)$$
$$+ E_3\alpha(\alpha\sin^2\beta^* - 2\cos\beta^*\sin\beta^* + 2\alpha\cos^2\beta^*)\}$$
$$= F(k)\{2(E_2 + E_3\alpha^2)\cos^2\beta^* - [E_0 + (E_1 + 2E_3)\alpha]\cos\beta^*\sin\beta^* + (E_1 + E_2 + E_3\alpha^2)\sin^2\beta^*\} \qquad [5.50]$$

where

$A_1 = 2(E_2 + E_3\alpha^2)$, $A_2 = -[E_0 + (E_1 + 2E_3)\alpha]$, $A_3 = (E_1 + E_2 + E_3\alpha^2)$.

With the aerofoil approximations $A_1 \approx 0$, $A_2 \approx -E_1\alpha$, $A_3 \approx E_1$

we have $\tan(2\varepsilon) \approx \alpha$, leading to $\varepsilon \approx \pi/2 + \alpha/2$.

We can then write for the damping coefficient due to pitch motion,

$b_{\theta\theta} \approx 0.5E_1[1 - (1 + 0.5\alpha^2)\cos(2\beta^* - \alpha)]$.

This expression is plotted in Fig. 5(e), and it can be seen that negative pitch damping will always occur near to $\beta^* = \alpha/2$ and $\beta^* = \pi - \alpha/2$ but these conditions can be avoided by having α negative for $\beta^* < \pi/2$ and α positive for $\beta^* > \pi/2$.

The inertia derivative,

$$\omega A_{\theta\theta} = \text{Imag}(Q_{\theta\theta}(\alpha, \beta^*, k)) = 0.5\rho V_A s^3 \int_r^{r+1} c\eta^2\,\{G(k)\,[-C_{l0}\sin\beta^*\cos\beta^*$$
$$+ a(\sin^2\beta^*\cos\alpha - \cos\beta^*\sin\alpha\sin\beta^*) + C_{d0}(\sin^2\beta^* + 2\cos^2\beta^*) + A\sin\alpha(\sin\alpha\sin^2\beta^*$$
$$- 2\cos\beta^*\sin\delta)] + 0.5ka(\sin^2\beta^*\cos^2\alpha - 2\sin\beta^*\cos\beta^*\sin\alpha\cos\alpha + \cos^2\beta^*\sin^2\alpha\}\,d\eta \qquad [5.51]$$

Using load grading integrals and assuming small α, the coefficient of pitch inertia derivative due to pitch velocity may be written as

$$\omega\, a_{\theta\theta}(\alpha, \beta^*) = G(k)\{-E_0\sin\beta^*\cos\beta^* + E_1(\sin^2\beta^* - \alpha\cos\beta^*\sin\beta^*) + E_2(\sin^2\beta^* + 2\cos^2\beta^*)$$
$$+ E_3\alpha(\alpha\sin^2\beta^* - 2\cos\beta^*\sin\beta^* + 2\alpha\cos^2\beta^*)\} + 0.5kE_1(\sin^2\beta^* - 2\alpha\sin\beta^*\cos\beta^* + \alpha^2\cos^2\beta^*)$$
$$= G(k)\{2(E_2 + E_3\alpha^2)\cos^2\beta^* - [E_0 + (E_1 + 2E_3)\alpha]\cos\beta^*\sin\beta^* + (E_1 + E_2 + E_3\alpha^2)\sin^2\beta^*\}$$
$$+ 0.5kE_1(\sin^2\beta^* - 2\alpha\sin\beta^*\cos\beta^* + \alpha^2\cos^2\beta^*) \qquad [5.52]$$

where

$B_1 = E_1\alpha^2$, $B_2 = -2E_1\alpha$, $B_3 = E_1$

This is plotted in Fig. 6(e), and is seen to be always negative.

5.3.3 Yaw moment component

The section yaw moment = M, so the total yaw moment is given by

$$Q_\psi = s\int_r^{r+1} M_u \, d\eta$$

Linearising to first order in q_θ yields

$$Q_\psi = 0.5\rho V_A^2 s^2 \int_r^{r+1} c^2 [C_{m0} + (\zeta - \chi)\{a(\eta)\sin\alpha\cos\alpha + C_{d0}\sin\alpha + A(\eta)\sin^3\alpha\}$$
$$+ q_\theta\tau\{C(k)\{-2C_{m0}\cos\beta^* + (\zeta-\chi)\{a(\eta)\sin(\beta-2\alpha) + C_{d0}\sin\beta^*\cos\alpha$$
$$+ A(\eta)\sin^2\alpha(3\sin\beta^*\cos\alpha - 2\sin\alpha\cos\beta^*)\}\} + 0.5ia(\eta)k(\zeta-0.5)\sin\delta\}]\,d\eta \qquad [5.53]$$

which may be written in the form

$$Q_\psi = Q_{\psi s} + Q_{\psi\theta}\,\theta'.$$

The damping derivative is

$$B_{\psi\theta} = \text{Real}(Q_{\psi\theta}(\alpha, \beta^*, k))$$
$$= 0.5\rho V_A s^2 \int_r^{r+1} c^2\eta\, F(k)[-2C_{m0}\cos\beta^* + (\zeta-\chi)\{a(\eta)\sin(\beta-2\alpha)$$
$$+ C_{d0}\sin\beta^*\cos\alpha + A(\eta)\sin^2\alpha(3\sin\beta^*\cos\alpha - 2\sin\alpha\cos\beta^*)]\,d\eta. \qquad [5.54]$$

Using load grading integrals and assuming small α, the coefficient of yaw damping derivative due to pitch velocity may be written as

$$b_{\psi\theta}(\alpha, \beta^*) = F(k)[-2E_4\cos\beta^* + \{E_5(\sin\beta^* - 2\alpha\cos\beta^*) + E_6\sin\beta^* + E_7\alpha^2(3\sin\beta^* - 2\alpha\cos\beta^*)]$$

For symmetric aerofoils, $C_{m0} = 0$, so

$$b_{\psi\theta}(\alpha, \beta^*) \approx F(k)\,E_5\,\sqrt{1+4\alpha^2}\cos(\beta^* - \varepsilon) \qquad [5.55]$$

where

$\tan\varepsilon = -1/2\alpha$ so $\varepsilon = \pi/2 + 2\alpha$

This expression is plotted in Fig. 5(f), and it can be seen that $b_{\psi\theta}$ will be positive unless α is very small.

The inertia derivative,

$$\omega A_{\psi\theta} = \text{Imag}(Q_{\psi\theta}(\alpha, \beta^*, k))$$
$$= 0.5\rho V_A s^2 \int_r^{r+1} c^2 h\{G(k)[-2C_{m0}\cos\beta^* + (\zeta-\chi)\{a(\eta)\sin(\beta-2\alpha)$$
$$+ C_{d0}\sin\beta^*\cos\alpha + A(\eta)\sin^2\alpha(3\sin\beta^*\cos\alpha - 2\sin\alpha\cos\beta^*)]$$
$$+ 0.5a(\eta)k(\zeta-0.5)(\sin\beta^*\cos\alpha - \cos\beta^*\sin\alpha\}\,d\eta. \qquad [5.56]$$

Using load grading integrals and assuming small α, the coefficient of yaw inertia derivative due to pitch velocity may be written as

$$\omega a_{\psi\theta}(\alpha, \beta^*) = G(k)[-2E_4\cos\beta^* + \{E_5(\sin\beta^* - 2\alpha\cos\beta^*) + E_6\sin\beta^*$$
$$+ E_7\alpha^2(3\sin\beta^* - 2\alpha\cos\beta^*)] + 0.5k(E_5 - 0.5E_8)(\sin\beta^* - \alpha\cos\beta^*)$$
$$\approx E_5\sqrt{1+4\alpha^2}\cos(\beta^* - \varepsilon) + 0.5k(E_5 - 0.5E_8)(\sin\beta^* - \alpha\cos\beta^*) \qquad [5.57]$$

This is plotted in Fig. 6(f), and is seen to be positive for most of the range.

5.4 Discussion

For the operation of a wind assisted ship in the maximised propulsion mode a large positive angle of incidence α would be chosen. As an example, values of $\pm 20^o$ have been used in the sample calculations. Fig. 5(a) shows the variation of the roll damping coefficient for roll motion $b_{\phi\phi}$, for $0 < \beta^* < 180^o$ and α values of 0 and $\pm 20^o$. An aspect ratio of 2 and a rectangular planform have been used (variations of these parameters are discussed later) as being representative of present practice. Apart from angles close to $\beta^* = (\pi + \alpha)/2$ the damping coefficient is always positive although the largest values of $b_{\phi\phi}$ correspond to $\alpha = + 20^o$ for $\beta^* < \pi/2$, but $\alpha = - 20^o$ for $\beta^* > \pi/2$. If these conditions are held, Fig. 5(b) shows that $b_{\theta\phi}$ for pitch damping due to roll is large and positive for $\beta^* < \pi/2$ but large and negative, i.e. negative damping for $\beta^* > \pi/2$.

Corresponding conflicts are seen for the remaining derivatives in Fig. 5 thus indicating that the requirements for large positive thrust from the rig are inconsistent with large positive damping for all angles of β^*. For example, $b_{\phi\phi}$ has a maximum value when $\beta^* = 0$ and 180^o, i.e. the apparent wind is directed along $\pm$ Cx and in either case thrust is very small negative or positive respectively. Maximum thrust occurs when β^* is approximately 90^o, a condition yielding small amounts of roll damping from roll, pitch and yaw motions. Pitch damping from pitch motions is, however, then effective as seen by the behaviour of $b_{\theta\theta}$ in Fig.5(e).

The effects of aspect ratio on the various aerodynamic damping coefficients are illustrated in Fig. 9 and for the purposes of demonstration an angle of incidence $\alpha = 15^o$ has been chosen as typical. The planform is rectangular with no sweepback corresponding to present marine aerofoils used on ships. It is clear that substantial departures from two - dimensional performance (AR = ∞) occur. Apart from the yaw derivatives, increases in aspect ratio give larger magnitudes for the remaining derivatives, although corresponding coincidences of values take place at the same β^*- axis crossing points as shown by the $\alpha = 20^o$ curves in Fig.5. The yaw derivatives $b_{\theta\phi}$ and $b_{\theta\psi}$ present interesting cases. The maximum magnitude for each of these occurs for AR = 3 and both become zero for AR = ∞, remaining positive for most β^* and all other aspect ratios. The principal benefits of roll damping occur for the higher aspect ratios but structural strength would tend to limit the span of marine aerofoils to, say, an aspect ratio of 5.

The planform shape can be described in terms of sweepback angle and taper ratio (top chord length/bottom chord length). Sweepback does not appear to offer any aerodynamic or structural advantages for wingsails but taper ratio, as used for yacht sails, is of interest. Figure 10 shows the variations of damping derivatives for taper =1 (rectangular planform) and taper = 0 (triangle with apex at top) of equal plan area with $\alpha = 20^o$, AR = 2. For all but the yaw derivatives, the introduction of taper reduces the magnitude of the derivatives, but the shape of the variation with β^* remains, and thus the capacity for positive damping is also reduced.

On the other hand, the variations of the yaw derivatives, Figs. 10(c) and (f) are reversed by the introduction of taper, but magnitudes always remain small.

The derivatives b_{mn} have been made dimensionless by using the apparent wind velocity V_A and are thus directly related to body axes and conditions seen by an observer moving with the ship. Data concerning ship propulsion and environmental conditions are inevitably connected with ship speed through the water V_S, true wind speed V_T and true wind direction γ (see Fig. 3). A re - plot of the results in Fig. 5 for various ratios of $V_S/V_T = \sigma$ is shown in Fig. 11 for $\alpha = 15^o$, AR = 2 and a rectangular planform. Maximum roll damping is achieved for all γ at the highest σ ratio whereas the contrary is true for pitch damping. Roll damping can, however, become negative for some values of σ in quartering seas, whereas pitch damping is substantially negative for a wider range of σ in bow seas. If $\sigma > 1$, as it usually is for cargo ships at sea, $b_{\phi\phi}(V_A/V_T)^2$ is positive for all γ, as the critical value of β^* will never be reached.

6. MOTION DAMPING OF OTHER WASP DEVICES - THEORY

6.1 Wingsails

As shown in the preceding chapter, by using load grading integrals and assuming small α, the derivative for roll damping due to roll velocity may be represented by
$C_B(\alpha, \beta^*) \approx 0.5\, E_1[(1 + 0.5\alpha^2) \cos(2\beta^* - \alpha) + 1]$.

A symmetric NACA 0015 aerofoil of rectangular planform with an aspect ratio of 2, and lift curve slope $\partial C_L/\partial\alpha = 2.6$ per radian has been used for this analysis as being representative of present practice. These data then give $C_L(\alpha) = 0$ and ± 0.9 and $C_D(\alpha) = 0.01$ and 0.06 for incidence angles α of 0 and $\pm 20^o$ respectively. To avoid the possibility of stall, the wingsail must be yawed around on its pivot so that α is always small, with the magnitude of 20^o representing a reasonable maximum limit for wingsails.

In steady conditions, the thrust coefficient is given by
$C_T = C_L \sin\beta^* - C_D \cos\beta^*$
and the heel moment coefficient is given by
$C_H \approx C_L \cos\beta^* + C_D \sin\beta^*$
The direction of the resultant aerodynamic force can be controlled by adjusting α.

The first order passive roll damping derivative is approximately
$C_B(\alpha, \beta^*) \approx (3.1 \cos\beta^* + 3.6\, \alpha \sin\beta^*) \cos\beta^*$ [6.1]
It can be seen from Fig. 12(c) that this parameter will be negligible in a beam wind, but will always be positive in a quartering wind. Negative damping always occurs near $\beta^* = (\pi+\alpha)/2$ and the minimum value $C_{B\,min} = -0.76\, \alpha^2$. Second-order drag terms become relevant here, but they are also small.

Alternatively, the aerofoil can be oscillated like an active fin, with $\alpha = \alpha_s + i\alpha_0 \exp i(\omega_e t + \varepsilon)$, in which case the damping coefficient has an additional increment of
$C_A = \{(2.6 \cos\beta^* + 0.37\, \alpha_s \sin\beta^*) \cos\varepsilon\} / q$ [6.2]

Figure 12(b) shows that C_H will be negligible in a beam wind, so the ship will roll about an upright position, and Fig. 12(c) indicates that C_B will also be negligible in a beam wind, but will always be positive in a quartering wind. For the operation of a wind assisted ship in the maximised propulsion mode, a large positive angle of incidence would be used in current practice. However, maximum roll damping can be obtained by ensuring that α is positive for $\beta^* < 90^o$ (giving positive thrust) and negative for $\beta^* > 90^o$ (giving negative thrust). A compromise must therefore be made between the requirements of thrust generation or roll damping. Again in a beam wind, Fig. 12(d) shows that qC_A will also be very small. To obtain a

positive increment in qC_A the phase must be controlled so that for $\beta^* < 90^o$, $\varepsilon = 0$ (in phase) and for $\beta^* > 90^o$, $\varepsilon = 180^o$ (in anti-phase).

The preceding results lead to the conclusion that negligible damping will always be provided by a wingsail in a beam wind.

6.2 Horizontal axis wind turbines (HAWT)

The forces and velocities on a yawed HAWT are shown in Fig. 13. Jackson (1986) measured the lift and drag forces on small two- and three-bladed model HAWTs at various yaw angles. The HAWT was a scale model of the Swansea University machine, as described by Herapath et al (1979), with blade profile NACA 4415, rated tip speed ratio of 5, maximum power coefficient of 0.45. A curve-fit to these experimental points yields equations of the form:

$$C_L = \lambda \sin\delta \, (a_1 \cos\delta - b_1 \lambda + c_1) \qquad [6.3a]$$

$$C_D = \lambda \cos\delta \, (a_2 \cos\delta - b_2 \lambda + c_2) \qquad [6.3b]$$

$$C_P = \lambda^2 \, (a_3 \cos\delta - b_3 \lambda + c_3) \qquad [6.3c]$$

where, for three blades,

$a_1 = 0.3$	$b_1 = 0.016$	$c_1 = 0.07$
$a_2 = 0.3$	$b_2 = 0.035$	$c_2 = 0.3$
$a_3 = 0.0132$	$b_3 = 0.0012$	$c_3 = 0.0002$

These lift, drag, power and resultant thrust coefficients for head winds ($\beta^* = 0$) are shown in Fig. 14 as a function of tip speed ratio, λ and in Fig. 15 as a function of yaw angle, δ. The direction of the resultant aerodynamic force can be controlled by adjusting the incidence. It can be seen that the resultant thrust, considering the wind turbine to be driving a propeller, is negative in head winds, due to the high drag coefficient.

For wind turbines, the resultant aerodynamic thrust can be resolved into overall 'lift' and 'drag' forces for the complete rotor. Unlike land-based wind turbines, the overall drag coefficient will be very important. In WASP applications it is the components resolved along and normal to the ship's axis of symmetry (i.e. direction of ship's propeller thrust) which are important, rather than lift and drag components. The torque transmitted to the rotor shaft may be used to drive a hydrodynamic propeller, either directly or indirectly through an electric generator/motor set, which enables the ship to sail directly upwind, if required.

Similar to the analysis for wingsails in the preceding section, the linear roll velocity is given by $v = V_A u$, where $u = h\phi' / V_A$.

Using the substitution

$$H = \sqrt{1 + 2u \sin\beta^* + u^2}$$

we may write

$\sin d\alpha = u \cos \beta^* / H$,

$\cos d\alpha = (1 + u \sin \beta^*) / H$

Again referring to Fig. 13 and linearising to first order in u gives

$V_U \approx V_A(1 + u \sin \beta^*)$,

$V_A \approx V_U (1 - u \sin \beta^*)$

The component of the section lift force measured perpendicular to the instantaneous apparent wind velocity vector V_U is given by,

$$L = 0.5\rho V_U^2 \pi R^2 (R\Omega/V_U) \sin(\delta + d\alpha) [a_1 \cos(\delta + d\alpha) - b_1 R\Omega/V_U + c_1]$$

$$= 0.5\rho V_U \pi R^3 \Omega (1/H^2) (\sin \delta - u \cos(\beta^* + \delta)) [a_1(\cos \delta + u \sin(\beta^* - \delta)) - b_1 \lambda + c_1(1 + u \sin \beta^*)] \quad [6.4]$$

and the lift coefficient is then

$$C_L = (\lambda/H) [\sin \delta + u \cos(\beta^* - \delta)] [a_1 \cos \delta - b_1\lambda + c_1 + u(a_1 \sin(\beta^* - \delta) + c_1 \sin \beta^*)]$$

$$= (\lambda/H) [\sin \delta(a_1 \cos \delta - b_1\lambda + c_1) + u (a_1 \cos(\beta^* - 2\delta) - b_1\lambda \cos(\beta^* - \delta) + c_1(\cos \beta^* \cos \delta + 2 \sin \delta \sin \beta^*))] \quad [6.5]$$

The corresponding component of section drag force is

$$D = 0.5\rho V_U \pi R^3 \Omega \cos(\delta + d\alpha) [a_2 \cos(\delta + d\alpha) - b_2 R\Omega/V_U + c_2] \quad [6.6]$$

and the drag coefficient is then

$$C_D = \lambda/H [\cos \delta + u \sin(\beta^* - \delta)] [a_2 \cos \delta - b_2\lambda + c_2 + u(a_2 \sin(\beta^* - \delta) + c_2 \sin \beta^*)].$$

$$= \lambda/H \{\cos \delta(a_2 \cos \delta - b_2\lambda + c_2) + u[2a_2 \sin(\beta^* - \delta) \cos \delta - b_2\lambda \sin(\beta^* - \delta) + c_2(2 \sin \beta^* \cos \delta - \sin \delta \cos \beta^*)]\}. \quad [6.7]$$

The section thrust component is given by

$$C_T = - C_L \sin(\beta^* + d\alpha) - C_D \cos(\beta^* + d\alpha)$$

$$= - (1/H) [C_L(\sin \beta^* + u) + C_D \cos \beta^*]$$

Assuming small δ gives

$$C_T \approx - (\lambda / H^2)\{\delta \sin \beta^*(a_1 - b_1\lambda + c_1) + \cos \beta^*(a_2 - b_2\lambda + c_2) + u ((a_1 + 2a_2) \sin \beta^* \cos \beta^* + \delta ((3 \sin^2\beta^* + \cos^2\beta^*) a_1 - 2 \cos^2\beta^* a_2) - (b_1 + b_2)\lambda \sin \beta^* \cos \beta^* - \lambda\delta (b_1(\cos^2\beta^* + 3 \sin^2\beta^*) + b_2 \cos^2\beta^*)) + (c_1 + 2 c_2) \cos \beta^* \sin \beta^* + (c_1(2 \sin^2\beta^* + \cos^2\beta^*) - c_2 \cos^2\beta^*) \delta\} \quad [6.8]$$

The section side force component is given by

$$C_S = - C_L \cos(\beta^* + d\alpha) + C_D \sin(\beta^* + d\alpha)$$

$$= (1/H) (- C_L \cos \beta^* + C_D(\sin \beta^* + u))$$

Assuming small δ gives

$$C_S \approx (\lambda / H^2) \{- \delta \cos \beta^* (a_1 - b_1\lambda + c_1) + \sin \beta^* (a_2 - b_2\lambda + c_2) + u [- (a_1 - a_2) \cos^2\beta^* + 3 a_2 \sin^2\beta^* - 2 \delta \sin \beta^* \cos \beta^* (a_1 + a_2) + \lambda ((b_1 - b_2) \cos^2\beta^* - 2 b_2 \sin^2\beta^* + (b_1 + b_2) \delta \sin \beta^* \cos \beta^*) - c_1 \cos^2\beta^* + c_2 (\cos^2\beta^* + 3 \sin^2\beta^*) - (2 c_1 + c_2) \delta \sin \beta^* \cos \beta^*]\}$$

$$= \lambda \{- \delta \cos \beta^* (a_1 - b_1\lambda + c_1) + \sin \beta^* (a_2 - b_2\lambda + c_2) + u [\{- a_1 + a_2 - c_1 + c_2 + \lambda (b_1 - b_2)\}\cos^2\beta^*$$

$$+ \{- 2\,a_1 - 2\,a_2 - 2\,c_1 - c_2 - \lambda\,(b_1 - b_2)\}\,\delta \sin\beta^* \cos\beta^* + \{a_2 + c_2\} \sin^2\beta^* \,]\} \qquad [6.9]$$

The side force is then given by

$S = 0.5\,\rho\,V_A^2\,\pi R^2\,C_S$

and the roll moment is given by $Q_\phi = hS$

that is,

$Q_\phi = Q_{\phi s} + Q_{\phi\phi}(\delta, \beta^*, \lambda)\,\phi'$

The steady part of the roll moment is given by

$$Q_{\phi s} = 0.5\,\rho\,V_A^2\,\pi R^2\,h\lambda\{-\delta\cos\beta^*\,(a_1 - b_1\lambda + c_1) + \sin\beta^*\,(a_2 - b_2\lambda + c_2)\} \qquad [6.10]$$

The damping derivative is

$$C_B(\delta, \beta^*, \lambda) = Q_{\phi\phi}(\delta, \beta^*, \lambda) \,/\, 0.5\,\rho\,V_A\,\pi R^2\,h^2$$

$$= \lambda\{- a_1 + a_2 - c_1 + c_2 + \lambda\,(b_1 - b_2)\}\cos^2\beta^* + \{- 2\,a_1 - 2\,a_2 - 2\,c_1 - c_2$$

$$- \lambda\,(b_1 - b_2)\}\,\delta \sin\beta^* \cos\beta^* + \{a_2 + c_2\} \sin^2\beta^*\}$$

$$= \lambda(A_1 \cos^2\beta^* + A_2 \cos\beta^* \sin\beta^* + A_3 \sin^2\beta^*)$$

$$= 0.5\lambda\{-\sqrt{(A_1 - A_3)^2 + A_2^2}\,\cos 2(\beta^* - \varepsilon) + A_1 + A_3\} \qquad [6.11]$$

where

$A_1 = - a_1 + a_2 - c_1 + c_2 + \lambda\,(b_1 - b_2)$ $\qquad = 0.23 - 0.019\,\lambda$

$A_2 = - \{2\,a_1 + 2\,a_2 + 2\,c_1 + c_2 + \lambda\,(b_1 - b_2)\}\,\delta$ $\qquad = - \delta\,(1.64 - 0.019\,\lambda)$

$A_3 = a_2 + c_2$ $\qquad = 0.6$

and

$\tan(2\varepsilon) = A_2 \,/\, (A_1 - A_3)$.

$$= \delta\,(1.64 - 0.019\,\lambda) \,/\, (0.37 + 0.019\,\lambda)$$

which, for these values of λ, is approximately $3\,\delta$.

From these data,

$$C_B \approx 0.5\lambda\{-\,(0.37 + 0.019\,\lambda)\cos\,(2\,\beta^* - 3\,\delta) + 0.83 - 0.019\,\lambda\} \qquad [6.12]$$

which is minimum, given by $C_{B\min} = 0.6\,\lambda$, when $\beta^* = 1.5\,\delta$.

The effective thrust coefficient, assuming the wind turbine to be driving a propeller, is given by

$C_T = (V_A \,/\, V_S)\,C_P - C_L \sin\beta^* - C_D \cos\beta^*$

where C_P is the power generated by the wind turbine.

The static heel moment coefficient is given by

$C_H = - C_L \cos\beta^* + C_D \sin\beta^*$

The first order passive roll damping derivative is

$$C_B(\lambda, \theta, \beta^*) = 0.02\,\lambda\,\{(12 - \lambda)\cos^2\beta^* - \delta\,(45 - \lambda)\sin\beta^* \cos\beta^* + 30\sin^2\beta^*\} \qquad [6.13]$$

The device could be used actively, with $\delta = \delta_s + i\delta_o \exp i(\omega_e t + \varepsilon)$, which adds an extra term to the damping derivative,

$$C_A = \{- 0.016\,\lambda\,(25 - \lambda)\,\delta_o \cos\beta^* \cos\varepsilon\} \,/\, q \qquad [6.14]$$

The variations of C_T, C_H, C_B and qC_A with wind heading are shown in Fig. 16 for several tip speed ratios at $\delta = 0$ and in Fig. 17 for several angles of incidence at $\lambda = 7$, a value which corresponds typically to the maximum power coefficient.

It can be seen from Fig. 17(a) that for this device, the resultant thrust (considering the wind turbine to be driving a propeller) is negative in head winds, as the result of a high drag coefficient. Alternatively, HAWT rotors may be optimised to give positive thrust in head winds, but this will give lower roll damping.

Figure 17(b) shows that C_H is large in beam winds, so the ship will roll about a small angle of heel (e.g. 2^o - 3^o). Also, a static angle of heel can only be produced to leeward. The damping coefficient is always positive, as may be seen in Fig. 17(c), and is highest in beam winds, where roll damping is usually most needed. This device can, therefore, be very beneficial as a roll stabiliser. As with wingsails, setting δ to give higher thrust will give lower damping for $\beta^* > 90^o$. To obtain a positive increment in qC_A, as indicated in Fig. 17(d), the phase must be controlled so that for $\beta^* < 90^o$, $\varepsilon = 180^o$ (in anti-phase) and for $\beta^* > 90^o$, $\varepsilon = 0$ (in phase).

6.3 Vertical axis wind turbines (VAWT)

The VAWT has lower transmission losses than the HAWT, especially if the wind turbine and the ship's propeller are on the same shaft.
A cross-wind ('lift') force can be produced by setting the blades at a pitch angle, ψ. Voith-Schneider and Kirsten-Boeing propellers consist of four or more blades projecting vertically from a horizontal disc, geared to the propeller drive shaft. Cam action keeps a positive blade angle when along the ship's axis and zero or 90^o when across the ship's axis. Varying the position of the cam can create reverse or side thrust, so the ship does not need a rudder. A wind turbine need not be limited by the elementary eccentric Voith-Schneider blade angle control.

The forces and velocities on a VAWT are shown in Fig. 18. The aerodynamic thrust, side force and power coefficients are shown in Fig. 19 with $\lambda = 3$, $\beta^* = 5^o$ and blade pitch angle $\psi = 0^o$. It can be seen that a two-bladed machine produces fluctuating thrust and side forces which are of little practical use for direct propulsion, but that three or more blades produce a steady force, the direction of which can be controlled by varying the pitch of the blades. The variation of the aerodynamic thrust and side force coefficients with wind heading for several pitch angles at a typical tip-speed ratio $\lambda = 7$ is shown in Fig. 20. It can be seen that wind headings of less than 90^o produce negative aerodynamic thrust. This device would probably be used to drive a propeller rather than using the aerodynamic force, but the stabilising forces will still operate. The direction of the resultant aerodynamic (autogyro) component of the thrust force can be controlled by using cyclic pitch variation, but this is unlikely to be worth the additional cost overall.

A representative machine having $N_B = 3$ straight blades of section NACA 0015; blade chord / radius = 0.1; blade span/diameter = 0.7, i.e. solidity, $\sigma = 0.14$; and lift curve slope $a = 5$, has been used for theoretical calculations.

From Fig. 18 it is seen by geometry that

$$V_E^2 = [\Omega R + V_A \cos(\theta - \beta^*)]^2 + V_A^2 \sin^2(\theta - \beta^*) = V_A^2\{\lambda^2 + 2\lambda \cos(\theta - \beta^*) + 1\} \quad [6.15]$$

therefore

$$V_E = V_A \sqrt{1 + 2\lambda \cos(\theta - \beta^*) + \lambda^2} \approx V_A[\lambda + \cos(\theta - \beta^*)]$$

and also

$$V_A = V_E [\lambda - \sin(\theta - \beta^*)] / \lambda^2$$

The linear roll velocity is given by

$$v = V_A u = h\phi'.$$

Also from Fig. 18 it is seen that

$$\begin{aligned} V_U^2 &= V_A^2 (\cos\beta^* + \lambda\cos\theta)^2 + \{V_A (\sin\beta^* + \lambda \sin\theta) + v\}^2 \\ &= V_A^2\{(\cos\beta^* + \lambda\cos\theta)^2 + \{\sin\beta^* + \lambda\sin\theta + u\}^2\} \\ &\approx V_A^2\lambda^2 \{1 + (2/\lambda)\cos(\beta^* - \theta) + 2(u/\lambda^2)\{\sin\beta^* + \lambda\sin\theta\}\} \\ V_U &\approx V_A\{\lambda + \cos(\theta - \beta^*) + (u/\lambda)\{\sin\beta^* + \lambda\sin\theta\}\} \end{aligned} \quad [6.16]$$

It can also be seen from Fig. 18 that the effective angle of incidence is

$$\alpha_e = \psi + \theta - d\alpha$$

where, by geometry,

$$V_U \sin d\alpha = V_A (\sin\beta^* + \lambda\sin\theta + u)$$

$$V_U \cos d\alpha = V_A (\cos\beta^* + \lambda\cos\theta)$$

therefore the effective angle of incidence is given by

$$\begin{aligned} \sin\alpha_e &\approx (V_A/V_U)\ (\sin(\psi + \theta)(\cos\beta^* + \lambda\cos\theta) - \cos(\psi + \theta)(\sin\beta^* + \lambda\sin\theta + u)) \\ &\approx (V_A/V_U)\ (\sin(\psi + \theta - \beta^*) + \lambda\sin\psi - u\cos(\psi + \theta)) \end{aligned} \quad [6.17]$$

where

$$(V_A/V_U) = [\lambda - \cos(\theta - \beta^*) - u\sin\theta] / \lambda^2$$

Therefore the component of the section lift force (measured perpendicular to the instantaneous apparent wind velocity vector V_U) is given by

$$\begin{aligned} dL(\eta) &= 0.5\rho V_U^2 ca \sin(\theta + \psi - d\alpha) \\ &= 0.5\rho V_A V_U ca \{\sin(\psi + \theta - \beta^*) + \lambda\sin\psi - u\cos(\psi + \theta)\} \end{aligned} \quad [6.18]$$

and the corresponding component of the section drag force is given by

$$\begin{aligned} dD(\eta) &= 0.5\rho V_U^2 c(C_{Do} + A\sin^2(\theta + \psi - d\alpha)) \\ &= 0.5\rho V_A^2 c(H^2 C_{Do} + A(\sin(\theta + \psi - \beta) + \lambda\sin\psi - u\cos(\theta + \psi))^2) \\ &= 0.5\rho V_A^2 cH(C_{Do}(\lambda + \cos(\theta - \beta^*) + u\sin\theta) + A[\lambda - \cos(\theta - \beta^*) - u\sin\theta](\sin^2(\theta + \psi - \beta) \\ &\quad + 2\sin(\theta + \psi - \beta)\lambda\sin\psi + \lambda^2\sin^2\psi - 2u\cos(\theta + \psi)\sin(\theta + \psi - \beta) \\ &\quad - 2u\cos(\theta + \psi)\lambda\sin\psi + u^2\cos^2(\theta + \psi))/\lambda^2) \end{aligned} \quad [6.19]$$

Linearising to first order in u and neglecting terms in $(1/\lambda^2)$ yields

$$= 0.5\rho V_A^2 cH\{C_{Do}(\lambda + \cos(\theta - \beta^*) + u \sin\theta) + A(\lambda \sin^2\psi + 2\sin(\theta + \psi - \beta^*)\sin\psi$$
$$- \cos(\theta - \beta^*)\sin^2\psi + (1/\lambda)\sin(\theta + \psi - \beta^*)[\sin(\theta + \psi - \beta^*) - 2\cos(\theta - \beta^*)\sin\psi]$$
$$- (1/\lambda^2)\sin^2(\theta + \psi - \beta^*)\cos(\theta - \beta^*) - u\sin\psi[2\cos(\theta + \psi) + \sin\theta\sin\psi]$$
$$- (2/\lambda)u[\cos(\theta + \psi)\sin(\theta + \psi - \beta^*) - \cos(\theta + \psi)\cos(\theta - \beta^*)\sin\psi$$
$$+ \sin\theta\sin(\theta + \psi - \beta^*)\sin\psi])\} \quad [6.20]$$

For high aspect ratio blades, C_D can be neglected in comparison with C_L for evaluating forces, but not for evaluating power.

The overall thrust force, side force, torque and power components are then given by

$dT(\eta) = -dL\sin d\alpha$

$dS(\eta) = -dL\cos d\alpha$

$dQ(\eta) = R[dL\sin(\theta - d\alpha) - dD\cos(\theta - d\alpha)]$

$P(\eta) = \Omega Q(\eta)$

Therefore

$$T(\eta) = -0.5\rho V_A^2 ca\{[\lambda\sin\psi + \sin(\theta - \beta^* + \psi)](\sin\beta^* + \lambda\sin\theta) - u[\sin(\psi + \theta)\cos\beta^*$$
$$- 2\cos(\psi + \theta)\sin\beta^* + \lambda(\sin\psi(1 + \sin^2\theta) - \cos\psi\cos\theta\sin\theta)]\}$$

$$S(\eta) = -0.5\rho V_A^2 ca\{[\lambda\sin\psi + \sin(\theta - \beta^* + \psi)](\cos\beta^* + \lambda\cos\theta) - u\cos(\theta + \psi)(\cos\beta^* + \lambda\cos\theta)\}$$

$$Q(\eta) = 0.5\rho V_A^2 cR(a\{\sin(\psi + \theta - \beta^*) + \lambda\sin\psi - u\cos(\psi + \theta)\}\{\sin(\theta - \beta^*) - u\cos\theta\}$$
$$- \{C_{Do}(\lambda + \cos(\theta - \beta^*) + u\sin\theta) + A(\lambda\sin^2\psi + 2\sin(\theta + \psi - \beta^*)\sin\psi$$
$$- \cos(\theta - \beta^*)\sin^2\psi + (1/\lambda)\sin(\theta + \psi - \beta^*)[\sin(\theta + \psi - \beta^*) - 2\cos(\theta - \beta^*)\sin\psi]$$
$$- (1/\lambda^2)\sin^2(\theta + \psi - \beta^*)\cos(\theta - \beta^*) - u\sin\psi[2\cos(\theta + \psi) + \sin\theta\sin\psi]$$
$$- (2/\lambda)u[\cos(\theta + \psi)\sin(\theta + \psi - \beta^*) - \cos(\theta + \psi)\cos(\theta - \beta^*)\sin\psi$$
$$+ \sin\theta\sin(\theta + \psi - \beta^*)\sin\psi])\}\{\cos(\theta - \beta^*) + \lambda + u\sin\theta\}$$

Linearising to first order in u and neglecting terms in $(1/\lambda)$ yields

$$Q(\eta) = 0.5\rho V_A^2 cR(a\{\sin(\psi + \theta - \beta^*)\sin(\theta - \beta^*) + \lambda\sin\psi\sin(\theta - \beta^*) - u[\cos(\psi + \theta)\sin(\theta - \beta^*)$$
$$+ \cos\theta\sin(\psi + \theta - \beta^*) + \lambda\cos\theta\sin\psi]\} - C_{Do}(\lambda^2 + 2\lambda\cos(\theta - \beta^*) + \cos^2(\theta - \beta^*)$$
$$+ 2u(\sin\theta\cos(\theta - \beta^*) + \lambda\sin\theta)) - A(\lambda^2\sin^2\psi + 2\lambda\sin(\theta + \psi - \beta^*)\sin\psi$$
$$- \cos^2(\theta - \beta^*)\sin^2\psi + \sin^2(\theta + \psi - \beta^*) - 2u[\lambda\sin\psi\cos(\theta + \psi)$$
$$+ \cos(\theta + \psi)\sin(\theta + \psi - \beta^*) + \cos(\theta - \beta^*)\sin^2\psi\sin\theta)\} \quad [6.21]$$

Summing over all the blades and assuming constant pitch and small ψ gives:

for 2 blades;

$$T(\eta) = -0.5\rho V_A^2 c\,2\lambda a\{(\psi(\sin\beta^* + \sin\theta\cos(\theta - \beta^*)) + \sin\theta\sin(\theta - \beta^*)) + u(\psi(1 + \sin^2\theta) - \sin\theta\cos\theta\}$$

$$S(\eta) = -0.5\rho V_A^2 c\,2\lambda a\{(\psi(\cos\beta^* + \cos\theta\cos(\theta - \beta^*)) + \cos\theta\sin(\theta - \beta^*)) - u\cos\theta(\cos\theta - \psi\sin\theta)\}$$

$$Q(\eta) = 0.5\rho V_A^2 cR^2(a\{\psi\sin(\theta - \beta^*)\cos(\theta - \beta^*) + \sin^2(\theta - \beta^*) - u[2\cos\theta\sin(\theta - \beta^*)$$
$$- \psi\cos(2\theta - \beta^*)]\} - C_{Do}[(\lambda^2 + \cos^2(\theta - \beta^*) + 2u\sin\theta\cos(\theta - \beta^*)]$$
$$- A(2\lambda^2\psi^2 + \sin^2(\theta - \beta^*) + \psi\sin 2(\theta - \beta^*) - 2u[\cos\theta\sin(\theta - \beta^*) + \psi\cos(2\theta - \beta^*)])\} \quad [6.22]$$

Time average:

$$Q(\eta) = 0.5\rho V_A^2 cR^2(a\{0.5 + u\sin\beta^*\} - C_{Do}(\lambda^2 + 0.5 + u\sin\beta^*) - A(\lambda^2\psi^2 + 0.5 + u\sin\beta)$$

and for N_B blades ($N_B > 2$);

$$T(\eta) = -0.5\rho V_A^2 c\, 0.5N_B\lambda\, a(\cos\beta^* + 3\psi\sin\beta^* + u\,3\psi)$$

$$S(\eta) = 0.5\rho V_A^2 c\, 0.5N_B\lambda\, a(\sin\beta^* - 3\psi\cos\beta^* + u)$$

$$Q(\eta) = 0.5\rho V_A^2 cR\,(N/2)\{a(1 + 2u\sin\beta^*) - C_{Do}(2\lambda^2 + 1 + 2u\sin\beta^*)$$
$$- A(2\lambda^2\psi^2 + 1 + 2u\sin\beta)\} \qquad [6.23]$$

All these quantities are independent of θ for more than two blades.

The steady component of the torque is given by

$$Q_S(\eta) = 0.5\rho V_A^2 cR\,(N/2)\{a - C_{Do}(2\lambda^2 + 1) - A(2\lambda^2\psi^2 + 1)\}. \qquad [6.24]$$

The power is given by

$$P = \Omega\, dQ = 0.5\rho V_A^2\, c\Omega R(N/2)\{a - C_{Do}(2\lambda^2 + 1) - A(2\lambda^2\psi^2 + 1)\}$$

which gives the power coefficient as

$$C_P = 0.5\,\sigma\lambda\,\{a - C_{Do} - A - 2\lambda^2(C_{Do} + A\psi^2)\}. \qquad [6.25]$$

This is maximum when $\lambda^2 = \dfrac{a - C_{Do} - A}{6(C_{Do} + A\psi^2)}$ at $\psi = 0$, where $\lambda_{opt} \approx 6.9$

The section roll moment may be written as

$$Q_\phi(\eta) = s\eta\, S(\eta)$$

and so the total roll moment component may be written in the form

$$Q_\phi = s^2\int_r^{r+1} \eta\, S(\eta)\, d\eta$$

i.e. for two blades,

$$Q_\phi = -0.5\rho V_A^2 c\, 2\lambda s^2\int_r^{r+1} \eta a\{(\psi(\cos\beta^* + \cos\theta\cos(\theta - \beta^*)) + \cos\theta\sin(\theta - \beta^*))$$
$$- (s\eta\phi'/V_A)\cos\theta(\cos\theta - \psi\sin\theta)\}\, d\eta$$

and for N_B blades,

$$Q_\phi = 0.5\rho V_A^2 c\, 0.5N_B\lambda s^2\int_r^{r+1} \eta\; a[\sin\beta^* - 3\psi\cos\beta^* + (s\eta\phi'/V_A)]\; d\eta$$

that is,

$$Q_\phi = Q_{\phi s} + Q_{\phi\phi}(\beta^*, \lambda, \theta)\,\phi'.$$

If active pitch control is used, with $\psi = \psi_s + \psi_o \exp i(\omega_e t + \varepsilon)$, then as before, the damping derivative, $B = \text{Real}(Q_{\phi\phi})$ where:

for 2 blades,

$$B = -0.5\rho V_A^2 c\, 2\lambda s^2\int_r^{r+1} \eta a\{((\psi_o/\omega\phi_o)\cos\varepsilon\,(\cos\beta^* + \cos\theta\cos(\theta - \beta^*))$$
$$+ \cos\theta\sin(\theta - \beta^*)) - (s\eta/V_A)\cos\theta(\cos\theta - \psi_s\sin\theta)\}\, d\eta$$

and for N_B blades,

$$B = 0.5\rho V_A^2 c\, 0.5N_B\lambda s^2\int_r^{r+1} \eta\; a[-3(\psi_o/\omega\phi_o)\cos\varepsilon\,\cos\beta^* + (s\eta/V_A)]\; d\eta$$

and using the load grading integrals

$$E = (s/h) \int_r^{r+1} a\eta \, d\eta \approx a$$

$$E' = (s/h)^2 \int_r^{r+1} a\eta^2 \, d\eta \approx a\,(r^2 + r + 0.333) / (r^2 + r + 0.25)$$

gives

for 2 blades,

$$B = -0.5\rho V_A^2 c\, 2\lambda sh\{((\psi_o/\omega\phi_o)\cos\varepsilon\,(\cos\beta^* + \cos\theta\cos(\theta - \beta^*)) + \cos\theta\sin(\theta-\beta^*))\}E - 0.5\rho V_A c\, 2\lambda sh^2\cos\theta(\cos\theta - \psi_s\sin\theta)E'$$

giving the passive damping coefficient

$$C_B = -(cs / \pi R^2)2\lambda\cos\theta(\cos\theta - \psi\sin\theta)\,E' \qquad [6.26a]$$

and the active damping coefficient

$$C_A = -(cs / \pi R^2)\,2\lambda\,\{(\psi_o\cos\varepsilon\,(\cos\beta^* + \cos\theta\cos(\theta - \beta^*)) + \cos\theta\sin(\theta-\beta^*))\}E\ /\ q \qquad [6.26b]$$

and for N_B blades,

$$B = -0.5\rho V_A^2 c\, 0.5N_B\lambda sh\ 3\,(\psi_o/\omega\phi_o)\ \cos\varepsilon\ \cos\beta^*\,E + 0.5\rho V_A^2 c\, 0.5N_B\lambda h^2(s/V_A)\,E'$$

giving the passive damping coefficient

$$C_B = (N_B cs / \pi R^2)\ 0.5\lambda\,E' \qquad [6.26c]$$

and the active damping coefficient

$$C_A = -(N_B cs / \pi R^2)\ 1.5\,\lambda\,\psi_o\ \cos\varepsilon\ \cos\beta^*\,E' / q \qquad [6.26d]$$

When driving a propeller, the effective thrust is

$$T(\eta) = 0.5\rho V_A^2 ch\,[(\Omega R/V_S)\,0.5\,N_B\,a - 0.5\,N_B\,\lambda\,a(\cos\beta^* + 3\psi\sin\beta^*)]$$

$$= 0.5\rho V_A^2\,A\,\sigma\,a\,\lambda\,[(V_A/V_S) - \cos\beta^* - 3\psi\sin\beta^*] \qquad [6.27]$$

Summing the blade element forces over all the blades gives

$$C_T = T / 0.5\rho V_A^2\pi R^2 \approx -0.25\,\sigma\,\lambda\,a\,(\cos\beta^* + 3\,\psi\sin\beta^*)$$

$$C_H = S\,h / 0.5\rho V_A^2\pi R^2 h \approx -0.25\,\sigma\,\lambda\,a\,(\sin\beta^* - 3\,\psi\cos\beta^* + h\phi' / V_A)$$

$$C_P \approx 0.25\,\sigma\,\lambda\,a$$

$$C_B(\lambda) = B / 0.5\rho V_A\pi R^2 h^2 \approx 0.25\,\sigma\,\lambda\,E$$

where, to allow for blade interference and tower shadow effects, only forces from the upwind blades have been included here. The resultant thrust coefficient, with the turbine driving a propeller, is given by

$$C_T \approx 0.25\,\sigma\,\lambda\,a\,((V_A / V_S) - \cos\beta^* - 3\,\psi\sin\beta^*)$$

and the static heel moment coefficient by

$$C_H \approx 0.25\,\sigma\,\lambda\,a(\sin\beta^* - 3\,\psi\cos\beta^*)$$

The coefficient C_H is large in a beam wind, so the ship will roll about a small angle of heel (e.g. 2^o - 3^o). As with a HAWT, a static angle of heel can only be produced to leeward. As for wingsails, higher heeling moments correspond to lower thrusts for $\beta^* > 90^o$. Figure 21(c) shows that C_B has the advantage of always being positive and does not vary with wind heading or

pitch angle. This makes the VAWT more effective as a stabiliser than wingsails or Flettner rotors, as damping is provided even in a beam wind. To obtain a positive increment in qC_A, as shown in Fig. 21(d), the same phase control as for HAWT must be used.

6.4 Flettner rotors

Flettner rotors (i.e. vertical cylinders that rotate about the generator axis) use the Magnus effect to develop large lift forces by preventing separation of the boundary layer, thus maintaining very low pressure on the lift side. End plates are needed to prevent air being drawn back into this region. The are generally of constant diameter, but could be made conical. If two or more rotors are used, the ship can be manoeuvred by rotating them in opposite directions or at different speeds. The principle is displayed in Fig. 23.
Fig. 24 shows some typical C_L and C_D curves, for infinite aspect ratio from Swanson (1961) and for AR = 10 from Clayton (1985), with end plates (top and bottom) of diameters 1.4 and 2 times the cylinder diameter. Behaviour for tip speed ratios greater than 4 is strongly dependent on Reynolds number and end plate diameter. A lift coefficient of 10 can be achieved for $\lambda > 10$. As there is no sharp trailing edge to fix a stagnation point on the cylinder, the response of the lift force to an apparent wind which fluctuates in both magnitude and direction is uncertain. It has been assumed here that the lift and drag forces follow the fluctuations, but in practice there would be a time lag, which should increase the damping forces and moments.

From the measurements given by Clayton(1985), for a rotor with aspect ratio = 10 and end disks of twice the rotor diameter, the C_L and C_D curves yield equations of the form:

$C_L = a_1 \lambda - a_2$

$C_D = A_1 \lambda - A_2$

where $\lambda = \Omega D / 2V_A$ and

$a_1 = 3.86$, $a_2 = 3.47$, $A_1 = 1.22$, $A_2 = 1.52$

The direction of the resultant aerodynamic force can be controlled by adjusting the rotational speed.

Following an analysis similar to that of wingsails in Chapter 5, using the notation $u = h\phi' / V_A$ and $\lambda = \Omega c / 2V_A$:
The roll induced component of the section lift force measured perpendicular to the instantaneous apparent wind velocity vector V_U is given by,

$L(\eta) = 0.5\rho V_U^2 c[a_1 \Omega c/2V_U - a_2)]$.

Linearising to first order in u yields

$L(\eta) = 0.5\rho V_U V_A c\,[a_1 |\lambda| - a_2(1 + u \sin\beta^*)]$. [6.28a]

The corresponding component of section drag force is

$D(\eta) = 0.5\rho V_U^2 c(A_1 \Omega c/2V_U - A_2)]$

and linearising to first order in u yields

$$D(\eta) = 0.5\rho V_U V_A c\,[A_1\,|\lambda| - A_2(1 + u\sin\beta^*)]. \qquad [6.28b]$$

The section thrust force component is given by

$L\sin(\beta^* + d\alpha) - D\cos(\beta^* + d\alpha)$

and so the total thrust force is given by

$$T = s\int_r^{r+1}(L\sin(\beta^* + d\alpha) - D\cos(\beta^* + d\alpha))\,d\eta$$

Linearising to first order in u yields

$$T = 0.5\rho V_A^2 cs\int_r^{r+1}\{(a_1\lambda \pm a_2)\sin\beta^* \pm (A_1\lambda \pm A_2)\cos\beta^* + [(a_1\lambda \pm a_2(1 + \sin^2\beta^*) + A_2\sin\beta^*\cos\beta^*]\}\,d\eta$$

and therefore

$$C_T = (3.86\,\lambda \pm 3.47)\sin\beta^* \pm (1.22\,\lambda \pm 1.52)\cos\beta^* \qquad [6.29]$$

where the plus sign refers to $\lambda < 0$ (i.e. anticlockwise in Fig. 23) and the minus sign to $\lambda > 0$ (clockwise).

The section side force component is given by

$L\cos(\beta^* + d\alpha) + D\sin(\beta^* + d\alpha)$

and so the total side force is given by

$$S = s\int_r^{r+1}(L\cos(\beta^* + d\alpha) + D\sin(\beta^* + d\alpha))\,d\eta.$$

Linearising to first order in u yields

$$S = 0.5\rho V_A^2 cs\int_r^{r+1}[(a_1 \pm a_2)\cos\beta^* - (\pm A_1\lambda + A_2)\sin\beta^* \pm u(a_2\sin\beta^*\cos\beta^* - A_1\lambda - (\pm A_2)(1 + \sin^2\beta^*))]\,d\eta \qquad [6.30]$$

with the plus and minus signs as above.

The static heel moment coefficient is given by

$$C_H = -(3.86\,\lambda \pm 3.47)\cos\beta^* \pm (1.22\,\lambda \pm 1.52)\sin\beta^*$$

whence, C_H is low in beam winds and so the ship rolls about a small angle of heel.

The section roll moment component about the Cy axis is given by

$s\eta\,S(\eta)$

and so the total roll moment component may be written in the form

$$Q_\phi = s^2\int_r^{r+1}\eta\,S(\eta)\,d\eta.$$

Linearising to first order in u yields

$$Q_\phi = 0.5\rho V_A^2 cs^2\int_r^{r+1}\eta\,\{(a_1\lambda - a_2)\cos\beta^* + (A_1\lambda - A_2)\sin\beta^* + u[-a_2\sin\beta^*\cos\beta^* + A_1\lambda - A_2(1 + \sin^2\beta^*)]\}\,d\eta \qquad [6.31]$$

that is,

$$Q_\phi = Q_{\phi s} + Q_{\phi\phi}(\lambda, \beta^*)\,\phi'.$$

The damping derivative is

$$B = Q_{\phi\phi}(\lambda, \beta^*) = 0.5\rho V_A\,cs^2h\int_r^{r+1}\eta^2\,[\pm(a_2\sin\beta^*\cos\beta^* - A_1\lambda) - A_2(1 + \sin^2\beta^*)]\,d\eta$$

Using load grading integrals (as defined in Appendix 2), the derivative for roll damping due to roll velocity may be represented by

$$C_B(\lambda, \beta^*) = \pm (E_1 \cos\beta^* \sin\beta^* - E_2 \lambda) - E_3(1 + \sin^2\beta^*)$$
$$= 0.5 \{\sqrt{E_1^2+E_3^2} \cos 2(\beta^* + \varepsilon) - 3E_3 - (\pm 2E_2\lambda)\} \quad [6.32]$$

where

$\tan(2\varepsilon) = - (\pm E_1) / E_3$.

It can be seen that C_B may become negative in the region near $\beta^* = \pi/2 - \varepsilon$ if

$\lambda < (3E_3 + \sqrt{E_1^2+E_3^2}\ )/2E_2$

The minimum value of C_B is

$C_{Bmin} = - 0.5(\sqrt{E_1^2+E_3^2} + 3 E_3 - 2 E_2\lambda)$.

The variations of the roll damping coefficient with wind heading for different tip-speed ratios and directions of rotation are shown in Fig. 25. Low rotational speeds may produce negative damping in bow winds, particularly in the range $40^o < \beta^* < 60^o$, which could cause problems if the cylinders are left in position and stationary when the ship is in harbour. It is here considered that no really feasible techniques could be adopted for the active control of large rotating cylinders, although one could conceive of speed or height changes, for small variable geometry devices, where response times might be acceptably fast. The thrust coefficients are high, especially at high rotational speeds in beam winds. Unlike the other devices, the conflict between thrust and damping occurs for $\beta^* < 90^o$ instead of $\beta^* > 90^o$.

6.5 Cousteau device ('Turbosail')

This WASP device is being developed by the Fondation Cousteau, as reported by Constans (1985). The Turbosail is shown schematically in Fig. 26, from Constans (1985), and consists of a thick, hollow, elliptical cylinder profile fixed to the ship but with a facility for incidence angle adjustment. Inside and near the top of the cylinder is a fan which draws air through perforated regions of the cylinder along its span, near the trailing edge and either side of the chord line. The slot on the upwind (lift) side is left open, that on the downwind side is closed with a moveable flap, to provide a sharp trailing edge. This reduction of the boundary layer thickness increases lift and decreases drag with the results shown in Fig. 27, from Malavard (1984), for different angles of inclination to the apparent wind.

From the data given by Malavard(1984), the lift and drag coefficients for the Turbosail are given by

$C_L = 1.6 + 50 C_q + 9.2 \alpha$

$C_D = 0.6 + 3 \alpha^2$

where C_q is the suction coefficient. The thrust and static heel moment coefficients are given by

$C_T = C_L \sin\beta^* - C_D \cos\beta^*$

$C_H \approx C_L \cos\beta^* + C_D \sin\beta^*$

The direction of the resultant aerodynamic force can be controlled by adjusting the incidence or the suction rate.

The analysis is exactly the same as for wingsails, but with $E_0 \neq 0$, as $C_{l0} \neq 0$. Therefore using load grading integrals and assuming small α, the derivative for roll damping due to roll velocity may be represented by

$$C_B(\alpha, \beta^*) = 0.5\{\sqrt{(A_1-A_3)^2 + A_2^2}\ \cos 2(\beta^*- \varepsilon) + A_1 + A_3\} \qquad [6.33]$$

where

$A_1 = E_1 + E_2 + E_3\alpha^2$, $A_2 = E_0 + (E_1 + 2E_3)\alpha$, $A_3 = 2(E_2 + E_3\alpha^2)$

and

$\tan(2\varepsilon) = A_2 / (A_1 - A_3)$.

For the Turbosail, E_2 can be neglected compared with E_0, E_1 and E_3 as the profile drag is low compared with the other terms.

The variations of C_T, C_H, C_B and qC_A with wind heading for several angles of inclination to the apparent wind are shown in Fig. 28. It can be seen that for $\beta^* > 90^o$, the setting of $\alpha = 20^o$ (which gives increased thrust) will give a lower damping coefficient than for a setting $\alpha = -20^o$ (which gives reduced thrust). A choice must therefore be made between maximising either thrust or damping coefficients, at the cost of the other.

From these data the first order passive roll damping derivative can be found as

$$C_B(\alpha, \beta^*) = 10\cos^2\beta^* + (1.8 + 15\,\alpha)\cos\beta^*\sin\beta^* + 1.8\sin^2\beta^* \qquad [6.34]$$

Active control could be used, using $\alpha = \alpha_s + i\alpha_o \exp i(\omega_e t + \varepsilon)$, with the result that

$$C_A = \alpha_o\,(9.2\cos\beta^* + 6\,\alpha_s \sin\beta^*)\cos\varepsilon / q \qquad [6.35]$$

Evidently, C_H is small and positive at $\beta^* = 90^o$, so the ship will roll about a small angle of heel (e.g. 1^o - 2^o). As with wingsails, setting α to give higher thrust provides reduced damping for $\beta^* > 90^o$. To obtain a positive increment in qC_A, as shown in Fig. 28, the phase must be controlled so that for $\beta^* < (\pi/2 + 0.65\,\alpha_s)$, $\varepsilon = 0$ (in phase) and for $\beta^* > (\pi/2 + 0.65\,\alpha_s)$, $\varepsilon = 180^o$ (in anti-phase), where α_s represents the mean angle of incidence.

6.6 Hydrodynamic stabilisers

Figure 29 shows the forces and velocities on fin and rudder stabilisers.
Both fin and rudder coefficients are defined with reference to the ship speed V_S. It can be seen in Figs. 30 and 31 that the dependence of the passive damping coefficient C_B on wave heading angle μ^*, is very slight, and is usually taken as zero in conventional theories.

6.6.1 Fin stabilisers

Fins must be symmetrical to give equal moments in both directions. High lift and low drag are required. They may be:
a) one high aspect ratio hydrofoil per side, retractable or folding, with a trailing edge flap and low deflection angle (as made by Sperry or Denny Brown), as used on fast passenger liners. These give a high lift force per unit area up to the stall angle, but are easily damaged.
b) several low aspect ratio hydrofoils per side, with a blunt trailing edge and a high deflection angle (as made by Vosper Thorneycroft) which may also have a flap. These have delayed stall, but higher drag also. The blunt trailing edge gives good results due to a transient lift effect.

The magnification factor is defined as
MF = (roll amplitude of ship with fins) / (roll amplitude of ship without fins).
Typically this may be between 4 and 7. With a typical static heel angle of 5^o, and a magnification factor of 6, a 30^o roll amplitude can be reduced to 5^o residual roll angle.

Following an analysis similar to that for wingsails in Chapter 5;
from Fig. 29, the linear roll velocity is given by
$V_S\, u = h\phi' = i\omega_e s\eta\, \phi_o\, \tau$

The wave orbital velocity is given by:
$\xi' = i\omega\xi_o \exp[ik(x \cos\mu \pm y \sin\mu) + i\omega t + kz]$
The centre of gravity of the ship moves in a vertical circular orbit with diameter equal to the wave height, so therefore the relative velocity between the fin and the water is given by
$\xi'_{rel} = i\omega\xi_o\, \tau\, \{\exp[ik(x \cos\mu \pm y \sin\mu) + kz] - 1\}$, [6.36]
where the plus sign refers to the starboard fin and the minus sign to the port fin.

The horizontal component of the relative velocity is given by
$\xi_H' = V_S\, v_\pm = i\omega\xi_o\, \tau\, \{\exp[ik(x \cos\mu \pm y \sin\mu)] \exp(kz) - 1\}$
and the vertical component by
$\xi_V' = V_S\, w_\pm = \omega\xi_o\, \tau \exp[ik(x \cos\mu \pm y \sin\mu)] \exp(kz)$

Referring to Fig. 29, with $y = s\eta \cos\gamma$, $z = s\eta \sin\gamma$, and

$\exp [ks\eta \sin\gamma] \approx 1 + ks\eta \sin\gamma$

$\exp [\pm iks\eta \cos\gamma \sin\mu] \approx 1 \pm iks\eta \cos\gamma \sin\mu$

therefore,

$V_S\, v_\pm = i\omega\xi_o\, \tau \{\exp i[k(x \cos\mu \pm y \sin\mu)] \exp(kz) - 1\}$

$= i\omega\xi_o\, \tau \{\exp (ikx \cos\mu) (1 \pm iks\eta \cos\gamma \sin\mu) (1 + ks\eta \sin\gamma) - 1\}$

To first order in $ks\eta$,

$= i\omega\xi_o\, \tau \{\exp (ikx \cos\mu) (1 \pm iks\eta \cos\gamma \sin\mu + ks\eta \sin\gamma) - 1\}$

and so

$V_S(v_+ + v_-) = 2i\omega\xi_o\, \tau \{\exp (ik\, x \cos\mu) (1 + ks\eta \sin\gamma) - 1\}$

$V_S(v_+ - v_-) = 2i\omega\xi_o\, \tau \exp (ik\, x \cos\mu)\ iks\eta \cos\gamma \sin\mu$

Similarly,

$V_S\, w_\pm = \omega\xi_o\, \tau \exp [ik(x \cos\mu \pm y \sin\mu)] \exp(kz)$

To first order in $ks\eta$,

$\approx \omega\xi_o\, \tau \exp [ikx \cos\mu] (1 \pm iks\eta \cos\gamma \sin\mu + ks\eta \sin\gamma)$

Therefore,

$V_S(w_+ + w_-) = 2\omega\xi_o\, \tau \exp (ikx \cos\mu) (1 + ks\eta \sin\gamma)$

$V_S(w_+ - w_-) = 2\omega\xi_o\, \tau \exp (ikx \cos\mu)\, iks\eta \cos\gamma \sin\mu$

Considering the incident velocity on the fin, and ignoring spanwise components,

horizontal component, $V_H = V_S + \xi_H' \cos\mu = V_S (1 + v_\pm \cos\mu)$ [6.37a]

vertical component, $V_V = h\phi' \pm (-\xi_V') \cos(\gamma \pm \phi) - \xi_H' \sin\mu \sin(\gamma \pm \phi)$

$= V_S(u \pm (-w_\pm) \cos(\gamma \pm \phi) - v_\pm \sin\mu \sin(\gamma \pm \phi))$ [6.37b]

whence

$V_U^2 = V_H^2 + V_V^2 \approx V_S^2(1 + 2\, v_\pm \cos\mu) = V_S^2\, H^2$,

so $H \approx 1$.

$\tan d\alpha = (u \pm (-w_\pm) \cos(\gamma \pm \phi) - v_\pm \sin\mu \sin(\gamma \pm \phi)) / (1 + v_\pm \cos\mu)$

$\sin(d\alpha) \approx (u \pm (-w_\pm) \cos(\gamma \pm \phi) - v_\pm \sin\mu \sin(\gamma \pm \phi))$

$\cos(d\alpha) \approx 1 + v_\pm \cos\mu$

The roll induced component of the section lift force measured perpendicular to the instantaneous apparent wind velocity vector V_U is given by,

$L(\eta) = 0.5\rho V_U^2 c\, a \sin(\delta + d\alpha)$.

$= 0.5\rho V_S^2\, c\, a [\sin\delta (1 + v_\pm \cos\mu) + \cos\delta (u \pm (-w_\pm) \cos(\gamma \pm \phi) - v_\pm \sin\mu \sin(\gamma \pm \phi))]$ [6.38]

The corresponding component of section drag force is

$D(\eta) = 0.5\rho V_U^2 c(C_{d0} + A \sin^2(\delta + d\alpha))$

$= 0.5\rho V_S^2 c\, (C_{d0} + A\, (\sin\delta (1 + v_\pm \cos\mu) + \cos\delta (u \pm (-w_\pm) \cos(\gamma \pm \phi)$

$- v_\pm \sin\mu \sin(\gamma \pm \phi)))^2]$

$$\approx 0.5\rho V_S^2 c\,[C_{d0} + A\,(\sin^2\delta + 2v_\pm \sin\delta\cos\mu + u^2\cos^2\delta)]$$

$$\approx 0.5\rho V_S^2 c[C_D + 2A\,v_\pm \sin\delta\cos\mu] \qquad [6.39]$$

The thrust force is given by

$$T = L\sin d\alpha - D\cos d\alpha$$

$$= 0.5\rho V_S^2 s \int_r^{r+1} c\{a\,(u \pm (-w_\pm)\cos(\gamma \pm \phi)$$

$$- v_\pm \sin\mu \sin(\gamma \pm \phi)) * [\sin\delta\,(1 + v_\pm\cos\mu) + \cos\delta\,(u \pm (-w_\pm)\cos(\gamma\pm\phi)$$

$$- v_\pm \sin\mu\sin(\gamma\pm\phi))] - [C_D + 2A\,v_\pm\sin\delta\cos\mu]\,(1 + v_\pm\cos\mu)\}\,d\eta$$

$$= 0.5\rho V_S^2 s \int_r^{r+1} c\{-C_D + u(a\sin\delta) - v_\pm\,(a\sin\mu\sin(\gamma\pm\phi)\sin\delta + C_D\cos\mu$$

$$+ 2A\sin\delta\cos\mu) \pm (-w_\pm)\,(a\cos(\gamma\pm\phi)\sin\delta)\}\,d\eta.$$

The total thrust is given by

$$T = 0.5\rho V_S^2 s \int_r^{r+1} c\{-2C_D + 2u(a\sin\delta) - a\sin\mu\sin\delta\,(v_+\sin(\gamma+\phi) + v_-\sin(\gamma-\phi))$$

$$- (v_+ + v_-)\,(C_D\cos\mu + 2A\sin\delta\cos\mu) - a\sin\delta\,(w_+\cos(\gamma+\phi) - w_-\cos(\gamma-\phi))\}\,d\eta.$$

and the steady component by

$$T = -0.5\rho V_S^2 cs\,2C_D$$

so the thrust coefficient is therefore

$$C_T = -2\,C_D. \qquad [6.40]$$

The section roll moment component about the Cy axis is given by

$$s\eta\,(L\cos d\alpha + D\sin d\alpha)$$

and so the total roll moment component may be written in the form

$$Q = s^2 \int_r^{r+1} \eta\,(L\cos d\alpha + D\sin d\alpha)\,d\eta.$$

Using $\delta = \delta_s + i\,\delta_0 \exp i(\omega t + \varepsilon)$, the damping component will be given by the component in-phase with the roll velocity.

The roll moment is given by

$$Q = 0.5\rho V_S^2 s^2 \int_r^{r+1} c\eta\{a\,(1 + v_\pm\cos\mu)\,[\sin\delta\,(1 + v_\pm\cos\mu) + \cos\delta\,(u \pm (-w_\pm)\cos(\gamma\pm\phi)$$

$$- v_\pm\sin\mu\sin(\gamma\pm\phi))] + (u \pm (-w_\pm)\cos(\gamma\pm\phi)$$

$$- v_\pm\sin\mu\sin(\gamma\pm\phi))\,(C_D + 2A\,v_\pm\sin\delta\cos\mu)\}\,d\eta$$

$$= 0.5\rho V_S^2 s^2 \int_r^{r+1} c\eta\{a\sin\delta + u(a\cos\delta + C_D) + v_\pm\,[2a\sin\delta\cos\mu - a\cos\delta\sin\mu\sin(\gamma\pm\phi)$$

$$- C_D\sin\mu\sin(\gamma\pm\phi)] \pm (-w_\pm)\,(a\cos\delta + C_D)\cos(\gamma\pm\phi)\}\,d\eta. \qquad [6.41]$$

The total roll moment,

$$Q = 0.5\rho V_S^2 s^2 \int_r^{r+1} c\eta\{2a\sin\delta + 2u(a\cos\delta + C_D) + 2a\sin\delta\cos\mu\,(v_+ + v_-)$$

$$- (a\cos\delta + C_D)\,\{\sin\mu\,[v_+\sin(\gamma+\phi) + v_-\sin(\gamma-\phi)] - [w_+\cos(\gamma+\phi) - w_-\cos(\gamma-\phi)]\}\}\,d\eta.$$

Considering only lift components and linearising for small δ and ϕ,

$$Q \approx 0.5\rho V_S^2 s^2 \int_r^{r+1} ca\eta \{2\,(\delta_s + i\,\delta_o\, e^{i\varepsilon\tau}) + 2\,u + 2\,(\delta_s + i\,\delta_o\, e^{i\varepsilon\tau})\,\cos\mu\,(v_+ + v_-)$$
$$- \sin\mu\,[(v_+ + v_-)\sin\gamma + \phi_o\,\tau\,(v_+ - v_-)\cos\gamma] + [\phi_o\,\tau\,(w_+ + w_-)\sin\gamma - (w_+ - w_-)\cos\gamma]\}\,d\eta.$$
$$\approx 0.5\rho V_S s^2 \int_r^{r+1} ca\eta \{2\,V_S(\delta_s + i\,\delta_o\, e^{i\varepsilon\tau}) + 2i\omega_e s\eta\phi_o\,\tau$$
$$+ 4i\omega\xi_o\,\tau\,(\delta_s + i\,\delta_o\, e^{i\varepsilon\tau})\,\cos\mu\,\{\exp(ik\,x\cos\mu)\,(1 + ks\eta\sin\gamma) - 1\}$$
$$- 2i\omega\xi_o\,\tau\sin\mu\,[\exp(ik\,x\cos\mu)\,\{(1 + ks\eta\sin\gamma)\sin\gamma + iks\eta\,\phi_o\,\tau\cos^2\gamma\sin\mu\}\} - \sin\gamma]$$
$$+ 2\omega\xi_o\,\tau\exp(ikx\cos\mu)\,[(1 + ks\eta\sin\gamma)\sin\gamma\,\phi_o\,\tau - iks\eta\cos^2\gamma\sin\mu]\}\,d\eta. \qquad [6.42]$$

Ignoring terms in τ^2 and above gives the first order expression:

$$Q \approx 0.5\rho V_S s^2 \int_r^{r+1} ca\eta\,(2\,V_S\delta_s)\,d\eta$$
$$+ 0.5\rho V_S s^2\,\tau \int_r^{r+1} ca\eta\{-2\,V_S\,\delta_o\sin\varepsilon - 4\omega\xi_o\,\delta_s\,\cos\mu\sin(kx\cos\mu)\,(1 + ks\eta\sin\gamma)$$
$$+ 2\omega\xi_o\sin\mu\sin(kx\cos\mu)\,(1 + ks\eta\sin\gamma)\sin\gamma\}\,d\eta$$
$$+ 0.5\rho V_S s^2\,i\tau \int_r^{r+1} ca\eta\{2\,V_S\,\delta_o\cos\varepsilon + 2\,\omega_e s\eta\phi_o$$
$$+ 4\omega\xi_o\,\delta_s\cos\mu\,\{\cos(kx\cos\mu)\,(1 + ks\eta\sin\gamma) - 1\}$$
$$- 2\omega\xi_o\sin\mu\,[\cos(kx\cos\mu)\,(\sin\gamma + ks\eta) - \sin\gamma]\,d\eta. \qquad [6.43]$$

that is,

$$Q = Q_S + Q_{\phi\phi}(\delta, \mu)\,\omega_e\phi_o\tau$$

Therefore the damping derivative is

$$B_{\phi\phi} \approx 0.5\rho V_S s^2 \int_r^{r+1} ca\eta\{2\,V_S\,\delta_o\cos\varepsilon\,/(\omega_e\phi_o) + 2\,s\eta$$
$$+ 4(\omega\xi_o\,\delta_s\,/\phi_o)\,\cos\mu\,\{\cos(kx\cos\mu)\,(1 + ks\eta\sin\gamma) - 1\}$$
$$- 2(\xi_o\,/\phi_o)\sin\mu\,[\cos(kx\cos\mu)\,(\sin\gamma + ks\eta) - \sin\gamma]\}\,d\eta. \qquad [6.44]$$

and the inertia derivative is given by

$$\omega A_{\phi\phi} = 0.5\rho V_S\,s^2 \int_r^{r+1} ca\eta\{-2V_s\,\delta_o\sin\varepsilon - 4(\xi_o\,\delta_s\,/\phi_o)\,\cos\mu\,[\sin(kx\cos\mu)\,(1$$
$$+ ks\eta\sin\gamma) + 2(\xi_o\,/\phi_o)\sin\mu\sin(kx\cos\mu)\,(1 + ks\eta\sin\gamma)\sin\gamma\}\,d\eta. \qquad [6.45]$$

Using the load grading integrals,

$$E = (s/\hat{c}h) \int_r^{r+1} ca\eta\,d\eta \approx a$$

$$E' = (1/\hat{c})\,(s/h)^2 \int_r^{r+1} ca\eta^2\,d\eta \approx a(r^2 + r + .333)\,/\,(r^2 + r + .25) \approx a$$

The static heel moment coefficient is then

$$C_H = 2E\sin\delta$$

The first order damping derivative is

$$B_{\phi\phi} = \text{Real}(Q_{\phi\phi}(\delta, \mu))$$
$$\approx 0.5\rho V_S\,\hat{c}sh^2\,\{2\,E\,V_S\,\delta_o\cos\varepsilon\,/(h\omega_e\phi_o) + 2\,E'$$
$$+ 4(\omega\xi_o\,\delta_s\,/\phi_o)\,\cos\mu\,\{\cos(kx\cos\mu)\,(E/h + k\,E'\sin\gamma) - E/h\}$$

$- 2(\xi_o / \phi_o) \sin \mu [\cos(kx \cos \mu) (E \sin \gamma / h + kE') - E \sin \gamma / h]\}$.

and so the roll damping coefficient is

$C_B = 2E\{V_S \delta_o \cos \varepsilon / (h \omega_e \phi_o)$

$+ 2(\omega \xi_o \delta_s / h\phi_o) \cos \mu \{\cos (kx \cos \mu) - 1\} - 2(\xi_o / h\phi_o) \sin \mu [\cos(kx \cos \mu) - 1] \sin \gamma\}$

$+ 2E' \{1 + 2(\omega \xi_o \delta_s / \phi_o) \cos \mu \cos (kx \cos \mu) \; k \sin \gamma - (k\xi_o / \phi_o) \sin \mu \cos (kx \cos \mu)\}$. [6.46]

In beam winds, this becomes

$C_B = 2EV_S \delta_o \cos \varepsilon / (h\omega_e \phi_o) + 2E' \{1 - k\xi_o / \phi_o\}$.

The first order passive roll damping component is

$C_B = 2E'[1 - k\xi_o / \phi_o]$

and active oscillation gives

$C_B = 2E\, V_S \delta_o \cos \varepsilon / (h\omega_e \phi_o) = 2E \delta_o \cos \varepsilon / q$.

The fins are taken to extend at an angle γ (assumed 45°) from the horizontal. An aspect ratio of 2 has been used which, on the basis of thin aerofoil theory with empirical boundary layer corrections, gives the slope of the lift curve as a = 2.6 per radian. Typical values of roll period = 9 s (i.e. ω = 0.7 rad/s), wavelength = 180 m (i.e. k = 0.035), wave amplitude ξ_o = 3 m, ship speed V_S = 6 m/s, roll amplitude ϕ_o = 25° and fin deflection angle δ_o = 15° were used. Also ship beam = 11 m and fin length = 0.5 m, which gives s = 0.5, r = 11. Results are shown in Fig. 30.

6.6.2 Rudders

A rudder can be used to stabilise roll in the same manner as an active fin because the centre of pressure of the rudder is below the roll axis. The rudder has a very small lever arm, and therefore develops small roll moments as indicated by the results shown in Fig. 31. It is seen that as with fin stabilisers, setting $\varepsilon = 0$ gives a positive value for qC_A at all wave angles.

The linear roll velocity is given by

$V_S u = i\omega_e s\eta \phi_o \tau$

and the wave orbital velocity is given by

$\xi' = i\omega\xi_o \exp[ikx_R \cos \mu + i\omega t + kz]$

The centre of gravity of the ship moves in a vertical circular orbit with diameter equal to the wave height, so therefore, ignoring terms of order k^2,

the relative velocity between the rudder and the water is given by

$\xi'_{rel} = i\omega\xi_o \tau \{\exp[ikx_R \cos \mu + kz] - 1\}$

The horizontal component of the relative velocity is given by

$\xi_{H'} = V_S v = i\omega\xi_o \tau \{\exp [ikx_R \cos \mu] \exp(kz) - 1\}$

and the vertical component is

$\xi_V' = V_S\, w = \omega \xi_o \tau \exp[ikx_R \cos\mu] \exp(kz)$

Ignoring spanwise components,

component in direction of flow $= V_S + \xi_H' \cos\mu = V_S (1 + v \cos\mu)$ [6.47a]

component across flow $= -h\phi' + \xi_H' \sin\mu \cos\phi - \xi_V' \sin\phi = V_S(-u + v \sin\mu - w \sin\phi)$ [6.47b]

whence

$V_U^2 = V_S^2(1 + 2v \cos\mu + v^2 - 2uv \sin\mu + u^2) = V_S^2 H^2$

$\tan d\alpha = (-h\phi' + \xi_H' \sin\mu - \xi_V' \sin\phi) / (V_S + \xi_H' \cos\mu)$

$= (-u + v \sin\mu - w \sin\phi) / (1 + v \cos\mu)$

$H \sin(d\alpha) = -u + v \sin\mu - w \sin\phi$

$H \cos(d\alpha) = 1 + v \cos\mu$

where

$H = \sqrt{1 + 2v \cos\mu + v^2 - 2\, uv \sin\mu + u^2} \approx 1.$

The roll induced component of the section lift force measured perpendicular to the instantaneous apparent wind velocity vector V_U is given by,

$L(\eta) = 0.5\rho V_U^2 c\, a \sin(\delta - d\alpha).$

$= 0.5\rho V_S^2 c\, a[\sin\delta (1 + v \cos\mu) - \cos\delta (-u + v \sin\mu - w \sin\phi)]$

$= 0.5\rho V_S^2 c\, a[\sin\delta + v(\sin\delta \cos\mu - \cos\delta \sin\mu) + u \cos\delta + w \cos\delta \sin\phi]$ [6.48]

The corresponding component of section drag force is

$D(\eta) = 0.5\rho V_U^2 c(C_{d0} + A \sin^2(\delta - d\alpha))$

$= 0.5\rho V_S^2 c[C_{d0} + A(\sin\delta + v(\sin\delta \cos\mu - \cos\delta \sin\mu) + u \cos\delta + w \cos\delta \sin\phi)^2]$

$\approx 0.5\rho V_S^2 c[C_{d0} + A \sin\delta (\sin\delta + 2v (\sin\delta \cos\mu - \cos\delta \sin\mu) + 2u \cos\delta + 2w \cos\delta \sin\phi)]$

$\approx 0.5\rho V_S^2 c\{C_{d0} + A \sin^2\delta + 2A\, v \sin\delta (\sin\delta \cos\mu - \cos\delta \sin\mu) + 2Au \sin\delta \cos\delta$

$+ 2Aw \sin\delta \cos\delta \sin\phi\}$ [6.49]

The thrust force is given by

$T = -L \sin d\alpha - D \cos d\alpha$

$= -0.5\rho V_S^2\, s \int_r^{r+1} ca\ (-u + v \sin\mu - w \sin\phi) * [\sin\delta + v(\sin\delta \cos\mu$

$- \cos\delta \sin\mu) + u \cos\delta + w \cos\delta \sin\phi] + (1 + v \cos\mu) [C_{d0} + A \sin^2\delta$

$+ 2A\, v \sin\delta (\sin\delta \cos\mu - \cos\delta \sin\mu) + 2Au \sin\delta \cos\delta + 2Aw \sin\delta \cos\delta \sin\phi]\, d\eta$

$= -0.5\rho V_S^2 s \int_r^{r+1} c\ \{C_D - u(a + 2A \cos\delta) \sin\delta + v(a \sin\mu \sin\delta$

$+ C_{d0} \cos\mu + 2A \sin\delta (\sin\delta \cos\mu - \cos\delta \sin\mu)) - w(a + 2A \cos\delta) \sin\delta \sin\phi\}\, d\eta.$

The steady component is then given by

$T = -0.5\rho V_S^2 s C_D \int_r^{r+1} c\, d\eta$

$\approx -0.5\rho V_S^2 s\, \hat{c} C_D$ [6.50]

and so the thrust coefficient is given by

$C_T = -C_D.$

Roll moment component

The section roll moment component about the Cy axis is given by

$s\eta(L \cos d\alpha - D \sin d\alpha)$

and so the total roll moment component may be written in the form

$$Q = s^2 \int_r^{r+1} \eta(L \cos d\alpha - D \sin d\alpha)\ d\eta.$$

$$= 0.5\rho V_S^2 s^2 \int_r^{r+1} c\eta \{a(1 + v \cos \mu)[\sin \delta + v(\sin \delta \cos \mu - \cos \delta \sin \mu) + u \cos \delta + w \cos \delta \sin \phi] - (-u + v \sin \mu - w \sin \phi)[C_D + 2A v \sin \delta (\sin \delta \cos \mu - \cos \delta \sin \mu) + 2Au \sin \delta \cos \delta + 2Aw \sin \delta \cos \delta \sin \phi]\} d\eta.$$

$$= 0.5\rho V_S^2 s^2 \int_r^{r+1} c\eta \{a \sin \delta + v(a(2 \sin \delta \cos \mu - \cos \delta \sin \mu) - C_D \sin \mu) + u(a \cos \delta + C_D) + w(a \cos \delta + C_D) \sin \phi\} d\eta.$$

$$= 0.5\rho V_S^2 s^2 \int_r^{r+1} ca\eta \{\delta_s + i\delta_o e^{i\varepsilon\tau} + v(2(\delta_s + i\delta_o e^{i\varepsilon\tau}) \cos \mu - \sin \mu) + u + w \phi_o \tau\} d\eta.$$

$$= 0.5\rho V_S s^2 \int_r^{r+1} ca\eta \{V_S(\delta_s + i\delta_o e^{i\varepsilon\tau}) + V_S v(2(\delta_s + i\delta_o e^{i\varepsilon\tau}) \cos \mu - \sin \mu) + V_S u + V_S w \phi_o \tau\} d\eta.$$

$$= 0.5\rho V_S s^2 \int_r^{r+1} ca\eta \{V_S(\delta_s + i\delta_o e^{i\varepsilon\tau}) + i\omega\xi_o \tau \{\exp[ikx_R \cos \mu] \exp(kz) - 1\}(2(\delta_s + i\delta_o e^{i\varepsilon\tau}) \cos \mu - \sin \mu) + i\omega_e s\eta\phi_o\tau + \omega\xi_o \tau \exp[ikx_R \cos \mu] \exp(kz)\ \phi_o\tau\} d\eta.$$

To first order in τ,

$$= 0.5\rho V_S s^2 \int_r^{r+1} ca\eta\ V_S \delta_s\, d\eta$$

$$+ 0.5\rho V_S s^2 i\tau \int_r^{r+1} ca\eta \{V_S \delta_o \cos \varepsilon + \omega\xi_o \{\cos[kx_R \cos \mu] \exp(kz) - 1\}(2\delta_s \cos \mu - \sin \mu) + \omega_e s\eta\phi_o + \omega\xi_o\ i \sin[kx_R \cos \mu] \exp(kz)(2\delta_s \cos \mu - \sin \mu)\} d\eta. \qquad [6.51]$$

that is,

$$Q = Q_s + Q_{\phi\phi}(\delta, \mu)\, i\omega_e\phi_o\, \tau$$

The damping derivative is

$$B_{\phi\phi} = \text{Real}(Q_{\phi\phi}(\delta, \mu))$$

$$= 0.5\rho V_S s^2 \int_r^{r+1} ca\eta \{V_S\delta_o \cos \varepsilon / (\omega_e\phi_o) + (\xi_o/\phi_o) \{\cos[kx_R \cos \mu] \exp(kz) - 1\}(2\delta_s \cos \mu - \sin \mu) + s\eta\} d\eta.$$

and as $\exp ks\eta = 1 + ks\eta$,

$$= 0.5\rho V_S s^2 \int_r^{r+1} ca\eta \{V_S\delta_o \cos \varepsilon / (\omega_e\phi_o) + (\xi_o/\phi_o) \{(1 + ks\eta) \cos[kx_R \cos \mu] - 1\}(2\delta_s \cos \mu - \sin \mu) + s\eta\} d\eta. \qquad [6.52]$$

Putting $E = (s/\hat{c}h) \int_r^{r+1} c\eta a\, d\eta \approx a$

$$E' = (1/\hat{c})(s/h)^2 \int_r^{r+1} c\eta^2 a\, d\eta \approx a(r^2 + r + 0.33) / (r^2 + r + 0.25)$$

For values of r near to $r = -1$, $E' \approx (3 + 1.63\, r)\, a$

Therefore the first order damping derivative is given by

$$B = 0.5\rho V_S c s h^2\{EV_S\delta_o \cos\varepsilon /(h\omega_e\phi_o) + (\xi_o/\phi_o)\{(E/h + kE')\cos[kx_R\cos\mu] - E/h\}(2\delta_s\cos\mu - \sin\mu) + E'\}$$

$$C_B = EV_S\delta_o \cos\varepsilon /(h\omega_e\phi_o) + (\xi_o/\phi_o)\{(E/h + kE')\cos[kx_R\cos\mu] - E/h\}(2\delta_s\cos\mu - \sin\mu) + E' \quad [6.53]$$

In a beam wind,

$$C_B = EV_S\delta_o \cos\varepsilon /(h\omega_e\phi_o) - E'\{k\xi_o/\phi_o - 1\}$$

The first order passive roll damping derivative,

$$C_B(\delta, \mu^*) = E'(k\xi_o/\phi_o)(2\delta_s\cos\mu - \sin\mu) + E'$$

$$= 1.5a\{(k\xi_o/\phi_o)(2\delta_s\cos\mu - \sin\mu) + 1\} \quad [6.54]$$

and active oscillation yields

$$C_A = EV_S\delta_o \cos\varepsilon /(h\omega_e\phi_o) = \delta_o\, a\cos\varepsilon / q$$

An aspect ratio of 2 has been used which, on the basis of thin aerofoil theory with empirical boundary layer corrections, gives the slope of the lift curve as a = 2.6 per radian.
Typical values of roll period = 9 s (i.e. ω = 0.7 rad/s), wavelength = 180 m (i.e. k = 0.035), wave amplitude ξ_o = 3 m, ship speed V_S = 6 m/s, roll amplitude $\phi_o = 25^o$ and rudder deflection angle $\delta_o = 5^o$ were used. Also x_R = 40 m, rudder span = 4.2 m, and vertical position of centre of gravity is 0.2 m below top of rudder, which gives s = 4.2, r = - 0.95. Results are shown in Fig. 31.

7. OFFSHORE WIND TURBINES.

7.1 Structural considerations

Most wind engineering research has concentrated on the design of the rotor, with arbitrary choice of tower structure. The market for wind turbines grew rapidly from 1981 to 1985, mostly in California, although the tendency was for mass production of similar machines rather than for innovative development. The market halved in 1986, when the end of U.S. Energy Tax Credits coincided with the fall in the oil price resulting from the Middle East war, and there has been little further development since then, due to lack of financial investment. There is very little data available relating to masts and towers, as the existing databases (e.g. EUROWIN) concentrate entirely on windspeeds and performance characteristics.

The type of structure depends on environmental conditions, the seabed state dictating the foundations or moorings. Ideally, the structure should have the least possible resistance to wave loads near the water surface, with underwater members slender to minimise diffraction and the waterplane area as low as possible to reduce wave slamming effects. These requirements are difficult to achieve as the water level varies with the tide, and support has to be provided somewhere. Three legs may be good enough for stability on land or in the deep sea, but damage stability considerations in shallow water show a need for duplication. The soil in the Wash is fine clay with 10 - 15 m sedimentary deposit on the surface, so a piled structure would be required. Other sites, such as Morecambe Bay and Carmarthen Bay have firmer soil conditions, and gravity structures would be possible.

There are now over 250 offshore oil or gas platforms in European waters, 95% of which are fixed steel jackets. The concrete industry has recently been making developments in shallow water fields, e.g. the main platform of the recent 30 m depth North Ravenspurn field in the southern North Sea, mainly owing to unfavorable estimates of the cost of fabricated steel jackets. Steel has been used extensively in the earlier phases of wind turbine development, both for the rotating components and the support structures. A few large prototype installations have been built with concrete towers. In the following calculations, a concrete structure has been included for comparison.

Stiff towers are becoming obsolete for economic reasons. Rigid lattice towers are being replaced by flexible cylinder towers. Some towers cater for blade deflection by tapering the tower, others by offsetting the rotor, although this gives eccentric forces on the tower.

Possible options are

a) piled tubular steel jacket (space frame) or tripod in steel

This has less wave loading than a gravity structure, owing to the smaller diameters of the members. However, it is much more expensive, and may be less economic to manufacture and install. The piles need to be deeply driven, particularly if there is a deep layer of sand on the sea bed.
b) Concrete gravity structure with a concrete or steel pillar, which may be straight or tapered, with a polygonal or circular section. The weight of the heavy base gives stability against the overturning moment due to waves and aerodynamic loading, but it will be more affected by wave scour than (a). Concrete is more durable than steel in the offshore environment.
c) Articulated column or guyed tower.

Compliant structures withstand environmental loads by deflecting from their equilibrium position, and are reasonably cost effective to build, whereas rigid structures of high stiffness are expensive.

Many manufacturers (e.g. the Wind Energy Group) do not design or manufacture their own structures, but provide the separate manufacturers of each part with 'expected' loads. This has the result that all components are designed separately to different standards in isolation and their interractions are largely ignored in the design process.
Other manufacturers (e.g. James Howden Wind Turbines) use an integrated process to design the whole structure fully, and then manufacture all parts together to the same standards, although this did not apply to the underwater support of their proposed offshore wind turbine.

Certification, when performed for wind turbines at all, is usually for the requirements of a subsidy and not for the requirements of any of the classification societies.

7.2 Forces on the structure

Forces in the horizontal plane are:
a) Wave and current forces on the tower,
b) Wave forces on foundations,
c) Wind force on the tower, and
d) Resultant lift and drag forces from the turbine blades and nacelle.
As most of these forces are time-dependent, the equations of motion will contain both structural, and fluid dynamic damping factors.

Environmental forces are relatively more important in the design of offshore structures than with any other type of structure. A fundamental prerequisite to the design of an offshore installation is an accurate assessment of the wind and wave environment. The loads likely to be imposed by wind, waves, currents and tides must be calculated from these, and then the

behaviour of the structure under extreme loading conditions and prolonged exposure can be predicted.

The data which need to be considered before the structure can be designed are:
a) wind speeds and directions, averaged over various different time periods (i.e. with influence extending over various areas), as functions of height above L.A.T. (lowest astronomical tide);
b) probability spectra for wave heights and periods, as modified by seabed topography and current;
c) variations in water depth due to tides; and
d) thickness of marine growth.

These quantities are randomly varying, and expected extreme values are chosen statistically. The '50 year return' value is commonly used for offshore structures - i.e. an average of 50 years occurs between exceedances of this value.

7.2.1 Wave forces

The majority of British studies have been concentrated in the area of the Wash, around Burnham Flats. Others have been mainly in Swedish inland waters where ice formation can present additional hazards. Off the north-east coast of Norfolk, the prevailing winds come from the land, so wind-driven waves should be fairly small, although severe East or South East gales over the North Sea are not unusual. The tidal range in the Wash is higher than for open sea locations, at about ± 6 m. The 50-year storm surge is also high, at about 2.5 m. This gives a much greater diurnal variation of depth than on a deep-sea installation.
The most extreme loading is given by the design wave, i.e. the highest wave expected to occur in 50 years, which is calculated by extrapolating from measurements taken over a shorter time period.

The U.K. Department of Energy (1990) gives guidance notes on the design, construction and certification of offshore structures. The design wave used should have an amplitude equal to the 50-year amplitude and a range of wave periods. For the Wash, the recommended value for the 50-year significant wave height is 9 m, and the mean period about 9.6 secs. This wave will break in depths less than 11.5 m, and the 100-year breaking wave height is 18 m. Wave propagation in shallow waters is modified by shoaling (refraction) due to the topography of the sea bed.

For the area classified as A6 - 03 (near Burnham Flats), Burton and Roberts (1985) give the lowest astronomical tide as 10 m - 20 m and the 50-year design storm waveheight as 11 m - 13.5m. Considering the centre of this area, taking minimum depth = 15 m, i.e. high tide still water level, d = 27 m, and maximum wave amplitude, ξ = 6 m, with a design wave period of

10 s, we have frequency, $\omega = 0.628$ rad/s; wave number, $k = 0.047\ m^{-1}$; wavelength = 133 m. The storm waves will not be scattered, and diffraction can be neglected, as $D/\lambda < 0.2$. Shorter waves, corresponding to lower waveheights and higher frequencies, will be scattered, but the forces from these will be comparatively small and so may be ignored.

For storm waves at high tide, Morison's equation will be valid for calculating the loads. If the forces from shorter waves in shallower water are required, diffraction theories would need to be used, particularly if forces on a large-diameter gravity base are required. Non-linear wave theories, such as Dean's 5th order stream function, can model a near-breaking shallow water wave in isolation, but do not account for diffraction.

For all but storm waves, the orbital diameter of fluid particle motion does not remain in a given direction long enough for the flow to separate or shed vortices before it changes direction again, so the drag forces are fairly small, and inertia forces dominate, and therefore potential flow theories can be used with a linearised equivalent viscous drag factor. The linearised Morison's equation can be used for inertia-dominated members in long waves, which predominate, and so diffraction and radiation effects can be neglected. However, this does not apply for a large-diameter gravity base, where drag will predominate. For storm waves, nonlinear effects and flow separation must be considered. Vortices will be shed, and the forces will be in the transitional range where drag and inertia effects are both important.

For sites close to land, the JONSWAP fetch-limited wave spectrum given by Hasselman et al (1973) should be used. This is sharply peaked about the modal frequency, so only a small range of wavelengths and periods need to be considered. Wave size depends on wind speed, fetch, and duration and also on the state of the tide, water depth, topography of the sea bed, etc. For the area mentioned above, the dominant periods will be about 5 s, with wave periods 1 s - 14 s. The sea states are usually low, as the wind blows mainly from the land over a small fetch. The dominant wave period will be about 5 s, which at mean sea level gives $\omega = 1.25$ rad/s; $k = 0.16\ m^{-1}$, wavelength = 40 m, with the maximum wave orbital velocity = 3.77 m/s.

If drag is significant, Morison's equation gives the tower loads more accurately than diffraction formulae.

Morison's equation for wave load:

Assuming a uniform unsteady flowfield, normal force per unit length in wave direction (due to the ambient pressure gradient) on a thin cylinder ($D < 0.2\lambda$) is $F = F_D + F_M$

where the drag term, $F_D = 0.5\rho\, D\, C_D\, u\, |u|\, dz = 0.5\rho\, D\, C_D\, |u|\, dz$

and the inertia term, $F_M = 0.25\rho\, \pi D^2\, C_M\, u'\, dz$ for added mass

The fluid force consists of :

a) Froude-Krylov force (undisturbed pressure) = $\rho \nabla\, u'$

b) disturbance pressure, i.e. added mass and diffraction (wave scatter) = $C_m \rho \nabla u'$

At high tide in a design wave, the wave force on the tower is given by Morison's equation as:

$$F = 0.5\rho_w \int_{-d}^{\xi} \{D C_D u|u| + 0.5 \pi D^2 C_M u'\} dz$$

$$= \frac{0.5 \rho_w D C_D \xi^2 \omega^2}{4k \sinh^2 kd} \cos\theta |\cos\theta| [\sinh 2k(\xi+d) + 2k(\xi+d)] + \frac{0.25 \rho_w \pi D^2 C_M \xi \omega^2}{k \sinh kd} \sin\theta [\sinh k(\xi+d)] \quad [7.1]$$

Circular cylinders give periodic lift forces, due to vortex shedding. The surface of a wind turbine tower will be rough, owing to marine corrosion, so the flow will always be turbulent, with high drag. Taking values given by Patel (1989) for Reynold's number $\approx 4 \times 10^7$:
For low aspect ratio, smooth, cylindrical inertia-dominated members,
$C_M = 1 + 1/\{1 + (D/d)^2\}$.
In shallow, sheltered waters marine fouling will be considerable, and a layer of mussels 100 mm thick could form within 2 - 3 years of installation, extending from the spring tide level to the seabed. Estimating the roughness height $\varepsilon = 0.1$ m, the basic drag coefficient will be
$C_{Do} = 1.46 (\varepsilon / D)^{0.08} (1 + 2\varepsilon / D)$.
Using a typical concrete tower diameter of D = 7 m gives $C_{Do} = 1.07$, whereas a typical steel diameter of d = 4 m has $C_{Do} = 1.135$.
For short members, $C_D = C_{Do}(0.5 + d/10D)$.
Therefore, the concrete tower has $C_D = 0.95$ and $C_M = 1.94$, whereas the steel tower has $C_D = 1.33$ and $C_M = 1.98$. Therefore with the preceding values of k, d, ω and ξ,
$F_{concrete} = 1.462 \cos^2 \omega t + 5.3 \sin \omega t$ (MN)
$F_{steel} = 1.106 \cos^2 \omega t + 1.76 \sin \omega t$ (MN)

And the corresponding moment about the ocean floor is given by

$$M = \int_{-d}^{\xi} 0.5\rho \{D C_D u|u| + 0.5 \pi D^2 C_M u'\} (z + d) dz$$

$$M = \left\{ \frac{0.5\rho D C_D \xi^2 \omega^2}{4k \sinh^2 kd} \cos\theta |\cos\theta| [(\xi + d - 1/2k) \sinh 2k(\xi+d) + 2k(\xi+d)^2] + \frac{0.25\rho \pi D^2 C_M \xi \omega^2}{k \sinh kd} \sin\theta (\xi + d - 1/k) \sinh k(\xi+d) \right\} \quad [7.2]$$

$M_{concrete} = 36 \cos^2 \omega t + 62 \sin \omega t$ (MNm)
$M_{steel} = 27 \cos^2 \omega t + 20.7 \sin \omega t$ (MNm)

The drag force lever arm is 25 m, and the inertia force lever arm is 12 m. The drag force has a higher lever arm, as it acts mainly near the crest. There will also be impact loads and wave slamming loads at wave crest level. There is as yet no established method for evaluating the

forces on large structures in shallow water waves, and the treatment of breaking waves is also an uncertain science. Wave impact loads may be estimated by assuming that all the kinetic energy of the wave is converted into strain energy. Swift and Dixon (1982) report that impact forces are nearly in phase with the drag force. For the present case, the impact force is taken as 3 cos ωt (MN), with a lever arm of 33 m. Although the impact force will be less than the inertia component, the moment about the sea bed will be comparable, owing to a higher lever arm. The wind force on the exposed tower and current forces on the submerged tower are likely to be negligible in comparison with the wave forces and the wind forces on the blades.

7.2.2 Steady wind forces on the structure

The small amount of offshore wind data which exists comes from light vessels, ships, oil and gas platforms and coastal meteorological stations (e.g. Bell Rock). The are all measured at low altitudes from large structures which interfere with the flow, and there are as yet no reliable theories for the variation of windspeed with height or with fetch offshore.
Estimates of 50-year return windspeeds are required with averaging times from 3 seconds upwards, referenced to a standard height of 10 m above still water level. With large waves, a distance of 10 m above still water level may be below the wave crest level, so this concept is only representative.
The wind velocity distribution with height is usually given by the approximate expression $(V_h/V_{10}) \approx (h/10)^{0.1}$, where h is in meters,
as the wind velocity profile is less steep offshore than over land.
The survival storm windspeed in the North Sea is quoted by Patel (1989) as 51.5 m/s.
The U.K. Department. of Energy (1984) recommends that the 50-year 3-s gust speed at 10 m height in the Wash area is taken as 47 m/s which is increased to 58 m/s at an altitude of 80m. The maximum 1-minute sustained windspeed at 10 m is given as 36 m/s, which increases to 44 m/s at 80 m.

The British Standards Institute Code of Practice for the design of buildings gives the following rules for calculating wind loads:
The design wind speed, $V_S = S_1 S_2 S_3 V$
where V is the 50-year 3-second gust speed at 10 m above ground level;
S_1 = topography factor = 1;
S_3 = design life factor = 1; and
S_2 = factor for structure size and height above ground level.

A 3 second gust affects an area of 20 m diameter only, and not the entire structure simultaneously. It is used for localised forces, e.g. the force on one blade.
$S_{2\,3sec} = 0.723\ h^{0.105}$

A 5 second mean is used for calculating forces on members up to 50 m, and a 15 second mean is used for calculating forces on members over 50 m

A 1 minute mean ('sustained windspeed') is used for calculating forces on the whole structure, when calculating the wind force to go with the maximum wave force.

$S_{2\,1\,min} = 0.668\,h^{0.1152}$

The turbines need to be at least of megawatt scale for commercial viability. Apart from the recent prototype design described by Davies (1988), all references suggest at least 3 MW capacity.

Roughly, a 50m diameter rotor generates 1 MW, rising to 6 MW, 100 m diameter for rated windspeeds of about 15 m/s.

Considering the wind forces on a 100m diameter turbine at the A6-03 site:

The hub height from the sea bed must allow for the sum of water depth, tide, storm crest, storm surge, blade radius, spray clearance, greenhouse effect (which may raise the sea level) and a gap for safety, which gives a minimum of 90 m, i.e. the minimum height from mean sea level is 70 m. A greater height may be required, to capture higher wind speeds so for the following example, the hub height from the sea bed is taken as 100m.

For a HAWT, the rotational speed is usually quoted as about 20 rpm, i.e. a tip speed of 105 m/s and an angular velocity, Ω of 0.33 Hz, At the shutdown windspeed of 25 m/s, this gives a minimum tip-speed ratio of $\lambda = 4.2$, and at the rated windspeed of 15 m/s, $\lambda = 7$.

For a VAWT, the rotational speed is usually quoted as about 9 rpm, i.e. a tip speed of 47 m/s and $\Omega = 0.15$ Hz. At the shutdown windspeed of 25 m/s, this gives a minimum tip-speed ratio of $\lambda = 1.9$. At the rated windspeed of 15 m/s, $\lambda = 3$.

There is cyclic loading transmitted to the tower by the rotor due to cyclic variations in the aerodynamic loads, particularly for two-bladed machines, although to some extent also on three bladed machines, due to wind shear, tower shadow and yaw. Two bladed machines are often teetered to reduce the transmission of the cyclic loading, but this is very expensive and the use of three bladed machines to eliminate most of the loading would generally be more efficient.

a) Steady aerodynamic forces on a yawed horizontal axis wind turbine (HAWT)

The forces and velocities on a yawed HAWT are shown in Fig. 13. The wind blows at an angle of yaw δ to the wind turbine axis of rotation, and the waves are at an angle γ to the wind.

These can be treated analogously to HAWTs on ships (see Section 6.2), with v replaced by x', V_A replaced by V_T and β replaced by $(90^o - \gamma)$.

Also, X force replaces side force and Y force replaces thrust force.

The section X force coefficient is given by

$C_X = C_L \sin\gamma + C_D \cos\gamma$

$= \lambda \{\sin\gamma \sin\delta (a_1 \cos\delta - b_1 \lambda + c_1) + \cos\gamma \cos\delta (a_2 \cos\delta - b_2 \lambda + c_2)\}$

The section Y force coefficient is given by

$C_Y = - C_L \cos\gamma + C_D \sin\gamma$

$= \lambda [- \cos\gamma \sin\delta (a_1 \cos\delta - b_1\lambda + c_1) + \sin\gamma \cos\delta (a_2 \cos\delta - b_2\lambda + c_2)]$

For small δ and γ this will be

$C_Y = - \lambda\{- \delta (a_1 - b_1\lambda + c_1) + \gamma (a_2 - b_2\lambda + c_2)\}$ [7.3]

C_X and C_Y are shown in Fig. 32 as functions of wave angle γ for several angles of yaw δ. When $\lambda = 4$, and $\gamma = \delta = 0$ then $C_D = 1.84$, $C_L = 0$, $C_X = 1.84$ and $C_Y = 0$. The force in the wave direction at V = 25 m/s (cutout value) is given by $F_A = 5.5$ MN.

b) Steady aerodynamic forces on a vertical axis wind turbine (VAWT)

The aerodynamic coefficients C_X and C_Y are shown in Fig. 19 as functions of azimuth angle θ, with various numbers of blades. It can be seen that a two-bladed machine produces fluctuationg C_X and C_Y, which give unsteady loading to the tower, but that three or more blades produce comparatively steady forces, the direction of which can be controlled by varying the pitch of the blades. The same coefficients are shown in Fig. 33 as functions of wave angle for several tipspeed ratios. There is no resultant lift unless the blades are set at a pitch angle ψ.

By analogy with VAWTs on ships (see section 6.3), with V_A replaced by V_T, β replaced by $(90^o - \gamma)$, and $\psi = 0$:

The force coefficients on each blade are given by

$C_X = \sigma\lambda a \cos(\theta + \gamma) (\sin\gamma + \lambda \cos\theta)$ [7.4a]

$C_Y = \sigma\lambda a \cos(\theta + \gamma) (\cos\gamma + \lambda \sin\theta)$ [7.4b]

Summing over all the blades and resolving in the wave direction gives :

for 2 bladed rotors:

$C_X = \sigma\lambda a \cos\theta \cos(\theta+\gamma)$

$C_Y = \sigma\lambda a \sin\theta \cos(\theta+\gamma)$

which give the average values

$C_X = 0.5\sigma \lambda a \cos\gamma$

$C_Y = 0.5\sigma \lambda a \sin\gamma$

for more than two blades, the forces are constant,

$C_X = 0.5\sigma\lambda a \cos\gamma$ [7.5a]

$C_Y = 0.5\sigma\lambda a \sin\gamma$ [7.5b]

For a representative machine with three straight blades, with $\lambda = 4$, $\gamma = 0$, $\sigma = 0.1$, $a = 4$, $V = 25$ m/s (cut-out value), the force in the wave direction is given by $F_A = 2.4$ MN.

7.3 Dynamic response

The dynamic response of the rotor blades is a dominant factor in the design. The natural frequency of the tower and blades must avoid vortex shedding, wave loading and blade rotation frequencies. Dynamically 'soft' towers are designed to have a natural frequency of less than the blade passing frequency , i.e. about 0.7 Hz - 1 Hz. (about 2 - 3 times the rotational frequency of the turbine.

Assuming for simplicity two cases, both of height 100 m:
a) a reinforced homogeneous concrete tower, with outer diameter = 7 m, Young's modulus $E = 30000$ MN/m^2 and density $\rho = 3$ tonne/m^3.
b) a steel pillar with outer diameter = 4 m, Young's modulus $E = 210000$ MN/m^2 and density $\rho = 7.85$ tonne/m^3. This could be made out of unstiffened plate, but the thickness required for offshore use would be excessive. Longitudinal stiffeners have been assummed.
N_s equally spaced stiffeners of area A have second moment of area $I_s = N_s A D^2 / 8$

Second moment of area of the tube, $I_t = \pi (D_1^4 - D_2^4)/ 64$
Modulus, $Z = 2I / D_1$
mass per unit length of the tube, $m_t = \rho\pi(D_1^2 - D_2^2)/ 4$
The bending moment is given by
$EI\, y = F_A z + 3[z - z_I] \cos \omega t + F_D[z - z_D] \cos^2\omega t + F_M [z - z_M] \sin \omega t.$
Taking a representative position at z = 50 m (half way up), the bending stress is given by
$\sigma = 275 \times 10^9 / Z.$
The permissible bending stress for Grade 55 steel is 265 N/mm^2, so at this point, $Z > 1.04$ m^3.
For relative deflection at z in y due to force F in the y-direction:
$EI\, y = F_A z^3/6 + 3[z - z_I]^3 \cos \omega t / 6 + F_D[z - z_D]^3 \cos^2\omega t / 6 + F_M [z - z_M]^3 \sin \omega t / 6 + A_1 z + A_2$
using the forces calculated above, as shown in Fig. 34, this gives:
for concrete,
$EI\, y = 0.917 z^3 + 0.5 [z - 73]^3 \cos \omega t + 0.244 [z - 75]^3 \cos^2\omega t + 0.877 [z - 88]^3 \sin \omega t + A_1 z + A_2$
where
$A_1 = -27500 - 1093 |\cos \omega t| - 457 |\cos^2\omega t| - 378 |\sin \omega t|$ (MN m^2)
$A_2 = 1834000 + 99458 |\cos \omega t| + 41860 |\cos^2\omega t| + 36325 |\sin \omega t|$ (MN m^3)
and for steel,
$EI\, y = 0.917 z^3 + 0.5 [z - 73]^3 \cos \omega t + 0.184 [z - 75]^3 \cos^2\omega t + 0.293 [z - 88]^3 \sin \omega t + A_1 z + A_2$
where
$A_1 = -27500 - 1093 |\cos \omega t| - 346 |\cos^2\omega t| - 127 |\sin \omega t|$ (MN m^2)
$A_2 = 1834000 + 99458 |\cos \omega t| + 31720 |\cos^2\omega t| + 12193 |\sin \omega t|$ (MN m^3)

Therefore, the relative deflection at any point z on the tower is given by

for concrete:

$$EI\,y = \{0.917\,z^3 - 27500\,z + 1834000\} + \{0.5\,[z - 73]^3 - 1093\,z + 99458\}\cos\omega t + \{0.244\,[z - 75]^3 - 457\,z + 41860\}\cos^2\omega t + \{0.877\,[z - 88]^3 - 378\,z + 36325\}\sin\omega t \quad [7.6a]$$

for steel:

$$EI\,y = \{0.917\,z^3 - 27500\,z + 1834000\} + \{0.5\,[z - 73]^3 - 1093\,z + 99458\}\cos\omega t + \{0.184\,[z - 75]^3 - 346\,z + 31720\}\cos^2\omega t + \{0.293\,[z - 88]^3 - 127\,z + 12193\}\sin\omega t \quad [7.6b]$$

and the deflection at the top,

for concrete:

$$y = (1834000 + 99458\cos\omega t + 41860\cos^2\omega t + 36325\sin\omega t) / EI$$

for steel:

$$y = (1834000 + 99458\cos\omega t + 31720\cos^2\omega t + 12193\sin\omega t) / EI$$

The natural frequency, ω is given by

$$\omega_n^2 = 12.46 \times 10^3\,EI / m\,L^4$$

The tower stiffness, $K = 3EI / L^3$

Critical damping, $B^* = 2\sqrt{AK} = 2K / \omega_n = \sqrt{2.9 \times 10^{-3}\,mEI / L^2}$

The structural damping, B can be estimated as = $0.02 \times B^*$

Therefore, for various tower wall thicknesses, in concrete:

thickness (m)	1.00	0.75	0.5	0.25
I (m^4)	87.2	72.9	54.2	30.2
m (tonne/m)	56.5	44.1	30.6	15.9
steady y (m)	0.70	0.84	1.13	2.02
dynamic y (mm)	38	45	61	110
ω_n (rad/sec)	2.40	2.49	2.57	2.66
f_n (Hz)	0.38	0.40	0.41	0.42
B^*($\times 10^6$ kg/s)	6.55	5.29	3.80	2.04
B ($\times 10^6$ kg/s)	0.13	0.11	0.08	0.04

and in steel:

plate thickness (m)	0.05	0.04	0.03	0.02
Z (m^3)	2.85	2.74	2.62	2.50
I_t (m^4)	1.21	0.98	0.74	0.50
I_s (m^4)	4.48	4.48	4.48	4.48
I (m^4)	5.69	5.46	5.22	4.98
m_t (tonne/m)	4.87	3.91	2.94	1.96
m_s (tonne/m)	31.0	31.0	31.0	31.0

m (tonne/m)	35.87	34.91	33.94	32.96
steady y (m)	1.53	1.60	1.67	1.75
dynamic y (mm)	83	87	91	95
ω_n (rad/sec)	2.04	2.02	2.01	2.00
f_n (Hz)	0.32	0.32	0.32	0.316
B*(x 10^6 kg/s)	3.52	3.41	3.29	3.162
B (x 10^6 kg/s)	0.071	0.068	0.065	0.063

7.4 Aerodynamic damping

a) HAWT:

These can be treated analogously to HAWTs on ships, as in sections 6.2 and 7.2.1.

The linear roll velocity is given by $x' = V_T u$, where $u = x' / V_T$.

The section X force component is given by

$$C_X = C_L \sin(\gamma - d\alpha) + C_D \cos(\gamma - d\alpha)$$

$$= (1/H)\,(C_L \sin\gamma + C_D(\cos\gamma + u))$$

$$= (\lambda / H^2)\,\{\sin\gamma \sin\delta\,(a_1 \cos\delta - b_1\lambda + c_1) + \cos\gamma\cos\delta\,(a_2\cos\delta - b_2\lambda + c_2)$$

$$+ u\,(-a_1\,(\sin^2\gamma\cos 2\delta - \sin\gamma\cos\gamma\sin 2\delta) + a_2\,(2\cos^2\gamma\cos^2\delta + 2\sin\gamma\cos\gamma\sin\delta\cos\delta$$

$$+ \cos^2\delta) + b_1\lambda\,(\sin^2\gamma\cos\delta - \sin\gamma\cos\gamma\sin\delta) - b_2\lambda\,(\cos^2\gamma\cos\delta + \sin\gamma\cos\gamma\sin\delta + \cos\delta)$$

$$- c_1(\sin^2\gamma\cos\delta - 2\sin\gamma\sin\delta\cos\gamma) + c_2\,(2\cos^2\gamma\cos\delta + \cos\gamma\sin\delta\sin\gamma + \cos\delta)$$

$$= \lambda\,\{\sin\gamma\sin\delta\,(a_1\cos\delta - b_1\lambda + c_1) + \cos\gamma\cos\delta\,(a_2\cos\delta - b_2\lambda + c_2)$$

$$+ u\,(-a_1\sin^2\gamma\cos 2\delta + a_2\,(2\cos\gamma\sin\gamma\sin\delta\cos\delta + \cos^2\delta)$$

$$+ (b_1 - b_2)\lambda\,(\sin^2\gamma\cos\delta + \sin\gamma\cos\gamma\sin\delta)$$

$$- c_1\sin^2\gamma\cos\delta + c_2\,(\cos\gamma\sin\delta\sin\gamma + \cos\delta) \qquad [7.7]$$

The damping derivative is given by

$$C_B = \lambda\{-a_1\sin^2\gamma\cos 2\delta + a_2\,(\cos\gamma\sin\gamma\sin 2\delta + \cos^2\delta)$$

$$+ (b_1 - b_2)\lambda\,(\sin^2\gamma\cos\delta + \sin\gamma\cos\gamma\sin\delta)$$

$$- c_1\sin^2\gamma\cos\delta + c_2\,(\cos\gamma\sin\delta\sin\gamma + \cos\delta\}$$

$$= \lambda\{\sin^2\gamma\,(-a_1\cos 2\delta + (b_1 - b_2)\lambda\cos\delta - c_1\cos\delta) + \cos\gamma\sin\gamma\,(a_2\sin 2\delta + (b_1 - b_2)\lambda\sin\delta$$

$$+ c_2\sin\delta) + a_2\cos^2\delta + c_2\cos\delta\}$$

For small δ and γ, this is approximately

$$C_B = \lambda\{-\gamma^2\,(a_1 - (b_1 - b_2)\lambda + c_1) + \delta\gamma\,(2a_2 + (b_1 - b_2)\lambda + c_2) + a_2 + c_2\}$$

$$= \lambda\{-\gamma^2\,(0.37 + 0.019\,\lambda) + \delta\gamma\,(0.9 - .019\lambda) + 0.6\} \qquad [7.8]$$

Thus, for any given γ, the maximum damping is obtained when

$$\delta = (2a_2 + (b_1 - b_2)\lambda + c_2)\;\gamma\,/\,(2a_2 + c_2 - (4a_1 + (b_1 - b_2)\lambda - c_1)\gamma^2) \qquad [7.9]$$

which gives the optimum angle as approximately

$$\delta_{opt} \approx (1 - 0.023\,\lambda)\,\gamma$$

At V = 25m/s, $\lambda = 4$, $\gamma = \delta = 0$, the damping derivative is

$B = 0.5\rho V_T \pi R^2 C_B = 0.29 \times 10^6$ kg/s. [7.10]

The variation of damping coefficient with wind direction is shown in Fig. 35 for different tip speed ratios at $\delta = 0$ and for different angles of incidence at $\lambda = 6$. It can be seen that the damping coefficient is always positive and is highest when wind and wave directions coincide. B is highest when $\delta = \gamma$, i.e. when the turbine axis is pointing in the wave direction, not the wind direction. In a high wind, i.e. above the rated wind speed, when excess wind is being spilt anyway, it will be beneficial to yaw the turbine around to face the waves, which will increase the stability of the tower without losing power. This would require some sort of sensing device (e.g. an inclinometer) to be included in the control system. The increase in fatigue susceptibility which comes from operating in yaw should be compensated by a decrease due to removing the vibrations from the wave loading.

Although there will be damping in the direction of the turbine axis, there will be excitation in the perpendicular direction. However, this will be much smaller and probably not a problem.

b) <u>VAWT</u>:

By analogy with VAWTs on ships, similarly to sections 6.3 and 7.2.2:

Linearising to first order in u and neglecting terms in $(1/\lambda)$ yields

$X = 0.5\rho V_T^2 ca\{\cos(\theta + \gamma)(\sin\gamma + \lambda\cos\theta) + u\cos\theta(\sin\gamma + \lambda\cos\theta)\}$

$Y = 0.5\rho V_T^2 ca\{\cos(\theta + \gamma)(\cos\gamma + \lambda\sin\theta) + u[\sin\theta\sin\gamma - 2\cos\theta\cos\gamma - \lambda\cos\theta\sin\theta]\}$ [7.11]

Summing over all the blades gives:

for 2 blades:

$X = 0.5\rho V_T^2 c\, 2\lambda a\cos\theta\{\cos(\theta + \gamma) + u\cos\theta\}$

$Y = 0.5\rho V_T^2 c\, 2\lambda a\sin\theta\{\cos(\theta + \gamma) + u\cos\theta\}$

which gives the time average

$X = 0.5\rho V_T^2 c\,\lambda a\{\cos\gamma + u\}$

$Y = -0.5\rho V_T^2 c\,\lambda a\sin\gamma$ [7.12]

for N_B blades ($N_B > 2$):

$X = 0.5\rho V_T^2 c\, 0.5N_B\,\lambda\, a(\cos\gamma + u)$

$Y = -0.5\rho V_T^2 c\ 0.5N_B\,\lambda\, a\sin\gamma$

The total X force component may be written in the form

$X = X_s + B_X(\lambda, \theta)\, x'$.

For 2 blades, $B_X = 0.5\rho V_T ch\, 2\lambda a\cos^2\theta$

For N_B blades, $B_X = 0.5\rho V_T ch\, 0.5N_B\lambda\, a$ [7.13]

The total Y force component may be written in the form

$Y = Y_S + B_Y(\lambda, \theta)\, x'$.

For 2 blades, $B_Y = 0.5\rho V_T ch\, 2\lambda a \cos\theta \sin\theta$

For N_B blades, $B_Y = 0$

The damping derivative has the advantage that it is always positive and does not vary with the wave direction.

The damping derivative, $C_B(\theta, \lambda) = \sigma \lambda a \cos^2\theta$ for 2 blades, which averages at $C_B = 0.5\sigma\lambda a$.

For more than two blades, it is constant at $C_B = 0.5\sigma\lambda\, a$

Thus, when V = 25m/s, $\lambda = 4$, $\mu = 0$, $\sigma = 0.1$, the damping derivative is

$B = 0.5\rho V_T ch\, 0.5N_B\lambda\, a = 0.096 \times 10^6$ kg/s.

As with the HAWT, the aerodynamic damping is of the same order of magnitude as the structural damping, allowing a less stiff tower to be used.

8. MEASUREMENTS AT SEA ON A FISHING BOAT

M.F.V. Resolution is an 11.3 m Whitby keel boat, used as a long-liner. It is shown in Figs. 36 and 37. John Brennan, the Skipper and previous owner, had wanted a sail to control the drift of the boat which would not need much attention from the crew during fishing, or obstruct activities on deck. A spritsail mizzen was fitted by James Byam Shaw in 1985, which reduced the drift and rolling motions and improved the directional stability, as well as saving fuel. The sail is trapezoidal, of height 3.9 m, bottom width 2.54 m and top width 1.43 m. The following year, the Sea Fish Industry Authority (previously the White Fish Industry Authority) sponsored James Byam Shaw to design and build a full sail rig as an experiment, and selected *Resolution* on which to retrofit it. The boat has a fully battened Gunter/sprit mainsail of height 6.7 m and base width 6.36 m and a jib sail of height 5.8 m and base width 2.54 m. Tests performed by the Sea Fish Industry Authority before the mast was installed had given a mean roll period of 2.98 secs.

Measurements of the rolling motion were made on this boat in March 1989 at Whitby.

The following measurements were made:

a) 15.07 - 15.15 p.m., (8 mins)
With all the sails up and the engine on 3/4 throttle, boat speed varied from 5.1 knots to 8.3 knots. Sailing close hauled with an apparent wind direction of approximately 60°.

b) 16.10 - 16.24 p.m., (16 mins)
With all the sails up and the engine switched off.

c) 16.50 - 17.06 p.m., (16 mins)
With all the sails down and the engine on full.

A Sperry AccuStar electronic inclinometer was used to measure the roll, connected to a datalogger and a Toshiba T3200 mini computer, as shown in Fig. 38. The computer was run off the boat's 24 V starter battery, converted to 240 V a.c. using an inverter.
The data was filtered while digitising, and all frequencies above 2 Hz were filtered out.
The calibration factor for the inclinometer is 60 millivolts per degree, and for the datalogger is 12.28 datalogger units per degree (i.e. 205 datalogger units per volt).

After subtracting the mean values and calibrating the readings from the datalogger, the data appears as in Figs. 39 to 41. It can be seen that case (a) (i.e. sail and motor together) has the smallest amplitude and case (c) (i.e. motor alone) has the largest.
The time history measurements were analysed using a Fast Fourier Transform to give the spectral density,

$$S(\omega) = \int_0^\infty \phi(t) \exp(-i\omega t)\, dt$$

as shown in Fig. 42. A smoothed version is shown in Fig. 43, which was obtained by summing the data points in batches. It can be seen that case (a) gives a broad band response of lower amplitude, whereas case (c) is sharply peaked about the natural frequency.

Taking spectral moments about the origin, i.e.

$m_k = \int_0^\infty \omega^k S(\omega)\, d\omega$

gives the following quantities:

m_o = area under curve

$\hat{\omega} = m_1 / m_o$ = mean (observed) frequency

σ = variance (r.m.s. frequency) = $\sqrt{m_2 / m_o}$

skewness (i.e. symmetry) = m_3 / σ^3

kirtosis (i.e. flatness) = m_4 / σ^4.

Results from the Fourier analysis give:

	both	sail	motor
	(a)	(b)	(c)
m_o	0.038	0.034	0.038
m_1	0.070	0.064	0.070
m_2	0.152	0.143	0.153
m_3	10.282	10.459	9.316
m_4	30.283	29.978	24.898
mean frequency (rad/sec)	1.841	1.904	1.847
zero crossing (r.m.s.) frequency (rad/sec)	2.011	2.048	1.992
skewness	1.265	1.217	1.179
kirtosis	1.853	1.703	1.582
r.m.s. roll amplitude (deg)	3.66	4.04	4.48

Therefore, the addition of a sail makes little difference to the mean roll frequency, but increases the skewness of the spectrum, and increases the damping, as shown by the increased kirtosis, and by the reduced peak and r.m.s. amplitudes. In fact, the damping was greater with the sails and engine together than with the sails alone.

The spectra are of the standard form $S(\omega) = (A/\omega^5) \exp(-B/\omega^4)$, where

	both	sail	motor
	(a)	(b)	(c)
ω_o (dominant frequency)	1.76	1.82	1.88
A	14.00	19.19	19.85
B	5.30	5.88	5.24

The amplitude, A is lower with the sail than without it, although the presence of the sail makes very little difference to B.

9. EXPERIMENTAL PROGRAMME

The aim of the experimental programme was to understand the unsteady flow behaviour of aerofoil sections and wind turbines subjected to harmonic oscillatory rolling motions with parametric variation of the mean incidence angle, wind heading and frequency.
The main objectives were:
a) to measure the roll damping and inertia moments of aerofoils and wind turbines;
b) to derive roll damping coefficients from the measurements;
c) to deduce parametric equations from them; and
d) to demonstrate the viability of the performance of these devices as roll stabilisers.

9.1 Scale requirements:

In order to calculate coefficients which can be scaled up to full size, it is necessary to preserve the characteristics of the flow behaviour. Therefore the viscous and inertia components of the force must be scaled equally.

One significant parameter is the Reynolds Number, $Re = Vc / \nu$. In these model tests, the maximum wind speed that could be provided by the open jet wind tunnel equipped with the low-speed nozzle was 13 m/s. Therefore, it was not possible to raise the wind velocity, V in proportion to the reduction in the chord length, c, as in fact V was approximately equal for both cases. Therefore it was not possible to preserve the same Reynolds number, and all the aerofoil tests were performed at approximately Re = 250,000. Although this gave lift forces which were too small and drag forces which were too large, as the viscous forces were too large, many characteristics of the flow were preserved, e.g. the separation point remained at the sharp trailing edge. Tests were not performed on Flettner rotors, Cousteau Turbosails or slotted multiwings because these characteristics would not be preserved. The open jet has a turbulence level of 5%, and the surface of the aerofoil was slightly rough, owing to the grain of the wood showing through the paint, so the boundary layer was turbulent throughout.

For fluctuating forces, it is also necessary to scale the frequency.
The inertia moments are proportional to
$F_I = \rho\omega^2\phi h^2 c^3$
and viscous moments are proportional to
$F_V = \rho V \omega c^3 h$.
Therefore, denoting full-scale quantities by subscript f and model-scale quantities by subscript m, for inertia and viscous forces to be scaled equally requires that

$$\frac{\omega_f^2\phi_f h_f^2 c_f^3}{\omega_m^2\phi_m h_m^2 c_m^3} = \frac{V_f\omega_f c_f^3 h_f}{V_m\omega_f c_m^3 h_m}$$

$$\text{i.e. } \frac{h_f\omega_f\phi_f}{V_f} = \frac{h_m\omega_m\phi_m}{V_m} = \text{constant, q.} \qquad [9.1]$$

Therefore, for equality of velocity ratio q, the frequency of excitation, ω was increased in proportion to the reduction in size, h. The roll angle amplitude (ϕ_o) was kept small for assumptions of linearity.

Average ocean windspeeds lie in the range 5 - 10 m/s.
For the vessels considered for wind assistance, the following values are typical;

	Fishing boats	Container ships
roll period (s)	5	20
ω_f (rad/s)	1.25	0.3
V_f (m/s)	6	10
full-scale chord length (m)	2	6
for a model chord length of 0.25 m, this gives		
scale	1/8	1/24

The wind tunnel velocity, V_m is 13 m/s, so for equality of velocity ratio, $q = h\omega\phi_o / V$:
Minimum q is for container ships, requiring ω_m = 9.4 rad/s = 1.5 Hz.
Maximum q is for fishing boats, requiring ω_m = 22 rad/s = 3.5 Hz.
Roll frequencies of 1.5 Hz, 2.5 Hz and 3.5 Hz were therefore used in the model tests. A sampling frequency of 33 Hz was used, with all frequencies higher than 17 Hz filtered out to prevent aliasing and to reduce noise. This allows analysis of data up to the 3rd. harmonic of the highest forcing frequency.

9.2 Equipment

The numbers in square brackets refer to descriptions of each piece of equipment, which are found in Appendix 2.

The wind tunnel [1] is a 1m square open jet, and the devices were located 0.5 m downstream from the exit nozzle plane.

Consideration of the various options for producing the forced sinusoidal motions led to a choice of a simplified planar motion mechanism concept, consisting of a scotch yoke driven by a 1 kW motor [2], as shown in the general arrangement in Fig. 44. The forces and moments are recorded by a purpose-built six-component balance [3], shown in Fig. 45, consisting of strain gauges wired into Wheatstone bridges, connected via amplifiers [4] and filters [5] to the datalogger [6]. Data acquisition and processing were controlled using the microcomputer [7].
The motor, balance and linear bearing [8] were mounted on a base plate which could be rotated through 90° in 15° increments, to give parametric variation of the angle between driving force and wind direction.

The models were mounted on an aluminium shaft passing through a spherical bearing at 70 mm below the wind tunnel floor. This bearing supported the weight of the specimen, and transmited free movement in rotary motions only. It was situated 0.5 m downstream of the tunnel exit plane. The shaft was attached to the balance so that it could measure forces normal to the shaft and yaw rotations only, which can be resolved to give roll, pitch and yaw moments. The balance was driven in simple harmonic motion, restrained to one degree of freedom along the linear bearing. The ship hull was not modelled, but was represented as a stationary flat plane (i.e. the tunnel groundboard).
The lever arm from the spherical bearing to the pivot on the balance was 0.37 m.

The wind tunnel had an exit plane of width 1 m and the wind velocity was constant over the middle 80% of the exit area. It is necessary for the entire specimen to remain within this area at all points during its oscillation. To keep the specimen in the centre of the tunnel, the tests were performed with a gap of 300 mm between the bottom of the aerofoil (in its mean position) and the tunnel floor, and a gap of 500 mm between the wind turbine hub and the tunnel floor. The maximum possible roll amplitude, allowing for this restriction, was then $\phi_o = 15^o = 0.24$ radians.
Therefore the maximum amplitude of motion = 0.37 tan (0.24) = 90 mm.
The linear bearing was selected to allow a total travel of up to 200 mm.

The forces and moments were measured on a purpose-built six-component balance, which was designed to specifications put forward on the basis of the following theoretical estimates of forces and moments:

Expected maximum aerodynamic loads:
It was originally the intention to use a windspeed of 15 m/s and an aerofoil of chord = 0.25 m and span = 0.75 m. The maximum static lift coefficient was expected to be 2, and it was expected that the dynamic loads would be about 1.5 times the static loads. These estimates gave a maximum expected dynamic lift force of 78 N, and therefore a maximum expected dynamic roll moment of 78 x 0.37 = 28.8 Nm.
For the wind turbine, of diameter = 0.67 m, the maximum static lift coefficient was estimated as 0.8, and the drag coefficient as 2.3, based on the wind turbine measurements in Figs. 14 and 15 (which were actually for a different wind turbine). This gave the maximum expected dynamic lift force as 58 N and the drag force as 165 N, with the maximum possible resultant force = 175 N. Therefore, the maximum expected dynamic roll moment = 175 x 0.37 = 65 Nm.

Expected maximum inertia loads:
The section mass of the aerofoil = 0.5 kg/m. For the largest aerofoil, with an estimated gap of 200 mm to the bearing, the moment of inertia is I = 0.14 kg m^2. Therefore at $\omega = 22$ rad/sec and $\phi_o = 0.24$ radians, the inertia moment is given by $I\phi'' = 0.14 \times 22^2 \times 0.24 = 16.44$ Nm.

The wind turbine has mass = 0.48 kg, and lever arm = 0.57 m to the bearing, so the moment of inertia is given by I = 0.156 kg m^2. Therefore at ω = 15 rad/s and ϕ_o = 0.24 radians, the inertia moment is given by $I\phi'' = 0.156 \times 15^2 \times 0.24 = 8.4$ Nm.

Therefore maximum expected dynamic roll moment about spherical bearing is given by 45.24 Nm for the aerofoil and 73.4 Nm for the wind turbine.
The maximum force to be transmitted to the balance is therefore 73.4 / 0.37 = 198 N.

The balance does not measure its own inertia load, but only the difference between the motion of the top and bottom plates, which will be small.
Therefore the balance was designed with linear ranges of
FX and FY channels = 200 N
Yaw moment channel = 200 x 0.04 = 8 Nm.
Vertical force channel = 200 sin 0.25 = 50 N.
Note: Due to a design fault, (i.e. weight of top plate under-estimated), the vertical channel can only measure downward forces up to the weight of top plate plus 5 N, which corresponds to FX forces up to 20 N only, i.e. a small fraction of the measuring range. It was designed to measure ± 25 N, and should have been designed for 10 N ± 50 N. Because of this, the balance became overstrained in the vertical direction early in the test programme and the results from the FZ channel became unusable.

The total mass of moving parts below pivot, including the balance, connection plates and linear bearing, was 4.1 kg. The maximum acceleration = 50 m/s^2. Therefore the maximum required force was 4.1 x 50 + 198 = 403 N. From a scotch yoke of radius 90 mm, this requires a torque of 36 Nm. As the maximum rotational speed of the motor, Ω = 22 rad/s, the power required = 0.8 kW.

9.3 Models.

9.3.1 Aerofoils.

Following the theoretical investigations detailed in Chapter 5, it was not considered worth while to investigate the effect of variations of planform, such as taper, or of different sections. Two aerofoils of section NACA 0015, chord length of 0.25m, spans of 0.25m and 0.5m and masses 0.22 kg and 0.32 kg were supplied by Miro Model Products.
A spanwise shaft was fitted at 0.08 m from leading edge (32% of chord, i.e. mass centre) to eliminate inertial yawing moments. To keep the inertia forces low, the aerofoils were made from expanded polystyrene foam glued to the shaft, covered with thin plywood. The shaft was a thin-walled aluminium tube of diameter = 13 mm, stiffened by filling with expanded polyurethane foam.

The section was chosen because NACA 0015 aerofoils have been used by several investigators in wind assisted ship propulsion, although only at higher aspect ratios than were used here. The aspect ratios of 1 and 2 were chosen because the Japanese WASP program used those aspect ratios, although with a different section.
The models are shown in the wind tunnel in Figs. 46 and 47.

9.3.2 Wind turbine

Following the theoretical investigations detailed in Chapter 6, it was decided to use a three-bladed HAWT only. The HAWT used was a 1/60 scale model of the Nibe-B wind turbine with diameter 0.67 m. It had 3 wooden blades of length 306 mm and section NACA 4412 - 4434 with 11^{o} twist and adjustable pitch. The full-scale rated windspeed was 13 m/s, and the rated tip-speed ratio, λ was 5.4. The blades and hub weigh 0.1 kg. The motor supplied with the wind turbine was heavy, and produced an inertia force which was too high for the balance, so a bicycle dynamo of mass 0.34 kg was used to measure the power. The dynamo could only turn clockwise, owing to its design for use on bicycles, whereas the wind turbine had been designed as an anticlockwise upwind machine. It therefore had to be used as a clockwise downwind machine, and so its performance is not ideal, but should be sufficient for the purpose of these tests. It is shown in the wind tunnel in Fig. 48.
The dynamo produces a.c. at a frequency of four times the rotational frequency, which therefore required a very small timestep to record its output. It was not possible to vary λ and ψ independently, as it was not possible to vary the electrical load across the dynamo.

9.4 Calibration.

A calibration rig was built, which is shown in Fig. 51.
Forces were measured by deflections of the balance, as recorded by the strain gauges. Force was applied in one loading mode at a time, by hanging masses on pulleys. The masses used were all found to be underweight, and so were ballasted up by taping on small bolts. The loading in each mode was lined up by adjusting the position of the pulleys until a zero reading was achieved in the opposite direction. The calibration was performed using the same datalogger and voltage supply as were used for the tests, so that any errors would be consistent. For each load increment, the logger scanned each of the six channels by taking 10 readings at 30 millisec intervals and averaging, which allowed faults and drifting channels to be spotted.

An applied force F_n, in mode n, is taken to give a reading on the datalogger of R_m in mode m. For each loading mode, a best-fit gradient was deduced for each of the six channels, as voltage per unit load, i.e. $G_{mn} = R_m / F_n$, where G is the gradient. When all the loading modes had been completed, the matrix G was then inverted to produce the response matrix. The force applied could then be calculated from the readings by applying the equation $F_n = (G)^{-1}{}_{mn} R_m$.

There was found to be strong coupling between the FX and MY channels, and also the FY and MX channels, but as the MX and MY channels were not used for these tests, it was ignored. Fortunately, it was found that coupling between the four channels which were to be used was negligible, and was probably due to slight non-alignments of the calibration equipment, so only the diagonal terms of the matrix were used.
The results were:
$G_{11} = 50$, $G_{22} = 53$, $G_{33} = 342$, $G_{44} = 864$, where the units are Newtons per datalogger unit.

9.5 Software

The software consisted of three separate main programs, listings of which are found in Appendix 2.

9.5.1 Program LOG performs real-time A/D conversion of the output from the FX, FY, FZ and MZ channels of the balance and the power from the dynamo (for the wind turbine only), and also from a revolution counter during testing, and stores the results on disk for processing as a file of raw data measurements. To avoid zero drift on the datalogger, the zero was reset at the beginning of each test. The tunnel wind speed, nominal frequency, aerofoil aspect ratio or wind turbine blade pitch angle, angles of orientation (β) and incidence (α) or yaw (δ) and lever arm were entered before each test. The wind turbine rotational speed, read from an oscilloscope, was also entered.
For the aerofoils, 10 cycles were measured at 30 millisec intervals.
For the wind turbines, 2 cycles were measured at 5 millisec intervals, in order to record the higher frequency oscillations of the order of the blade passing frequency.

9.5.2 Program PROC processes the raw data produced by program LOG.
The true frequency and phase of the excitation were calculated from the revolution counter.

a) For the aerofoils, the readings from each channel were then interpolated to give evenly spaced data points, which were averaged over 10 cycles, to increase the signal-to-noise ratio.
b) For the wind turbine, the readings from each channel were interpolated over one cycle to give 128 data points, for use in a subsequent Fourier analysis.

The data were then converted to moments about the spherical bearing, using the calibration matrix and the relations
Roll moment = 0.37 FX , Pitch moment = 0.37 FY and Yaw moment = MZ.
The results were stored on disk. Printouts and graphs of the raw data were obtained at this stage.

9.5.3 Program FOURIER processes the data output by program PROC.

a) For the aerofoils, harmonic analysis was used to obtain the first three Fourier components in the roll, pitch and yaw modes of motion.
Summations were taken over one cycle of N points, at $\omega t_n = 2\pi\,(n-1)/(N-1)$ in the range n = 1 to N, with integration by the trapezium rule for points at $\omega t_m = \pi\,(2m-1)/(N-1)$ in the range m = 1 to N-1. The frequency points for integration were taken as
$f_m = 0.5(f(\omega t_m) + f(\omega t_{m+1}))$
which gives the Fourier series
$f(\omega t) = a_o + \Sigma_m\,(a_m \cos(n\omega t) + b_m \sin(n\omega t))$
where the Fourier components are given by
$a_o = (1/N)\,\Sigma_m\, f_m$, $a_m = (2/N)\,\Sigma_m\, f_m \cos(n\omega t)$, $b_m = (2/N)\,\Sigma_m\, f_m \sin(n\omega t)$.

b) For the wind turbines, it was necessary to do a full Fast Fourier Transform using 128 points, as there are high frequency components in the readings due to the rotation of the wind turbine. As the MZ channel had become overstrained, only the FX and FY channels and the power from the dynamo were recorded. The dynamo produces alternating current at a frequency of 4 times the rotation frequency of the turbine, for which reason a small timestep of 5 millisecs had to be used to measure its output.

9.5.4 Output

Typical samples of the output are shown in Figures 52 to 66.
Fig. 52 is a typical sample of raw data from the steady flow on an aerofoil with no oscillation, showing some turbulence of a small amplitude imposed on the steady values.
Figs. 53 and 54 are typical samples of raw and processed data for the smaller aerofoil, and Figs. 55 and 56 for the larger one. The dotted lines are the curve fits produced by the Fourier analysis. It can be seen that the roll, consisting largely of structural components, is roughly sinusoidal, whereas the pitch has a sharp trough and a rounded peak (reversed in the second case, which is for negative α), owing to the increased forces when moving towards the tunnel and the decreased forces when moving away from it. Similarly, the yaw moment appears as a saw-tooth.

Figs. 57 and 58 are the steady flow on a wind turbine with no oscillation, showing a periodic force owing to the blade rotation. The frequency of the pitch moment is equal to the rotational frequency, the roll force is at twice this frequency, and the dynamo produces a.c. at four times the rotational frequency. In Fig. 58, the top two graphs show curve fits to the raw data calculated by Fourier analysis. The dotted line is the mean steady value. The lower three graphs are the Fourier analysis coefficients displayed as functions of frequency. The solid line is the cos term (damping) and the dotted line is the sin term (inertia). The peaks in these curves correspond to the frequencies of the original signals.

Figs. 59, 60, 61 and 62 are for axial flow on a wind turbine rolling in line with the wind direction, Figs. 63 and 64 are for a wind turbine rolling parallel to the wind direction at an angle of yaw, and Figs. 65 and 66 are for a wind turbine with no angle of yaw, but rolling at an angle to the wind direction .
It can be seen that the pitch moment varies in amplitude, being larger when the wind turbine is travelling towards the wind tunnel. The Fourier analysis curve-fits in the top two graphs of Figs. 60, 62, 64 and 66 contain only the lower harmonics of the rolling frequency, and ignore the rotational frequency fluctuations. The last 3 graphs in the same Figures show that the roll now has a high peak about the roll frequency and a small one about the rotational, whereas the pitch has a higher peak about the rotational and a lower one about the roll frequency.

Test Procedures.
In order to calibrate out stiffnesses, structural damping, added mass etc., the following tests were performed:
a) Oscillation of the balance and shaft without the aerofoil to measure the stiffness, damping and inertia of the restraints.
b) Oscillation with the aerofoil but with no wind to measure the added mass and the structural damping and inertia of the aerofoil.
c) With the wind on but no oscillation to measure the steady aerodynamic forces.
d) Oscillating with the wind on to measure the aerodynamic damping.

Because mains noise and vibrations were considerable during the day, when other machinery was in use in the laboratory, all these tests were performed at off-peak times when other activity in the laboratory was minimal.

9.6 Aeroelastic and structural effects.

The forces which must be taken into account are inertial, aerodynamic, structural and the applied force. The applied force is known and the remaining forces depend on the displacements and velocities of the aerofoil and shaft. There are three degrees of freedom - roll, pitch and yaw about the spherical bearing. For wind turbines, yaw moments were not measured, as the yaw channel on the balance was broken. The resultant forces FX and FY at the balance due to the roll and pitch moments were measured. Only steady-state motions were measured. Only the first bending mode of the aerofoil or shaft was considered, as higher frequencies were filtered out from the measurements.

9.6.1 Structural flexibility of the aerofoils.

Referring to Fig. 49, the aerofoil extends from $0 < z < s$, and has Young's modulus E_1 and second moment of area I_1. The shaft continues from $s < z < d$, with corresponding E_2 and I_2.

The flexibility of the aerofoils was measured by clamping the shaft horizontal and hanging weights on the free end, where the deflection was measured. Photographs of the deflections are shown in Fig. 50. The self weight of the aerofoil can be ignored, as the deflection due to it is constant.

The flexibility of the shaft was measured:
for length, $d = 0.675$ m, the deflection was measured as $y = 0.02736\ M$
and given theoretically by $y = Mgd^3 / 3E_2I_2$
so $E_2I_2 = gd^3 / 0.0821 = 36.75\ N\,m^2$
and for length, $d = 0.43$ m, the deflection was measured as $y = 0.006977\ M$
so $E_2I_2 = 37.26\ N\,m^2$
Therefore the flexibility of the shaft was taken as $E_2I_2 = 37\ N\,m^2$.

For the combination of aerofoil and shaft, the deflection at $z = 0$ due to a force Mg at $z = 0$ is given by standard beam theory as

$$y = \frac{Mg}{3}\left(\frac{d^3 - s^3}{E_2I_2} + \frac{s^3}{E_1I_1}\right)$$

For the shorter aerofoil, with AR = 1, $s = 0.25$ m, $d = 0.62$ m, the deflection was measured as $y = 0.02008\ M$ and given theoretically by
$y = Mg(0.223 / E_2I_2 + 0.0156 / E_1I_1) / 3$
Therefore, $E_1I_1 = 136\ N\,m^2$.

For the longer aerofoil, with AR = 2, $s = 0.5$ m, $d = 0.87$ m, the deflection was measured as $y = 0.04938M$ and given theoretically by
$y = Mg(0.5335 / E_2I_2 + 0.125 / E_1I_1) / 3$
Therefore $E_1I_1 = 183\ N\,m^2$.

9.6.2 Structural flexibility of the wind turbine shaft.

For length $h = 0.54$ m, the deflection was measured as $y = 0.002191\ M$ and given theoretically by
$y = Mgh^3 / 3EI$
so the flexibility of the shaft, $EI = 235\ N\,m^2$

9.6.3 Deflections of the aerofoil

There are three degrees of freedom - roll, pitch and yaw about the spherical bearing.
The steady-state resultant forces F_x and F_y and moment M_θ at the balance are being measured.
The aerofoils used were of light construction, connected to a very light shaft, which deforms under load. As the aerofoil is stiffer than the shaft, the shaft takes most of the bending. Only the first bending mode will be considered, as higher frequencies will be filtered out from the measurements.

Referring to Fig. 49, at a distance z from the top of the aerofoil, the displacements are x, y and θ, relative to moving axes in the undeflected position of the aerofoil. The deflection has steady and time-dependent components, i.e. $y = y_o(z) + y_1(z, t)$.
The forces are:
a) a uniformly distributed force F_o due to the steady components of aerodynamic force due to the freestream wind velocity, V, where $F_o = 0.5\,\rho\,V^2\,c\,C_L\cos\beta$;
b) a time-varying force $F_D(d - z)\tau$ due to the unsteady components of aerodynamic force due to the roll velocity, $(d - z)\,\phi'$, where $F_D = 0.5\rho\,V\,c\,i\omega\phi_o\,a\cos\beta$;
c) a structural inertia force in the roll direction only.

Thus the sectional aerodynamic force at z can be written as $[F_o + F_D\,(d - z)\tau]\,dz$
and the corresponding sectional inertia force at z on the aerofoil as $-\,m\omega^2\,\phi_o\tau\,(d - z)\,dz$.
The inertia force on the shaft below the aerofoil is negligible.
Therefore, putting $F_1 = [F_D - m\omega^2\,\phi_o]$ in the following:

The relative deflection at z in the y direction due to a force $F = F_o + F_1(d - z)\tau$ in the y-direction can thus be obtained using standard beam theory. There are two geometric conditions;

i) $0 < z < s$,

$$M = F_o\,z^2 / 2 + F_1\,\tau\,(3\,z^2 d - z^3) / 6$$

$$E_1 I_1 (dy/dz) = F_o\,z^3/6 + F_1\,\tau\,(4\,z^3\,d - z^4) / 24 + A_1$$

$$E_1 I_1\,y = F_o\,z^4/24 + F_1\,\tau\,(5\,z^4\,d - z^5)/ 120 + A_1\,z + B_1$$

ii) $s < z < d$,

$$M = F_o\,(2z - s)\,s / 2 + F_1\,\tau\,s(3z(2d - s) - 3sd + 2s^2) / 6$$

$$E_2 I_2 (dy/dz) = F_o\,(z^2 - sz)s / 2 + F_1\,\tau\,zs(3z(2d - s) - 6sd + 4s^2) / 12 + A_2$$

$$E_2 I_2\,y = F_o\,z^2\,(2z - 3s)s / 12 + F_1\,\tau\,z^2 s(z(2d - s) - 3sd + 2s^2) / 12 + A_2\,z + B_2$$

at $z = d$, $(dy/dz) = y = 0$, so

$$A_2 = -\,F_o\,(d - s)sd / 2 - F_1\,\tau\,sd(6d^2 - 9sd + 4s^2) / 12$$

$$B_2 = F_o\,sd^2\,(4\,d - 3\,s) / 12 + F_1\,\tau\,d^2 s[4\,d^2 - 5\,sd + 2\,s^2] / 12$$

Therefore, at z = s,

$E_2I_2(dy/dz) = -F_o(d-s)sd/2 + F_1\tau s[s^3 - 6d^3 + 9sd^2 - 4s^2d]/12$

$E_2I_2\, y = F_o s(-s^3 - 9sd^2 + 6s^2d + 4d^3)/12 + F_1\tau s(s^4 - 5s^3d + 11d^2s^2 - 11sd^3 + 4d^4)/12$

and so equating the gradient and deflection at z = s gives

$$A_1 = -\frac{F_o s^3}{6} - \frac{F_1\tau}{24}s^3(4d-s) + \frac{sE_1I_1}{12E_2I_2}\{-6F_o(d-s)d + F_1\tau[s^3 - 6d^3 + 9sd^2 - 4s^2d]\}$$

and

$$B_1 = \frac{F_o s^4}{8} + F_1\tau\frac{s^4(15d-4s)}{120} + \frac{sE_1I_1}{12E_2I_2}\{F_o(-s^3 - 3sd^2 + 4d^3) + F_1\tau d(-s^3 + 2ds^2 - 5sd^2 + 4d^3)\}$$

The relative deflection at any point z on the blade is then given by

$$y = \frac{1}{E_1I_1}\left(\frac{F_o(z^4 - 4zs^3 + 3s^4)}{24} + \frac{F_1\tau}{120}(5z^4d - z^5 - zs^3(20d - 5s) + 15s^4d - 4s^5)\right)$$
$$+\frac{F_o s}{12E_2I_2}\{-6zd(d-s) - s^3 - 3sd^2 + 4d^3\}$$
$$+\frac{F_1\tau s}{12E_2I_2}\{[s^3 - 6d^3 + 9sd^2 - 4s^2d]z - s^3d + 2s^2d^2 - 5sd^3 + 4d^4\}$$

The deflection due to the bending of the aerofoil is the $(1/E_1I_1)$ term, which is a very small part of the total, as can be seen from the photographs in Fig. 50, and it can be ignored to give

$$y = \frac{F_o s}{12E_2I_2}(-6zd(d-s) - s^3 - 3sd^2 + 4d^3)$$
$$+\frac{F_1\tau s}{12E_2I_2}([s^3 - 6d^3 + 9sd^2 - 4s^2d]z - s^3d + 2s^2d^2 - 5sd^3 + 4d^4)$$
$$= y_o(z) + y_1(z)\tau.$$

The corresponding deflection on the shaft below the aerofoil is

$$y = \frac{sF_o}{12E_2I_2}[2z^3 - 3sz^2 - 6(d-s)zd + d^2(4d - 3s)]$$
$$+\frac{sF_1\tau}{12E_2I_2}[2z^3d - 3z^2sd - sz^3 + 2s^2z^2 - zd(6d^2 - 9sd + 4s^2) + d^2[4d^2 - 5sd + 2s^2]]$$

9.6.4 Deflections of the wind turbine shaft

Similarly to the aerofoils, with the forces;

a) a steady force F_o at the hub due to the steady components of aerodynamic force due to the freestream wind velocity, V;

b) a time-varying force $F_D\tau$ at the hub due to the unsteady components of aerodynamic force due to the roll velocity, $h\phi'$;

c) a structural inertia force in the roll direction only, $= -m\omega^2\phi_o\tau z\,dz$

Thus the aerodynamic force at the hub, F_A is given by $[F_o + F_D\tau]$

and the corresponding inertia force at the hub is given by $-M\omega^2\phi_o\tau h$ in the y direction only.

The inertia force on the shaft is given by - $m\omega^2 \phi_o \tau$ (h - z) dz in the y direction only,
where M = 0.44 kg and m = 0.8 kg / m.
Therefore putting $F_1 = - m\omega^2 \phi_o$ and $F_2 = [F_D - M \omega^2 \phi_o h]$ in the following:

From Fig. 49, the relative deflection in the y direction at height z due to force
$F = F_o + F_2 \tau + F_1 (h - z)\tau$ in the y-direction can be obtained using beam theory:

$$EI(d^2y/dz^2) = (F_o + F_2 \tau)\, z + F_1 \tau \int_0^z (h - \zeta)\,(z - \zeta)\, d\zeta$$

$$= (F_o + F_2 \tau)\, z + F_1 \tau\, (hz^2/2 - z^3/6)$$

$$EI(dy/dz) = (F_o + F_2 \tau)\, z^2/2 + F_1 \tau\, (hz^3/6 - z^4/24) + A$$

$$EI\, y = (F_o + F_2 \tau)\, z^3/6 + F_1 \tau\, (hz^4/24 - z^5/120) + Az + B$$

At z = h, y = 0 = (dy/dz), so

$$A = - (F_o + F_2 \tau)\, h^2/2 - F_1 \tau\, h^4/8$$

$$B = (F_o + F_2 \tau)\, h^3/3 + 11\, F_1 \tau\, h^5/120$$

The relative deflection at any point z on the shaft is then given by

$$EI\, y = (F_o + F_2 \tau)\, (z^3 - 3\, h^2 z + 2h^3) / 6 + F_1 \tau\, (5hz^4 - z^5 - 15\, h^4 z + 11\, h^5) / 120$$

$$= y_o(z) + y_1(z)\, \tau + y_2(z)\, \tau.$$

where $y_o = \dfrac{F_o}{6EI}\,(z^3 - 3zh^2 + 2\, h^3)$

$$y_2 = \frac{F_2}{6EI}\,(z^3 - 3zh^2 + 2\, h^3)$$

$$y_1 = \frac{F_1}{120EI}\,(- z^5 + 5hz^4 - 15\, h^4 z + 11h^5)$$

As h = 0.54 m and EI = 235 N m^2, tip deflections are:

$$y_o = 0.2233\, F_o = 8.150\, \lambda\, (a - b\lambda)\ mm$$

$$y_2 = 0.2233\, F_2 = 0.2828\, f^3\ mm$$

$$y_1 = 0.0179\, F_1 = 0.1413\, f^2\ mm.$$

9.6.5 Natural frequency of the aerofoil

For natural free vibrations, the kinetic energy is given by

$$T = 0.5\, my'^2 \approx \frac{- m\omega_n^2\, [F_D - m\omega^2 \phi_o]^2\, s^2}{288\, E_2^2 I_2^2} \int_0^s \{z^2(s^3 - 6d^3 + 9sd^2 - 4s^2d)^2 + 2z(s^3 - 6d^3$$

$$+ 9sd^2 - 4s^2d)\,(- s^3d + 2s^2d^2 - 5sd^3 + 4d^4) + (- s^3d + 2s^2d^2 - 5sd^3 + 4d^4)^2\}\, dz$$

$$\approx \frac{- m\omega_n^2\, [F_D - m\omega^2 \phi_o]^2\, s^3}{864\, E_2^2 I_2^2} (s - d)^2\, \{s^6 - 9s^5d + 36s^4d^2 - 81s^3d^3 + 117s^2d^4$$

$$- 96sd^5 + 48d^6\}$$

and so for

$$AR = 1;\ T \approx - 2.452\, m\omega_n^2\, [F_D - m\omega^2 \phi_o]^2 \times 10^{-9}\ N\,m$$

$$AR = 2;\ T \approx - 1.223\, m\omega_n^2\, [F_D - m\omega^2 \phi_o]^2 \times 10^{-7}\ N\,m$$

and the potential energy by

$$V = 0.5\, F\, y \approx \frac{[F_D - m\omega^2 \phi_o]^2\, s}{24\, E_2 I_2} \int_0^s (d - z)\, \{z(s^3 - 6d^3 + 9sd^2 - 4s^2 d) - s^3 d + 2s^2 d^2 - 5sd^3 + 4d^4\}\, dz$$

$$\approx \frac{-[F_D - m\omega^2 \phi_o]^2\, s^2}{72\, E_2 I_2} (s - d)\, \{s^4 - 6s^3 d + 15s^2 d^2 - 18sd^3 + 12d^4\}$$

and so for

$AR = 1;\ V \approx 8.74\, [F_D - m\omega^2 \phi_o]^2 \times 10^{-6}$ N m

$AR = 2;\ V \approx 1.11\, [F_D - m\omega^2 \phi_o]^2 \times 10^{-4}$ N m

Therefore, the natural frequency is given by

$$\omega_n^2 = \frac{12 E_2 I_2}{ms(d - s)} \frac{\{s^4 - 6s^3 d + 15s^2 d^2 - 18sd^3 + 12d^4\}}{\{s^6 - 9s^5 d + 36s^4 d^2 - 81s^3 d^3 + 117s^2 d^4 - 96sd^5 + 48d^6\}}$$

which is approximately $3.432\, E_2 I_2 / msd^2(d - s)$

and so for

$AR = 1;\ \omega_n^2 = 7143,\ \omega_n = 84.5$ rad/s $= 13.5$ Hz

$AR = 2;\ \omega_n^2 = 1814,\ \omega_n = 42.6$ rad/s $= 6.8$ Hz

This natural frequency is several times larger than the forcing frequency, so resonance will be avoided.

9.6.6 Natural frequency of the wind turbine shaft

For natural free vibrations, the kinetic energy is given by

$$T = 0.5\, my'^2 \approx \frac{m\omega^2 F_2^2}{72\, E^2 I^2} \int_0^h \{z^6 - 6z^4 h^2 + 2z^3 h^3 + 9z^2 h^4 - 6zh^5 + h^6\}\, dz$$

$$+ \frac{m\omega^2 F_1^2}{28800\, E^2 I^2} \int_0^h \{z^{10} - 10hz^9 + 25h^2 z^8 + 30\, h^4 z^6 - 172\, h^5 z^5 + 110\, z^4 h^6$$

$$+ 225\, h^8 z^2 - 330\, zh^9 + 121\, h^{10}\}\, dz$$

$$\approx m\omega^2 h^7 (0.00615\, F_2^2 + 0.00106\, F_1^2 h^4) / E^2 I^2$$

and the potential energy by

$$V = 0.5\, F\, y \approx \frac{F_2^2 h^3}{12\, EI} + \frac{F_1^2}{240\, EI} \int_0^h (h - z)\, (-z^5 + 5hz^4 - 15\, h^4 z + 11h^5)\, dz$$

$$\approx \frac{F_2^2 h^3}{12\, EI} + \frac{F_1^2}{240\, EI} \int_0^h (z^6 - 6hz^5 + 5\, h^2 z^4 + 15h^4 z^2 - 26\, h^5 z + 11\, h^6)\, dz$$

$$\approx h^3 (0.0833\, F_2^2 + 0.013\, F_1^2 h^4) / EI$$

Therefore, the natural frequency is given by

$$\omega_n^2 = (EI / mh^4)\, \{0.083\, F_2^2 + 0.013\, F_1^2 h^4\} / \{0.00615\, F_2^2 + 0.00106\, F_1^2 h^4\}$$

for the structural effects with no wind, $F_1 = -m\omega^2 \phi_o = -7.9 f^2$ N/m^2

and $F_2 = -M\omega^2 \phi_o h = -2.435 f^2$ N, so

$\omega_n^2 = 13.30\,EI / mh^4$

and $\omega_n = 192$ rad/s(= 31 Hz)

This natural frequency is several times larger than the roll forcing and rotational frequencies, so resonance will be avoided.

9.6.7 Structural damping of the aerofoil

The damping derivative is given by $B = 2A\,\omega_n = 2m(d - z)\nu\omega_n\,dz$, so the sectional damping moment due to the deflection of the aerofoil can be estimated as $S(z) = B\,y' = 2\nu\,m\,\omega_n\,(d - z)\,(i\omega y_1\,\tau)\,dz$.

and the total structural damping moment is given by

$$S = 2\nu m\,\omega_n\,i\omega\tau \int_0^d y_1\,(d - z)\,dz$$

and putting $P = \int_0^d y_1\,(d - z)\,dz$, i.e.

$$P = \frac{F_1\,s}{12\,E_2I_2}\int_0^s (d - z)\,[z(s^3 - 6d^3 + 9sd^2 - 4s^2d) - s^3d + 2s^2d^2 - 5sd^3 + 4d^4]\,dz$$

$$+\frac{s\,F_1}{12\,E_2I_2}\int_s^d (d - z)\,[2z^3d - 3z^2sd - sz^3 + 2s^2z^2 - zd(6d^2 - 9sd + 4s^2) + d^2(4\,d^2 - 5\,sd + 2\,s^2)]\,dz$$

$$= \frac{F_1\,s^2}{36\,E_2I_2}[-s^5 + 7\,s^4d - 21\,s^3d^2 + 33\,s^2d^3 - 30\,sd^4 + 12\,d^5]$$

$$+\frac{s\,F_1}{120\,E_2I_2}[11\,d^6 - 53\,sd^5 + 105\,s^2d^4 - 110\,s^3d^3 + 65\,s^4d^2 - 21\,s^5d + 3\,s^6]$$

so for

AR = 1; $P = 2.07 \times 10^{-5}\,F_1$

AR = 2; $P = 2.33 \times 10^{-4}\,F_1$

This gives $S = 2\nu m\,\omega_n\,i\omega\tau\,P$

For AR = 1; $S = 0.011\,\nu\,f\,\tau\,F_1$

For AR = 2; $S = 0.062\,\nu\,f\,\tau\,F_1$

with the wind off, $F_1 \approx -m\omega^2\phi_o = -4.935\,f^2$ N/m^2 so the structural damping moment is given by

For AR = 1; $S = -0.054\,\nu\,f^3$ Nm

For AR = 2; $S = -0.306\,\nu\,f^3$ Nm

9.6.8 Structural damping of wind turbine shaft

As for the aerofoils;

The sectional damping derivative due to the deflection of the shaft is given by $B = 2A\,\omega_n$ $= 2\nu m(h - z)\omega_n\,dz$, so the sectional damping moment can be estimated as

$S = B\,y' = 2\nu m\,\omega_n\,(h - z)\,(i\omega y\,\tau)\,dz$.

so the total structural damping moment is given by

$$S = 2\nu m\omega_n i\omega\tau \int_0^h (h - z)\, y\, dz$$

and putting $P = \int_0^h (h - z)\, y\, dz$

$$= \frac{F_2}{6EI}\int_0^h (h - z)(z^3 - 3zh^2 + h^3)\, dz + \frac{F_1}{120EI}\int_0^h (h - z)\,(-z^5 + 5hz^4 - 15\, h^4 z + 11h^5)\, dz$$

$$= \frac{F_2}{6EI}\int_0^h (h^4 - 4\, zh^3 + 3z^2h^2 + hz^3 - z^4)\, dz$$

$$+ \frac{F_1}{120EI}\int_0^h (11h^6 - 26\, h^5 z + 15\, h^4 z^2 + 5h^2 z^4 - 6hz^5 + z^6)\, dz$$

$$= \{0.008333\ F_2 + 0.0262\, h^2 F_1\}h^5 / EI$$

so therefore,

Structural damping moment, $S = 2\omega\, \omega_n \nu\, mP$

with the wind off, $F_1 = - m\omega^2\phi_o = 7.89\, f^2\ N/m^2$ and $F_2 = - M\omega^2\phi_o h = 2.345\, f^2\ N$, so this is

$S = - 2\omega\, \omega_n \nu\, m(0.008333\, M + 0.0262\, mh)\, \omega^2\phi_o\, h^6 / EI = - 0.04\, \nu\, f^3$ Nm.

10. TEST RESULTS

These experiments were performed in the Fluids Laboratory at University College London between 27th March and 23rd September 1989.

10.1 Aerofoil tests

These tests were all performed at a nominal windspeed of V ≈ 13 m/s (except where stated) and at roll frequencies of f = 0, 1.5, 2.5 and 3.5 Hz. There was a gap of 300 mm between the wind tunnel floor and the bottom of the aerofoil in its mean position.
The parameters which were varied in the tests were:
Aspect ratio = 1 and 2.
Orientation angles, β = 0 to 90° in 15° intervals.
Frequencies, f = 0, 1.5 Hz, 2.5 Hz, 3.5 Hz.
Mean incidence angles, α = - 20° to 20° in 5° increments.
Orientation angles from 90° to 180° (i.e. following winds) can be calculated from these results by reversals, as shown in Fig. 67.

The following tests were performed:

AR	Orientation, β	mean incidence, α	Results Fig
1	45°	±5°, ±10°, ±15°, 20°	72, 73
2	45°	0, ±5°, ±10°, ±15°, ±20°	74, 75
1	0, 15°, 30°, 45°, 60°, 75°	- 15°	76, 77
1	0, 15°, 30°, 45°, 60°, 75°, 90°	15°	78, 79
2	0, 15°, 30°, 45°, 60°, 75°, 90°	-10°	80, 81
2	0, 15°, 30°, 45°, 60°, 75°, 90°	10°	82, 83

10.1.1 Steady force and moment coefficients

The steady lift and drag over the unstalled range are given by (at β = 45° and f = 0):
For AR = 1,
$C_L = 1.215 \sin \alpha$
$C_D = 0.01 + 1.498 \sin^2 \alpha$
$C_M = 0.2 \sin \alpha$
lever arm = 0.495 m
stall angle = 15°
which can be seen in Figs. 68 and 70. The yaw and drag do not fit very well, but that may be because they are small numbers, below the accuracy of the measuring technique.

For AR = 2,

$C_L = 1.8 \sin \alpha$

$C_D = 0.007 + 1.177 \sin^2\alpha$.

$C_M = 0.324 \sin \alpha$

lever arm = 0.62 m

stall angle = 20^o

which can be seen in Figs. 69 and 71.

These coefficients are shown as functions of α in Fig. 70 for AR = 1 and in Fig. 71 for AR = 2, for varying roll frequencies. The steady component is barely affected by the rolling.
The lift coefficients are 70 % of the theoretical value, and the drag coefficients are 115% of it, due to low Reynolds number effects and turbulence.

10.1.2 Structural inertia and added mass measurements

For the dynamic tests, the equipment does not record most of the inertia of the balance or any of its stiffness, as it is the difference between the motion of the top and bottom plates of the balance which is recorded.

Measurements of the structural moments with the wind off, (with $\alpha = \beta = 45^o$) gave:
(moments in Nm):

For AR = 1,

Roll inertia = $1.454\ f^2 - 0.033$

roll damping = $0.1335\ f^3 + 0.2$

Pitch inertia = $0.1\ f^2 + 0.284$

pitch damping = $- 0.078 + 0.1\ f$

Yaw inertia = $- 0.015\ f^2 + 0.0298$

yaw damping = $0.022 - 0.012\ f$

For AR = 2,

Roll inertia = $2.694\ f^2 + 0.17$

roll damping = $0.234\ f^3 - 0.5$

Pitch inertia = $- 0.044\ f^2 + 0.403$

pitch damping = $- 0.7 + 0.5\ f$

Yaw inertia = $0.0033\ f^2 - 0.005$

yaw damping = $0.025 + 0.02\ f$

These forces are due mainly to structural inertia forces and partly to aerodynamic added mass effects.

10.1.3 Damping and inertia coefficients

The results of the tests, showing the aerodynamic moments, with the structural components subtracted, are shown in Figs. 72 to 83.

Roll or pitch damping coefficient = roll or pitch damping moment / $0.5\rho V cs^3 f$

Roll or pitch inertia coefficient = roll or pitch inertia moment / $0.5\rho Vcs^3 f^2$

Yaw damping coefficient = yaw damping moment / $0.5\rho V c^2s^2 f$

Yaw inertia coefficient = yaw inertia moment / $0.5\rho V c^2s^2 f^2$

Fitting curves of the same form as in the theory of Chapter 5 to the measured data gives the experimental values:

Figs 72 and 74 are damping coefficients as functions of α, with curves of the theoretical form fitted. They follow the theoretical curve forms fairly well, although the coefficients are slightly different from their theoretical values.

Figs 73 and 75 are inertia coefficients as functions of α. Although the values for the longer aerofoil follow the theoretical curve forms fairly well, (except for drag, which is higher), the values for the shorter aerofoil have more scatter and it was not possible to fit curves of the correct form accurately, particularly for pitch and drag.

Figs 76, 78, 80, and 82 are damping coefficients as functions of β. It was possible to fit curves of the theoretical form for roll, pitch, lift and drag, although yaw behaved in a slightly different manner so that the data did not quite follow the curves.

Figs 77, 79, 81 and 83 are inertia coefficients as functions of β. Here, attempts to fit curves with the same coefficients to two different data sets have produced a compromise which does not quite fit either set. The fits for the longer aerofoil (Figs 81 and 83) are more successful than the fits for the shorter aerofoil.

10.1.4 Comparison of theoretical and experimental results

Using the theory of Chapter 5, with the above values of C_L, C_D and gap ratios, gives the following theoretical values.

$$\text{Roll damping moment} = 0.5\rho V s^3 \phi' \int_r^{r+1} F(k)\, c\eta^2 [a \cos\delta \cos\beta + C_{d0}(\cos^2\beta + 2\sin^2\beta) + A \sin\alpha(\cos^2\beta + 2\cos\delta \sin\beta)]\, d\eta.$$

$$= 0.5\rho V csh^2 \phi' F(k) \{E_1(\cos^2\beta + \alpha \sin\beta \cos\beta) + E_2(\cos^2\beta + 2\sin^2\beta) + E_3(\alpha \cos^2\beta + 2\alpha \cos\beta \sin\beta + 2\alpha^2 \sin^2\beta)\}$$

$$\text{Roll damping coefficient} = 2\pi\phi F(k) \{(E_1 + E_2 + E_3\alpha^2)\cos^2\beta + (E_1 + 2E_3)\alpha \cos\beta \sin\beta + 2(E_2 + E_3\alpha^2)\sin^2\beta\}$$

The aerodynamic inertia derivative,

$$\omega A_{\phi\phi} = 0.5\rho V s^3 \phi' \int_r^{r+1} c\eta^2 G(k) [a \cos\delta \cos\beta + C_{d0}(\cos^2\beta + 2\sin^2\beta) + A \sin\alpha(\cos^2\beta + 2\cos\delta \sin\beta)] d\eta.$$

$$\approx 0.5\rho V csh^2 \phi' G(k) \{E_1(\cos^2\beta + \alpha \sin\beta \cos\beta) + E_2(\cos^2\beta + 2\sin^2\beta) + E_3(\alpha \cos^2\beta + 2\alpha \cos\beta \sin\beta + 2\alpha^2 \sin^2\beta)\}$$

$$\text{Roll inertia coefficient} \approx \phi G(k) \{(E_1 + E_2 + E_3\alpha^2) \cos^2\beta + (E_1 + 2E_3) \alpha \cos\beta \sin\beta + 2(E_2 + E_3\alpha^2) \sin^2\beta\}$$

Using the following values;

AR = 1, r = 1.48, h = 0.495, F(k) = 0.5

AR = 2, r = 0.74, h = 0.62, F(k) = 0.8

gives:

	AR = 1		AR = 2	
Damping terms:	Theor.	Exp.	Theor.	Exp.
$E_1^* = 2\pi\phi F(k)\int a\eta^2 d\eta =$	5.408	5.8842	5.720	6.032
$E_2^* = 2\pi\phi F(k)\int C_{d0}\eta^2 d\eta =$	0.031	0.1286	0.020	0.0804
$E_3^* = 2\pi\phi F(k)\int A\eta^2 d\eta =$	3.336	3.9228	2.022	3.0547
$E_5^* = 2\pi\phi F(k)\int a\chi\eta d\eta =$	-0.142	0.2572	-0.039	0.3416
$E_6^* = 2\pi\phi F(k)\int C_{d0}\chi\eta d\eta =$	-0.001	0.0096	0.00	0.008
$E_7^* = 2\pi\phi F(k)\int A\chi\eta d\eta =$	1.463	0.75	1.508	0.6
Inertia terms:				
$I_1^* = \phi F(k)\int a\eta^2 d\eta =$	-0.861	-2.12	-0.910	-1.1254
$I_2^* = \phi F(k)\int C_{d0}\eta^2 d\eta =$	-0.005	-0.005	-0.0032	-0.012
$I_3^* = \phi F(k)\int A\eta^2 d\eta =$	-0.531	-0.65	-0.322	-0.5024
$I_5^* = \phi F(k)\int a\chi\eta d\eta =$	0.023	0.1286	0.0062	-0.1206
$I_6^* = \phi F(k)\int C_{d0}\chi\eta d\eta =$	0.0001	-0.0032	0.00	0.0015
$I_7^* = \phi F(k)\int A\chi\eta d\eta =$	-0.233	-0.0964	-0.240	0.0659

The E_1^* values are slightly higher than predicted because of dynamic stall delay. This is particularly noticeable in the inertia coefficients. The E_2^* and E_3^* values are higher, owing to the rough surface of the aerofoil and to dynamic drag effects such as shed vorticity from the top of the wingsail. The yawing moments are not well predicted, partlicularly the lift term, but this may be due to some structural inertia effects owing to the lack of homogeneity of the internal construction of the aerofoils.

10.2 Wind Turbine tests

All these tests were performed at roll frequencies of f = 0, 1, 1.5 and 2 Hz, as the structure of the model would not stand up to higher frequencies.

Lever arm = 0.57 m. Blade diameter = 0.67 m.

Note - the blade pitch ψ was measured at the root of the blade, where the adjustment was performed.

The parameters which were varied in the tests were:

Wind velocities, V = 4.5 m/s and 9.3 m/s.

blade root pitch angles, $\psi = 20^o, 30^o, 40^o$.

Orientation angles, $\gamma = 0^o, 15^o, 30^o$.

Frequencies, f = 1, 1.5 and 2 Hz.

Yaw angles, $\delta = -10^o, 0, 10^o, 20^o, 30^o$.

The tests performed, and the measured blade rotation frequencies and tip speed ratios for each test, are listed below:

			V = 4.5 m/s (1.6" collar)		V = 9.3 m/s (1.25" collar)	
ψ	γ	δ	Ω (Hz)	λ	Ω (Hz)	λ
20°	0	0	9.19	4.29	22.00	4.98
30°	0	0	6.51	3.04	14.03	3.18
40°	0	0	4.49	2.10	9.81	2.22
20°	0	10°	7.66	3.57	21.62	4.90
30°	0	10°	5.34	2.49	11.64	2.64
40°	0	10°	4.48	2.10	10.10	2.29
20°	0	20°	7.11	3.32	19.88	4.50
30°	0	20°	5.46	2.55	13.77	3.12
40°	0	20°	4.26	1.99	8.93	2.02
20°	0	-10°	9.80	4.57	17.66	4.00
30°	0	-10°	6.74	3.15	14.82	3.36
40°	0	-10°	4.51	2.11	10.01	2.27
20°	15°	0	10.27	4.79	18.98	4.30
30°	15°	0	7.71	3.60	13.59	3.08
40°	15°	0	4.84	2.26	9.91	2.24
20°	15°	10°	9.37	4.38	18.38	4.16
30°	15°	10°	6.59	3.08	12.84	2.91
40°	15°	10°	4.81	2.24	9.41	2.13
20°	15°	20°	8.86	4.14	16.81	3.81
30°	15°	20°	6.38	2.98	13.26	3.00
40°	15°	20°	4.79	2.24	9.63	2.18

From the above, it can be seen that (approximately) the tip-speed ratio, $\lambda \approx 88/\psi$.
The wind turbine did not always self-start at $\psi = 20^o$, and sometimes required a push.

10.2.1 Steady moment and power coefficients

The steady roll and pitch moment coefficients and the power output coefficient are shown in Figs. 84 to 93, as indicated in the following table.

Figure	x axis	γ	V (m/s)	variable
84	δ	0	4.5	$\psi = 20^o, 30^o, 40^o$
85	λ	0	4.5	$\delta = 0, \pm 10^o, 20^o$
86	δ	0	9.3	$\psi = 20^o, 30^o, 40^o$
87	λ	0	9.3	$\delta = 0, \pm 10^o, 20^o$
88	δ	15^o	4.5	$\psi = 20^o, 30^o, 40^o$
89	λ	15^o	4.5	$\delta = 0, 10^o, 20^o$
90	δ	15^o	9.3	$\psi = 20^o, 30^o, 40^o$
91	λ	15^o	9.3	$\delta = 0, 10^o, 20^o$
92	δ	30^o	9.3	$\psi = 20^o, 30^o, 40^o$
93	λ	30^o	9.3	$\delta = 0, 10^o, 20^o, 30^o$

Figures 84, 86, 88, 90 and 92 are steady moment and power coefficients as functions of the yaw angle, δ. The roll and power coefficients are approximately constant, and pitch is proportional to δ for $\gamma = 0$. Figures 92 and 93 have no pitch measurements because the pitch gauge on the balance became damaged.
Figs. 85, 87, 89, 91 and 93 are steady moment and power coefficients as functions of the tip speed ratio, λ. There is some scatter on the data, but it follows the theory reasonably, enabling the following equations to be derived from the results:

For $\gamma = 0^o$, f = 0, the steady lift and drag coefficients are given by:
For V = 4.5 m/s;
$C_L = -\lambda \sin\delta\,(0.50 - 0.35\lambda)$
$C_D = -\lambda \cos\delta\,(0.258 - 0.132\,\lambda)$
$C_P = \lambda^2\,(0.221 - 0.029\,\lambda)$
For V = 9.3 m/s;
$C_L = \lambda \sin\delta\,(0.11 - 0.10\,\lambda)$
$C_D = -\lambda \cos\delta\,(0.042 - 0.09\,\lambda)$
$C_P = \lambda^2\,(0.108 - 0.0144\,\lambda)$
which indicates that the optimum value of λ to yield the highest C_P is between $\lambda = 7.5$ and 7.6.

10.2.2 Structural and added mass measurements

Measurements of the structural and added mass moments with the wind switched off (with $\delta = \gamma = 0$) gave: (moments in Nm)

Roll inertia = $2.261f^2 - 0.182$

roll damping = $-0.242 f^3 + 0.6035$

Pitch inertia = $0.051 f^2 + 0.29$

pitch damping = $-0.177 f + 0.263$

which are mainly structural inertia and damping moments.

10.2.3 Damping and inertia coefficients

The results of these tests, showing the aerodynamic moments after the structural components have been subtracted, are shown in figs. 94 to 117, as listed in the following table:

x axis	γ	ψ	δ	Figure number (V = 4.5 m/s)	Figure number (V = 9.3 m/s)
δ	0	20°	-	94	106
δ	0	30°	-	95	107
δ	0	40°	-	96	108
λ	0	-	-10°	97	109
λ	0	-	0	98	110
λ	0	-	10°	99	111
δ	15°	20°	-	100	112
δ	15°	30°	-	101	113
δ	15°	40°	-	102	114
λ	15°	-	0°	103	115
λ	15°	-	10°	104	116
λ	15°	-	20°	105	117

Figs 94 to 117 present non-dimensionalised coefficients, and should therefore all be the same. They agree generally, although there are slightly higher values for $\psi = 20°$ than for $\psi = 40°$, and for V = 4.5 m/s than for V = 9.3 m/s, which may be due to slight variations in the measurement of ψ and V.

The constraint of fitting the same coefficients to two different data sets prevents any of the curves from fitting any of the data absolutely when taken in isolation, but by considering the two data sets together, the curves can be seen to fit between them.

The curves fitted to the data have the following equations. For forces in the direction of the mean force (not the instantaneous force);

For V = 4.5 m/s:

'Drag' damping coefficient = $0.62 (1 - 0.081 \lambda + 0.419 (1 - 0.308 \lambda) \sin \delta) \lambda f$

'Lift' damping coefficient = $0.28 (1 - 0.161 \lambda + (1 - 0.357 \lambda) \sin \delta) \lambda f$

'Drag' inertia coefficient = $- 0.4 (1 - 0.075 \lambda + 0.375 (1 + 0.20 \lambda) \sin \delta) \lambda f^2$

'Lift' inertia coefficient = $- 0.17 (1 - 0.117 \lambda + 2.06(1 - 0.114 \lambda) \sin \delta) \lambda f^2$

For V = 9.3 m/s:

'Drag' damping coefficient = $0.28 (1 - 0.25 \lambda + 0.536 (1 - 0.27 \lambda) \sin \delta) \lambda f$

'Lift' damping coefficient = $0.37 (1 - 0.23 \lambda + 0.27 (1 - 0.62 \lambda) \sin \delta) \lambda f$

'Drag' inertia coefficient = $- 0.3 (1 - 0.133 \lambda + 0.117 (1 - 0.571 \lambda) \sin \delta) \lambda f^2$

'Lift' inertia coefficient = $- 0.16 (1 - 0.125 \lambda - 0.375 (1 - 0.583 \lambda) \sin \delta) \lambda f^2$

Therefore, for V = 4.5 m/s:

Roll damping coefficient = $(- 0.28 \sin \gamma + 0.62 \cos \gamma + 0.045 \lambda \sin \gamma - 0.05 \lambda \cos \gamma$
$- (0.28 - 0.1 \lambda) \sin \gamma \sin \delta + (0.26 - 0.08 \lambda) \cos \gamma \sin \delta) \lambda f h$
$\approx 0.3534 (1 - 0.081 \lambda - 0.452(1 - 0.2 \lambda) \gamma + 0.419(1 - 0.307 \lambda) \delta - 0.452 (1 - 0.357 \lambda) \gamma \delta) \lambda f$

Pitch damping coefficient = $(0.28 \cos \gamma + 0.62 \sin \gamma - 0.045 \lambda \cos \gamma - 0.05 \lambda \sin \gamma$
$+ (0.28 - 0.1 \lambda) \cos \gamma \sin \delta + (0.26 - 0.08 \lambda) \sin \gamma \sin \delta) \lambda f h$
$\approx 0.16 (1 - 0.16 \lambda + 2.214(1 - 0.081 \lambda) \gamma + (1 - 0.357 \lambda) \delta + 0.93 (1 - 0.308 \lambda) \gamma \delta) \lambda f$

Roll inertia coefficient = $(- 0.4 \cos \gamma + 0.17 \sin \gamma + 0.03 \cos \gamma \lambda - 0.02 \lambda \sin \gamma$
$- (0.15 + 0.03 \lambda) \cos \gamma \sin \delta + (0.35 - 0.04 \lambda) \sin \gamma \sin \delta) \lambda f^2 h$
$\approx - 0.228 (1 - 0.075 \lambda - 0.425 (1 - 0.117 \lambda) \gamma + 0.875 (1 - 0.11 \lambda) \delta - 0.375 (1 + 0.2 \lambda) \gamma \delta) \lambda f^2$

Pitch inertia coefficient = $(- 0.4 \sin \gamma - 0.17 \cos \gamma + 0.03 \sin \gamma \lambda + 0.02 \lambda \cos \gamma$
$- (0.15 + 0.03 \lambda) \cos \gamma \sin \delta - (0.35 - 0.04 \lambda) \sin \gamma \sin \delta) \lambda f^2 h$
$\approx - 0.097 (1 - 0.147 \lambda + 2.35(1 - 0.075 \lambda) \gamma + 0.88(1 + 0.2 \lambda) \delta + 2.06 (1 - 0.11 \lambda) \gamma \delta) \lambda f^2$

For V = 9.3 m/s:

Roll damping coefficient = $(0.28 \cos \gamma - 0.37 \sin \gamma - 0.07 \lambda \cos \gamma + 0.085 \lambda \sin \gamma$
$+ 0.15 (1 - 0.27 \lambda) \cos \gamma \sin \delta - 0.1 (1 - 0.62 \lambda) \sin \gamma \sin \delta) \lambda f h$
$\approx 0.16 (1 - 0.25 \lambda - 1.32 (1 - 0.23 \lambda) \gamma + 0.536 (1 - 0.27 \lambda) \delta - 0.357 (1 - 0.62 \lambda) \gamma \delta) \lambda f$

Pitch damping coefficient = $(0.28 \sin \gamma + 0.37 \cos \gamma - 0.07 \lambda \sin \gamma - 0.085 \lambda \cos \gamma$
$+ 0.15 (1 - 0.27 \lambda) \sin \gamma \sin \delta + 0.1 (1 - 0.62 \lambda) \cos \gamma \sin \delta) \lambda f h$
$\approx 0.211 (1 - 0.23 \lambda + 0.756 (1 - 0.25 \lambda) \gamma + 0.405 (1 - 0.27 \lambda) \delta + 0.27 (1 - 0.62 \lambda) \gamma \delta) \lambda f$

Roll inertia coefficient = $(- 0.3 \cos \gamma + 0.16 \sin \gamma + 0.04 \lambda \cos \gamma - 0.02 \lambda \sin \gamma$
$- 0.035(1 - 0.571 \lambda) \cos \gamma \sin \delta - 0.06 (1 - 0.583 \lambda) \sin \gamma \sin \delta) \lambda f^2 h$
$\approx - 0.171 (1 - .133 \lambda - 0.532 (1 - 0.125 \lambda) \gamma + 0.117 (1 - 0.571 \lambda) \delta + 0.2 (1 - 0.583 \lambda) \gamma \delta) \lambda f^2$

Pitch inertia coefficient = $(- 0.3 \sin \gamma - 0.16 \cos \gamma + 0.04 \lambda \sin \gamma + 0.02 \lambda \cos \gamma$
$- 0.035 (1 - 0.571 \lambda) \cos \gamma \sin \delta + 0.06(1 - 0.583 \lambda) \sin \gamma \sin \delta) \lambda f^2 h$
$\approx - 0.0912 (1 - 0.125 \lambda + 1.875(1 - 0.133 \lambda) \gamma + 0.219 (1 - 0.57 \lambda) \delta - 0.375 (1 - 0.583 \lambda) \gamma \delta) \lambda f^2$

10.3 Comparison with theory

Revised theory gives the steady coefficients as:

$C_L = \lambda \sin\delta\,(a_1 - b_1\lambda)$

$C_D = \lambda \cos\delta\,(a_2 - b_2\lambda)$

and experiment gives these coefficients as:

For V = 4.5 m/s;

$a_1 = -0.500$ $\quad b_1 = -0.350$

$a_2 = -0.258$ $\quad b_2 = -0.132$

For V = 9.3 m/s;

$a_1 = -0.110$ $\quad b_1 = -0.10$

$a_2 = -0.042$ $\quad b_2 = -0.090$

Analogous to the theory of section 6.2, the component of the section lift force measured perpendicular to the instantaneous apparent wind velocity vector V_U is given by

$$L = 0.5\rho V_U^2 \pi R^2 (R\Omega/V_U)\sin(\delta + d\alpha)\,[a_1 - b_1 R\Omega/V_U]$$

$$\approx 0.5\rho\, V_A^2 \pi R^2 \lambda\,[a_1 \sin\delta - b_1\lambda\sin\delta + u\,[a_1(\sin\delta\cos\gamma + \cos\delta\sin\gamma) - b_1\lambda\cos\delta\sin\gamma]$$

The corresponding component of section drag force is

$$D = 0.5\rho V_U \pi R^3 \Omega\cos(\delta + d\alpha)\,[a_2 - b_2 R\Omega/V_U]$$

$$\approx 0.5\rho V_A^2 \pi R^2 \lambda[a_2\cos\delta - b_2\lambda\cos\delta + u\,(a_2[\cos\gamma\cos\delta - \sin\gamma\sin\delta] + b_2\lambda\sin\delta\sin\gamma)]$$

The roll moment coefficient is given by

$$R = h(L\sin(\gamma - d\alpha) - D\cos(\gamma - d\alpha))$$

$$= h\,(1/H)\,[L\sin\gamma - D\,(\cos\gamma + u)]$$

$$= 0.5\rho\, V_A^2 \pi R^2 \lambda\, h\{a_1\sin\delta\sin\gamma - b_1\lambda\sin\delta\sin\gamma - a_2\cos\delta\cos\gamma + b_2\lambda\cos\delta\cos\gamma$$

$$+u\,[a_1\cos\delta\sin^2\gamma - b_1\lambda(\cos\delta\sin^2\gamma - \sin\delta\sin\gamma\cos\gamma) - a_2(-\sin\gamma\cos\gamma\sin\delta + \cos\delta)$$

$$- b_2\lambda(\sin\delta\cos\gamma\sin\gamma - \cos\delta\sin^2\gamma)]\}$$

The roll damping derivative is

$$C_B(\delta, \gamma, \lambda) = \lambda\,\{(a_1 - b_1\lambda)\cos\delta\sin^2\gamma + (a_2 + b_1\lambda - b_2\lambda)\sin\delta\sin\gamma\cos\gamma - (a_2 - b_2\lambda)\cos\delta$$

$$- b_2\lambda\cos\delta\cos^2\gamma\}$$

Assuming small δ gives

$$= \lambda\{-a_2\cos^2\gamma + (a_2 + b_1\lambda - b_2\lambda)\delta\sin\gamma\cos\gamma + (a_1 - b_1\lambda - a_2 + b_2\lambda)\sin^2\gamma\}$$

$$= \lambda(A_1\cos^2\gamma + A_2\cos\gamma\sin\gamma + A_3\sin^2\gamma)$$

where	V = 4.5 m/s	V = 9.3 m/s
$A_1 = -a_2$	$= 0.258$	$= 0.042$
$A_2 = (a_2 + (b_1 - b_2)\lambda)\,\delta$	$= -\delta(0.258 + 0.218\lambda)$	$= -\delta(0.042 + 0.01\lambda)$
$A_3 = (a_1 - a_2 - \lambda(b_1 - b_2))$	$= (-0.242 + 0.218\lambda)$	$= (-0.068 + 0.01\lambda)$

The pitch moment coefficient is given by

$$C_P = - C_L \cos(\gamma - d\alpha) - C_D \sin(\gamma - d\alpha)$$

$$= - 0.5\rho V_A^2 \pi R^2 \lambda h(a_1 \sin\delta \cos\gamma - b_1 \lambda \sin\delta \cos\gamma + a_2 \cos\delta \sin\gamma - b_2 \lambda \cos\delta \sin\gamma$$
$$+ u [a_1 (\cos\delta \sin\gamma \cos\gamma + \sin\delta) - b_1 \lambda (\cos\delta \sin\gamma \cos\gamma + \sin\delta \sin^2\gamma)$$
$$- a_2 \sin^2\gamma \sin\delta + b_2 \lambda (\sin\delta \sin^2\gamma + \cos\delta \sin\gamma \cos\gamma)])$$

The pitch damping derivative is

$$C_B(\delta, \gamma, \lambda) = - \lambda [a_1 (\cos\delta \sin\gamma \cos\gamma + \sin\delta) - b_1 \lambda (\cos\delta \sin\gamma \cos\gamma + \sin\delta \sin^2\gamma)$$
$$- a_2 \sin^2\gamma \sin\delta + b_2 \lambda (\sin\delta \sin^2\gamma + \cos\delta \sin\gamma \cos\gamma)]$$
$$= - \lambda h [(a_1 - b_1 \lambda + b_2 \lambda) \cos\delta \sin\gamma \cos\gamma + a_1 \sin\delta - (a_2 + b_1 \lambda - b_2 \lambda) \sin\delta \sin^2\gamma]$$

Assuming small δ gives

$$= - \lambda [a_1 \delta \cos^2\gamma + (a_1 - b_1 \lambda + b_2 \lambda) \sin\gamma \cos\gamma + (a_1 - a_2 - b_1 \lambda + b_2 \lambda) \delta \sin^2\gamma]$$
$$= \lambda(A_1 \cos^2\gamma + A_2 \cos\gamma \sin\gamma + A_3 \sin^2\gamma)$$

where	V = 4.5 m/s	V=9.3 m/s
$A_1 = - a_1 \delta$	$= 0.5 \delta$	$= 0.11 \delta$
$A_2 = - (a_1 - (b_1 - b_2)\lambda)$	$= 0.5 - 0.218 \lambda$	$= 0.11 + 0.01 \lambda$
$A_3 = - (a_1 - a_2 - (b_1 - b_2)\lambda) \delta$	$= - (0.242 - 0.218 \lambda) \delta$	$= (0.068 - 0.01 \lambda) \delta$

Figures 118 - 121 demonstrate the comparison of this theory with the experimemtal data. The upper two graphs on each page are for V = 4.5 m/s and the lower two are for V = 9.3 m/s. It can be seen that the reduction in roll damping at higher λ is not always predicted by the theory. The prediction of roll damping is reasonable, although the prediction of pitch damping is not very close. This may to some extent be accounted for by an experimental innaccuracy in the measurement of the δ angle, which was set by hand and measured by eye.

The values at $\gamma = 15^o$ were better predicted than the values at $\gamma = 0$. This may be because rolling the wind turbine produces apparent incidence effects other than those accounted for by the quasistatic theory.

11. DISCUSSION

11.1 Theoretical Results

The conflict mentioned earlier between maximum propulsive performance and optimum damping requirements is demonstrated in Figures 12, 13 and 16, where settings of α which give a higher thrust will give a lower damping coefficient for $\beta^* > 90^o$.

Figure 122 shows the performance coefficients C_T, C_H, C_B and qC_A generated by all seven devices, with the following representative mean settings:

	$\beta^* < 90^o$		$\beta^* > 90^o$	
a) Wingsail	$\alpha = 20^o$	$\varepsilon = 0$	$\alpha = -20^o$	$\varepsilon = 180^o$
b) HAWT, $\lambda = 7$	$\delta = -20^o$	$\varepsilon = 180^o$	$\delta = 20^o$	$\varepsilon = 0$
c) VAWT, $\lambda = 7$	$\psi = -10^o$	$\varepsilon = 180^o$	$\psi = 10^o$	$\varepsilon = 0$
d) Flettner rotor	$\lambda = -4$	-	$\lambda = 4$	-
e) Turbosail	$\alpha = 15^o$	$\varepsilon = 0$	$\alpha = -15^o$	$\varepsilon = 180^o$
f) Fin stabiliser	$\delta = 10^o$	$\varepsilon = 0$	$\delta = 10^o$	$\varepsilon = 0$
g) Rudder stabiliser	$\delta = 10^o$	$\varepsilon = 0$	$\delta = 10^o$	$\varepsilon = 0$

It can be seen that the highest roll damping coefficients in beam winds are achieved by wind turbines and fin stabilisers.

Even though a wind turbine produces less thrust per unit frontal (swept) area than a Flettner rotor, this deficiency is offset by the corresponding reduction of hydrodynamic resistance of the hull produced by better roll damping. Also, although wind turbines develop less roll damping than fin stabilisers, they do generate an additional thrust force. For a given ship, a wind turbine should provide more damping with less disadvantages than fin stabilisers, e.g. no cavitation, plus a propulsive increment. Although a wind turbine will produce a more stable ship, this will be at the cost of a small angle of heel (2^o - 3^o) in a beam wind.

The stabilising characteristics of aerodynamic devices depend mainly on the apparent wind direction. High-lift devices such as wingsails, Flettner rotors and Cousteau Turbosails, like soft sails, produce very little damping in beam winds, and so do not make effective stabilisers. On the other hand, high-drag devices, such as wind turbines, will give a high passive damping moment, but very low active damping in beam winds and so it is probably not worthwhile to use these devices actively.

For all hydrodynamic devices, the roll damping moment is generated by the ship speed, V_S. The roll damping is virtually independent of wave direction, but it is zero when V_S is zero.

Wind turbines can work in harbour when wind speeds are higher than the cut-in value necessary to drive the rotor to its design speed of rotation. Although wind turbines may be less efficient stabilisers than fins at high ship speeds, they will be more efficient at low ship speeds. As can be seen from Fig. 123, comparing a fin stabiliser with a HAWT, the fin stabiliser can only be effective when the ship is moving, and produces very little damping at very low ship speeds (e.g. in harbour). The HAWT, however, will produce damping at zero ship speed, as long as the wind is blowing.
In the example in the figure, the HAWT had D = 10 m, h = 2.83 m, $C_B = 4.2$,
so $B_A = 1616 \sqrt{V_S^2 + V_T^2}$.
The fin had area = 0.6 m^2, h = 2.42 m, $C_B = 3$, so $B_H = 5403\ V_S$.

For combinations of aero- and hydro-dynamic stabilisers, the magnification factor is $1 / \omega_e (B_S + B_A + B_H)$ and the fractional reduction in resonant roll amplitude caused by the device is $\delta B = (B_A + B_H) / (B_S + B_A + B_H)$. For active fins, representative values are $B_H \approx 10 B_S$, and so $\delta B = 0.91$ for operation with active fins alone. For aerodynamic devices alone, if $B_A = B_S$ then $\delta B = 0.5$, a value which is comparable with bilge keels alone. For combinations of devices, if $B_A = B_S$ then $\delta B = 0.92$, and it is seen that aerodynamic stabilisers produce little additional increase in damping when used in combination.

The first Japanese wind assisted motor ship, SHIN AITOKU MARU, has been described by Matsumoto et al (1982). The principal particulars of the ship are:

Length between perpendiculars	66 m
Beam	10.6 m
Draught	4.2 m
Block coefficient	0.67
Metacentric height GM	0.78 m
Natural roll period	9 s
Natural roll frequency, ω_ϕ	0.7 rad/s
Service speed, V_S	6 m/s
Deadweight	1600 tonnes
Weight displacement, Δ = 2000 tonnes	19.62 MN
Wingsail area	194 m^2
Roll lever arm h_a	8 m
Bilge keel area (each side)	11.3 m^2
Rudder area	7.2 m^2

On this experimental ship, the rudder and bilge keels were made rather larger than usual. The large inertia of a high block coefficient ship requires the installation of substantial anti-rolling capacity.

Assuming also that:

Hydrodynamic roll lever arm h_h	6 m
True wind speed V_T	12 m/s
Apparent wind speed V_A	15 m/s
Wave amplitude ξ_o	3 m
Wavelength	180 m
Wave number k	0.035
Static heel angle, $\phi_s = k\,\xi_o$	$0.105 = 6^o$

the static heeling moment required to produce a 6^o heel in still water is $\Delta\ GM\ \phi_s = 1.6$ MNm. The equivalent heeling moment produced by stabilisers is given by $0.5\rho V^2 A\ h\ C_H$ which becomes, for hydrodynamic devices, $110.7\ A_h\ C_H$ (kN/m) and for aerodynamic devices, $1.1\ A_a\ C_H$ (kN/m). Thus, in order to obtain the *total* required moment from hydrodynamic devices we require $A_hC_H = 14.5\ m^2$ compared with $A_aC_H = 1460\ m^2$ from aerodynamic devices.

The total moment can be provided by the following hydrodynamic devices,

(i) 8 low aspect ratio fins, with $C_H = 0.5$, area $3.62\ m^2$ each;

(ii) 4 high aspect ratio fins, with $C_H = 1.5$, area $2.41\ m^2$ each.

In a beam wind, the following aerodynamic devices, suitability sized for the SHIN AITOKU MARU,

(a) HAWT with $C_H = 2.34$, diameter $D_0 = 10$ m;

(b) VAWT with $C_H = 1.22$, $D_0 = 12$ m, span = 8.5 m;

(c) Flettner rotor with $C_H = 2.2$, $D_0 = 2$ m, height = 20 m;

(d) Turbosail with $C_H = 1.8$, $D_0 = 2$ m, height = 20 m;

can thus each contribute 12.6%, 8.5%, 6% and 5% respectively, to the required static heeling moment, and produce static heel angles of 0.7^o, 0.5^o, 0.35^o and 0.3^o respectively. These will be additive, for the case of multiple devices. It should be noted that wingsails generate low heeling moments in beam winds and make insignificant contributions to the roll damping.

By definition, the damping derivatives are given by

$B_H = 0.5\ \rho_w V_S A_h h_h^2\ C_{Bh}$

$B_A = 0.5\ \rho_a V_A A_a h_a^2\ C_{Ba}$

As $\rho_w \approx 840\ \rho_a$, $V_A \approx 2.5\ V_S$ and $h_a \approx 1.33\ h_h$, equality of damping derivatives requires $A_aC_{Ba} = 190\ A_hC_{Bh}$. Therefore, comparing the preceding aerodynamic devices with hydrodynamic fin stabilisers having

(i) low AR and $C_B = 3$;

(ii) high AR and $C_B = 8$

yields the following results:

Device		Equivalent to a fin of area	
		(i)	(ii)
(a) HAWT:	$C_B = 4.2, D_0 = 10$ m	0.6 m^2	0.22 m^2
(b) VAWT:	$C_B = 1.22, D_0 = 12$ m, H = 8.5 m	0.22 m^2	0.08 m^2
(c) Flettner rotor:	$C_B = 1.84, D_0 = 2$ m, H = 20 m	0.13 m^2	0.05 m^2
(d) Turbosail:	$C_B = 1.8, D_0 = 2$ m, H = 20 m	0.13 m^2	0.05 m^2

11.2 Comparison of Theoretical and Experimental Results

11.2.1 Aerofoils

For aerofoils, owing to dynamic effects, both lift and drag derivatives are higher than predicted by quasistatic theory. The experimental results produced curves of approximately the same form as the theoretical curves, but of slightly higher magnitude. All conclusions drawn from the theoretical results are still valid, and the theory can be made realistically accurate by the inclusion of a simple dynamic factor.

11.2.2 Wind turbines

The wind turbine experimental results were not so close to those given by the somewhat crude wind turbine theory used. However, as was revealed by the literature survey, most work on propellers has been for axial flow only, and the small amount of work which has covered wind turbines at an angle of yaw has been for steady flow only. Therefore, there had been very little on which to base the original theory. Attempts to rewrite rotor theory with angles of yaw were not considered to be worthwhile while there was no data to check them against, and there was no time to do so later, but this is where any further work should commence.

The yawed flow induces a velocity difference across the face of the wind turbine, and the rolling motion also produces a fluctuating velocity difference. The actual damping therefore varies from the quasisteady damping in having extra components which will be functions of the yaw angle, δ. These extra components complicate the flow and create unsteady effects, some of which contribute to the damping. However, the experimental results are broadly similar to the theoretical predictions, so the foregoing conclusions should still hold in general. A full finite element rotor theory analysis taking into account all apparent velocity and incidence effects due to the yaw and roll would cost a fairly large amount of computer time without producing very much better overall results than the crude theory, as there would still be factors which would not be picked up correctly, such as dynamic stall effects on the rotating blades, concerning which different authors in the literature theory disagree, even for steady axial flow. Further experiments are likely to be of more use than rotor theory in predicting the actual overall behaviour of wind turbines rolling at an angle of yaw. For the aerodynamic design of the turbine

design of the turbine blades, i.e. the distribution of chord thickness, twist and section, a finite element (or equivalent) analysis would be necessary, but should be augmented with empirical dynamic stall data.

A wind turbine subjected to random excitations may not necessarily behave according to the superposition theory, and no measurements have yet been performed from which any conclusions may be drawn as to whether it will do so. The wind turbine differs from those objects on which the superposition theory has been validated in that it is rotating itself in addition to the motion of its supporting ship or tower. It is likely that the ratio of the turbine rotation frequency to the frequency of the support motion may have the effect of weighting the superposition function.

12. Conclusions and implications

The aerodynamic theory and experimental characteristics of wind energy devices have been illustrated in the contexts of motion damping of wind assisted ships and offshore wind turbines.

The pursuit of oscillatory motion reduction techniques is likely to bring large rewards in fuel savings since substantial reductions in ship resistance and improvements in propeller efficiency should take place. Reduction of the motions is always beneficial, even if no thrust is generated.
Further work is necessary to determine reliable hull hydrodynamic derivatives so that in combination with the aerodynamic derivatives estimates of induced resistance can be made. The reduced motion of the ship in a seaway will then provide an equivalent augment of thrust thus reducing the overall fuel consumption of the ship.

For wind assisted ships, there is a conflict between maximum propulsion performance and the most effective damping requirements. In apparent wind directions of greater than 90°, there is a conflict of requirements between the yaw angle setting to give maximum roll damping and that for maximum thrust. The principal benefits of roll damping occur for the higher aspect ratios but structural strength would tend to limit the span of marine aerofoils to, say, an aspect ratio of 5. Sweepback does not appear to offer any aerodynamic or structural advantages for wingsails. Taper reduces the magnitude of the roll damping derivative. Maximum roll damping is achieved for all true wind directions, γ, at the highest ship speed to wind speed ratio, σ. Roll damping can become negative for some values of σ in quartering seas. However, if $\sigma > 1$, as it usually is for cargo ships at sea, the roll damping derivative is positive for all γ, as the critical value of β^* will never be reached.

Horizontal axis wind turbines appear to be the most effective devices for wind assisted ships, and will certainly produce a more stable ship. Whether or not other operational disadvantages of wind turbines on ships can be accepted is a matter for debate and would need to be the subject of another investigation.

Even though a wind turbine produces less thrust per unit frontal (swept) area than a Flettner rotor, this deficiency is offset by the corresponding reduction of resistance produced by better roll damping. The benefits are further increased if other types of stabilisers can be eliminated. Present stabilisation methods either take up cargo space (e.g. tanks) or else create additional resistance (e.g. fins and bilge keels) and a wind turbine should be able to provide more damping with less of these disadvantages, plus a propulsive increment also.

For offshore wind turbines, the damping provided by the turbine is of the order of magnitude of the structural damping, which means that fixed towers may be made less stiff (and therefore cheaper) than would be necessary without the turbine present. When the wind speed is above the rated speed, it may be advantageous to yaw the turbine into the wave direction to damp the wave motions, gaining damping without losing power.

It is to be expected that further advances in wind assisted ship propulsion will, in general, result from retrofitting wind assist devices to existing ships. It is necessary to combine hull motion derivatives for existing ships with the aerodynamic derivatives previously examined. Wind assisted ships require hulls that possess sufficient static stability to support the sails in a combination of strong winds and large waves. Consequently, high block coefficients and low slenderness ratios are required but for this type of geometry, reliable measurements of hydrodynamic derivatives are scarce, and so the relevant hydrodynamic derivatives have not been determined. The implications of these results require further study when reliable values of the hull damping derivatives can be determined.

12.1 Suggestions for Further Research

Areas in which further research needs to be done are:

a) Materials, considering stiffness and fatigue effects.

b) Aerodynamic effects such as dynamic stall on rotating blades, and its structural effect on the tower or ship.

c) Wind and wave data for offshore areas.

d) Interference effects, for multiple devices on ships or for windfarms.

e) Reliability and low maintenance requirements.

f) Wind turbines in yaw.

other parameters which should be varied if the work is extended are:

a) Tunnel velocity V, for Reynolds number effects.

b) Roll amplitude ϕ.

c) Lever arm.

d) Higher roll frequencies.

e) Static heel angle ϕ_o.

f) Twist, taper, sweep, profile and planform of aerofoils.

g) Flexibility for aeroelastic effects.

h) Wind shear, turbulence and surface roughness.

i) Number of blades for wind turbine.

REFERENCES

Abbott, I.H. and Von Doenhoff, A.E.; Theory of wing sections, Dover, 1949

Aertssen, G.; *Proc. 12th ITTC*, 1969, p. 210
Service performance and trials at sea.

Anderson, M.B.; *Proc. 1st. British Wind Energy Assoc. Workshop*, 1979, p. 57 - 67
Horizontal axis wind turbines in yaw.

Anderson, M.B.; *Proc. 3rd. BHRA Int. Symp. Wind Energy Systems*, 1980, p. 357 - 374
A vortex wake analysis of a HAWT and a comparison with a modified blade element theory.

Atkinson, G.T., Wilmshurst, S.M.B. and Wilson, D.M.A.; *Proc..8th. British Wind Energy Assoc. Conf.*, Cambridge, 1986, p. 187 - 196
Blade dynamics and yawing activity of a HAWT in a sheared wind.

Atkinson, G.T., Wilmshurst, S.M.B. and Wilson, D.M.A.; *Proc. 9th British Wind Energy Assoc. Conf.*, Edinburgh, 1987, p. 71 - 78
The aerodynamics of rotors in yaw.

Baree, M.S.; Ph.D. thesis, Newcastle University, 1985
Added power required by ships in bad weather.

Basu and Hancock; *J. Fluid Mech.* 87, 1978, p. 159
Unsteady motion of two-dimensional aerofoils in incompressible inviscid flow.

Bauer, A.B.; *Proc. 3rd. AIAA Symp. on Aero/Hydronautics of sailing*, 1971
Sailing at all points of the compass.

Bauer, D.; *Proc. Seminar Offshore Wind Power Mega Project*, R.Ae.Soc, 1988, Ch. 6, 25pp
Design, fabrication and installation implications for offshore wind turbine support structures.

Bearman, P.W., Downie, M.J. and Graham, J.M.R.; *Proc. 14th. Naval Hydro. Symp.*, 1983
Calculation method for seperated flows with applications to oscillatory flow past cylinders and roll damping of barges.

Bergeson, L., Greenwald, C.K. and Hanson, T.F.; *Proc. 13th AIAA Symp. on Aero/Hydronautics of sailing*, 1983, p. 125 - 137
Magnus rotor test and evaluation for auxiliary propulsion.

Bergeson, L. and Greenwald, C.K.; *Proc. Int. Symp. Windship Technology*, Southampton, 1985, Vol. A., p. 45 - 114
Sail-assist developments 1979-1985.

Bishop, R.E.D., Price, W.G. and Temarel, P.; *Int. Ship. Prog.* 27, 1980, p.54 - 65
Hydrodynamic coefficients of some swaying and rolling cylinders of arbitrary shape.

Blackford, B.L.; *Proc. Int. Conf. Sail-assisted Comercial Fishing Vessels*, 1983, p.393 - 409
Windmill thrusters for commercial fishing craft.

Blackford, B.L.; *Proc. Int. Symp. Windship Technology*, Southampton, 1985, Vol. B, p. 267 - 282
Windmill thrusters: a comparison of theory and experiment.

Bose, N. and Small, G.H.; *Proc. Int. Symp.Windship Tech.*,Southampton,1985, Vol.B, p.283-296
Wind turbine drives - test results from the FALCON.

Bose, N. and Wilkinson, J.A.; *Wind Engineering,* Vol 9, 1985, p. 9 - 23
Performance tests on the wind turbine powered catamaran REVELATION.

Bratt, J.B.; Aeronatical Research Council *Report and Memo.* 2773, 1950
Flow patterns in the wake of an oscillating aerofoil.

British Standards Institute; Code of Practice CP3, Chapter V, Part 2 (1972, amended 1986)
Code of basic data for the design of buildings - wind loads.

Brooke, A.K.; *Trans. RINA,* Vol. 132, 1990
Evaluation of theoretical methods for determining roll damping coefficients.

Broome, D.R.; *Trans. RINA,* Vol. 124, 1982, p.193-204
Roll/yaw coupling measurements from an autopilot-controlled free-running ship model.

Brown, C.H.; 'Nicholl's Seamanship and Nautical Knowledge', 18th Ed, 1953, Brown, Son and Ferguson

Brown, D.T., Eatock Taylor, R. and Patel, M.H.; *J. Fluid Mech.*, Vol. 129, 1983, p. 385 - 407
Barge motions in random seas - a comparison of theory and experiment.

Burton, A.L. and Roberts, S.C.; *Proc. 7th BWEA Conf.*, Oxford, 1985, p. 269-277
The outline design and costing of 100m diameter wind turbines in an offshore area.

Carley, J.B.; *Proc. 4th. Ship Control Systems Symp.*, 1975 p.2/172 - 2/194
Feasibility study of steering and stabilising by rudder.

Chadwick, J.H.; *Trans. SNAME,* Vol. 63, 1955 p.237 - 280
On the stabilisation of roll.

Charrier, B., Constans, J., Cousteau, J.Y., Daif, A, Malavard, L., and Quinio, J.L.; *Proc. Int. Symp. Windship Technology,* Southampton, 1985, Vol. B, p. 39 - 60.
The Fondation Cousteau and wind ship propulsion, 1980 - 85.

Clayton, B.R. and Filby, P.; *Proc. 3rd BritishWind Energy Assoc. Conf.*, 1981, p. 172-184
Wind turbine wake studies.

Clayton, B.R. and Filby, P.; *Proc. 4th Brit.ish Wind Energy Assoc. Conf.*, 1982, p. 214 - 224
Measured effects of oblique flows and change in blade pitch angles on the performance and wake developments of model wind turbines.

Clayton, B.R.; *Proc. Int. Symp. Windship Technology,* Southampton, 1985, Vol.A, p. 251 - 276
BWEA initiative on wind assisted ship propulsion.

Clayton, B.R. and Sinclair, F.M.; UCL Mech. Eng. Dept. Report no. 88/10, 1988, 37pp.
Motion damping of ships fitted with marine aerofoils.

Clayton, B.R. and Sinclair, F.M.; *Trans. RINA,* Vol. 131, 1989, p. 121 - 133
Motion damping of ships fitted with marine aerofoils.

Clayton, B.R. and Sinclair, F.M.; *Trans. RINA* , Vol. 132, 1990, p.339 - 348
A comparison of the effectiveness of aerodynamic and hydrodynamic roll stabilisation methods.

Connoly, J.E.; *Trans. RINA* , Vol. 111, 1969, p. 21-48
Rolling and its stabilisation by active fins.

Constans, J.; *Proc. Regional Conf. Sail-Motor Propulsion,* Manila, 1985, p. 49 - 70
Alcyone, daughter of the wind - the ship of the future.

Cowley, W.E. and Lambert, T.H.; *Proc. 4th Ship Control Systems Symp.,* 1975, Vol.2, p.195 - 213
Sea trials on a roll stabiliser using the ship's rudder.

Cox, G.G. and Lloyd, A.R.; *Trans. SNAME,* Vol. 85, 1977, p. 51-93
Hydrodynamic design basis for navy ship roll motion stabilisation.

Dahlberg, J.A., Ronsten, G, Dexin, H. and Jinyin, W.; *Proc. European Wind Energy Conf.,* Glasgow, 1989
Wind tunnel measurements of load variations for a yawed wind turbine with different hub configurations.

Davies, D.E.; *Aeronautical Research Council Report and Memo.* 3804, 1978
Theoretical determination of subsonic oscillatory airforce coefficients.

Davies, T.O.; *Proc. Seminar Offshore Wind Power Mega Project,* R.Ae.Soc, 1988, Ch.3, 8pp
Configuration and design of a offshore wind turbine generator.

Denise, J.P.F.; *Trans. RINA,* Vol. 125, 1983, p. 255 - 268
On the roll motion of barges.

Desmarais, R.N.; *J.Aircraft* Vol. 16, 1979, p. 441 - 447
Accurate numerical evaluation of modified Struve functions occurring in unsteady aerodynamics.

Det Norske Veritas (DnV); Rules for the design, construction and inspection of offshore structures. Part 3, Chapter 1, July 1989.

Dixon, J.C.; *Proc. 3rd British Wind Energy Assoc. Conf.,* Cranfield, 1981, p. 80-87
Large offshore wind turbines: System design and economics.

Dixon, J.C. and Swift, R.H.; *Proc. 4th Brit. Wind Energy Assoc. Conf.,* 1982, p. 299-306
Structure design for compliant-tower offshore wind turbines.

Dixon, J.C. and Swift, R.H.; *Wind Engineering,* Vol.10, 1986, p. 21-30
Wave forces and scaling effects on offshore wind turbines.

Dixon, J.C. and Swift, R.H.; *Wind Engineering,* Vol. 10, 1986, p. 64-77
Offshore wind power systems: a review of developments and comparison of National studies.

Ewing, J.A.; *Int. Symp. Dynamics Marine Vehicles and Structures in waves,* 1974, p. 41-46
Some results from the Joint North Sea Wave Project of interest to engineers.

Falkner, V.M.; Aeronautical Research Council, *Report and Memo.* 2591, 1947
The solution of lifting-plane problems by vortex-lattice theory.

Faltinsen, O.M. and Michelsen, F.C.; *Int. Symp. Dynamics of Marine Vehicles and Structures in Waves*, 1974, p.91 - 106
Motions of large structures in waves at zero Froude number.

Firestein, G.; *Proc. Int. Symp. Windship Technology*, Southampton, 1985, Vol. B, p.23 - 38
Dynamic response of a wingsail mast to unsteady aerodynamic loads including ship motion effects.

Frank, W.; NSRDC Rept. 2357, Washington, 1967.
Oscillation of cylinders in or below the free surface of deep fluids.

Fujii, H. and Takahashi, T.; *Proc. Int. Conf. on Stability of ships*, 1975
Experimental study on lateral motions of a ship in waves.

Fujino, M. and Yoon, B.S.; *Int. Ship Prog.* Vol. 33, 1986, p. 159-172
A practical method of estimating ship motions and wave loads in large amplitude waves.

Garrad, A.D.; *Proc. 9th British Wind Energy Assoc. Conf.*, Edinburgh, 1987, p. 79-84
The use of finite element methods for wind turbine dynamics.

Giesing, J.P.; *J.Aircraft*, Vol. 5, 1968 p.135
Non-linear two-dim. unsteady potential flow with lift.

Gifford, E.W.H.; *Proc. Int. Conf. Sail Assisted Commercial Fishing Vessels*, 1983, p. 386-392
The Tunny rig - a variable camber flexible wingsail.

Gigliobianco, G.; *Proc. 16th AIAA/SNAME Symp. on Aero/Hydro. of sailing*, 1986, p.106-119
A vertical axis propelled catamaran.

Grim, O.; Proc. 12th ITTC, 1969, p. 688
Nonlinear phenomena in the behaviour of a ship in a seaway.

Hamada, N.; *Proc. Regional Conf. Sail-motor propulsion*, 1985, p.117 - 132
The development in Japan of modern sail asisted ships for energy conservation.

Hardell, R. and Ljungstrom, O.; *Proc. 2nd BHRA Int. Symp. Wind Energy Systems*, 1978, Vol. B, p. 8.85-113, also in *Wind Engineering* Vol. 3, 1979, p. 23-51
Offshore based wind turbine systems, OS-WTS for Sweden - a systems concept study.

Hasselman, K. et al; *Deutsche Hydro. Zeitschr.* Reihe A8.12, 1973, p. 1-95
Measurements of wind wave growth and swell decay during the Joint North Sea Wave Project, JONSWAP.

Herapath, R.G., Woolard, M.G. and Griffiths, M.G.; *Proc. 1st Brit. Wind Energy Assoc.Conf.*, Cranfield, 1979, p.68 - 77
Blade design and construction for a HAWT.

Hess, J.L. and Smith, A.M.O.; *Prog. Aero. Sci.* Vol. 8, 1966 p.1
Calculation of potential flow about arbitrary bodies.

Inglis, R.B. and Price, W.G.; *Trans. RINA* Vol. 124, 1982, p.141-158
A three dimensional ship motion theory - comparison between theoretical predictions and experimental data of the hydrodynamic coefficients with forward speed.

Jackson, I.A.; Mech. Eng. Proj. Rep., University College London, 1986, 95pp.
Wind Assisted Ship Propulsion.

Jacobs, W.R. and Tsakonas, S.; *J. Ship. Res* Vol. 17, 1973, p. 129 - 139
Propeller loading-induced velocity field by means of unsteady lifting surface theory.

Jordan, P.F.; *J.Aircraft* Vol. 15, 1978, p. 626 - 633
Reliable lifting surface solutions for unsteady flow.

Jφrgensen, H.D. and Prohaska, C.W.; *Proc. 11th ITTC*, 1966, p. 123 - 125
Wind resistance.

K'allström, C.G.; *Proc. 6th. Ship Control Syst. Symp.*, 1981, Vol 2.
Control of yaw and roll by a rudder / fin - stabiliser system.

Kaplan, P.; *Proc. 11th ITTC*, 1966, p. 393-396
Lecture notes on nonlinear theory of ship roll motions in a random seaway.

Kerr, D.; *Wind Engineering* , Vol. 10, 1986, p. 47-61
Support structures for an offshore array of VAWTs.

Kerwin, J.E. and Lee, C.S.; *Trans. SNAME*, Vol. 86, 1978, p. 218-253
Prediction of steady and unsteady marine propeller performance by numerical lifting surface theory.

Kountzeris, A., Roberts, J.B. and Gawthrop, P.J.; *Trans. RINA*, Vol. 132, 1990
Estimation of ship roll parameters from motion in irregular seas.

Lan, C.E.; *J. Aircraft* Vol. 11, 1974 , p. 518 - 527
A quasi-vortex-lattice method in thin wing theory.

Lewis, E.V. and Numata, E.; *Trans. SNAME*, Vol. 68, 1960, p. 510-547
Ship motions in oblique seas.

Lindley, D., Simpson, P.B., Hassan, U. and Milborrow, D.; *Proc. 3rd Int. Symp. Wind Energy Systems*, Copenhagen, 1980
Assessment of offshore siting of wind turbine generators.

Lloyd, A.J.R.M.; *Trans. RINA* , Vol. 117, 1975, p. 233-254
Roll stabiliser fins - a design procedure.

Loukakis, T.A. and Sclavounos, P.D.; *J.Ship.Res*, Vol. 22, 1978, p. 1 - 19
Some extensions of the classical approach to strip theory of ship motions, including the calculation of mean added forces and moments.

MacCamy, R.C. and Fuchs, R.A.; U.S. Army Corps of Engineers, Beach Erosion Board, Tech. Memo. 69.11954
Wave forces on piles, a diffraction theory.

Madsen, H.A.; *Proc. 7th British Wind Energy Assoc. Conf.*, Oxford, 1985, p.147 - 154
The actuator cylinder: a flow model for vertical axis wind turbines.

Malavard, L.; *Comptes Rendus de L'Acad. des Sciences.* La Vie des Sciences 1, 1984, p.57 - 72
Un nouveau propulseur èolien de navire.

Mandel, P.; 'Principles of Naval Architecture', 1967, Ed. J.P. Comstock, SNAME, Ch. 8

Manners-Spencer, J. and Edmunds, A.; *Proc. Int. Conf. Sail Assisted Fishing Vessels,* Tarpon Springs, 1983, p. 410-424
Fishing vessels with the Aerosystems wingsail.

Mathisen, J.B. and Price, W.G.; *Trans. RINA* Vol. 127, 1985, p. 295-307
Estimation of ship roll damping coefficients.

Matsumoto, N., Inoue, M. and Sudo, M.; *Proc. 2nd. Int. Conf. Stability of Ships and Ocean Vehicles,* Tokyo, 1982, p. 451 - 464
Operating performance of a sail equipped tanker in waves and wind.

Milborrow, D.J.; *Proc. 7th British Wind Energy Assoc. Conf.*, Oxford, 1985, p. 85-94
Changes in areofoil characteristics due to radial flow on rotating blades.

Morino, L., Chan, L.T. and Suciu, E.O.; *AIAA J.* , Vol. 13, 1975, p. 368-374
Steady and oscillatory subsonic and supersonic aerodynamics around complex configurations.

Morison, J.R., O'Brien, M.P., Johnson, J.W. and Schaaf, S.A.; *Petrol. Trans. Am. Inst. Mining Metal. Eng.* Vol. 189, 1950, p. 149-154.
The forces exerted by surface waves on piles.

Morisseau, K.C.; *Proc. Int. Conf. Sail Assisted Fishing Vessels,* 1983, p. 362 - 385
Advanced wind propulsion devices - current status and potential.

Murata, M., Tsuji, M., and Watanabe, T.; *Trans. NECIES* ,Vol. 98, 1981, p.75 - 85
Aerodynamic characteristics of a 1600 dwt sail-assisted tanker.

Nance, C.T.; *Proc. Int. Symp. Windship Technology,* Southampton, 1985, Vol. A, p. 1-18
Outlook for wind assistance.

Nielsen, P.; *Proc 4th BHRA Int. Symp. Wind Energy Systems,* 1982, p. 35-46
The wind power programme of the Ministry of Energy and the electric utilities in Denmark.

Ochi, M.K.; *2nd. Int. Conf. Behaviour of Offshore Structures,* 1979, p. 75 - 86.
A series of JONSWAP wave spectra for offshore structure design.

Patel, M.H.; 1989, 'Dynamics of Offshore structures', Butterworths.

Rainey, R.C.T.; *Proc. RINA Symp. Wind Prop. of Commercial Ships,* London, 1980, p. 97-116
The wind turbine ship.

Robinson, R.W., Stoddart, A.W. and Rainey, R.C.T.; *The Naval Architect*, 1984 , p. 284-285
The prediction of extreme roll motions in irregular beam seas.

Robinson, R.W. and Stoddart, A.W.; *Trans. RINA* Vol. 129, 1987 p.65-79
An engineering assessment of the role of non linearities in transportation barge roll response.

Rowe, W.S. and Cunningham, H.J.; *J. Aircraft* Vol. 21, 1984 , p. 420
On the convergence of unsteady generalised aerodynamic forces.

Sakata, R., Yamagami, Y, Okamoto, H., Ikebuchi, T. and Nema, K.; *Naval Arch. and Ocean Eng.* Vol. 21, 1983, p. 98 - 112
On the hydrodynamic forces acting on box type vessels and their motions.

Salvesen, N., Tuck, E.O. and Faltinsen, O.; *Trans. SNAME*, Vol. 78, 1970, p. 250
Ship motions and sea loads.

Satchwell, C.J. and Mays, J.H.; *Proc. Int. Conf. Sail Assisted Commercial Fishing Vessels*, Tarpon Springs, 1983, p. 259-291
Linearised performance analysis of sailing and motor sailing vessels.

Satchwell, C.J.; *Proc. Int. Symp. Windship Technology*, Southampton, 1985, Vol. B, p. 1-22
Aerodynamic design of marine aerofoils.

Satchwell, C.J.; Ship Science Rept. 27, Southampton University, 1986, 40pp.
Marine aerofoil motion damping and related propulsive benefits.

Satchwell, C.J.; *Proc. Seminar Offshore Wind Power Mega Project*, R.Ae.Soc, 1988, Ch.13, 27pp
Moored floating platforms for wind turbines.

Schwanecke, H.; 14th ITTC, Vol. 3, 1975, p. 357 - 397
Comparative calculation on unsteady propeller blade forces.

Sharpe, D.J.; *Proc. 6th. British Wind Energy Association Conf.*, Reading, 1984, p.146 - 159
Requirements and developments of the multiple streamtube theory for the aerodynamic performance of VAWTs.

Simpson, P.B. and Lindley, D.; *Proc. 2nd BWEA Conf.*, Cranfield, 1980, p. 173-185
Offshore siting of wind turbine generators in U.K. waters.

Simpson, P.B.; *Proc. Seminar Offshore Wind Power Mega Project*, R.Ae.Soc, 1988, Ch.2, 20pp
Turbine configuration and design.

Sinclair, F.M.; MSc. Thesis, Imperial College, 1982
Blade interference in vertical axis wind energy machines.

Sinclair, F.M. and Clayton, B.R.; *Proc. 10th. British Wind Energy Association Conf.*, London, 1988, p. 269 - 276
The use of wind energy devices as ship stabilisers.

Sinclair, F.M. and Clayton, B.R.; *Proc. European Wind Energy Assoc. Conf.*, Glasgow, 1989
The effects of wave loading on offshore wind turbines.

Sinclair, F.M. and Clayton, B.R.; *Wind Engineering* Vol 13, no.6, 1990, p. 276 - 292
Excitation and damping forces on offshore wind turbines.

Skogman, A.; *Proc. Int. Symp. Windship Technology*, Southampton, 1985, p. B 201 - 226
The practical meaning of lateral balance for a sail assisted research vessel.

Small, G.; Rept. NAOE-85-47, Glasgow University, 1985
Performance calculations for a wind turbine using liftline theory.

Smith, A.M.O.; *Proc. 7th ONR Symp. on Naval Hydro*, 1968
Recent progress in the calculation of potential flows.

Strickland, J.H.; *Proc. 5th ASME Wind Energy Symp*, 1986, p. 7-17
A review of aerodynamic analysis methods for vertical axis wind turbines.

Swanson, W.M.; *ASME J.Basic Eng.* Vol. 83, 1961, p. 461-470
The Magnus effect: a summary of investigations to date.

Swift, R.H. and Dixon, J.C.; *Proc. 4th Brit. Wind Energy Assoc.*, Cranfield, 1982, p. 291-298
Design wave forces for offshore structures.

Takagi, M; *Int. Symp. Mar. Vehicles and Struct. in waves*, 1974
An examination of the ship motion theory as compared with experiments

Tasai, F.; *Proc. 12th ITTC*, 1969 p.677
Improvements in the theory of ship motions in longitudinal waves.

Tasai, F.; *Proc. 13th ITTC*, 1972 p.918
The state of the art of calculations for lateral motions.

Townsin, R.L. and Kwon, Y.J.; *Trans. RINA* , Vol. 125, 1983, p. 199-208
Approximate formula for speed loss due to added resistance in wind and waves.

Ueno, K., Nakamura, J., Satoo, N. and Tachiki, M.; *Proc. 11th ITTC*, 1966, p.103
Some experiments of rolling effect on the ahead resistance of ships.

U.K. Dept. Energy; Offshore installations: Guidance on design, construction and certification, 4th. Ed, HMSO, 1990

Van Berlekom, W.B., Tråg̊ardh, P. and Dellhag, A.; *Trans. RINA* Vol. 117, 1975 p.41-60
Large tankers - wind coefficients and speed loss due to wind and sea.

Van Berlekom, W.B.; *Trans. NECIES* Vol. 97, 1981 p.123-134
Wind forces on modern ship forms - effects on performance.

Van Oortmersson, G.; *Proc. 9th ONR Symp. on Naval Hydro.*, 1972, p.957-1002
Some aspects of very large structures in waves.

Vassilopoulos, L;. *J. Ship. Res.* Vol. 15, 1971 p. 289-294
Ship rolling at zero speed in random beam seas with nonlinear damping and restoration.

Vaughan, H.; *Trans. RINA* Vol. 127, 1985, p. 247-256
Three-dimensional motions of ships and platforms in waves.

Vossers, G., Swaan, W.A. and Rijken, H.; *Trans. SNAME*, Vol. 68, 1960, p. 364-450
Experiments with series 60 models in waves.

Vugts, J.H.; *Proc. 12th ITTC*, 1969, p.758

The coupled roll-sway-yaw performance in oblique waves.

Walker, J.G.; *Proc. Int. Symp. Windship Technology*, Southampton, 1985, Vol. B, p. 83-96

A high performance automatic wingsail auxiliary propulsion system for commercial ships.

Walker, J.G.; Lecture to Southern Branch of RINA/I.Mar.E., 4/12/86

Watanabe, T., Endo, Y., Nakanishi, K. and Takeda, K.; *Proc. 12th AIAA Symp. on Aero/ hydronautics of sailing*, 1982, p. 238 - 249

Sail-equipped motorship 'Shin Aitoku Maru' and studies on a larger ship.

Watkins, C.E., Runyan, H.L. and Woolston, D.S.; NACA Rept. 1234, 1955

On the kernel function of the integral equation relating the lift and downwash distributions of oscillating finite wings in subsonic flow.

Watkins, C.E., Woolston, D.S. and Cunningham, H.J.; NASA Report R-48, 1959

A systematic kernel function procedure for determining aerodynamic forces on oscillating or steady finite wings at subsonic speeds.

Welnicki, W.; *Trans. RINA* ,Vol. 110, 1968, p. 479 - 484

Method of estimation of wind influence upon the course keeping ability of ships with large superstructures.

Wilkinson, J.A.; Amateur Yacht Research Society no. 105 , 1989, p.9 - 24

Windmill boat 'Revelation'. The ideal performance of the wind turbine propelled boat.

Wilkinson, J.A.; Private communication, 1989

Williams, A. and Liljenberg, H.; *Trans. SNAME*, Vol. 91, 1983, p.125 - 148

Revival of the Flettner rotor - beneficial or not for merchant vessels, fishing boats and recreational craft.

Yamanouchi, Y. and Ando, S.; *Proc. 11th ITTC*, 1966, p. 404

Experiments on a Series 60, $C_B = 0.7$ ship model in oblique regular waves.

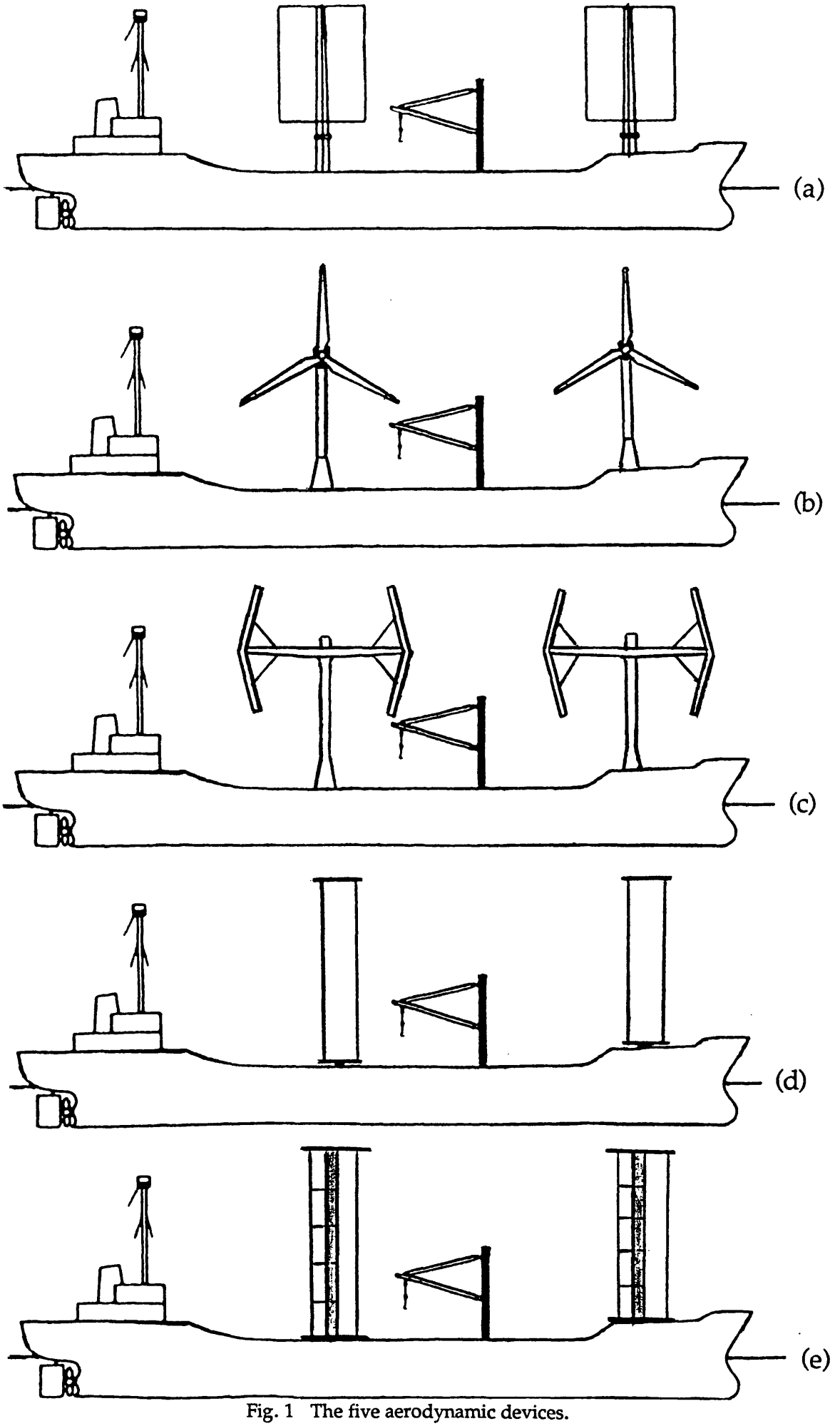

Fig. 1 The five aerodynamic devices.

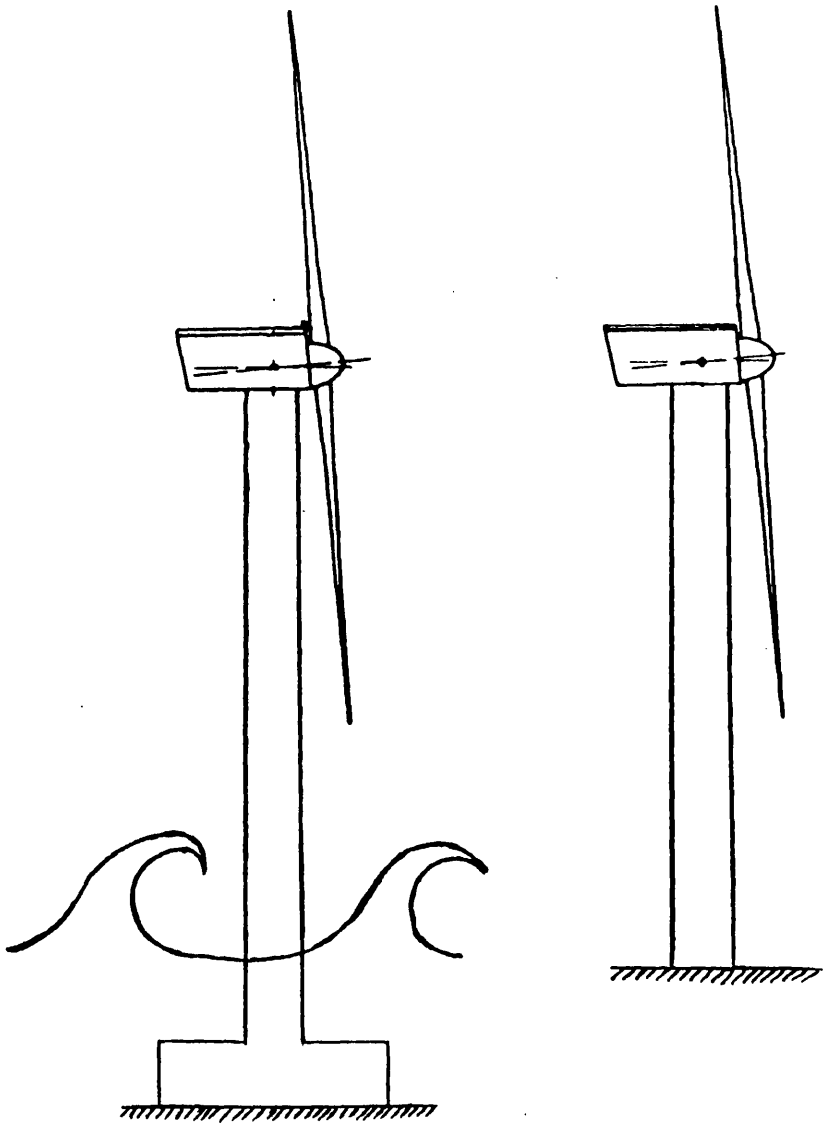

Fig. 2a Comparison of offshore and land based wind turbines.

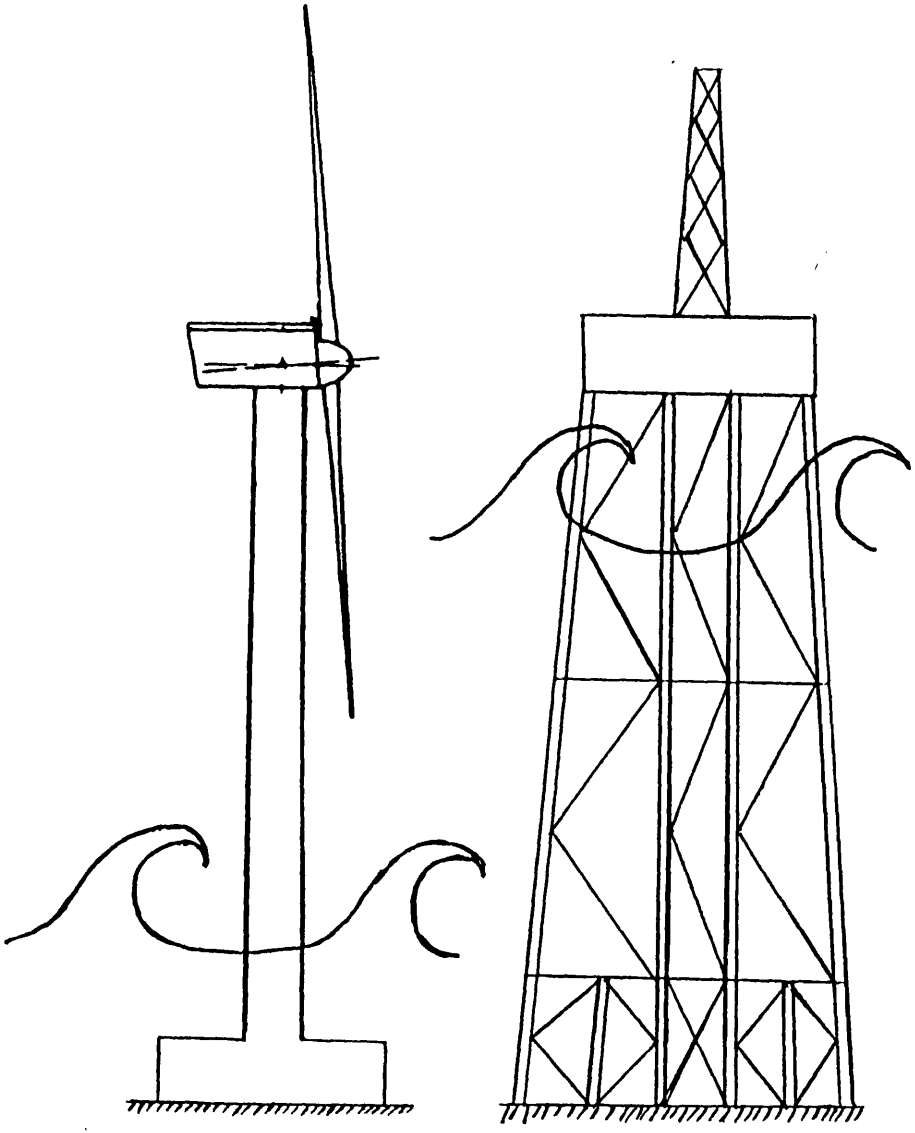

Fig. 2b Comparison of oil rig and offshore wind turbine.

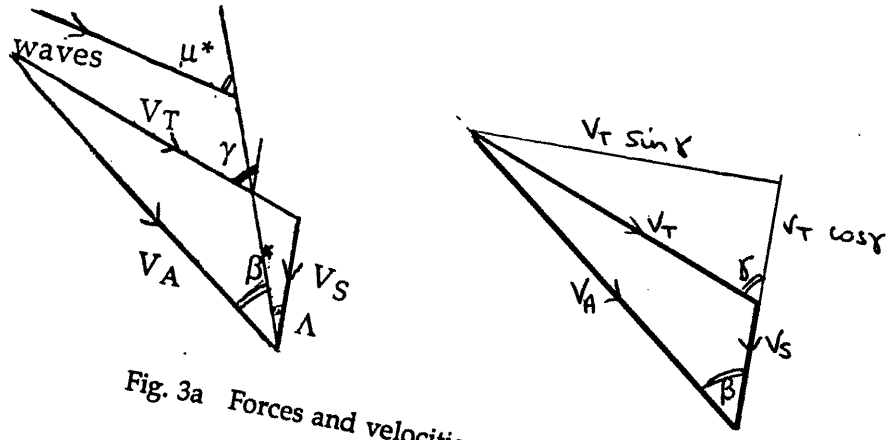

Fig. 3a Forces and velocities on a ship fitted with a WASP device.

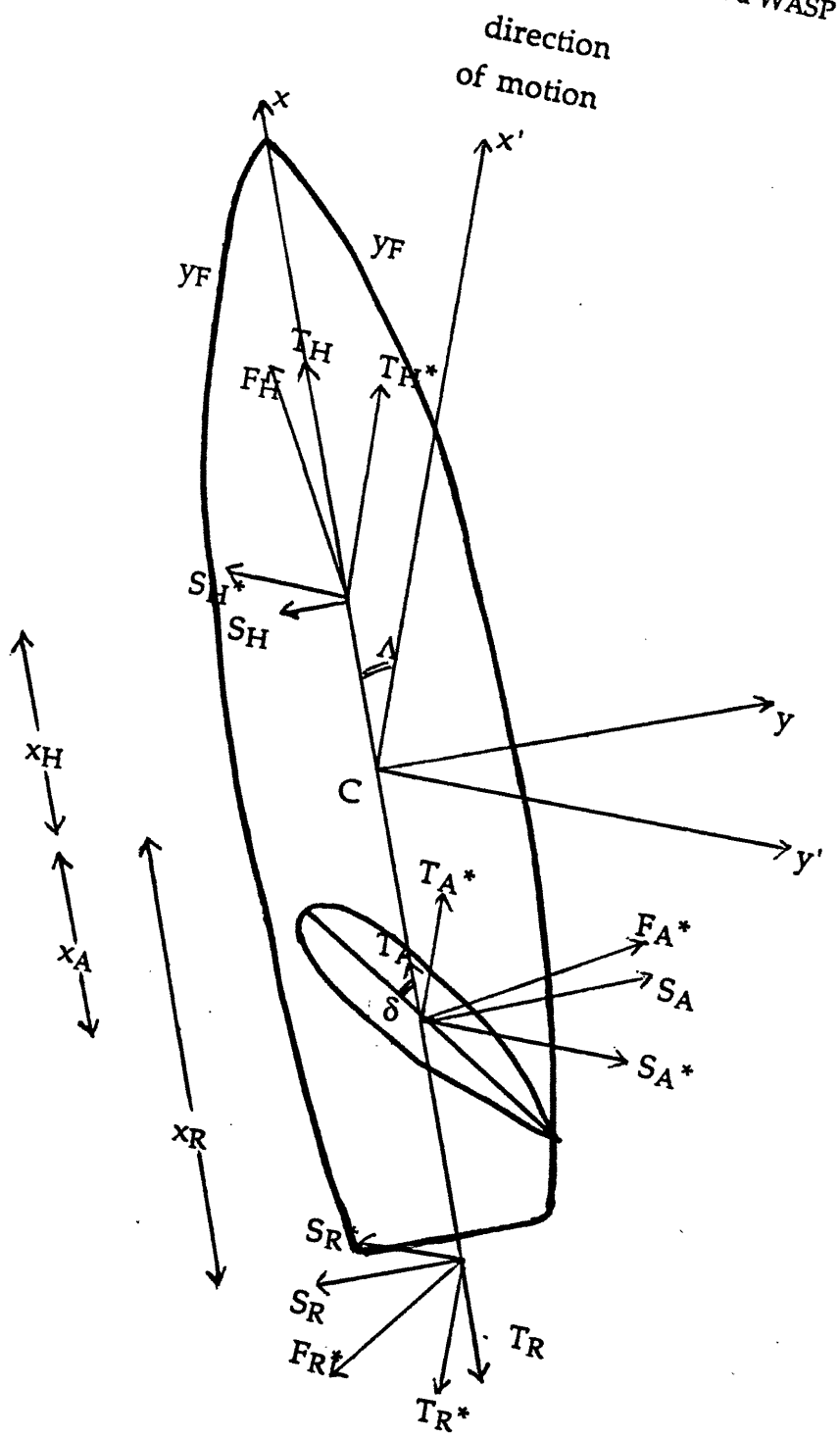

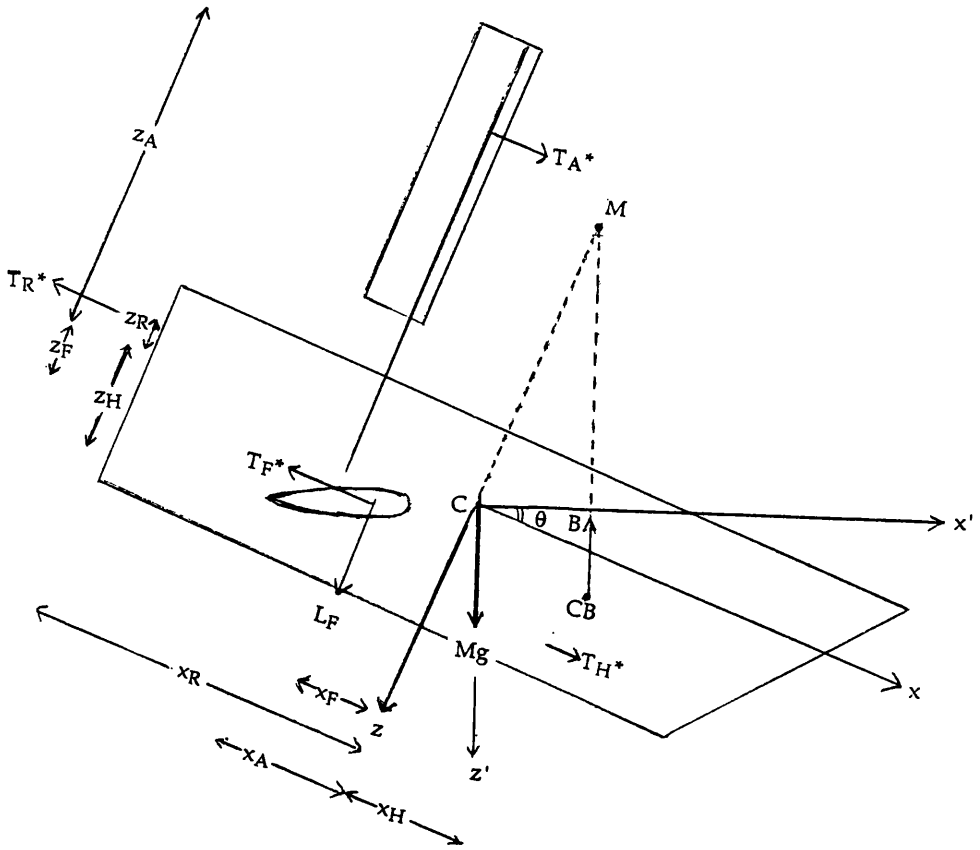

Fig. 3b Forces and velocities on a ship fitted with a WASP device.

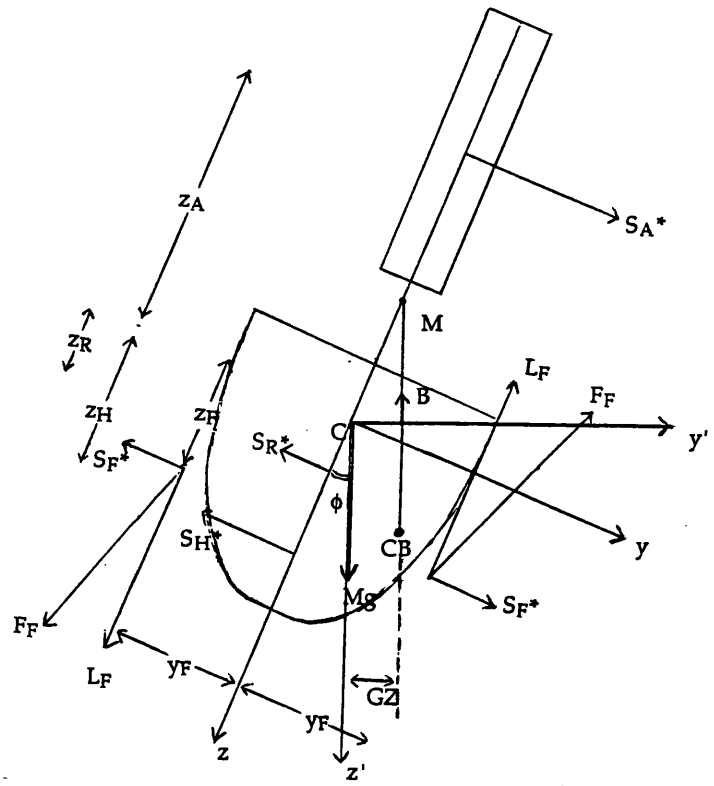

Fig. 3c Forces and velocities on a ship fitted with a WASP device.

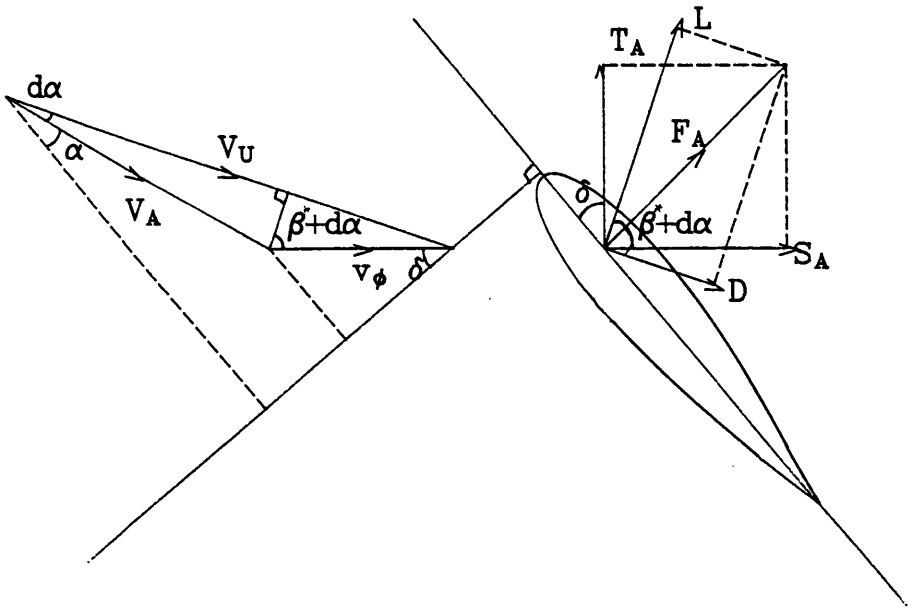

Fig. 4a Forces and velocities induced by roll motions.

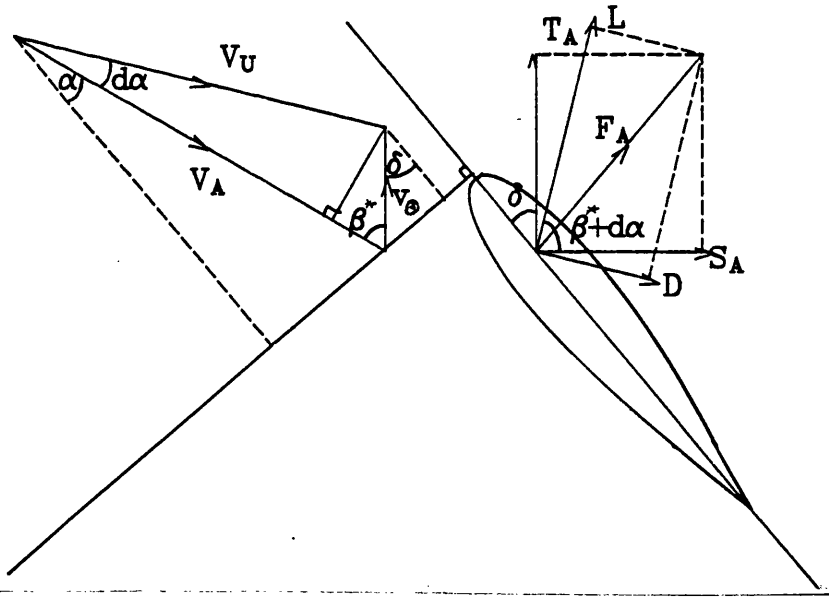

Fig. 4b Forces and velocities induced by pitch motions.

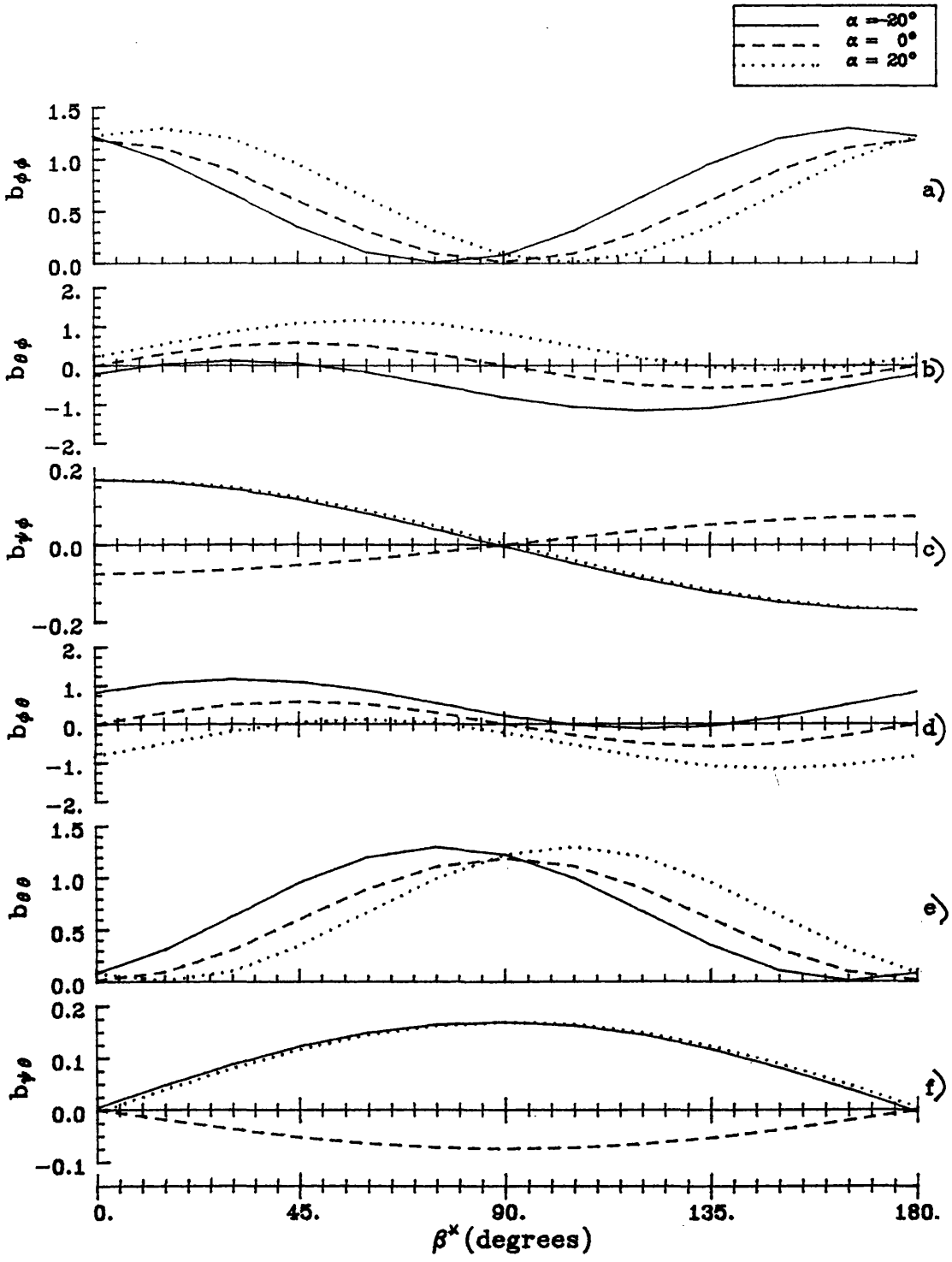

Fig. 5 Variations of damping derivatives as functions of wind heading β^* for a wingsail of aspect ratio of 1 and mean incidence $\alpha = 0, \pm 20^o$.

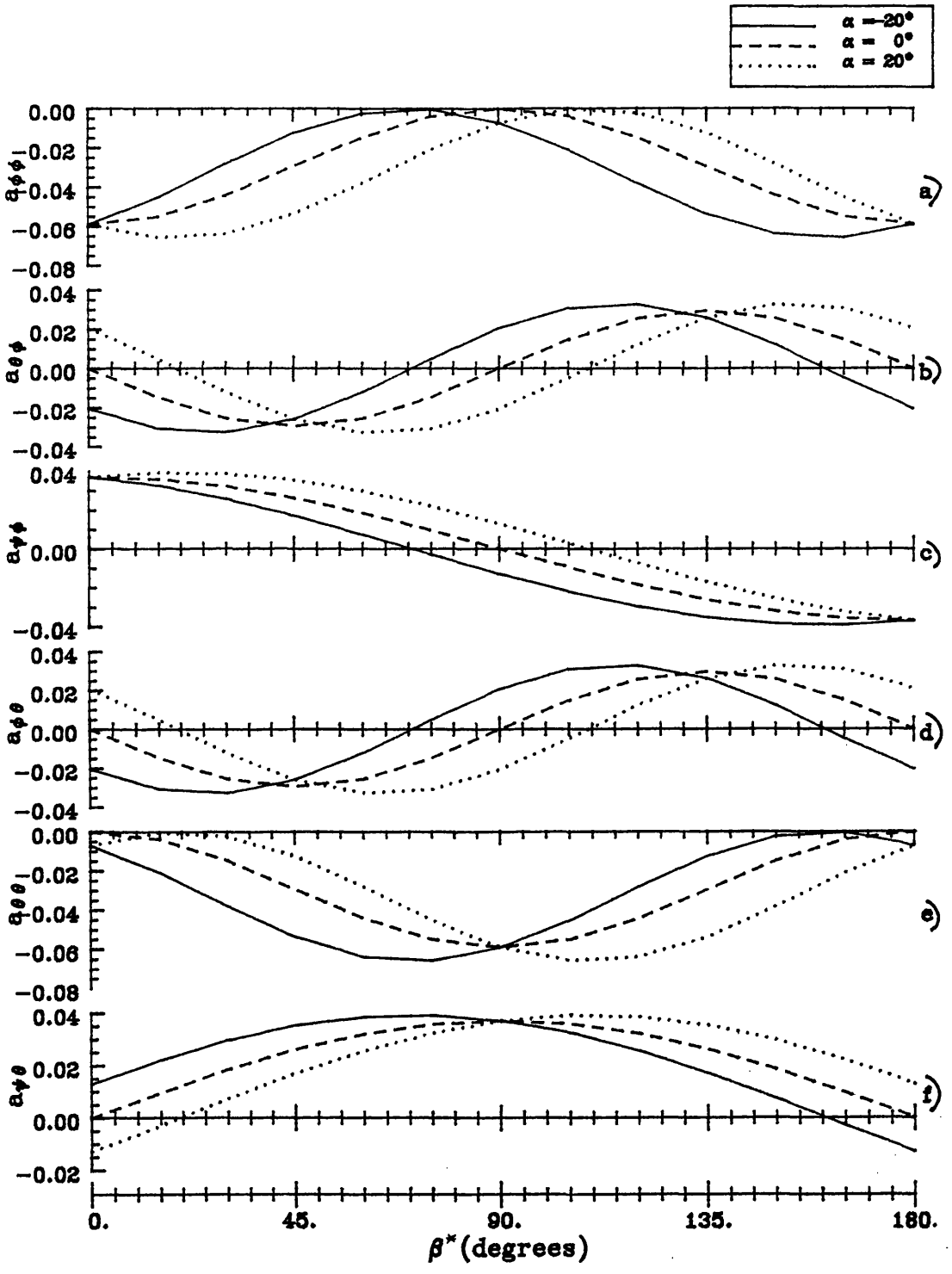

Fig. 6 Variations of inertia derivatives as functions of wind heading β^* for a wingsail of aspect ratio of 1 and mean incidence $\alpha = 0, \pm 20^0$ at reduced frequency $k = 0.1$.

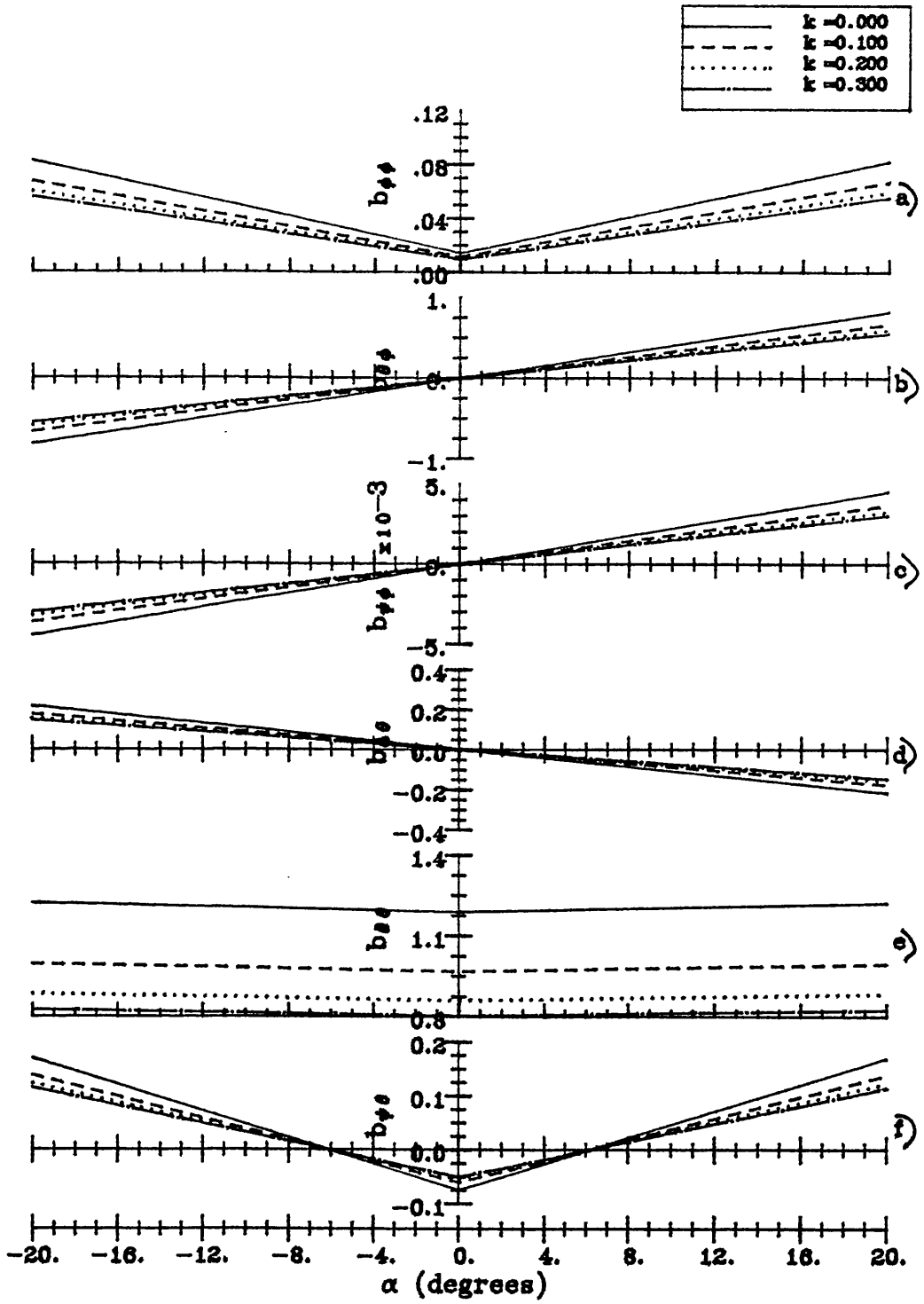

Fig. 7 Variations of damping derivatives as functions of mean incidence α for a wingsail of aspect ratio of 1 at wind heading $\beta^* = 90^o$ and reduced frequency k = 0.1, 0.2, 0.3.

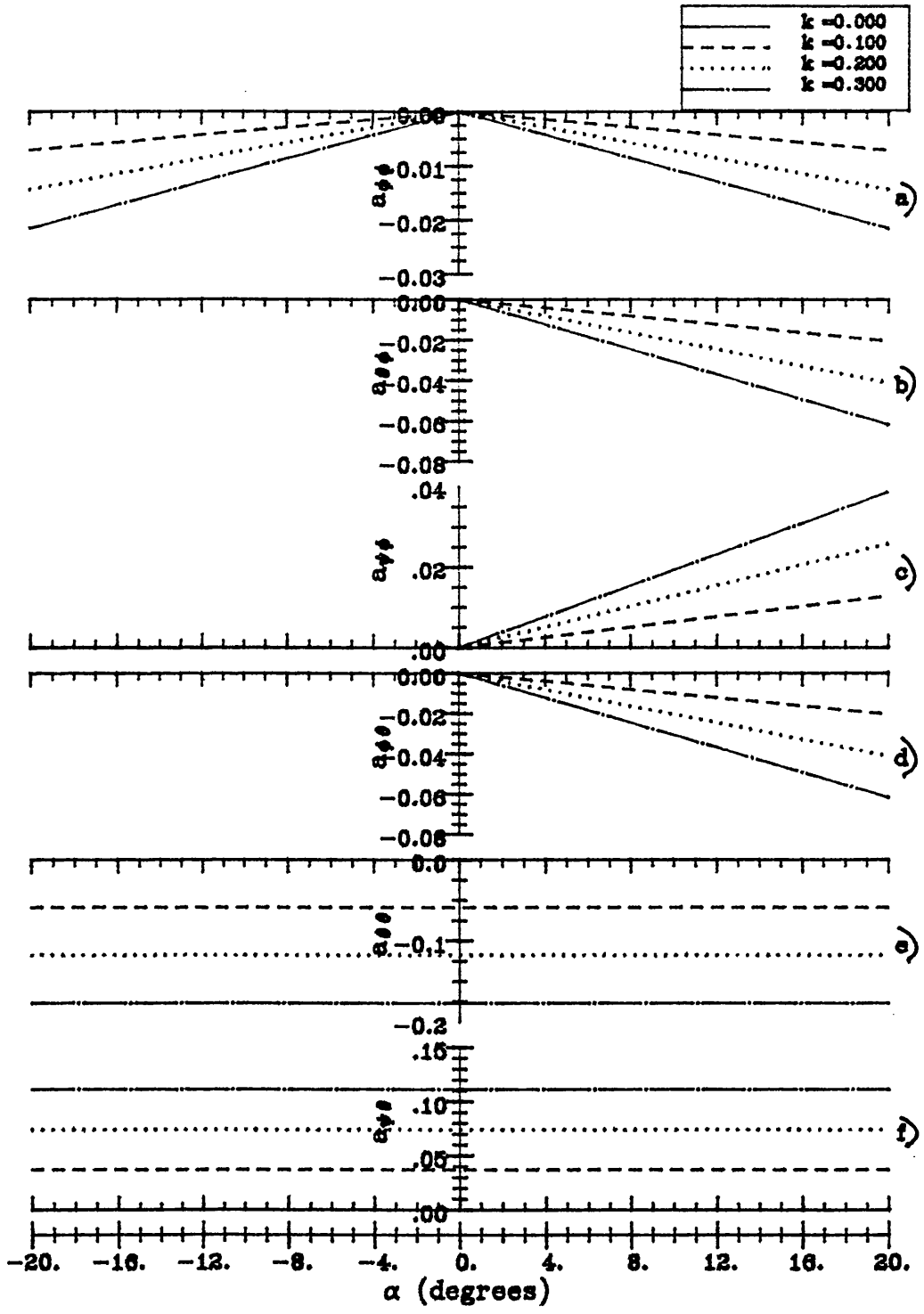

Fig. 8 Variations of inertia derivatives as functions of mean incidence α for a wingsail of aspect ratio of 1 at wind heading $\beta^* = 90^o$ at reduced frequency k = 0.1, 0.2, 0.3.

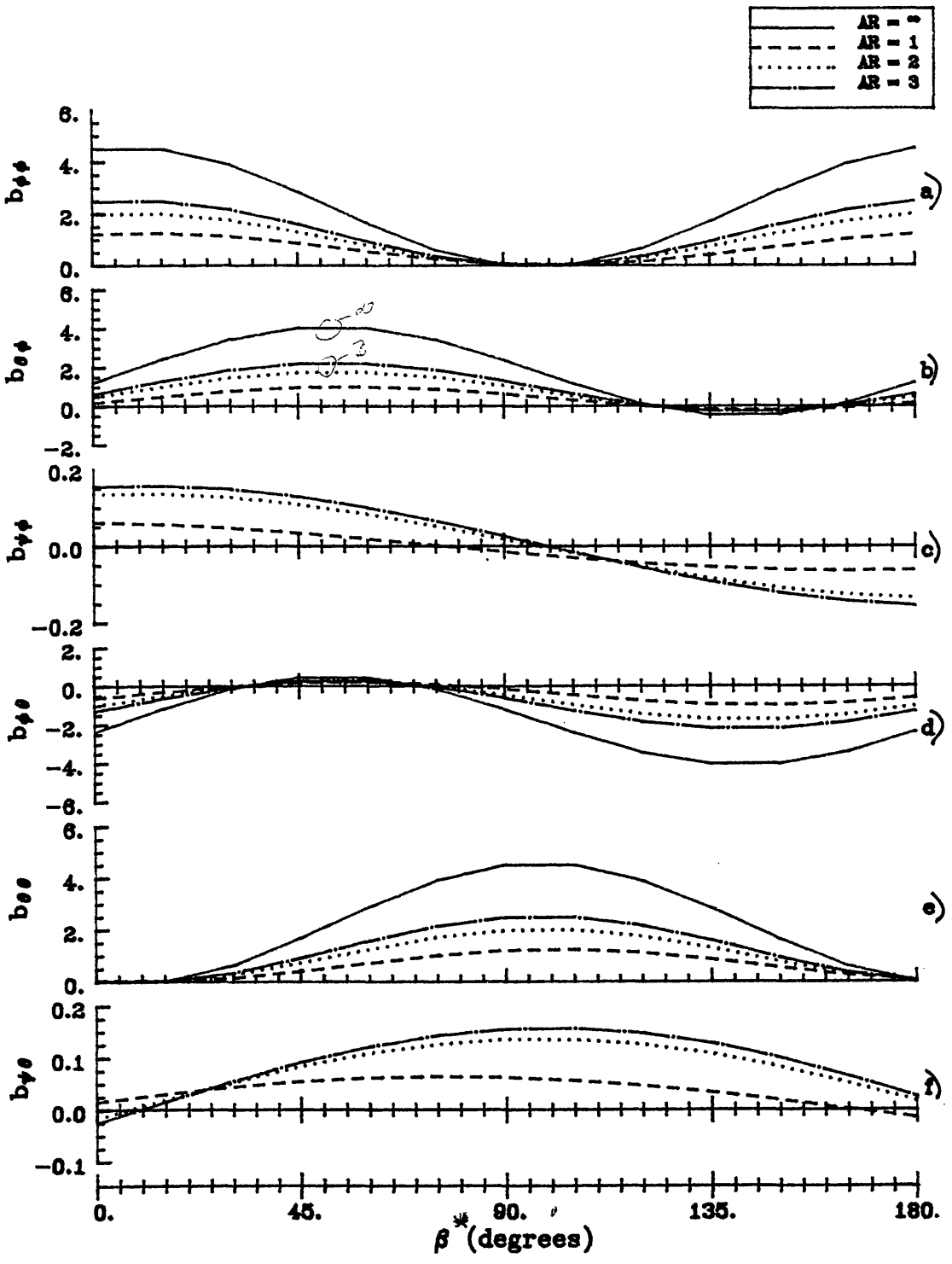

Fig. 9 Variations of damping derivatives as functions of wind heading β^* for a wingsail with mean incidence $\alpha = 15^o$ at aspect ratios 1, 2, 3 and infinity.

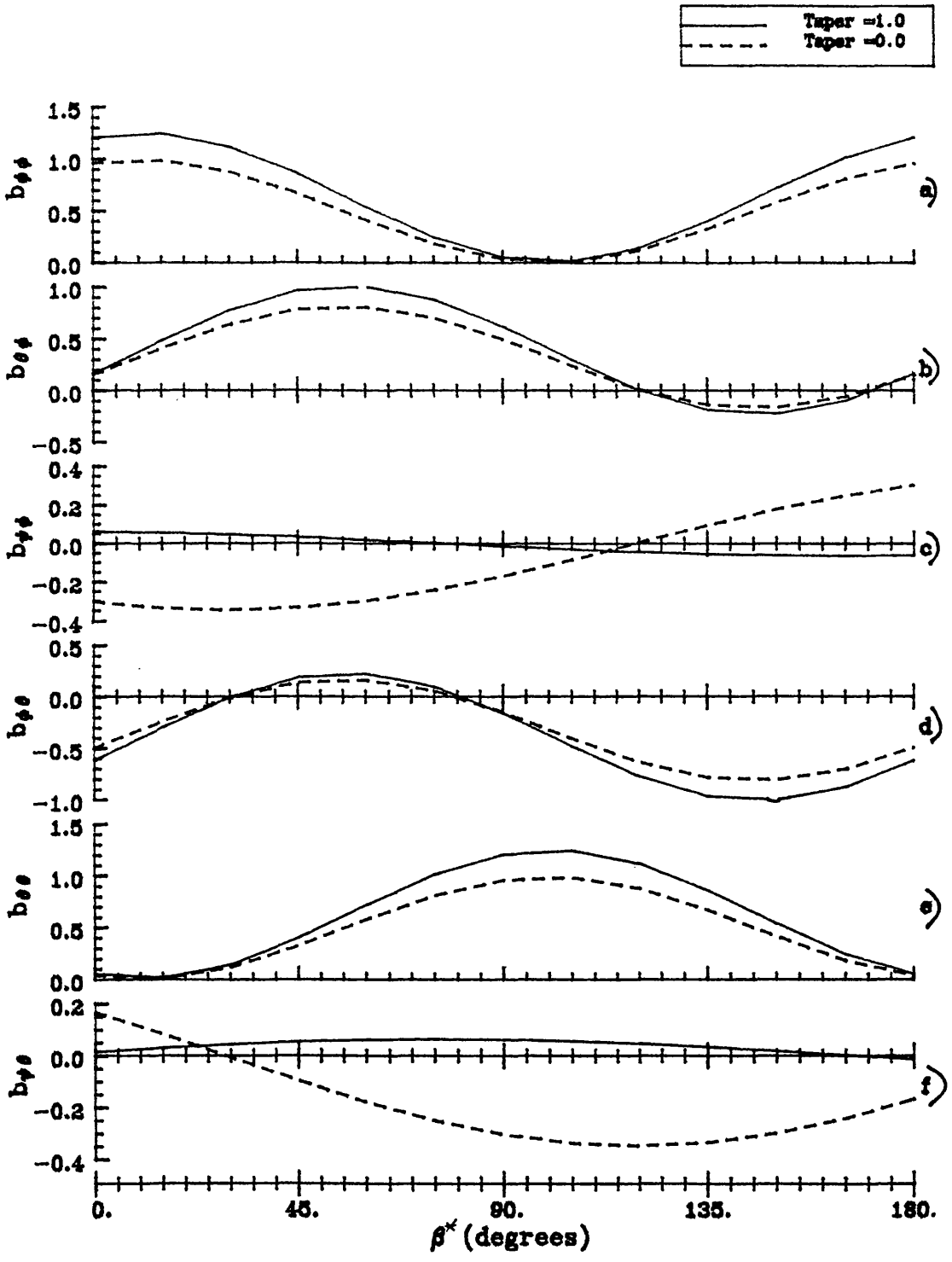

Fig. 10 Variations of damping derivatives as functions of wind heading β^* for a wingsail of aspect ratio of 1 with mean incidence $\alpha = 15^o$ and taper ratios of 0 and 1.

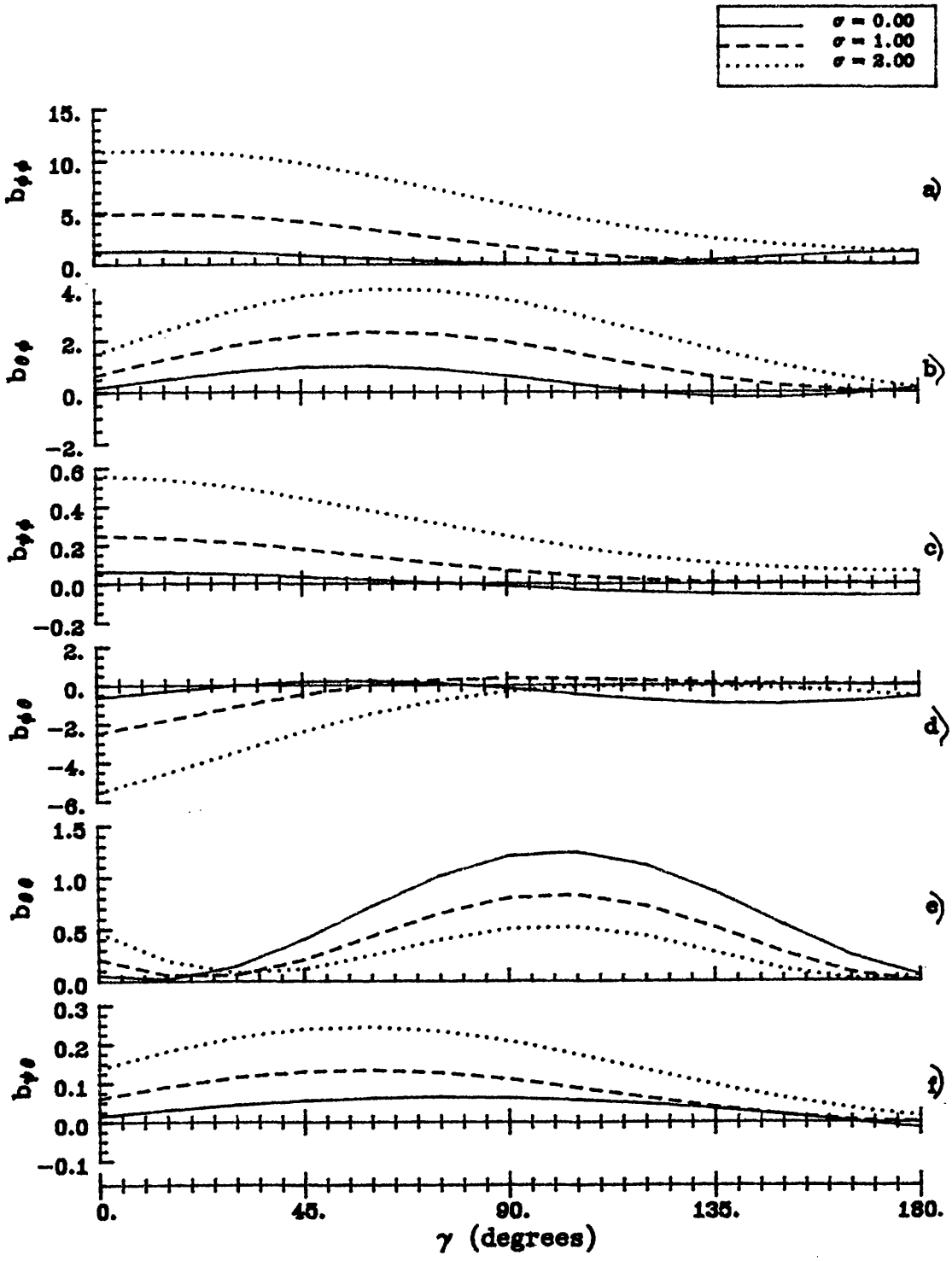

Fig. 11 Variations of damping derivatives as functions of true wind direction γ for a wingsail of aspect ratio of 1 with mean incidence $\alpha = 15^{o}$ and ship speed/wind speed ratios, $\sigma = 0, 1$ and 2.

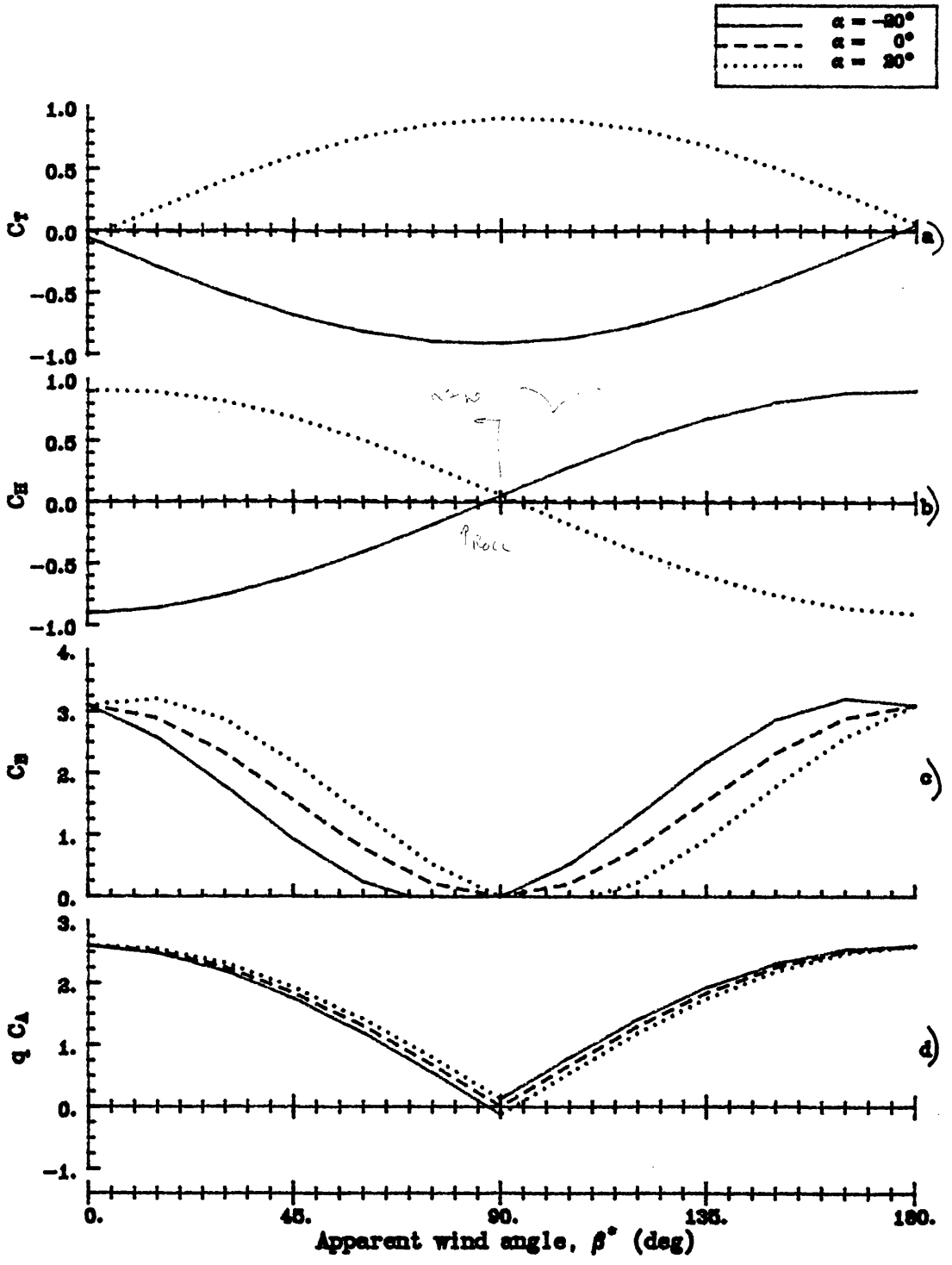

Fig. 12 Variations of C_T, C_H, C_B and qC_A as functions of wind heading β^* for a wingsail and mean incidence $\alpha = 0, \pm 20^o$.

Fig. 13 Forces and velocities on a yawed HAWT.

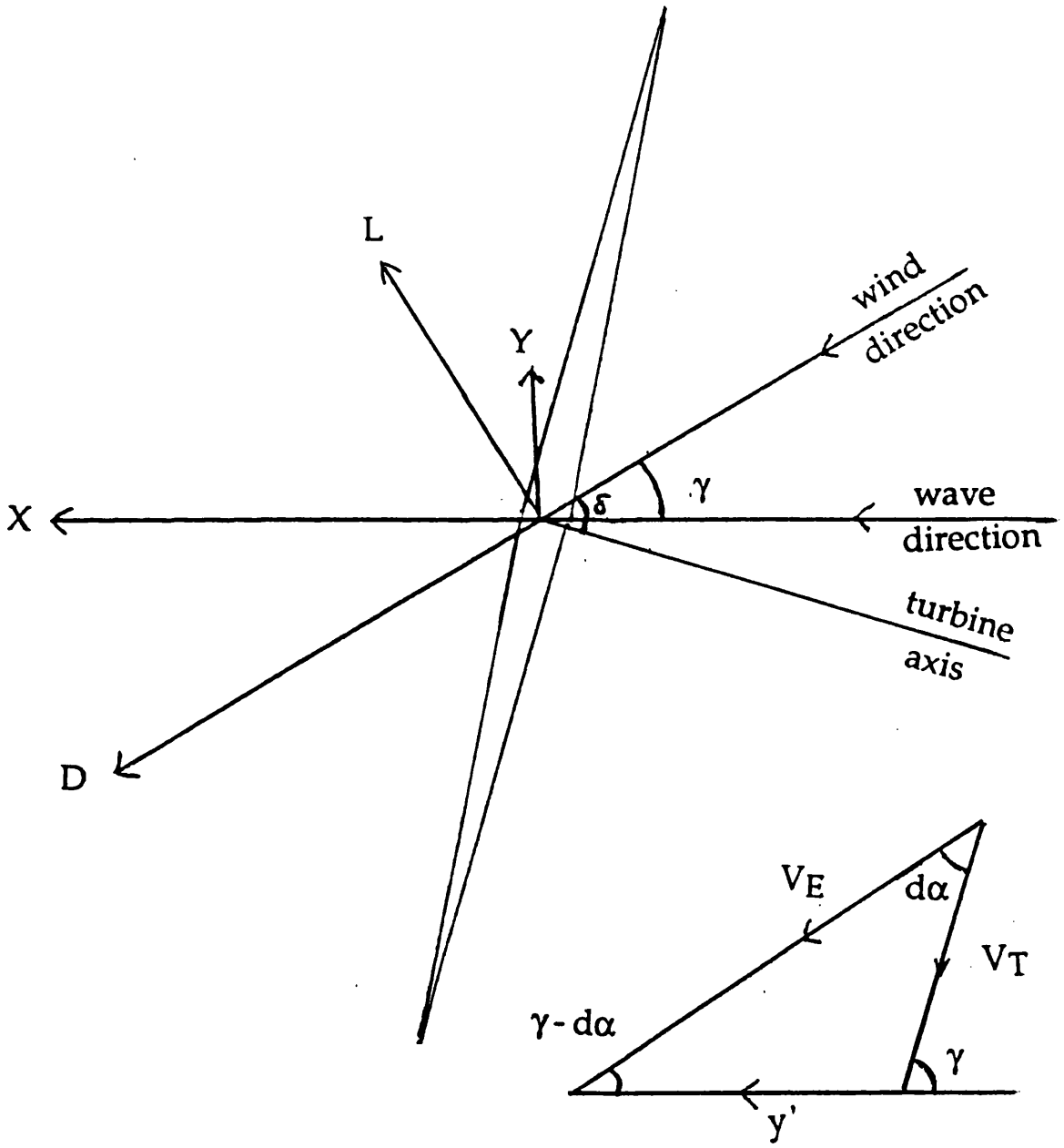

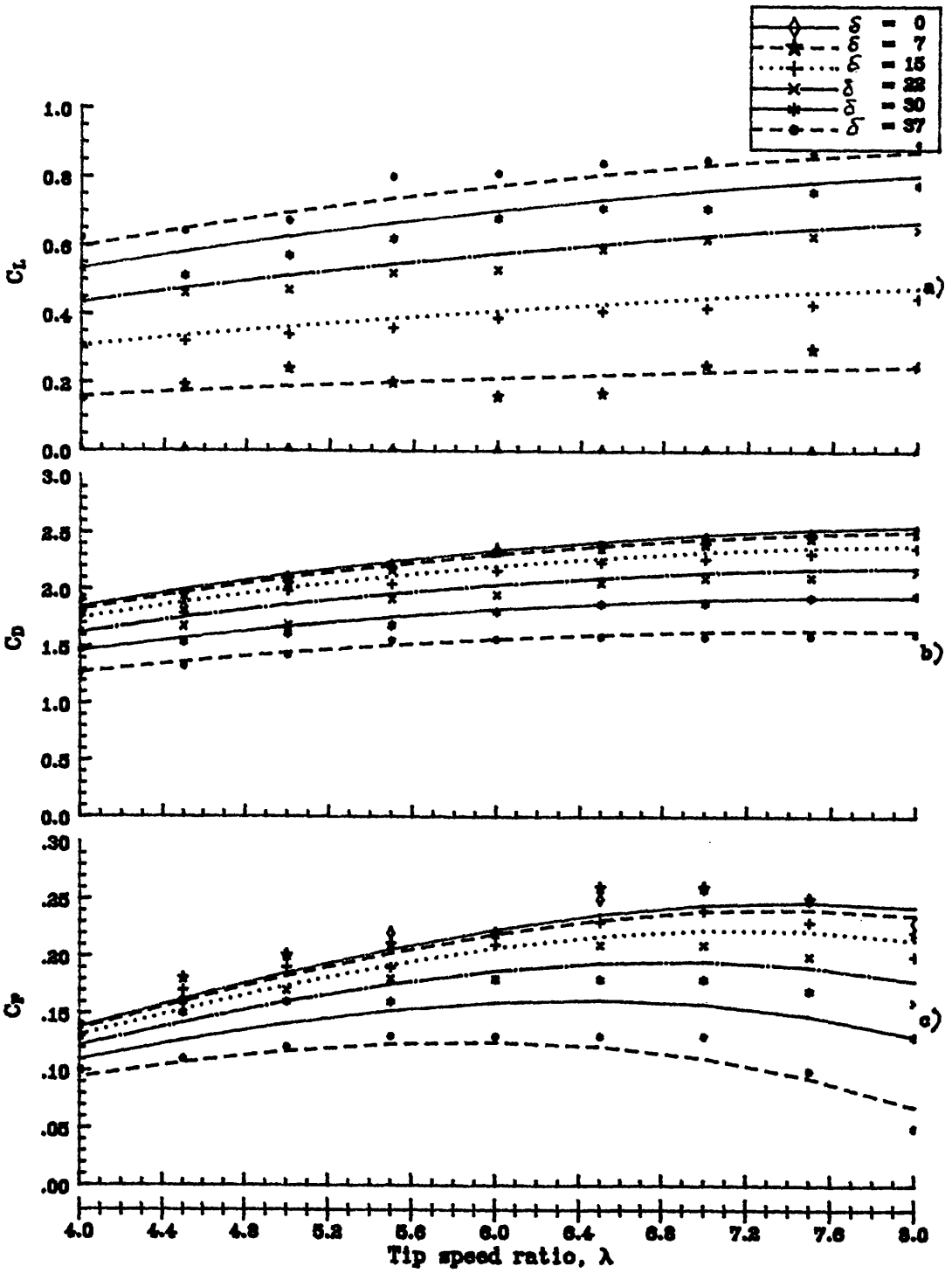

Fig. 14 Lift, drag and power coefficients as functions of tip speed ratio λ for a HAWT for yaw angles $\delta = 0, 7^o, 15^o, 22^o, 30^o, 37^o$.

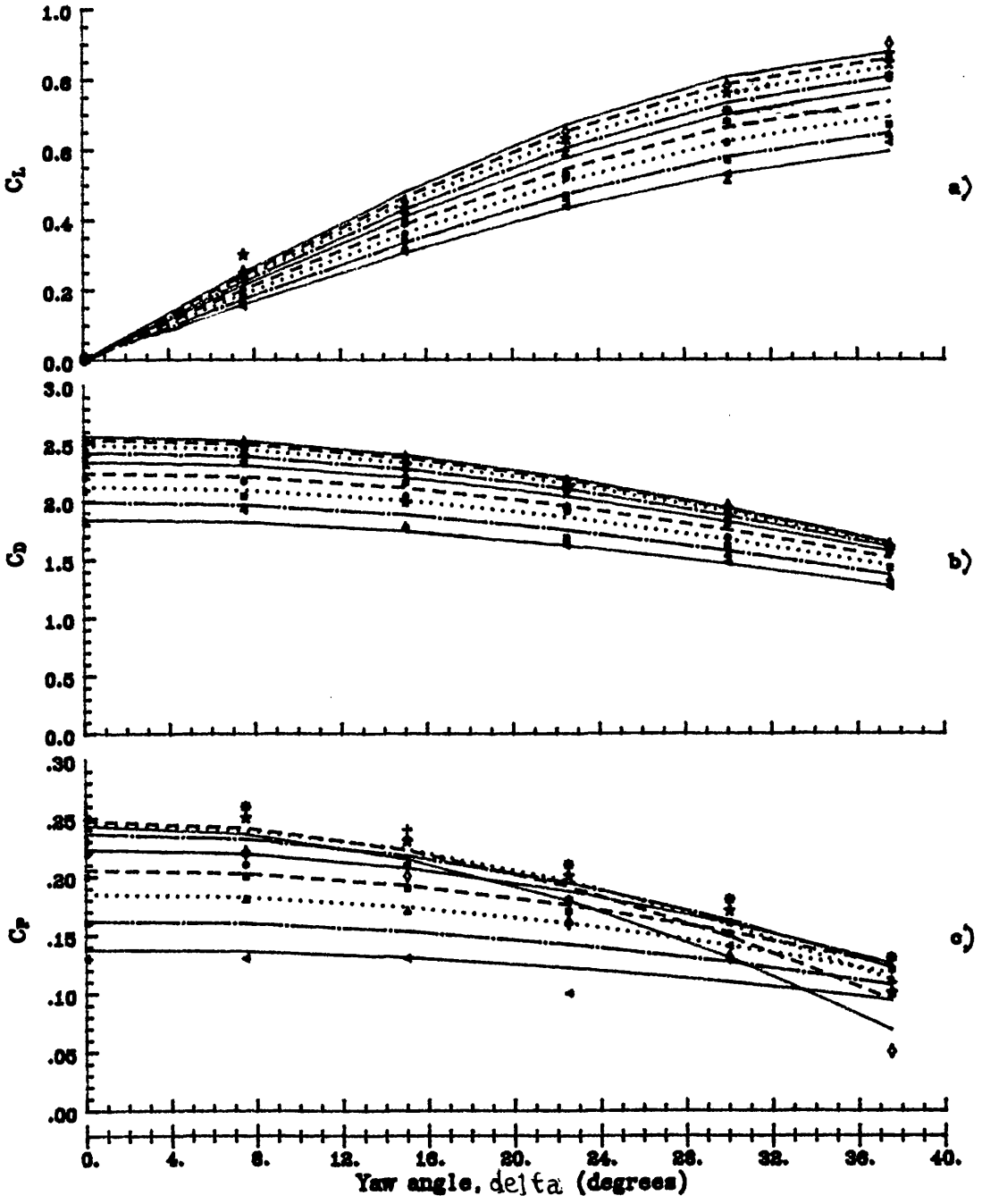

Fig. 15 Lift, drag and power coefficients as functions of yaw angle δ for a HAWT for tip-speed ratios, λ = 4.5, 5, 5.5, 6, 6.5, 7, 7.5, 8.

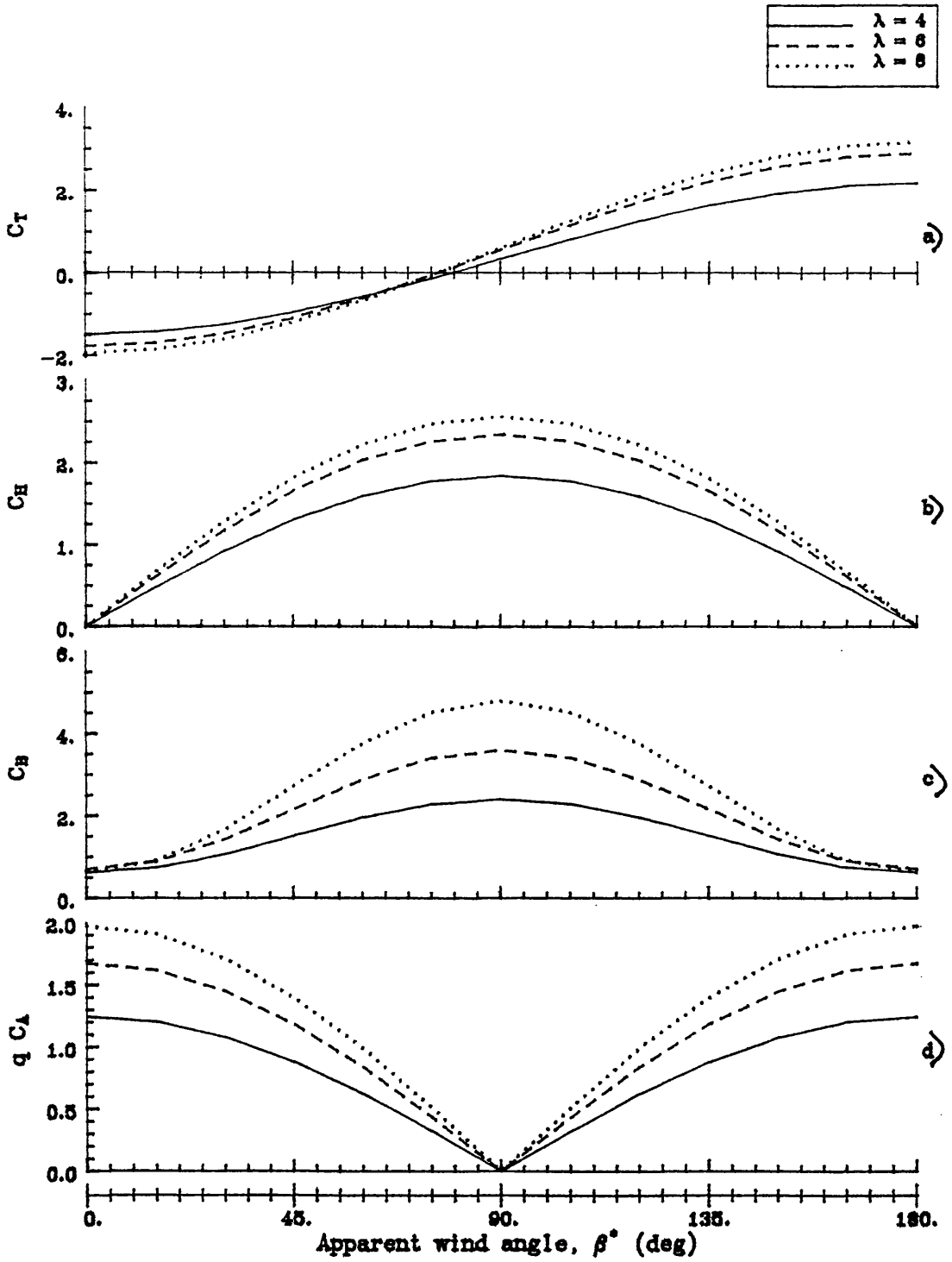

Fig. 16 Variations of C_T, C_H, C_B and qC_A as functions of wind heading β^* for a HAWT with yaw angle $\delta = 0$ for tip speed ratios $\lambda = 4, 6, 8$.

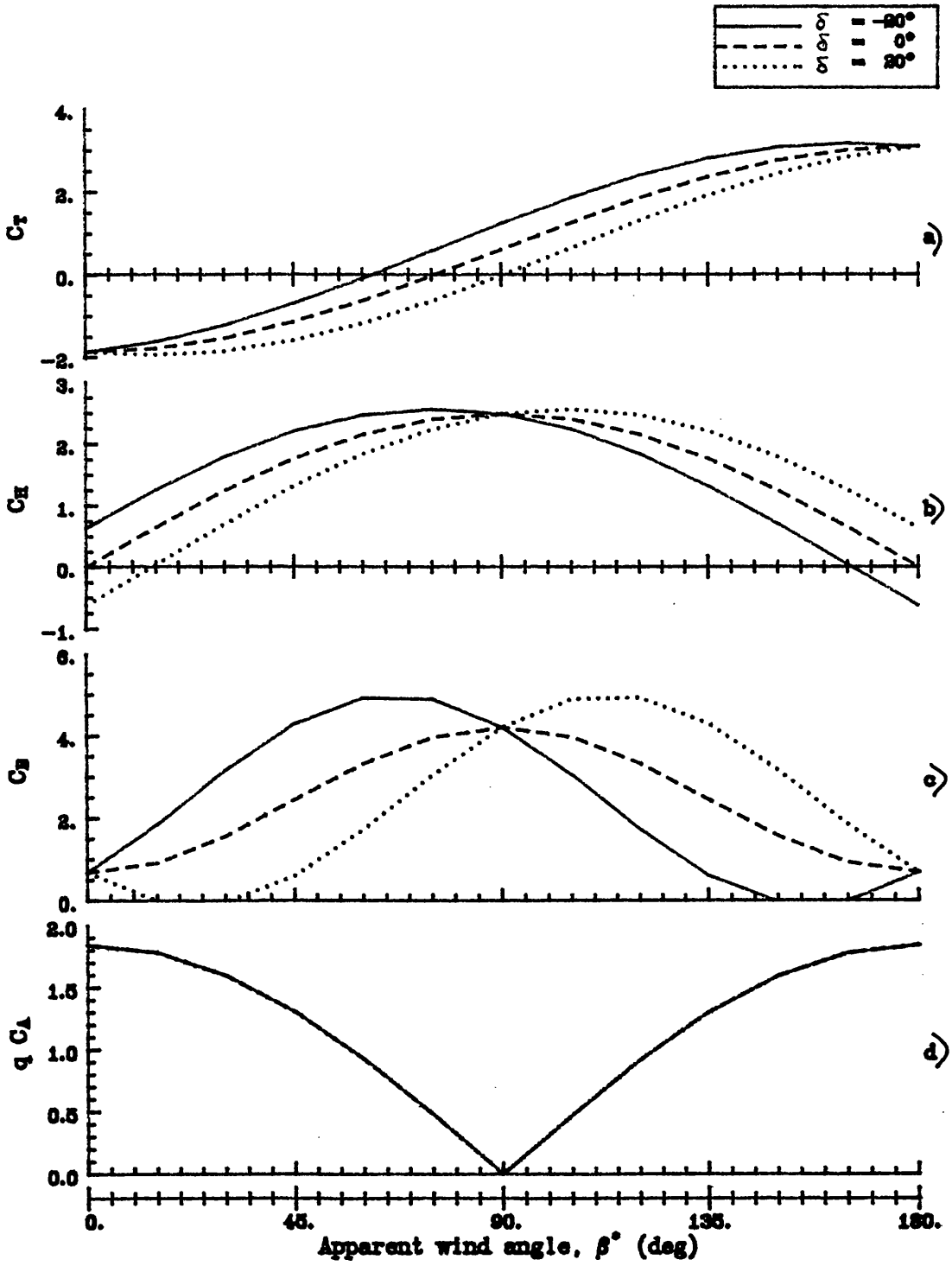

Fig. 17 Variations of C_T, C_H, C_B and qC_A as function of wind heading β^* for a HAWT at tip-speed ratio $\lambda = 6$ with yaw angles $\delta = 0, \pm 20^o$.

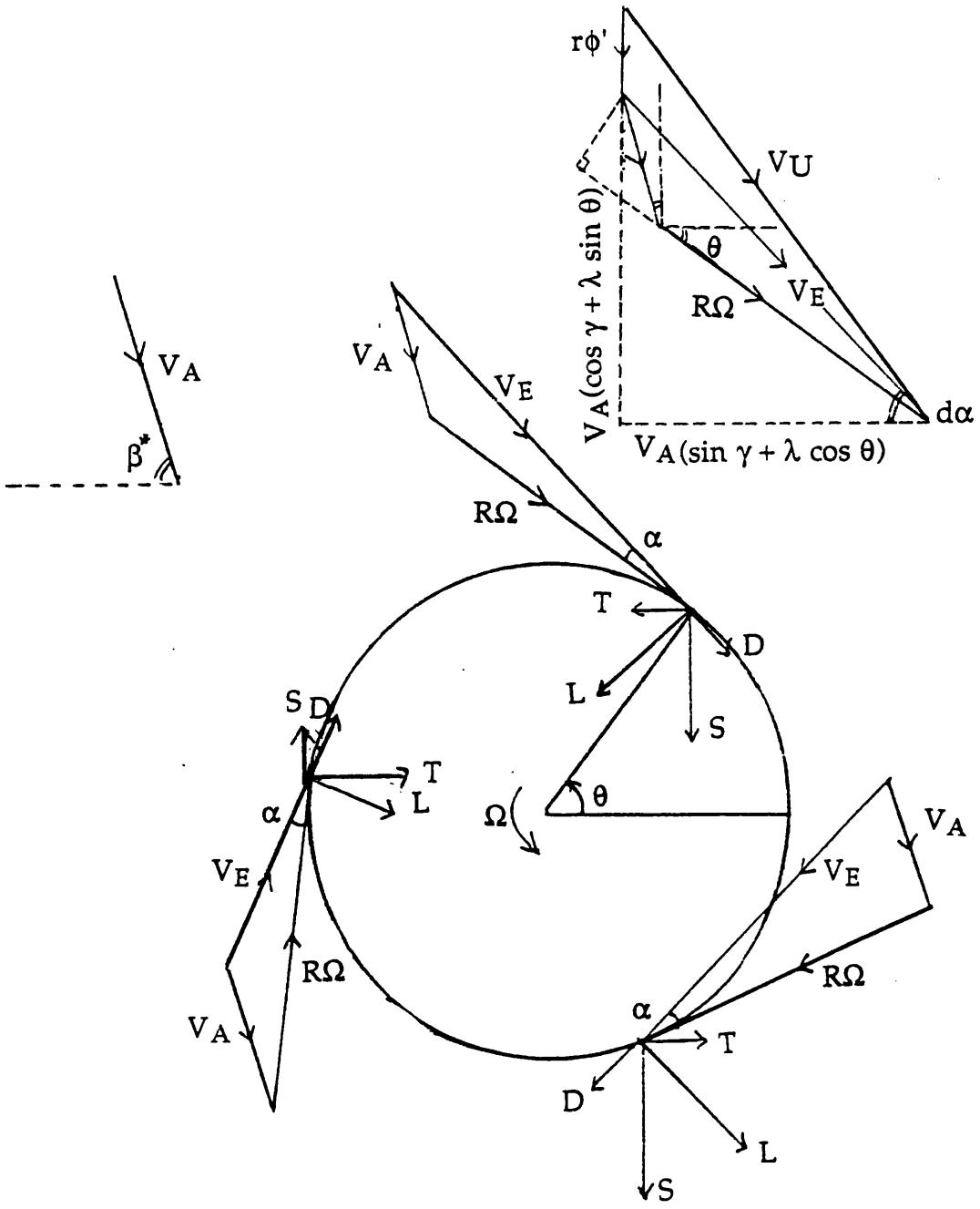

Fig. 18 Forces and velocities on a VAWT.

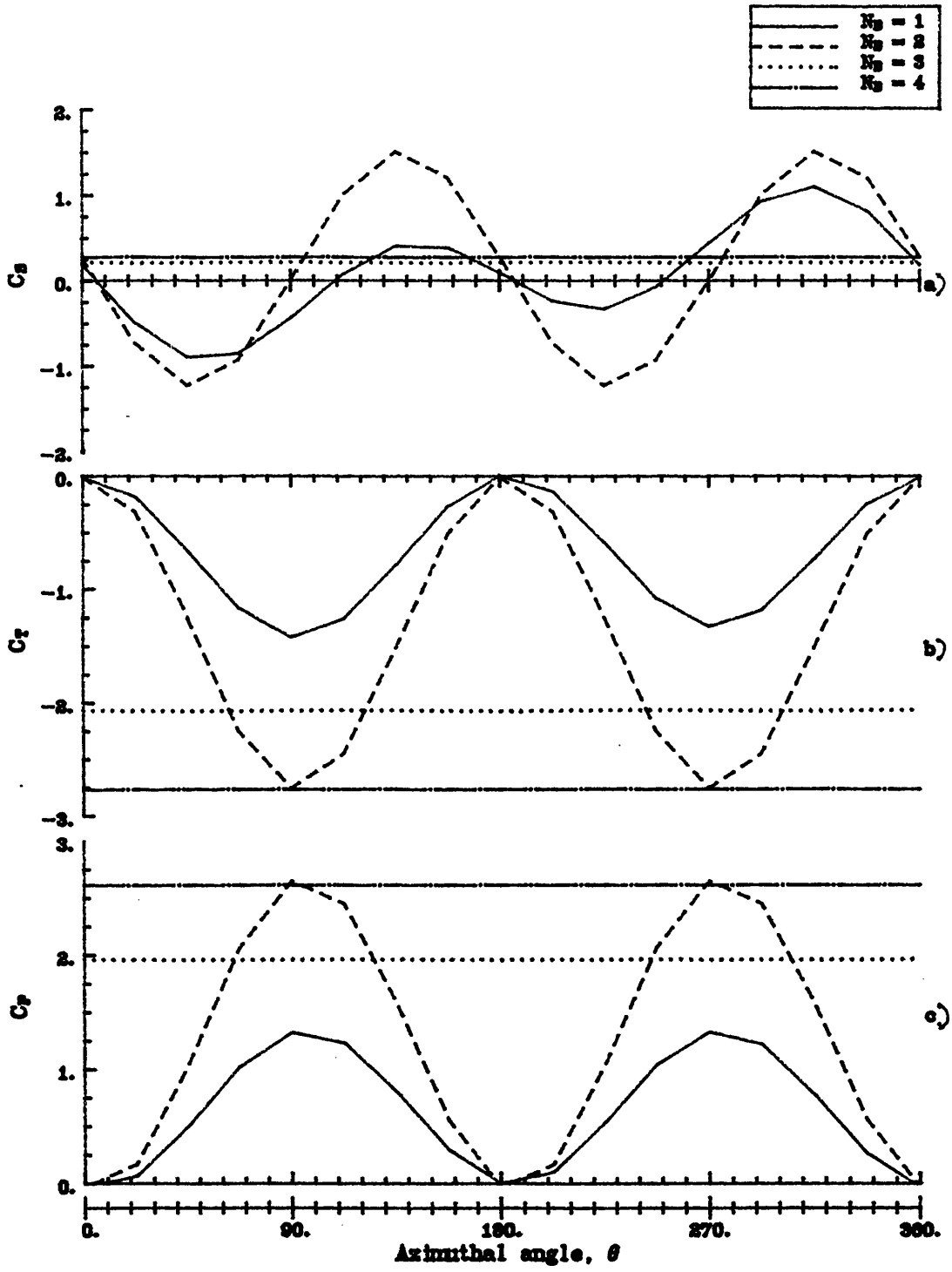

Fig. 19 Side force, thrust and power coefficients versus azimuthal angle for a VAWT with 1, 2, 3 and 4 blades.

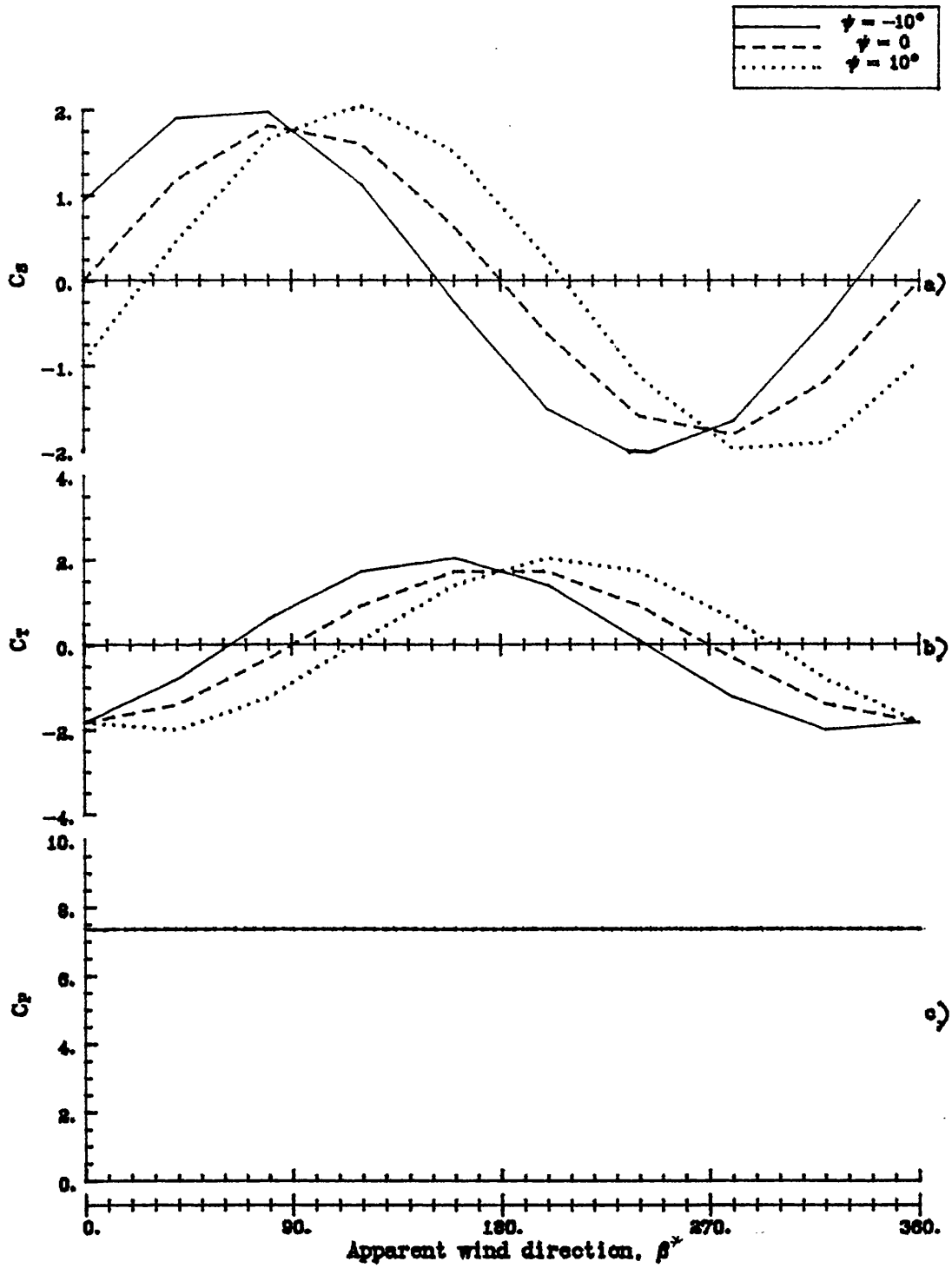

Fig. 20 Thrust, side force and power coefficients versus wind heading angle for a VAWT for blade pitch angles $\psi = 0, \pm 10^{o}$.

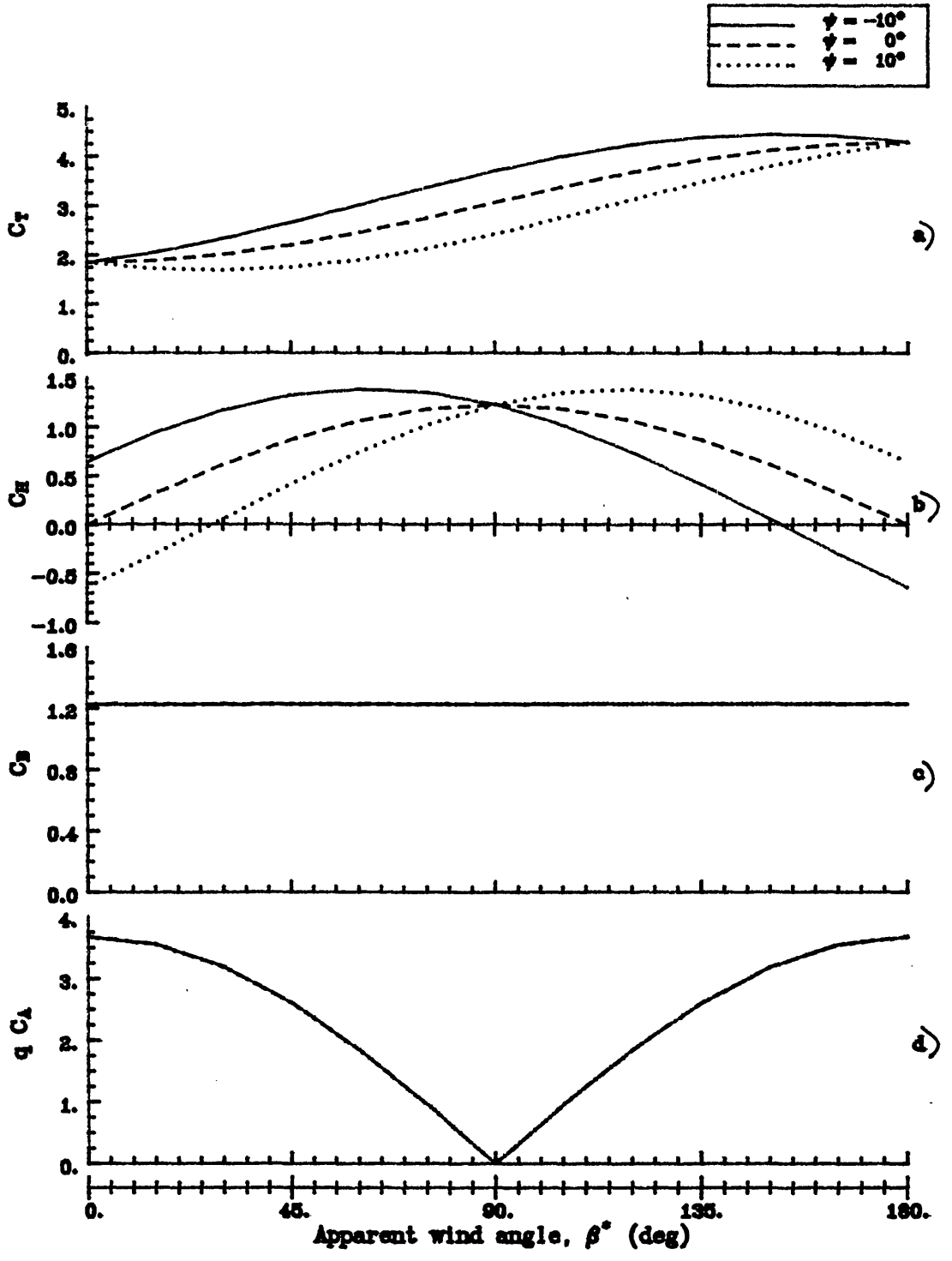

Fig. 21 Variations of C_T, C_H, C_B and qC_A as functions of wind heading β^* for a VAWT and blade pitch angles $\psi = 0, \pm 10^o$.

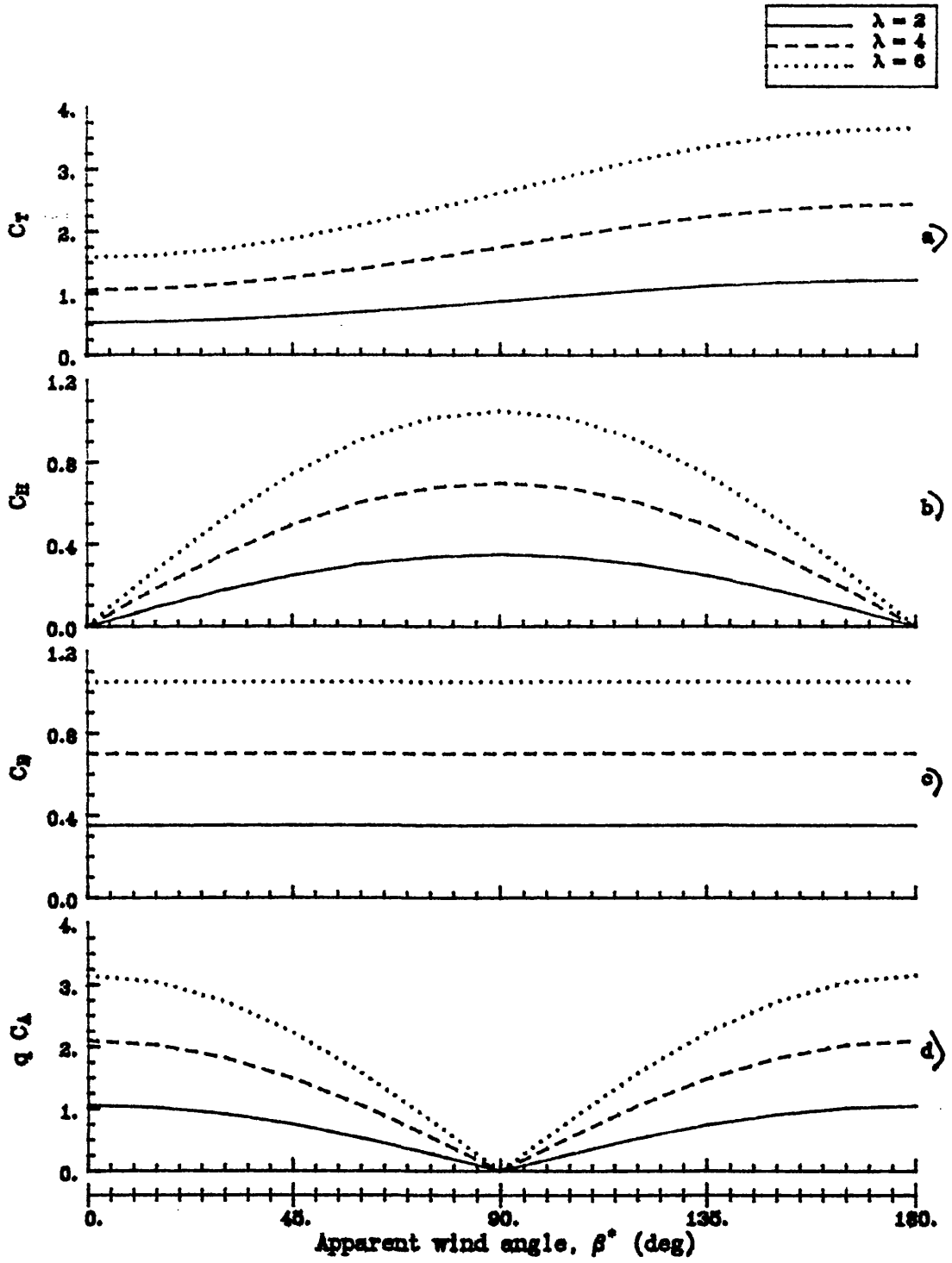

Fig. 22 Variations of C_T, C_H, C_B and qC_A as functions of wind heading β^* for a VAWT and tip-speed ratios $\lambda = 2, 4, 6$.

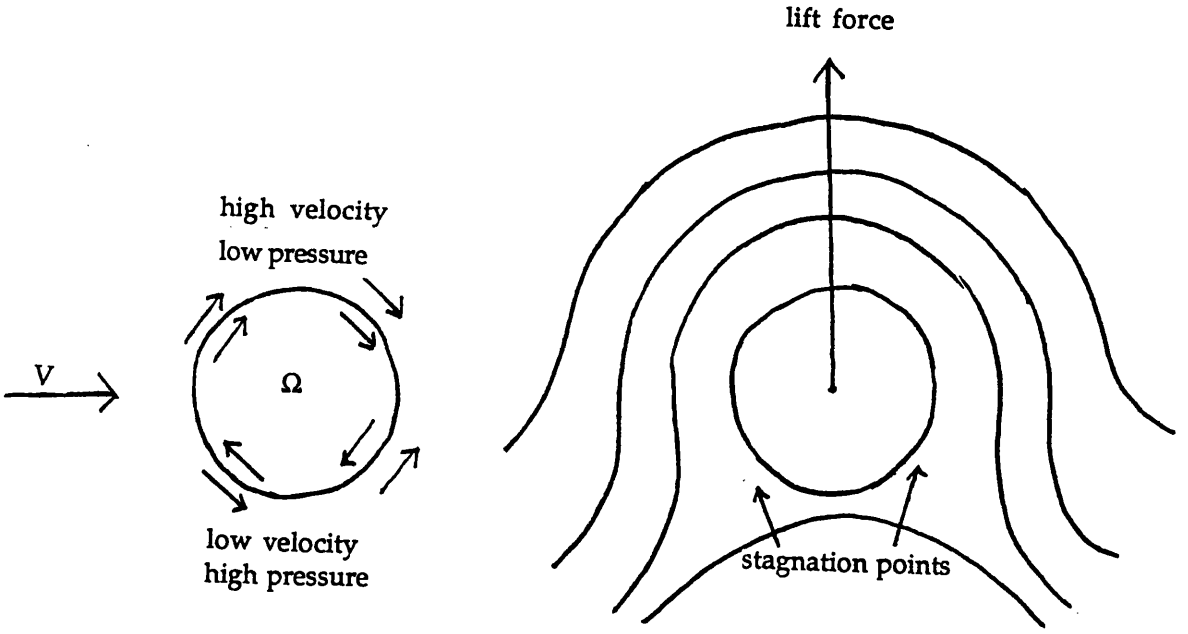

Fig. 23 Working principle of the Flettner rotor.

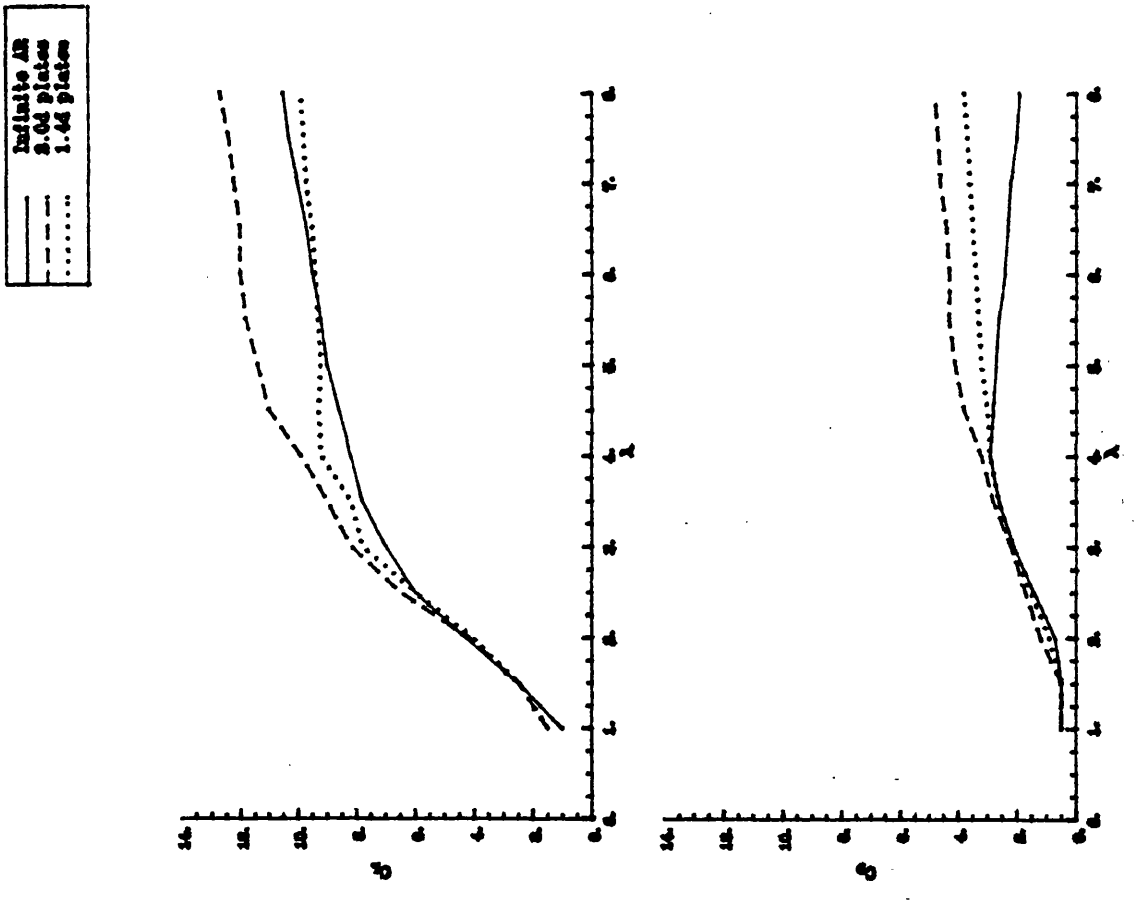

Fig. 24 Lift and drag coefficient curves for a Flettner rotor.

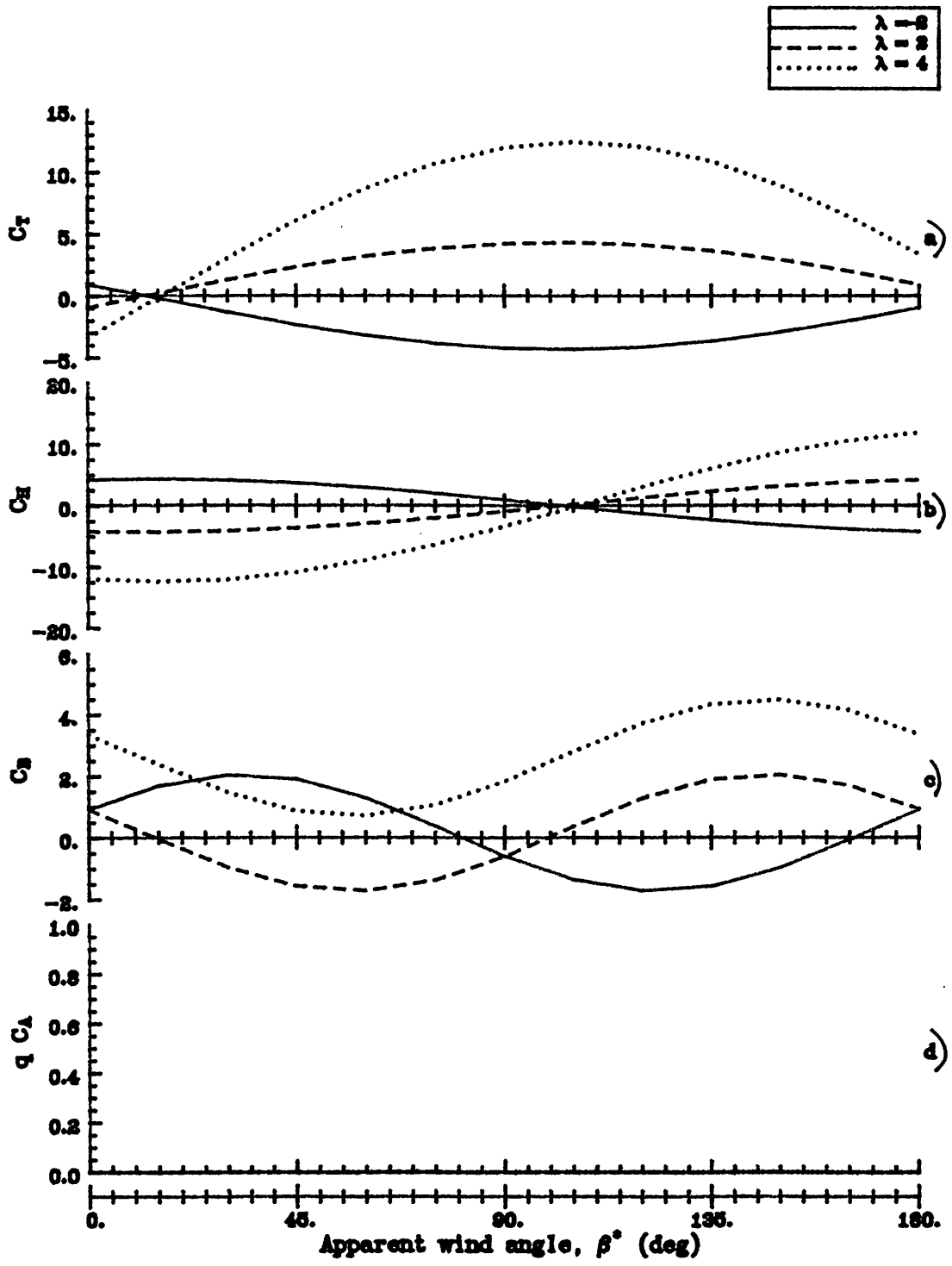

Fig. 25 Variations of C_T, C_H, C_b and qC_A as function of wind heading β^* for a Flettner rotor at tip-speed ratios $\lambda = \pm 2$ and 4.

Schematic View of the Main Components of
the Cousteau-Pechiney Turbosail System

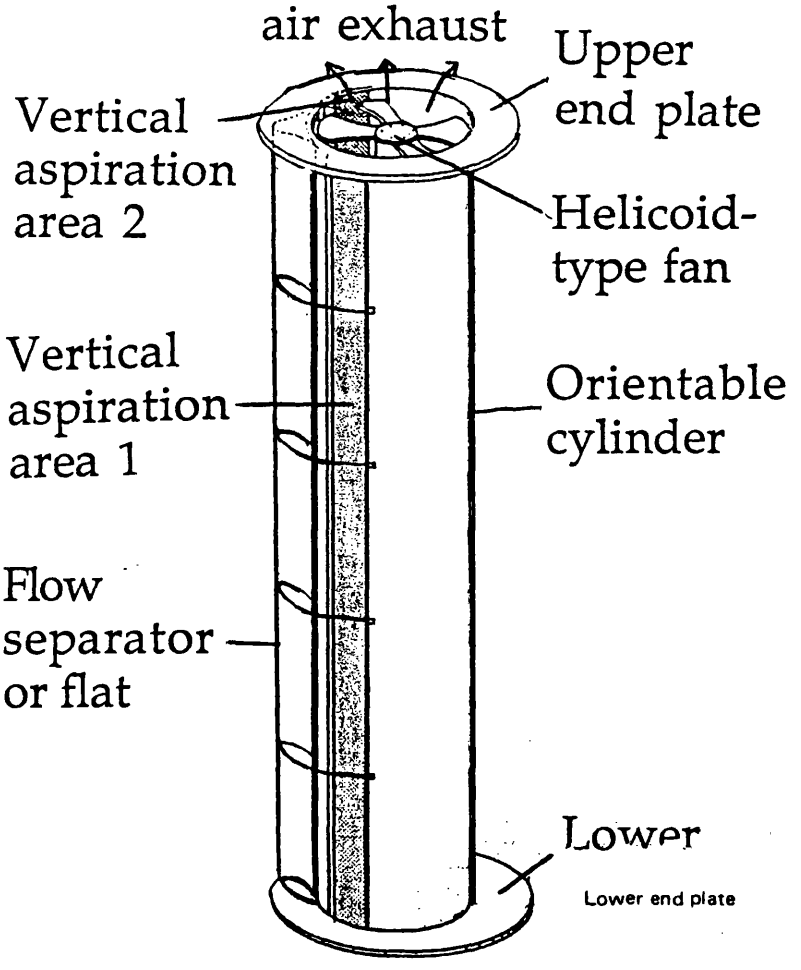

Basic Working Principle of the Turbosail System

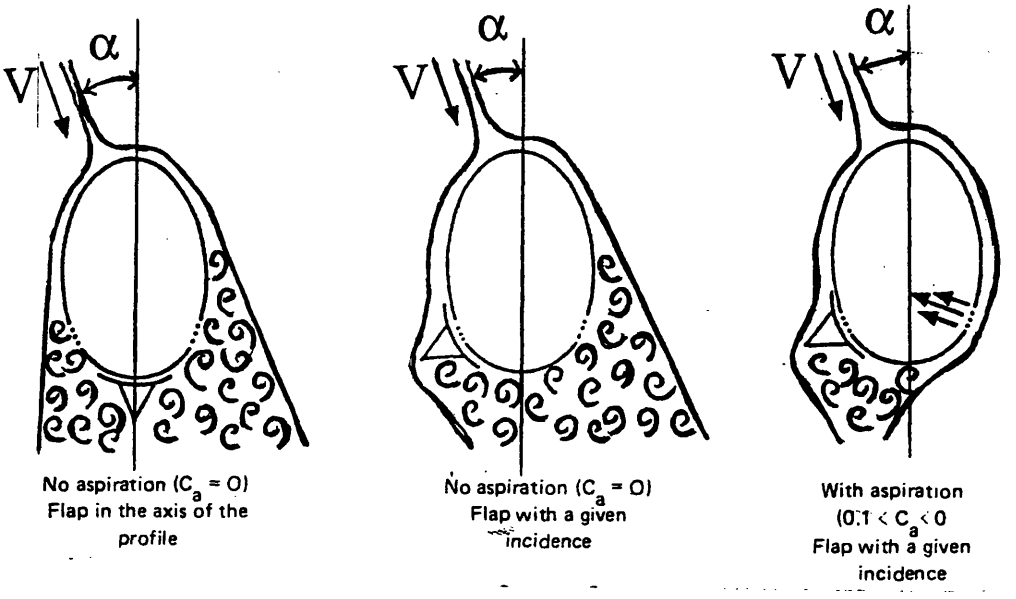

Fig. 26 The Cousteau Turbosail, from Constans (1985).

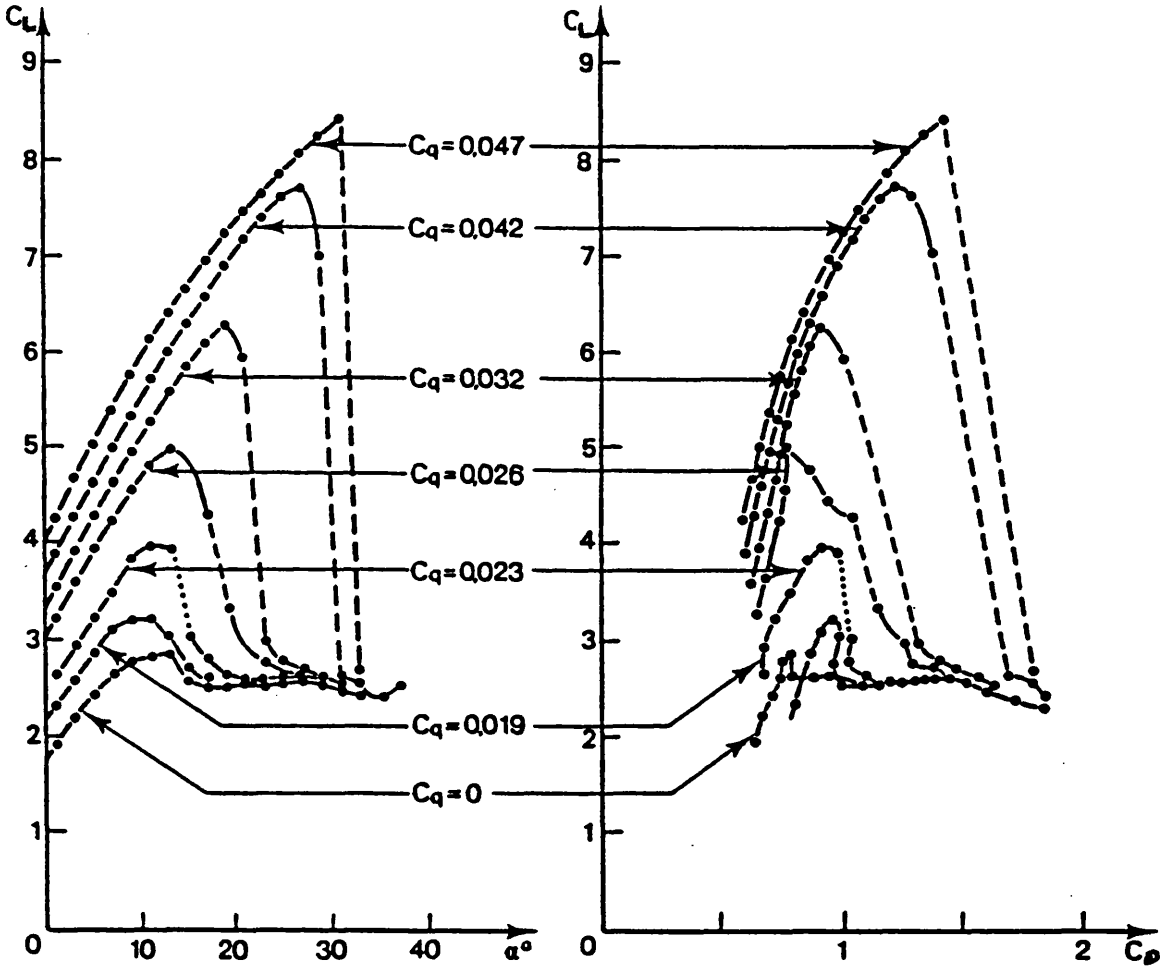

Fig. 27 Lift and drag coefficient curves for the Cousteau Turbosail, from Malavard (1984).

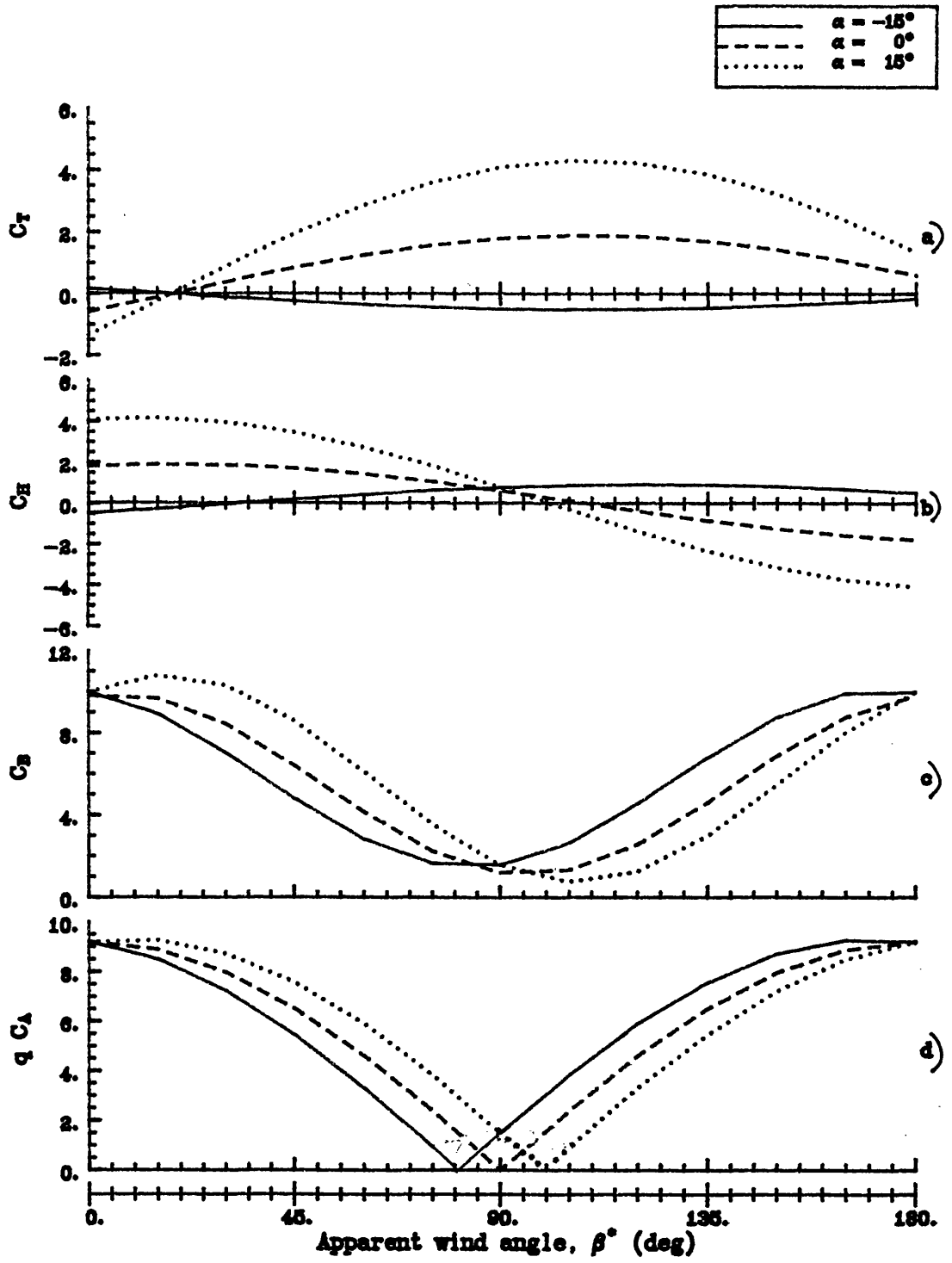

Fig. 28 Variations of C_T, C_H, C_B and qC_A as functions of wind heading β^* for a Cousteau Turbosail and mean incidence $\alpha = 0, \pm 15^o$.

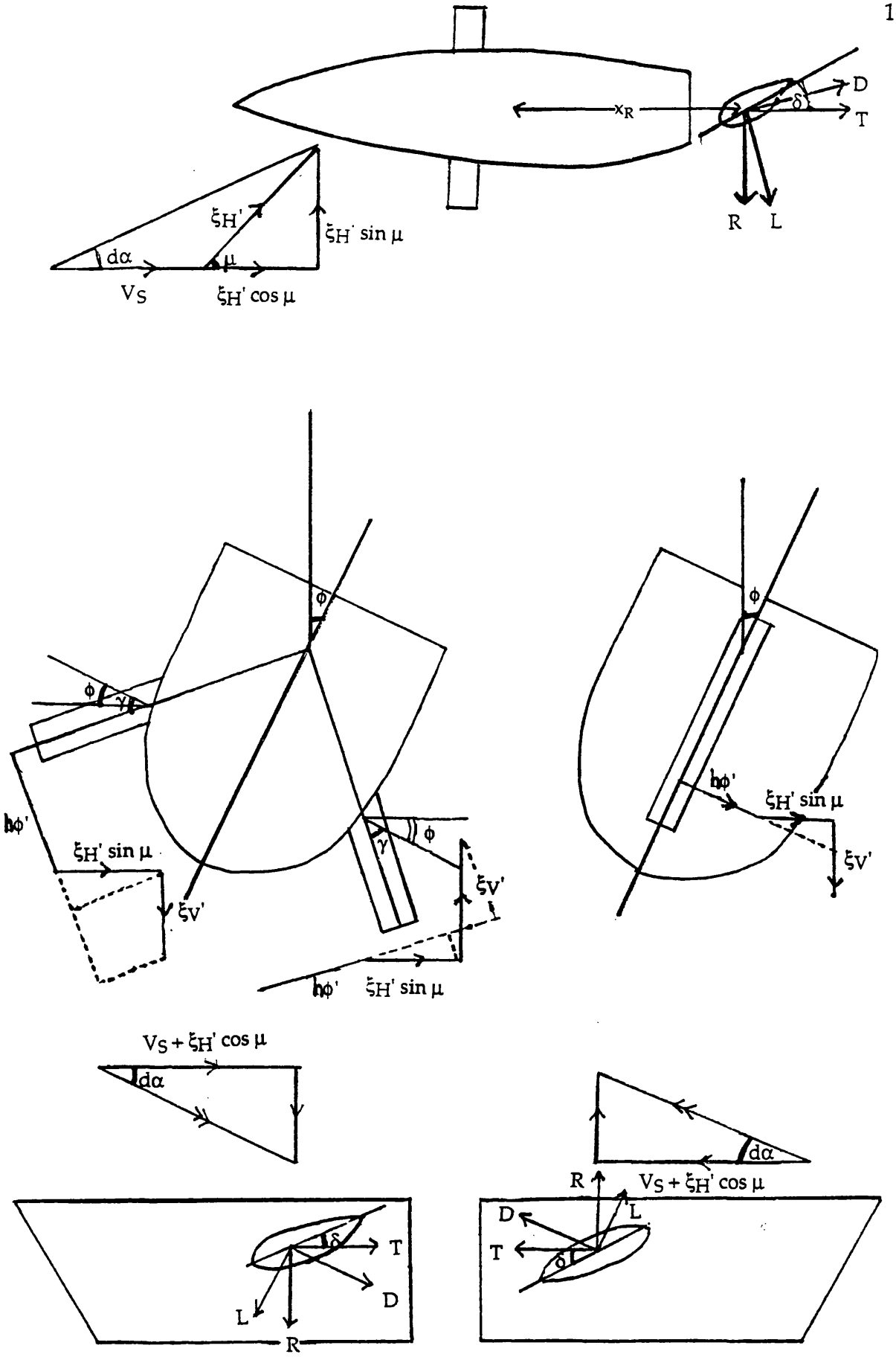

Fig. 29 Forces and velocities on fin and rudder stabilisers.

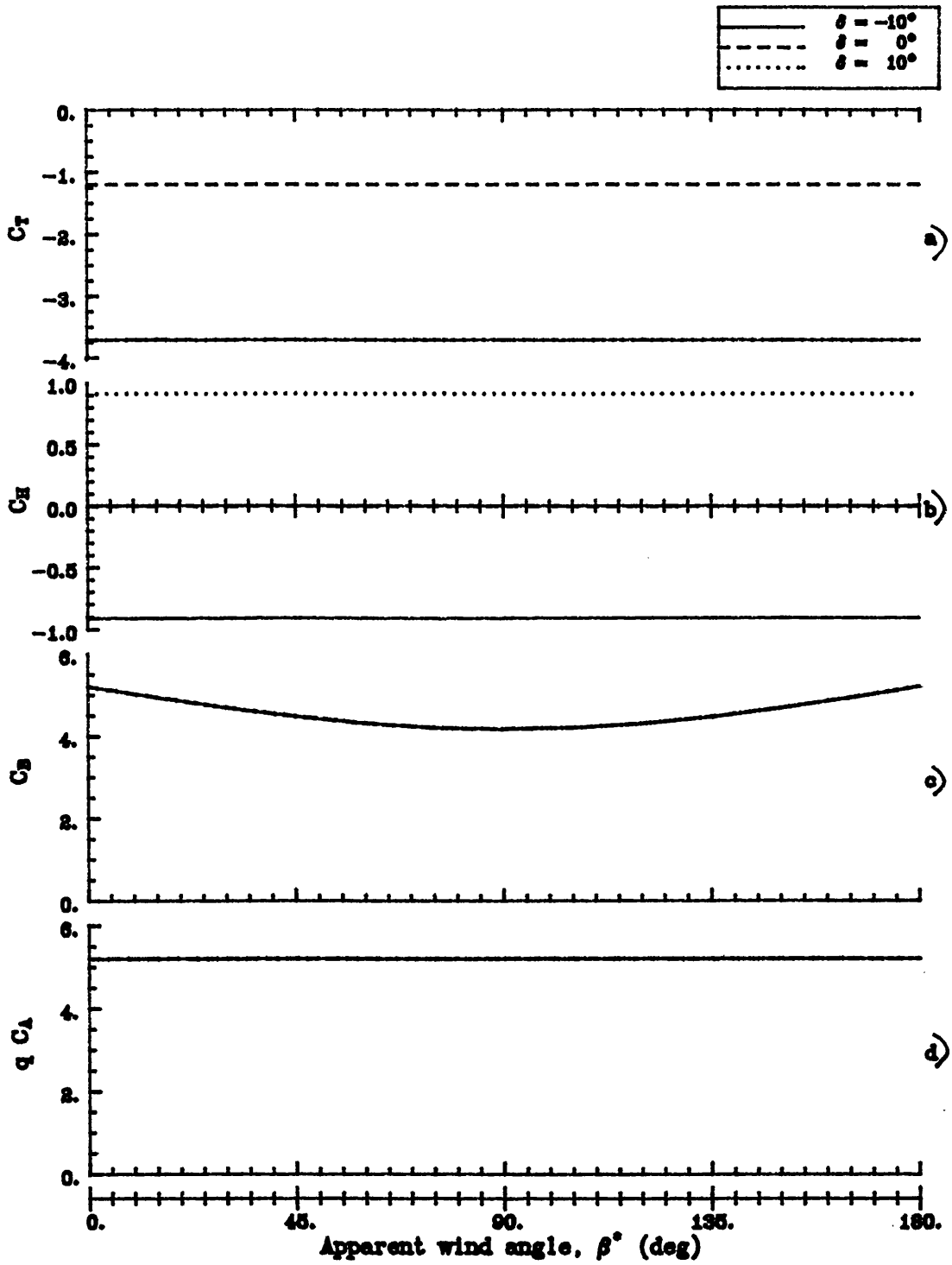

Fig. 30 Variations of C_T, C_H, C_B and qC_A as functions of wave heading μ^* for a fin stabiliser at deflection $\delta = 0, \pm 10^o$.

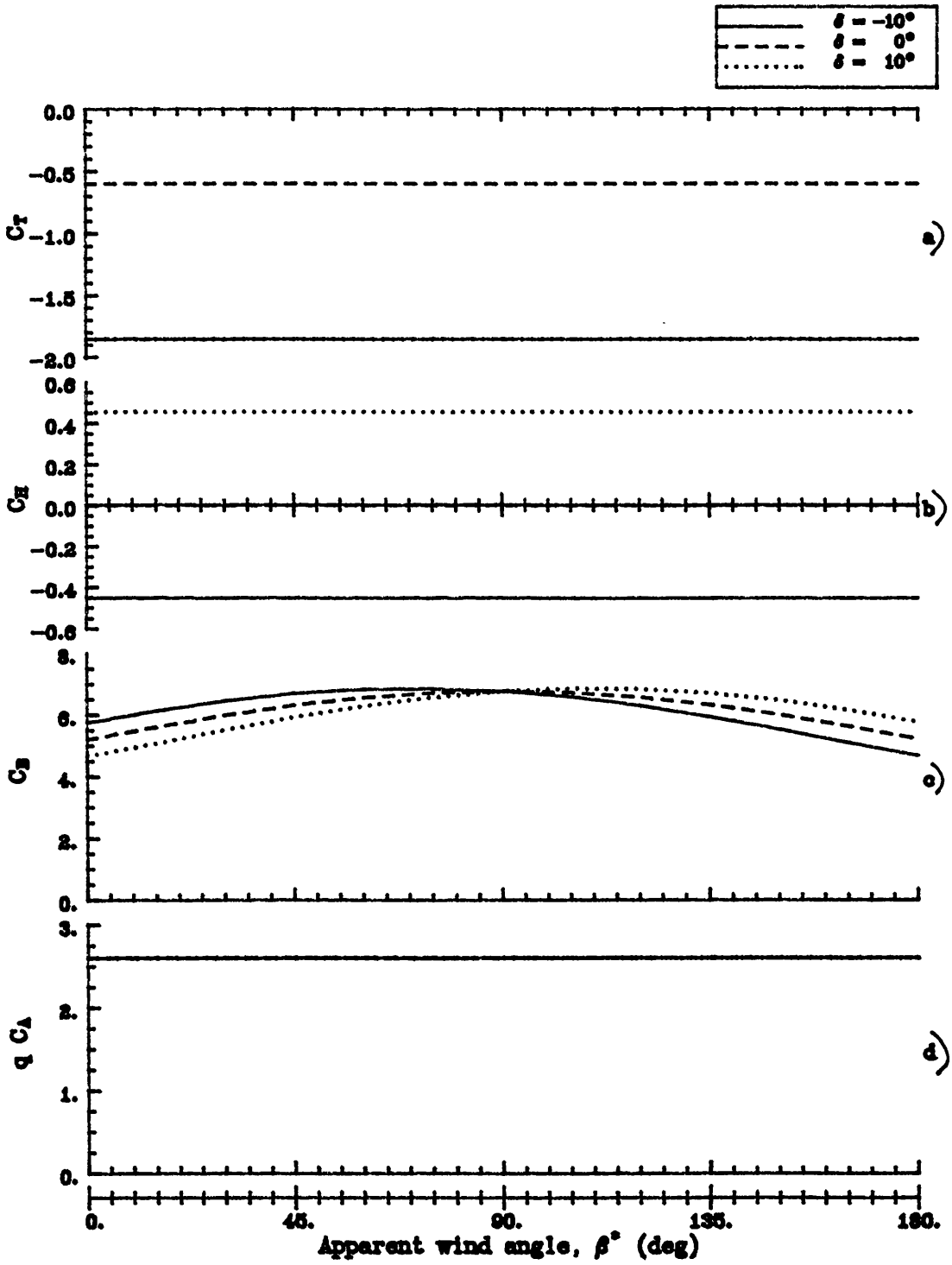

Fig. 31 Variations of C_T, C_H, C_B and qC_A as functions of wave heading μ^* for a rudder stabiliser at deflection $\delta = 0, \pm 10^o$.

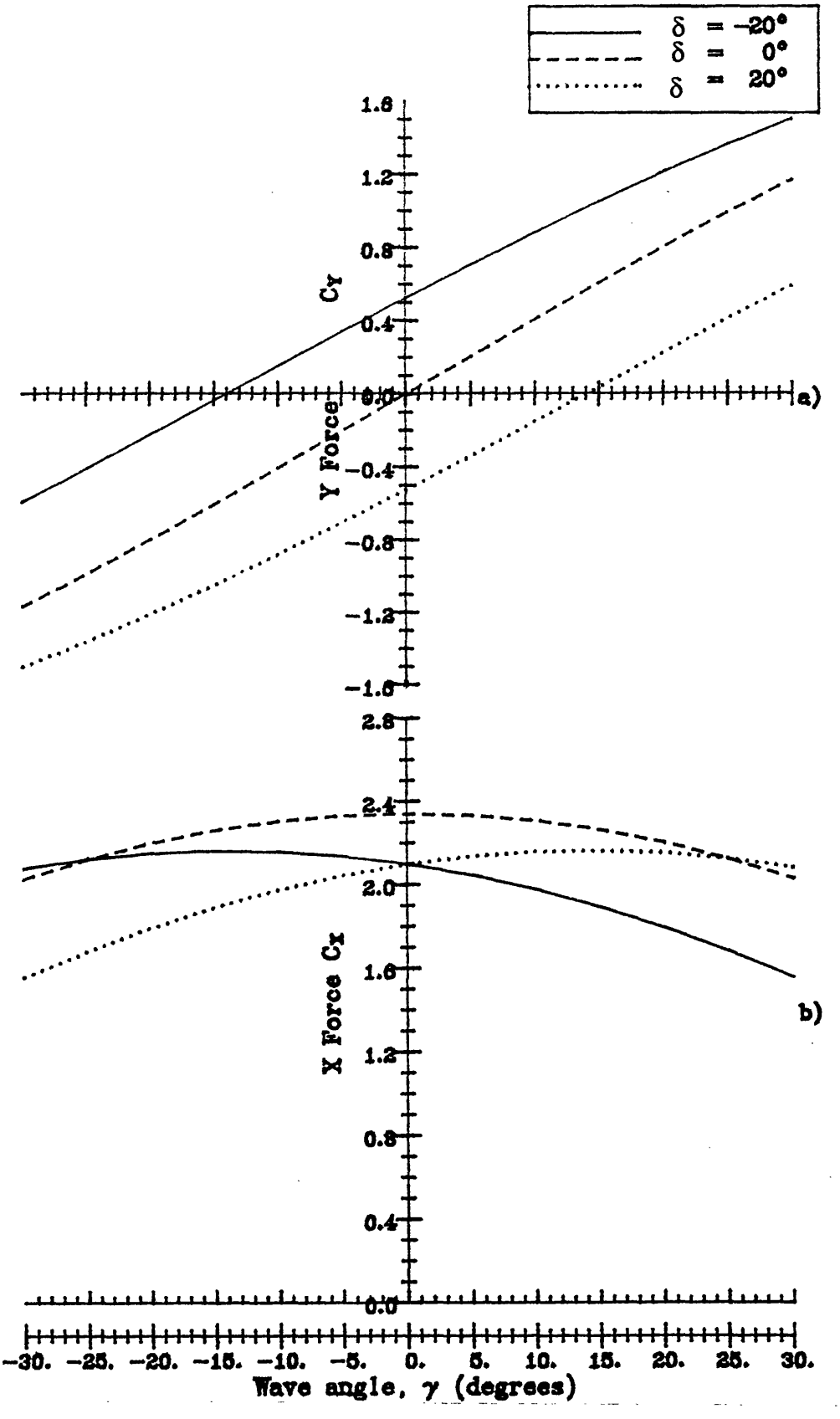

Fig. 32 X and Y force coefficients for a HAWT against wave angle, γ at yaw angles $\delta = 0, \pm 20^{o}$.

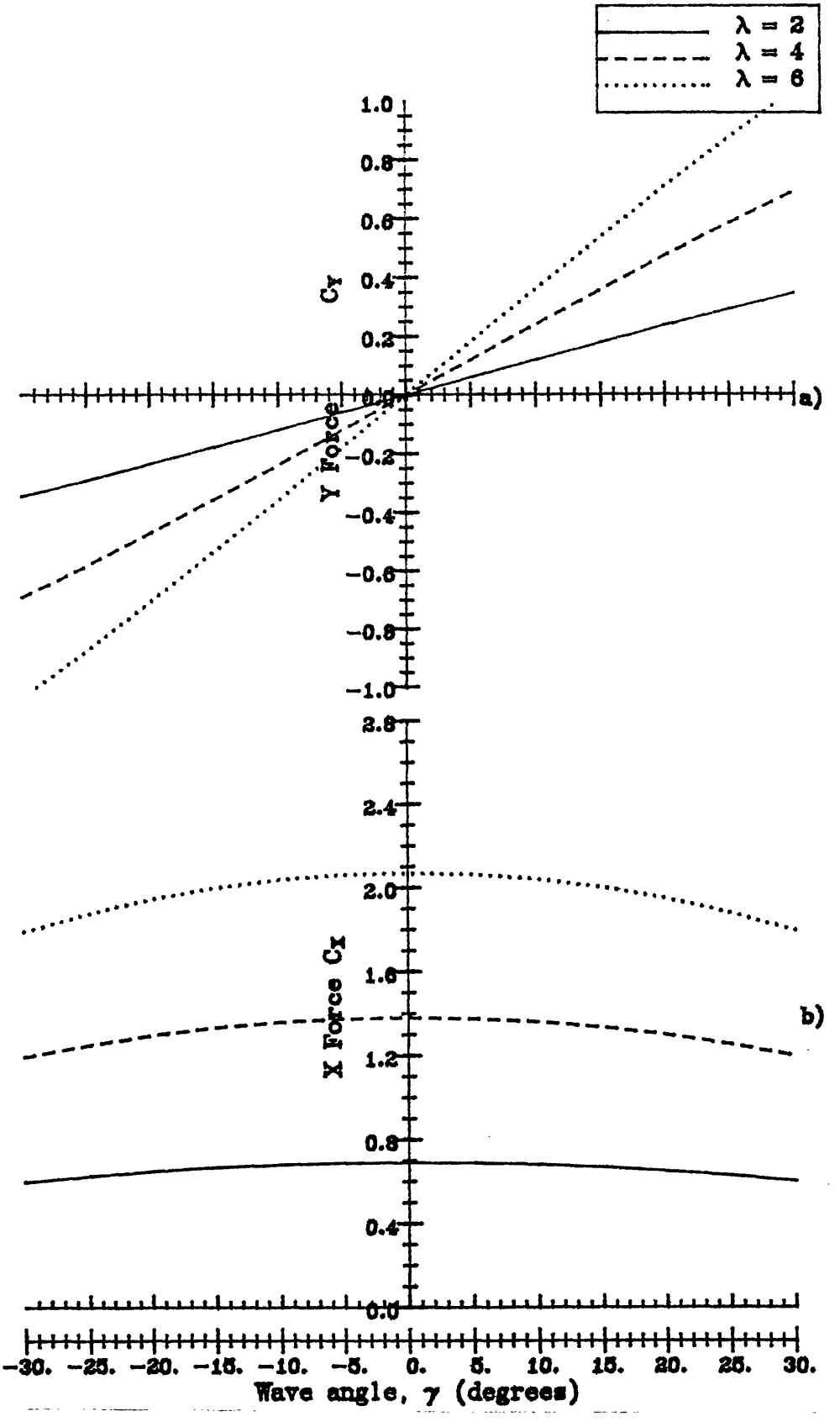

Fig. 33 X and Y force coefficients for a VAWT against wave angle, γ.

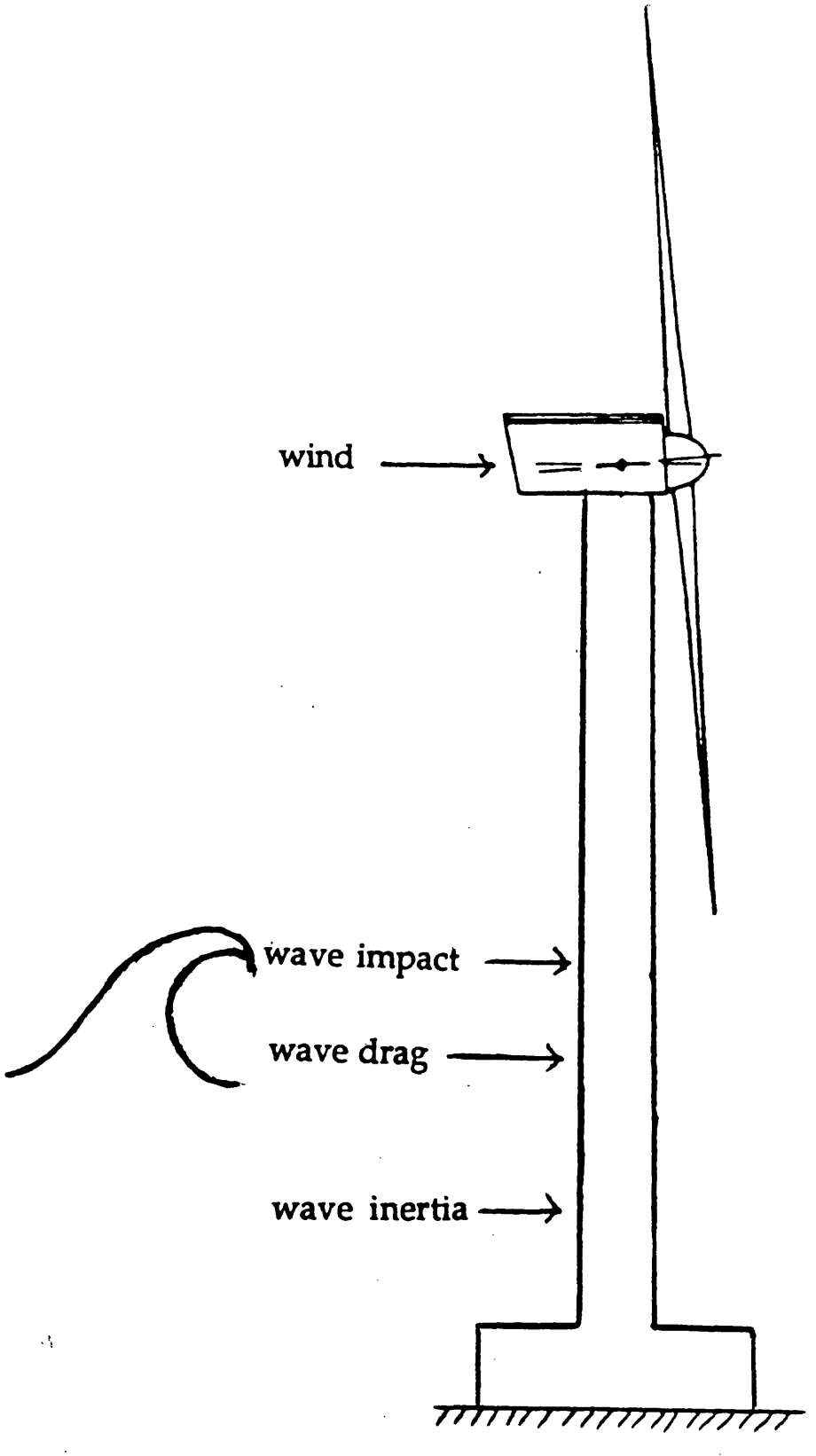

Fig. 34 Forces on the structure.

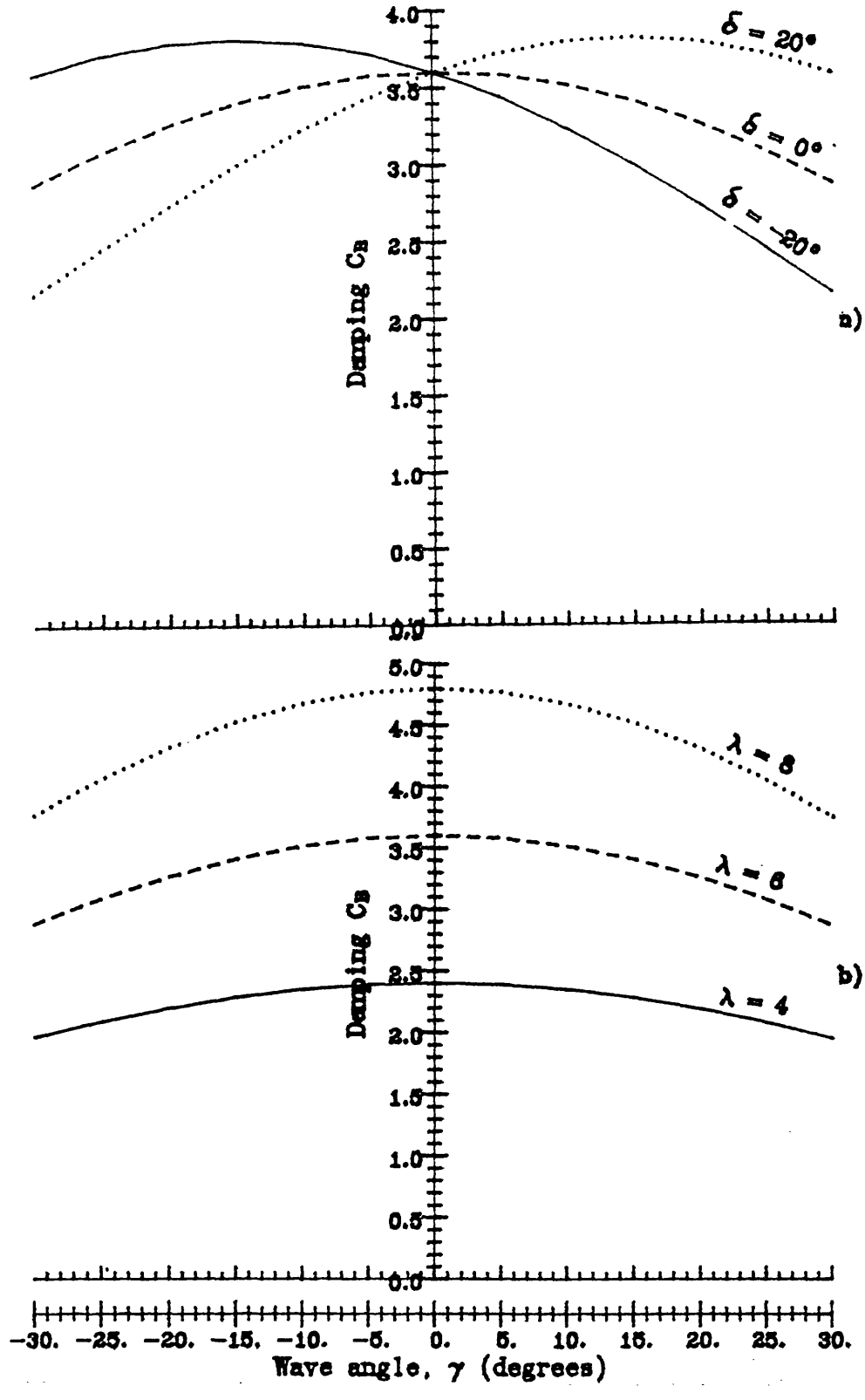

Fig. 35 Damping coefficients for a HAWT against wave angle, γ for yaw angle $\delta = 0, \pm 20^{o}$ and tip-speed ratio $\lambda = 4, 6, 8$.

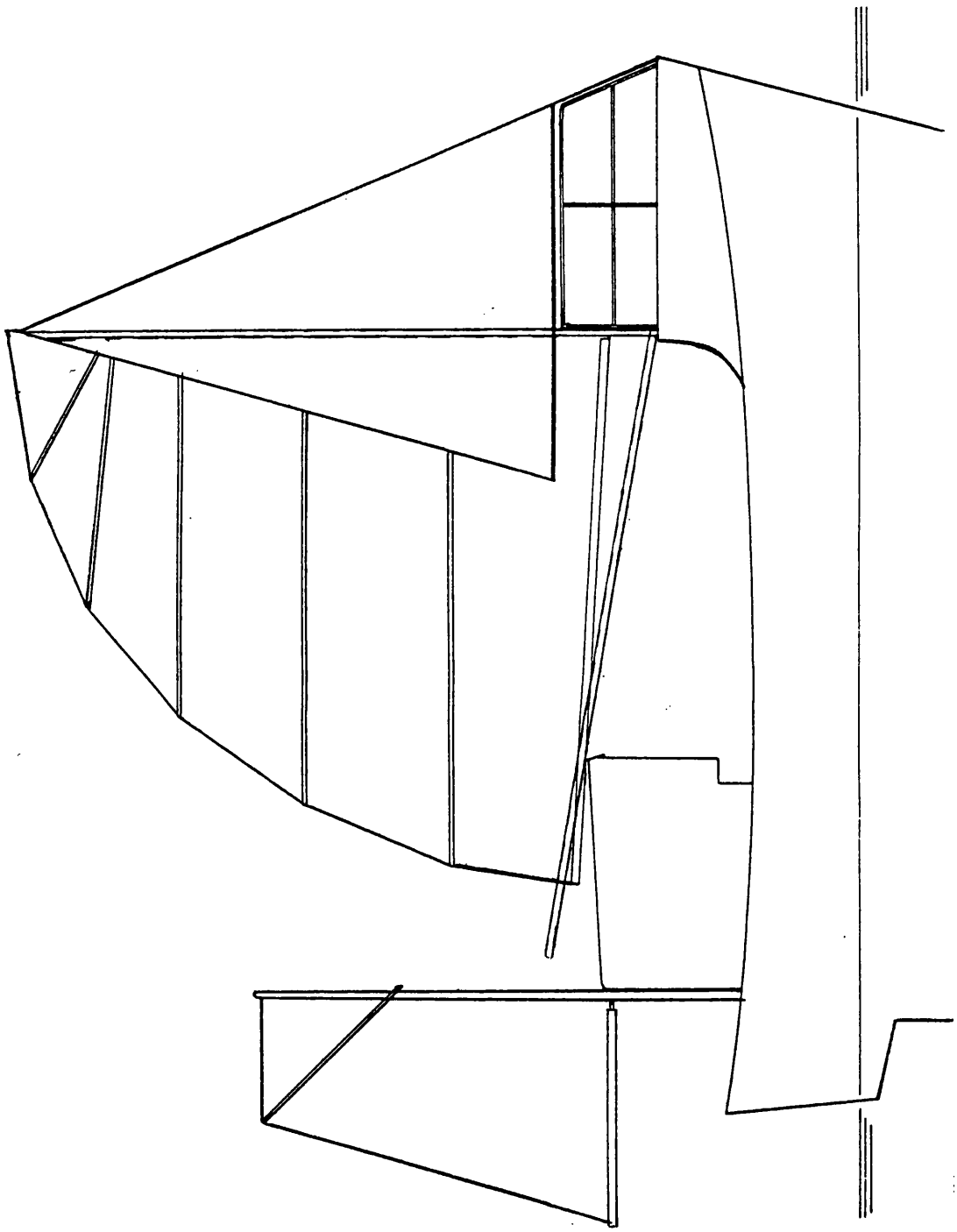

Fig. 36 Sketch of MFV Resolution.

Fig. 37 Photographs of MFV Resolution.

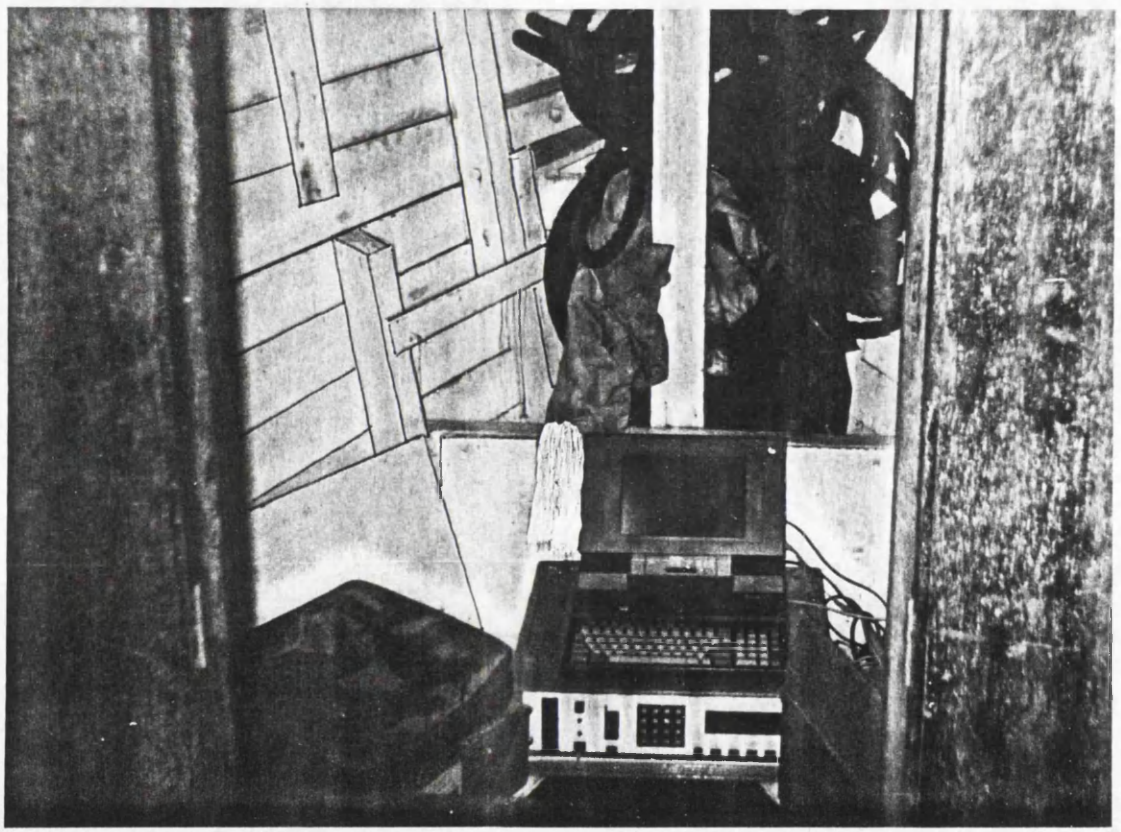

Fig. 38 The computer and datalogger on board MFV Resolution.

Fig. 39 Time history of roll angle from MFV Resolution travelling with sails and motor together.

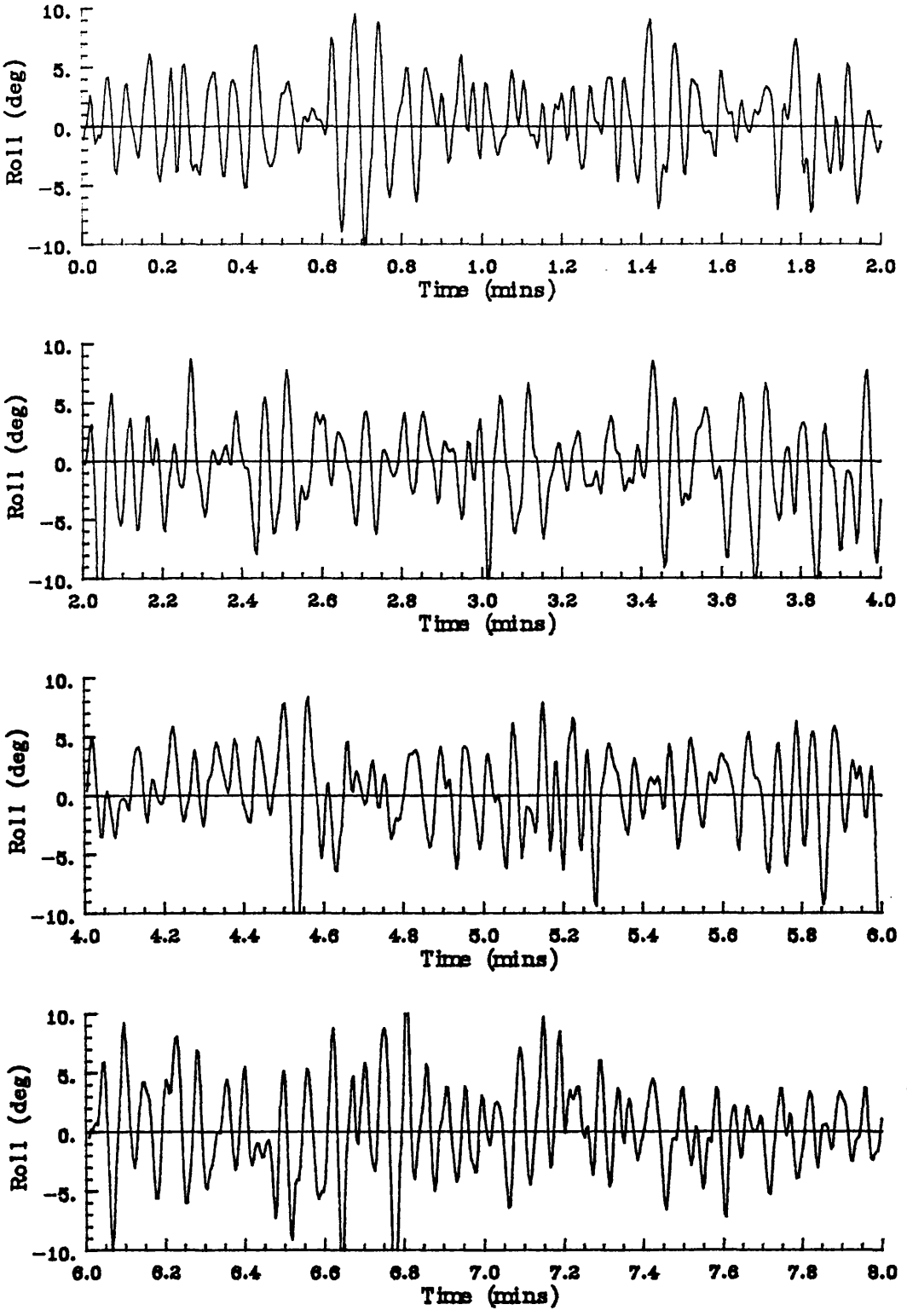

Fig. 40 Time history of roll angle from MFV Resolution travelling with sails alone.

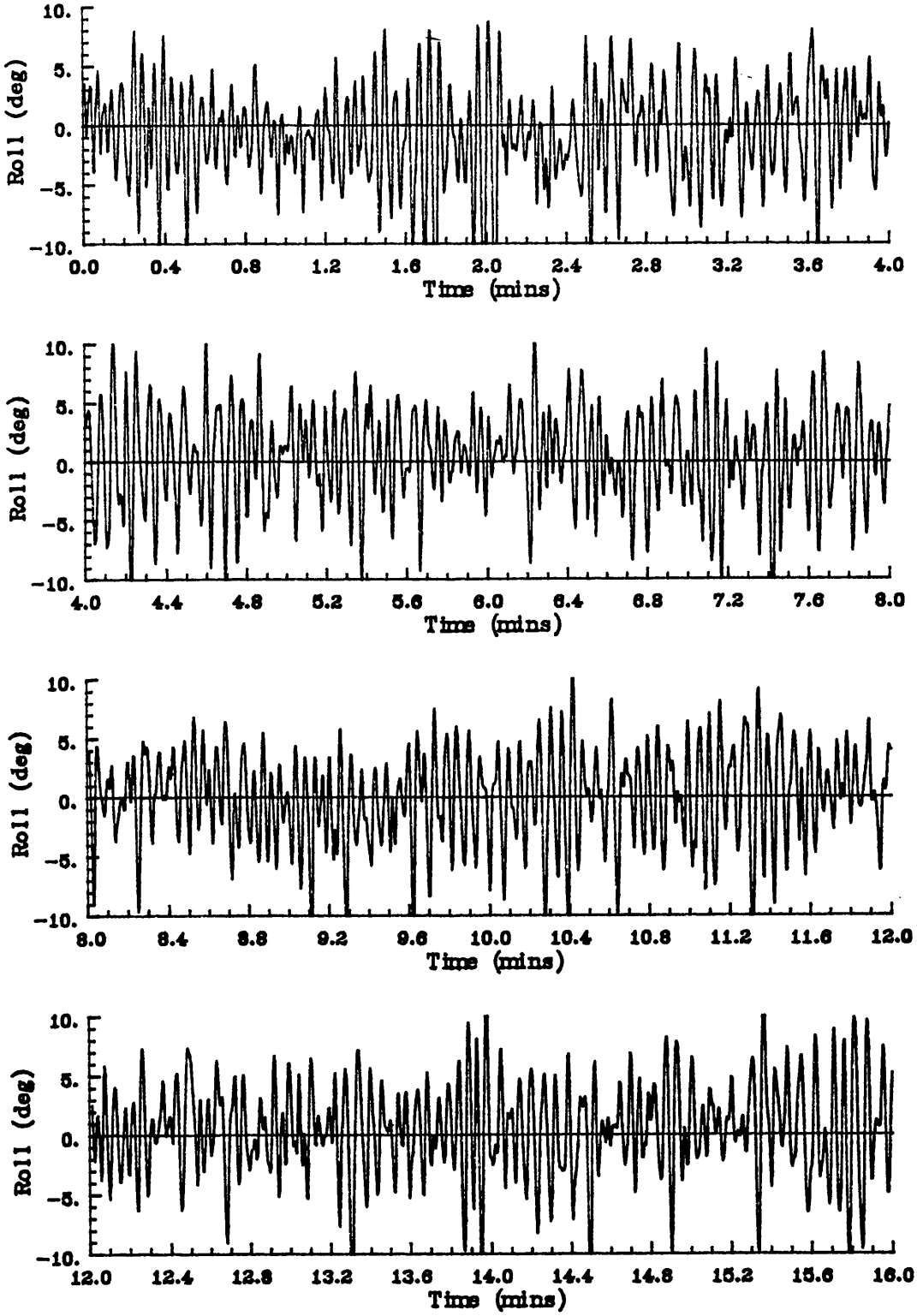

Fig. 41 Time history of roll angle from MFV Resolution travelling with motor alone.

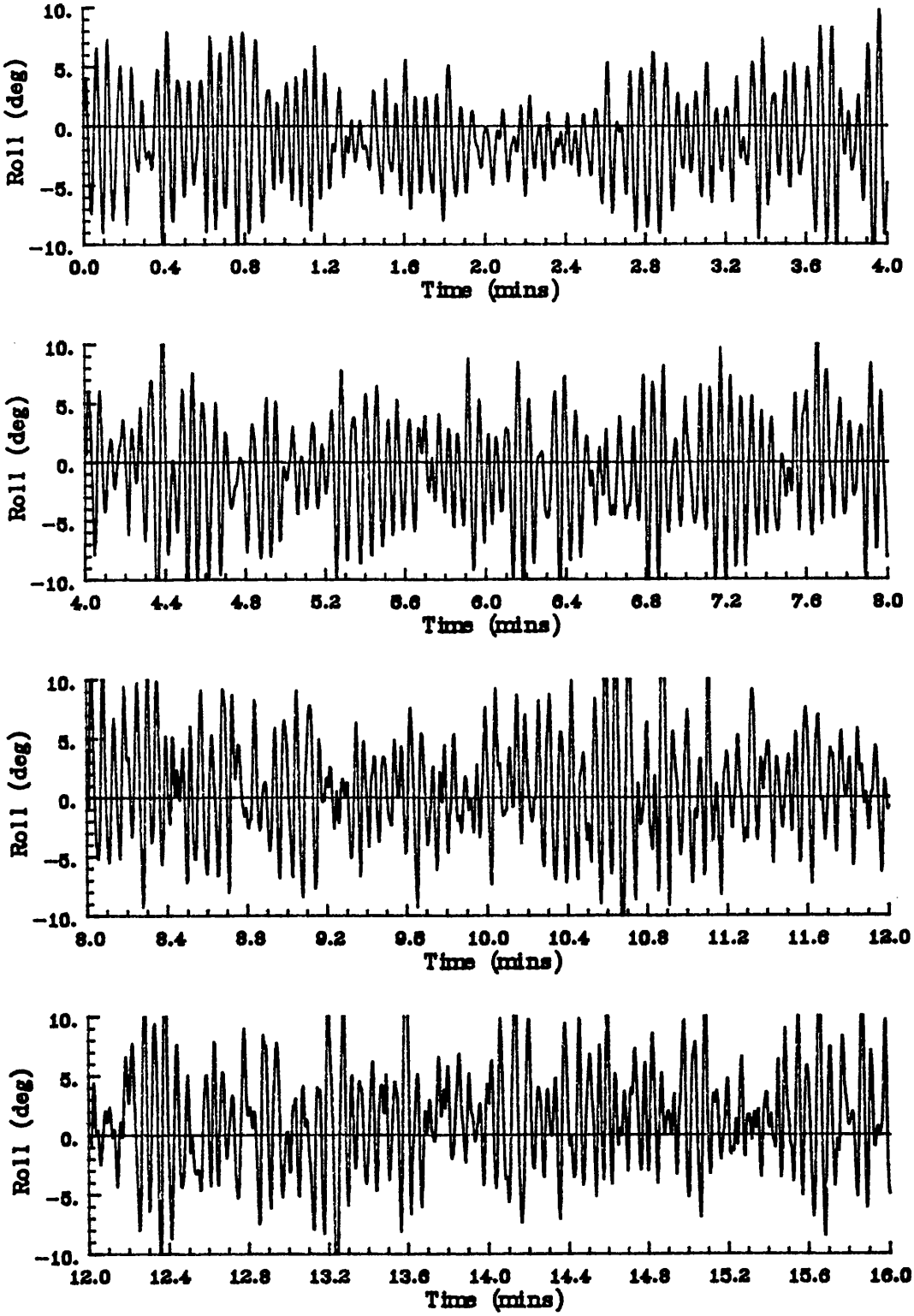

Fig. 42 Analysis of roll spectral density from measurements on MFV Resolution.

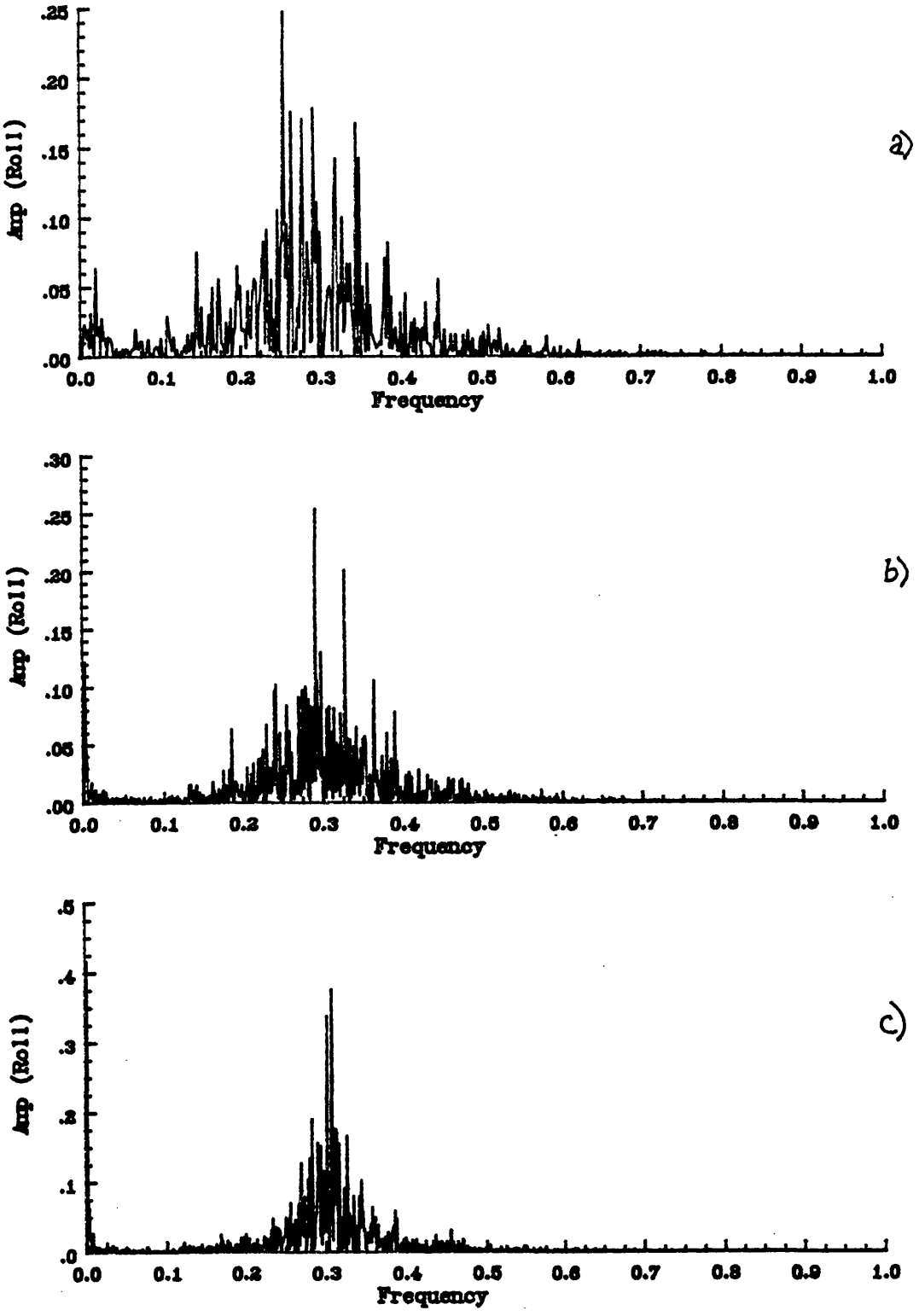

Fig. 43 Smoothed roll spectral density from measurements on MFV Resolution.

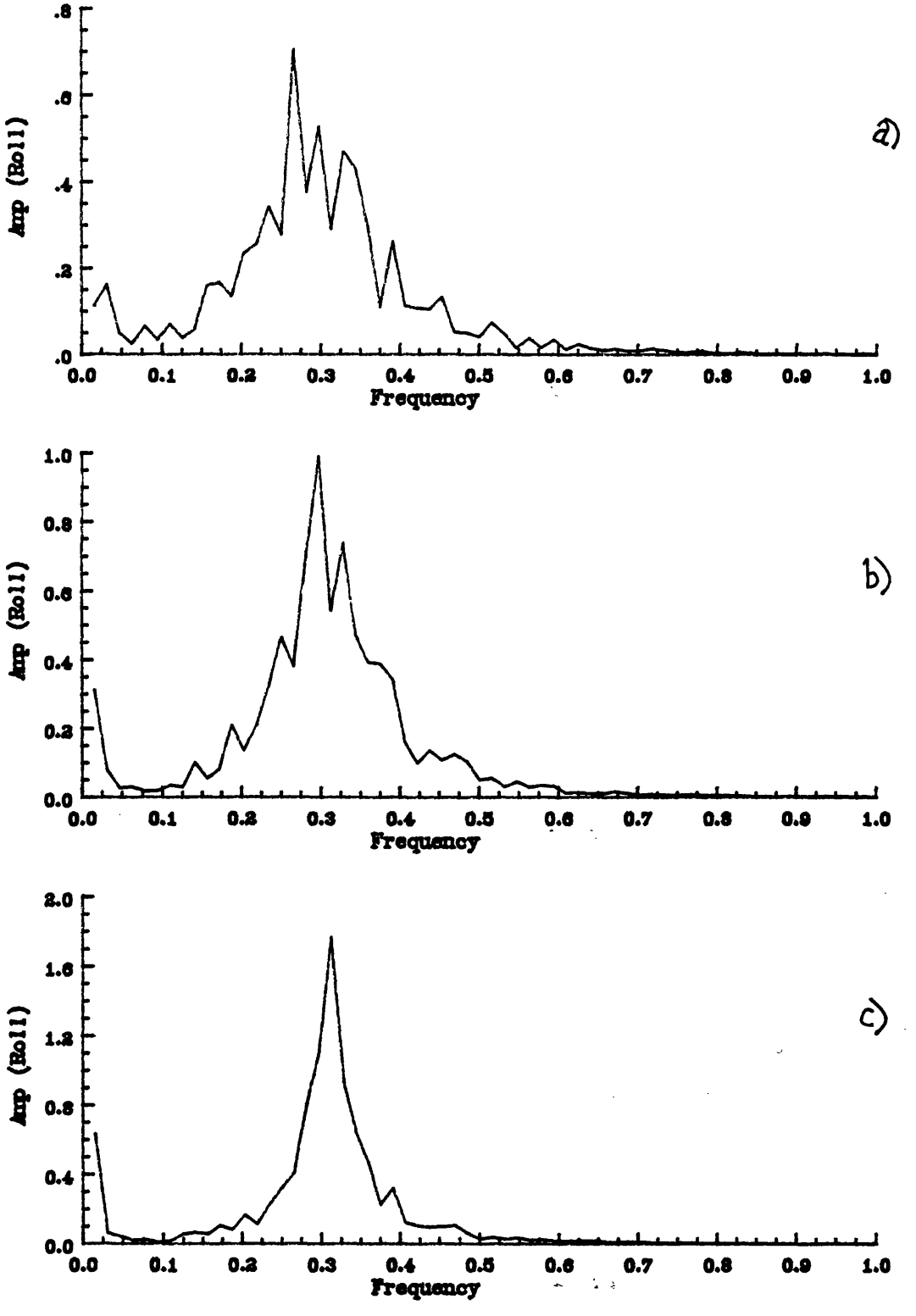

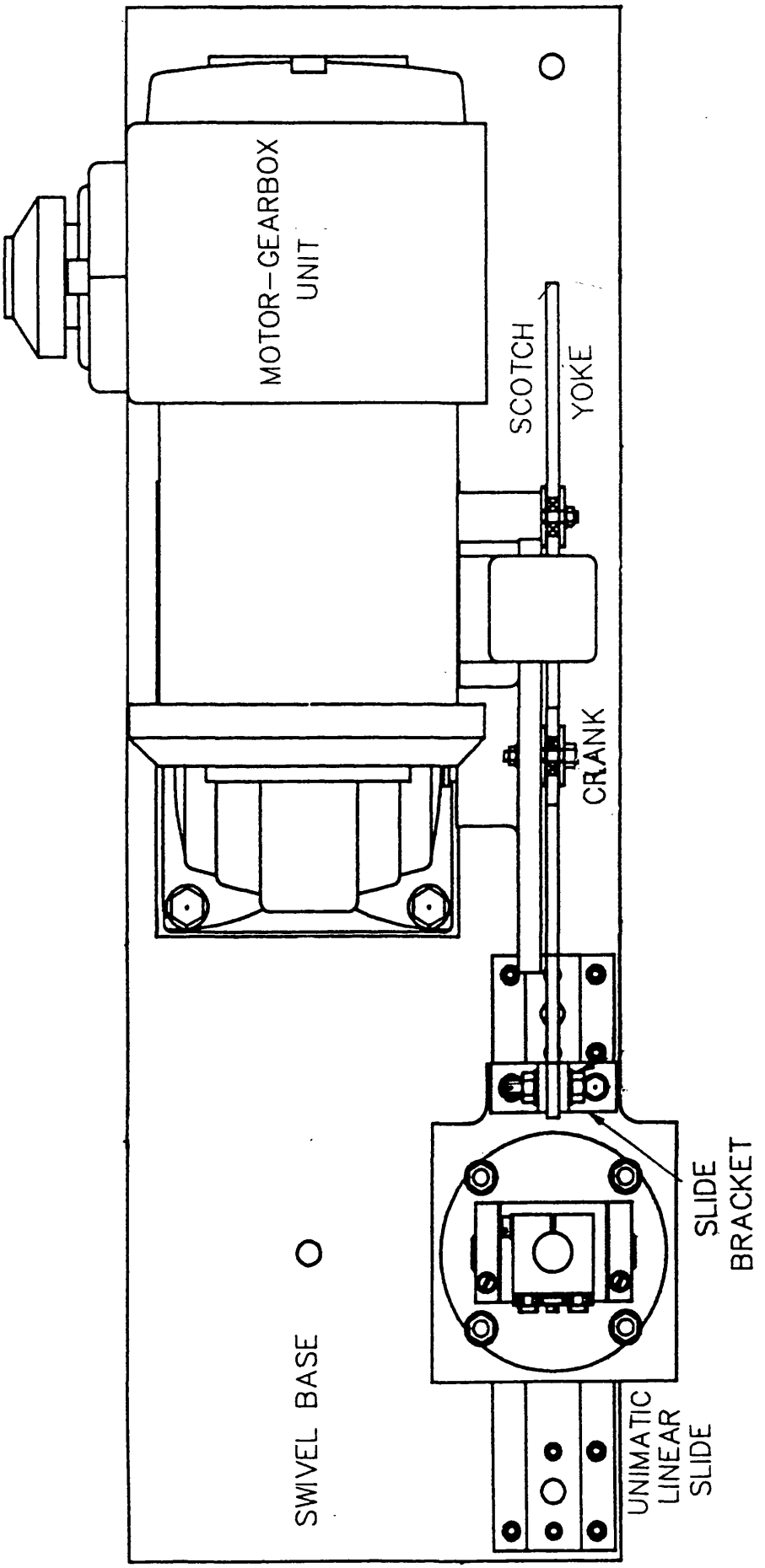

Fig. 44 General arrangement of the test rig.

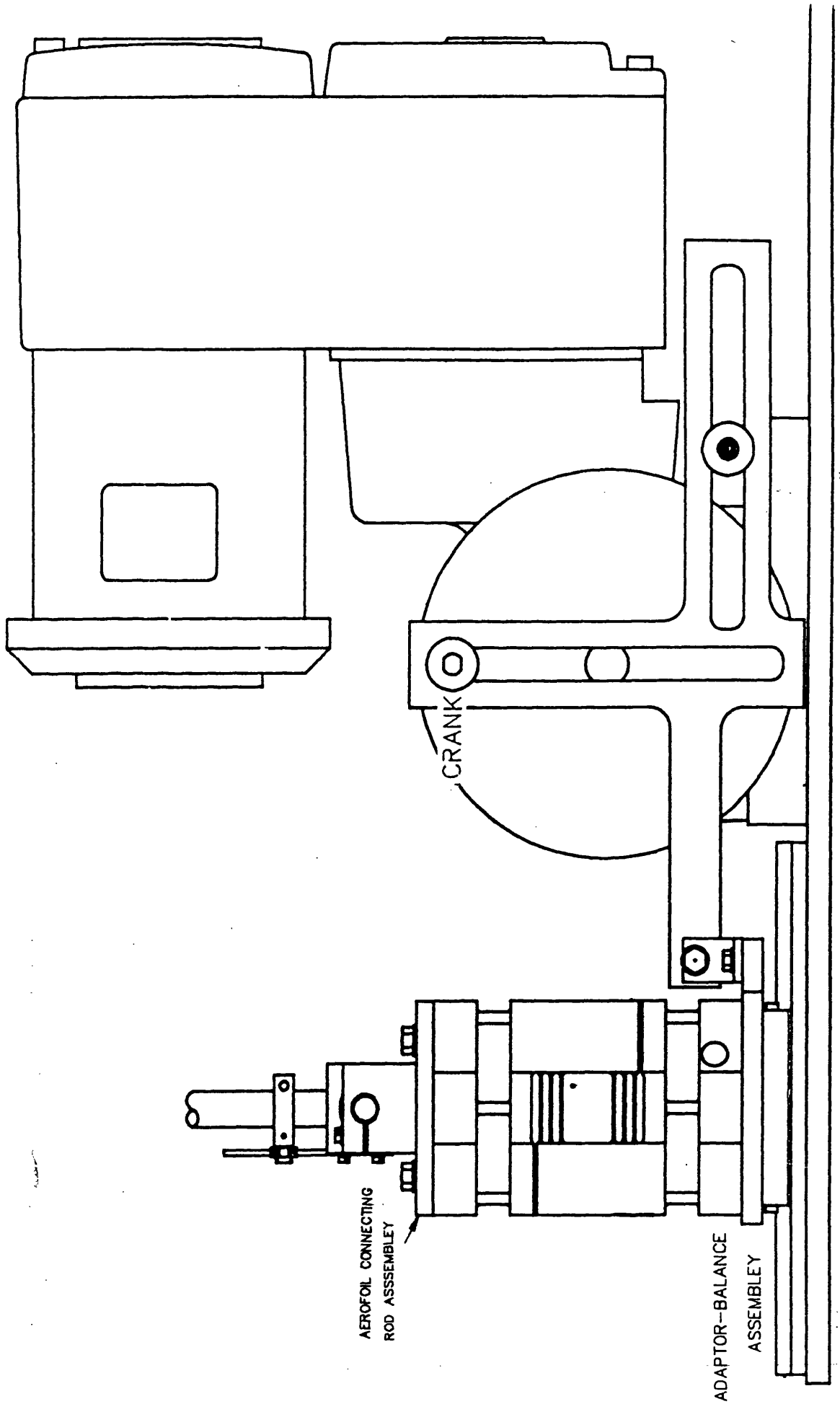
CRANK
AEROFOIL CONNECTING
ROD ASSSEMBLEY
ADAPTOR--BALANCE
ASSEMBLEY

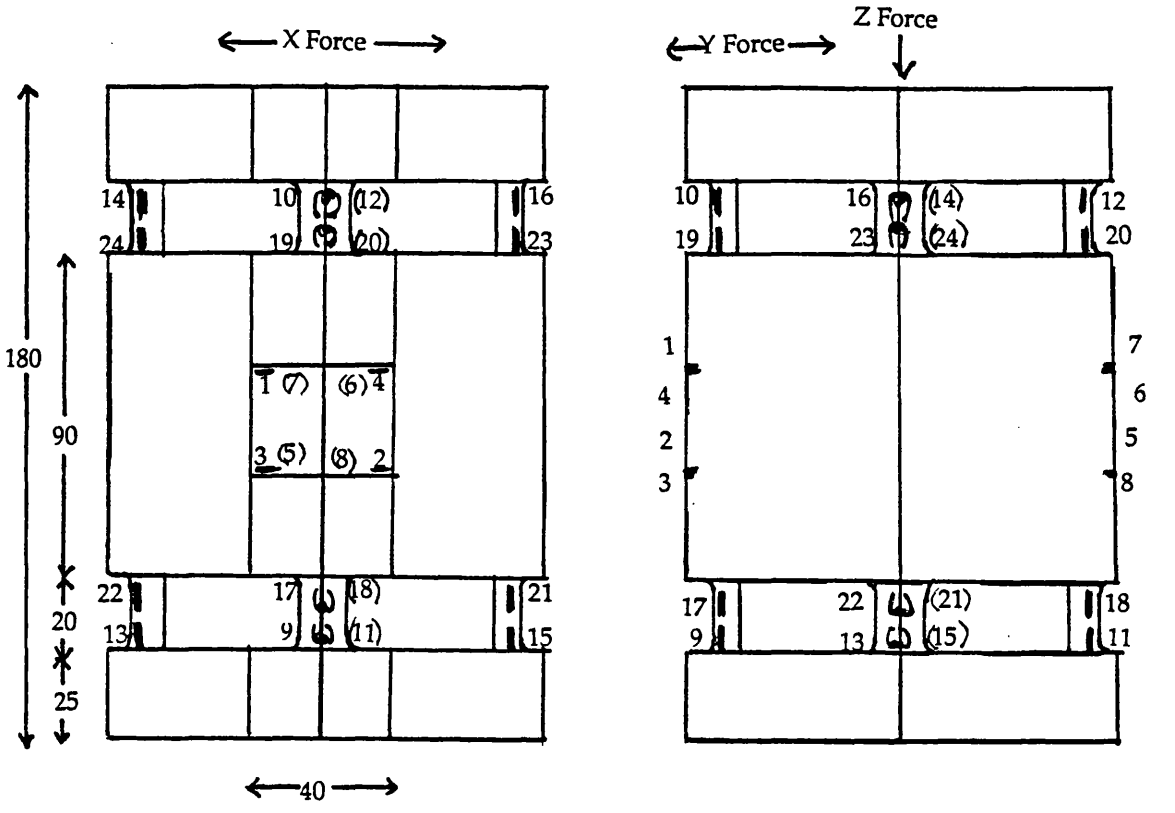

Fig. 45 The force balance.

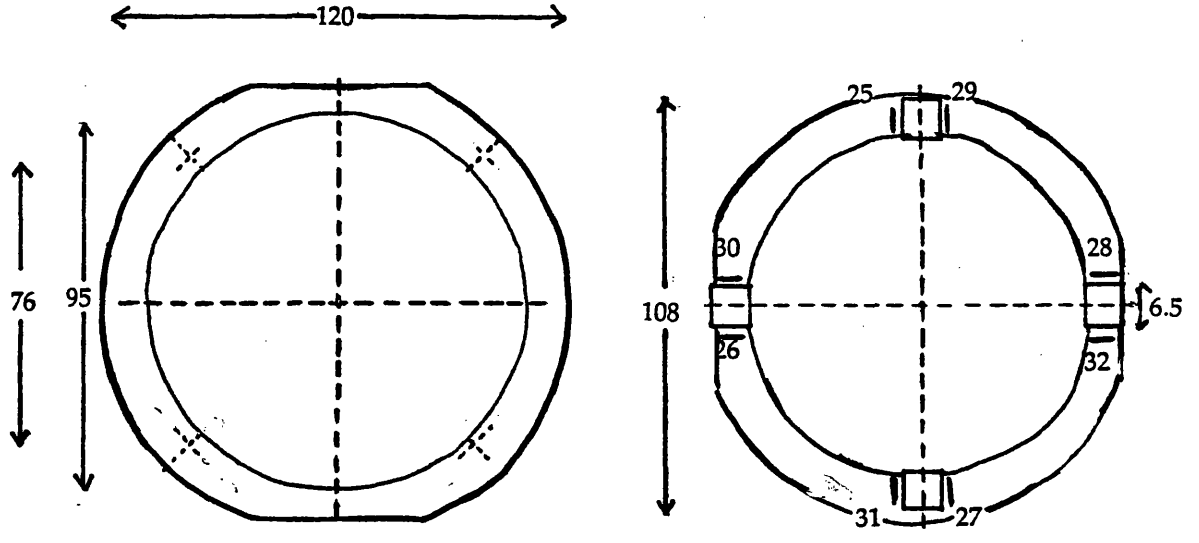

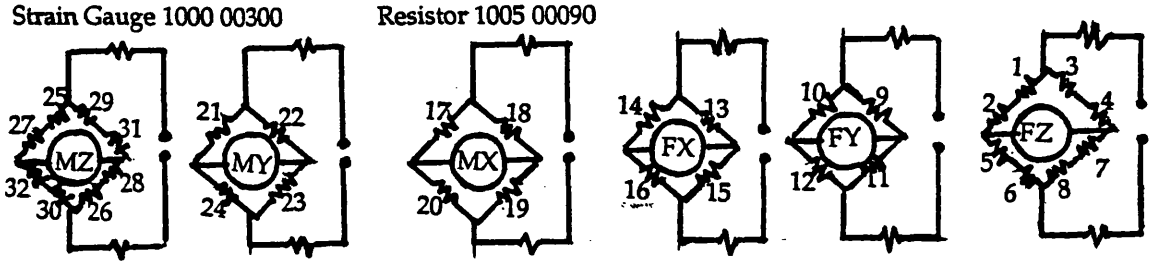

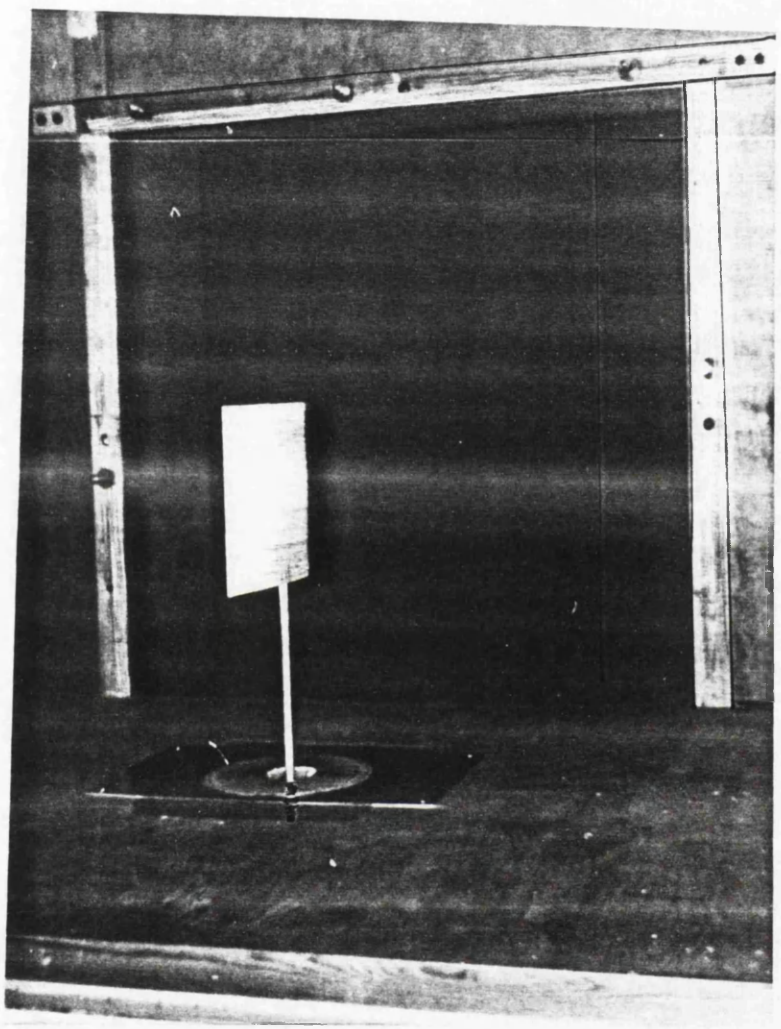

Fig. 46 Aerofoil of aspect ratio 1 under test.

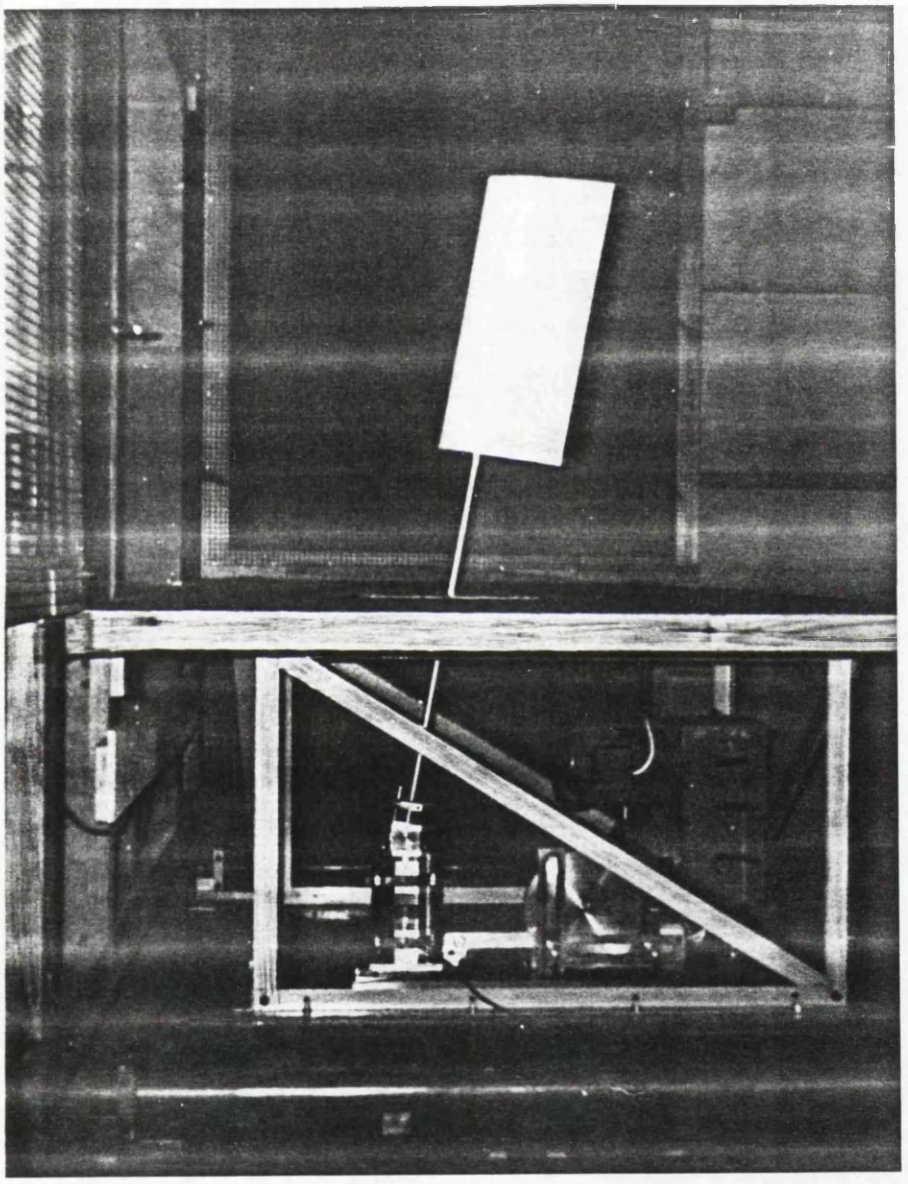

Fig. 47 Aerofoil of aspect ratio 2 under test.

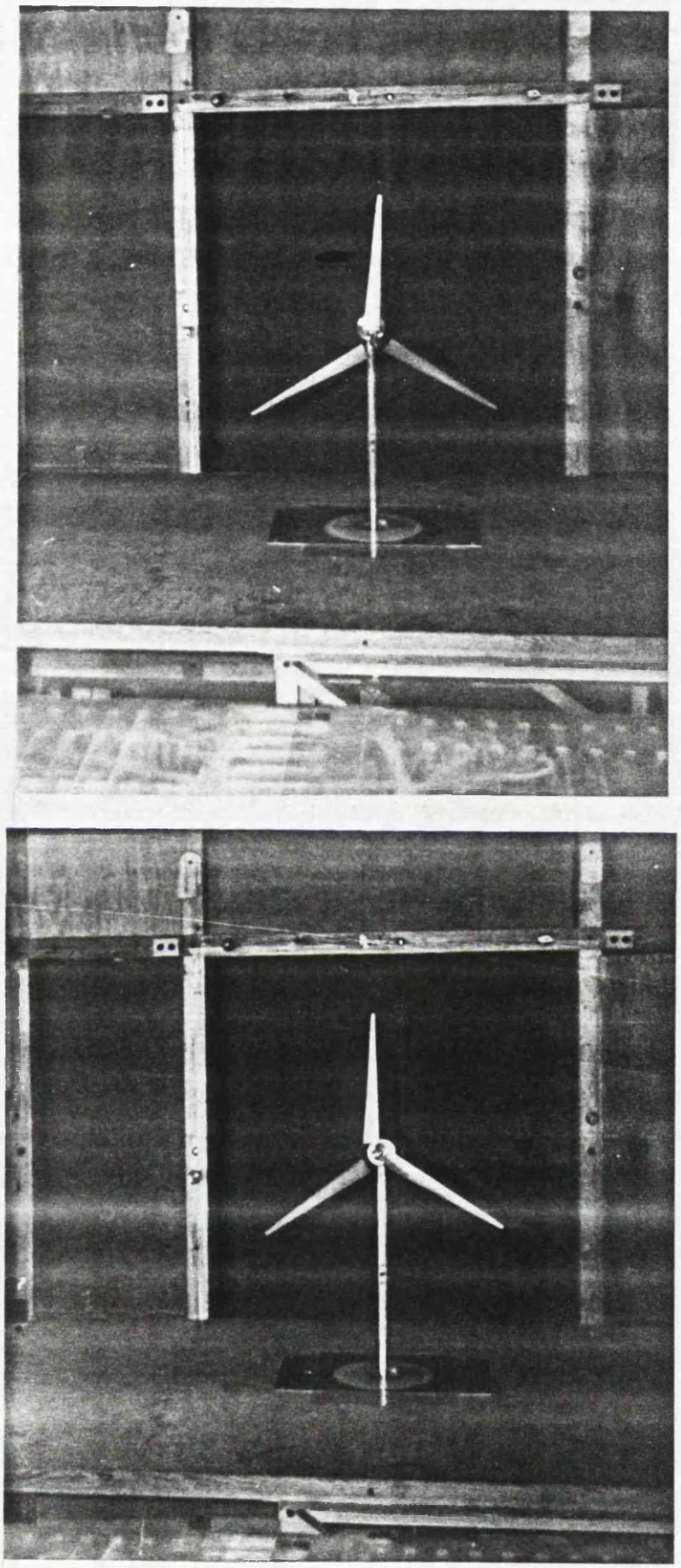

Fig. 48 Wind turbine under test.

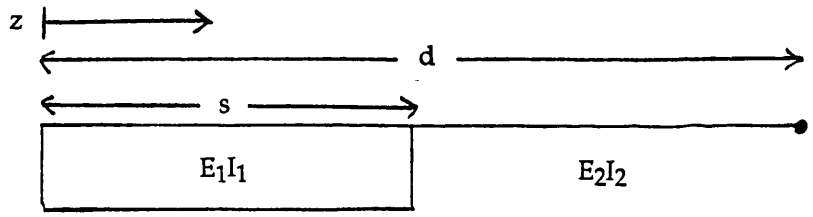

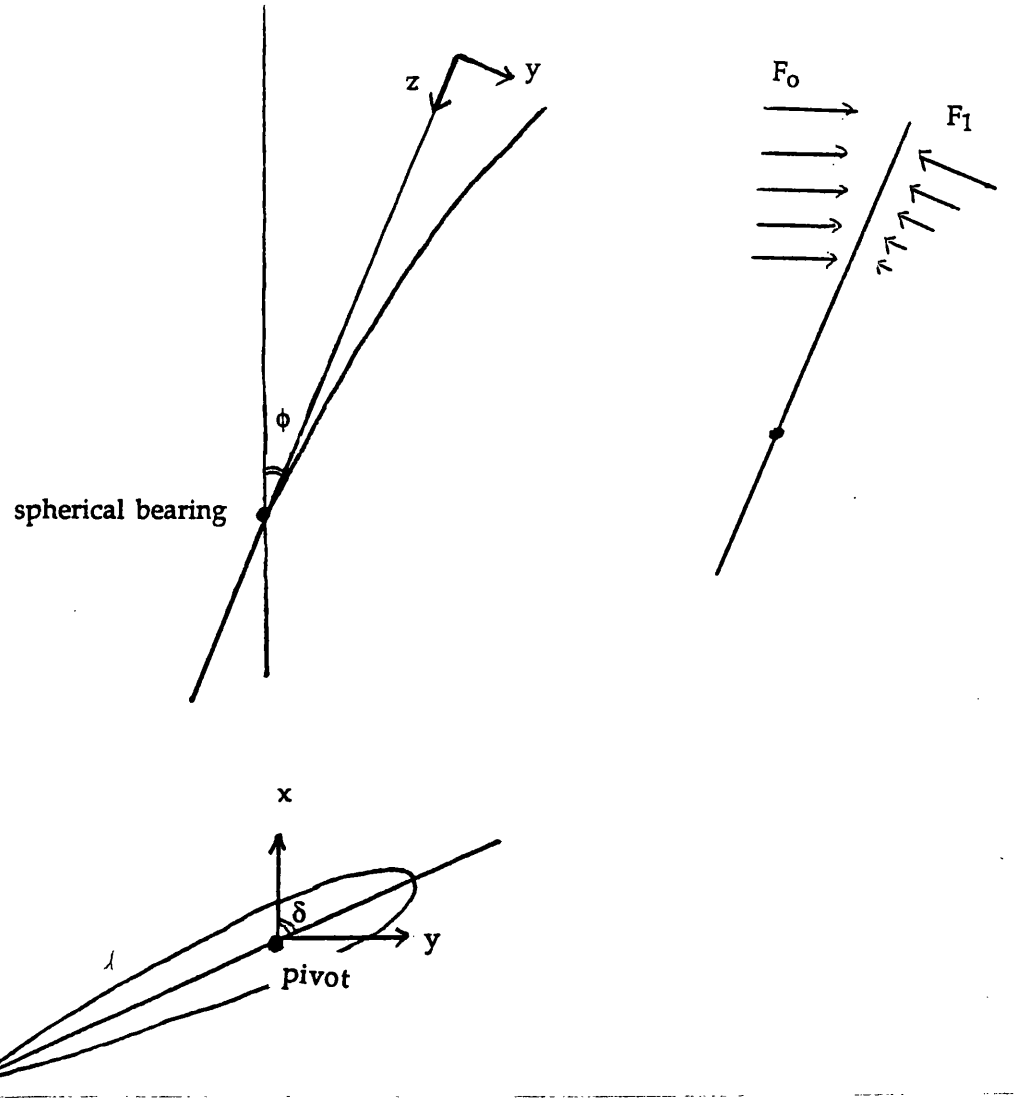

Fig. 49 Axes for the deflection of the aerofoil.

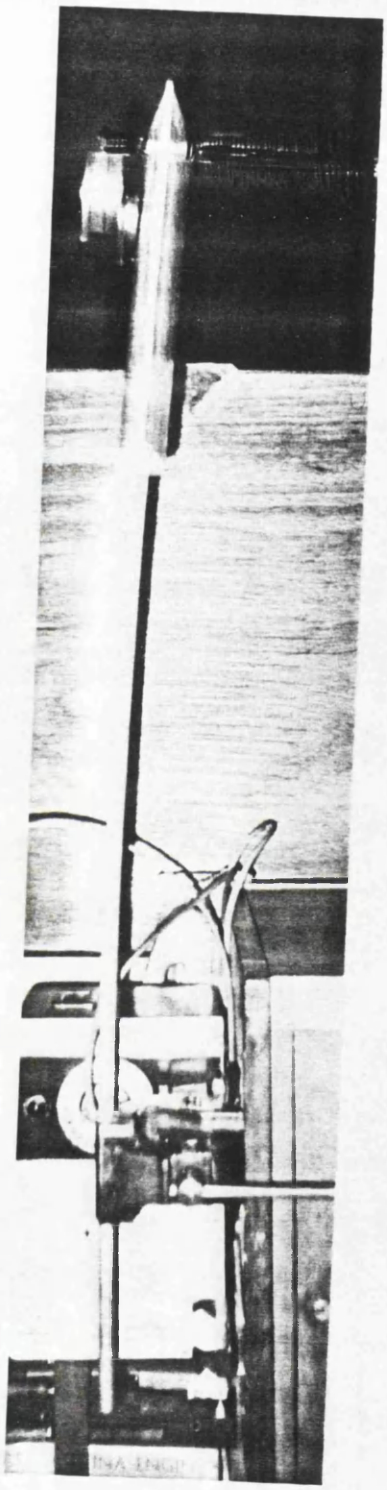

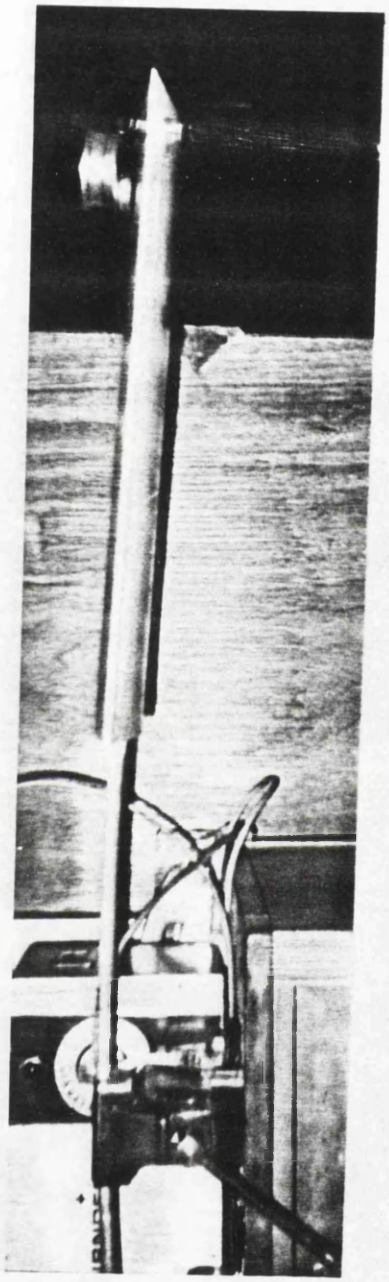

Fig. 50 The deflection tests.

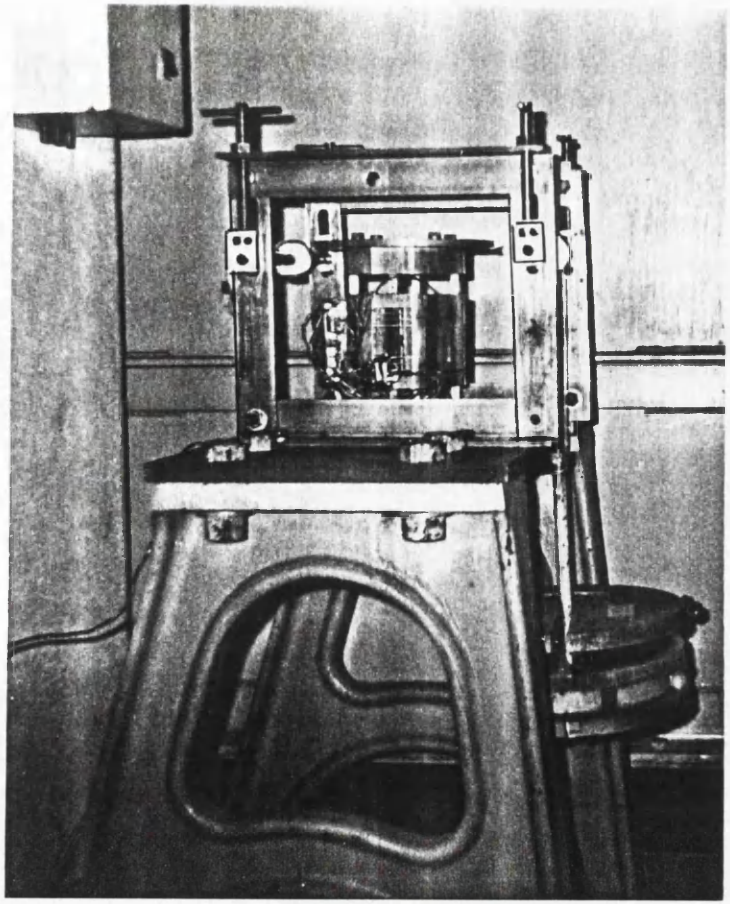

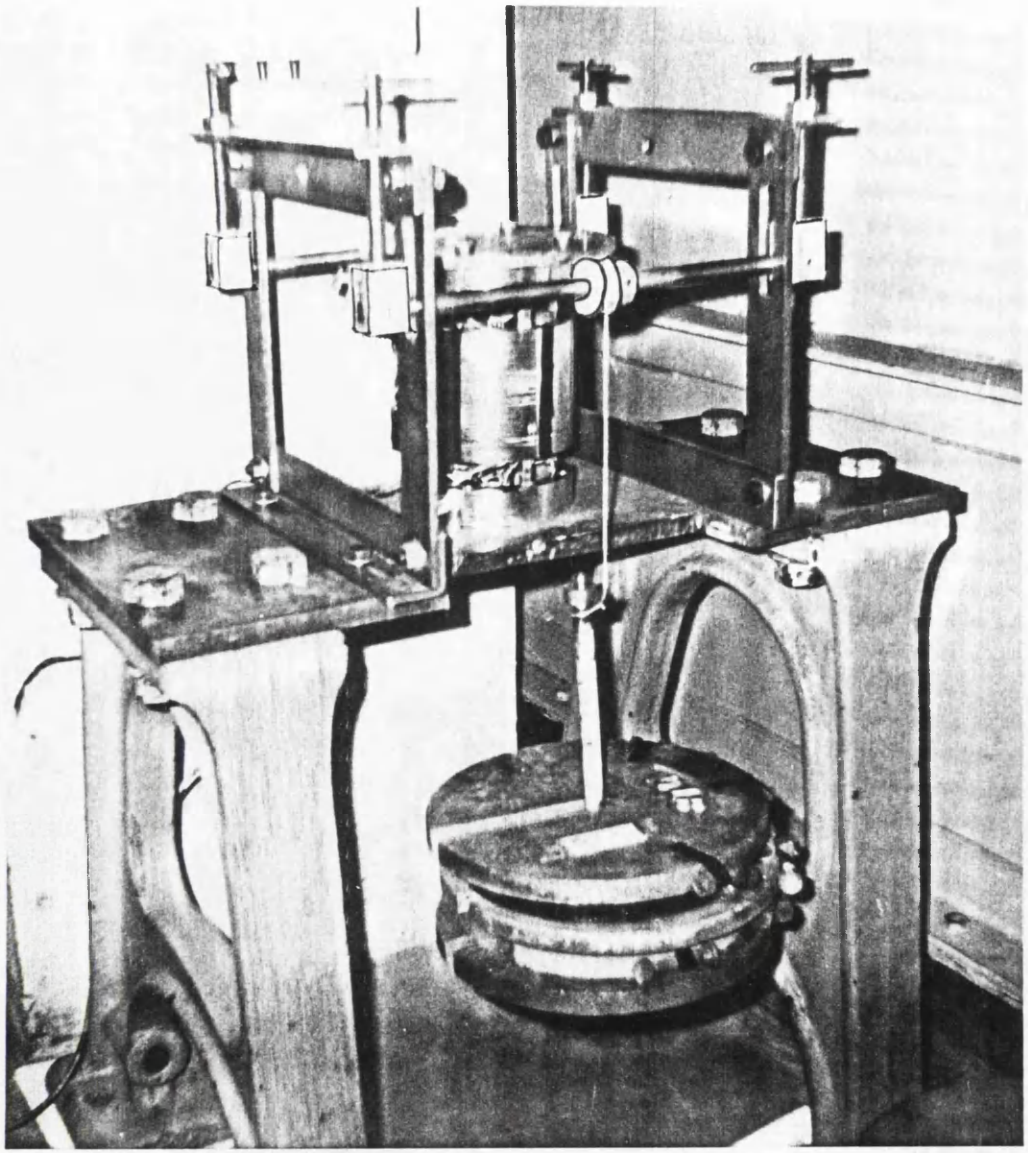

Fig. 51 The calibration rig.

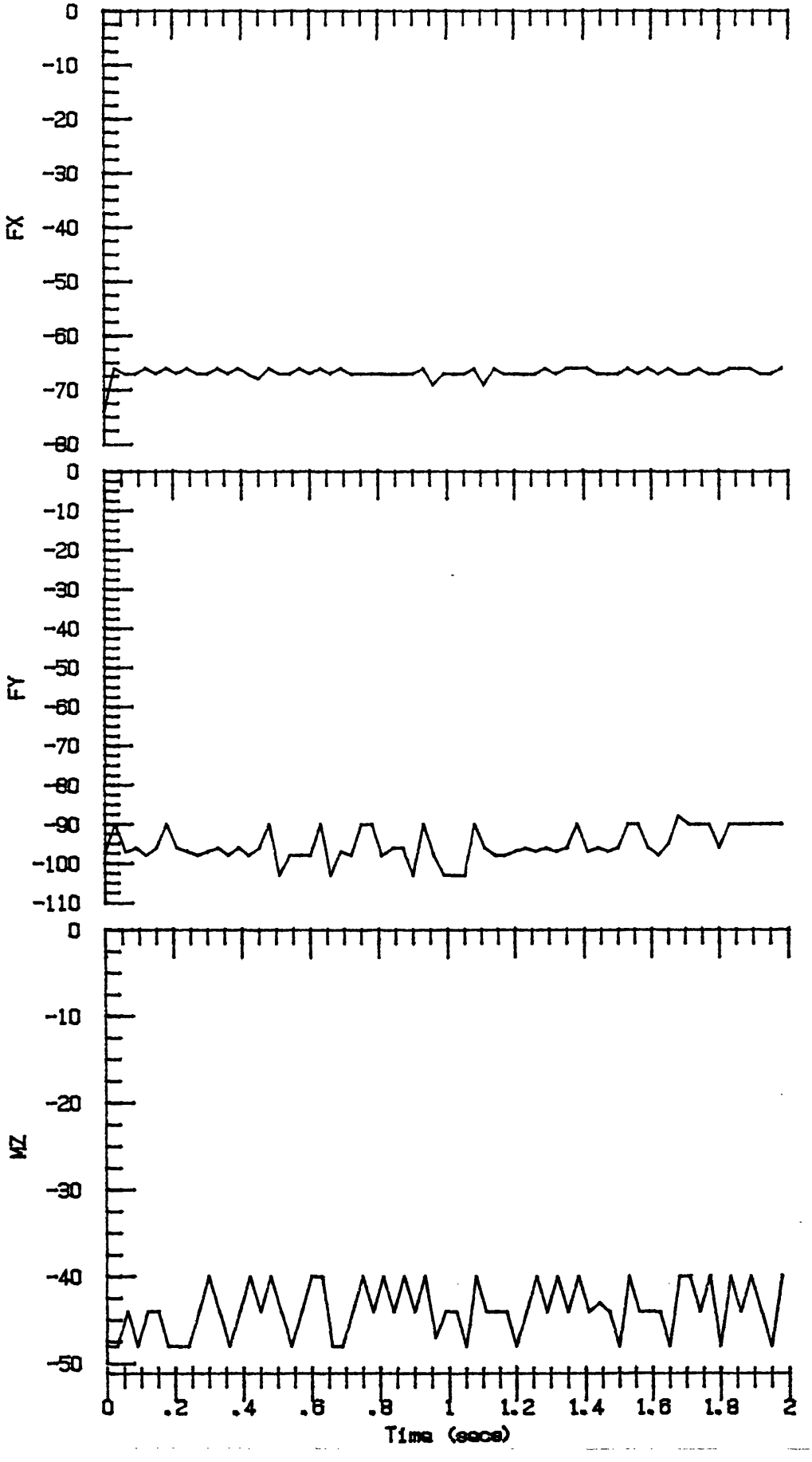

Fig. 52 Typical sample of raw data for steady flow on an aerofoil with no oscillation.

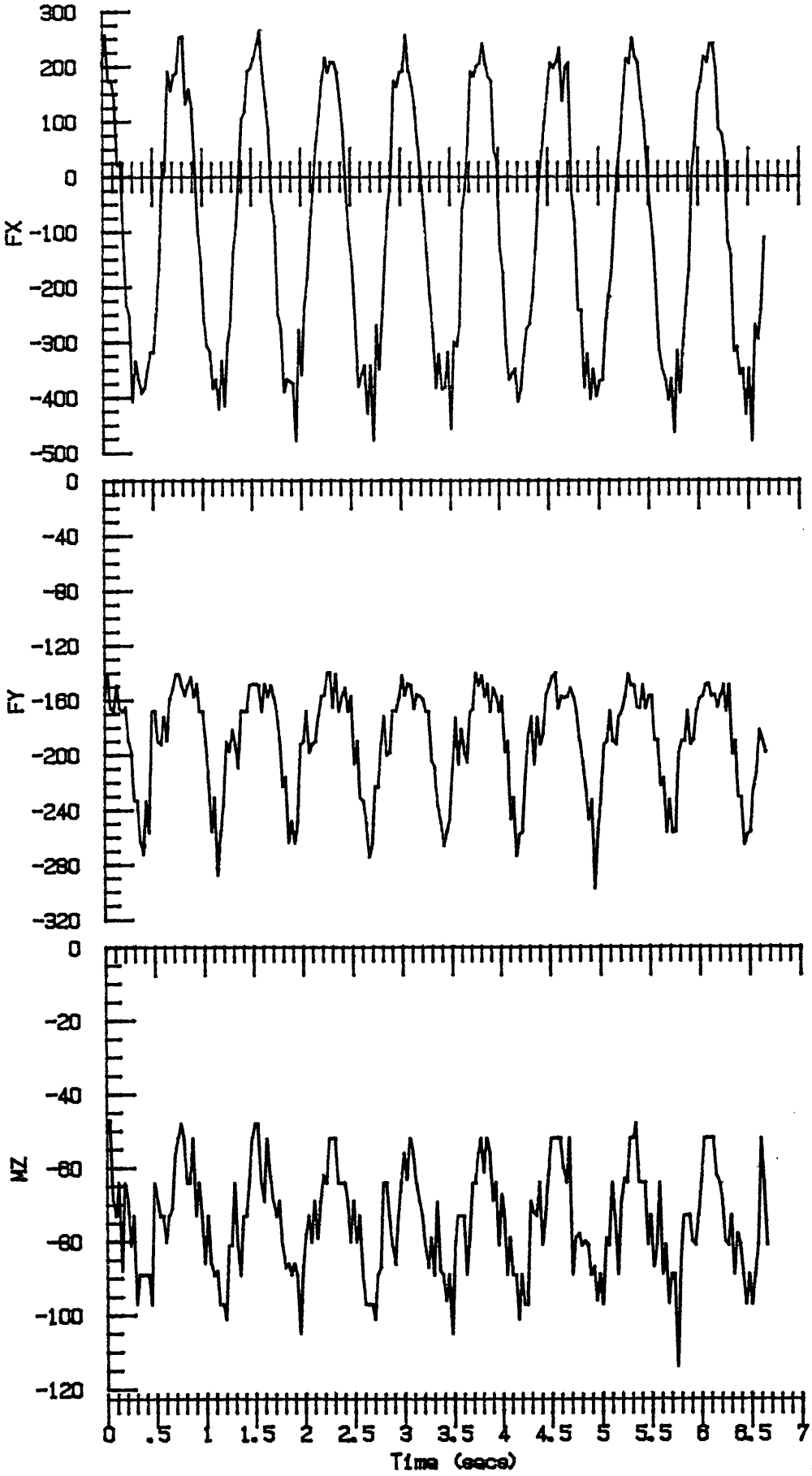

Fig. 53 Typical sample of raw data for the aerofoil of aspect ratio of 1 at frequency f = 1.5 Hz, wind heading $\beta^* = 45^o$, mean incidence $\alpha = 20^o$.

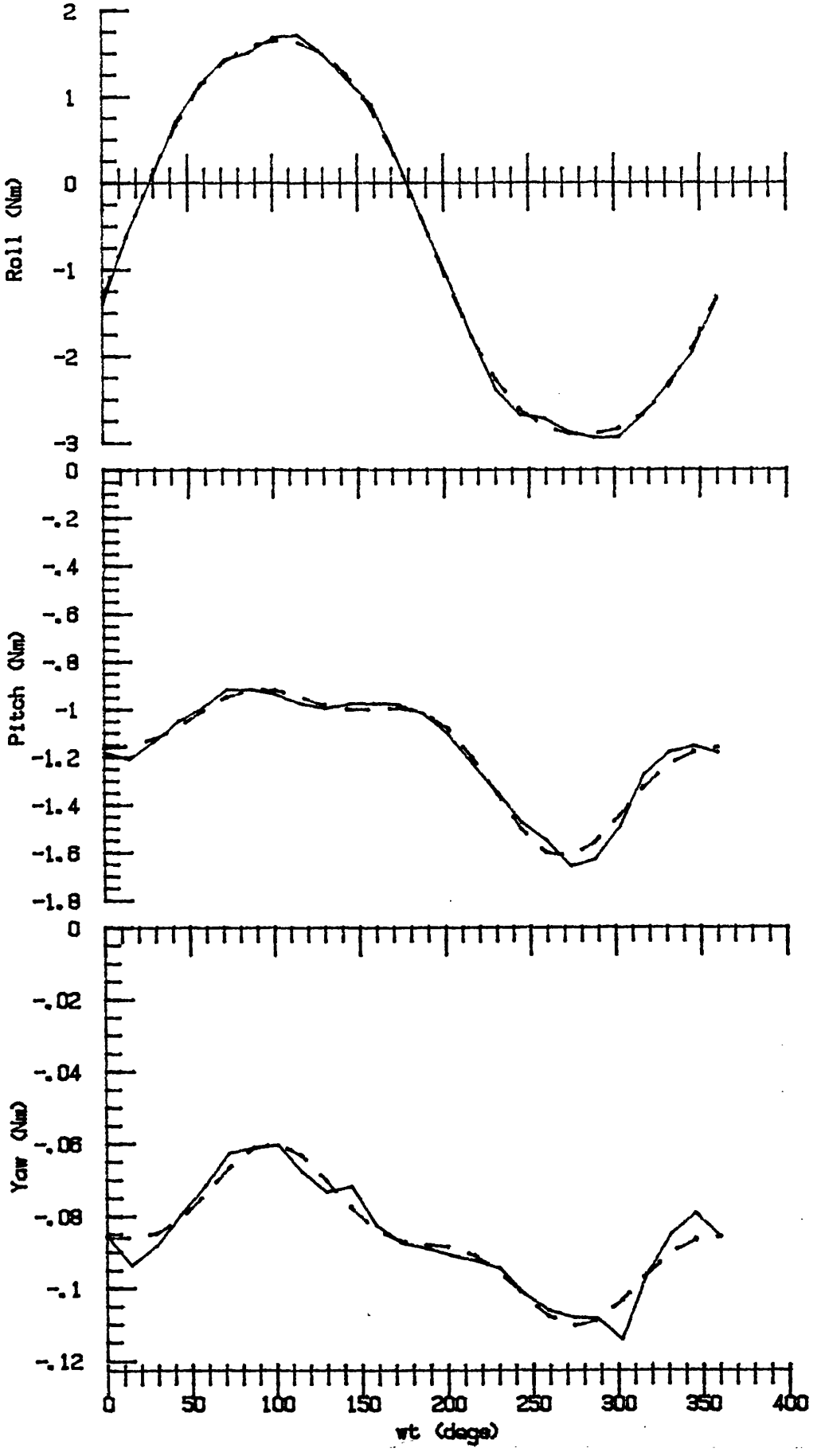

Fig. 54 Typical sample of processed data for the aerofoil of aspect ratio of 1 at frequency f = 1.5 Hz, wind heading $\beta^* = 45^o$, mean incidence $\alpha = 20^o$.

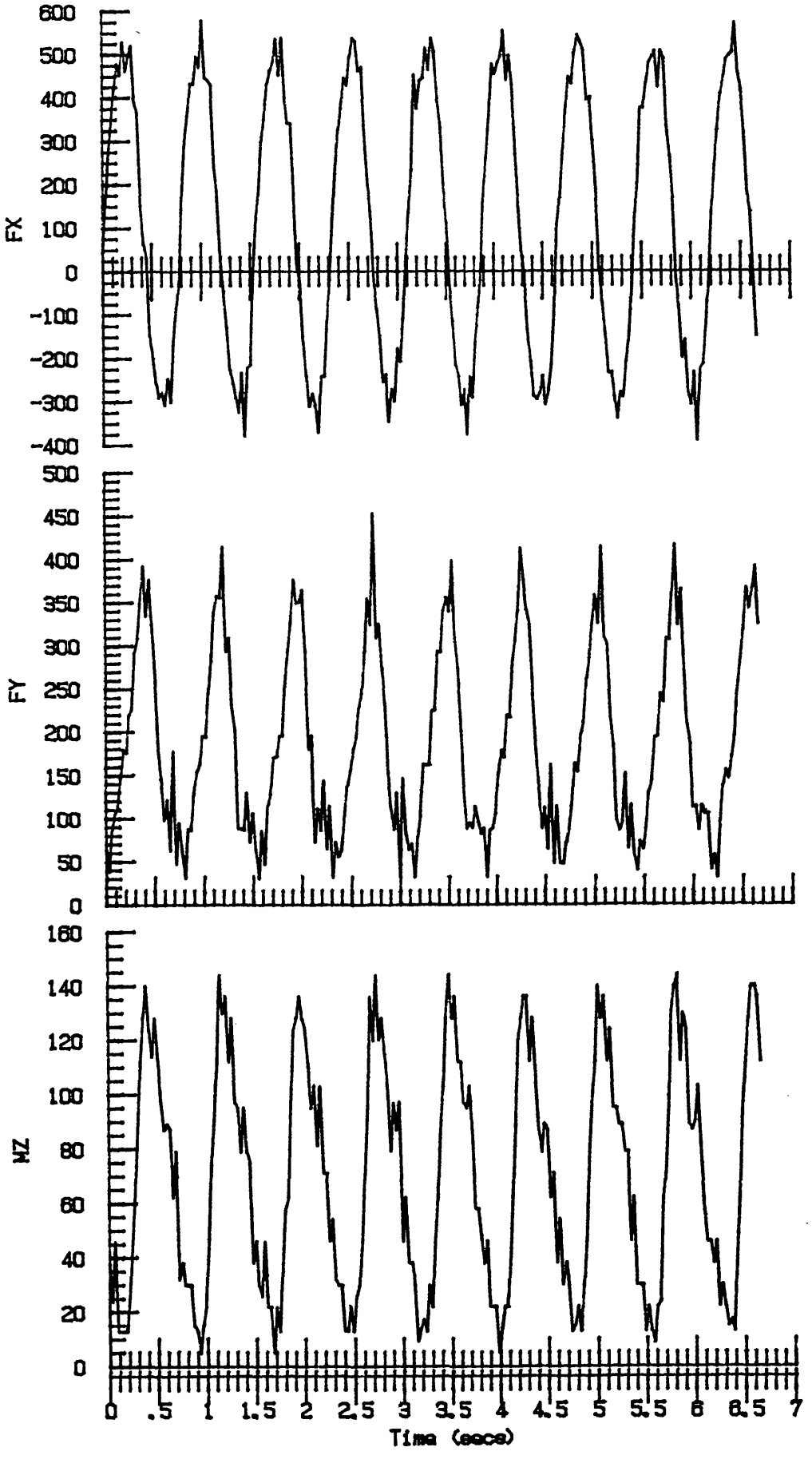

Fig. 55 Typical sample of raw data for the aerofoil of aspect ratio of 2 at frequency f = 1.5 Hz, wind heading $\beta^* = 60^\circ$, mean incidence $\alpha = -10^\circ$.

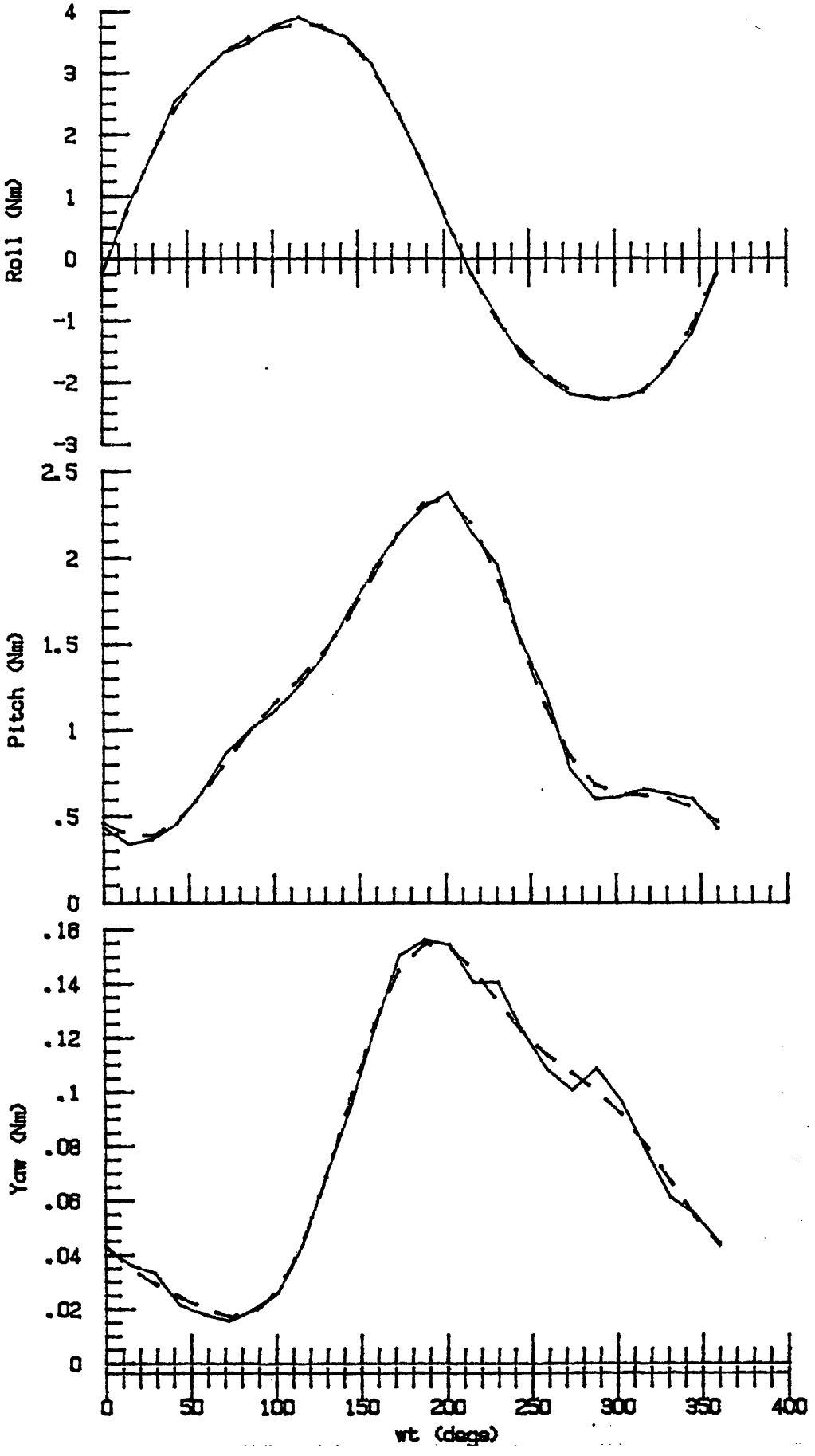

Fig. 56 Typical sample of processed data for the aerofoil of aspect ratio of 2 at frequency f = 1.5 Hz, wind heading $\beta^* = 60^o$, mean incidence $\alpha = -10^o$.

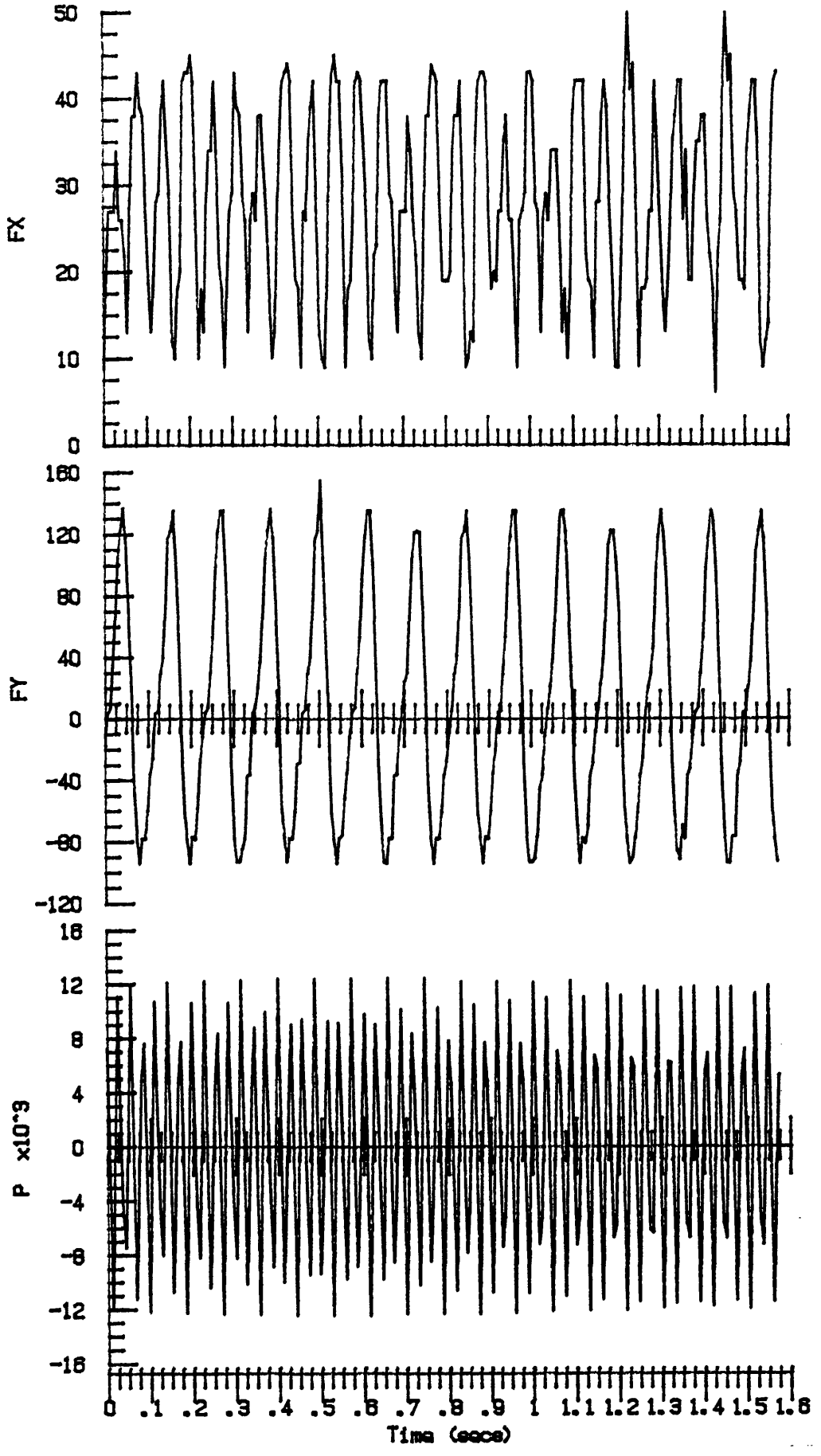

Fig. 57 Typical sample of raw data for steady flow on a wind turbine with no oscillation at blade pitch angle $\psi = 20^{o}$, wind heading $\beta^{*} = 90^{o}$, yaw angle $\delta = 10^{o}$ and wind velocity = 4.5 m/s.

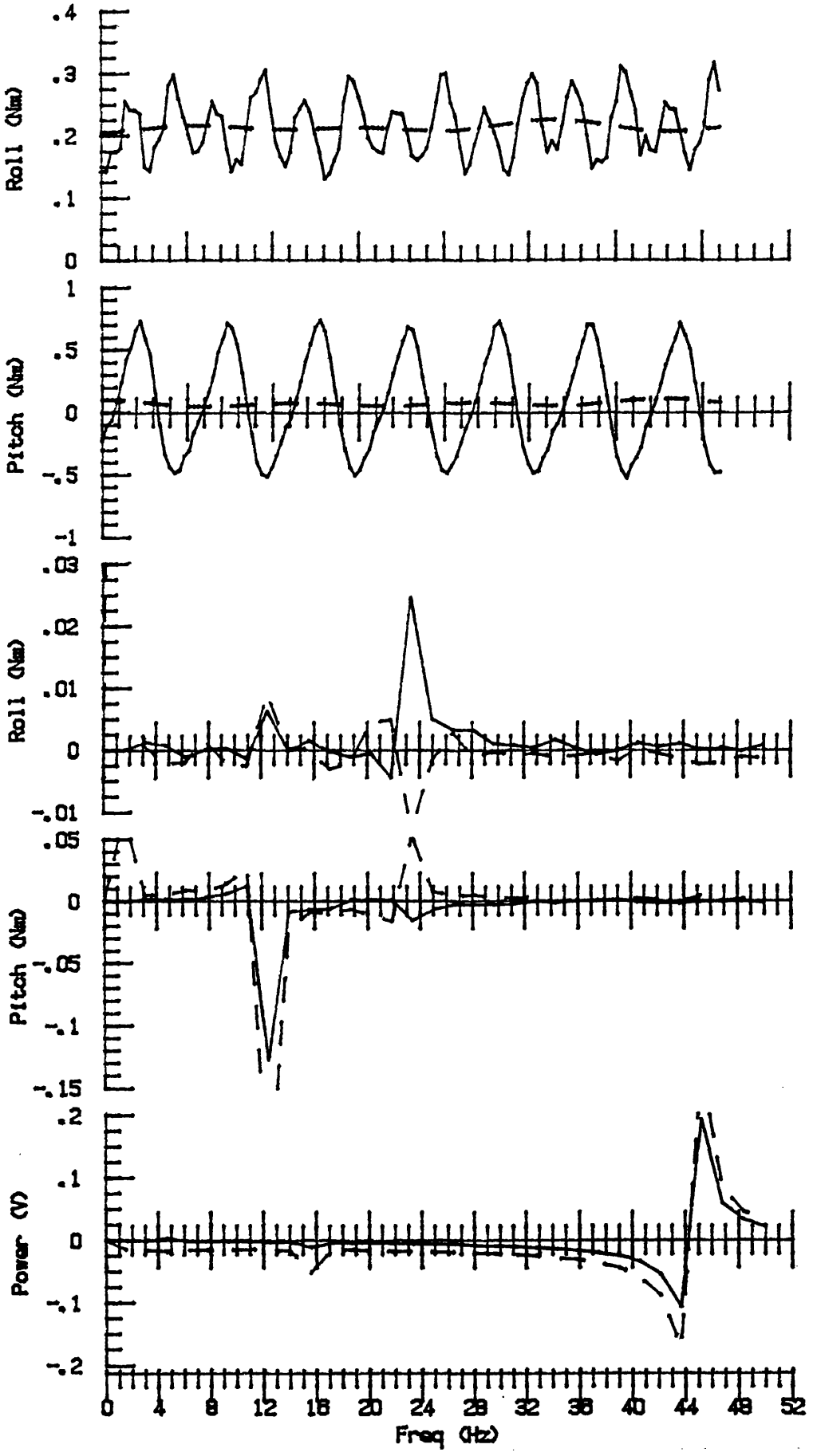

Fig. 58 Typical sample of processed data for steady flow on a wind turbine with no oscillation at blade pitch angle $\psi = 20^{o}$, wind heading $\beta^{*} = 90^{o}$, yaw angle $\delta = 10^{o}$ and wind velocity = 4.5 m/s.

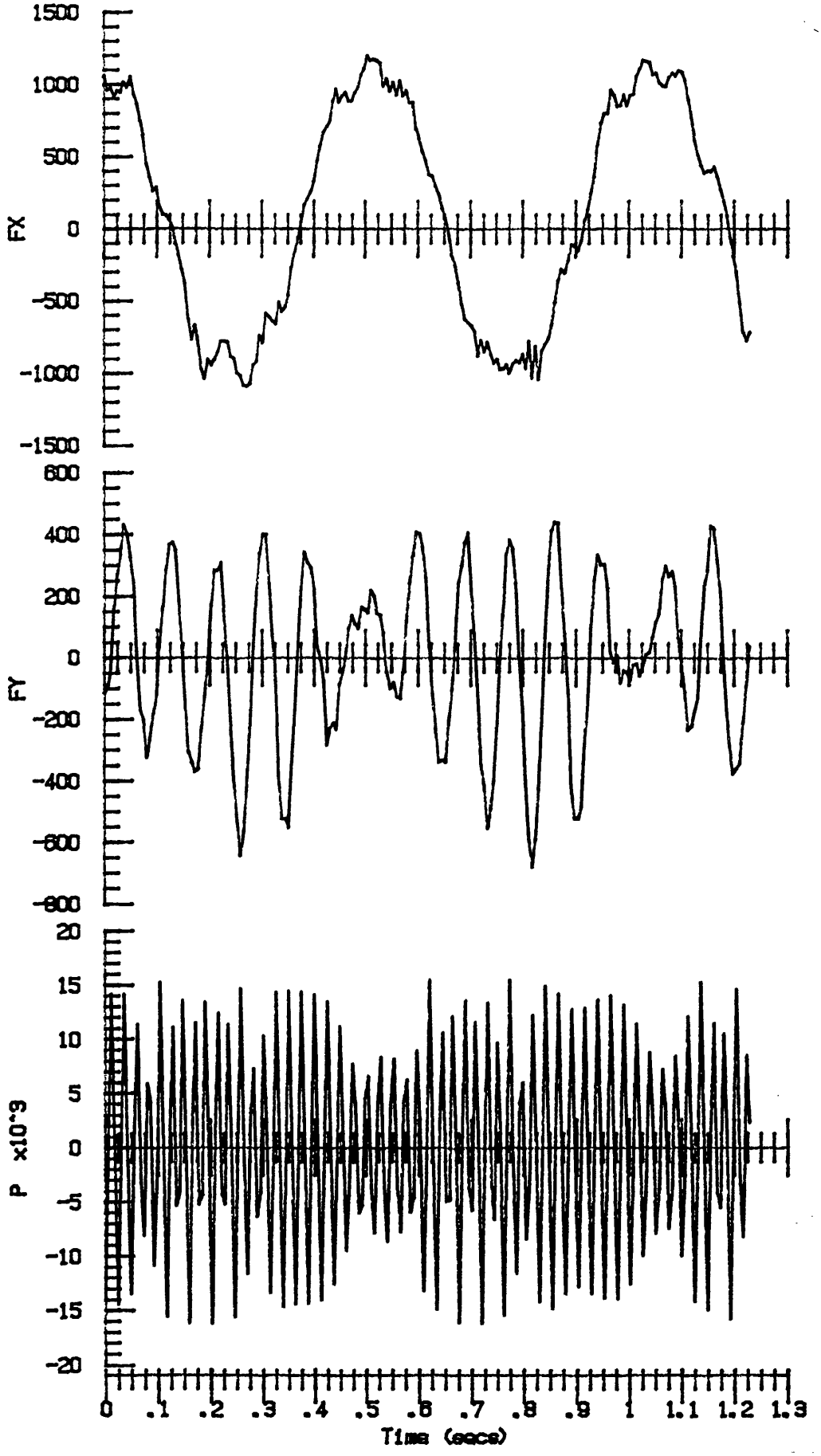

Fig. 59 Typical sample of raw data for axial flow on a HAWT at roll frequency f = 2 Hz, blade pitch angle $\psi = 40^{o}$, wind heading $\beta^{*} = 90^{o}$, yaw angle $\delta = 0$ and wind velocity = 9.3 m/s.

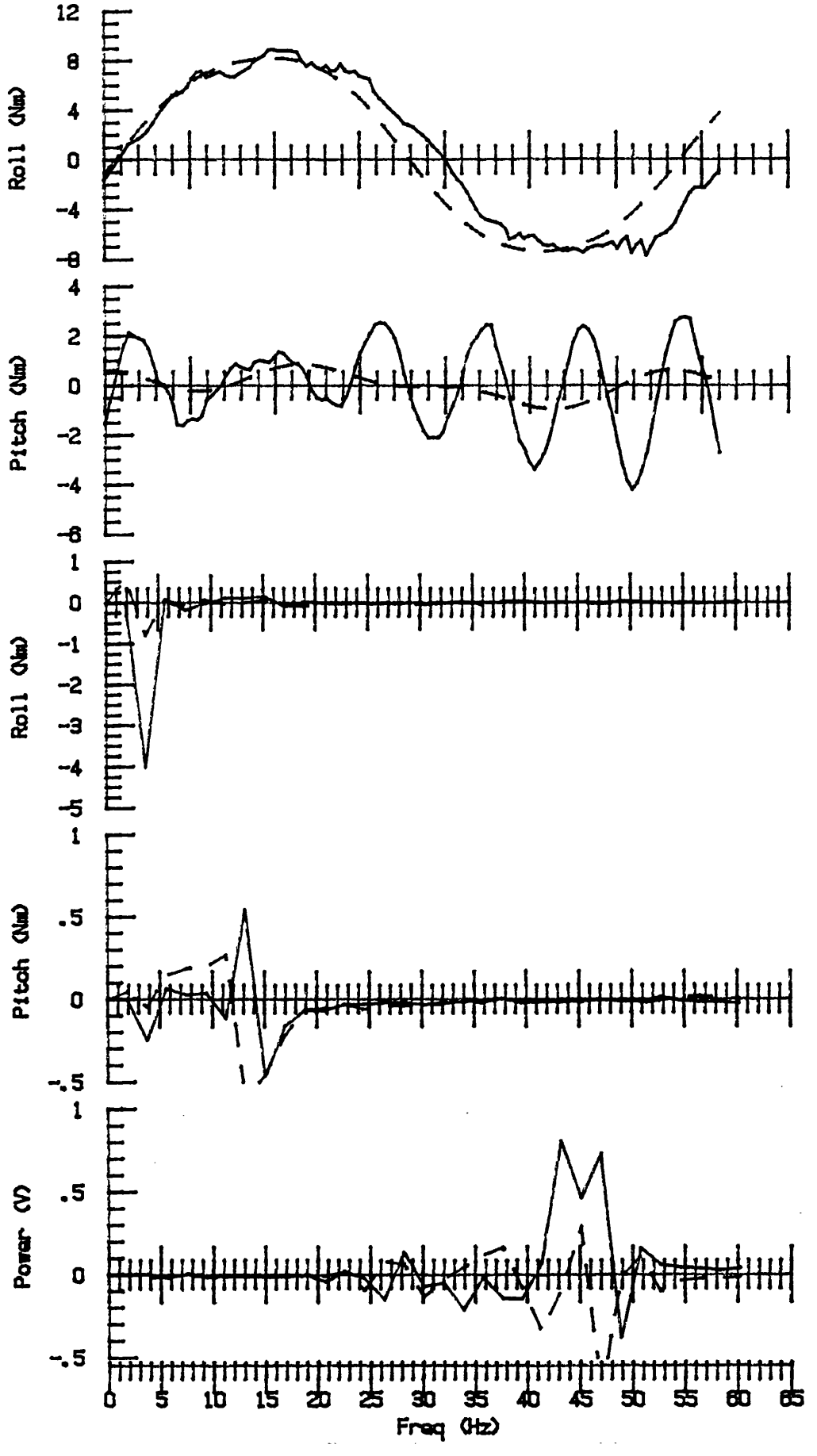

Fig. 60 Typical sample of processed data for axial flow on a HAWT at roll frequency f = 2 Hz, blade pitch angle $\psi = 40^{o}$, wind heading $\beta^{*} = 90^{o}$, yaw angle $\delta = 0$ and wind velocity = 9.3 m/s.

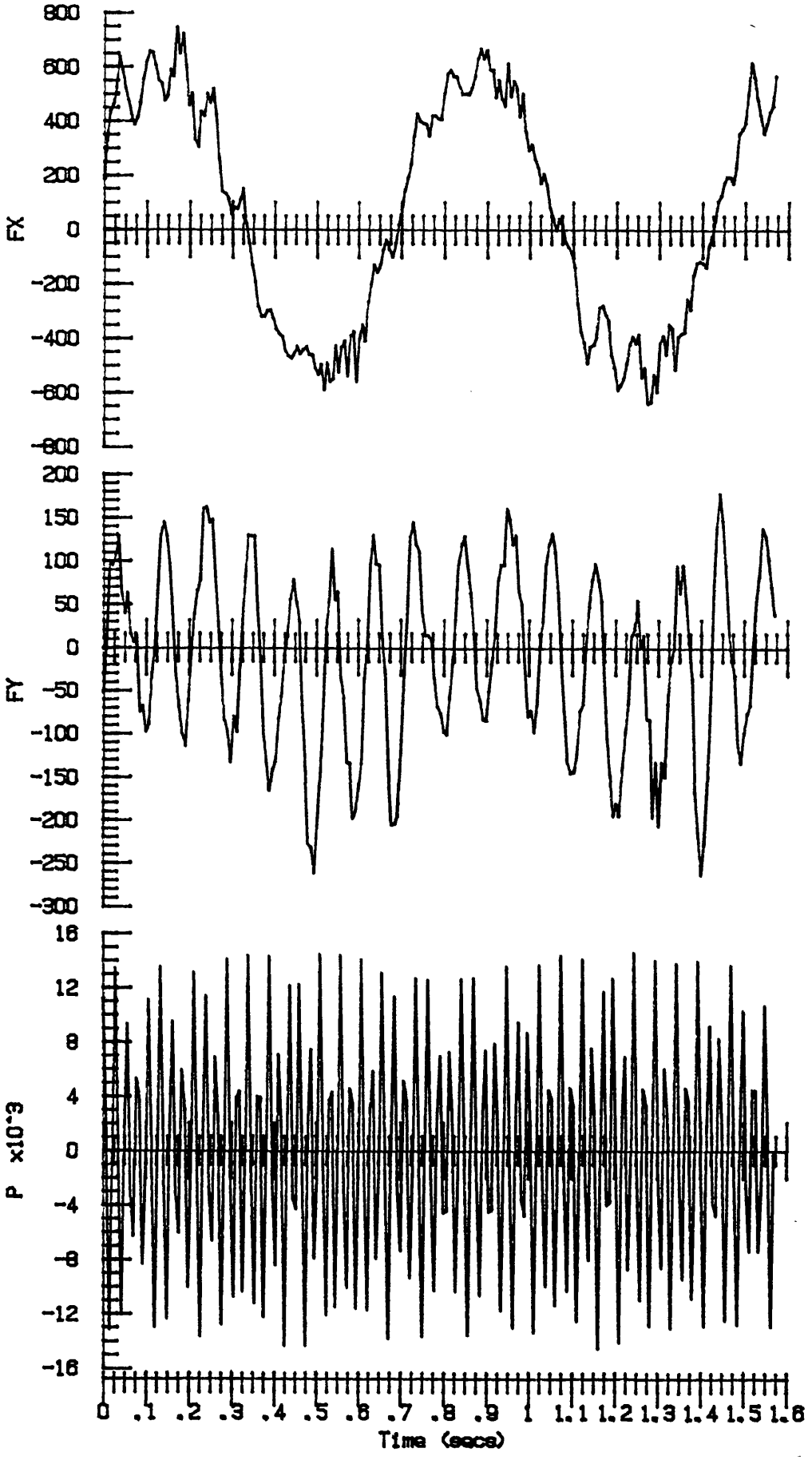

Fig. 61 Typical sample of raw data for axial flow on a HAWT at roll frequency f = 1.5 Hz, blade pitch angle $\psi = 20^o$, wind heading $\beta^* = 90^o$, yaw angle $\delta = 0$ and wind velocity = 4.5 m/s.

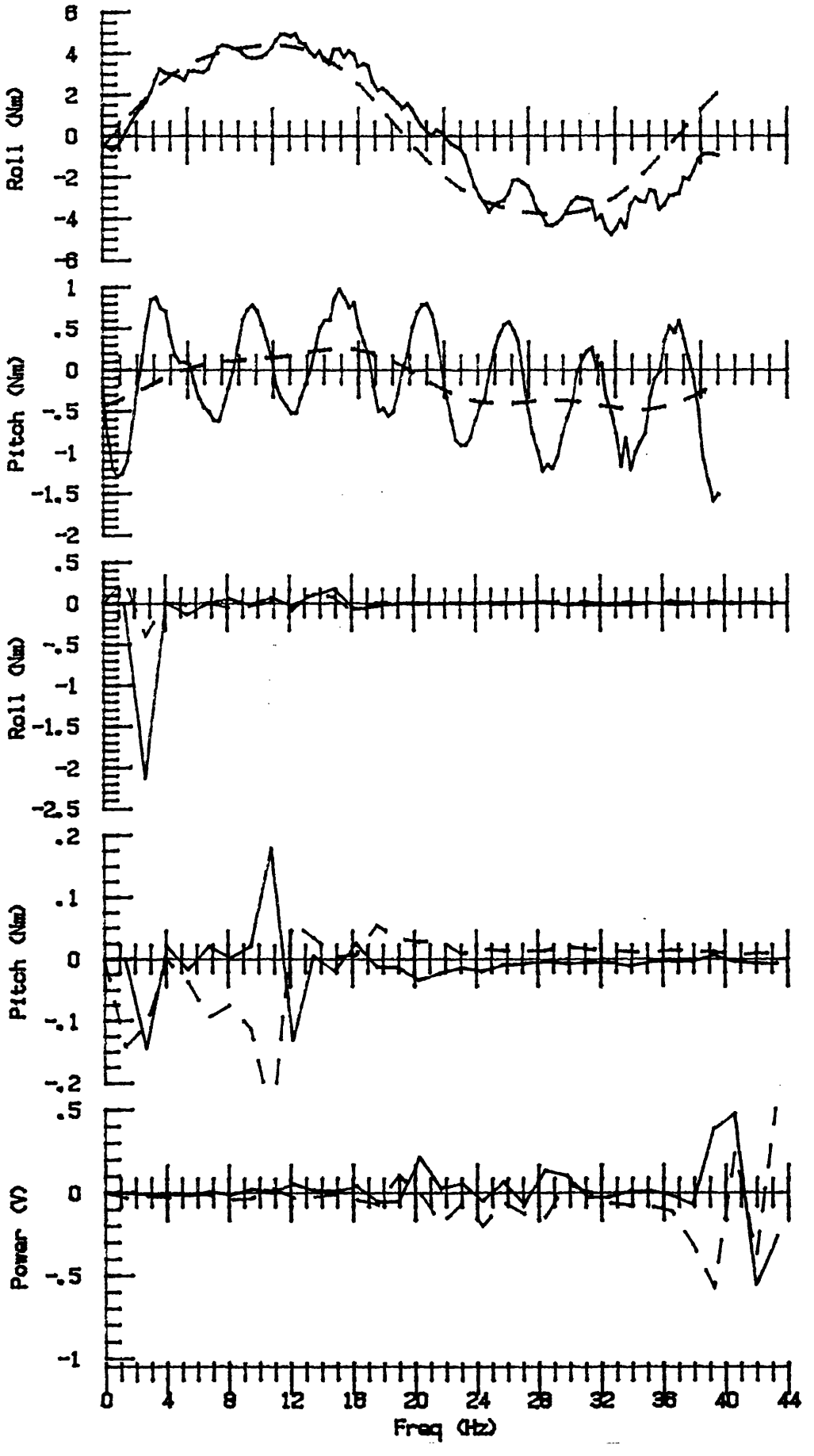

Fig. 62 Typical sample of processed data for axial flow on a HAWT at roll frequency f = 1.5 Hz, blade pitch angle $\psi = 20^{o}$, wind heading $\beta^{*} = 90^{o}$, yaw angle $\delta = 0$ and wind velocity = 4.5 m/s.

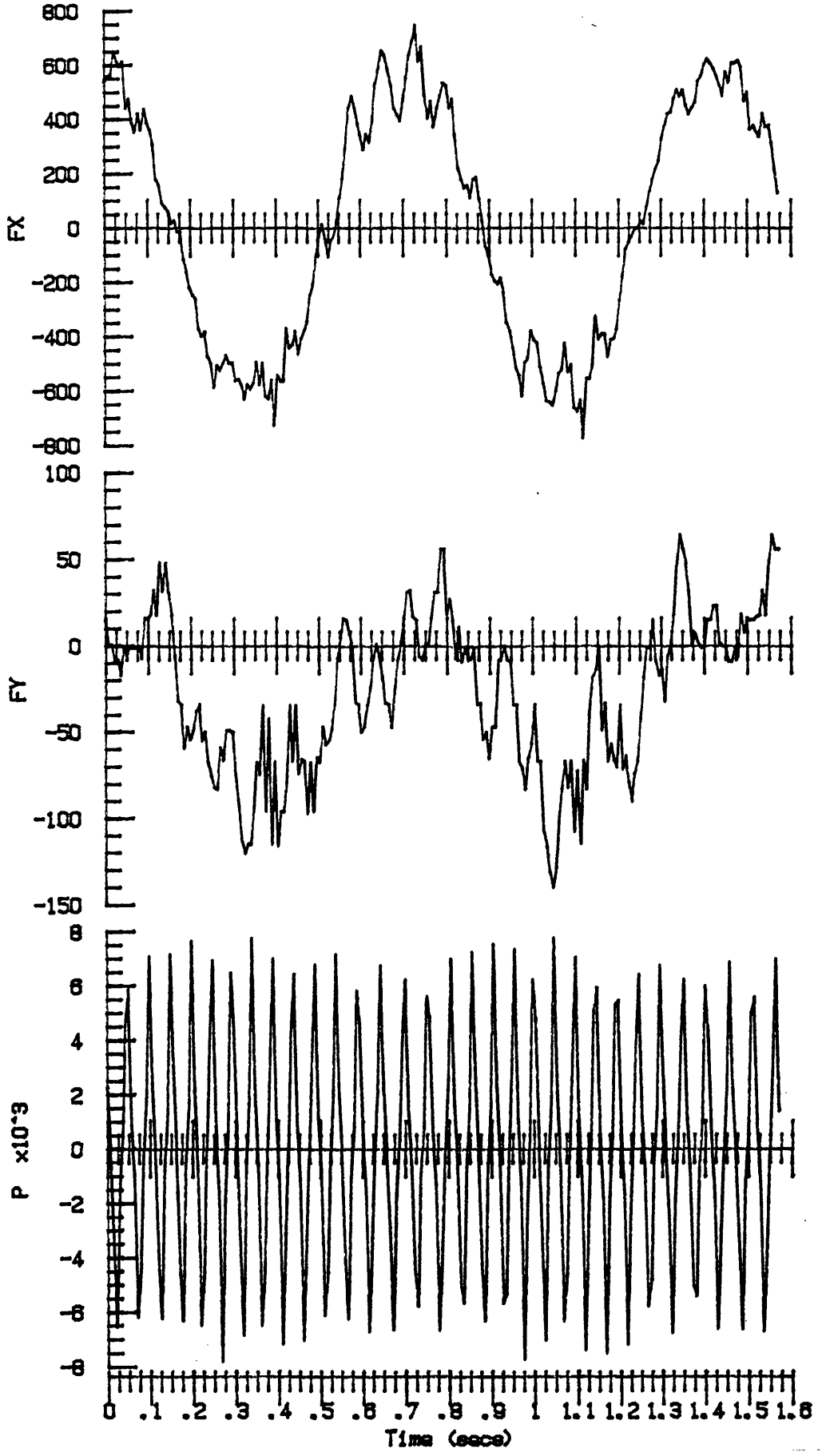

Fig. 63 Typical sample of raw data for a HAWT rolling parallel to the wind direction at an angle of yaw at roll frequency f = 1.5 Hz, blade pitch angle $\psi = 40^{o}$, wind heading $\beta^{*} = 90^{o}$, yaw angle $\delta = 10^{o}$ and wind velocity = 4.5 m/s.

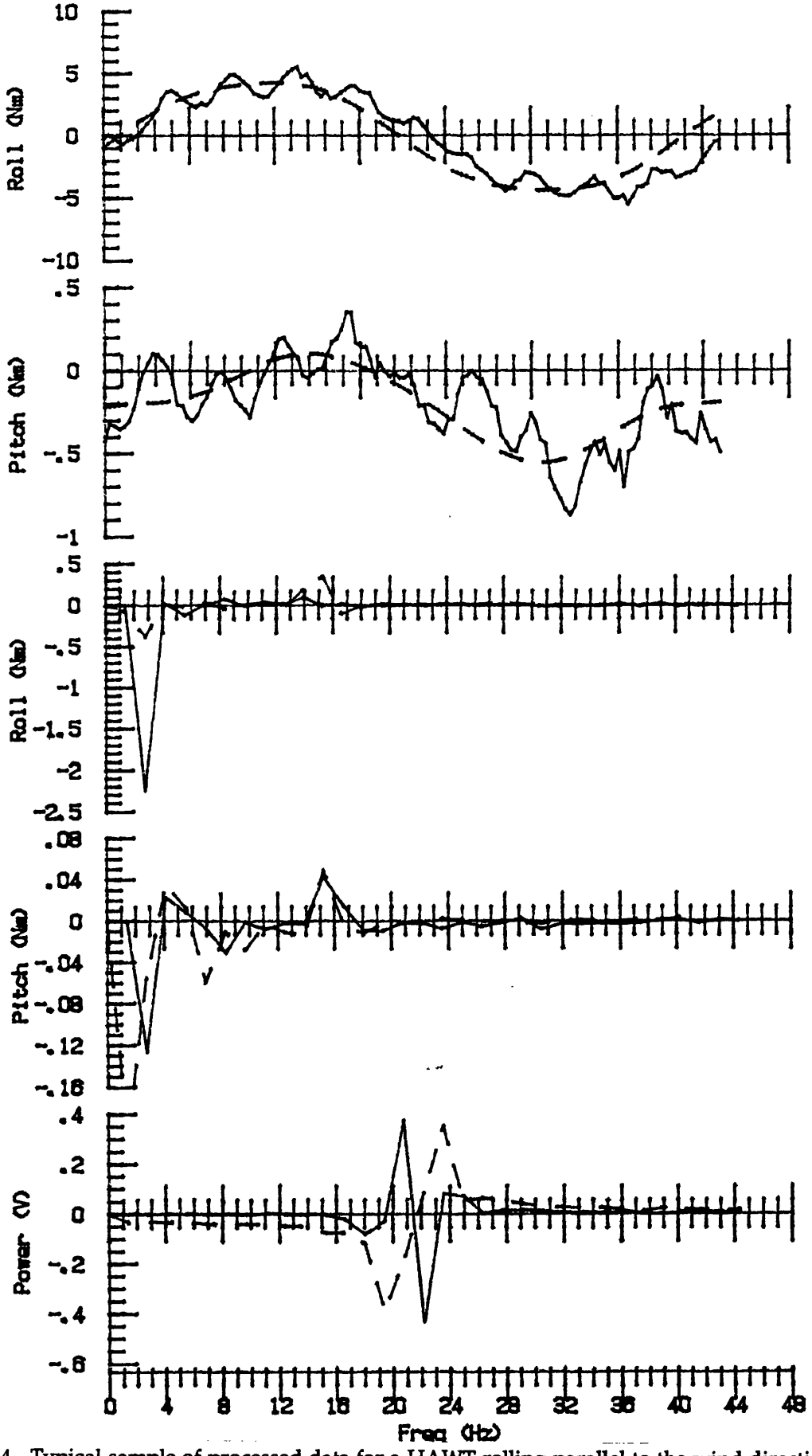

Fig. 64 Typical sample of processed data for a HAWT rolling parallel to the wind direction at an angle of yaw at roll frequency f = 1.5 Hz, blade pitch angle $\psi = 40^{o}$, wind heading $\beta^{*} = 90^{o}$, yaw angle $\delta = 10^{o}$ and wind velocity = 4.5 m/s.

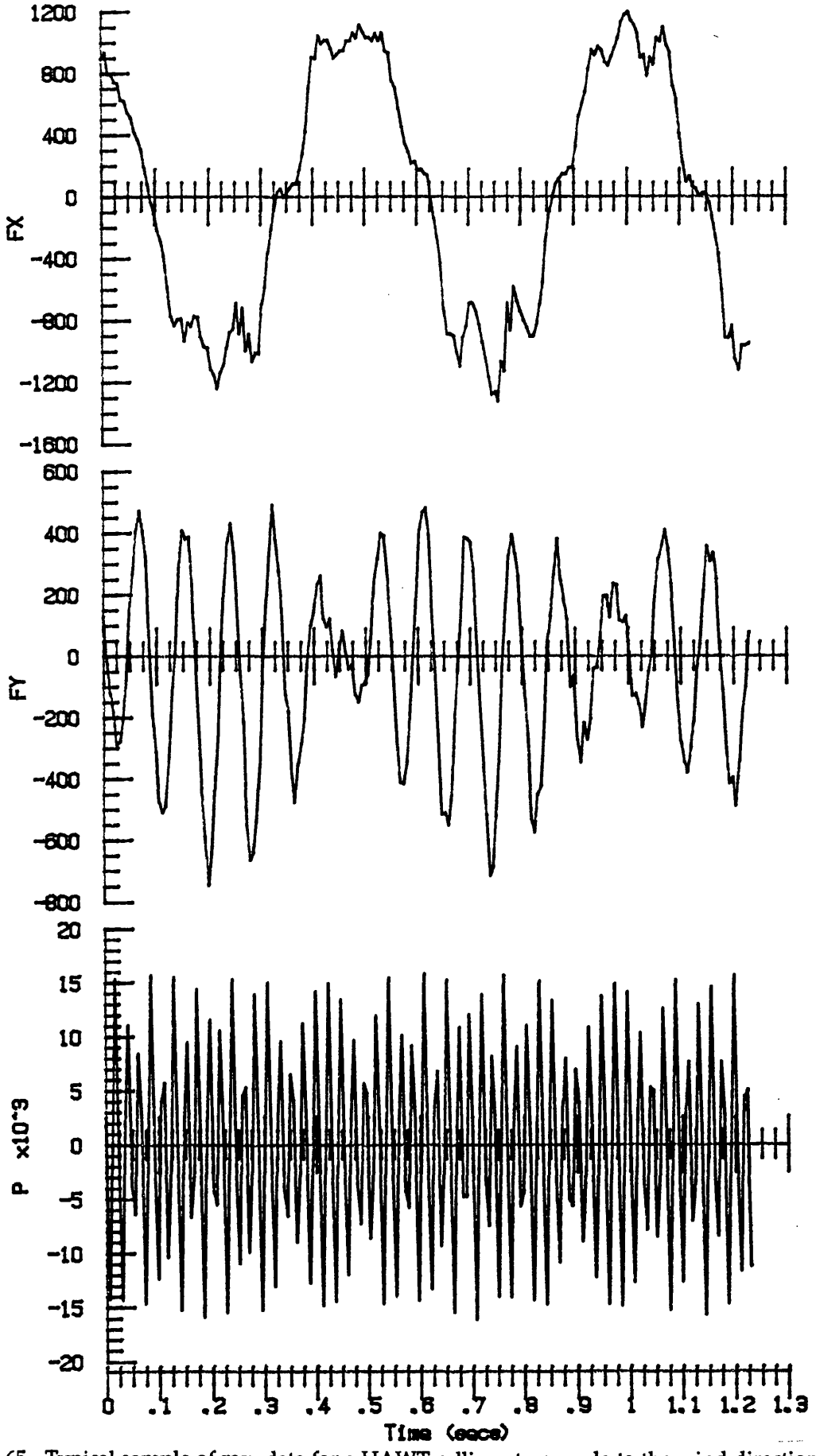

Fig. 65 Typical sample of raw data for a HAWT rolling at an angle to the wind direction with no angle of yaw at roll frequency f = 2 Hz, blade pitch angle $\psi = 20^{o}$, wind heading $\beta^{*} = 75^{o}$, yaw angle $\delta = 0$ and wind velocity = 4.5 m/s.

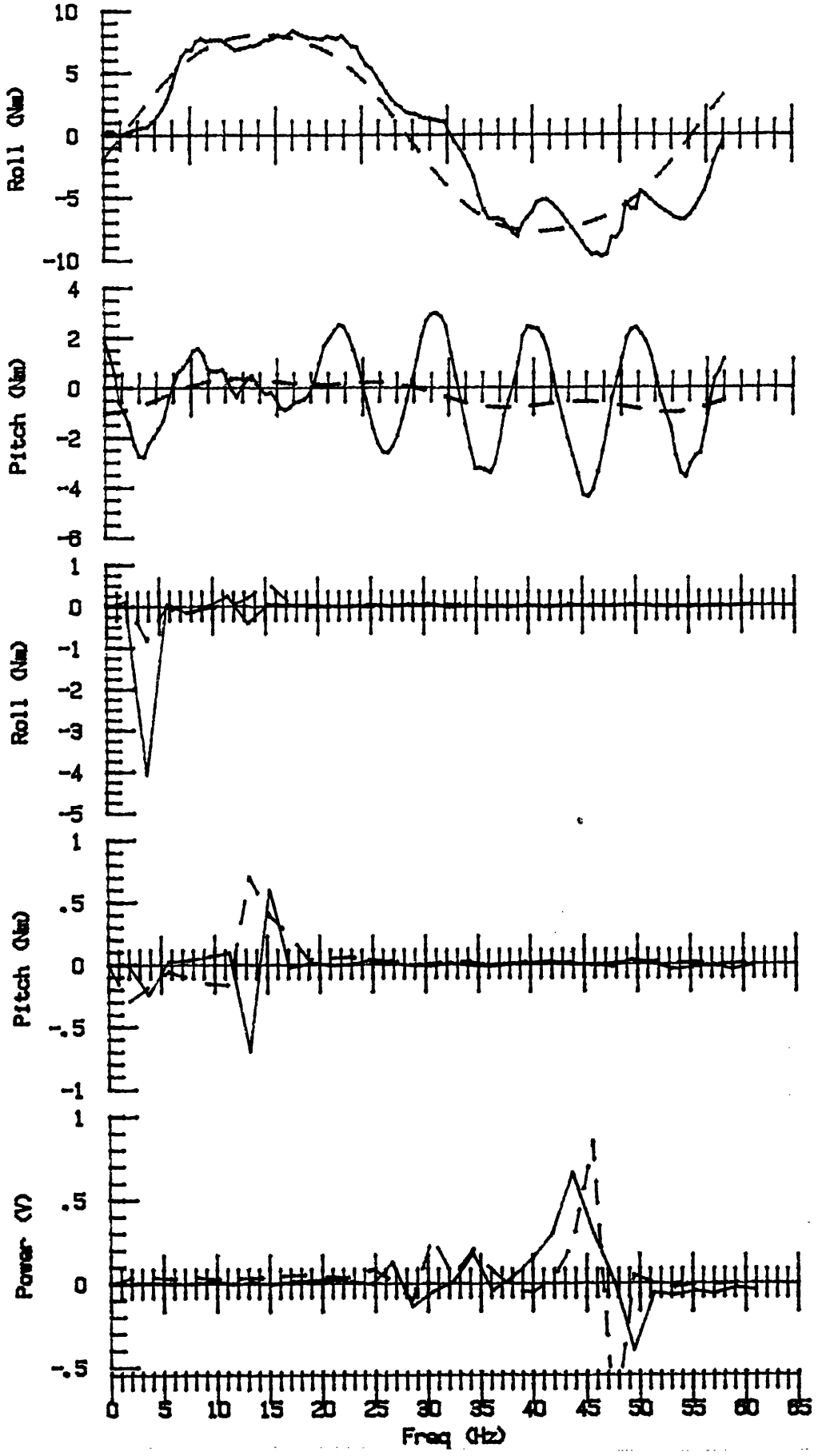

Fig. 66 Typical sample of processed data for a HAWT rolling at an angle to the wind direction with no angle of yaw at roll frequency f = 2 Hz, blade pitch angle $\psi = 20^{o}$, wind heading $\beta^{*} = 75^{o}$, yaw angle $\delta = 0$ and wind velocity = 4.5 m/s.

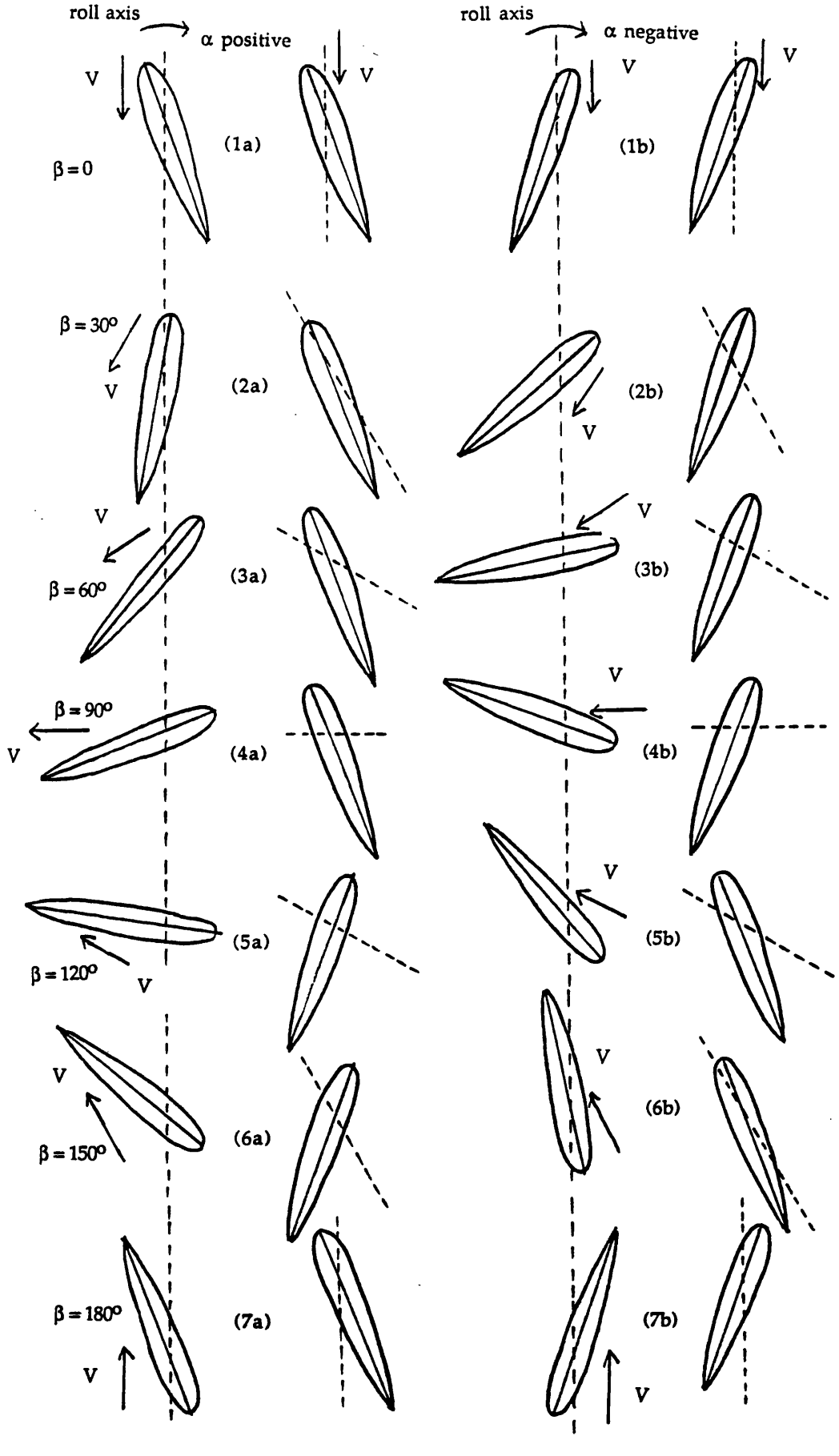

Fig. 67 Reversals for wind heading angles $90^o < \beta^* < 180^o$.

Note that (5), (6) and (7) correspond to (3), (2) and (1) reversed, so that only (1) to (4) need to be measured.

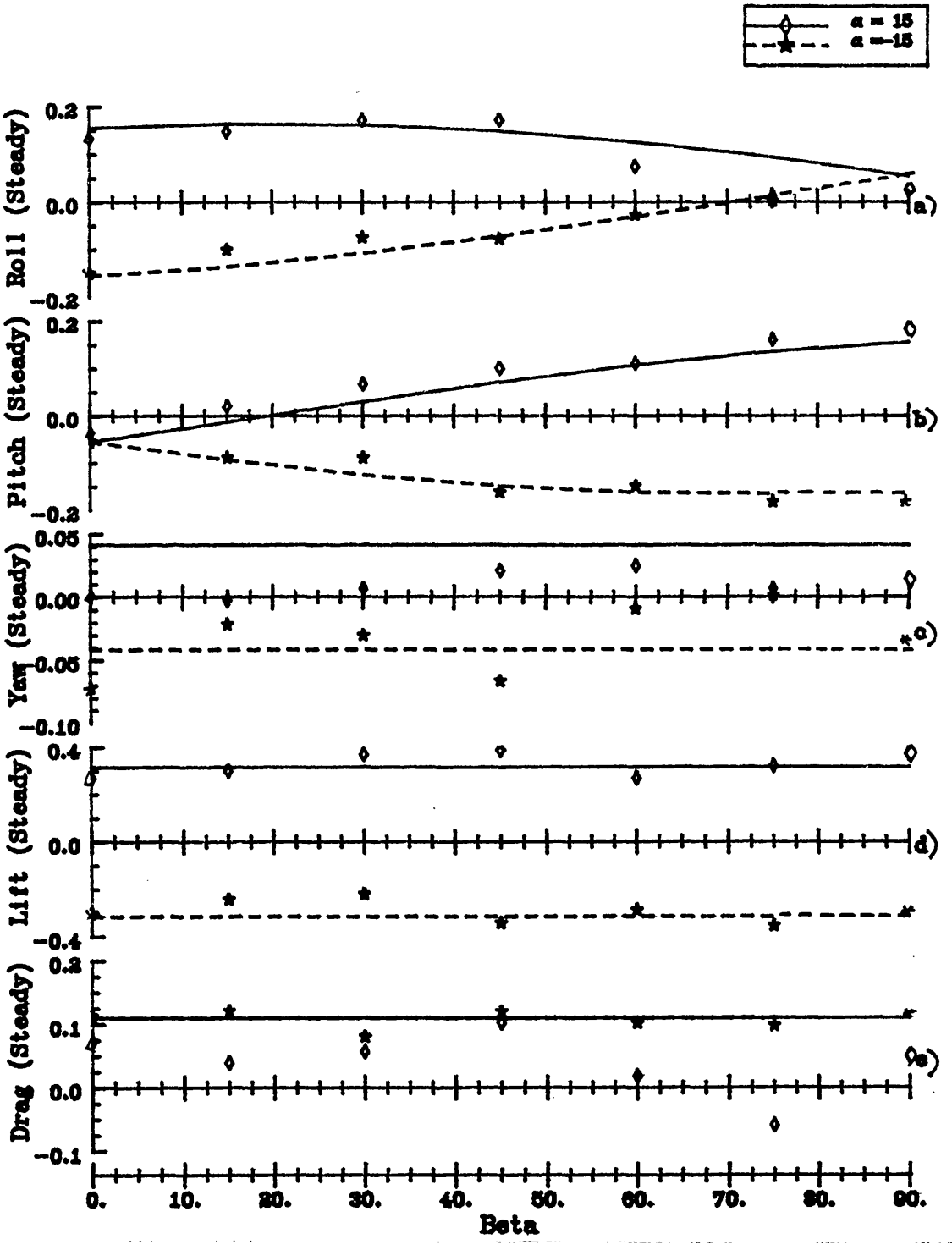

Fig. 68 Steady forces and moments on an aerofoil as functions of wind heading β^* on an aerofoil of aspect ratio of 1, mean incidence $\alpha = \pm 15^o$.

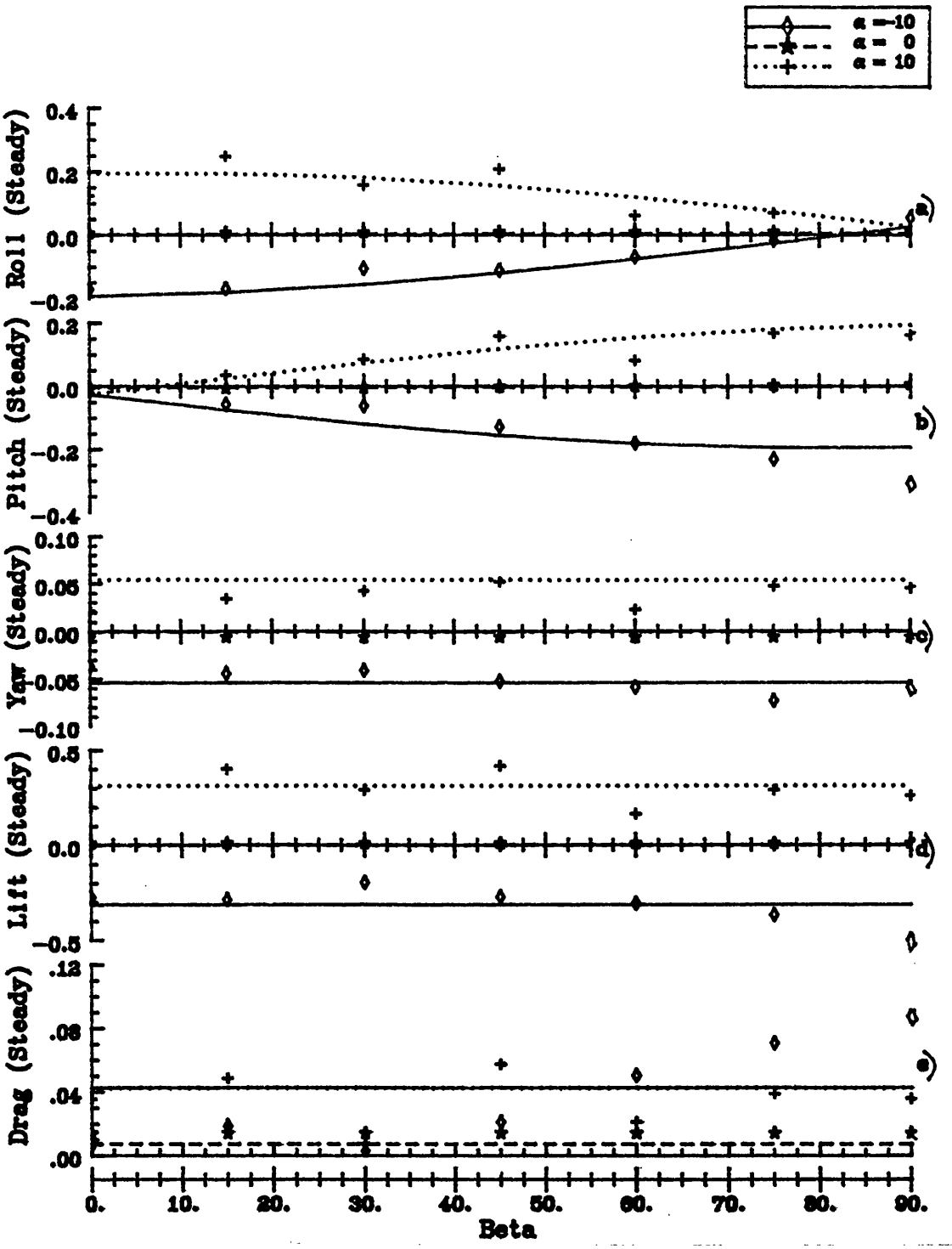

Fig. 69 Steady forces and moments on an aerofoil as functions of wind heading β^* on an aerofoil of aspect ratio of 2, mean incidence $\alpha = 0, \pm 10^o$.

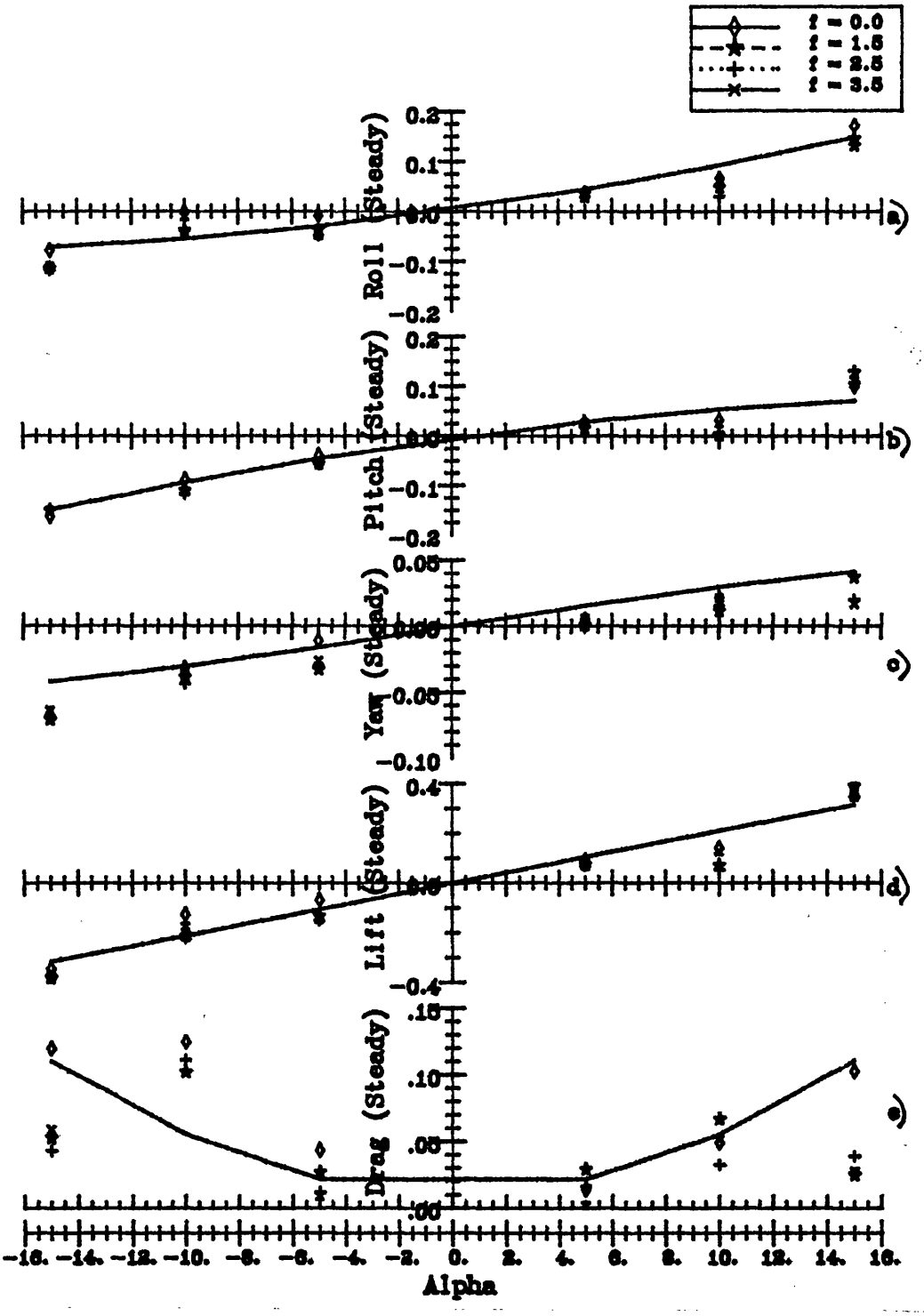

Fig. 70 Steady forces and moments on an aerofoil as functions of mean incidence α on an aerofoil of aspect ratio of 1, wind heading $\beta^* = 45^o$.

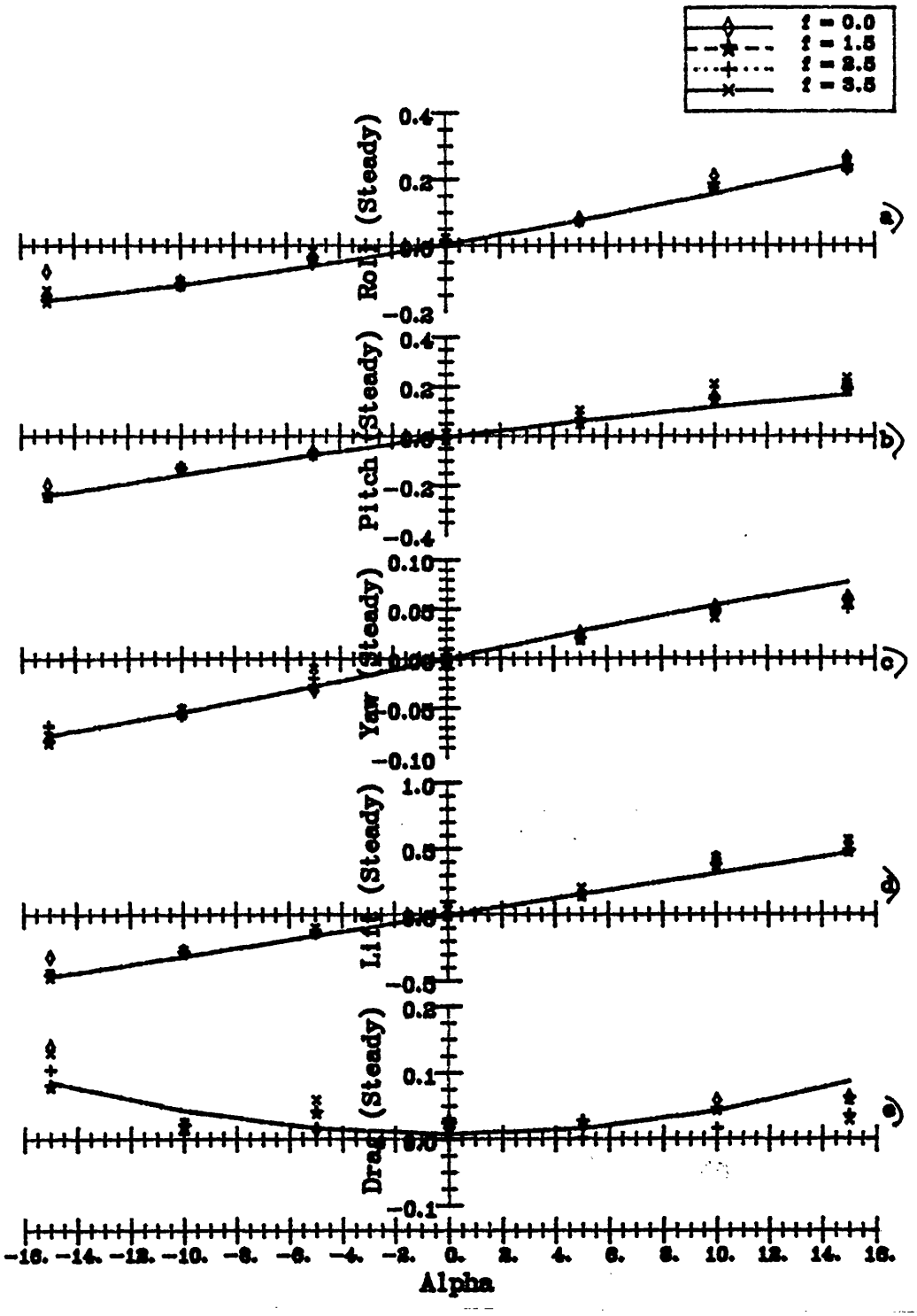

Fig. 71 Steady forces and moments on an aerofoil as functions of mean incidence α on an aerofoil of aspect ratio of 2, wind heading $\beta^* = 45^o$.

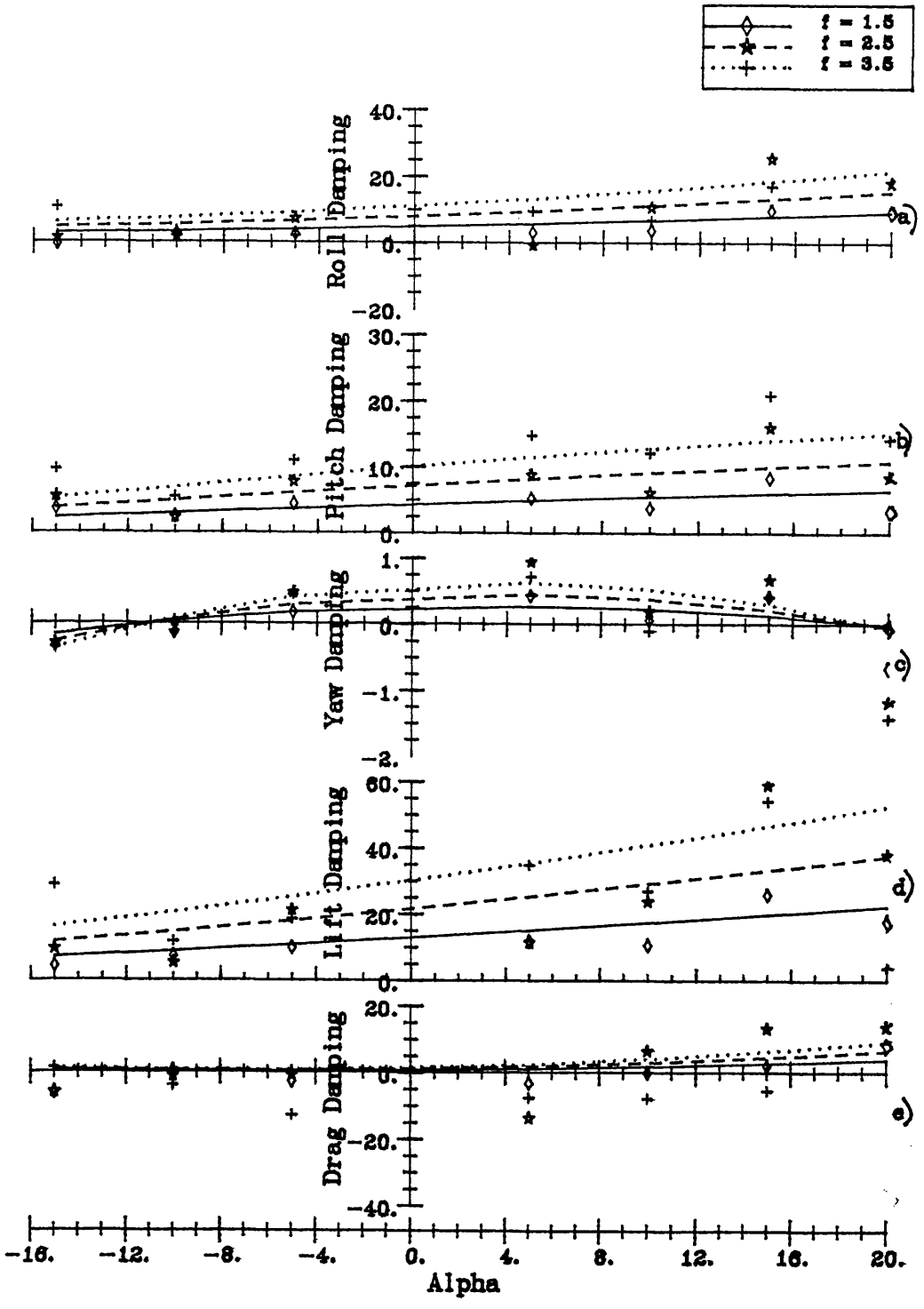

Fig. 72 Damping forces and moments on an aerofoil as functions of mean incidence α for aspect ratio of 1, wind heading $\beta^* = 45^o$, roll frequency f = 1.5, 2.5, 3.5 Hz.

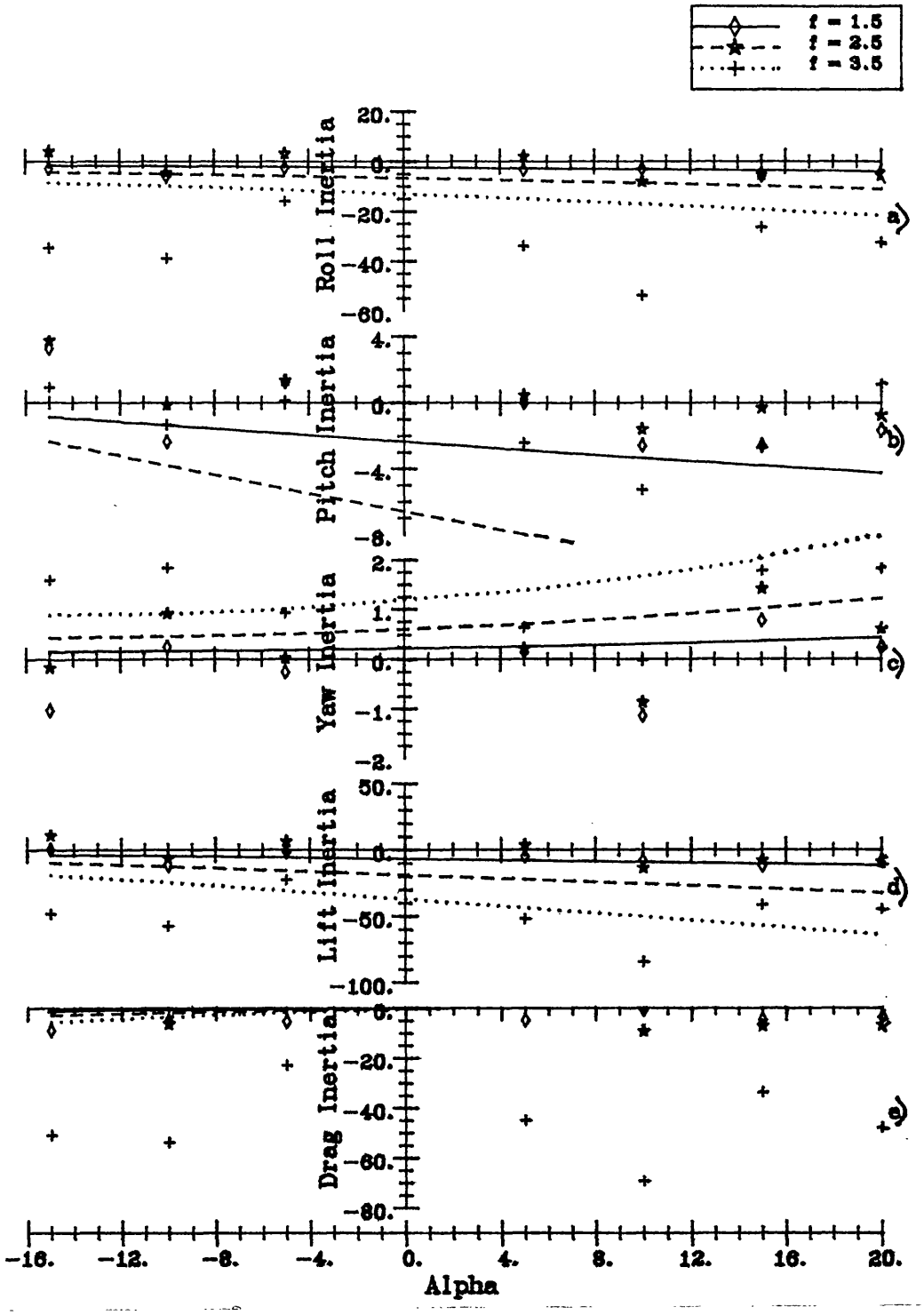

Fig. 73 Inertia forces and momentson an aerofoil as functions of mean incidence α for aspect ratio of 1, wind heading $\beta^* = 45^o$, roll frequency f = 1.5, 2.5, 3.5 Hz.

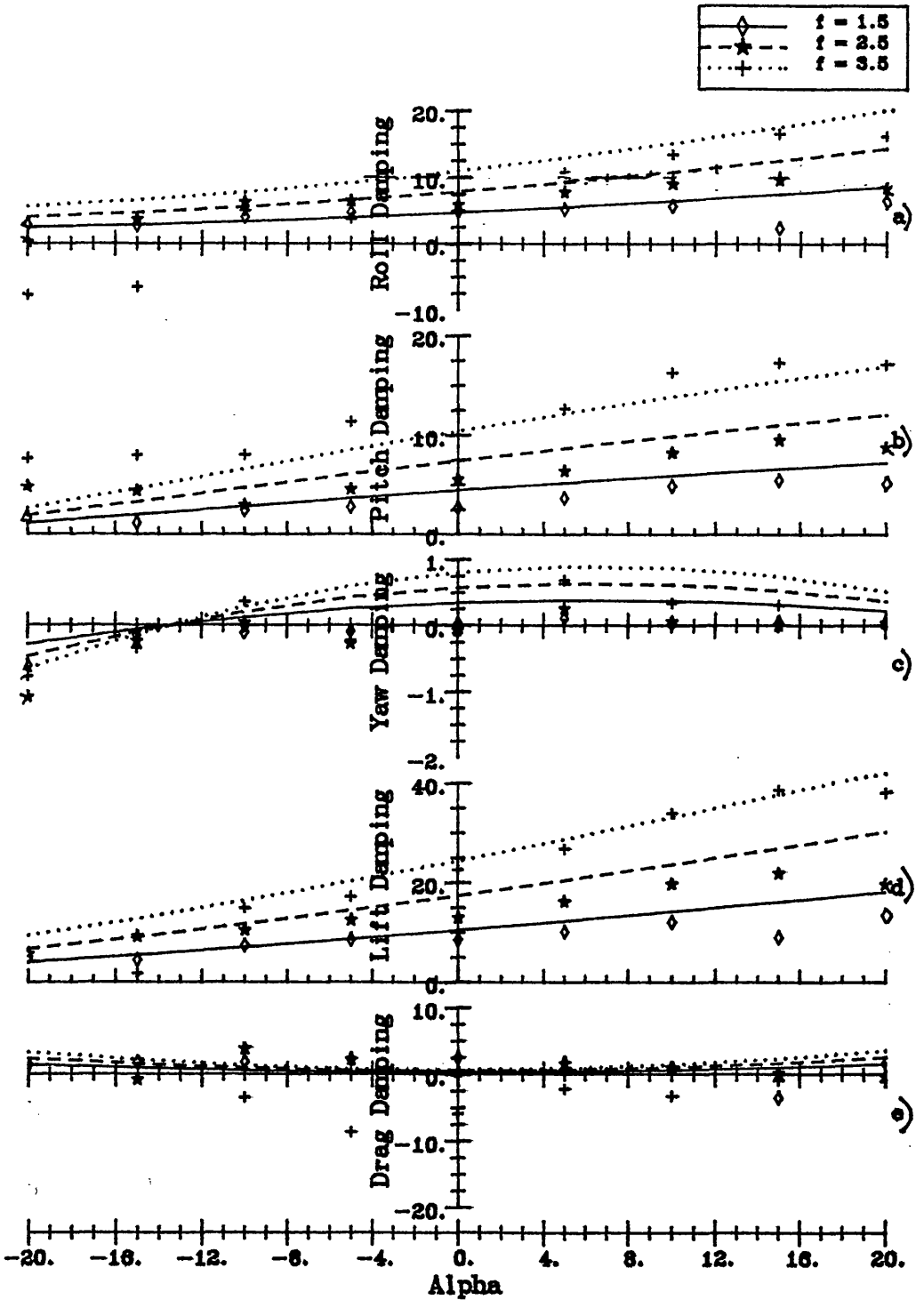

Fig. 74 Damping forces and moments on an aerofoil as functions of mean incidence α for aspect ratio of 2, wind heading $\beta^* = 45^o$, roll frequency f = 1.5, 2.5, 3.5 Hz.

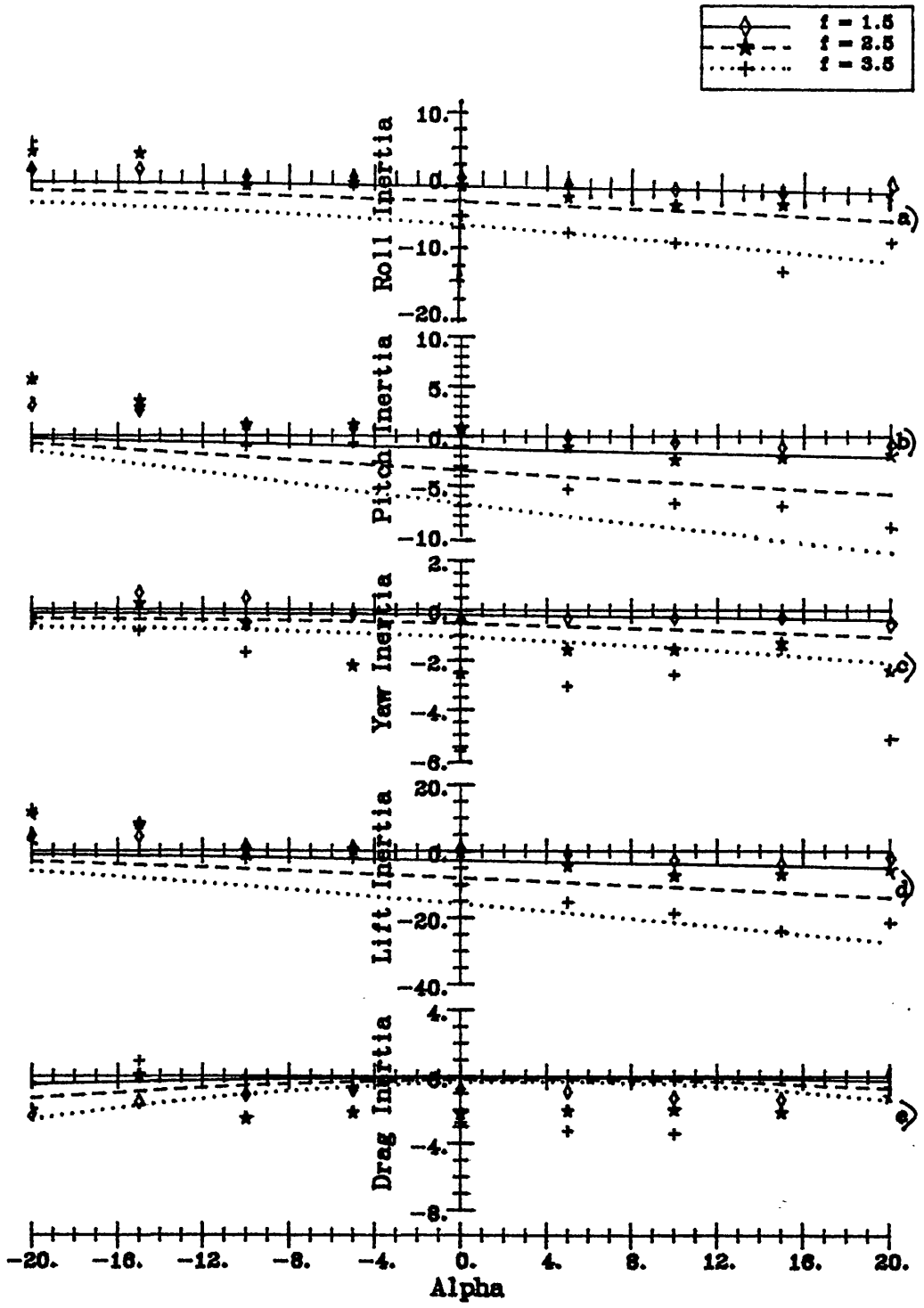

Fig. 75 Inertia forces and moments on an aerofoil as functions of mean incidence α for aspect ratio of 2, wind heading $\beta^* = 45^\circ$, roll frequency f = 1.5, 2.5, 3.5 Hz.

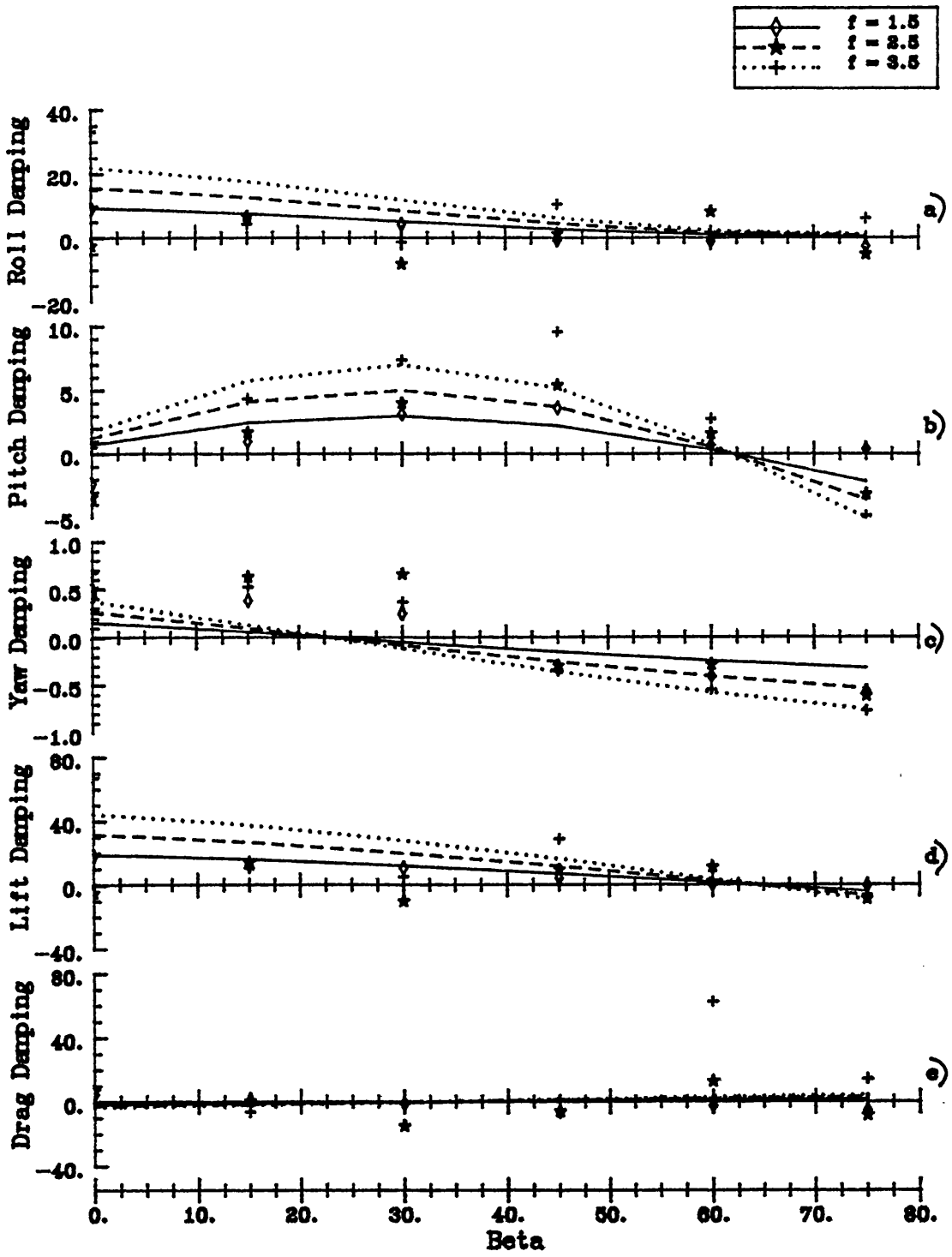

Fig. 76 Damping forces and moments on an aerofoil as functions of wind heading β^* for aspect ratio of 1, mean incidence $\alpha = -15^o$, roll frequency f = 1.5, 2.5, 3.5 Hz.

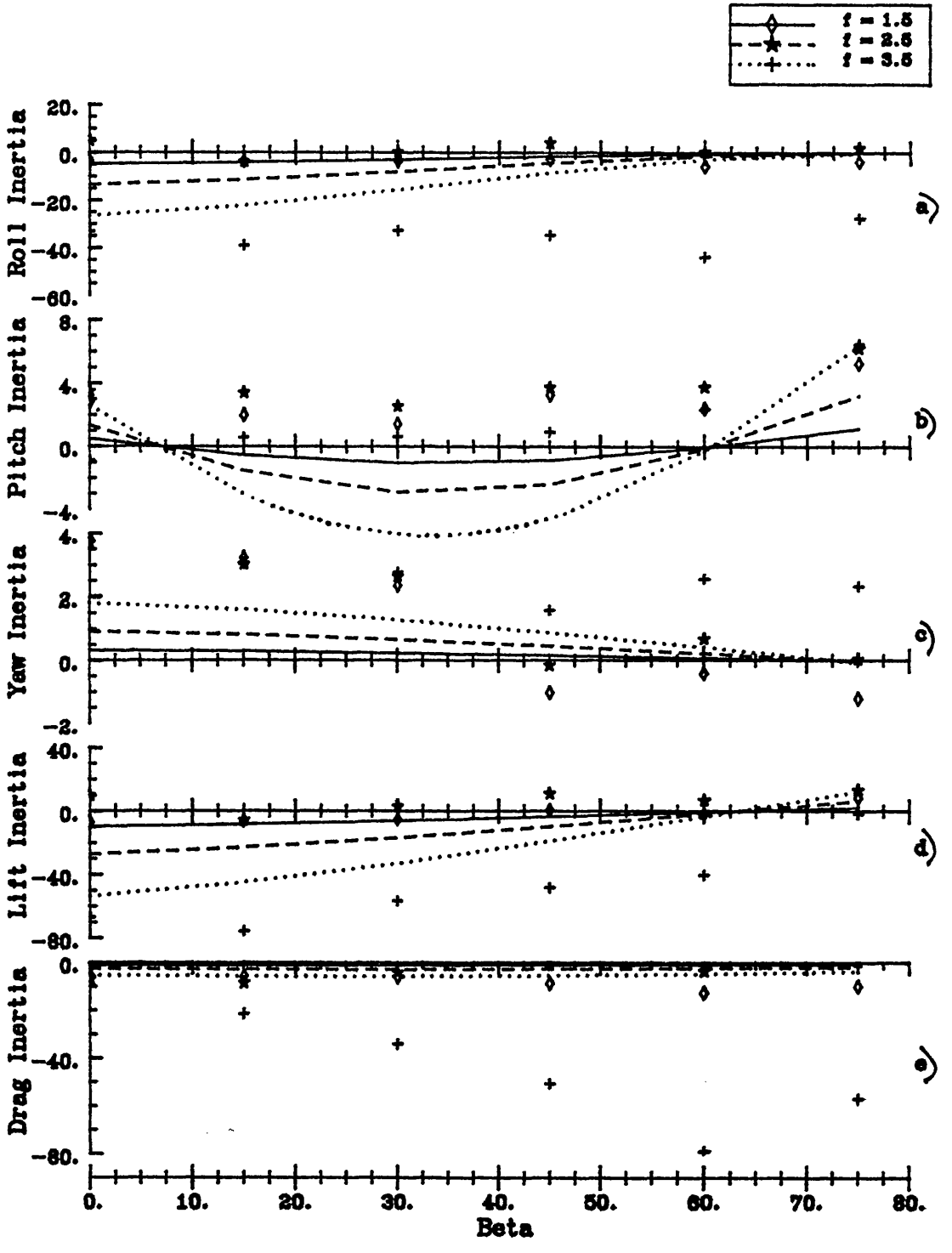

Fig. 77 Inertia forces and moments on an aerofoil as functions of wind heading β^* for aspect ratio of 1, mean incidence $\alpha = -15^o$, roll frequency f = 1.5, 2.5, 3.5 Hz.

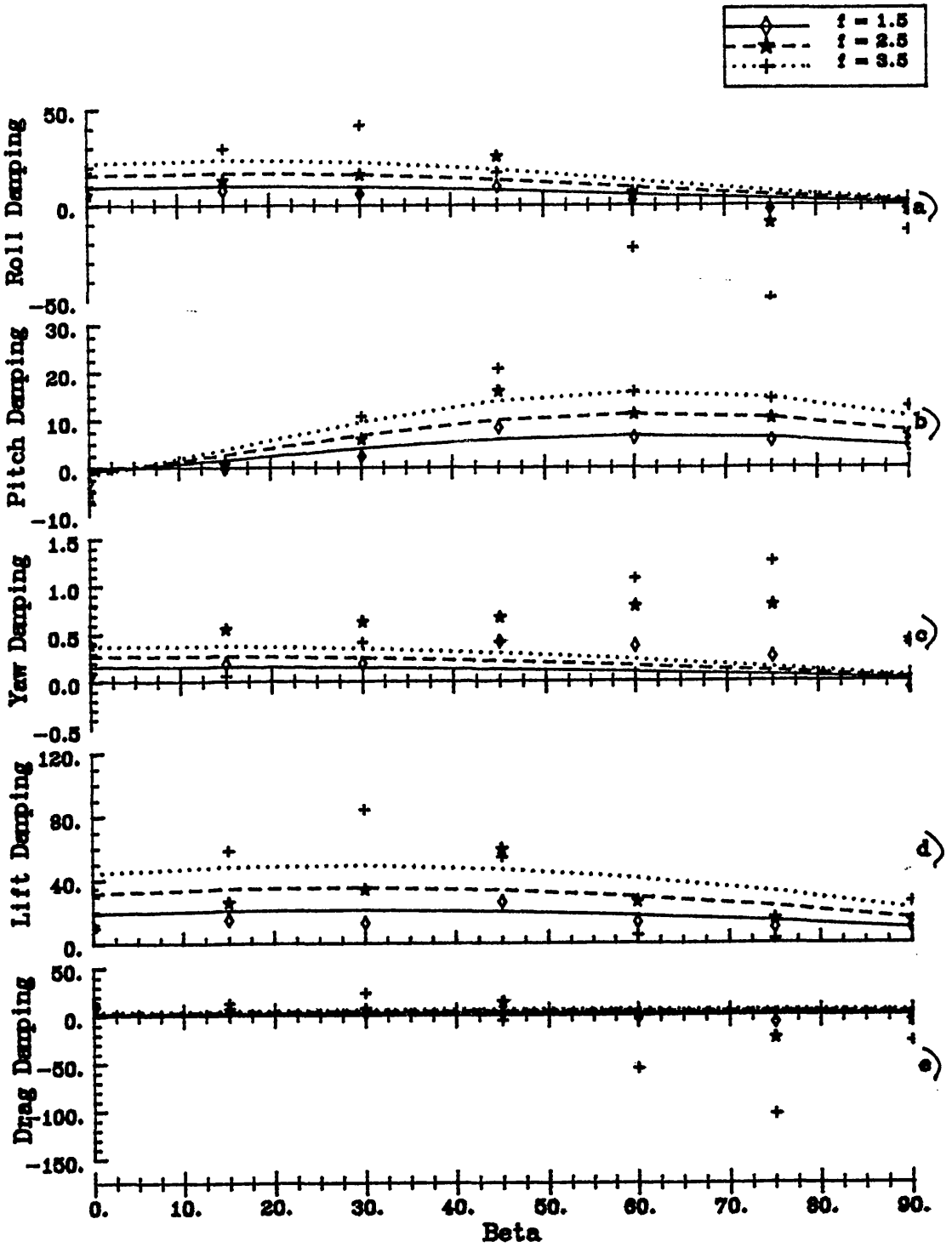

Fig. 78 Damping forces and moments on an aerofoil as functions of wind heading β^* for aspect ratio of 1, mean incidence $\alpha = 15^o$, roll frequency f = 1.5, 2.5, 3.5 Hz.

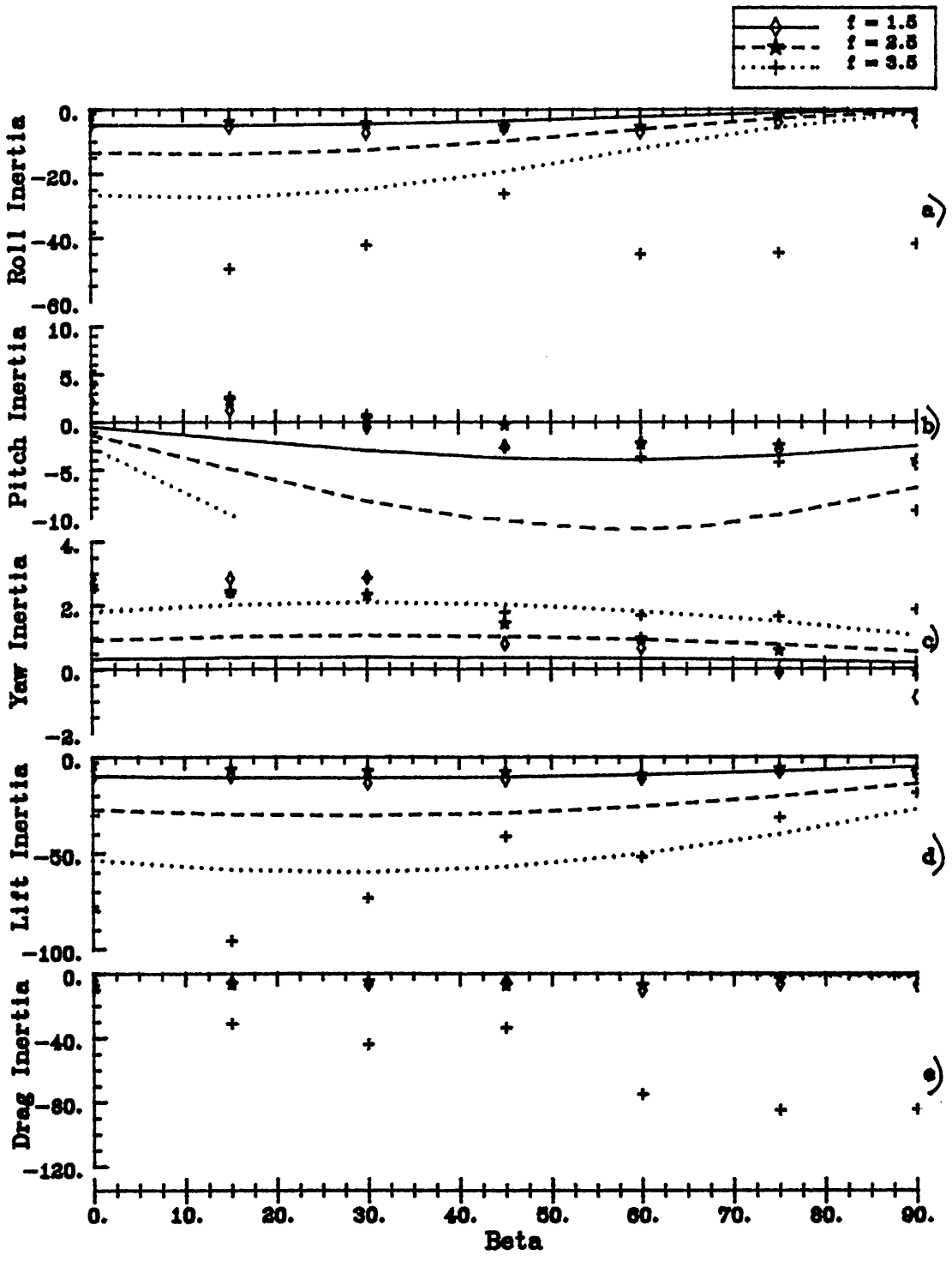

Fig. 79 Inertia forces and moments on an aerofoil as functions of wind heading β^* for aspect ratio of 1, mean incidence $\alpha = 15^o$, roll frequency f = 1.5, 2.5, 3.5 Hz.

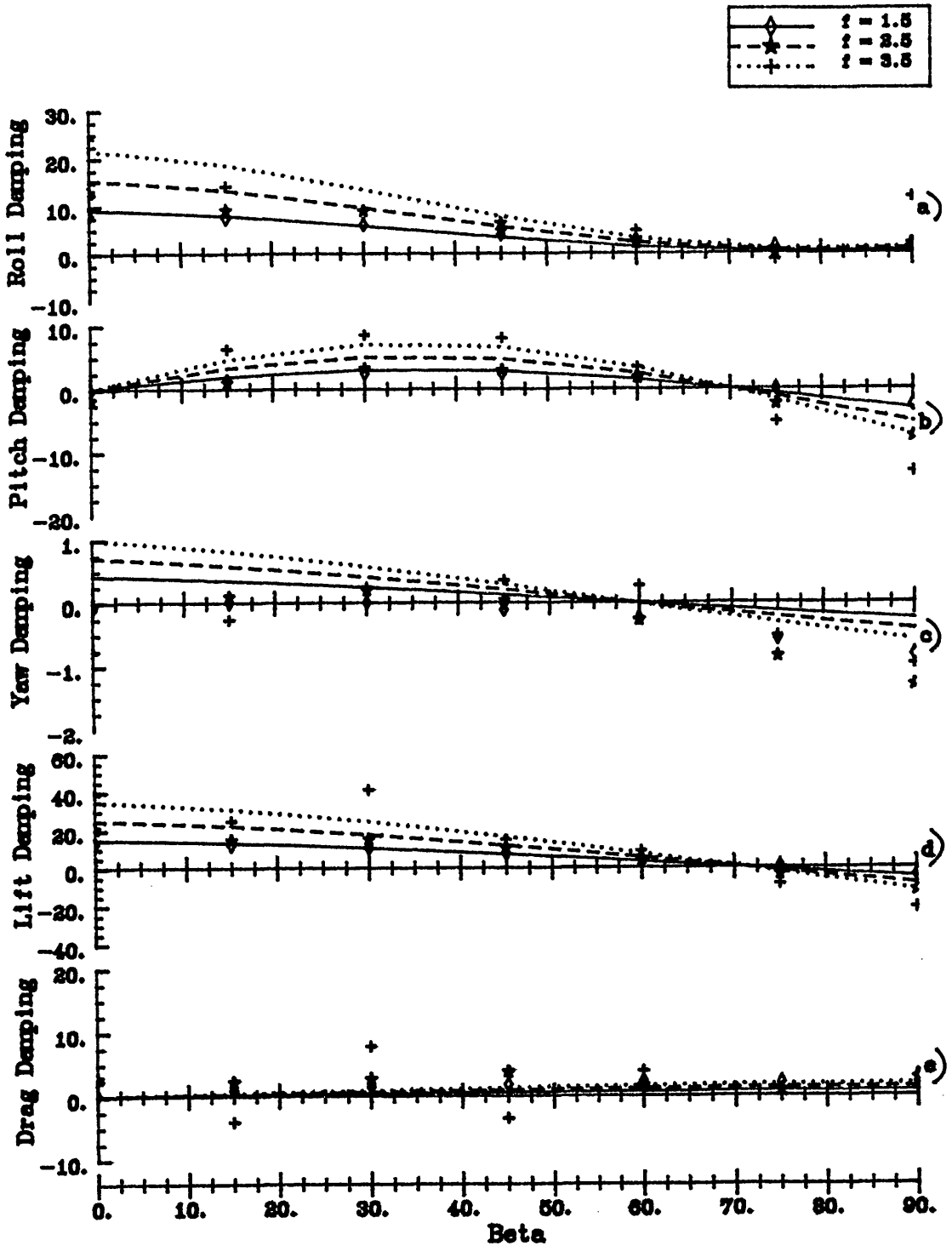

Fig. 80 Damping forces and moments on an aerofoil as functions of wind heading β^* for aspect ratio of 2, mean incidence $\alpha = -10^o$, roll frequency f = 1.5, 2.5, 3.5 Hz.

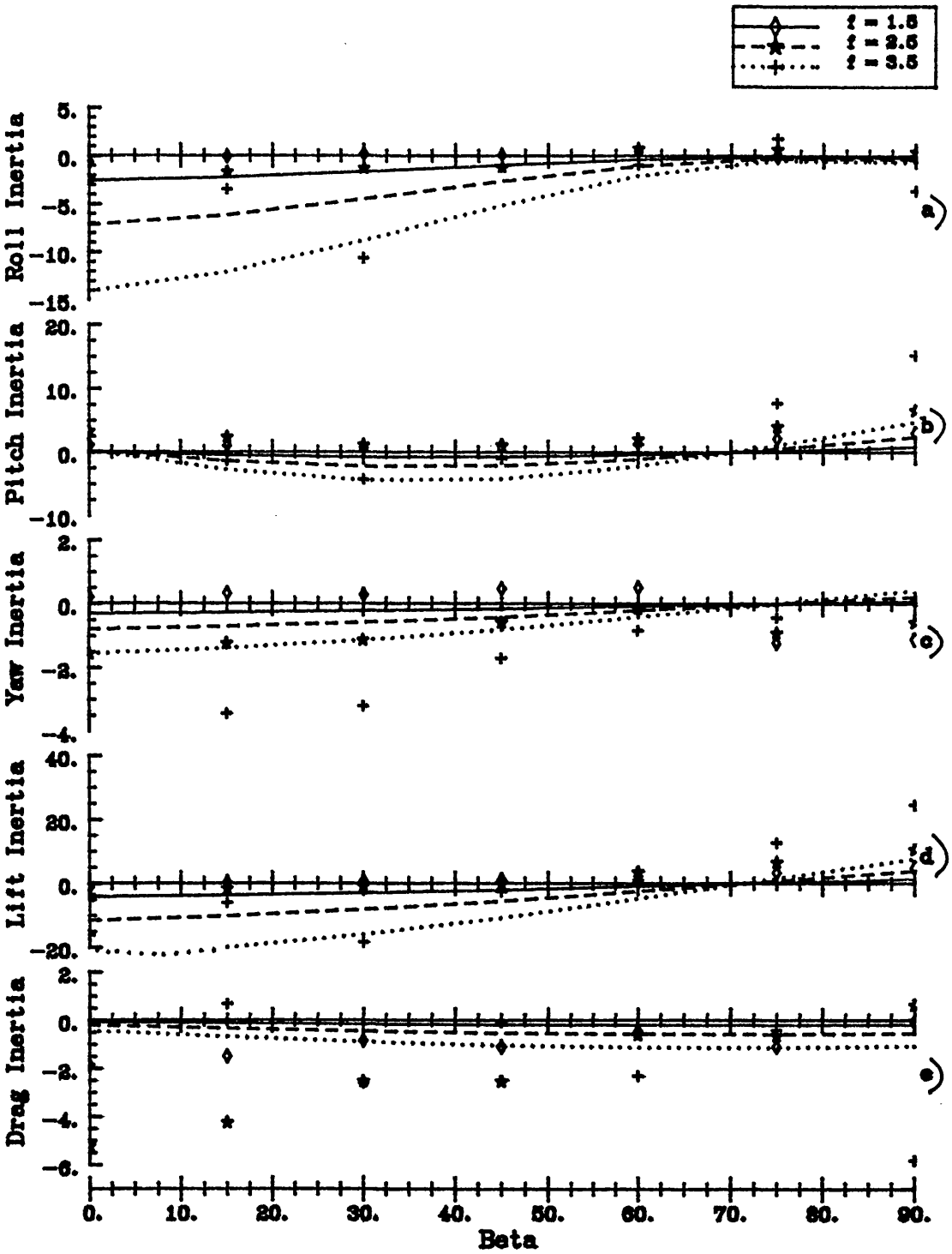

Fig. 81 Inertia forces and moments on an aerofoil as functions of wind heading β^* for aspect ratio of 2, mean incidence $\alpha = -10^o$, roll frequency f = 1.5, 2.5, 3.5 Hz.

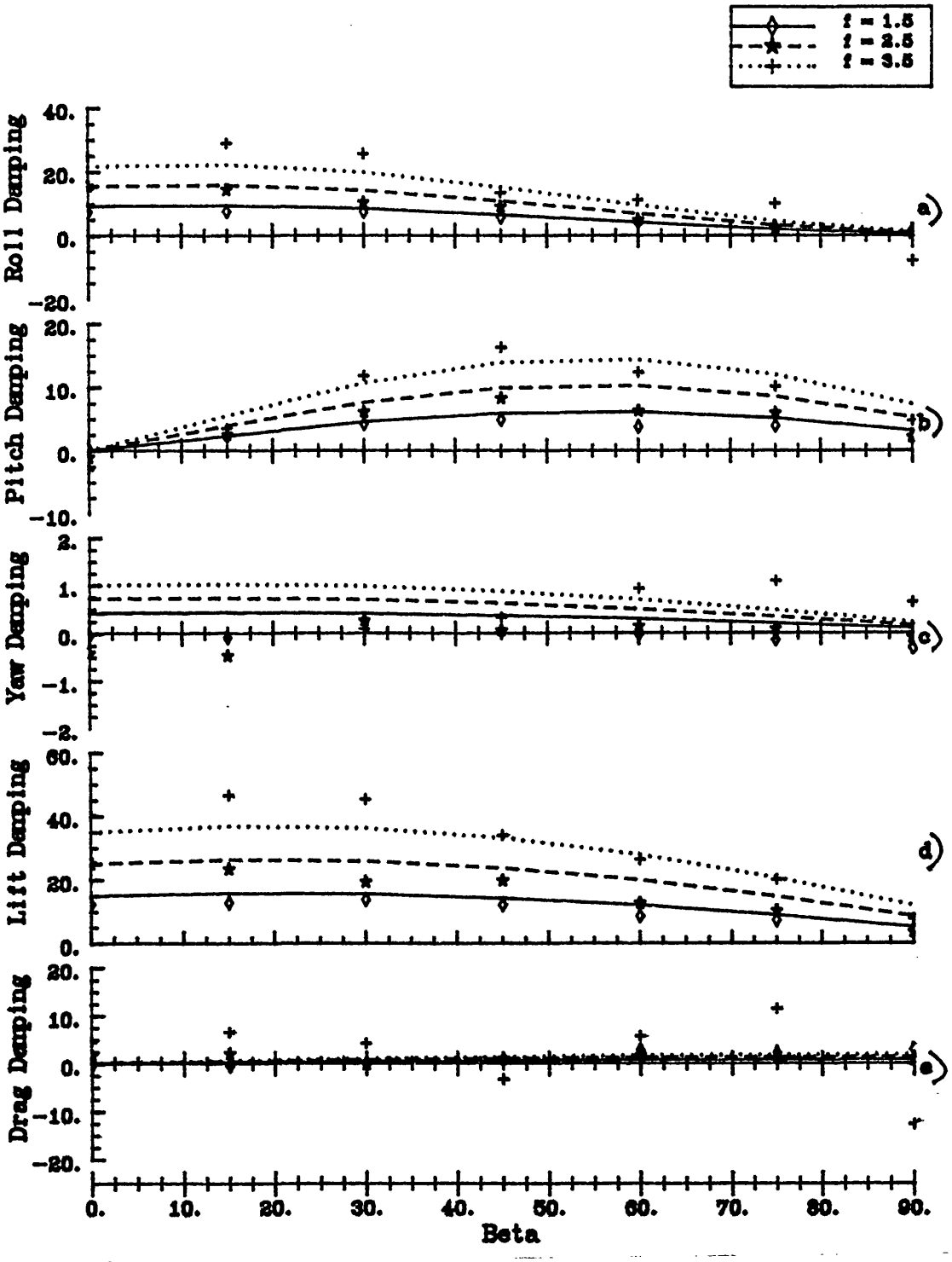

Fig. 82 Damping forces and moments on an aerofoil as functions of wind heading β^* for aspect ratio of 2, mean incidence $\alpha = 10^o$, roll frequency f = 1.5, 2.5, 3.5 Hz.

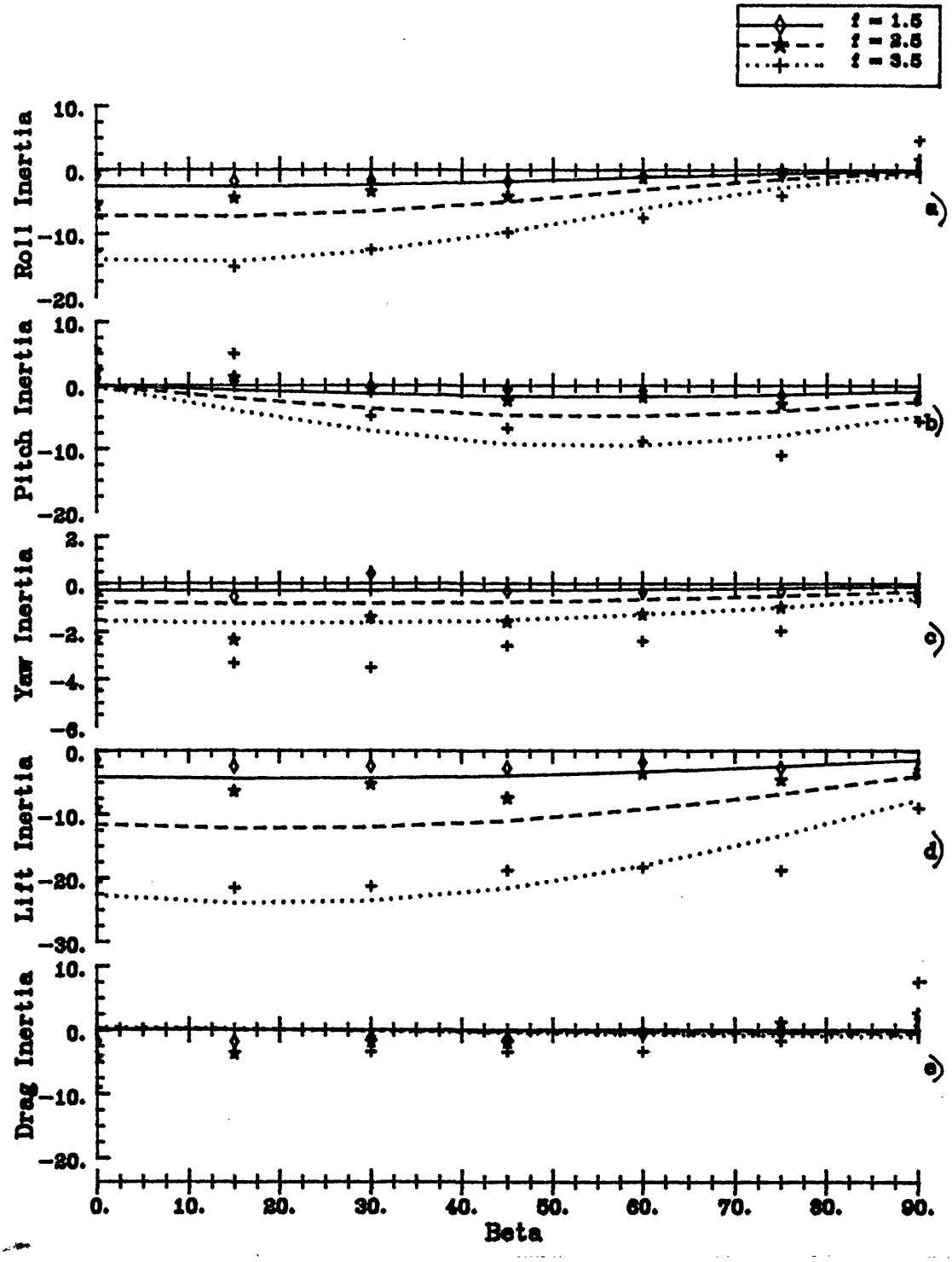

Fig. 83 Inertia forces and moments on an aerofoil as functions of wind heading β^* for aspect ratio of 2, mean incidence $\alpha = 10^o$, roll frequency f = 1.5, 2.5, 3.5 Hz.

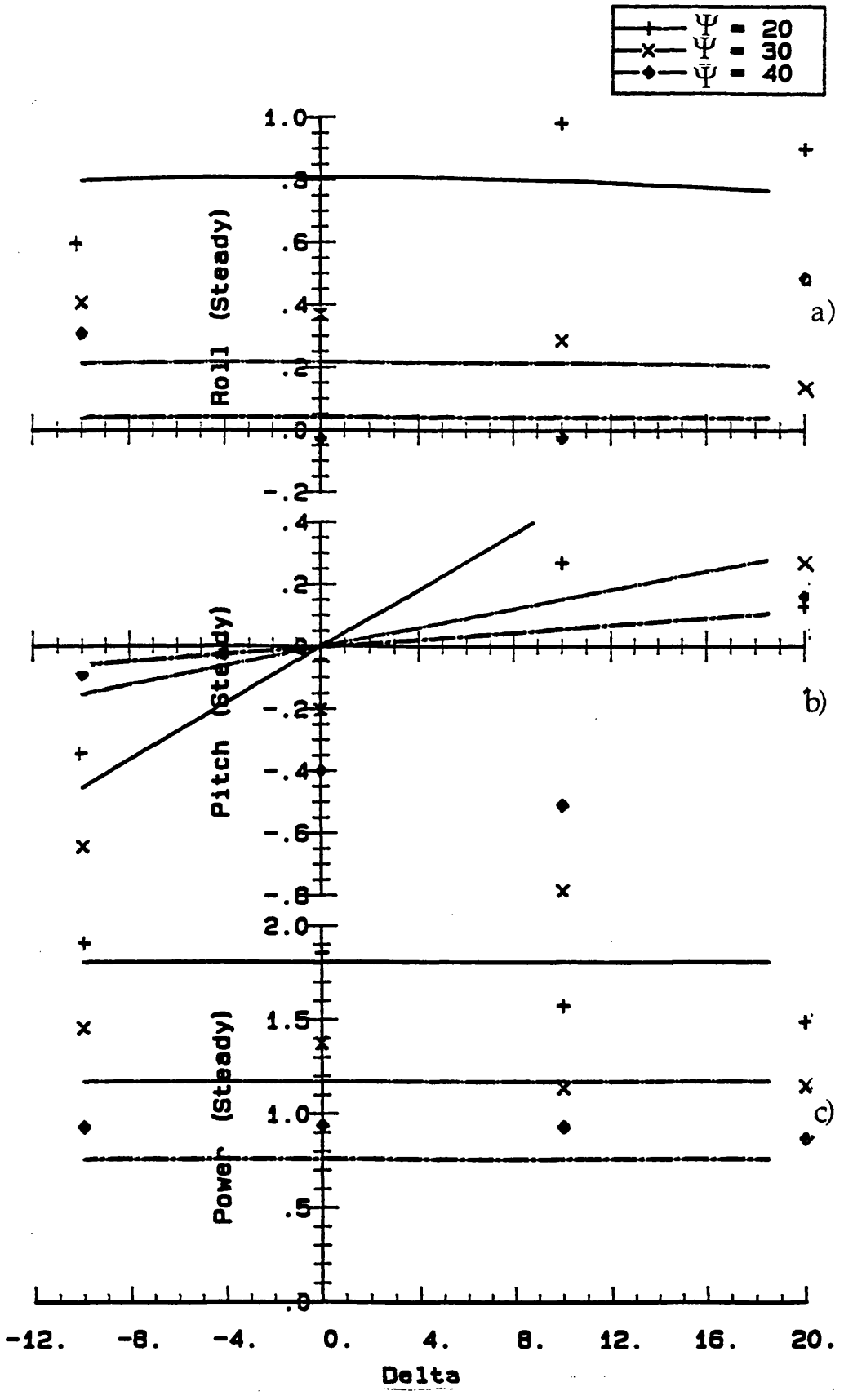

Fig. 84 Steady moments and power on a HAWT as functions of yaw angle δ at wind heading $\beta^* = 90^o$, wind velocity = 4.5 m/s for blade pitch angles $\psi = 20^o, 30^o, 40^o$.

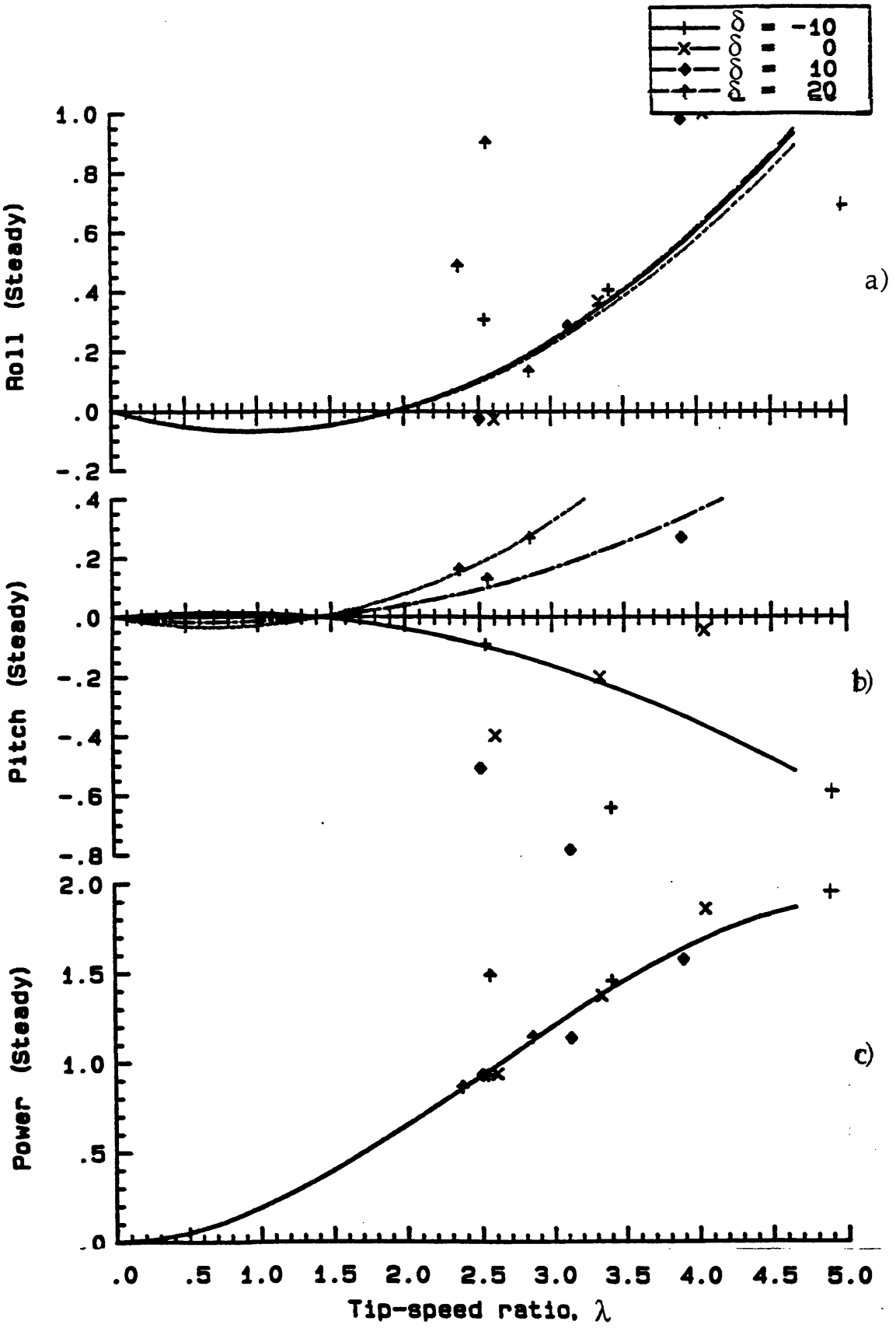

Fig. 85 Steady moments and power on a HAWT as functions of tip-speed ratio λ at wind heading $\beta^* = 90^o$, wind velocity = 4.5 m/s for yaw angles $\delta = -10^o, 0, 10^o, 20^o$.

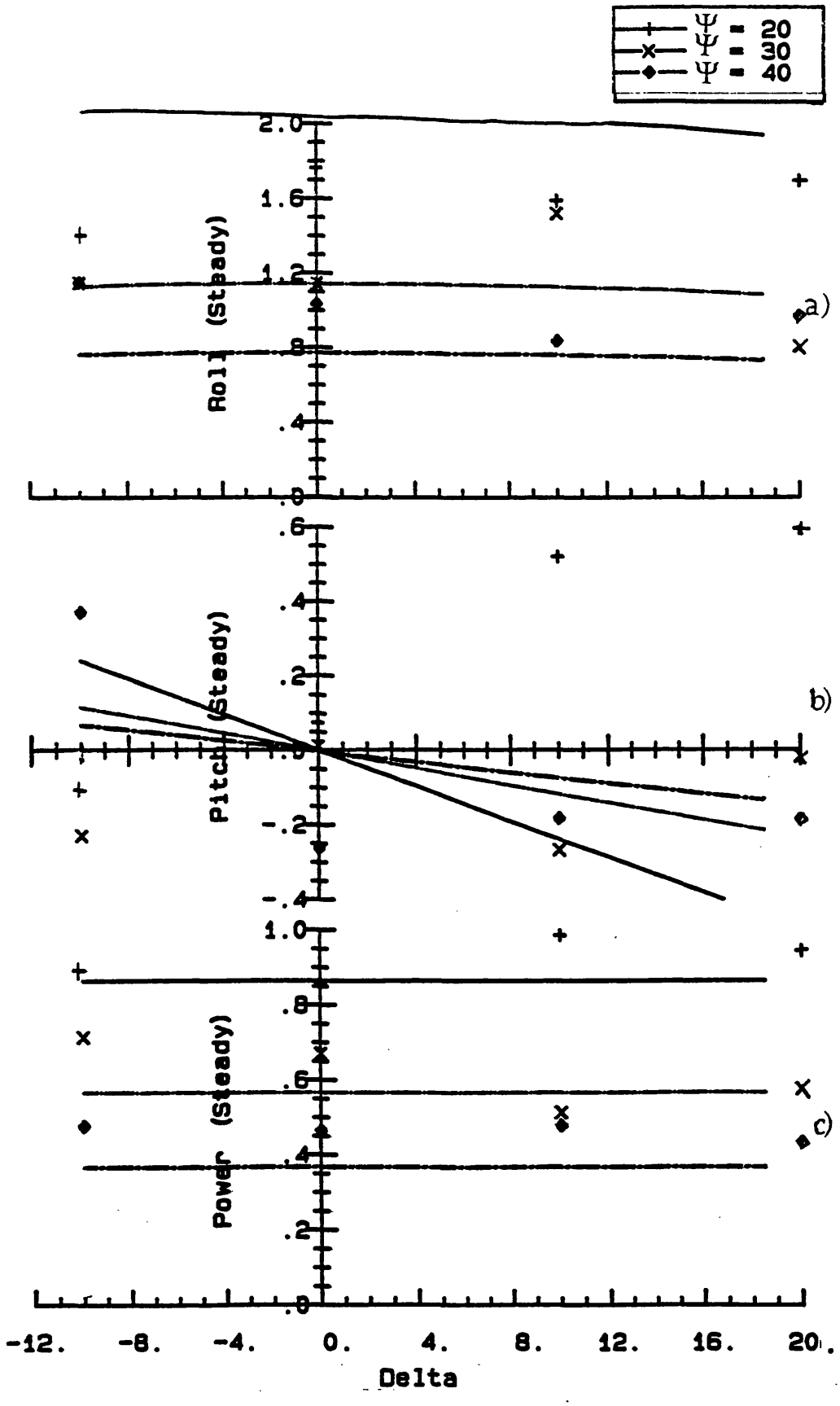

Fig. 86 Steady moments and power on a HAWT as functions of yaw angle δ at wind heading $\beta^* = 90^o$, wind velocity = 9.3 m/s for blade pitch angles $\psi = 20^o, 30^o, 40^o$.

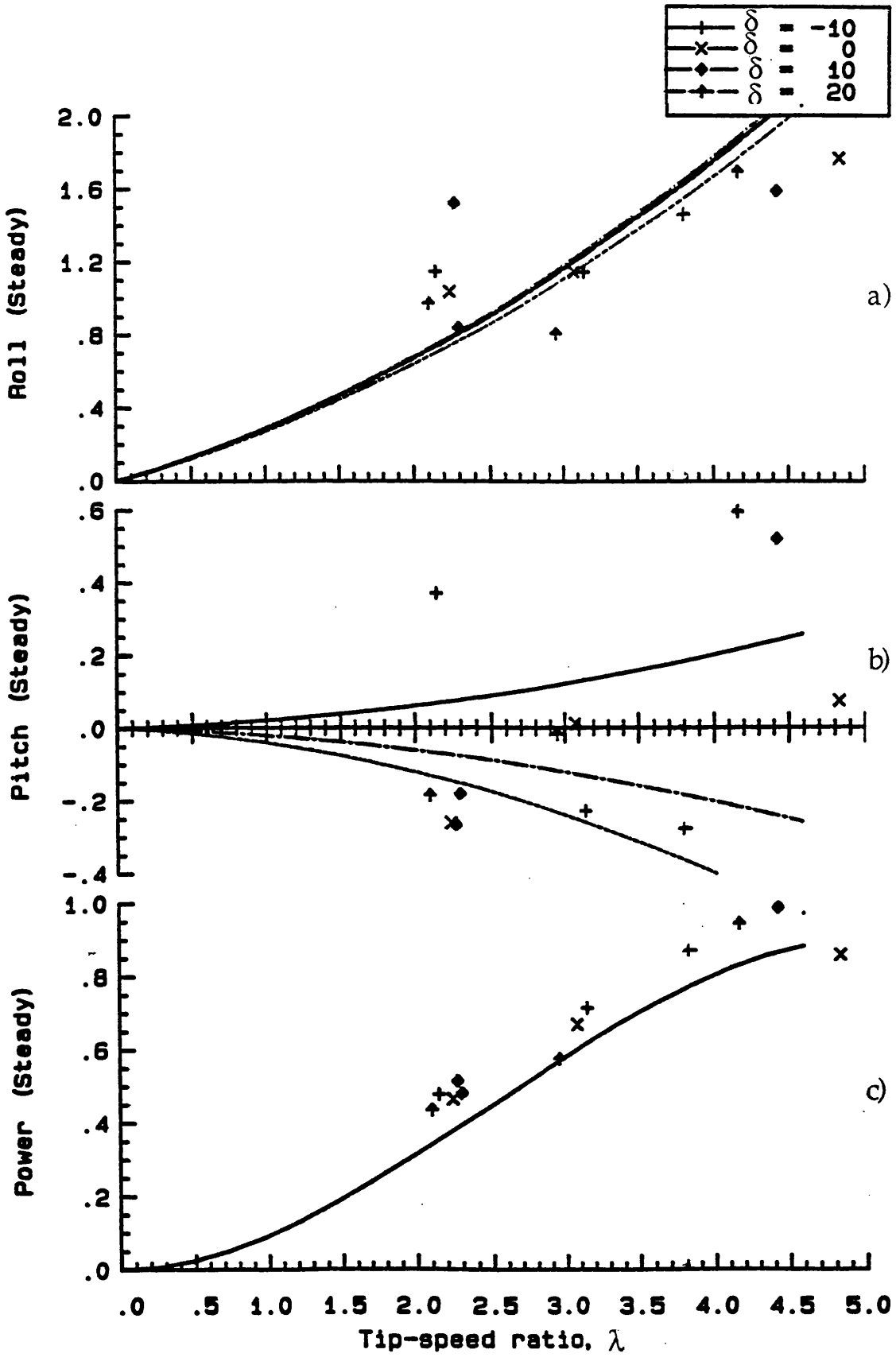

Fig. 87 Steady moments and power on a HAWT as functions of tip-speed ratio λ at wind heading $\beta^* = 90^\circ$, wind velocity = 9.3 m/s for yaw angles $\delta = -10^\circ, 0, 10^\circ, 20^\circ$.

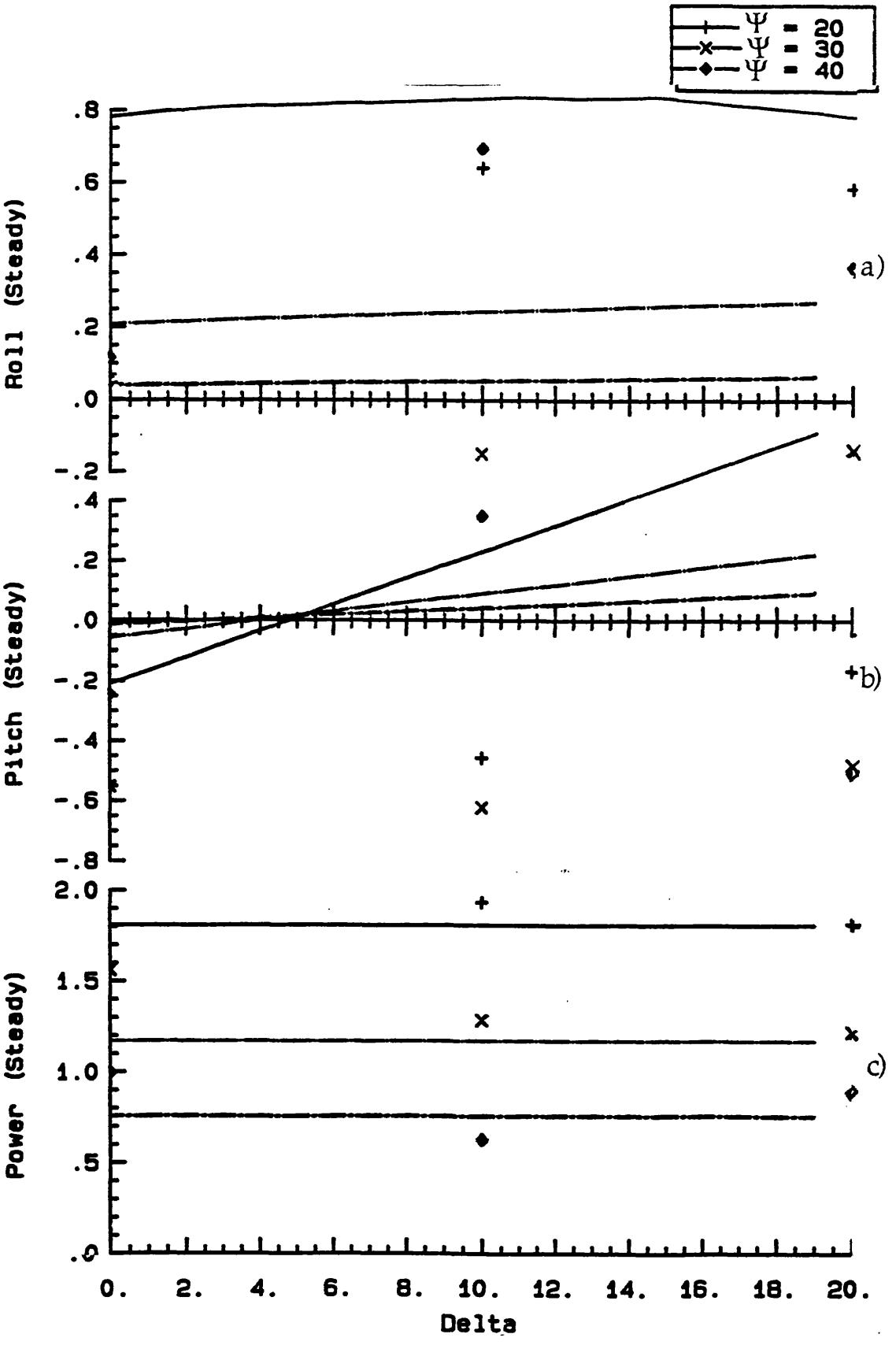

Fig. 88 Steady moments and power on a HAWT as functions of yaw angle δ at wind heading $\beta^* = 75^o$, wind velocity = 4.5 m/s for blade pitch angles $\psi = 20^o, 30^o, 40^o$.

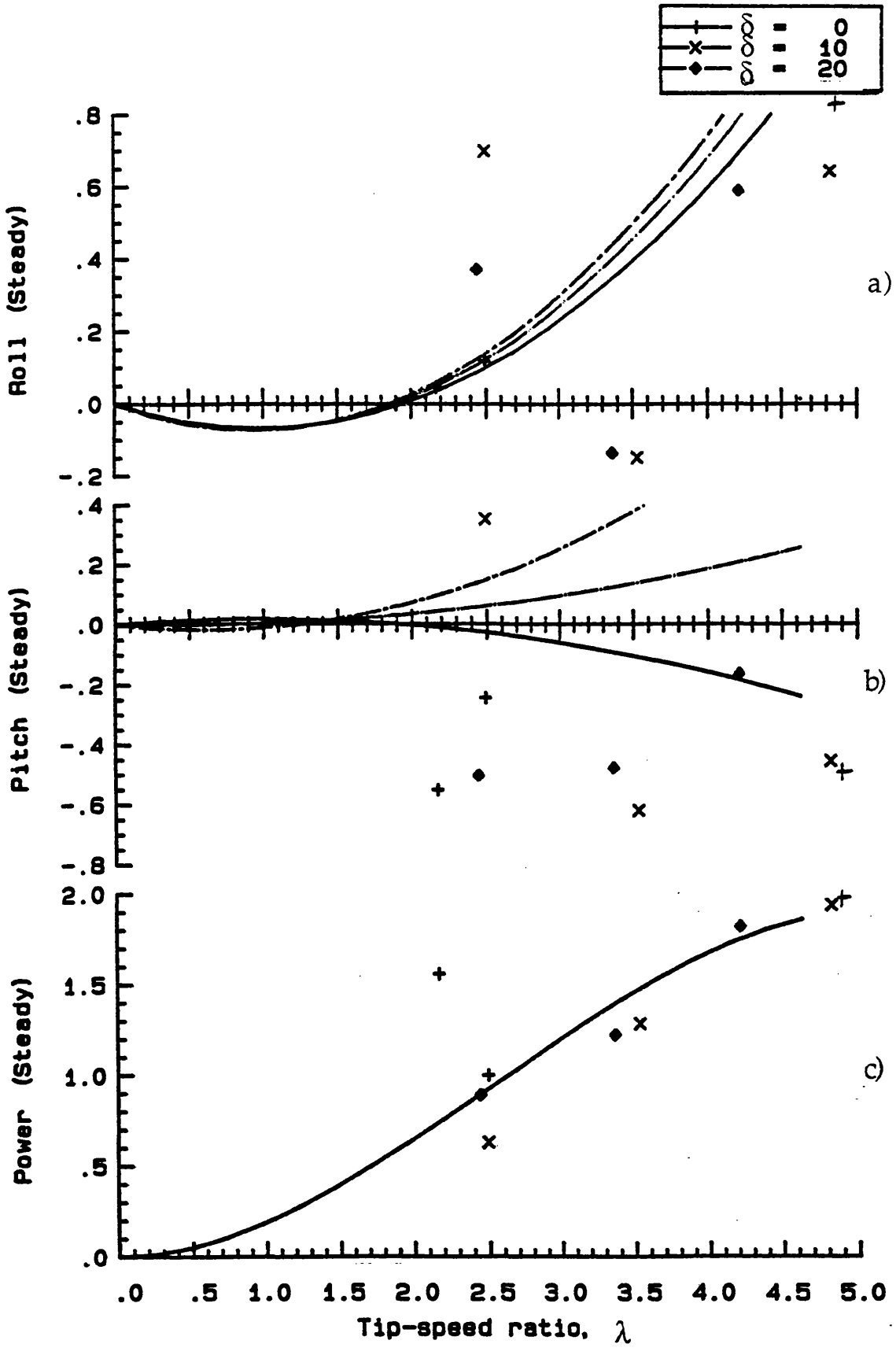

Fig. 89 Steady moments and power on a HAWT as functions of tip-speed ratio λ at wind heading $\beta^* = 75^\circ$, wind velocity = 4.5 m/s for yaw angles $\delta = 0, 10^\circ, 20^\circ$.

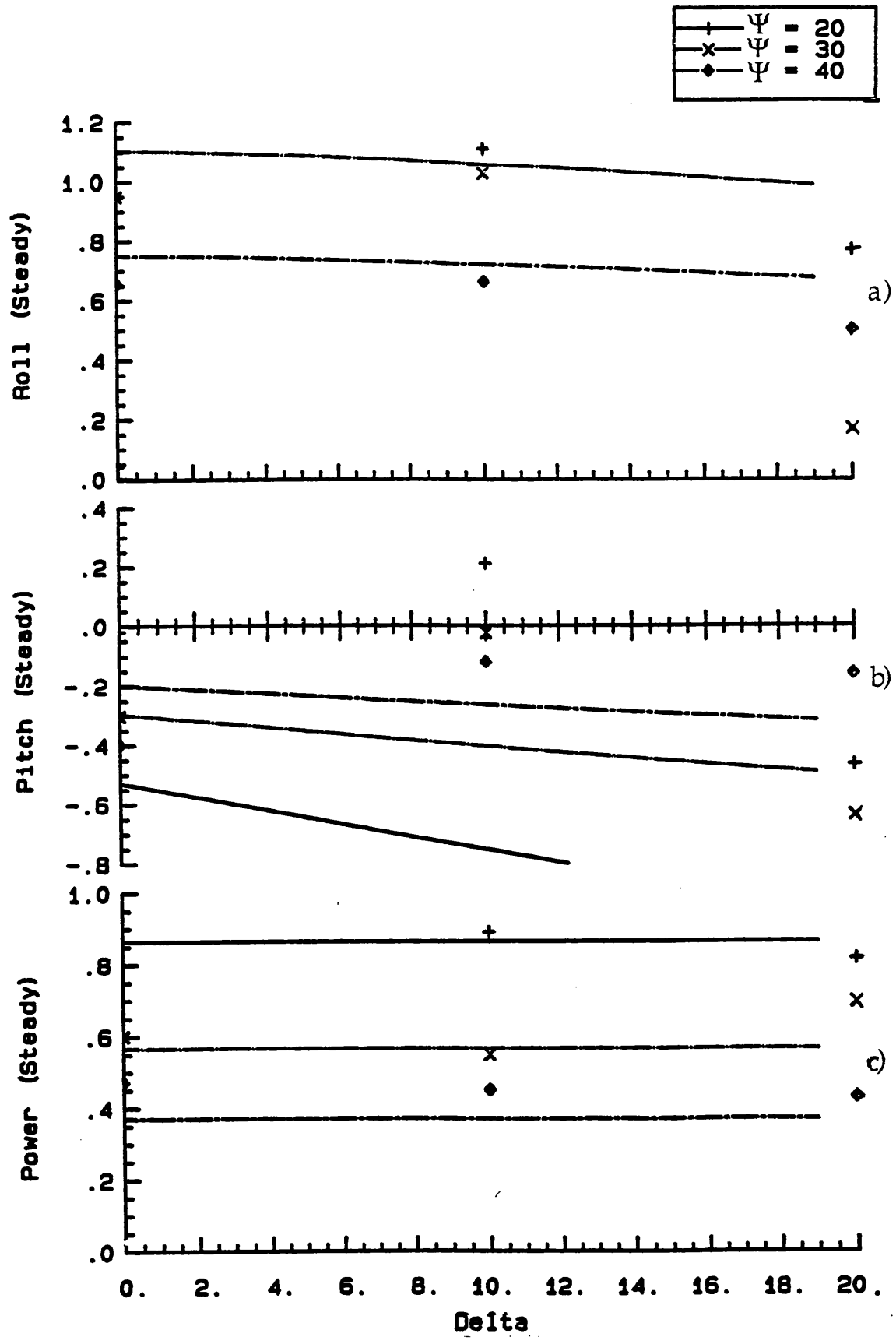

Fig. 90 Steady moments and power on a HAWT as functions of yaw angle δ at wind heading $\beta^* = 75^o$, wind velocity = 9.3 m/s for blade pitch angles $\psi = 20^o, 30^o, 40^o$.

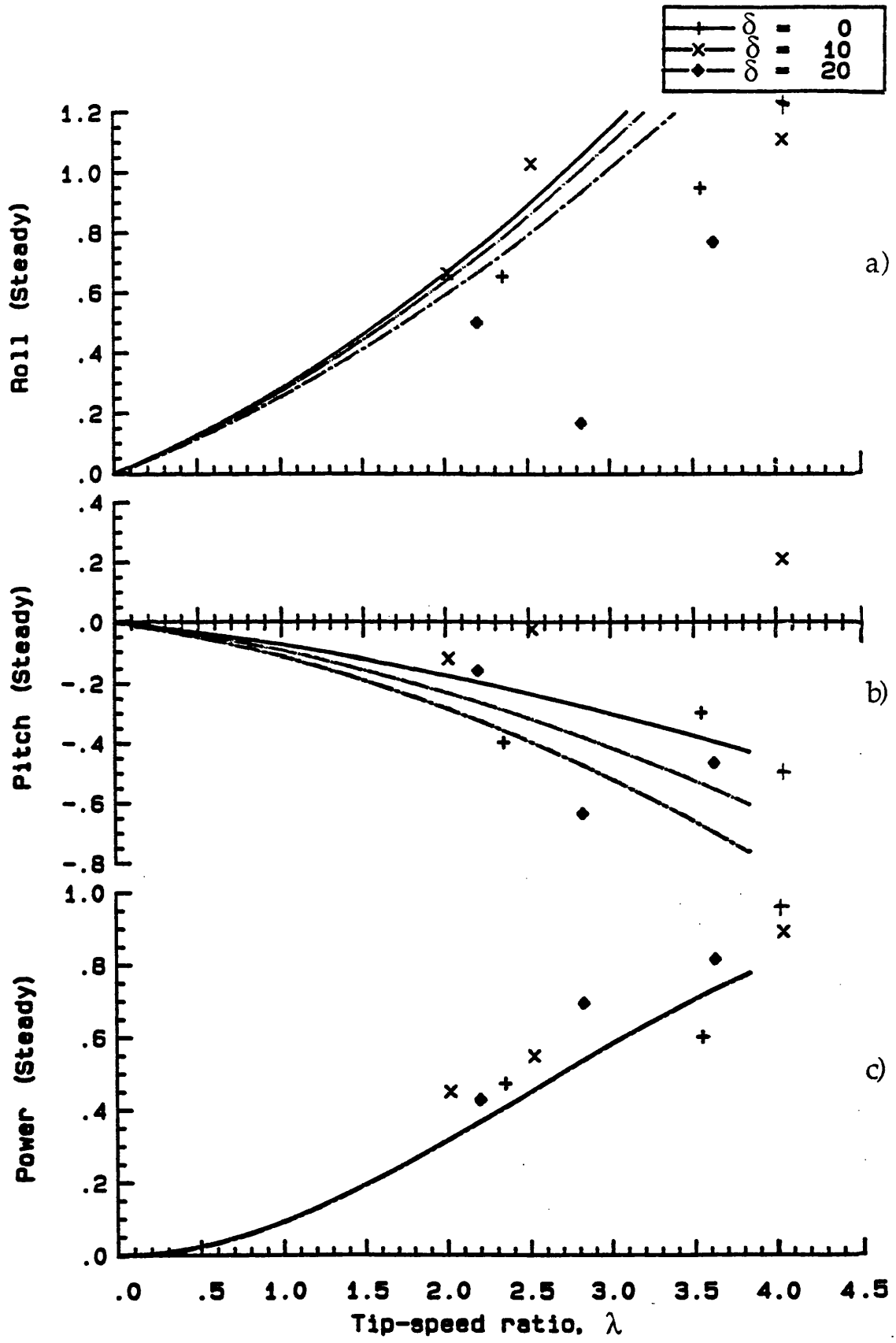

Fig. 91 Steady moments and power on a HAWT as functions of tip-speed ratio λ at wind heading $\beta^* = 75^\circ$, wind velocity = 9.3 m/s for yaw angles $\delta = 0, 10^\circ, 20^\circ$.

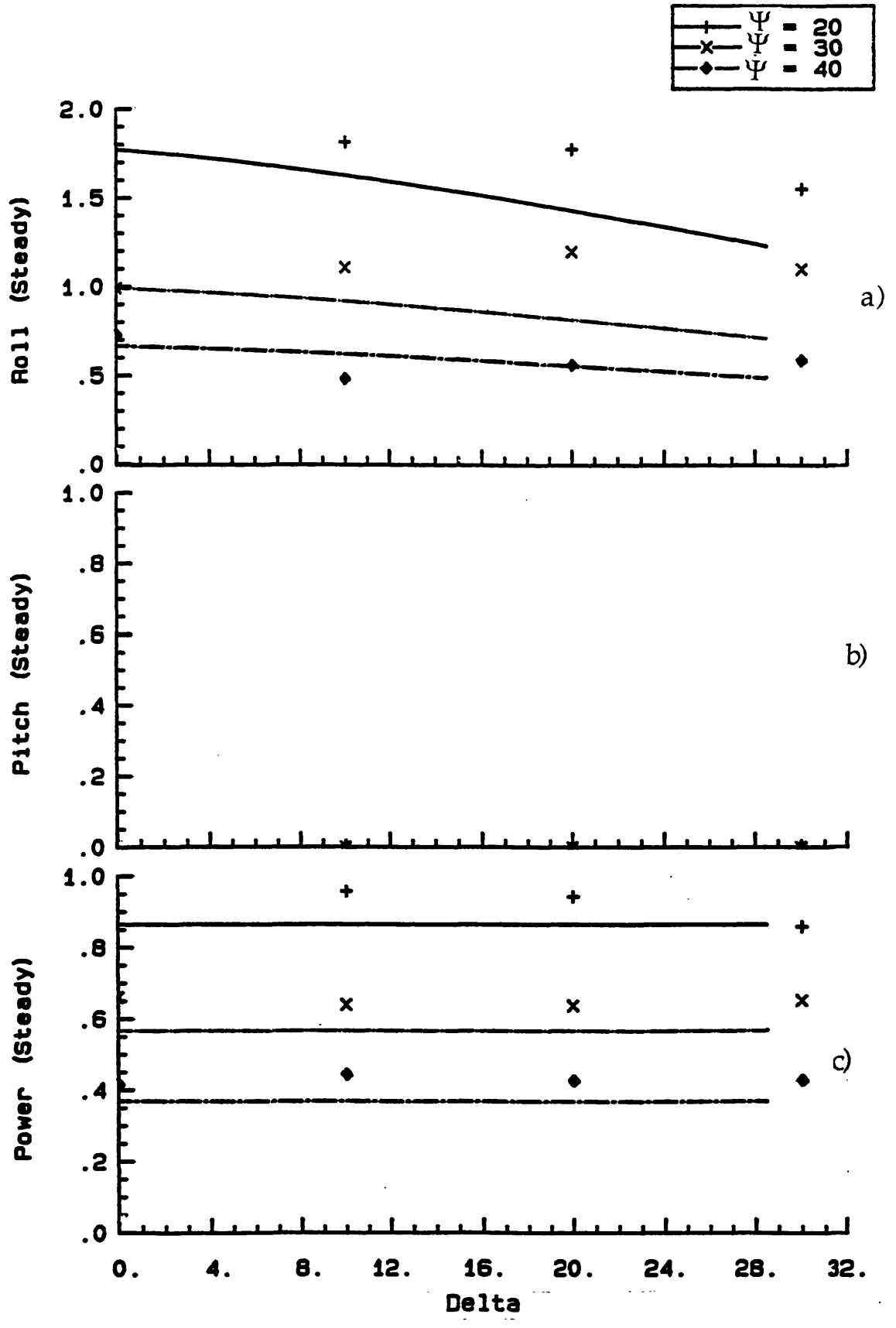

Fig. 92 Steady moments and power on a HAWT as functions of yaw angle δ at wind heading $\beta^* = 60^\circ$, wind velocity = 9.3 m/s for blade pitch angles $\psi = 20^\circ, 30^\circ, 40^\circ$.

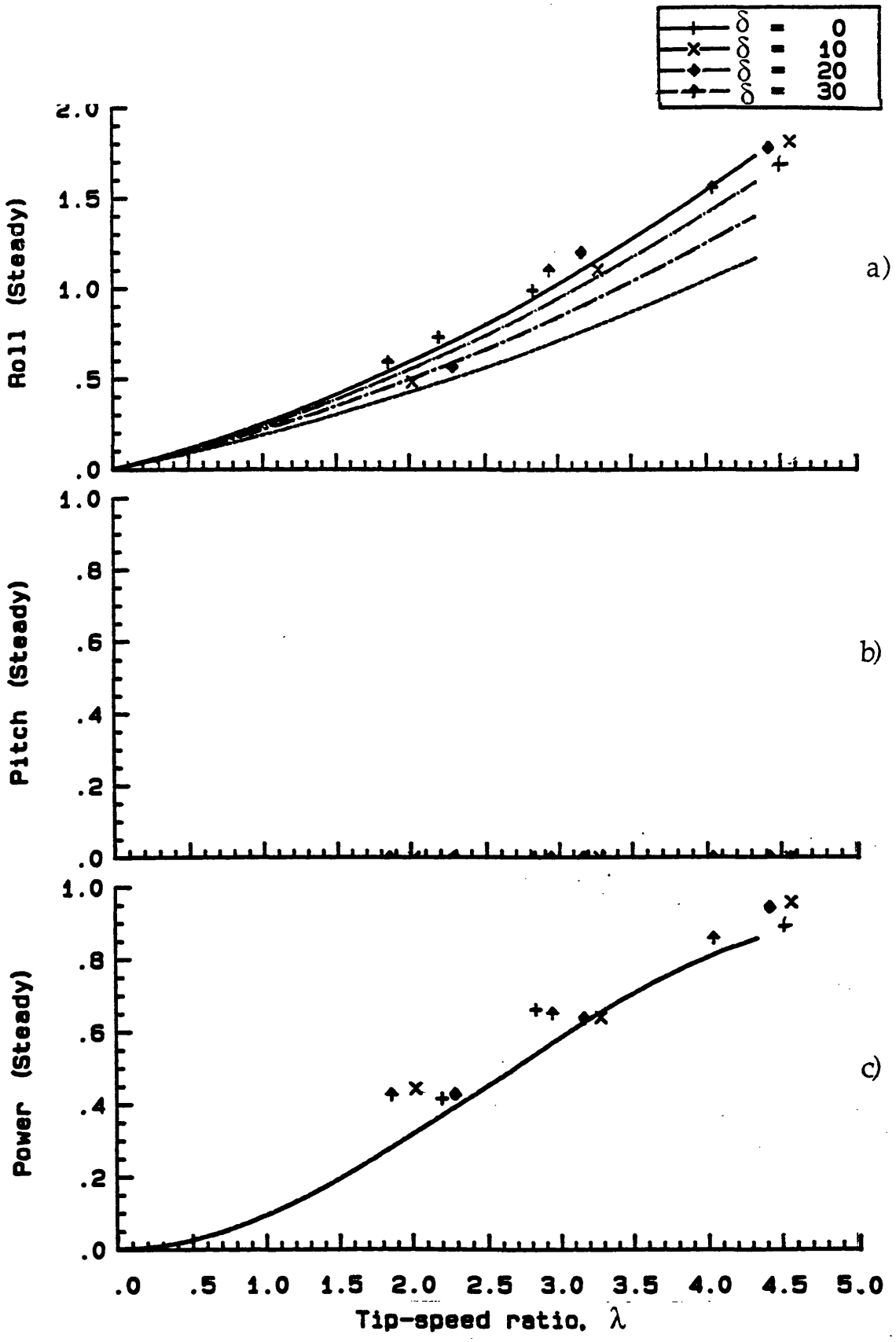

Fig. 93 Steady moments and power on a HAWT as functions of tip-speed ratio λ at wind heading $\beta^* = 60^o$, wind velocity = 9.3 m/s for yaw angles $\delta = 0, 10^o, 20^o, 30^o$.

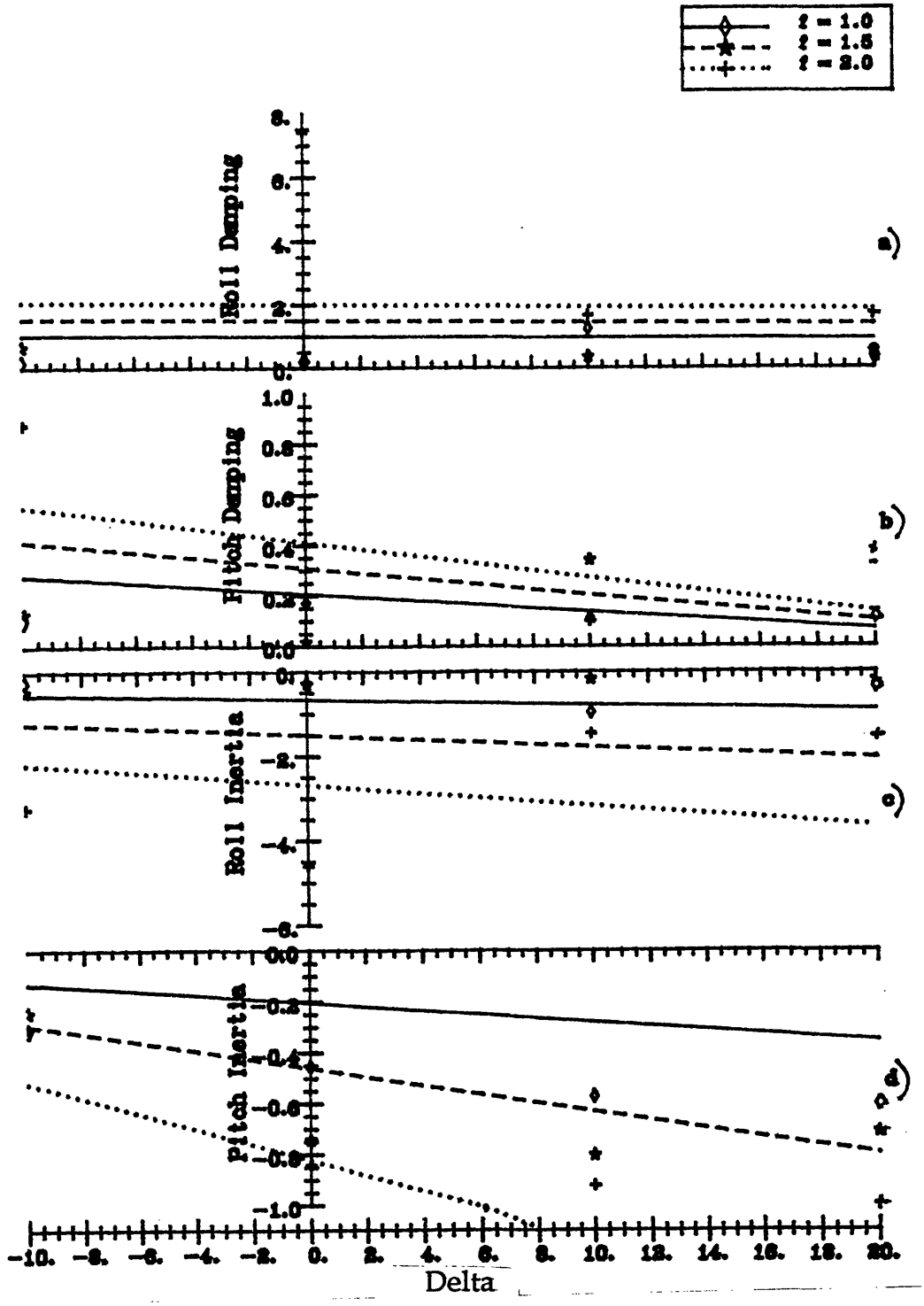

Fig. 94 Damping and inertia moments on a HAWT as functions of yaw angle, δ for wave angle $\gamma = 0$, blade pitch angle $\psi = 20^{o}$, windspeed = 4.5 m/s and roll frequency f = 1, 1.5 and 2 Hz.

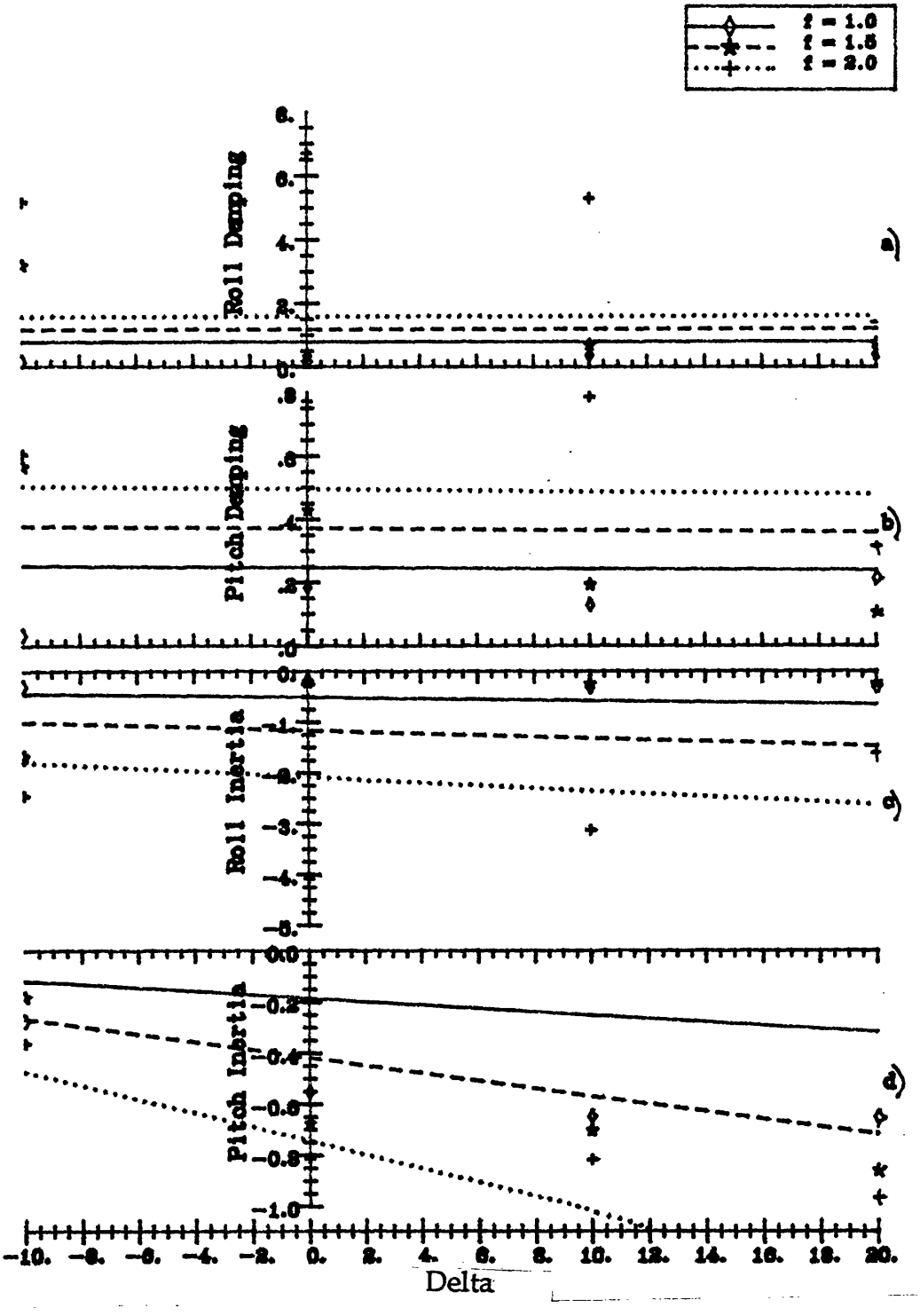

Fig. 95 Damping and inertia moments on a HAWT as functions of yaw angle, δ
for wave angle $\gamma = 0$, blade pitch angle $\psi = 30^{o}$
windspeed = 4.5 m/s and roll frequency f = 1, 1.5 and 2 Hz.

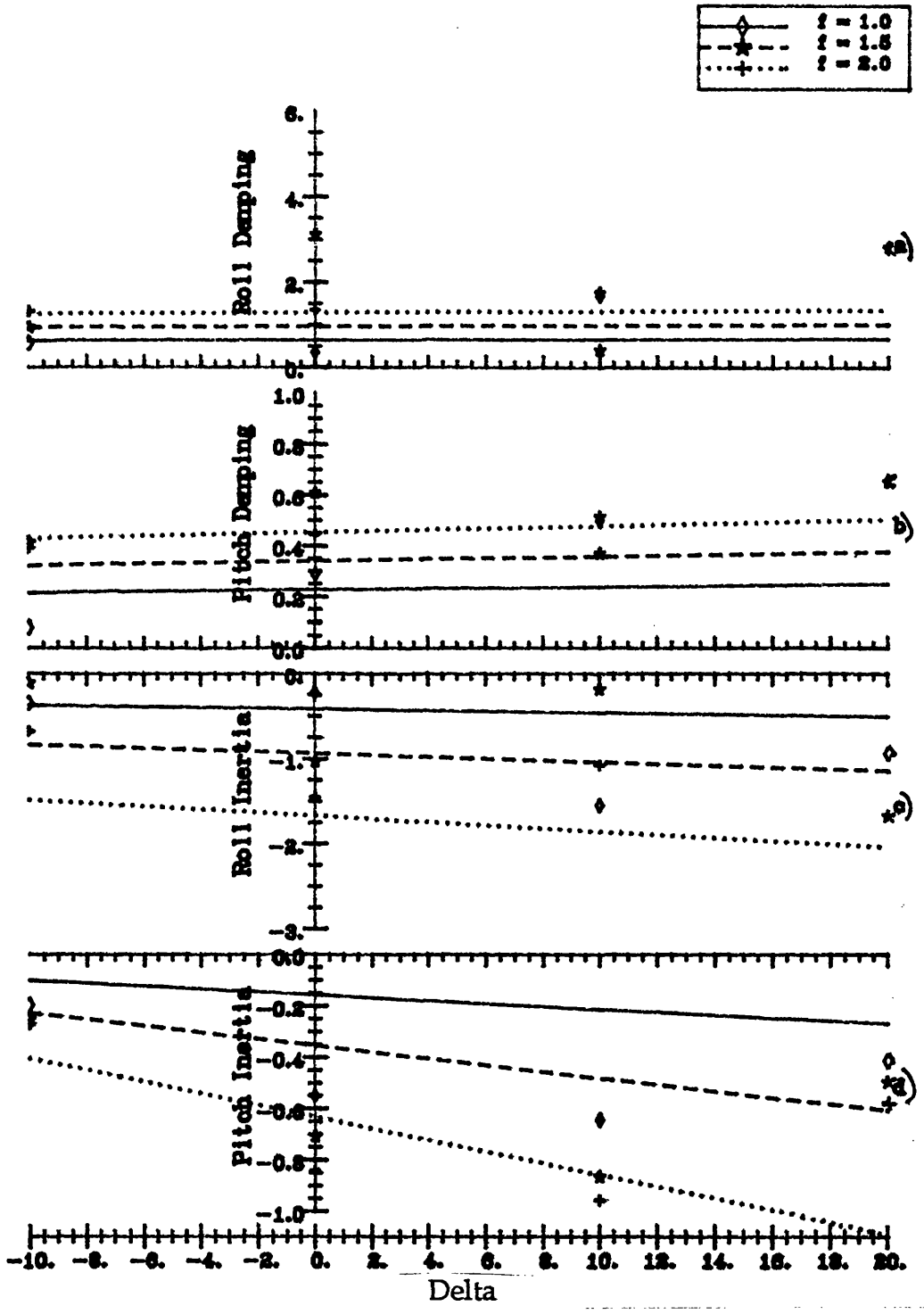

Fig. 96 Damping and inertia moments on a HAWT as functions of yaw angle, δ
for wave angle $\gamma = 0$, blade pitch angle $\psi = 40^o$
windspeed = 4.5 m/s and roll frequency f = 1, 1.5 and 2 Hz.

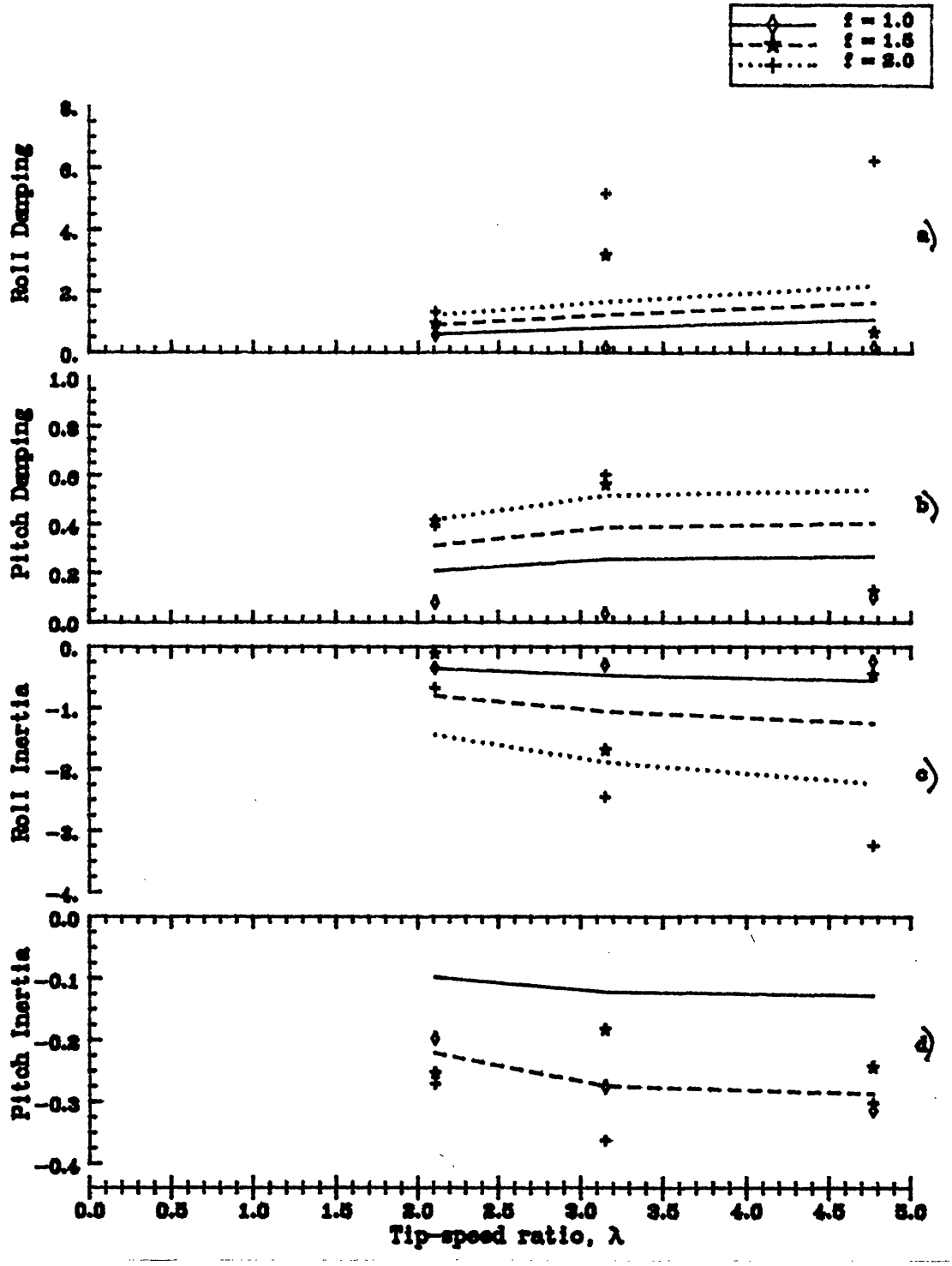

Fig. 97 Damping and inertia moments on a HAWT as functions of tip-speed ratio, λ
for wave angle, $\gamma = 0$, yaw angle $\delta = -10^{o}$
windspeed = 4.5 m/s and roll frequency f = 1, 1.5 and 2 Hz.

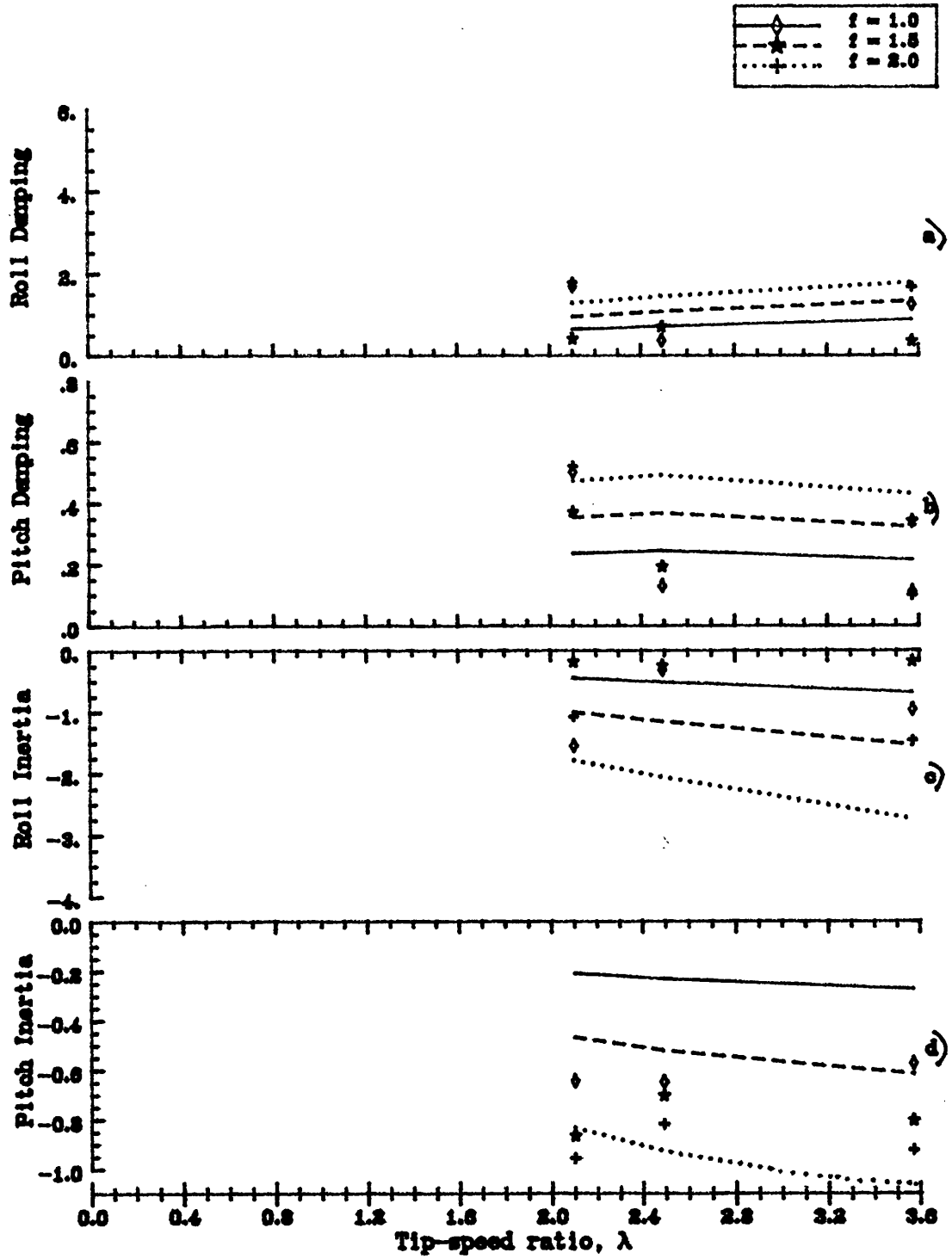

Fig. 98 Damping and inertia moments on a HAWT as functions of tip-speed ratio, λ for wave angle, $\gamma = 0$, yaw angle $\delta = 10^{o}$ windspeed = 4.5 m/s and roll frequency f = 1, 1.5 and 2 Hz.

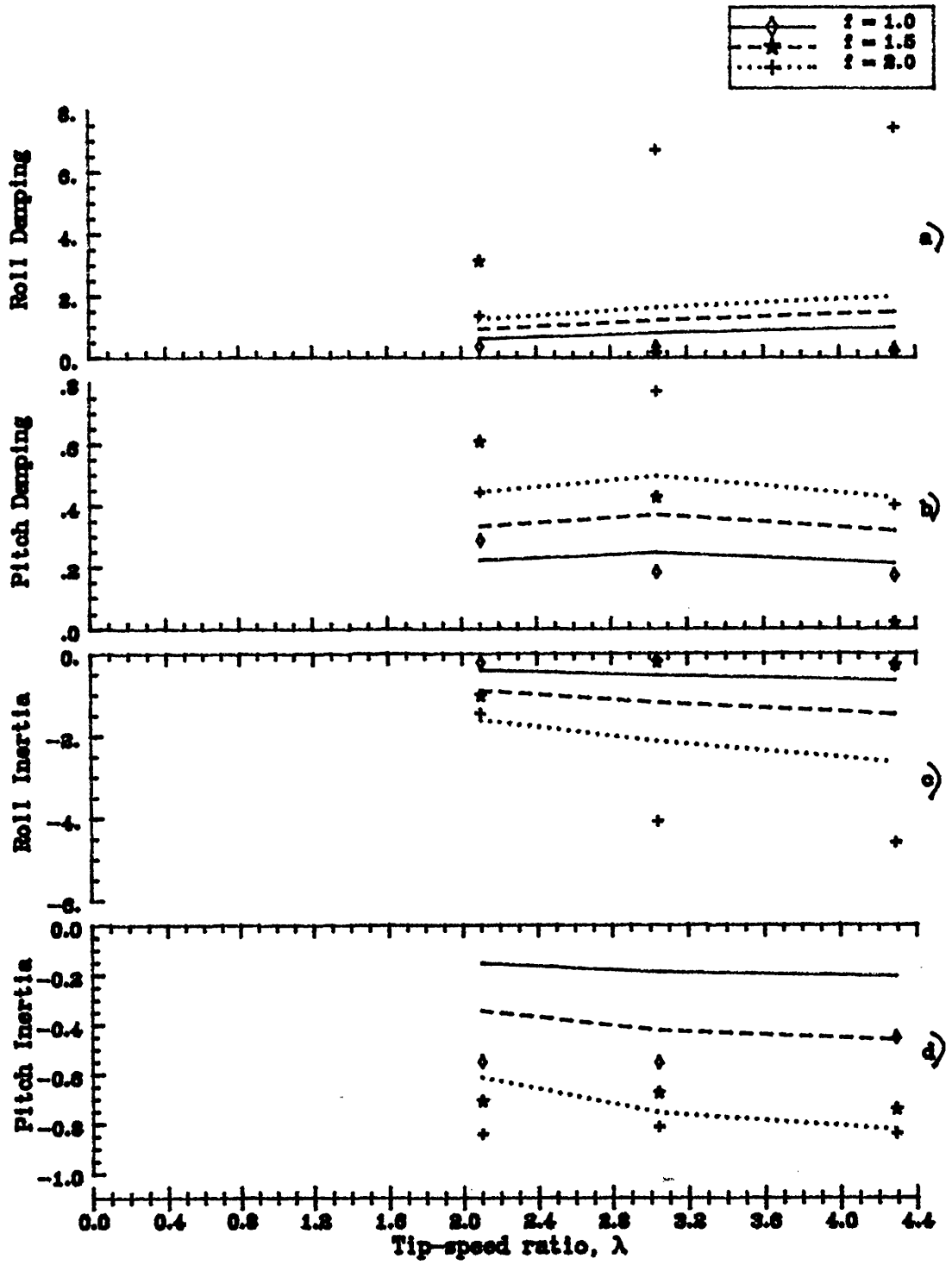

Fig. 99 Damping and inertia moments on a HAWT as functions of tip-speed ratio, λ for wave angle, $\gamma = 0$, yaw angle $\delta = 0^o$ windspeed = 4.5 m/s and roll frequency f = 1, 1.5 and 2 Hz.

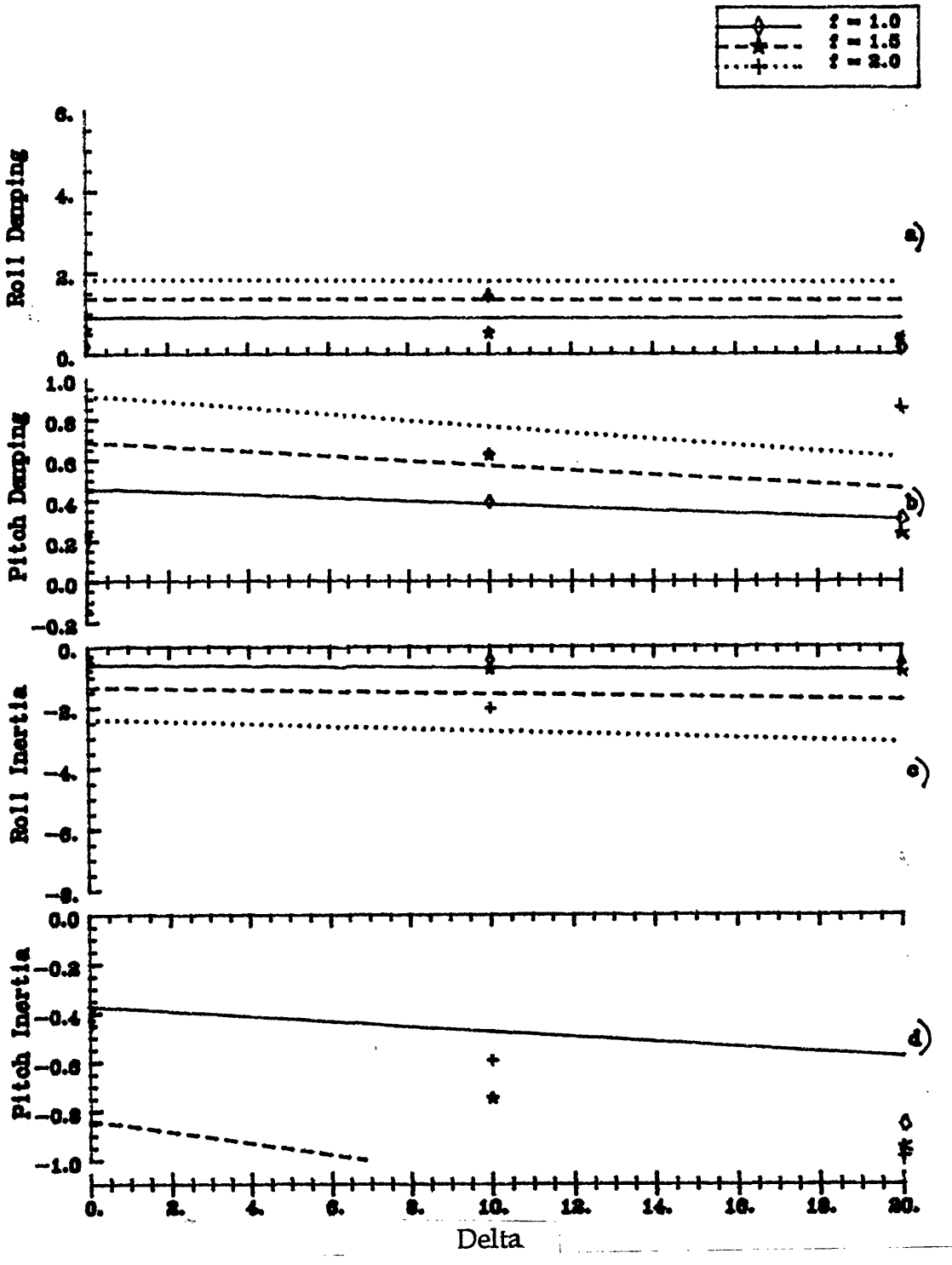

Fig. 100 Damping and inertia moments on a HAWT as functions of yaw angle, δ for wave angle $\gamma = 15^{o}$, blade pitch angle $\psi = 20^{o}$ windspeed = 4.5 m/s and roll frequency f = 1, 1.5 and 2 Hz.

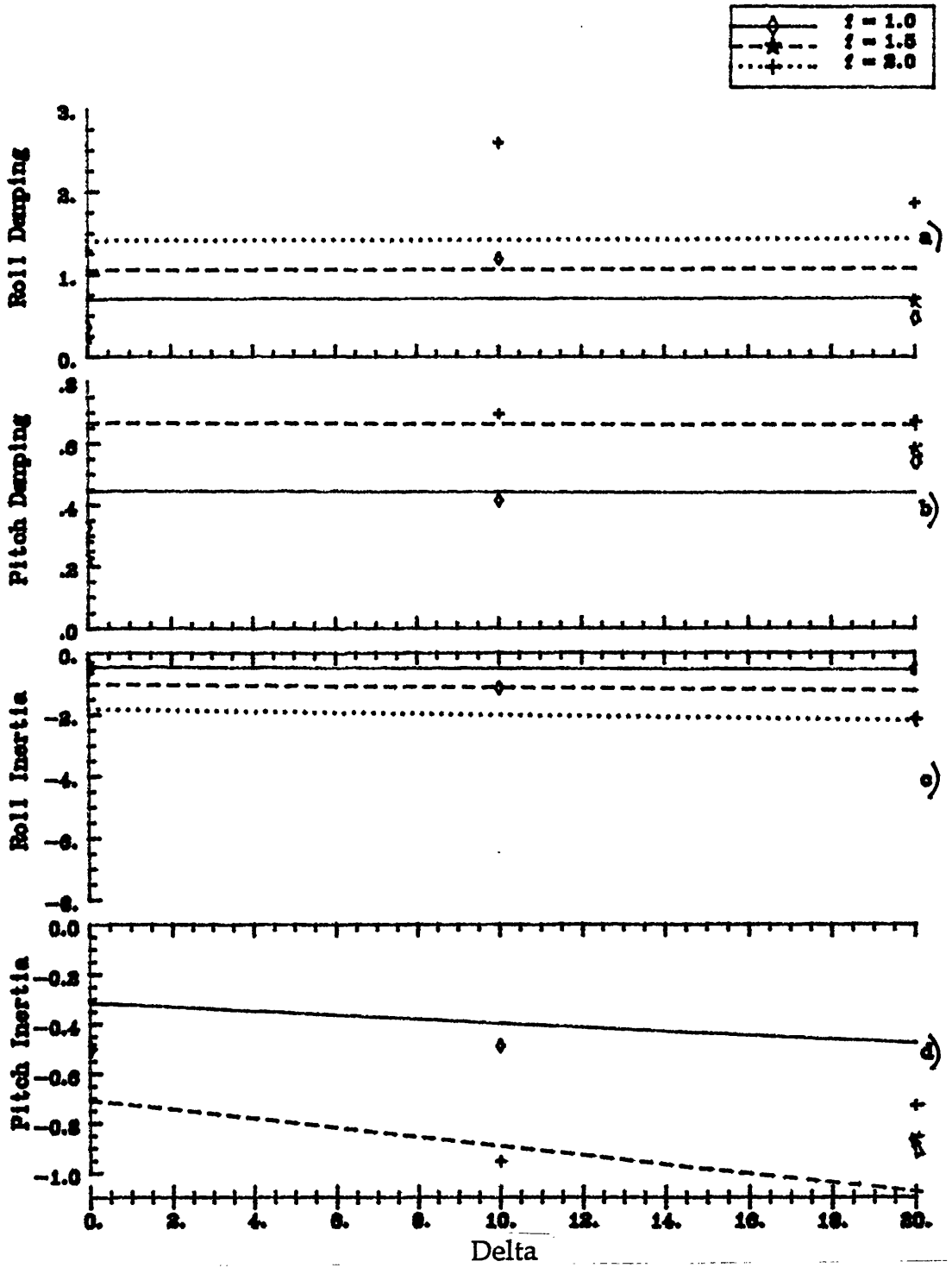

Fig. 101 Damping and inertia moments on a HAWT as functions of yaw angle, δ
for wave angle $\gamma = 15^{o}$, blade pitch angle $\psi = 30^{o}$
windspeed = 4.5 m/s and roll frequency f = 1, 1.5 and 2 Hz.

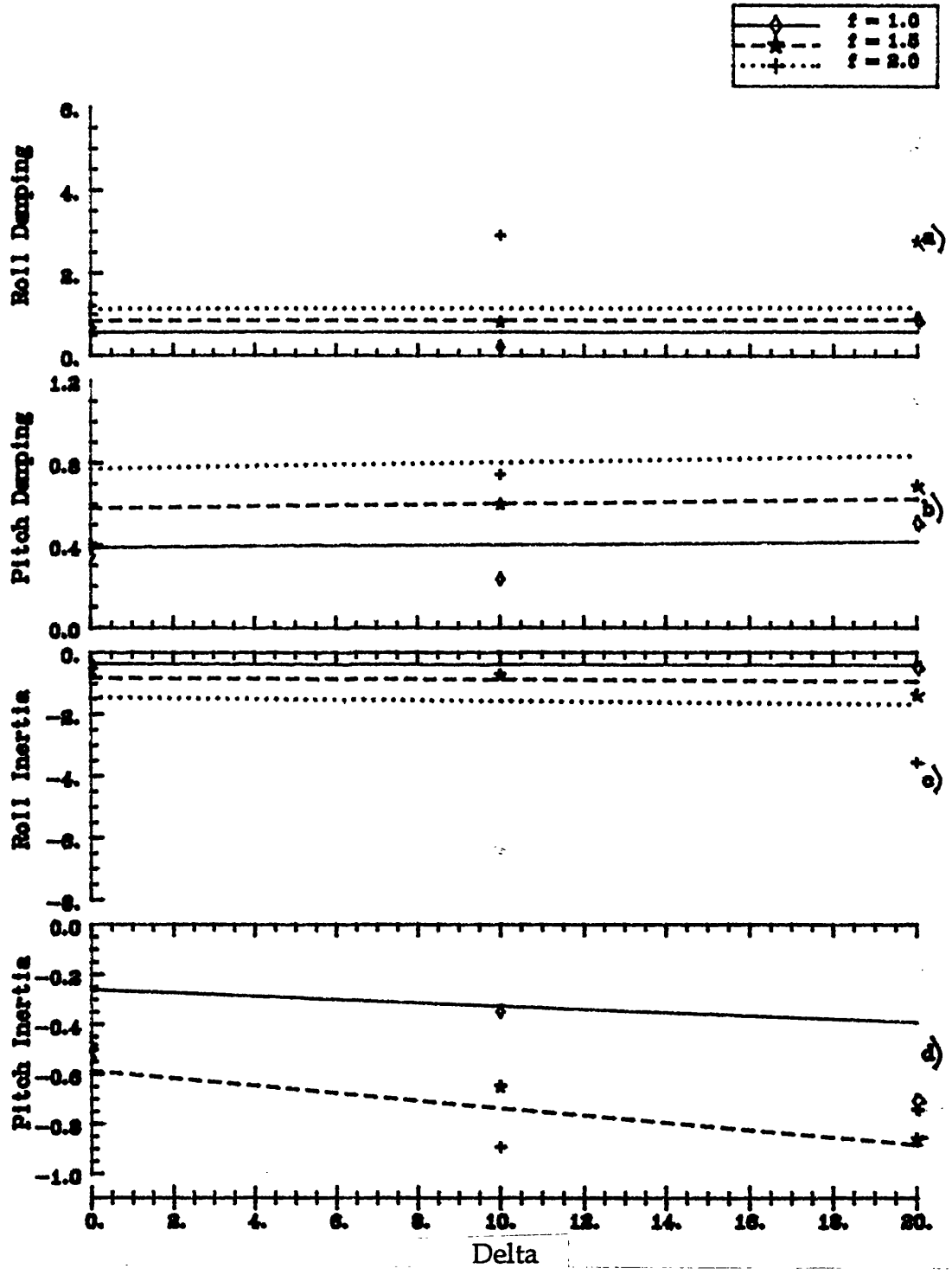

Fig. 102 Damping and inertia moments on a HAWT as functions of yaw angle, δ for wave angle $\gamma = 15^{o}$, blade pitch angle $\psi = 40^{o}$ windspeed = 4.5 m/s and roll frequency f = 1, 1.5 and 2 Hz.

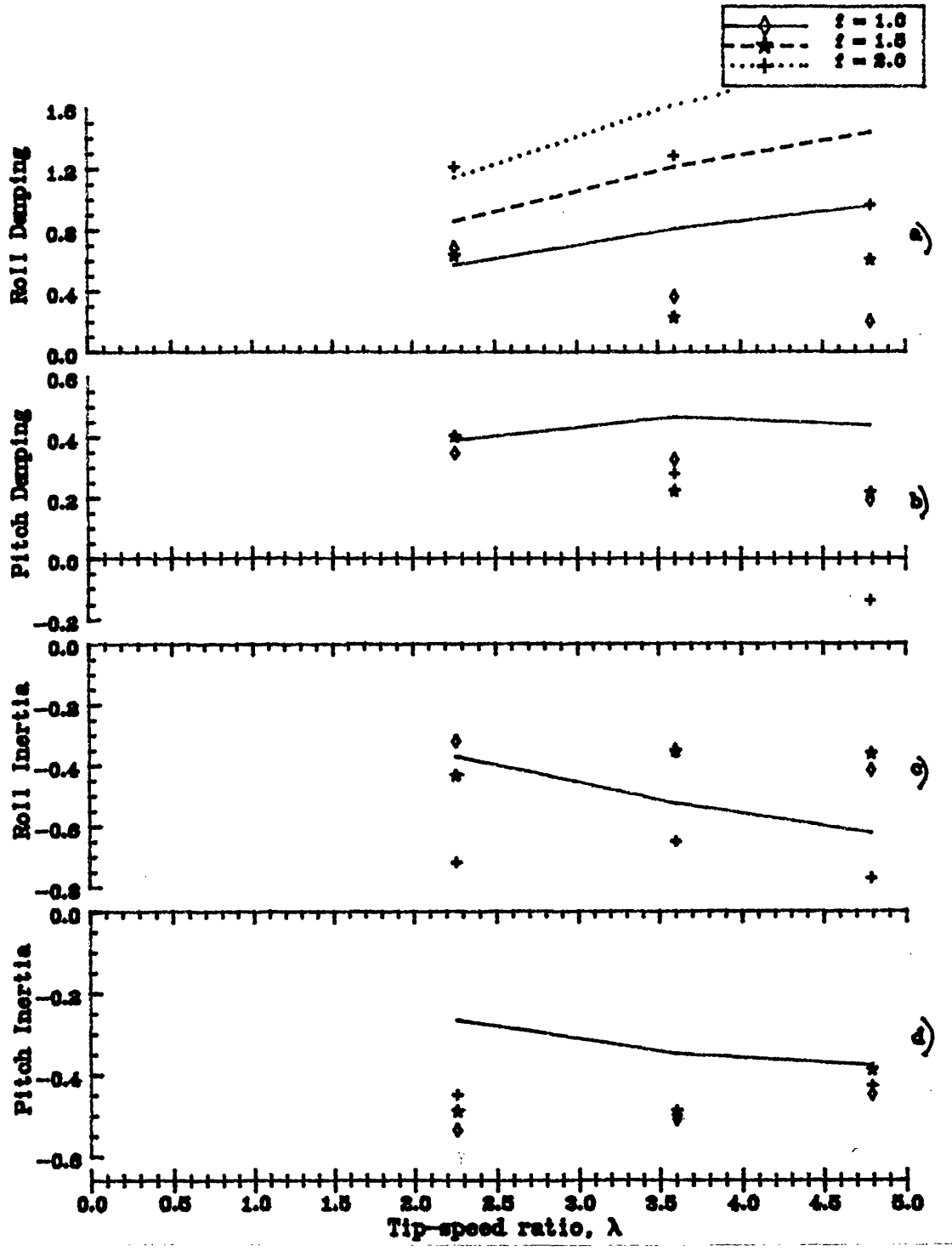

Fig. 103 Damping and inertia moments on a HAWT as functions of tip-speed ratio, λ
for wave angle, $\gamma = 15^{o}$, yaw angle $\delta = 0^{o}$
windspeed = 4.5 m/s and roll frequency f = 1, 1.5 and 2 Hz.

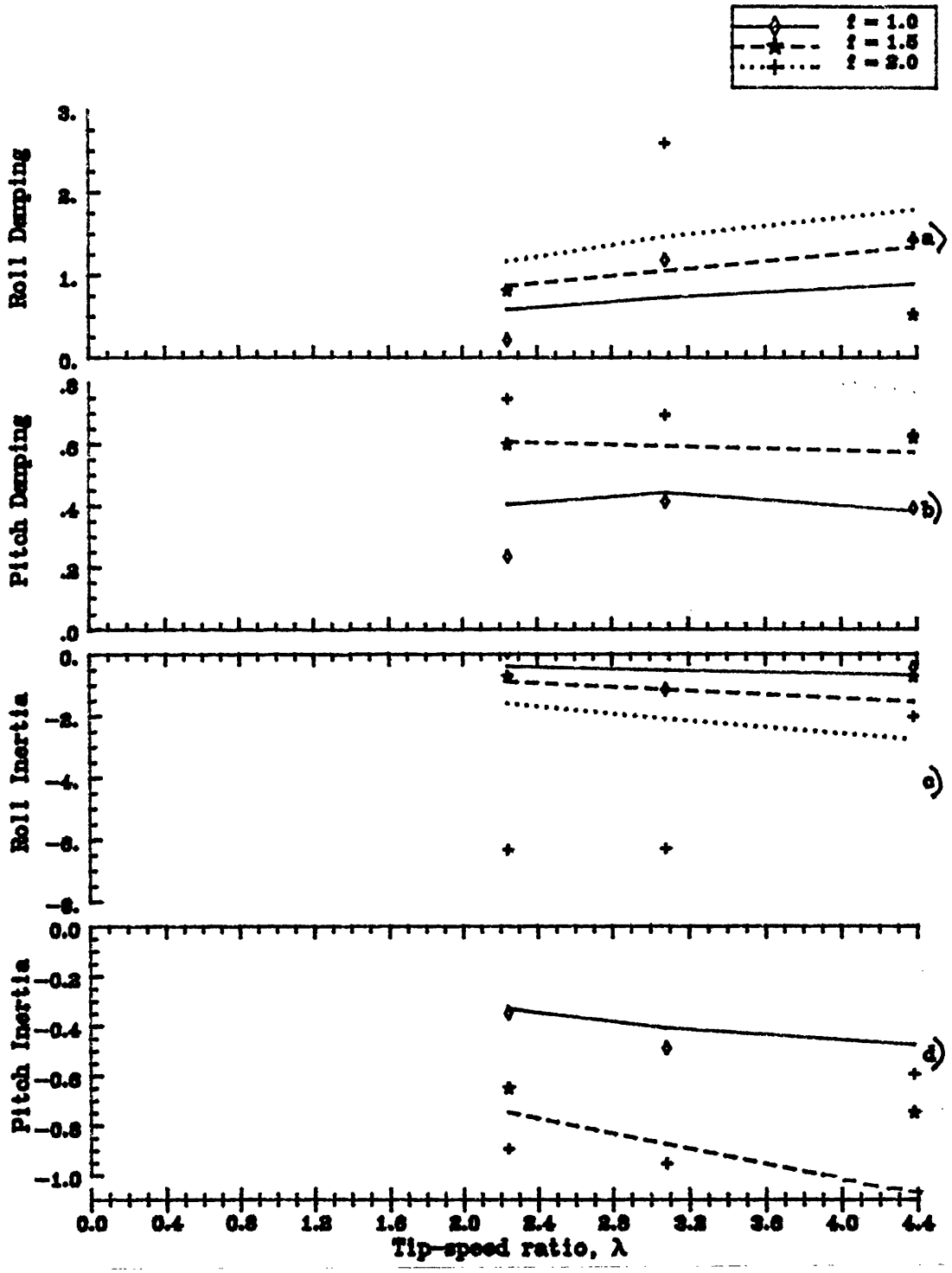

Fig. 104 Damping and inertia moments on a HAWT as functions of tip-speed ratio, λ for wave angle, $\gamma = 15^{o}$, yaw angle $\delta = 10^{o}$ windspeed = 4.5 m/s and roll frequency f = 1, 1.5 and 2 Hz.

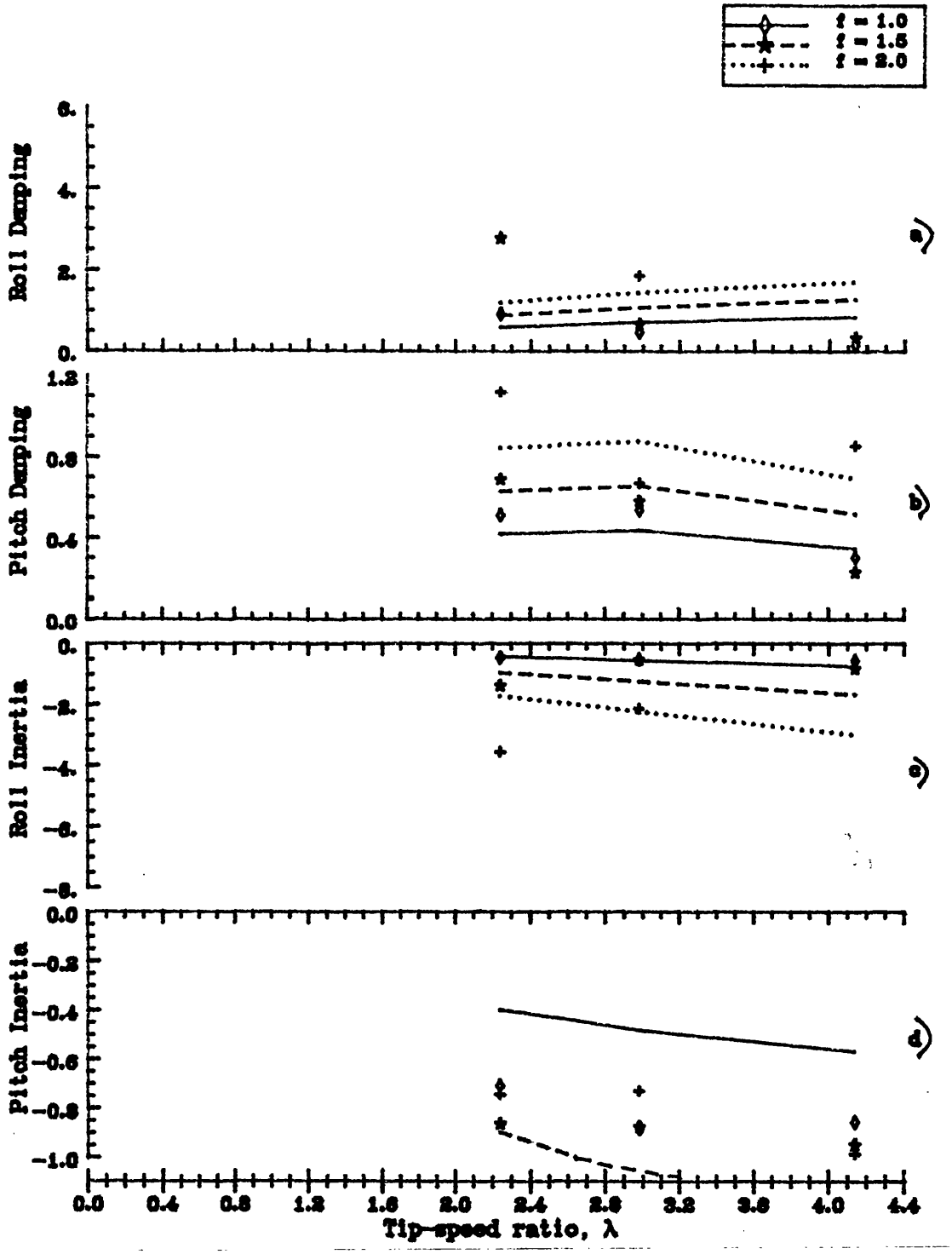

Fig. 105 Damping and inertia moments on a HAWT as functions of tip-speed ratio, λ
for wave angle, $\gamma = 15^o$, yaw angle $\delta = 20^o$
windspeed = 4.5 m/s and roll frequency f = 1, 1.5 and 2 Hz.

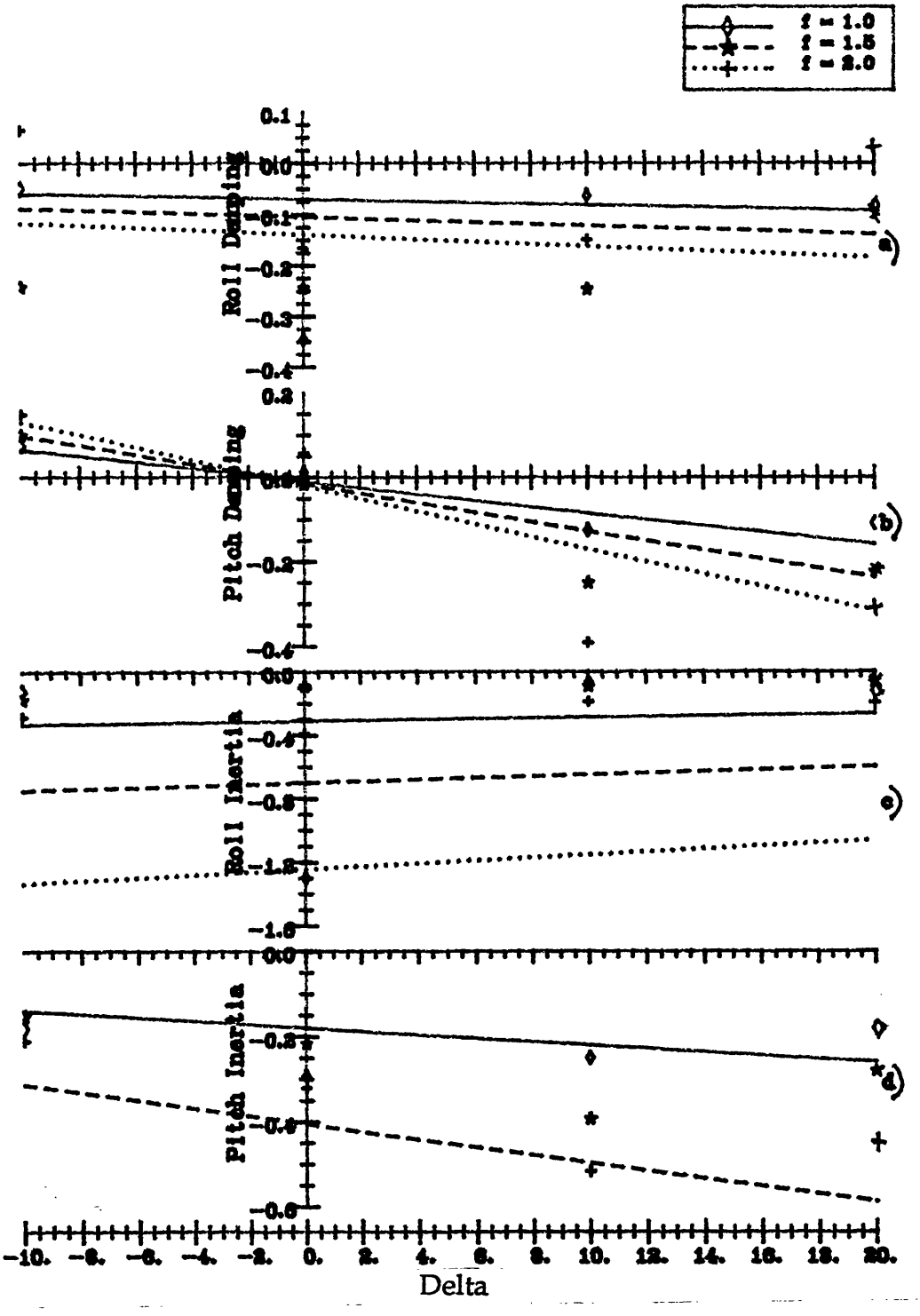

Fig. 106 Damping and inertia moments on a HAWT as functions of yaw angle, δ for wave angle $\gamma = 0$, blade pitch angle $\psi = 20^o$ windspeed = 9.3 m/s and roll frequency f = 1, 1.5 and 2 Hz.

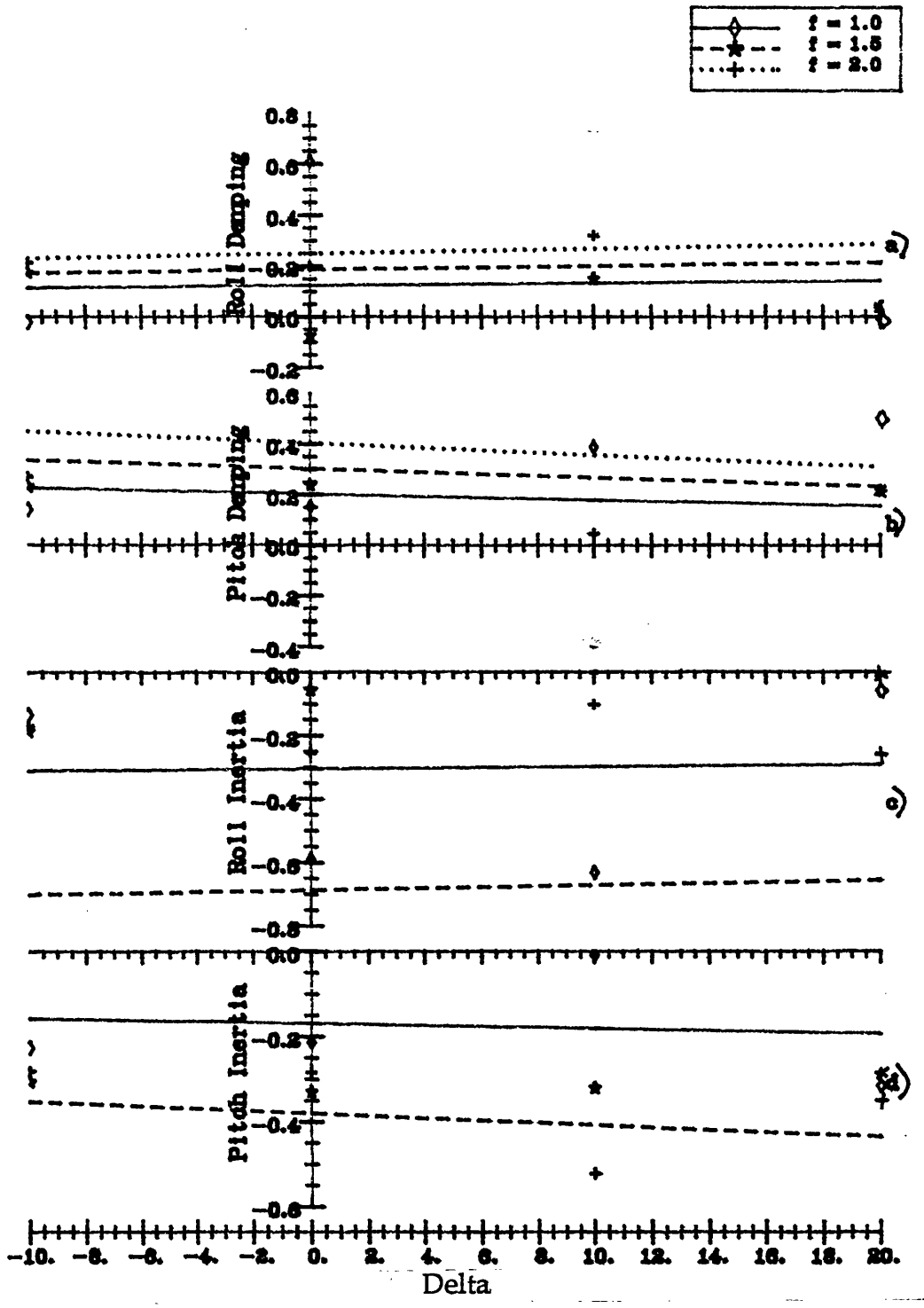

Fig. 107 Damping and inertia moments on a HAWT as functions of yaw angle, δ
for wave angle $\gamma = 0$, blade pitch angle $\psi = 30^{o}$
windspeed = 9.3 m/s and roll frequency f = 1, 1.5 and 2 Hz.

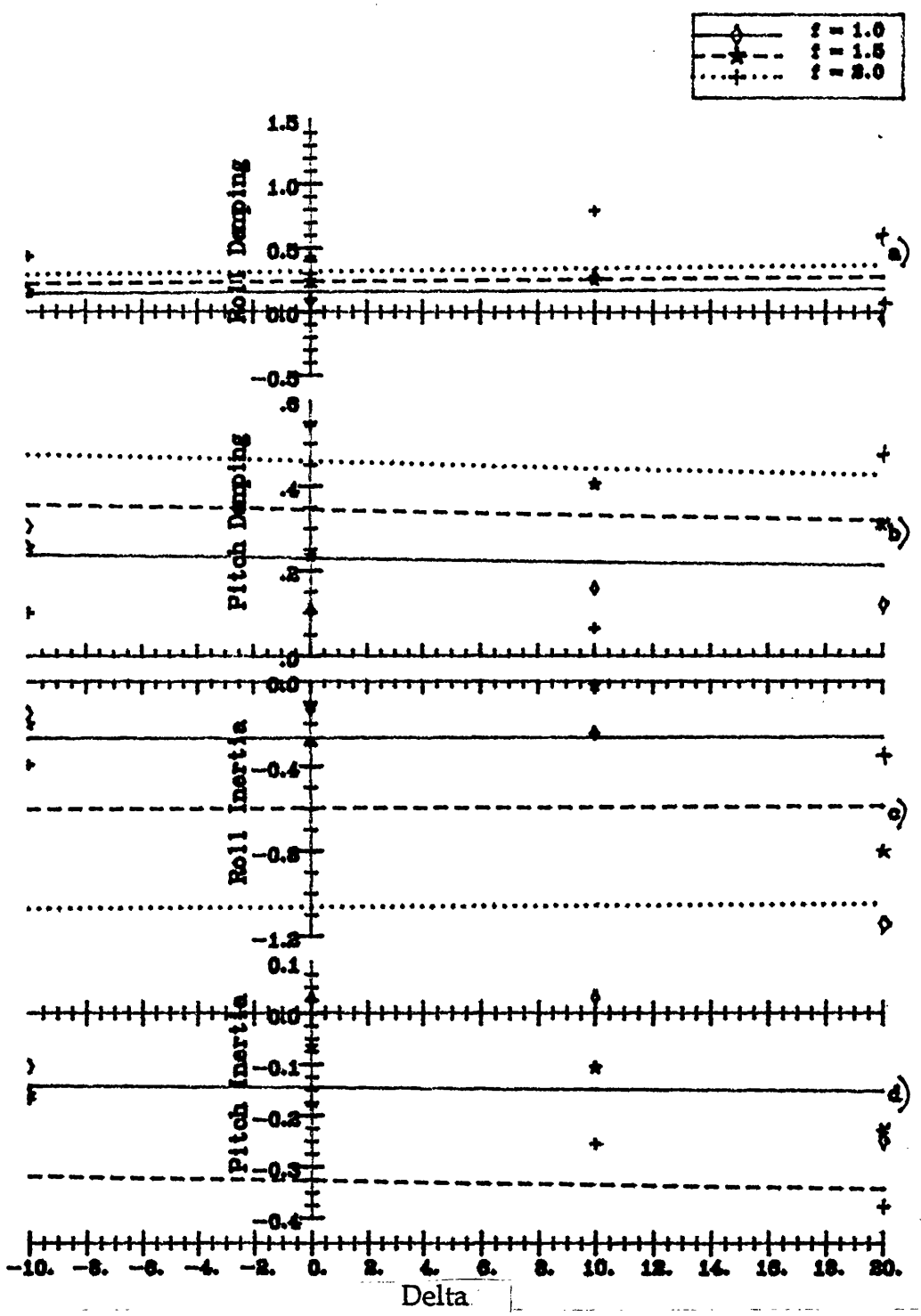

Fig. 108 Damping and inertia moments on a HAWT as functions of yaw angle, δ for wave angle $\gamma = 0$, blade pitch angle $\psi = 40^{o}$ windspeed = 9.3 m/s and roll frequency f = 1, 1.5 and 2 Hz.

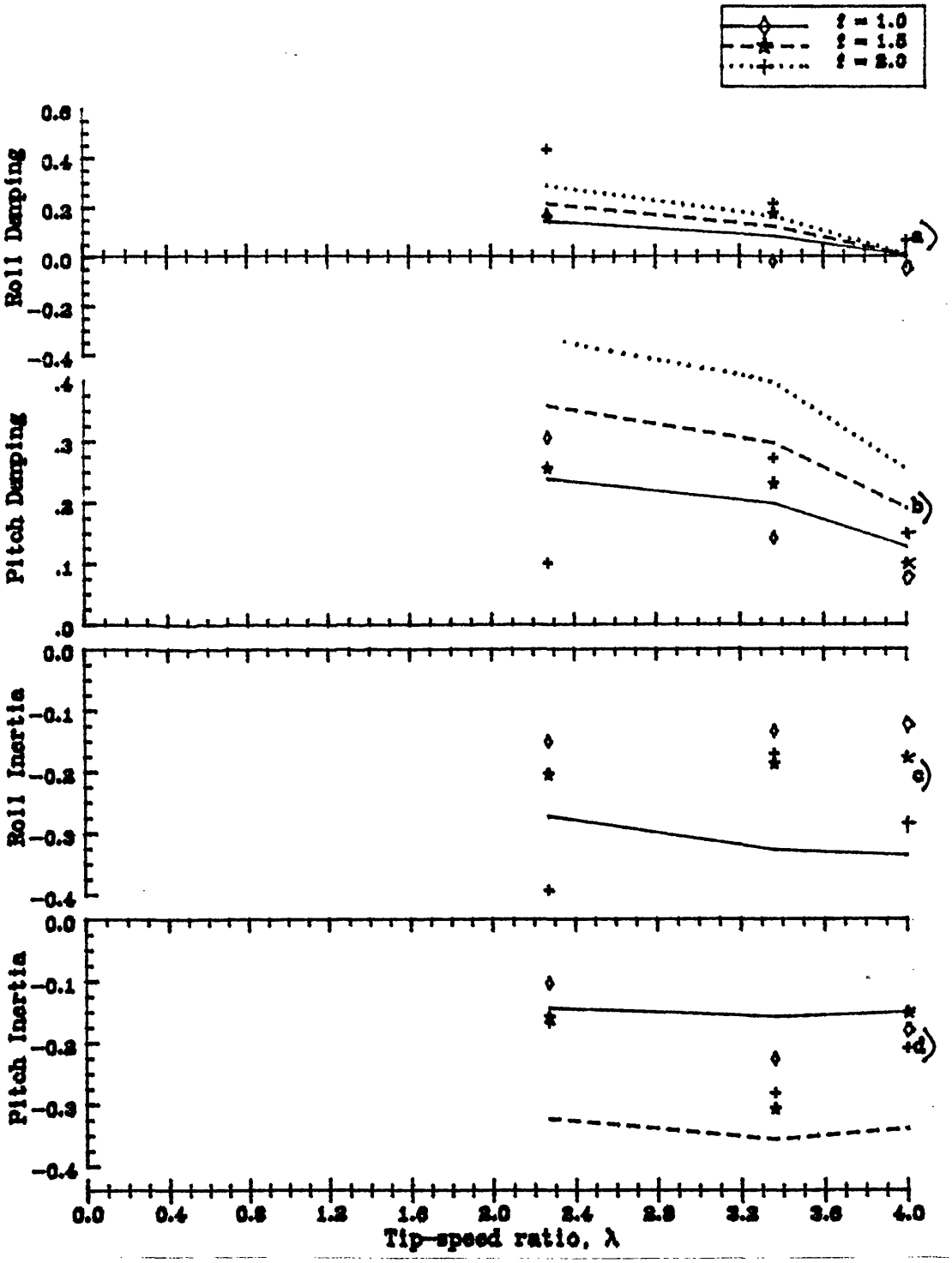

Fig. 109 Damping and inertia moments on a HAWT as functions of tip-speed ratio, λ for wave angle, $\gamma = 0$, yaw angle $\delta = -10^{o}$ windspeed = 9.3 m/s and roll frequency f = 1, 1.5 and 2 Hz.

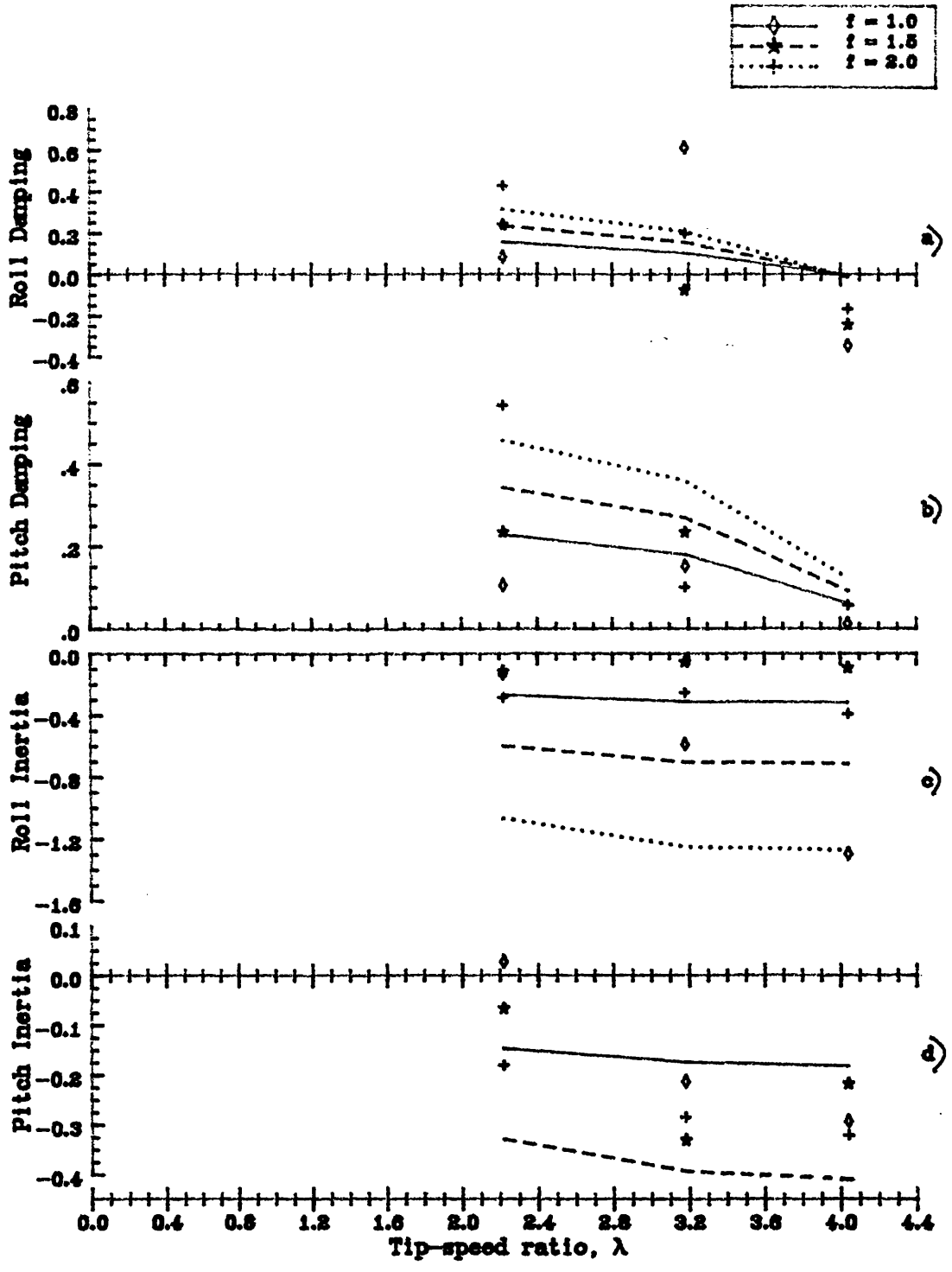

Fig. 110 Damping and inertia moments on a HAWT as functions of tip-speed ratio, λ for wave angle, $\gamma = 0$, yaw angle $\delta = 0^o$ windspeed = 9.3 m/s and roll frequency f = 1, 1.5 and 2 Hz.

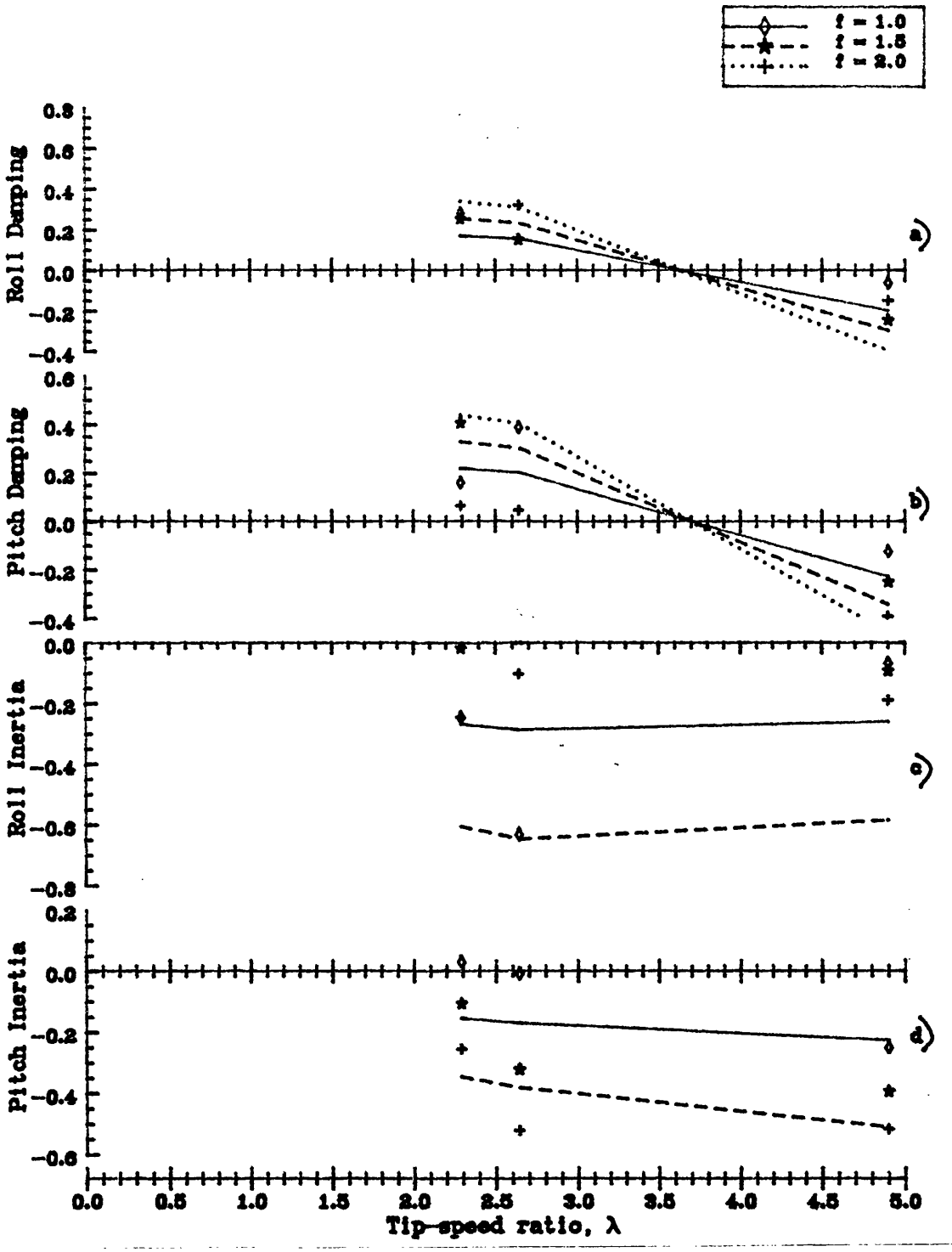

Fig. 111 Damping and inertia moments on a HAWT as functions of tip-speed ratio, λ for wave angle, $\gamma = 0$, yaw angle $\delta = 10^{o}$ windspeed = 9.3 m/s and roll frequency f = 1, 1.5 and 2 Hz.

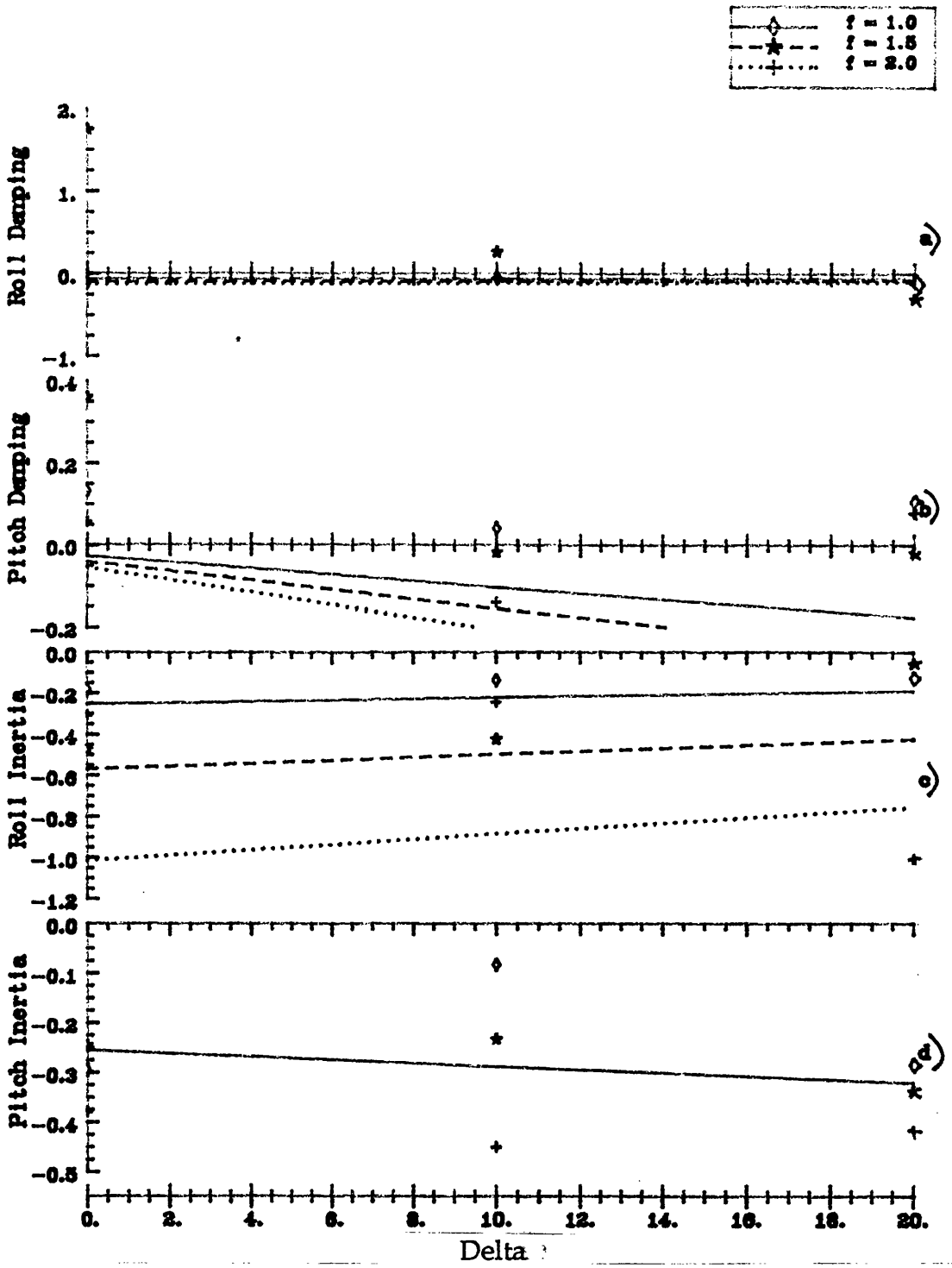

Fig. 112 Damping and inertia moments on a HAWT as functions of yaw angle, δ for wave angle $\gamma = 15^{o}$, blade pitch angle $\psi = 20^{o}$ windspeed = 9.3 m/s and roll frequency f = 1, 1.5 and 2 Hz.

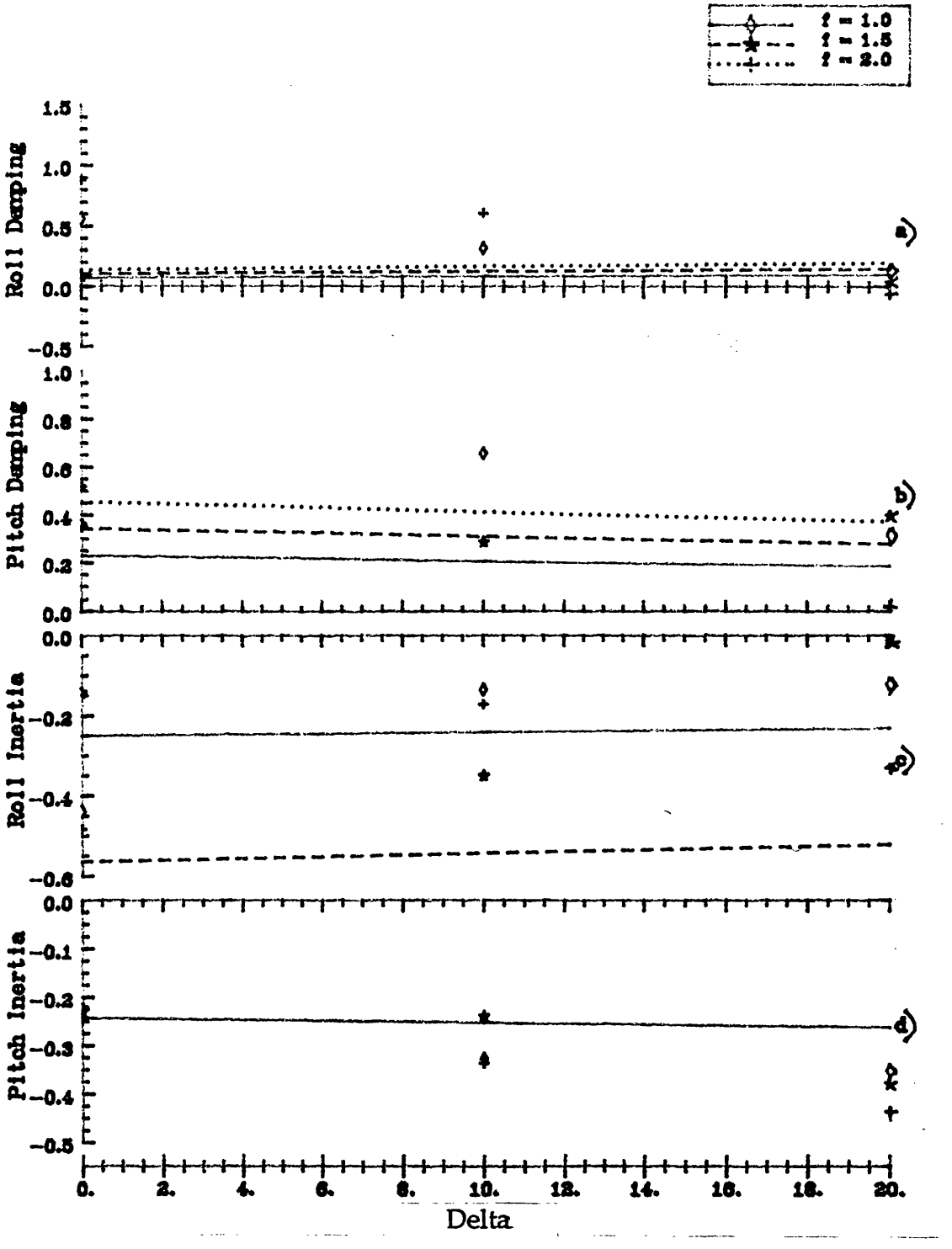

Fig. 113 Damping and inertia moments on a HAWT as functions of yaw angle, δ for wave angle $\gamma = 15^{o}$, blade pitch angle $\psi = 30^{o}$ windspeed = 9.3 m/s and roll frequency f = 1, 1.5 and 2 Hz.

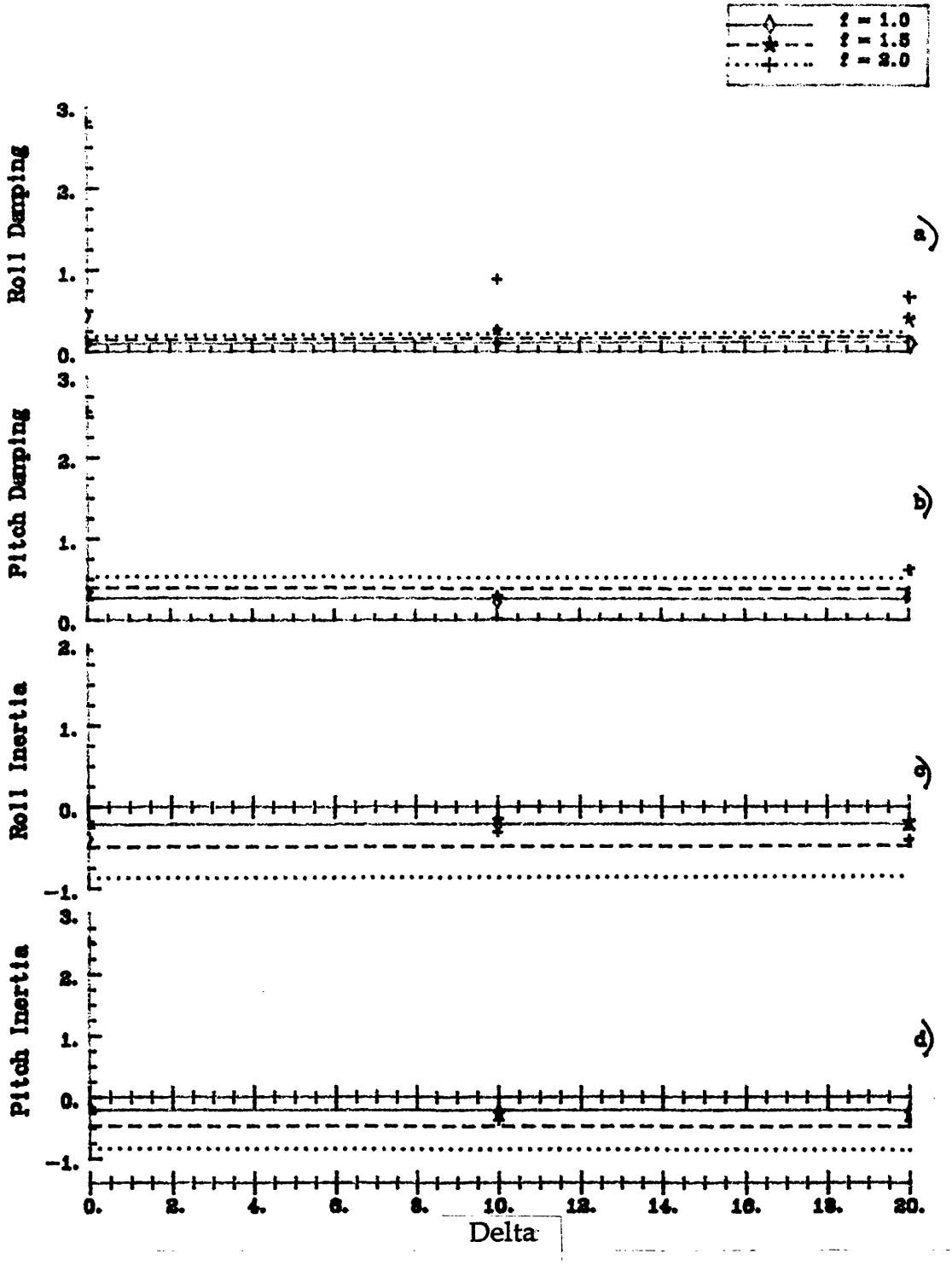

Fig. 114 Damping and inertia moments on a HAWT as functions of yaw angle, δ for wave angle $\gamma = 15^{o}$, blade pitch angle $\psi = 40^{o}$ windspeed = 9.3 m/s and roll frequency f = 1, 1.5 and 2 Hz.

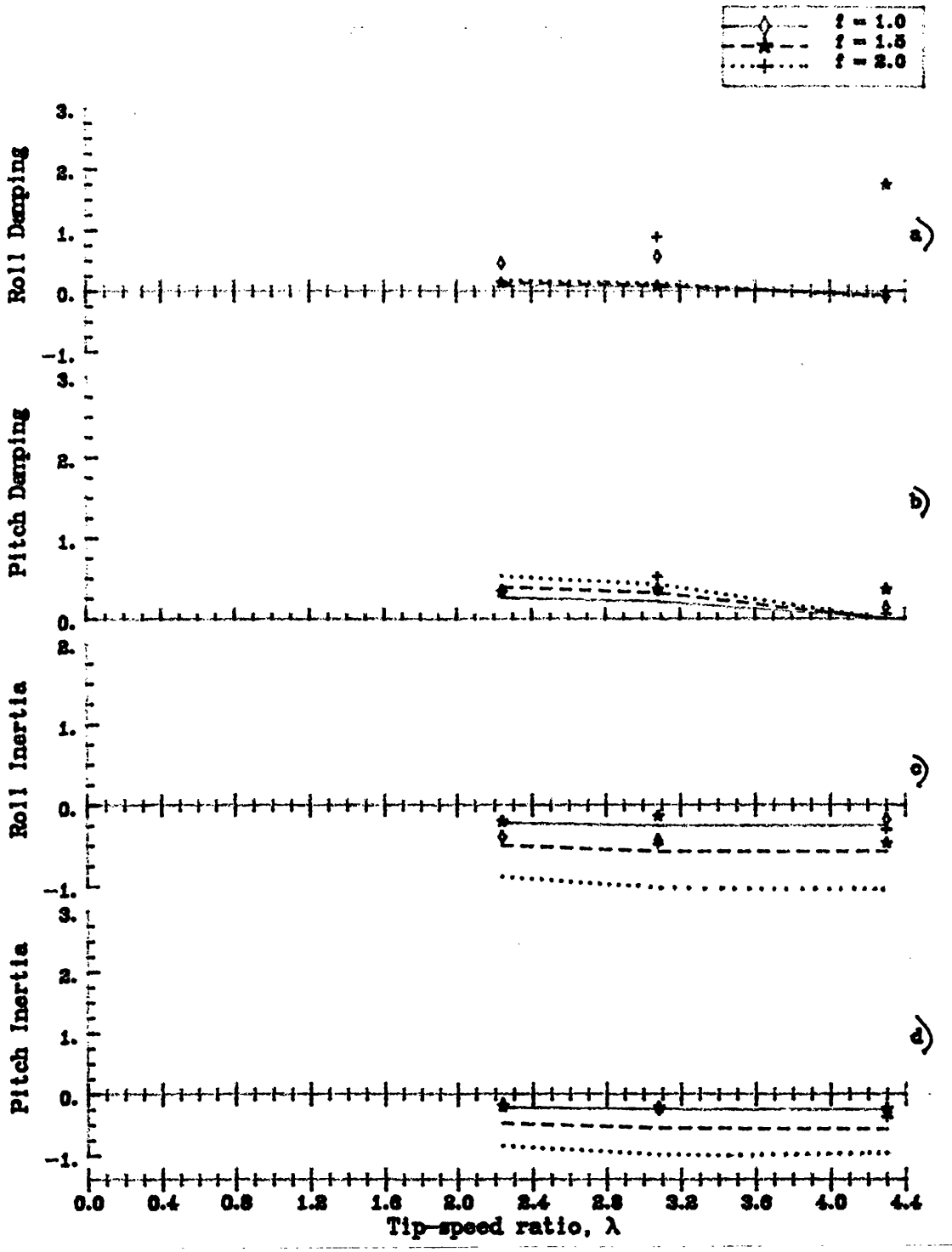

Fig. 115 Damping and inertia moments on a HAWT as functions of tip-speed ratio, λ
for wave angle, $\gamma = 15^{o}$, yaw angle $\delta = 0^{o}$
windspeed = 9.3 m/s and roll frequency f = 1, 1.5 and 2 Hz.

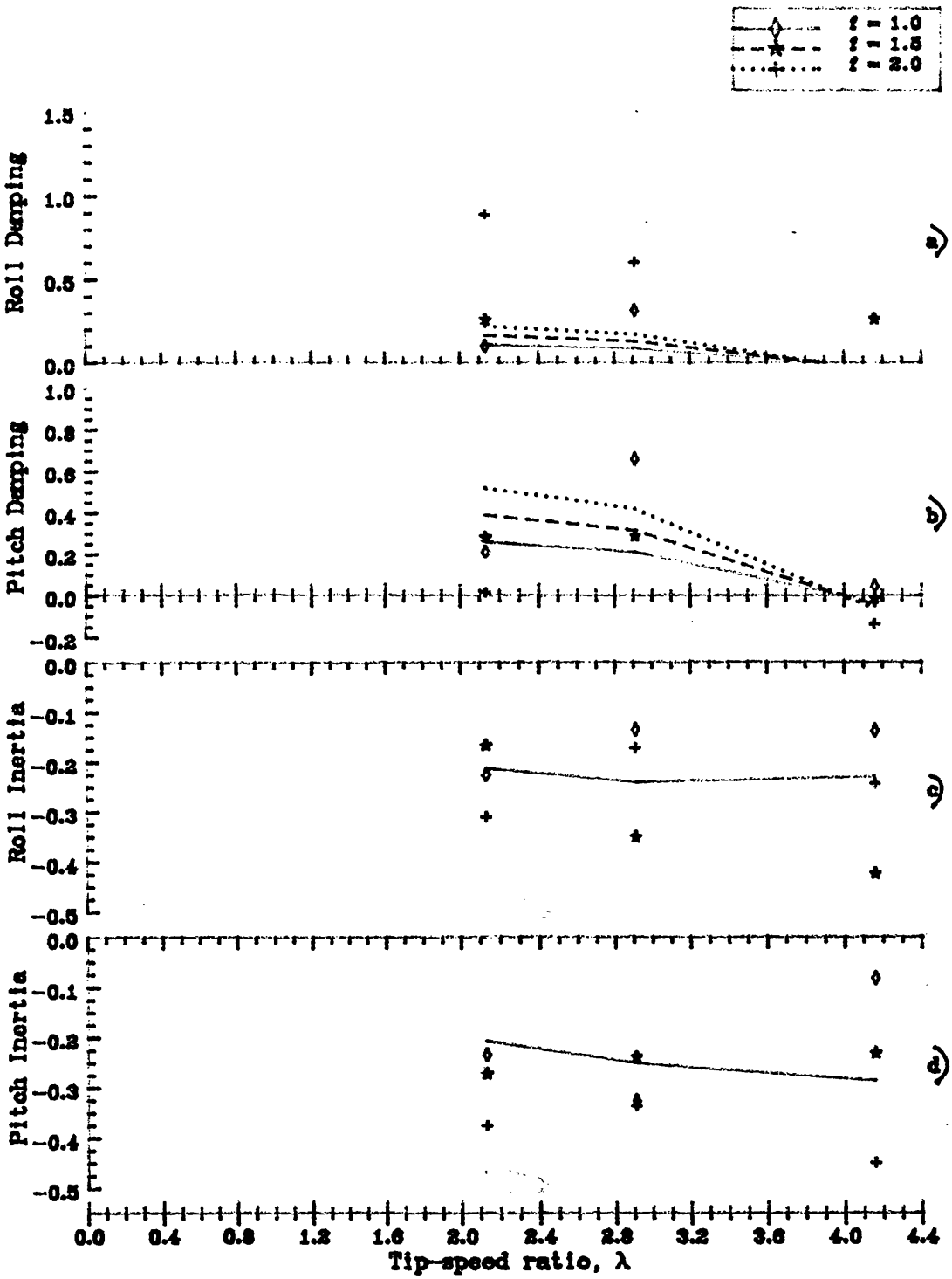

Fig. 116 Damping and inertia moments on a HAWT as functions of tip-speed ratio, λ for wave angle, $\gamma = 15^{o}$, yaw angle $\delta = 10^{o}$ windspeed = 9.3 m/s and roll frequency f = 1, 1.5 and 2 Hz.

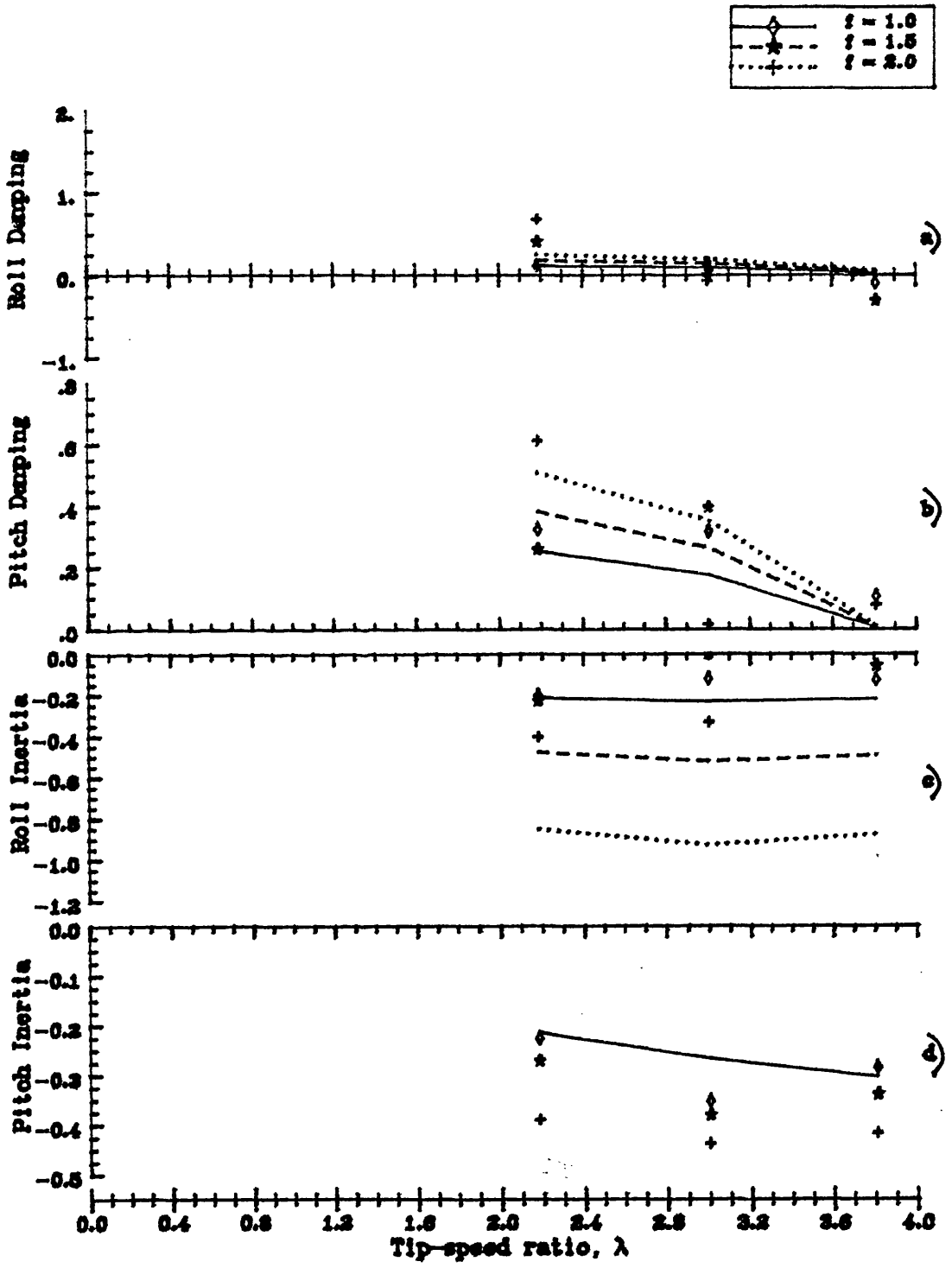

Fig. 117 Damping and inertia moments on a HAWT as functions of tip-speed ratio, λ for wave angle, $\gamma = 15^{o}$, yaw angle $\delta = 20^{o}$ windspeed = 9.3 m/s and roll frequency f = 1, 1.5 and 2 Hz.

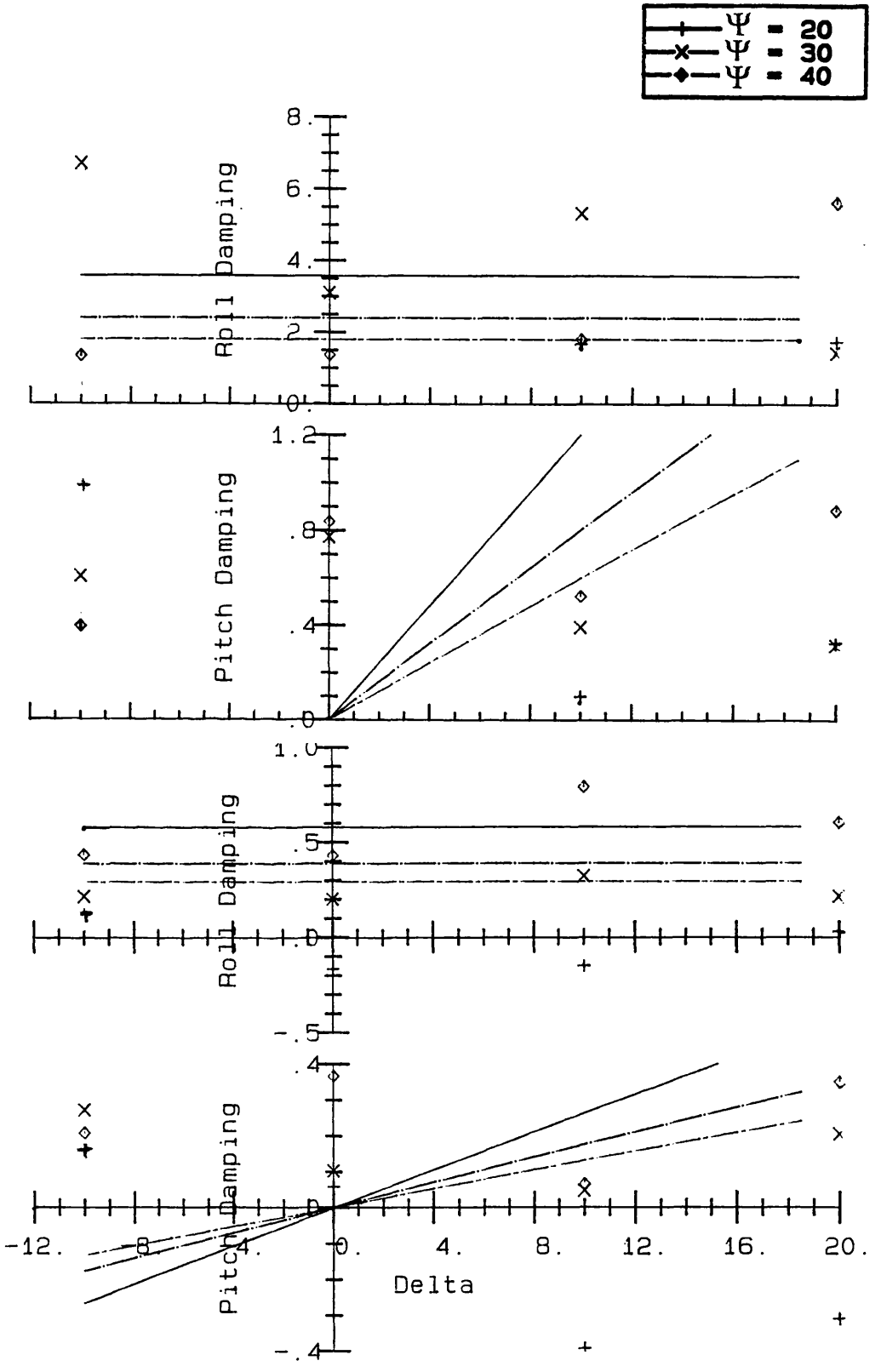

Figure 118 Roll and pitch damping coefficients as functions of yaw angle, δ for wave angle, $\gamma = 0$, windspeed = 4.5 m/s (above) and 9.3 m/s (below).

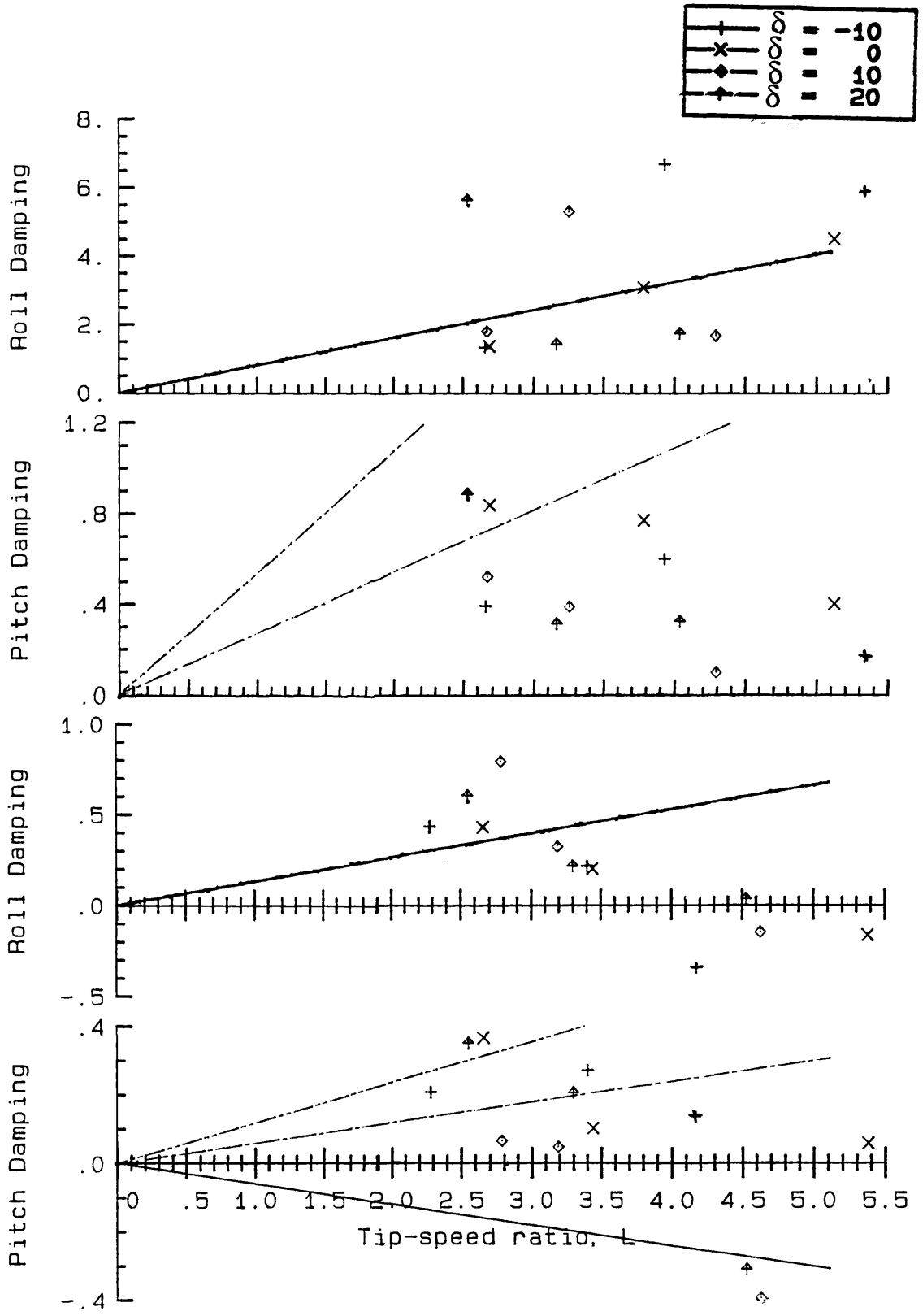

Figure 119 Roll and pitch damping coefficients as functions of tip speed ratio, λ for wave angle, $\gamma = 0$, windspeed = 4.5 m/s (above) and 9.3 m/s (below).

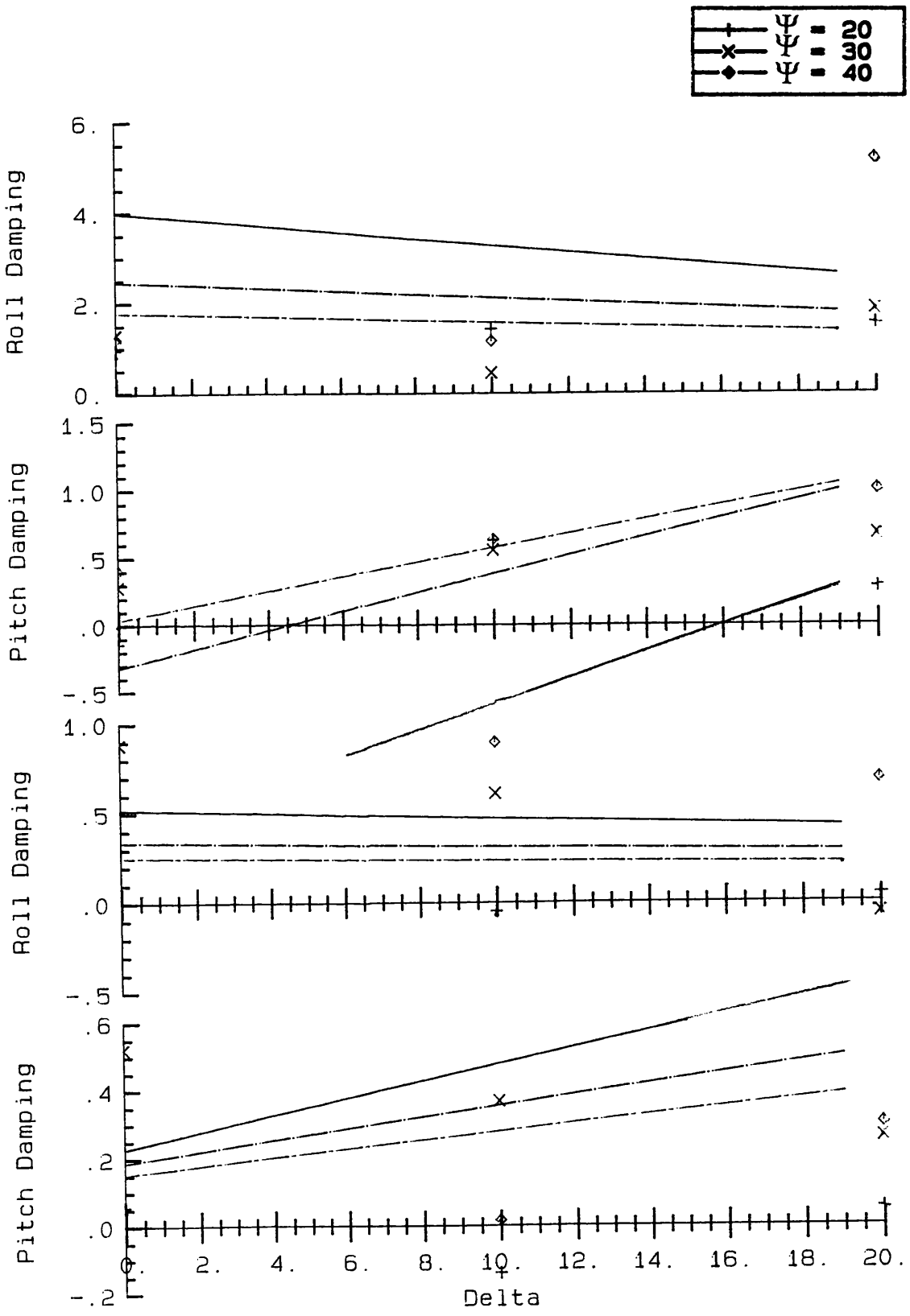

Figure 120 Roll and pitch damping coefficients as functions of yaw angle, δ for wave angle, $\gamma = 15^{o}$, windspeed = 4.5 m/s (above) and 9.3 m/s (below).

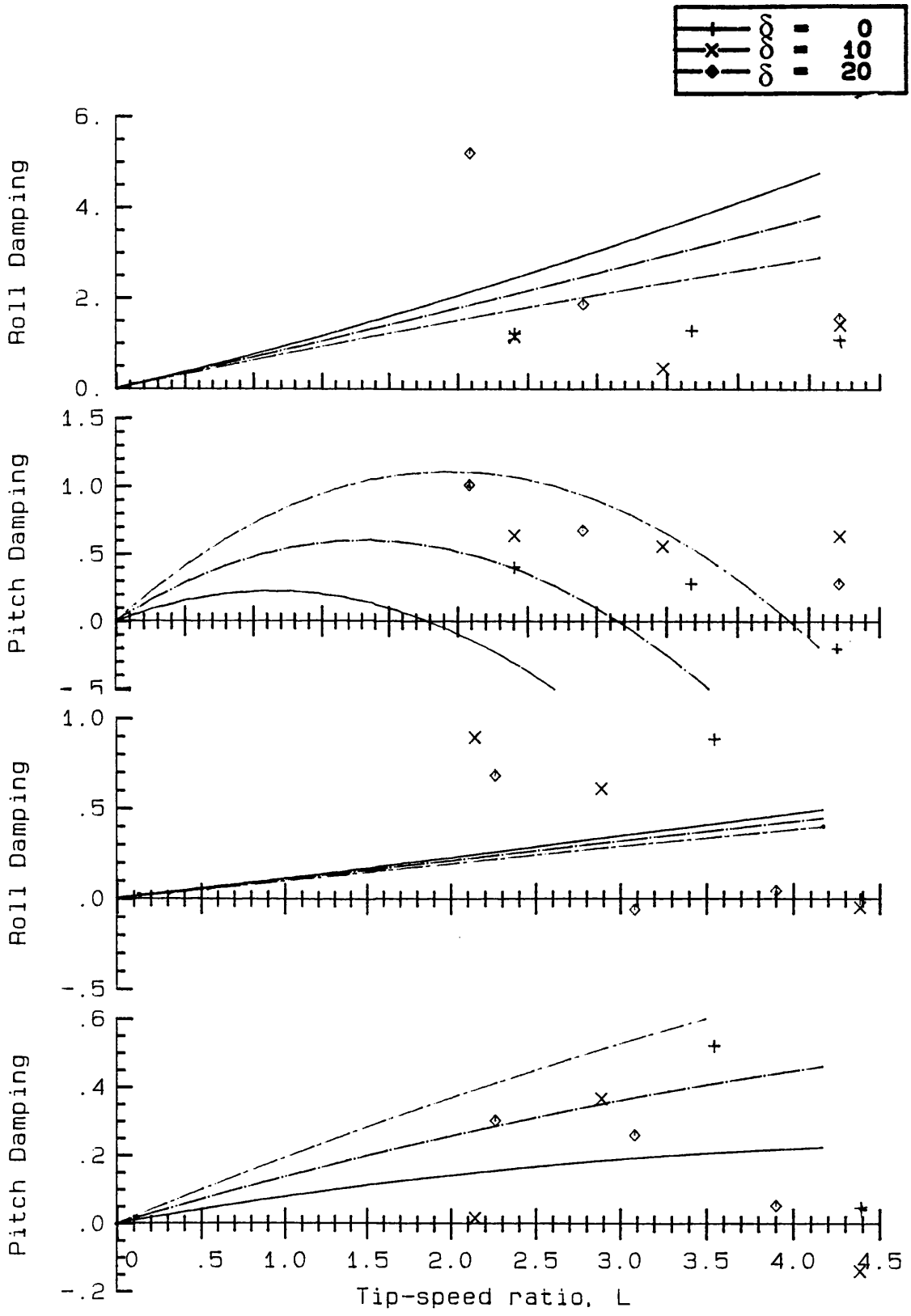

Figure 121 Roll and pitch damping coefficients as functions of tip speed ratio, λ for wave angle, $\gamma = 15^{o}$, windspeed = 4.5 m/s (above) and 9.3 m/s (below).

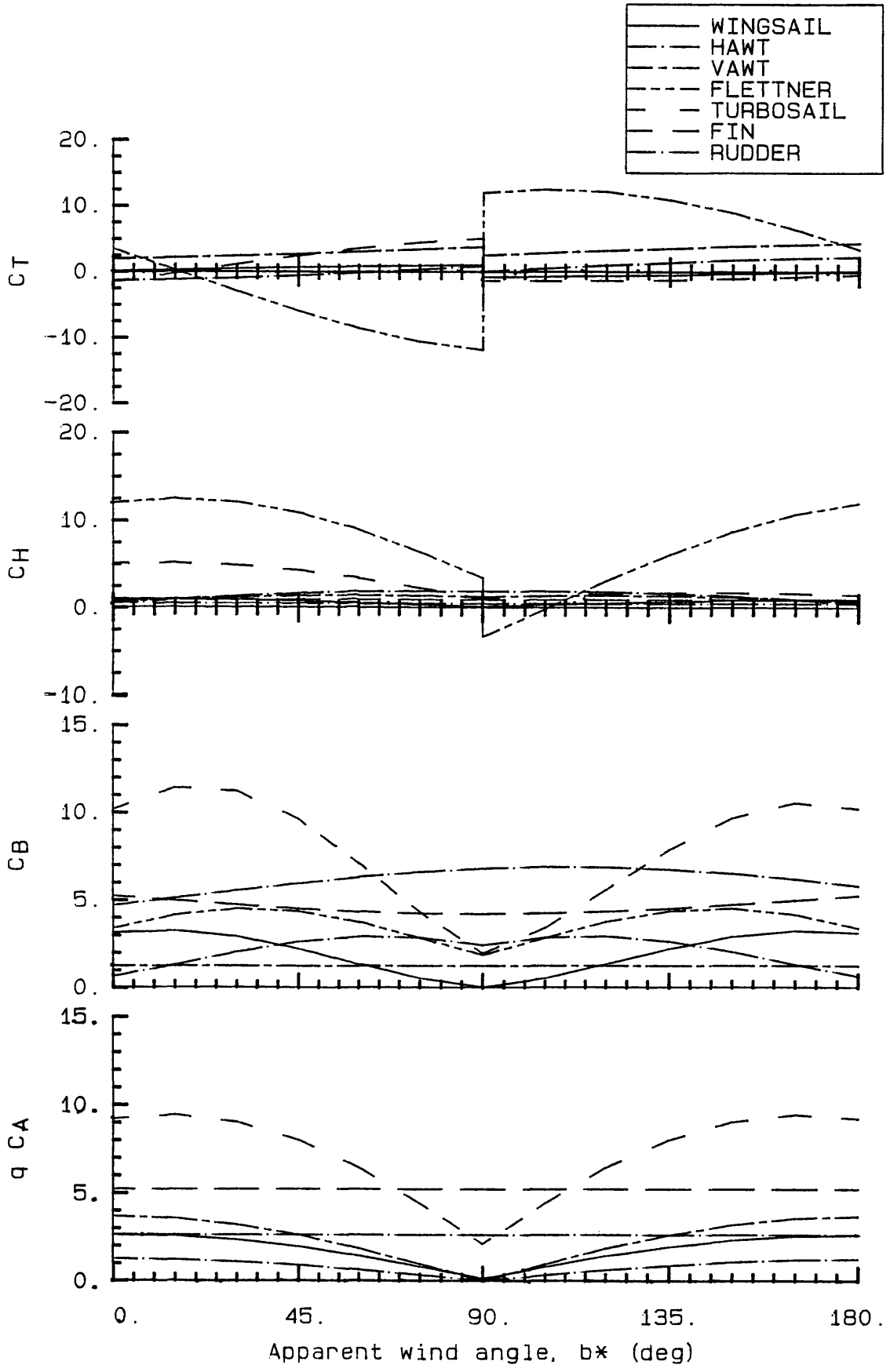

Figure 122 Variations of C_T, C_H, C_B and qC_A as functions of wind heading β^* for the seven devices.

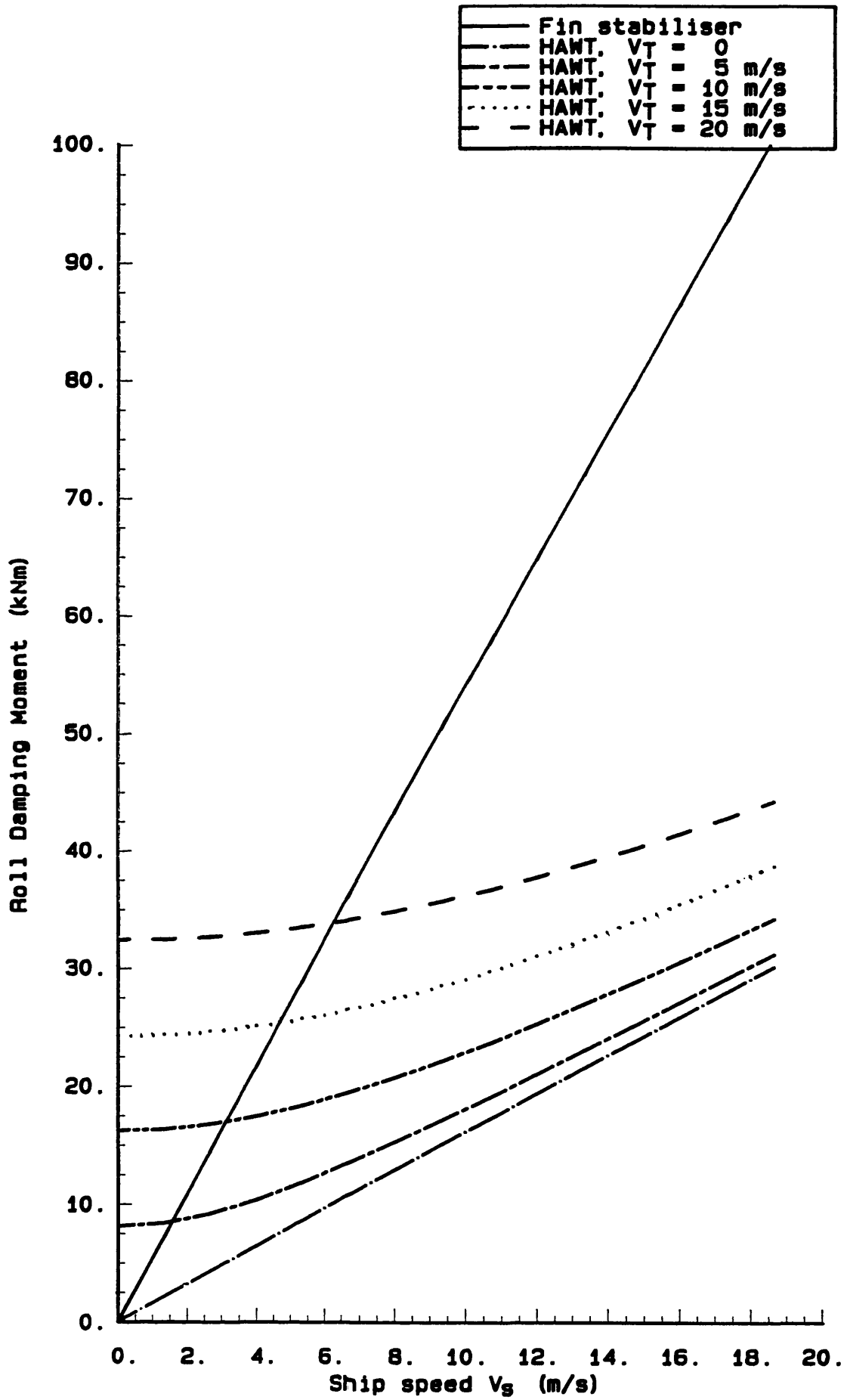

Figure 123 Comparison of the performances of a fin stabiliser and a HAWT at different ship and wind speeds.

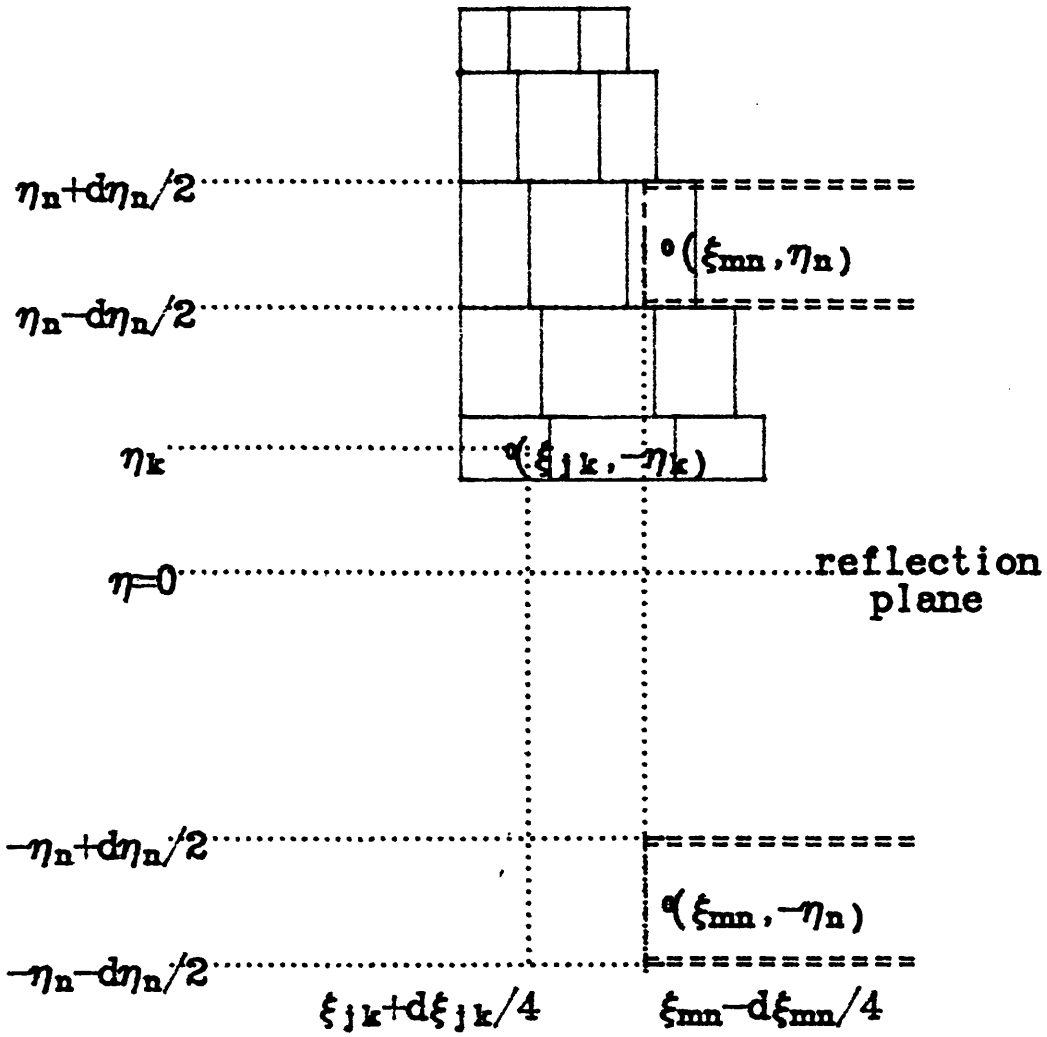

Figure 124 Coordinate system for vortex lattice calculation.

APPENDIX 1

Load Grading Integrals

The integrals required for the calculation of the aerodynamic derivatives are:

$$E_0 = (1/\hat{c})\,(s/h)^2 \int_r^{r+1} c\,C_{l0}(\eta)\eta^2 d\eta \qquad [A1.1]$$

$$E_1 = (1/\hat{c})\,(s/h)^2 \int_r^{r+1} c\,a(\eta)\,\eta^2 d\eta \qquad [A1.2]$$

$$E_2 = (1/\hat{c})\,(s/h)^2 \int_r^{r+1} c\,C_{d0}(\eta)\eta^2 d\eta \qquad [A1.3]$$

$$E_3 = (1/\hat{c})\,(s/h)^2 \int_r^{r+1} c\,A(\eta)\,\eta^2 d\eta \qquad [A1.4]$$

$$E_4 = (s / h\hat{c}^2) \int_r^{r+1} c^2 C_{m0}(\eta)\eta\, d\eta \qquad [A1.5]$$

$$E_5 = (s / h\hat{c}^2) \int_r^{r+1} c^2\, a(\eta)\,(\zeta - \chi)\,\eta\, d\eta \qquad [A1.6]$$

$$E_6 = (s / h\hat{c}^2) \int_r^{r+1} c^2\, C_{d0}\,(\zeta - \chi)\,\eta\, d\eta \qquad [A1.7]$$

$$E_7 = (s / h\hat{c}^2) \int_r^{r+1} c^2\, A(\eta)\,(\zeta - \chi)\,\eta\, d\eta \qquad [A1.8]$$

Note that h is the lever arm of the steady roll moment, not of the roll damping moment, i.e.

$h = s(r + 0.5)$

Apart from E_4 and E_5 which may be negative or positive, the remaining integrals are all positive.

For aerofoil sections (for which $E_0 = 0$), the integrals were calculated using quasistatic lifting surface theory by dividing the aerofoil plane into N_η (spanwise) and N_ξ (chordwise) elements (see Fig. 124). Defining $\Theta_\eta = \pi/(N_\eta + 1)$, the kth spanwise element has thickness

$$d\eta_k = (1 - \cos\Theta_\eta)\sin k\Theta_\eta / \sin\Theta_\eta \qquad [A1.9]$$

and is centred at

$$\eta_k = r + 0.5\,(1 - \cos k\Theta_\eta). \qquad [A1.10]$$

For straight-edged planforms of taper t, where $t = c\,(1 + r)/c(r)$

$$c(\eta_k) = c_k = 2c[1 - (\eta_k - r)(1 - t)] / (1 + t) \qquad [A1.11]$$

and for elliptic planforms,

$$c_k = (4c/\pi)\sqrt{1 - (\eta_k - r)^2}. \qquad [A1.12]$$

Chordwise elements are positioned similarly,

i.e. defining $\Theta_\xi = \pi/(N_\xi + 1)$, the jth chordwise element has thickness

$$d\xi_{jk} = c_k\,(1 - \cos\Theta_\xi)\sin j\Theta_\xi / \sin\Theta_\xi \qquad [A1.13]$$

and is centred at

$$x_{jk} = 0.5\,c_k\,(1 - \cos j\Theta_\xi) - \zeta(\eta_k). \qquad [A1.14]$$

Using Falkner's (1947) Vortex lattice method, the circulation of each element (m, n) is represented by a horseshoe vortex, with its spanwise arm along $\xi = \xi_{mn} - d\xi_{mn}/4$ and its chordwise arms stretching to infinity along $\eta = \eta_n + d\eta_n/2$, as shown in Fig. 124.

The normal velocity increment at $(\xi_{jk} + d\xi_{jk}/4, \eta_k)$ due to unit load γ_{mn} on element (m, n) and its image reflected in a plane at $\eta = 0$ is given by $dv_{jk} = C_{jkmn}\,\gamma_{mn}$

where

$$C_{jkmn} = \frac{1}{4\pi}\left\{\Sigma_i\left(\int_0^{\infty}\frac{\eta_{kn(i)}\,d\xi}{[(\xi+\xi_{jkmn})^2+\eta_{kn(i)}^2]^{3/2}}\right) - \int_{-\eta_{kn(2)}}^{\eta_{kn(1)}}\frac{\xi_{jkmn}\,d\eta}{[\xi_{jkmn}^2+\eta^2]^{3/2}} + \int_{\eta_{kn(4)}}^{-\eta_{kn(3)}}\frac{\xi_{jkmn}\,d\eta}{[\xi_{jkmn}^2+\eta^2]^{3/2}}\right\}$$

$$= \frac{1}{4\pi}\Sigma_i\left\{\frac{1}{\eta_{kn(i)}}\left(1 - \frac{\xi_{jkmn}}{R_{jkmn(i)}}\right) - \frac{\eta_{kn(i)}}{\xi_{jkmn}\,R_{jkmn(i)}}\right\}. \qquad [A1.15]$$

where

$\eta_{kn(1)} = \eta_n + d\eta_n/2 - \eta_k$ [A1.16a]

$\eta_{kn(2)} = -\eta_n + d\eta_n/2 + \eta_k$ [A1.16b]

$\eta_{kn(3)} = \eta_n - d\eta_n/2 + \eta_k$ [A1.16c]

$\eta_{kn(4)} = -\eta_n - d\eta_n/2 - \eta_k$ [A1.16d]

$\xi_{jkmn} = \xi_{mn} - d\xi_{mn}/4 - \xi_{jk} - d\xi_{jk}/4$ [A1.16e]

$R_{jkmn(i)} = \sqrt{\xi_{jkmn}^2 + \eta_{kn(i)}^2}$. [A1.16f]

Therefore total normal velocity at element (j, k) due to circulation distribution γ, over the aerofoil surface is given by

$v_{jk} = \Sigma\, C_{jkmn}\,\gamma_{mn}$. [A1.17]

Inversion of the matrix C gives the influence coefficient matrix $G = C^{-1}$. As the normal velocity distribution vmn is known for each element, the corresponding load on element (j, k) is given by

$\gamma_{jk} = \Sigma\, G_{jkmn}\, v_{mn}$. [A1.18]

The section circulation at spanwise station k is given by

$\Gamma_k = \Sigma\,\gamma_{jk}$. [A1.19]

The section yawing moment is given by

$\Psi_k = \Sigma\,\gamma_{jk}\,\xi_{jk}$. [A1.20]

We may now write

$a_k = a(\eta_k) = 2\Gamma_k/c_k$ [A1.21]

$(a\chi)_k = 2\Psi_k/c_k$ [A1.22]

$A_k = A(\eta_k) = a_k(1 - a_k/a_\infty)$ [A1.23]

where a_∞ is the sectional lift curve slope.

And putting $C_{l0}(\eta_k) = C_{l0k}$ etc., the integrals are then formed by summation, i.e.

$E_0 = \{\Sigma\, c_k\, C_{l0k}\, h_k^2\, d\eta_k\} / \hat{c}\,(r + 0.5)^2$ [A1.24]

$E_1 = \{\Sigma\, c_k\, a_k\, \eta_k^2\, d\eta_k\} / \hat{c}\,(r + 0.5)^2$ [A1.25]

$E_2 = \{\Sigma\, c_k\, C_{d0k}\, \eta_k^2\, d\eta_k\} / \hat{c}\,(r + 0.5)^2$ [A1.26]

$$E_3 = \{ \Sigma c_k \, A_k \, \eta_k^2 \, d\eta_k \} / \hat{c} \, (r + 0.5)^2 \qquad [A1.27]$$

$$E_4 = \{ \Sigma c_k^2 C_{m0k} \, \eta_k \, d\eta_k \} / \hat{c}^2 (r + 0.5) \qquad [A1.28]$$

$$E_5 = \{ \Sigma c_k^2 (a\chi)_k \eta_k \, d\eta_k \} / \hat{c}^2 (r + 0.5) \qquad [A1.29]$$

$$E_6 = \{ \Sigma c_k^2 \, (C_{d0}\chi)_k \, \eta_k \, d\eta_k \} / \hat{c}^2 (r + 0.5) \qquad [A1.30]$$

$$E_7 = \{ \Sigma c_k^2 \, (A\chi)_k \, \eta_k \, d\eta_k \} / \hat{c}^2 (r + 0.5) \qquad [A1.31]$$

For thin symmetric aerofoil sections, Abbot and von Doenhoff (1949) give

$a_\infty = 5.7$, $C_{l0} = 0.0$, $C_{d0} = 0.006$, $C_{m0} = 0.0$

which are functions of aspect ratio (AR), taper(t) and gap ratio (r).

For representative values, i.e. t = 1 and r = 0.2, values are approximately given by:

$E_0 = 0.0$

$E_1 = 2 \, (AR)^{0.6}$

$E_2 = 0.006$

$E_3 = 0.6(AR)^{-1.2} = 2.4 / E_1^2$

$E_4 = 0.0$

E_5 , E_6 and E_7 are more complicated functions of AR.

APPENDIX 2.

Equipment.

[1] Wind Tunnel.

The construction and calibration of the U.C.L. open jet wind tunnel is described by Clayton and Filby (1981). It produces a flow of speed 13 m/s at an open jet of 1 square metre area, which is uniform over the middle 80% of the jet at a turbulence level of 5%.

[2] Motor.

3 - phase, 1.5 hp motor supplied by U.S. Electrical Motors.
Unimount 125 enclosed high-efficiency motor module, model no. E188
Synchrogear module

[3] Force Balance.

A six-component strain-gauged dynamometer capable of following unsteady flow was designed and built by Maywood Instruments Ltd.
It contains 32 strain gauges and 12 resistors, wired into 6 Wheatstone bridges as shown in Fig. 45. Using 10 V input, the maximum output is 2mV per V = 20 mV. Therefore, amplification x 1000 was required to give full deflection on the datalogger. High forces are measured accurately, but for low forces the readings are unreliable, even for steady forces, as the signal to noise ratio of the combined equipment is not good. It was isolated electrically from the motor by a rubber bush at the connection to the scotch yoke. The connections at the linear bearing and spherical bearing do not involve metal contact.
Weight of balance = 1.6 kg.

[4] Amplifiers.

Six precision instrumentation strain-gauge amplifiers supplied by RS Components Ltd.
Serial no. RS - AD 524 AD. Stock no. 302-463.
Guaranteed offset voltage and offset voltage drift, low noise and high linearity.
Input offset voltage = 250 μV.
Output rating = ± 10 V at 5 mA.
Power supply = 15V d.c.
The amplifiers and filters were originally mounted on the balance, but the electromagnetic field of the motor caused so much noise and disturbance that they were dismounted again and connected at the other end of the cable, next to the datalogger, to remove the interference from the electric and magnetic fields of the motor.

[5] Filters.

Six low-pass filters supplied by Radio Spares

Serial no. P645 - UA 741 CP

[6] Datalogger.

PCI Series 80 datalogger supplied by CIL Microsystems.

Model no. PCI 1281, device no. 1248.

16 channel A/D converter, input ±10V.

The resolution of the datalogger is high, as the input range of ± 10 V is represented as ± 32000 units, but it has inherent noise.

[7] Computer.

Hewlett-Packard Series 80 personal computer.

HP86/B microcomputer.

[8] Linear Bearing.

A precision 'frictionless' linear bearing was supplied by Unimatic Engineers Ltd.

Maximum recommended linear speed = 5 m/s

Maximum recommended accelleration = 50 m/s^2.

Total weight of moving parts = 0.8 kg.

[9] Rev counter.

To measure frequency and phase accurately.

Power supply = 5V d.c.

[10] Supply.

D.C. constant voltage supplied by Weir Instruments Ltd. Model number 413 D.

Software

The following programs were written in Basic to run on the H.P. computer.

1) Program to read data from the datalogger for aerofoil tests.

```
10 !  PROGRAM LOG
20 !  This program reads data from datalogger for aerofoils.
30 !  Fiona Sinclair July 1987 and Jan 1989
40    DIM A$[99],B$[10],LM$(4)[2],FILNAM$[20],TITLE$[99],DAT$[8]
50    DIM A(4),ICHAN(4),Z(4),RAW(4,1000)
60 START: OFF KEY# @ CLEAR @ GCLEAR @ DISP "Program LOG" @ PRINTER IS 1
70    LM$(0)="FX" @ LM$(1)="FY" @ LM$(2)="FZ" @ LM$(3)="MZ" @ LM$(4)="RC"
80    NCHAN=4 @ DISP "Enter date";@ INPUT DAT$
90    FOR I=0 TO NCHAN @ ICHAN(I)=I+3 @ NEXT I
100   A$[1,12]="A,PA6144,GO," @ LA=12 @ ! Set command strings for datalogger
110   FOR I=0 TO NCHAN @ A$[LA+1,LA+3]="I"&VAL$ (ICHAN(I))&"," @ LA=LA+3
120   NEXT I @ A$[LA+1,LA+19]="QS10,QD30,F0,IC2,QE" @ B$="PA6144,QI"
130   FOR I=0 TO NCHAN @ Z(I)=0 @ NEXT I ! ************************************
140   DISP "Press CONT to begin initialising" @ PAUSE ! 809 = Datalogger
150   OUTPUT 809 ;A$ @ SEND 8 ; UNL @ RESUME 8 @ WAIT 1200
160   OUTPUT 809 ;B$ @ SEND 8 ; UNL @ RESUME 8
170   FOR J=0 TO 9 @ ENTER 809 ; A(0),A(1),A(2),A(3),A(4)
180   FOR I=0 TO NCHAN @ Z(I)=Z(I)+A(I) @ NEXT I
190   DISP USING "D,4X,5(M6D)" ; J,A(0),A(1),A(2),A(3),A(4)
200   SEND 8 ; UNT @ RESUME 8 @ NEXT J
210   FOR I=0 TO NCHAN @ Z(I)=INT (Z(I)/10) @ NEXT I
220   DISP USING "4A,X,5(M6D)" ; "Ave.",Z(0),Z(1),Z(2),Z(3),Z(4)
230.  DISP "Tunnel windspeed (m/s)";@ INPUT WVEL
240   DISP "Aspect ratio";@ INPUT AR@ AR$=CHR$ (64+AR)
250   DISP "Angle of orientation (degrees)";@ INPUT BETA
260   B=BETA/15 @ BETA$=CHR$ (65+B)
270   DISP "Gap (mm)";@ INPUT GAP
280   DISP "Angle of incidence (deg)";@ INPUT ALP
290   ALPH$=VAL$ (ABS (ALP)) @ S$="p" @ IF ALP<0 THEN S$="n"
300   ALP$=S$&ALPH$
310 TEST: DISP "Nominal frequency (Hz)";@ INPUT FRNOM
320   RPM=INT (FRNOM*60) @ RPM$=VAL$ (RPM)
330   TITLE$="AR = "&VAL$ (AR)&", "&RPM$&"rpm, Beta = "&VAL$ (BETA)&", Alpha =
&VAL$ (ALP)
340   FILNAM$=AR$&RPM$&BETA$&ALP$
350   NCYC=10 @ NSEC=30
360   IF FRNOM=0 THEN NSCAN=INT (NCYC*200/NSEC) @ GOTO 380
370   NSCAN=INT (NCYC*1000/NSEC/FRNOM) @ IF NSCAN>1000 THEN NSCAN=1000
380   A$[1,12]="A,PA6144,GO," @ LA=12 @ FOR I=0 TO NCHAN
390   A$[LA+1,LA+3]="I"&VAL$ (ICHAN(I))&"," @ LA=LA+3 @ NEXT I
400   L=LGT (NSCAN+1) @ A$[LA+1,LA+4+L]="QS"&VAL$ (NSCAN+1)&"," @ LA=LA+4+L
410   L=INT (LGT (NSEC)+1) @ A$[LA+1,LA+13+L]="QD"&VAL$ (NSEC)&",F0,IC2,QE"
420   B$="PA6144,QI"
430   FILNAM$=FILNAM$&"_R:D701" ! Store on disc
440 RAW: ON ERROR GOTO DISC_ERROR
450   NBYTE=8*((NCHAN+1)*(NSCAN+1)+14)+LEN (TITLE$)+40
460   RECLEN=256 @ NREC=INT (NBYTE/RECLEN+1) @ CREATE FILNAM$,NREC,RECLEN
470   ASSIGN# 1 TO  FILNAM$ @ TFR=0
480   PRINT# 1 ; WVEL,FRNOM,ALP,AR,BETA,GAP,TFR,NSEC,NSCAN
490   PRINT# 1 ; TITLE$,DAT$ @ FOR I=0 TO NCHAN @ PRINT# 1 ; LM$(I) @ NEXT I
500   FOR I=0 TO NCHAN @ PRINT# 1 ; Z(I) @ NEXT I
510   DISP "Press CONT to begin sampling" @ PAUSE
520   OUTPUT 809 ;A$ @ SEND 8 ; UNL @ RESUME 8 @ WAIT (NSCAN+1)*NSEC+1000
530   OUTPUT 809 ;B$ @ SEND 8 ; UNL @ RESUME 8 @ FOR I=0 TO NSCAN
540   ENTER 809 ; RAW(0,I),RAW(1,I),RAW(2,I),RAW(3,I),RAW(4,I)
550   SEND 8 ; UNT @ RESUME 8 @ NEXT I
560   FOR I=0 TO NSCAN @ FOR J=0 TO NCHAN @ PRINT# 1 ; RAW(J,I) @ NEXT J @ NEXT
I
570   ASSIGN# 1 TO  * @ OFF ERROR
580   OFF KEY# @ CLEAR @ BEEP @ GOTO TEST
590 DISC_ERROR: CALL "DISCERR" ( FILNAM$ ) @ GOTO RAW
600 STOPPER: CLEAR @ DISP "End of program LOG" @ STOP
610 END
```

2) Program to read data from the datalogger for wind turbine tests.

```
10 !  PROGRAM LOG
20 !  This program reads data from datalogger for wind turbines.
30 !  Fiona Sinclair July 1987 and Jan 1989
40 !  Adapted for wind turbines Aug 1989.
50    DIM A$[99],B$[10],LM$(3)[2],FILNAM$[20],TITLE$[99],DAT$[8]
60    DIM A(3),ICHAN(3),Z(3),RAW(3,1000)
70 START: OFF KEY# @ CLEAR @ GCLEAR @ DISP "Program LOG" @ PRINTER IS 1
80    LM$(0)="FX" @ LM$(1)="FY" @ LM$(2)="P " @ LM$(3)="RC"
90    NCHAN=3 @ DISP "Enter date ";@ INPUT DAT$
100   FOR I=0 TO NCHAN @ ICHAN(I)=I+3 @ NEXT I
110   A$[1,12]="A,PA6144,G0," @ LA=12 @ ! Set command strings for datalogger
120   FOR I=0 TO NCHAN @ A$[LA+1,LA+3]="I"&VAL$ (ICHAN(I))&"," @ LA=LA+3
130   NEXT I @ A$[LA+1,LA+19]="QS10,QD05,F0,IC2,QE" @ B$="PA6144,QI"
140   FOR I=0 TO NCHAN @ Z(I)=0 @ NEXT I ! ********************************
150   DISP "Press CONT to begin initialising" @ PAUSE ! 809 = Datalogger
160   OUTPUT 809 ;A$ @ SEND 8 ; UNL @ RESUME 8 @ WAIT 1200
170   OUTPUT 809 ;B$ @ SEND 8 ; UNL @ RESUME 8
180   FOR J=0 TO 9 @ ENTER 809 ; A(0),A(1),A(2),A(3)
190   FOR I=0 TO NCHAN @ Z(I)=Z(I)+A(I) @ NEXT I
200   DISP USING "D,4X,4(M6D)" ; J,A(0),A(1),A(2),A(3)
210   SEND 8 ; UNT @ RESUME 8 @ NEXT J
220   FOR I=0 TO NCHAN @ Z(I)=INT (Z(I)/10) @ NEXT I
230   DISP USING "4A,X,4(M6D)" ; "Ave.",Z(0),Z(1),Z(2),Z(3)
240   DISP "Tunnel windspeed (m/s)";@ INPUT WVEL
250   DISP "Pitch angle";@ INPUT AR@ AR$=CHR$ (65+AR/5)
260   DISP "Angle of orientation (degrees)";@ INPUT BETA
270   B=BETA/15 @ BETA$=CHR$ (65+B)
280   DISP "Gap (mm)";@ INPUT GAP
290   DISP "Angle of incidence (deg)";@ INPUT ALP
300   ALPH$=VAL$ (ABS (ALP)) @ S$="p" @ IF ALP<0 THEN S$="n"
310   ALP$=S$&ALPH$
320 TEST: DISP "Nominal frequency (Hz)";@ INPUT FRNOM
330   RPM=INT (FRNOM*60) @ RPM$=VAL$ (RPM)
340   TITLE$="Pitch="&VAL$ (AR)&","&RPM$&"rpm,Beta="&VAL$ (BETA)&",Alpha="&VAL$
(ALP)&",Wind="&VAL$ (WVEL)
350   FILNAM$=AR$&RPM$&BETA$&ALP$
360   NCYC=3 @ IF FRNOM>0 THEN NSEC=INT (1000/128/FRNOM+1)
370   IF FRNOM=0 THEN NSEC=5 @ NSCAN=256 @ GOTO 390
380   NSCAN=INT (NCYC*1000/NSEC/FRNOM) @ IF NSCAN>1000 THEN NSCAN=1000
390   A$[1,12]="A,PA6144,G0," @ LA=12 @ FOR I=0 TO NCHAN
400   A$[LA+1,LA+3]="I"&VAL$ (ICHAN(I))&"," @ LA=LA+3 @ NEXT I
410   L=LGT (NSCAN+1) @ A$[LA+1,LA+4+L]="QS"&VAL$ (NSCAN+1)&"," @ LA=LA+4+L
420   L=INT (LGT (NSEC)+1) @ A$[LA+1,LA+13+L]="QD"&VAL$ (NSEC)&",F0,IC2,QE"
430   B$="PA6144,QI"
440   FILNAM$=FILNAM$&"_R:D701" ! Store on disc
450 RAW: ON ERROR GOTO DISC_ERROR
460   NBYTE=8*((NCHAN+1)*(NSCAN+1)+13)+LEN (TITLE$)+40
470   RECLEN=256 @ NREC=INT (NBYTE/RECLEN+1) @ CREATE FILNAM$,NREC,RECLEN
480   ASSIGN# 1 TO  FILNAM$
490   DISP "Turbine frequency (Hz)";@ INPUT TFR
500   PRINT# 1 ; WVEL,FRNOM,ALP,AR,BETA,GAP,TFR,NSEC,NSCAN
510   PRINT# 1 ; TITLE$,DAT$ @ FOR I=0 TO NCHAN @ PRINT# 1 ; LM$(I) @ NEXT I
520   FOR I=0 TO NCHAN @ PRINT# 1 ; Z(I) @ NEXT I
530   DISP "Press CONT to begin sampling" @ PAUSE
540   OUTPUT 809 ;A$ @ SEND 8 ; UNL @ RESUME 8 @ WAIT (NSCAN+1)*NSEC+1000
550   OUTPUT 809 ;B$ @ SEND 8 ; UNL @ RESUME 8
560   FOR I=0 TO NSCAN @ ENTER 809 ; RAW(0,I),RAW(1,I),RAW(2,I),RAW(3,I)
570   SEND 8 ; UNT @ RESUME 8 @ NEXT I
580   FOR I=0 TO NSCAN @ FOR J=0 TO NCHAN @ PRINT# 1 ; RAW(J,I) @ NEXT J
590   NEXT I @ ASSIGN# 1 TO  * @ OFF ERROR
600   OFF KEY# @ CLEAR @ BEEP @ GOTO TEST
610 DISC_ERROR: CALL "DISCERR" ( FILNAM$ ) @ GOTO RAW
620 STOPPER: CLEAR @ DISP "End of program LOG" @ STOP
630 END
```

3) Program to process aerofoil data, forming an interpolated curve.

```
10 !  Program PROC
20 !  Fiona Sinclair January 1989
30 !  This program processes data collected by program LOG
40    DIM FILNAM$[20],LM$(4)[2],PM$(2)[10],TITLE$[99],DAT$[8]
50    DIM RAW(4,1000),Z(4),TEMP(3,100),PROC(2,100),XA(1000),YA(1000),CAL(3)
60    PM$(0)="Roll (Nm)" @ PM$(1)="Pitch (Nm)" @ PM$(2)="Yaw (Nm)"
70    GCLEAR @ OFF KEY# @ DISP "Program PROC" @ PRINTER IS 1 @ IPRINT=0
80  IN: ON ERROR GOTO DISC_ERROR
90    CAT ":D701" @ BEEP @ DISP "File name(without _R)?";@ INPUT FILE$
100   FILNAM$=FILE$&"_R:D701" @ ASSIGN# 1 TO  FILNAM$
110   READ# 1 ; WVEL,FREQ,ALP,AR,BETA,GAP,TFR,NSEC,NSCAN
120   READ# 1 ; TITLE$,DAT$@ FOR I=0 TO 4 @ READ# 1 ; LM$(I)@ NEXT I
130   FOR I=0 TO 4 @ READ# 1 ; Z(I)@ NEXT I
140   FOR J=0 TO NSCAN @ FOR I=0 TO 3 @ READ# 1 ; RAW(I,J)@ NEXT I
150   READ# 1 ; RAW(4,J)@ NEXT J @ ASSIGN# 1 TO  * @ FOR J=0 TO NSCAN
160   FOR I=0 TO 4 @ RAW(I,J)=RAW(I,J)-Z(I) @ NEXT I @ NEXT J
170   ARM=GAP/1000+AR*.125 @ Q=0 @ IF WVEL>0 THEN Q=ARM*FREQ/WVEL*1.508
180  PLOTR: CLEAR @ PLODEV=905 @ ON ERROR GOTO ERR
190    FOR I=0 TO NSCAN @ XA(I)=I*NSEC/1000 @ NEXT I
200    XLABEL$="Time (secs)"
210    FOR IC=0 TO 3 @ YLABEL$=LM$(IC)
220    FOR I=0 TO NSCAN @ YA(I)=RAW(IC,I) @ NEXT I
230    CALL "PLOTCH" ( PLODEV,1,4,1,IC+1,1,NSCAN,XLABEL$,YLABEL$,TITLE$,1,"",0,
A();1,YA() ) @ NEXT IC
240 FREQU: OFF KEY# @ CLEAR @ DISP "Calculating frequency" @ ON ERROR GOTO ERR
250   NCYC=-1 @ ISCAN=-1 @ C=0 @ D=0 @ E=0 @ F=0
260   ISCAN=ISCAN+1 @ IF ISCAN>= NSCAN THEN GOTO 340
270   IF RAW(4,ISCAN)>-1000 THEN GOTO 260
280   NCYC=NCYC+1 @ ITOT=-1 @ DISP "Cycle number ";NCYC
290   ITOT=ITOT+1 @ IF RAW(4,ISCAN+ITOT)>-1000 THEN GOTO 320
300   IF ISCAN+ITOT<NSCAN-1 THEN GOTO 290
310   NCYC=NCYC-1 @ GOTO 340
320   ZERO=.5*ITOT+ISCAN @ ISCAN=ISCAN+ITOT @ C=C+NCYC @ D=D+ZERO
330   E=E+NCYC*ZERO @ F=F+NCYC*NCYC @ GOTO 260
340   IF NCYC<1 THEN NCYC=10 @ FREQ=0 @ SAMP=NSCAN/10 @ AIND=0 @ GOTO INTERP
350   SAMP=((NCYC+1)*E-C*D)/(F*(NCYC+1)-C*C) ! Scans/cycle
360   FREQ=1000/SAMP/NSEC ! Cycles/sec
370   AIND=(C*E-F*D)/(C*C-F*(NCYC+1))+.25*SAMP ! Phase=0 at upright
380   IF AIND>SAMP THEN AIND=AIND-SAMP
390   IF AIND+NCYC*SAMP>NSCAN THEN NCYC=NCYC-1 @ GOTO 390
400 INTERP: NSAMP=INT (SAMP)
410   FOR J=0 TO NSAMP @ FOR IC=0 TO 3 @ TEMP(IC,J)=0 @ NEXT IC
420   FOR I=0 TO NCYC-1 @ A=AIND+SAMP*(I+J/NSAMP) @ IA=INT (A) @ FR=A-IA
430   FOR IC=0 TO 3
440   TEMP(IC,J)=TEMP(IC,J)+(1-FR)*RAW(IC,IA)+FR*RAW(IC,IA+1) @ NEXT IC
450   NEXT I @ FOR IC=0 TO 3 @ TEMP(IC,J)=TEMP(IC,J)/NCYC @ NEXT IC @ NEXT J
460 KEEP: DISP "Storing data" @ ON ERROR GOTO DISC_ERROR
470   FILNAM$=FILE$&"_P:D701"
480   NBYTE=8*(3*(NSAMP+1)+8)+LEN (TITLE$)+80
490   RECLEN=256 @ NREC=CEIL (NBYTE/RECLEN) @ CREATE FILNAM$,NREC+1,RECLEN
500   ASSIGN# 1 TO  FILNAM$ @ Q=0 @ IF WVEL>0 THEN Q=ARM*FREQ/WVEL*1.508
510   PRINT# 1 ; FREQ,Q,ALP,AR,BETA,GAP,EP,NSAMP
520   PRINT# 1 ; TITLE$,DAT$ @ FOR I=0 TO 4 @ PRINT# 1 ; PM$(I) @ NEXT I
530   DISP "Processing data"
540   CAL(0)=1/49 @ CAL(1)=1/59 @ CAL(2)=1/342 @ CAL(3)=1/864
550   FOR J=0 TO NSAMP @ FOR I=0 TO 1 @ PROC(I,J)=CAL(I)*TEMP(I,J)*.37 @ NEXT I
560   PROC(2,J)=CAL(3)*TEMP(3,J) @ NEXT J
570   FOR I=0 TO 2 @ FOR J=0 TO NSAMP @ PRINT# 1 ; PROC(I,J) @ NEXT J @ NEXT I
580   ASSIGN# 1 TO  * @ OFF ERROR @ GOTO IN
590 CHOICE: CLEAR @ GCLEAR @ BEEP @ IPRINT=0 @ PAP=0 @ ON ERROR GOTO ERR
600   ON KYBD AA,"1234567890" GOTO CHOICE
610   ON KEY# 1,"Disp raw" GOTO PAPDR
620   ON KEY# 2,"Print raw" GOTO PAPPR
630   ON KEY# 3,"Disp proc" GOTO PAPDP
640   ON KEY# 4,"Print Proc" GOTO PAPPP
650   ON KEY# 5,"Plot temp" GOTO PLOTT
660   ON KEY# 6,"Plot proc" GOTO PLOTP
```

```
670   ON KEY# 7,"Stop" GOTO STOPPER
680   KEY LABEL @ DISP "Press softkey"
690 HERE: GOTO HERE
700 PAPDP: PAP=1 @ GOTO PAPDR
710 PAPPP: PAP=1
720 PAPPR: PRINTER IS 901 @ IPRINT=1
730 PAPDR: PRINT "RESULTS FROM PROGRAM PROC" @ PRINT TITLE$
740   IF PAP=0 THEN NSAMP=NSCAN @ NCYC=NSCAN*NSEC/1000*FREQ
750   PRINT "Stored in file           ";FILE$
760   PRINT "Date                     ";DAT$
770   PRINT "Tunnel Velocity (V)    =";WVEL;"m/s"
780   PRINT "Frequency (f)          =";@ PRINT USING "X,2D.2D,X,7A" ; FREQ;"Hz"
790   PRINT "Velocity ratio (q)     =";@ PRINT USING "X,D.4D" ; Q
800   PRINT "Mean incidence (alpha) =";ALP;"degrees"
810   PRINT "Aspect ratio (AR)      =";AR
820   PRINT "Orientation (beta)     =";BETA;"degrees"
830   PRINT "Lever arm (h)          =";ARM;"m"
840   PRINT "Gap under aerofoil (r) =";GAP;"mm"
850   PRINT "Interval between scans =";NSEC;"millisecs"
860   PRINT NCYC;" cycles"
870   PRINT RPT$ ("-",48) @ IF PAP=0 THEN GOTO 930
880   PRINT USING FORM0 ; " wt (deg)","Roll","Pitch","Yaw"
890   PRINT RPT$ ("-",48)
900   FOR I=0 TO NSAMP
910   PRINT USING FORM2 ; I/NSAMP*360,PROC(0,I),PROC(1,I),PROC(2,I)
920   NEXT I @ PRINT RPT$ ("-",48) @ GOTO 970
930   PRINT USING FORM0 ; " Time(ms)","FX","FY","FZ","MZ","RC"
940   PRINT RPT$ ("-",48) @ FOR I=0 TO NSCAN
950   PRINT USING FORM1 ; I*NSEC,RAW(0,I),RAW(1,I),RAW(2,I),RAW(3,I),RAW(4,I)
960   NEXT I @ PRINT RPT$ ("-",48)
970   IF IPRINT=1 THEN PRINT CHR$ (12) @ PRINTER IS 1 @ GOTO CHOICE
980   DISP "Press CONT to continue" @ PAUSE @ GOTO CHOICE
990 PLOTP: CLEAR @ PLODEV=1 @ GCLEAR @ ON ERROR GOTO ERR
1000   FOR I=0 TO NSAMP @ XA(I)=I/NSAMP*360 @ NEXT I
1010   XLABEL$="wt (degs)"
1020   FOR IC=0 TO 2 @ YLABEL$=PM$(IC)
1030   FOR I=0 TO NSAMP @ YA(I)=PROC(IC,I) @ NEXT I
1040   CALL "PLOTCH" ( PLODEV,1,3,1,IC+1,1,NSAMP,XLABEL$,YLABEL$,TITLE$,1,"",0,
A(),1,YA() )
1050   NEXT IC @ PAUSE @ GOTO CHOICE
1060 PLOTT: CLEAR @ PLODEV=1 @ GCLEAR @ ON ERROR GOTO ERR
1070   FOR I=0 TO NSAMP @ XA(I)=I/NSAMP*360 @ NEXT I
1080   XLABEL$="wt (degs)"
1090   FOR IC=0 TO 3 @ YLABEL$=LM$(IC)
1100   FOR I=0 TO NSAMP @ YA(I)=TEMP(IC,I) @ NEXT I
1110   CALL "PLOTCH" ( PLODEV,1,4,1,IC+1,1,NSAMP,XLABEL$,YLABEL$,TITLE$,1,"",0,
A(),1,YA() )
1120   NEXT IC @ PAUSE @ GOTO CHOICE
1130 DISC_ERROR: CALL "DISCERR" ( FILNAM$ ) @ ON ERROR GOTO DISC_ERROR
1140   L=LEN (FILNAM$)
1150   IF FILNAM$[L-6,L]="_R:D701" THEN GOTO IN
1160   GOTO KEEP
1170 ERR: OFF ERROR @ DISP ERRN ,ERRL  @ PAUSE
1180 STOPPER: DISP "Program PROC ended" @ STOP
1190   FORM0: IMAGE 9A,5(3X,5A)
1200   FORM1: IMAGE X,6(M5D,2X)
1210   FORM2: IMAGE X,3D.3D,2X,3(M2D.3D,X)
1220 END
```

4) Program to calculate Fourier coefficients for aerofoils.

```
10 ! Program FOURIER
20 ! Fiona Sinclair July 1987 and January 1989
30 ! This program calculates Fourier coefficients
40 ! for aerofoils from data output by PROC.
50   DIM FILNAM$[20],PM$(4)[10],TITLE$[99],DAT$[8]
60   DIM PROC(4,100),P(4),A(4,6),XA(100),YA(100),ZA(100)
70   CLEAR @ DISP "Program FOURIER" @ PRINTER IS 901 ! @ CAT ":D701"
80   IN: BEEP @ ON ERROR GOTO DISC_ERROR
90    DISP "File name(without _P)";@ INPUT FILE$
100   FILNAM$=FILE$&"_P:D701" @ ASSIGN# 1 TO  FILNAM$
110   READ# 1 ; FREQ,Q,ALP,AR,BETA,GAP,TFR,NSAMP
120   READ# 1 ; TITLE$,DAT$@ FOR I=0 TO 4 @ READ# 1 ; PM$(I)@ NEXT I
130   FOR I=0 TO 4 @ FOR J=0 TO NSAMP @ READ# 1 ; PROC(I,J)@ NEXT J @ NEXT I
140   ASSIGN# 1 TO  *
150 FOUR: NCOEF=3 @ W=6.283185/NSAMP @ DISP "Calculating" @ ON ERROR GOTO ERR
160   FOR N=0 TO 6 @ FOR IC=0 TO 4 @ A(IC,N)=0 @ NEXT IC @ NEXT N
170   FOR L=1 TO NSAMP @ WT=W*(L-.5)
180   FOR IC=0 TO 4 @ P(IC)=(PROC(IC,L-1)+PROC(IC,L))/2
190   A(IC,0)=A(IC,0)+P(IC) @ NEXT IC
200   FOR N=1 TO NCOEF @ C=COS (N*WT) @ S=SIN (N*WT) @ FOR IC=0 TO 4
210   A(IC,N)=A(IC,N)+P(IC)*C @ A(IC,N+NCOEF)=A(IC,N+NCOEF)+P(IC)*S
220   NEXT IC @ NEXT N @ NEXT L
230   FOR IC=0 TO 4 @ A(IC,0)=A(IC,0)/NSAMP @ FOR N=1 TO 2*NCOEF
240   A(IC,N)=A(IC,N)*2/NSAMP @ NEXT N @ NEXT IC
250 PAPER: PRINT TITLE$;@ PRINT USING "M2D.3D" ; FREQ
260   PRINT "Analysis of file ";FILE$;" tested on ";DAT$
270   PRINT "Frequency (w)          =";@ PRINT USING "M2D.3D,X,2A" ; FREQ;"Hz"
280   PRINT "Velocity ratio (q)     =";@ PRINT USING "D.4D" ; Q
290   PRINT "Mean incidence (alpha) =";ALP;"degrees"
300   PRINT "Aspect ratio (AR)      =";AR
310   PRINT "Orientation (beta)     =";BETA;"degrees"
320   PRINT "Gap under aerofoil     =";GAP;"mm" @ PRINT
330   PRINT USING FORM0 ; " wt (deg)","Roll","Pitch","Yaw","Lift","Drag"
340   FOR I=0 TO NSAMP @ C=I/NSAMP*360
350   PRINT USING FORM2 ; C,PROC(0,I),PROC(1,I),PROC(2,I),PROC(3,I),PROC(4,I)
360   NEXT I @ PRINT
370   PRINT "               ";
380   FOR N=0 TO NCOEF @ PRINT "Real";N;" ";@ NEXT N
390   FOR N=1 TO NCOEF @ PRINT "Imag";N;" ";@ NEXT N @ PRINT
400   FOR IC=0 TO 4
410   PRINT USING FORM ; A(IC,0),A(IC,1),A(IC,2),A(IC,3),A(IC,4),A(IC,5),A(IC,6

420   NEXT IC @ PRINT RPT$ (CHR$ (10),3)
430 PLOTN: XLABEL$="wt (degs)" @ PLODEV=905 @ ON ERROR GOTO ERR
440   FOR I=0 TO NSAMP @ XA(I)=I/NSAMP*360 @ NEXT I
450   DISP "Please wait" @ W=6.283185/NSAMP
460   FOR IC=0 TO 4 @ YLABEL$=PM$(IC)
470   FOR I=0 TO NSAMP @ WT=W*I @ ZA(I)=A(IC,0) @ YA(I)=PROC(IC,I)
480   FOR J=1 TO NCOEF @ ZA(I)=ZA(I)+A(IC,J)*COS (J*WT)+A(IC,J+NCOEF)*SIN (J*WT

490   NEXT J @ NEXT I
500   CALL "PLOTCH" ( PLODEV,1,5,1,IC+1,1,NSAMP,XLABEL$,YLABEL$,TITLE$,1,"",0,X
(),2,YA(),ZA() )
510 NEXT IC @ BEEP @ GOTO IN
520 DISC_ERROR: CALL "DISCERR" ( FILNAM$ ) @ GOTO IN
530 ERR: OFF ERROR @ DISP ERRN ,ERRL
540 STOPPER: DISP "Program FOURIER ended" @ STOP
550 FORM: IMAGE X,8 (M2D.4D,X)
560 FORM0: IMAGE 9A,5(3X,5A)
570 FORM2: IMAGE X,3D.3D,2X,5(M2D.3D,X)
580 END
```

5) Program to process wind turbine data, forming an interpolated curve.

```
10 !  Program PROCFF
20 !  Fiona Sinclair August 1989
30 !  This program processes data collected by program LOG
40    DIM FILNAM$[20],LM$(3)[2],PM$(2)[10],TITLE$[99],DAT$[8]
50    DIM RAW(3,1000),Z(3),PROC(2,512),XA(1000),YA(1000),CAL(2)
60    PM$(0)="Roll (Nm)" @ PM$(1)="Pitch (Nm)" @ PM$(2)="Power (V)" @ NCHAN=3
70    GCLEAR @ OFF KEY# @ DISP "Program PROC" @ PRINTER IS 1 @ IPRINT=0
80  IN: ON ERROR GOTO DISC_ERROR
90    CAT ":D701" @ BEEP @ DISP "File name(without _R)?";@ INPUT FILE$
100   FILNAM$=FILE$&"_R:D701" @ ASSIGN# 1 TO  FILNAM$
110   READ# 1 ; WVEL,FREQ,ALP,AR,BETA,GAP,TFR,NSEC,NSCAN
120   READ# 1 ; TITLE$,DAT$@ FOR I=0 TO NCHAN @ READ# 1 ; LM$(I)@ NEXT I
130   FOR I=0 TO NCHAN @ READ# 1 ; Z(I)@ NEXT I
140   FOR J=0 TO NSCAN @ FOR I=0 TO NCHAN @ READ# 1 ; RAW(I,J)@ NEXT I @ NEXT J
150   ASSIGN# 1 TO  * @ FOR J=0 TO NSCAN
160   FOR I=0 TO NCHAN @ RAW(I,J)=RAW(I,J)-Z(I) @ NEXT I @ NEXT J
170   ARM=GAP/1000 @ Q=0 @ IF WVEL>0 THEN Q=ARM*FREQ/WVEL*1.508
180 PLOTR: GCLEAR @ PLODEV=905 @ ON ERROR GOTO ERR
190    FOR I=0 TO NSCAN @ XA(I)=I*NSEC/1000 @ NEXT I
200    XLABEL$="Time (secs)"
210    FOR IC=0 TO 2 @ YLABEL$=LM$(IC)
220    FOR I=0 TO NSCAN @ YA(I)=RAW(IC,I) @ NEXT I
230    CALL "PLOTCH" ( PLODEV,1,3,1,IC+1,1,NSCAN,XLABEL$,YLABEL$,TITLE$,1,"",0,
A();1,YA() ) @ NEXT IC @ GOTO IN
240 FREQU: OFF KEY# @ CLEAR @ DISP "Calculating frequency" @ ON ERROR GOTO ERR
250   NCYC=-1 @ ISCAN=-1 @ C=0 @ D=0 @ E=0 @ F=0 @ IFLAG=0
260   IF RAW(3,0)<-1000 THEN IFLAG=1 @ GOTO 270
270   ISCAN=ISCAN+1 @ IF ISCAN>= NSCAN THEN GOTO 360
280   IF RAW(3,ISCAN)>-1000 THEN GOTO 270
290   NCYC=NCYC+1 @ ITOT=-1 @ DISP "Cycle number ";NCYC
300   ITOT=ITOT+1 @ IF RAW(3,ISCAN+ITOT)>-1000 THEN GOTO 330
310   IF ISCAN+ITOT<NSCAN-1 THEN GOTO 300
320   NCYC=NCYC-1 @ GOTO 360
330   IF IFLAG=1 THEN NCYC=NCYC-1 @ IFLAG=0 @ GOTO 270
340   ZERO=.5*ITOT+ISCAN @ ISCAN=ISCAN+ITOT @ C=C+NCYC @ D=D+ZERO
350   E=E+NCYC*ZERO @ F=F+NCYC*NCYC @ GOTO 270
360   IF NCYC<0 THEN NCYC=1 @ FREQ=0 @ SAMP=NSCAN/2 @ AIND=0 @ GOTO INTERP
370   SAMP=((NCYC+1)*E-C*D)/(F*(NCYC+1)-C*C) ! Scans/cycle
380   FREQ=1000/SAMP/NSEC ! Cycles/sec
390   AIND=(C*E-F*D)/(C*C-F*(NCYC+1))+.25*SAMP ! Phase=0 at upright
400   IF AIND>SAMP THEN AIND=AIND-SAMP
410   IF AIND+(NCYC+1)*SAMP>NSCAN THEN NCYC=NCYC-1 @ GOTO 410
420 INTERP: NPROC=127 @ CONV=SAMP/NPROC
430   FOR J=0 TO NPROC @ FOR IC=0 TO NCHAN-1 @ PROC(IC,J)=0 @ NEXT IC
440   FOR N=0 TO NCYC @ A=AIND+J*CONV+SAMP*N @ IA=INT (A) @ FR=A-IA
450   FOR IC=0 TO NCHAN-1
460   PROC(IC,J)=PROC(IC,J)+(1-FR)*RAW(IC,IA)+FR*RAW(IC,IA+1)
470   NEXT IC @ NEXT N
480   FOR IC=0 TO NCHAN-1 @ PROC(IC,J)=PROC(IC,J)/(NCYC+1) @ NEXT IC @ NEXT J
490   RMS=0 @ FOR J=0 TO NSCAN @ RMS=RMS+RAW(2,J)*RAW(2,J) @ NEXT J
500   RMS=RMS/(NSCAN+1) @ RMS=SQR (RMS)
510 KEEP: DISP "Storing data" @ ON ERROR GOTO DISC_ERROR
520   FILNAM$=FILE$&"_P:D701"
530   NBYTE=8*(NCHAN*(NPROC+1)+8)+LEN (TITLE$)+80
540   RECLEN=256 @ NREC=NBYTE/RECLEN+1 @ CREATE FILNAM$,NREC,RECLEN
550   ASSIGN# 1 TO  FILNAM$ @ Q=0 @ IF WVEL>0 THEN Q=ARM*FREQ/WVEL*1.508
560   PRINT# 1 ; FREQ,Q,ALP,AR,BETA,GAP,TFR,NPROC,RMS
570   PRINT# 1 ; TITLE$,DAT$ @ FOR I=0 TO NCHAN-1 @ PRINT# 1 ; PM$(I) @ NEXT I
580   DISP "Processing data"
590   CAL(0)=1/49 @ CAL(1)=1/39 @ CAL(2)=1/3102
600   FOR J=0 TO NPROC @ FOR I=0 TO 1 @ PROC(I,J)=PROC(I,J)*CAL(I)*.37 @ NEXT I
610   PROC(2,J)=PROC(2,J)*CAL(2) @ NEXT J
620   FOR I=0 TO NCHAN-1 @ FOR J=0 TO NPROC @ PRINT# 1 ; PROC(I,J) @ NEXT J
630   NEXT I @ ASSIGN# 1 TO  * @ OFF ERROR @ GOTO IN
640 CHOICE: CLEAR @ GCLEAR @ BEEP @ IPRINT=0 @ PAP=0 @ ON ERROR GOTO ERR
```

```
650   ON KYBD AA,"1234567890" GOTO CHOICE
660   ON KEY# 1,"Disp raw" GOTO PAPDR
670   ON KEY# 2,"Print raw" GOTO PAPPR
680   ON KEY# 3,"Disp proc" GOTO PAPDP
690   ON KEY# 4,"Print Proc" GOTO PAPPP
700   ON KEY# 5,"Stop" GOTO STOPPER
710   KEY LABEL @ DISP "Press softkey"
720 HERE: GOTO HERE
730 PAPDP: PAP=1 @ GOTO PAPDR
740 PAPPP: PAP=1
750 PAPPR: PRINTER IS 901 @ IPRINT=1
760 PAPDR: PRINT "RESULTS FROM PROGRAM PROC" @ PRINT TITLE$
770   IF PAP=0 THEN NSAMP=NSCAN @ NCYC=NSCAN*NSEC/1000*FREQ
780   PRINT "Stored in file           ";FILE$
790   PRINT "Date                     ";DAT$
800   PRINT "Tunnel Velocity (V)    =";WVEL;"m/s"
810   PRINT "Frequency (f)          =";@ PRINT USING "X,2D.2D,X,7A" ; FREQ,"Hz"
820   PRINT "Velocity ratio (q)     =";@ PRINT USING "X,D.4D" ; Q
830   PRINT "Mean incidence (alpha) =";ALP;"degrees"
840   PRINT "Pitch angle            =";AR
850   PRINT "Orientation (beta)     =";BETA;"degrees"
860   PRINT "Turbine frequency      =";TFR;"Hz"
870   PRINT "Lever arm (h)          =";ARM;"m"
880   PRINT "Interval between scans =";NSEC;"millisecs"
890   PRINT NCYC+1;" cycles"
900   PRINT RPT$ ("-",48) @ IF PAP=0 THEN GOTO 960
910   PRINT USING FORM0 ; " wt (deg)","Roll","Pitch","Power"
920   PRINT RPT$ ("-",48)
930   FOR I=0 TO NPROC
940   PRINT USING FORM2 ; I/SAMP*360,PROC(0,I),PROC(1,I),PROC(2,I)
950   NEXT I @ PRINT RPT$ ("-",48) @ GOTO 1000
960   PRINT USING FORM0 ; " Time(ms)","FX","FY","P ","RC"
970   PRINT RPT$ ("-",48) @ FOR I=0 TO NSCAN
980   PRINT USING FORM1 ; I*NSEC,RAW(0,I),RAW(1,I),RAW(2,I),RAW(3,I)
990   NEXT I @ PRINT RPT$ ("-",48)
1000   IF IPRINT=1 THEN PRINT CHR$ (12) @ PRINTER IS 1 @ GOTO CHOICE
1010   DISP "Press CONT to continue" @ PAUSE @ GOTO CHOICE
1020 PLOTP: CLEAR @ PLODEV=1 @ GCLEAR @ ON ERROR GOTO ERR
1030   FOR I=0 TO NPROC @ XA(I)=I/SAMP*360 @ NEXT I
1040   XLABEL$="wt (degs)"
1050   FOR IC=0 TO NCHAN-1 @ YLABEL$=PM$(IC)
1060   FOR I=0 TO NPROC @ YA(I)=PROC(IC,I) @ NEXT I
1070   CALL "PLOTCH" ( PLODEV,1,3,1,IC+1,1,NPROC,XLABEL$,YLABEL$,TITLE$,1,"",0,
A(),1,YA() )
1080   NEXT IC @ PAUSE @ GOTO CHOICE
1090 DISC_ERROR: CALL "DISCERR" ( FILNAM$ ) @ ON ERROR GOTO DISC_ERROR
1100   L=LEN (FILNAM$)
1110   IF FILNAM$[L-6,L]="_R:D701" THEN GOTO IN
1120   GOTO KEEP
1130 ERR: OFF ERROR @ DISP ERRN ,ERRL  @ PAUSE
1140 STOPPER: DISP "Program PROCFF ended" @ STOP
1150   FORM0: IMAGE 9A,4(3X,5A)
1160   FORM1: IMAGE X,5(M5D,2X)
1170   FORM2: IMAGE X,3D.3D,2X,4(M2D.3D,X)
1180 END
```

6) Program to calculate Fourier coefficients for wind turbines.

```
10 ! Program FFT
20 ! Fiona Sinclair August 1989
30 ! This program calculates Fourier coefficients
40 !  for wind turbines from data output by PROCFF.
50   DIM FILNAM$[20],PM$(2)[10],TITLE$[99],DAT$[8]
60   DIM PROC(2,128),XA(128),R(128),S(128),A(2,6)
70   CLEAR @ DISP "Program FFT" @ PRINTER IS 901 @ CAT ":D701"
80   IN: ON ERROR GOTO STOPPER
90   DISP "File name(without _P)";@ INPUT FILE$
100   FILNAM$=FILE$&"_P:D701" @ ASSIGN# 1 TO  FILNAM$
110   READ# 1 ; FREQ,Q,ALP,AR,BETA,GAP,TFR,NPROC@ NPROC=NPROC+1
120   READ# 1 ; TITLE$,DAT$@ FOR I=0 TO 2 @ READ# 1 ; PM$(I)@ NEXT I
130   FOR I=0 TO 2 @ FOR J=1 TO NPROC @ READ# 1 ; PROC(I,J)@ NEXT J @ NEXT I
140   ASSIGN# 1 TO  * @ L=0 @ N=NPROC
150   FILNAM$=FILE$&"_F:D701" @ CREATE FILNAM$,7,256 @ ASSIGN# 1 TO  FILNAM$
160   PRINT# 1 ; FREQ,Q,ALP,AR,BETA,GAP,TFR,NPROC
170   PRINT# 1 ; TITLE$
180   N=N/2 @ L=L+1 @ IF N>1 THEN GOTO 180
190 FOUR: DISP "Calculating" @ ON ERROR GOTO ERR
200   R(0)=0 @ S(0)=0
210   FOR IC=0 TO 2 @ FOR I=1 TO NPROC @ R(I)=PROC(IC,I) @ S(I)=0 @ NEXT I
220   NA=NPROC @ NB=1 @ FOR IL=1 TO L
230   NA=NA/2 @ CALL "FFTSTP" ( R(),S(),NA,NB ) @ NB=NB*2 @ NEXT IL
240   CALL "TRAN" ( R(),S(),L,NPROC )
250   FOR N=0 TO NPROC/4 @ PRINT# 1 ; R(N) @ NEXT N
260   FOR N=0 TO NPROC/4 @ PRINT# 1 ; S(N) @ NEXT N
270   A(IC,0)=R(1) @ FOR I=1 TO 2 @ A(IC,I)=2*R(I+1) @ A(IC,I+3)=-(2*S(I+1))
280  NEXT I @ NEXT IC @ ASSIGN# 1 TO  *
290 PAPER: PRINT TITLE$;@ PRINT USING "M2D.3D" ; FREQ
300   PRINT "Analysis of file ";FILE$;" tested on ";DAT$
310   PRINT "Roll frequency (w)      =";@ PRINT USING "M2D.3D,X,2A" ; FREQ;"Hz"
320   PRINT "Velocity ratio (q)      =";@ PRINT USING "D.4D" ; Q
330   PRINT "Mean incidence (alpha) =";ALP;"degrees"
340   PRINT "Pitch angle (deg)       =";AR
350   PRINT "Orientation (beta)      =";BETA;"degrees"
360   PRINT "Gap under turbine       =";GAP;"mm" @ PRINT
370   PRINT "                  ";
380   FOR N=0 TO NCOEF @ PRINT "Real";N;" ";@ NEXT N
390   FOR N=1 TO NCOEF @ PRINT "Imag";N;" ";@ NEXT N @ PRINT
400   FOR IC=0 TO 2
410   PRINT USING FORM ; A(IC,0),A(IC,1),A(IC,2),A(IC,3),A(IC,4),A(IC,5),A(IC,6
420   NEXT IC @ PRINT RPT$ (CHR$ (10),3) @ BEEP @ GOTO IN
430 DISC_ERROR: CALL "DISCERR" ( FILNAM$ ) @ GOTO IN
440 ERR: OFF ERROR @ DISP ERRN ,ERRL
450 STOPPER: DISP "Program FFT ended" @ STOP
460 FORM: IMAGE X,8 (M2D.4D,X)
470 END
```

7) Program to plot graphs of output

```
10 ! Program FOURIER
20 ! Fiona Sinclair July 1987 and January 1989
30 ! This program plots Fourier graphs from data output by FFT.
40   DIM FILNAM$[20],PM$(2)[10],TITLE$[99],DAT$[8]
50   DIM PROC(2,32),P(2),A(2,6),XA(32),YA(32),ZA(32),R(2,32),S(2,32)
60   CLEAR @ DISP "Program FOURIER" @ PRINTER IS 901 ! @ CAT ":D701"
70   IN: BEEP @ ON ERROR GOTO DISC_ERROR
80   DISP "File name(without _P)";@ INPUT FILE$
90   FILNAM$=FILE$&"_P:D701" @ ASSIGN# 1 TO  FILNAM$
100   READ# 1 ; FREQ,Q,ALP,AR,BETA,GAP,TFR,NSAMP,RMS
110   READ# 1 ; TITLE$,DAT$@ FOR I=0 TO 2 @ READ# 1 ; PM$(I)@ NEXT I
120   FOR I=0 TO 2 @ FOR J=0 TO NSAMP @ READ# 1 ; PROC(I,J)@ NEXT J @ NEXT I
130   ASSIGN# 1 TO  *
140   FILNAM$=FILE$&"_F:D701" @ ASSIGN# 1 TO  FILNAM$
150   READ# 1 ; FREQ,Q,ALP,AR,BETA,GAP,TFR,NPROC
160   READ# 1 ; TITLE$
170   FOR IC=0 TO 2 @ FOR N=0 TO NPROC/4 @ READ# 1 ; R(IC,N)@ NEXT N
180   FOR N=0 TO NPROC/4 @ READ# 1 ; S(IC,N)@ NEXT N
190   A(IC,0)=R(IC,1) @ FOR I=0 TO 3 @ A(IC,I)=2*R(IC,I+1)
200   A(IC,I+3)=-(2*S(IC,I+1)) @ NEXT I @ NEXT IC
210   ASSIGN# 1 TO  *
220 PLOTN: XLABEL$="Freq (Hz)" @ PLODEV=905 @ ON ERROR GOTO ERR
230   FOR I=0 TO NSAMP @ XA(I)=I/NSAMP*360 @ NEXT I
240   FOR IC=0 TO 1 @ YLABEL$=PM$(IC)
250   FOR I=0 TO NSAMP @ WT=W*I @ ZA(I)=.5*A(IC,0) @ YA(I)=PROC(IC,I)
260   FOR J=1 TO NCOEF
270   ZA(I)=ZA(I)+A(IC,J)*COS (J*WT)+A(IC,J+NCOEF)*SIN (J*WT)
280   NEXT J @ NEXT I
290   CALL "PLOTCH" ( PLODEV,1,5,1,IC+1,1,NSAMP,XLABEL$,YLABEL$,TITLE$,1,"",0,X
(),2,YA(),ZA() ) @ NEXT IC
300   FOR IC=0 TO 2 @ YLABEL$=PM$(IC)
310   F=FREQ @ IF FREQ=0 THEN F=1.56
320   FOR I=0 TO NPROC/4 @ XA(I)=I*F @ ZA(I)=R(IC,I) @ YA(I)=S(IC,I) @ NEXT I
330   CALL "PLOTCH" ( PLODEV,1,5,1,IC+3,1,NPROC/4,XLABEL$,YLABEL$,TITLE$,1,"",0
XA(),2,YA(),ZA() )
340 NEXT IC @ BEEP @ GOTO IN
350 DISC_ERROR: CALL "DISCERR" ( FILNAM$ ) @ GOTO IN
360 ERR: OFF ERROR @ DISP ERRN ,ERRL
370 STOPPER: DISP "Program FOURIER ended" @ STOP
380 FORM: IMAGE X,8 (M2D.4D,X)
390 FORM0: IMAGE 9A,5(3X,5A)
400 FORM2: IMAGE X,3D.3D,2X,5(M2D.3D,X)
410 END
```

```
10 SUB "PLOTCH" (PLDV,NX,NY,IX,IY,ID,NTOT,XLAB$,YLAB$,TITLE$,L,S$,IASK,XA(),YNU
,YA(),ZA())
20 ! INPUT:PLDV Plotter device = 905 (hardcopy), =1 (screen)
30 !        NX,NY,IX,IY No. of plots required and position of this one
40 !        ID =0 (Landscape); =1 (Portrait)
50 !        XLAB$, YLAB$ Axis labels
60 !        TITLE$  Page title
70 !        L Line type (1=solid, 2=none, 3-8=dots and dashes)
80 !        S$ Marker for points (e.g. "*")
90 !        IASK = 0 (automatic), 1(interractive) scaling
100 !       YNUM = Number of Y arrays
110 !       XA = NTOT points to be plotted
120 !       YA,ZA = NTOT points to be plotted
130  DIM XLABEL$[99],YLABEL$[99]
140  ON ERROR GOTO 400
150  IF PLDV=905 THEN PLOTTER IS 905 @ IDIR=ID ELSE PLOTTER IS 1 @ IDIR=0
160  CALL "PLOTPOS" ( NX,NY,IX,IY,IDIR,PLDV,TITLE$,NHINC,NVINC,LHLAB,LVLAB,HHT,
HT )
170  IF IDIR=0 THEN NXINC=NHINC @ LXLAB=LHLAB @ XHT=HHT @ NYINC=NVINC @ LYLAB=L
LAB @ YHT=VHT
180  IF IDIR<> 0 THEN NXINC=NVINC @ LXLAB=LVLAB @ XHT=VHT @ NYINC=NHINC @ LYLAB
LHLAB @ YHT=HHT
190 CALL "AUTOSCALE" ( XA(),NTOT,NXINC,XMIN,XMAX,XINC,NXIND,XTICK,IASK,LXLAB,XL
B$,XLABEL$ )
200 CALL "AUTOSCALE" ( YA(),NTOT,NYINC,YMIN,YMAX,YINC,NYIND,YTICK,IASK,LYLAB,YL
B$,YLABEL$ )
210 IF IDIR=0 THEN SCALE XMIN,XMAX,YMIN,YMAX ELSE SCALE YMAX,YMIN,XMIN,XMAX
220 XHT=XHT*(XMAX-XMIN) @ YHT=YHT*(YMAX-YMIN)
230 IF XMIN>0 THEN XORIG=XMIN ELSE XORIG=0
240 IF XMAX<0 THEN XORIG=XMAX
250 IF YMIN>0 THEN YORIG=YMIN ELSE YORIG=0
260 IF YMAX<0 THEN YORIG=YMAX
270 YN=1 @ IF NX=1 AND NY>1 THEN XN=0 @ XLABEL$="" ELSE XN=1
280 CALL "AXISZ" ( IDIR,1,XMIN,XMAX,XINC,NXIND,XTICK,XLABEL$,YHT,XN,YORIG,YMIN

290 CALL "AXISZ" ( IDIR,2,YMIN,YMAX,YINC,NYIND,YTICK,YLABEL$,XHT,YN,XORIG,XMIN

300 IF IDIR=0 THEN CLIP XMIN,XMAX,YMIN,YMAX ELSE CLIP YMIN,YMAX,XMIN,XMAX
310 CALL "DATAPLOT" ( XA(),YA(),NTOT,IDIR,L,S$ )
320 IF YNUM=1 THEN GOTO 340
330 PEN 2 @ CALL "DATAPLOT" ( XA(),ZA(),NTOT,IDIR,L+3,S$ )
340 IF IY<NY THEN GOTO 390
345 IF NX>1 THEN GOTO 390
350  CALL "PLOTPOS" ( NX,NY,IX,NY+1,IDIR,PLDV,TITLE$,NHINC,NVINC,LHLAB,LVLAB,HH
,VHT )
360 PEN 1 @ LINE TYPE 1 @ IF IDIR=0 THEN YHT=VHT ELSE YHT=HHT
370 IF IDIR=0 THEN SCALE XMIN,XMAX,-1,.01 ELSE SCALE .01,-1,XMIN,XMAX
380 CALL "AXISZ" ( IDIR,1,XMIN,XMAX,XINC,NXIND,XTICK,XLAB$,YHT,1,0,0 )
390 SUBEXIT
400 OFF ERROR @ IF ERRN =126 THEN DISP "Switch on plotter and press CONT" @ PAU
E @ GOTO 150
410 DISP "Error no. ";ERRN ;" on line ";ERRL  @ PAUSE
420 SUBEND
```

```
10 SUB "FFTSTP" (R(),S(),NA,NB)
20 DIM X(512),Y(512)
30 ANGLE=3.141592654/NA @ U=COS (ANGLE) @ V=-SIN (ANGLE) @ A=1 @ B=0
40 FOR IA=1 TO NA
50 FOR IB=1 TO NB @ J=IA+(IB-1)*2*NA @ X(J)=R(J)+R(J+NA) @ Y(J)=S(J)+S(J+NA)
60 X(J+NA)=(R(J)-R(J+NA))*A-(S(J)-S(J+NA))*B
70 Y(J+NA)=(R(J)-R(J+NA))*B+(S(J)-S(J+NA))*A @ NEXT IB
80 A1=A*U-B*V @ B1=B*U+A*V @ A=A1 @ B=B1 @ NEXT IA
90 FOR I=1 TO NA*NB*2 @ R(I)=X(I) @ S(I)=Y(I) @ NEXT I
100 SUBEND
```

```
10 SUB "TRAN" (A1(),A2(),L,N)
20 DIM B1(512),B2(512),IND(512)
30 M=N/4 @ K=2 @ IND(1)=1 @ IND(2)=1+2*M @ IND(3)=1+M @ IND(4)=1+3*M
40 FOR I=3 TO L @ GOSUB 90
50 NEXT I
60 FOR I=1 TO N @ B1(I)=A1(IND(I)) @ B2(I)=A2(IND(I)) @ NEXT I
70 FOR I=1 TO N @ A1(I)=B1(I)/N @ A2(I)=B2(I)/N @ NEXT I
80 SUBEXIT
90 M=M/2 @ K=K*2
100 FOR J=1 TO K @ IND(K+J)=IND(J)+M @ NEXT J @ RETURN
110 SUBEND
```

```
10 SUB "DISCERR" (FILNAM$)
20  OFF ERROR @ OFF KEY# @ CLEAR
30  DISP "Disc error no. ";ERRN ;" on line ";ERRL ;" for file ";FILNAM$
40  IF ERRN =60 THEN GOTO 110
50  IF ERRN =63 THEN GOTO 130
60  IF ERRN =70 THEN GOTO 200
70  IF ERRN =71 THEN GOTO 220
80  IF ERRN =124 OR ERRN =128 THEN GOTO 230
90  IF ERRN =130 THEN GOTO 240
100 PAUSE @ SUBEXIT
110 DISP "This disc is write protected. Try another disc."
120 DISP "Press CONT when ready" @ PAUSE @ SUBEXIT
130 DISP "Duplicate file name"
140 ON KEY# 1,"Purge" GOTO PUR
150 ON KEY# 2,"Rename" GOTO RENM
160 DISP "Press softkey" @ KEY LABEL
170 GOTO 170
180 PUR: PURGE FILNAM$ @ GOTO 290
190 RENM: DISP "New filename (in quotes)?" @ INPUT FILNAM$@ GOTO 290
200 DISP "Try other disc drive.Press CONT when ready." @ PAUSE
210 MASS STORAGE IS ":D701" @ SUBEXIT
220 DISP "End of file reached" @ SUBEXIT
230 DISP "This disc is full. Use another disc. Press CONT when ready." @ PAUSE
240 ON KEY# 1,"Continue" GOTO 290
250 ON KEY# 2,"Initialise" GOTO INISE
260 DISP "Press softkey" @ KEY LABEL
270 GOTO 270
280 INISE: INITIALIZE
290 CLEAR @ OFF KEY# @ SUBEND
```